frontiers | Research Topics

Plant cuticle: From biosynthesis to ecological functions

Edited by
Eva Domínguez, Antonio Heredia, Isabel Molina and Amauri Bueno

Published in
Frontiers in Plant Science

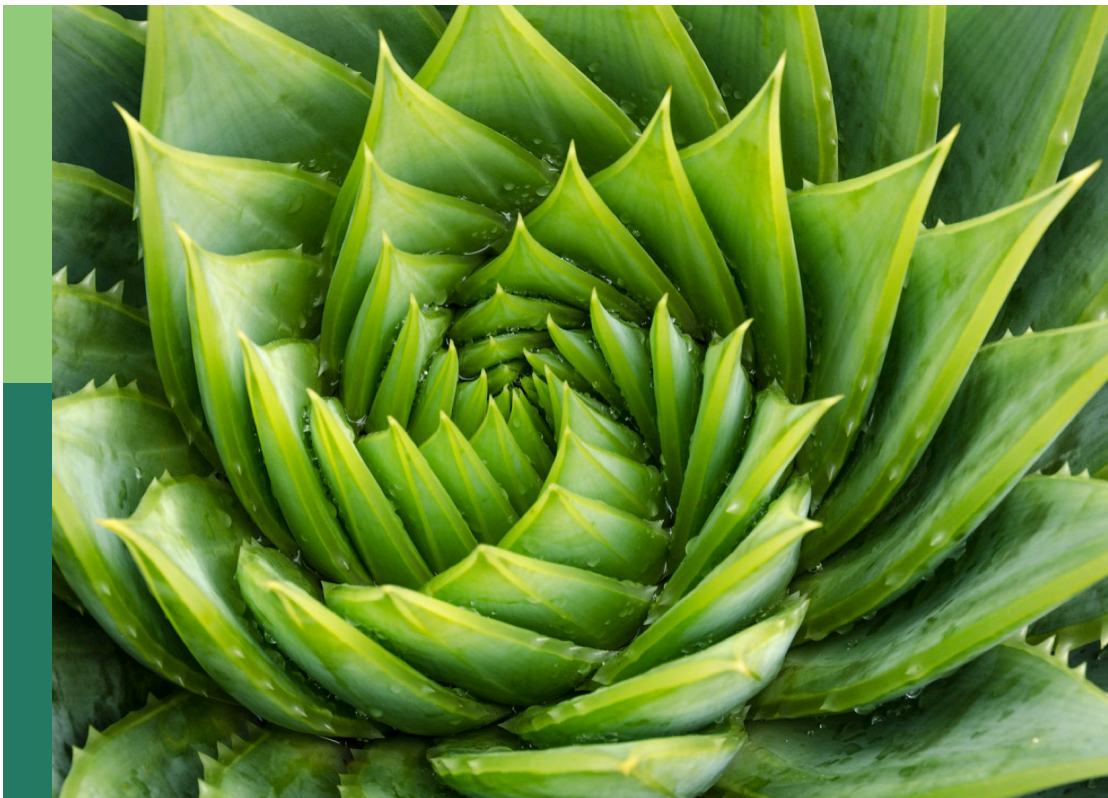

ISSN 1664-8714
ISBN 978-2-83251-793-2
DOI 10.3389/978-2-83251-793-2

About Frontiers

Frontiers is more than just an open access publisher of scholarly articles: it is a pioneering approach to the world of academia, radically improving the way scholarly research is managed. The grand vision of Frontiers is a world where all people have an equal opportunity to seek, share and generate knowledge. Frontiers provides immediate and permanent online open access to all its publications, but this alone is not enough to realize our grand goals.

Frontiers journal series

The Frontiers journal series is a multi-tier and interdisciplinary set of open-access, online journals, promising a paradigm shift from the current review, selection and dissemination processes in academic publishing. All Frontiers journals are driven by researchers for researchers; therefore, they constitute a service to the scholarly community. At the same time, the *Frontiers journal series* operates on a revolutionary invention, the tiered publishing system, initially addressing specific communities of scholars, and gradually climbing up to broader public understanding, thus serving the interests of the lay society, too.

Dedication to quality

Each Frontiers article is a landmark of the highest quality, thanks to genuinely collaborative interactions between authors and review editors, who include some of the world's best academicians. Research must be certified by peers before entering a stream of knowledge that may eventually reach the public - and shape society; therefore, Frontiers only applies the most rigorous and unbiased reviews. Frontiers revolutionizes research publishing by freely delivering the most outstanding research, evaluated with no bias from both the academic and social point of view. By applying the most advanced information technologies, Frontiers is catapulting scholarly publishing into a new generation.

What are Frontiers Research Topics?

Frontiers Research Topics are very popular trademarks of the *Frontiers journals series*: they are collections of at least ten articles, all centered on a particular subject. With their unique mix of varied contributions from Original Research to Review Articles, Frontiers Research Topics unify the most influential researchers, the latest key findings and historical advances in a hot research area.

Find out more on how to host your own Frontiers Research Topic or contribute to one as an author by contacting the Frontiers editorial office: frontiersin.org/about/contact

Plant cuticle: From biosynthesis to ecological functions

Topic editors

Eva Domínguez — La Mayora Experimental Station, Spanish National Research Council (CSIC), Spain

Antonio Heredia — University of Malaga, Spain

Isabel Molina — Algoma University, Canada

Amauri Bueno — Julius Maximilian University of Würzburg, Germany

Citation

Domínguez, E., Heredia, A., Molina, I., Bueno, A., eds. (2023). *Plant cuticle: From biosynthesis to ecological functions*. Lausanne: Frontiers Media SA.

doi: 10.3389/978-2-83251-793-2

Table of contents

frontiers | Frontiers in Plant Science

TYPE Editorial
PUBLISHED 15 February 2023
DOI 10.3389/fpls.2023.1154255

OPEN ACCESS

EDITED AND REVIEWED BY
Anna N Stepanova,
North Carolina State University,
United States

*CORRESPONDENCE
Eva Domínguez
edominguez@eelm.csic.es

SPECIALTY SECTION
This article was submitted to Plant Physiology, a section of the journal Frontiers in Plant Science

RECEIVED 30 January 2023
ACCEPTED 07 February 2023
PUBLISHED 15 February 2023

CITATION
Molina I, Bueno A, Heredia A and Domínguez E (2023) Editorial: Plant cuticle: From biosynthesis to ecological functions. *Front. Plant Sci.* 14:1154255. doi: 10.3389/fpls.2023.1154255

Editorial: Plant cuticle: From biosynthesis to ecological functions

Isabel Molina[1], Amauri Bueno[2], Antonio Heredia[3] and Eva Domínguez[4]*

[1]Department of Biology, School of Life Sciences and the Environment, Algoma University, Sault Ste Marie, ON, Canada, [2]Chair of Botany II – Ecophysiology and Vegetation Ecology, Julius von Sachs Institute of Biological Sciences, University of Würzburg, Würzburg, Germany, [3]Departamento de Biología Molecular y Bioquímica, Instituto de Hortofruticultura Subtropical y Mediterránea "La Mayora", Universidad de Málaga-Consejo Superior de Investigaciones Científicas, Universidad de Málaga, Málaga, Spain, [4]Departamento de Mejora Genética y Biotecnología, Instituto de Hortofruticultura Subtropical y Mediterránea "La Mayora", Universidad de Málaga-Consejo Superior de Investigaciones Científicas, Estación Experimental La Mayora, Málaga, Spain

KEYWORDS

plant cuticle, waxes, cutin, cell wall, phenolics, water transpiration, pathogens

Editorial on the Research Topic
Plant cuticle: From biosynthesis to ecological functions

At the interface between the plant and the environment, the cuticle functions as a barrier to water loss and as a protective layer against pathogens and UV light (Kunst and Samuels, 2009; Yeats and Rose, 2013). Over the last decades, numerous researchers from different fields have investigated the chemistry, structure, biosynthesis and functional properties of the plant cuticle, bringing new questions and insights, and significantly enriching our understanding of its structure, chemical composition, physical properties, natural variability, development, and functions.

In the current scenario of global climate change, it is crucial to understand the biophysical properties of the cuticle as well as how environmental factors, including temperature, UV radiation and relative humidity, modulate cuticle deposition and its functional properties (Domínguez et al., 2011). Seufert et al. report on the influence of different wax fractions on the water transpiration properties of isolated leaf cuticles. Using a differential extraction protocol, the authors studied the influence of triterpenoids and very-long-chain aliphatics (VLCA) on water permeability in cuticles from several species. Comparison of water permeance from isolated cuticles and selectively dewaxed cuticles showed that the cuticle components that greatly affect its transpiration barrier function are mainly VLCAs, and that triterpenoids barely contribute to the water barrier properties of the cuticle. Chen et al. compare adaxial and abaxial cuticle transpiration in detached tea leaves from eight different cultivars. Total leaf cuticle transpiration correlated with abaxial transpiration. Among the different wax classes, VLCA and glycol esters negatively correlated with leaf cuticle transpiration. Additionally, intracuticular waxes were the major water barrier in the adaxial leaf surface and epicuticular waxes in the abaxial side. Low water transpiration rate is also important for extending the life of cut ornamental flowers. Cheng et al. used oriental lily to investigate flower cuticle transpiration and wax chemical composition, showing a higher amount of waxes, largely *n*-alkanes, in tepals than in leaves. However, leaves presented lower water permeance than tepals, a result that the

authors attributed to differences in alkane chain length, with C27 and C29 predominating in tepals and C29 and C31 being more prevalent in leaves. Exploration of these results in other species could provide a tool to select for cultivars with extended vase life.

The Michaelis´ hypothesis states that inadequate cuticle development can cause increased transpiration rate in the treeline. Bueno et al. examine this hypothesis in populations of *Pinus uncinata* from the subalpine forest and the alpine tundra. The authors found higher minimum conductance, lower amounts of cuticle waxes and thinner cuticles in needles from the tundra trees than in those from the forest. These results support the notion that inadequate cuticle development could be one of the factors leading to increased water transpiration during winter in this species. Vega et al. describe water sorption and desorption of isolated leaf cuticles of three woody species. The presence of cutan in the cuticles of holly and cherry laurel was associated with higher water sorption. Differences in cuticle water sorption and water loss were detected among the three studied species, whereas an effect of leaf age on water desorption was only observed in eucalyptus.

The mechanical, thermal and optical properties of the tomato fruit cuticle were analyzed by Benítez et al. and Benitez et al. Cutinization of anticlinal cell walls during development plays a biomechanical role inducing cuticle softening. The increase in cuticle phenolic content with ripening was accompanied by a progressive stiffness that suggested a cooperative association of phenolics with both cutin and polysaccharide fractions. The heat regulation capacity of the cuticle varied with development and temperature and was mainly attributed to the cutin matrix. However, the glass transition temperature, the transition from a rigid glassy state to a relaxed rubbery conformation, was modulated by phenolics, polysaccharides and, to a minor extent, waxes. The observed increase in cuticle glass transition between fruit growth and ripening implies physical changes that can affect molecular diffusion through the cuticle. The authors also report that the highly efficient UV-B filtering capacity of the cuticle can be attributed to the accumulation of cinnamic acids, and that the deposition of the flavonoid chalconaringenin during ripening expands the blocking capacity of the cuticle to include UV-A light.

Tomato fruit has become a model for cuticle analysis due to its thick and easy-to-isolate cuticle, as well as to the genetic and genomic resources available in the form of natural and artificially induced mutants, germplasm collections, and intra and interspecies segregating populations (Petit et al., 2017). In their minireview, Petit et al. explore the recent advances in uncovering the genetic and molecular determinants of cuticle deposition and its implications in our understanding of tomato fruit cuticle and its relation to plant growth and performance. Future challenges and possible avenues of research such as investigating the regulation of cuticle phenolics and cell wall polysaccharides deposition, the correlation of cuticle deposition with epidermal cell development and organ growth, and the epigenetic regulation of cuticle biosynthesis are also considered.

Over the last years, there has been a shift in how the cuticle is envisioned, from an isolated outer layer to part of the more complex scenario of the outer epidermal cell wall (Ingram and Nawrath, 2017). In a mini-review, Reynoud et al. describe recent developments and hypotheses on how cuticle chemical composition can affect its architecture and the architecture-function relationships. Although plant cuticles have been typically described as an assembly of lipids, namely waxes and cutin, a far more complex architecture of the cuticle is depicted. It can be described as a hydrophobic, dynamic, chemically and spatially heterogeneous composite containing lipids, cell-wall-derived polysaccharides, phenolic acids and, in some instances such as ripe tomato, flavonoids. The relationship between cell wall pectin, cuticle permeability and *Botrytis cinerea* resistance was investigated by Lorrai et al. using *Arabidopsis thaliana* pectin mutants. Alteration of homogalacturonan integrity, a major pectin component, increased the accumulation of reactive oxygen species (ROS) dependent on the activity of the class III peroxidase AtPRX71. These changes in homogalacturonan structure also led to a notable increase in cuticle permeability and resistance to *B. cinerea*. Interestingly, neither cuticle permeability nor pathogen resistance were affected in cell wall mutants displaying changes in other polysaccharide components. In parallel, Aragon et al. report on the contribution of cutin and waxes to cuticle permeability, ROS accumulation and sensitivity to *B. cinerea* in *A. thaliana* mutants. Although mutants with altered cutin or wax composition displayed an increase in cuticle permeability and ROS levels, resistance to *B. cinerea* was only found in cutin mutants. These mutants displayed upregulation of genes related to pectin and ROS accumulation after *B. cinerea* inoculation. These observations point again to a relationship between pathogen resistance, the pectin domain of the epidermal cell wall, cuticle permeability and cutin composition that merits further study. Arya et al. review the complex and multidimensional interactions between the plant cuticle and pathogenic fungi, paying special attention to epicuticular waxes and cutin monomers, the two most studied cuticle components in relation to pathogens. Differences between pre-penetration and infection processes, fungi lifestyles, and epicuticular wax chemistry and structure make this topic particularly challenging. The authors further debate how composition, structure, permeability and released cutin monomers are perceived by plants and can elicit defense responses.

Ensuring peak fresh produce quality is one of the main current goals of the agri-food industry (Oltra-Mestre et al., 2021). The biophysical properties of the cuticle modulate traits related to postharvest life (Fernández-Muñoz et al., 2022). Si et al. study the radial growth of apple cuticle and its implications in mechanical strain build-up, a trigger for several fruit surface disorders. A combination of radioactive labelling and cuticle analysis was employed showing that cuticle deposition occurred in the inner cuticle region, close to the cell wall, thus creating an aging gradient across cuticle thickness. The authors suggest that this pattern of cuticle deposition could delay surface microcrack propagation to epidermal cells in species with continuous cuticle deposition throughout development. Hurtado and Knoche investigate the role of the cuticle in strawberry water soaking, a skin disorder that limits open field production. Moisture exposed areas were associated with the presence of cuticle microcracks, which acted as fast and localized water uptake areas, thus triggering a series of events leading to cell burst and cell content leakage. The relationship between cuticle chemical composition and postharvest fruit quality was investigated

in zucchini and wampee. Carvajal et al. compare cuticle waxes and transcriptomic changes in a cold-tolerant and a cold-sensitive variety of zucchini at harvest and after cold storage. A thicker cuticle and higher amount of waxes were found in the cold-tolerant variety. The authors conclude that in zucchini, cuticle thickness is related to chilling tolerance and helps to reduce water loss, highlighting the importance of the biosynthesis of very-long-chain alkanes and its transcriptional regulation during the adaptation of the zucchini fruit to low temperatures and in maintaining the postharvest quality of zucchini fruit during cold storage. Huang et al. report on wampee cuticle composition and fruit transpiration along ripening in two cultivars. The cutin matrix was chiefly composed of dihydroxy fatty acids and the main wax compounds were alkanes and triterpenoids. Cultivar differences and changes during ripening were observed for the amount of cuticle and waxes. Fruit transpiration decreased with ripening. A negative correlation was found between the water barrier properties and the alkane content of ripening wampee fruits.

Two contributions to this Research Topic focus on largely unexplored areas of plant cuticle research. Philipe et al. review known aspects and hypothetical scenarios of the mechanisms used for the transport of cutin precursors and waxes across the plasma membrane and through the cell wall. The authors summarize the well-documented mechanism of cutin precursor export through the plasma membrane-localized ATP-binding cassette transporters. The researchers also discuss more exploratory and unknown aspects of the cellular trafficking and export of cuticle components *via* vesicles and *via* a non-vesicular route, and how the cuticle precursors can traverse the polysaccharide cell wall before their incorporation into the cuticle. The method article by Bock et al. is focused on the use of Raman vibrational microscopy, a non-destructive and fast technique that can be employed in epidermal tissue samples, to elucidate the in-depth localization and distribution of cuticle components at the microscale. After application of the methodology to study cuticles from three species, the authors reveal common cuticle chemical distribution features as well as differences, and draw general conclusions on the localization of waxes, phenolics and cutin on a supramolecular polysaccharide matrix.

The original article by Liu et al. describes the functional characterization of a ubiquitin ligase named ABA-related RING-type E3 ligase (AtARRE) that negatively regulates cuticle wax biosynthesis in *A. thaliana*. Co-expression of AtARRE and candidate target proteins involved in alkane formation showed that the alkane biosynthetic enzymes CER1 and CER3 are targets of AtARRE and that CER1 can be ubiquitinated by AtARRE. The authors propose that AtARRE serves as a post-translational regulator that terminates wax biosynthesis *via* the alkane-forming pathway.

Many uncertainties remain regarding the biogenesis and functions of the plant cuticle. To gain a broader perspective on the role of the cuticle in plant performance, it will be crucial to understand the structural and functional properties of isolated cuticles in their natural scenario, and to also consider cuticle interactions with epidermal cells. Because of its heterogeneous and composite nature, the cuticle varies among species and is modified by environmental, developmental and hormonal cues (Yeats and Rose, 2013). Hence, a comprehensive analysis of the interactions among cuticle components, their involvement in the functions ascribed to the cuticle, and how such components change in response to internal and external signals is required. In this sense, the design of artificial cuticles could be a promising strategy to study the contributions of individual cuticle components to the supramolecular structure and properties of the cuticle.

Author contributions

All authors listed have made a substantial, direct, and intellectual contribution to the work and approved it for publication.

Conflict of interest

The authors declare that the research was conducted in the absence of any commercial or financial relationships that could be construed as a potential conflict of interest.

Publisher's note

References

Domínguez, E., Heredia-Guerrero, J. A., and Heredia, A. (2011). The biophysical design of plant cuticles: An overview. *New Phytol.* 189, 938–949. doi: 10.1111/j.1469-8137.2010.03553.x

Fernández-Muñoz, R., Heredia, A., and Domínguez, E. (2022). The role of cuticle in fruit shelf-life. *Curr. Opin. Biotechnol.* 78, 102802. doi: 10.1016/j.copbio.2022.102802

Ingram, G., and Nawrath, C. (2017). The roles of the cuticle in plant development: Organ adhesions and beyond. *J. Exp. Bot.* 68, 5307–5321. doi: 10.1093/jxb/erx313

Kunst, L., and Samuels, L. (2009). Plant cuticles shine: Advances in wax biosynthesis and export. *Curr. Opin. Plant Biol.* 12, 721–727. doi: 10.1016/j.pbi.2009.09.009

Oltra-Mestre, M. J., Hardagen, V., Coughlan, P., and Segura-García del Río, B. (2021). Innovation in the agri-food sector: Exploiting opportunities for industry 4.0. *Creat. Innov. Manage.* 30, 198–210. doi: 10.1111/caim.12418

Petit, J., Bres, C., Mauxion, J. P., Bakan, B., and Rothan, C. (2017). Breeding for cuticle-associated traits in crop species: traits, targets, and strategies. *J. Exp. Bot.* 68, 5369–5387. doi: 10.1093/jxb/erx341

Yeats, T. H., and Rose, J. K. C. (2013). The formation and function of plant cuticles. *Plant Physiol.* 163, 5–20. doi: 10.1104/pp.113.222737

frontiers in Plant Science

MINI REVIEW
published: 25 June 2021
doi: 10.3389/fpls.2021.663165

The Plant Cuticle: An Ancient Guardian Barrier Set Against Long-Standing Rivals

*Gulab Chand Arya[1], Sutanni Sarkar[1,2], Ekaterina Manasherova[1], Asaph Aharoni[3] and Hagai Cohen[1]**

[1]Department of Vegetable and Field Crops, Institute of Plant Sciences, Agricultural Research Organization (ARO), Volcani Center, Rishon LeZion, Israel, [2]Plant Pathology and Microbiology Department, Robert H. Smith Faculty of Agriculture, Food and Environment, The Hebrew University of Jerusalem, Rehovot, Israel, [3]Department of Plant and Environmental Sciences, Weizmann Institute of Science, Rehovot, Israel

The aerial surfaces of plants are covered by a protective barrier formed by the cutin polyester and waxes, collectively referred to as the cuticle. Plant cuticles prevent the loss of water, regulate transpiration, and facilitate the transport of gases and solutes. As the cuticle covers the outermost epidermal cell layer, it also acts as the first line of defense against environmental cues and biotic stresses triggered by a large array of pathogens and pests, such as fungi, bacteria, and insects. Numerous studies highlight the cuticle interface as the site of complex molecular interactions between plants and pathogens. Here, we outline the multidimensional roles of cuticle-derived components, namely, epicuticular waxes and cutin monomers, during plant interactions with pathogenic fungi. We describe how certain wax components affect various pre-penetration and infection processes of fungi with different lifestyles, and then shift our focus to the roles played by the cutin monomers that are released from the cuticle owing to the activity of fungal cutinases during the early stages of infection. We discuss how cutin monomers can activate fungal cutinases and initiate the formation of infection organs, the significant impacts of cuticle defects on the nature of plant–fungal interactions, along with the possible mechanisms raised thus far in the debate on how host plants perceive cutin monomers and/or cuticle defects to elicit defense responses.

Keywords: plant cuticle, pathogenic fungi, defense response, epicuticular wax, plant-pathogen interactions

OPEN ACCESS

Edited by:
Eva Domínguez, Consejo Superior de Investigaciones Científicas, Spanish National Research Council (CSIC), Spain

Reviewed by:
Mario Serrano, National Autonomous University of Mexico, Mexico
Christiane Nawrath, University of Lausanne, Switzerland, in collaboration with reviewer Ulrich Schaffrath

***Correspondence:**
Hagai Cohen
hagaic@volcani.agri.gov.il

Specialty section:
This article was submitted to Plant Physiology, a section of the journal Frontiers in Plant Science

Received: *02 February 2021*
Accepted: *31 May 2021*
Published: *25 June 2021*

Citation:
Arya GC, Sarkar S, Manasherova E, Aharoni A and Cohen H (2021) The Plant Cuticle: An Ancient Guardian Barrier Set Against Long-Standing Rivals. Front. Plant Sci. 12:663165. doi: 10.3389/fpls.2021.663165

INTRODUCTION

The aerial surfaces of plants are covered by a lipophilic protective shield called the cuticle. The cuticle acts as a diffusion barrier and, therefore, influences the diffusion of an array of molecules such as water, gases, and solutes (Isaacson et al., 2009; Chen et al., 2011). Yet, apart from enabling plants to survive in dry environments, the cuticle represents the first line of defense against biotic stresses triggered by a variety of pathogens and pests, including fungi, bacteria, and insects. Thus, the cuticle acts as the interface where the complex molecular interactions occur between plant surfaces and pathogens. Not surprisingly, many attributes of the cuticle, for example, its architecture, thickness, and biochemistry were associated with altered resistance or susceptibility to pathogens (Manandhar and Hartman, 1995; Gabler et al., 2003; Gomes et al., 2012; Martin and Rose, 2014).

Plant cuticles are made of lipophilic compounds that are deposited onto the outer cell walls of the epidermis layer (**Figure 1**). These include the solvent-extractable cuticular waxes and cutin, cuticle's main component, which cannot be extracted due to its polymeric nature. Cuticular waxes are typically deposited within (intracuticular) or on top (epicuticular) of the cutin matrix and are composed of a mixture of C_{20} to C_{40} very-long-chain-fatty-acids (VLCFAs), which are further modified to form corresponding alkanes, aldehydes, ketones, primary and secondary alcohols, and esters (Samuels et al., 2008; Buschhaus and Jetter, 2011). The polyester cutin is composed of C_{16} and C_{18} fatty acids modified with functional groups, such as terminal and mid-chain hydroxy, epoxy, and carboxy groups, which are cross-linked by ester bonds (Cohen et al., 2019; Philippe et al., 2020). Studies show that the structural and chemical nature of the cuticle varies greatly between plant species, genotypes, organs, and developmental stages (Jeffree, 2006; Domínguez et al., 2011; Yeats and Rose, 2013; Fernández et al., 2016; Jetter and Riederer, 2016).

The development of the cuticle facilitated the terrestrialization of land plants approximately 450 million years ago (Cohen et al., 2017). As most primary nutritional source of carbon for fungal species is living or dead plant tissue, it is hypothesized that the early colonizing plants paved the way to the foundation and divergence of the first fungal ancestries (Lutzoni et al., 2018). Indeed, the main concept opines that plants and fungi coevolved 400–600 million years ago (Heckman et al., 2001), and that during this period, these two kingdoms developed complex relationships. These include symbiotic interactions where both the host plant and the fungus benefit from their mutualistic relationship; saprotrophy, where the fungus obtains nourishment from dead or decaying plant tissues; and parasitism, practiced by most pathogenic fungi, which need to penetrate the host plant tissue in order to reach the nutritional contents of inner cells (Burdon and Thrall, 2009). Plant colonization by fungi strongly depends on their lifestyle. Spores of necrotrophic fungal species (e.g., *Botrytis cinerea*) land on the host plant cuticle surface, germinate *via* germ tubes that eventually become the primary hyphae that penetrate through the host cuticle (**Figure 2A**, upper panel). Following penetration, hyphae grow below the cuticle to some complex secondary hyphae that kills epidermal and inner tissue host cells (**Figure 2A**, bottom panel). At the early stages of infection, hemibiotrophic fungal (e.g., *Magnaporthe oryzae*) spores germinate on the cuticle surface and develop a specialized infection structure called appressorium, a flattened organ that pressures the host plant surface eventually penetrating it *via* a penetration peg. This stage is considered biotrophic as the bulged hyphae that colonize the infected cells do not kill it (**Figure 2B**, upper panel). However, at later infection stages, these hyphae adopt a necrotrophic lifestyle eventually killing epidermal and inner tissue host cells (**Figure 2B**, bottom panel). Biotrophic fungi (e.g., *Blumeria graminis*) germinate on the cuticle surface and typically develop an appressorium. This structure penetrates through the host plant cuticle and colonizes the intercellular space *via* a feeding structure called haustorium, which invades the host cell without piercing the plasma membrane and killing it (**Figure 2C**, upper panel). At the final stages of infection, the fungus produces dense mycelia on the cuticle surface and conidia (**Figure 2C**, bottom panel; Schulze-Lefert and Panstruga, 2003; Laluk and Mengiste, 2010; Lo-Presti et al., 2015).

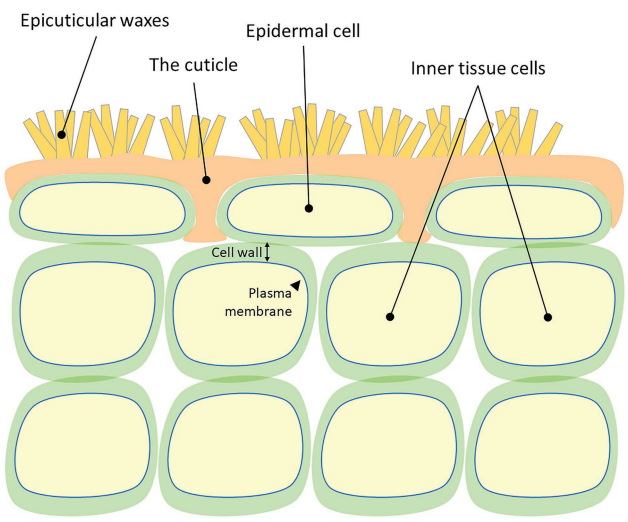

FIGURE 1 | A schematic representation of the cellular localization of the plant cuticle. Cell wall and plasma membrane are presented.

Pathogenic fungi have established a battery of strategies to overcome the cuticle barrier. These include the utilization of cuticle-derived signals that induce the spore germination on the plant surface, the formation of specialized infection organs, and penetration of the cuticle. Some fungal species enter through stomata or natural gaps, whereas others pierce the surface of the cuticle by applying mechanical pressure. Most pathogenic fungi, however, secrete a blend of specialized cell wall-degrading enzymes toward the plant surface, including pectate lyases, cellulases, and cutinases. The latter family of enzymes possesses a unique ability to release the ester bond-linked monomers that build the cutin polyester (Kubicek et al., 2014). Cutinase activity was shown in various pathogenic fungi to greatly impact the process of infection: from the initial stages of spore adhesion to the plant surface, through spore germination and the formation of specialized infection organs, to the breakdown of the cuticle and the colonization of the host plant (Kolattukudy, 1985).

Regardless of the kind of relationship, all the types of interaction between the aerial organs of plants and fungi take place at the cuticle surface – a hub of plant innate immunity and fungal infection responses. In the current review, we focus on the multidimensional roles of plant cuticle-derived components during the infection of pathogenic fungi. For additional information about the regulation of plant–bacteria interactions at the cuticle surface, we warmly refer readers to the excellent reviews of Aragón et al. (2017) and Ziv et al. (2018). Here, we first describe rudimentary evidence that establishes epicuticular waxes as major determinants of plant–fungal interactions and that certain wax components can affect various pre-penetration and infection processes of fungi with different lifestyles. We then shift our focus to the roles played by cutin monomers that are released from the cuticle owing

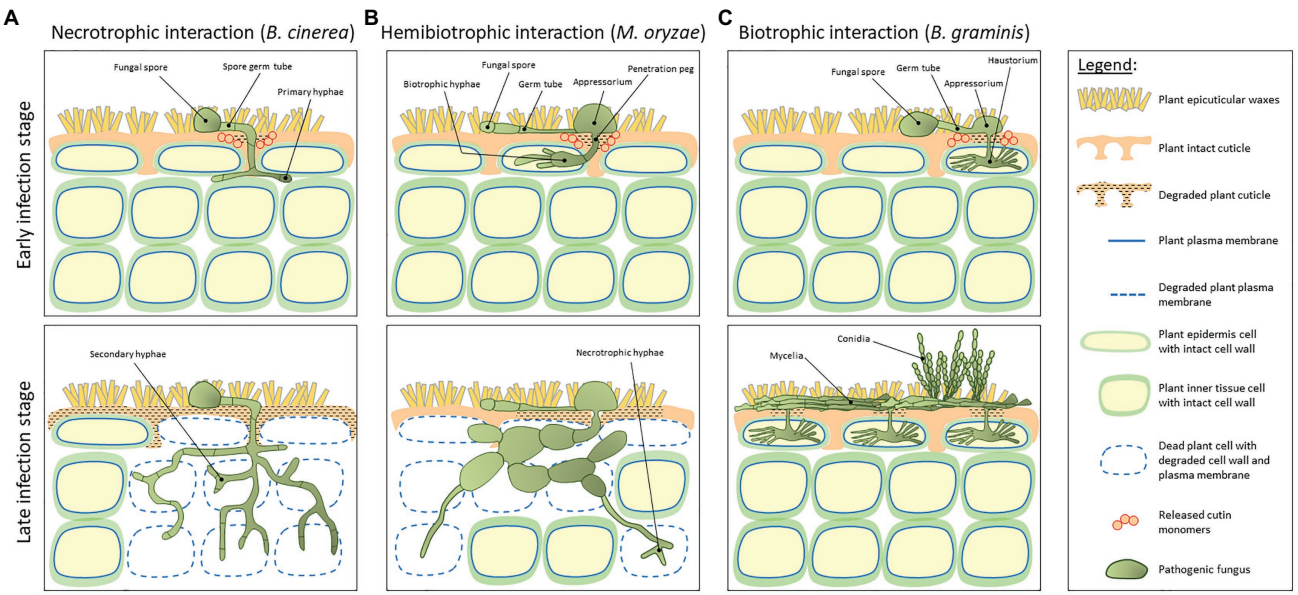

FIGURE 2 | A schematic representation of the host plant and pathogen fundamental structures during early and late stages of plant–fungal interaction. **(A)** Interaction with a necrotrophic fungus (e.g., *Botrytis cinerea*). Spores land on the host plant cuticle surface and generate a germ tube. These tubes become the primary hyphae that penetrate through the cuticle and grow below the cuticle into a complex secondary hyphae structure that kills epidermal and inner tissue host cells. **(B)** Interaction with a hemibiotrophic fungus (e.g., *Magnaporthe oryzae*). At early stages of infection, spores germinate on the cuticle surface and develop a specialized infection structure called appressorium, a flattened organ that pressures the host plant surface eventually penetrating it *via* a penetration peg. This stage is considered biotrophic as the bulged hyphae that colonize the infected cells do not kill it. However, at later infection stages, these hyphae adopt a necrotrophic life style. **(C)** Interaction with a biotrophic fungus (e.g., *Blumeria graminis*). At early infection stage, spores germinate on the cuticle surface and develop an appressorium. After penetration through the host plant cuticle, the fungus colonizes the intercellular space *via* a feeding structure called haustorium, which invades the host cell without piercing the plasma membrane and killing it. At final stages of infection, the fungus produces dense mycelia on the cuticle surface and conidia. Upper panels represent early infection stages, whereas bottom panels represent late infection stages.

to the activity of fungal cutinases during the early stages of infection. We describe how these monomers activate fungal cutinases and initiate the formation of infection organs. Finally, we mention key reports that revealed the significant impacts of imperfections in cuticle biochemistry and permeability on the nature of interactions between pathogenic fungi and host plants and discuss possible mechanisms by which host plants perceive released cutin monomers to elicit defense responses.

Epicuticular Waxes Are Major Determining Factors of Plant–Fungal Interactions

As epicuticular waxes are deposited on top of the outermost surface of the cuticle, they are the first to interact with any type of pathogen. It is, therefore, expected that changes to the patterns of crystallization, composition, and hydrophobicity of epicuticular waxes will significantly impact various aspects of plant–fungal interactions (Shepherd and Griffiths, 2006; Buschhaus and Jetter, 2011; Lewandowska et al., 2020). Extensive work on *B. graminis* has shown that this pathogenic fungus exploits components of the plant epicuticular wax to induce pre-penetration processes. For instance, silencing 3-ketoacyl-CoA synthase 6 (KCS6) and enoyl-CoA reductase (ECR) in wheat (*Triticum aestivum*), both of which are important for VLCFA biosynthesis and the elongation reactions required for cuticular lipid biosynthesis, attenuates *B. graminis* spore germination (Wang et al., 2019; Kong et al., 2020). In line with these findings, Feng et al. (2009) characterized Lip1, a lipase in *B. graminis* that is secreted onto the surface of fungal cell walls and possesses the ability to release alkanes and primary fatty alcohols from the epicuticular wax of wheat leaves. Remarkably, the pretreatment of wheat leaves with Lip1 resulted in the removal of surface wax, which, in turn, severely compromised conidial adhesion, appressorium formation, and secondary hyphal growth of the fungus (Feng et al., 2009). The spores of this fungus also hardly germinated on the barley (*Hordeum vulgare*) *emr1* mutant, which is depleted in the leaf surface waxes due to a mutation in KCS6 (Weidenbach et al., 2014). In the case of *Alternaria brassicicola*, it was shown that the removal of epicuticular waxes from cauliflower (*Brassica oleracea*) leaves affected spore adhesion and fungal penetration during the early stages of infection (Berto et al., 1999). An intriguing case that highlights the divergent effects of the wax composition on fungal infection is that of *Curvularia eragrostidis*, a cosmopolitan fungal pathogen that infects hosts from several botanical families (Ferreira et al., 2014). It was found that epicuticular waxes from its grass host plant, hairy crabgrass (*Digitaria sanguinalis*), significantly induced spore germination and germ tube elongation, but had no effect on appressorium differentiation. Yet, the epicuticular waxes of tall fescue grass (*Festuca arundinacea*), which represents a nonhost species of this fungus, hindered fungal spore germination and appressoria formation (Wang et al., 2008).

The aforementioned studies clearly demarcate the importance of the signaling roles of epicuticular wax components to the initiation of fungal infection processes. Complementing investigations sought to isolate the specific wax components that initiate these processes. *In vitro* assays have validated that very-long-chain (VLC) aldehydes trigger the spore germination and appressorium differentiation of *B. graminis* (Ringelmann et al., 2009; Hansjakob et al., 2010, 2011). Similarly, wax inducer 1 (WIN1) suppression in wheat negatively affected *B. graminis* germination by interfering with the VLC aldehyde wax biosynthesis. Remarkably, coating the leaves of WIN1-silenced lines with typical wild-type (WT) epicuticular waxes fully restored the spore germination of the fungus (Kong and Chang, 2018). More specifically, the C_{28} aldehyde of wheat was shown to endorse the spore germination in *Puccinia graminis* f. sp. *tritici* (Reisige et al., 2006). Apart from the wax aldehydes, primary alcohols were also shown to play critical roles in the fungal infection initiation. Namely, the C_{24} primary alcohol on the surface of avocado (*Persea americana*) fruit triggers the spore germination and appressorium differentiation in *Colletotrichum gloeosporioides* (Podila et al., 1993). Higher levels of the C_{30} primary alcohol in the Arabidopsis *cer1* line, which is mutated in the ECERIFERUM 1 (CER1) enzyme, were able to suppress the growth and reproduction of *Golovinomyces orontii* (Jenks et al., 1995; Inada and Savory, 2011). Interestingly, the overexpression of CER1 in Arabidopsis promoted the VLC alkane biosynthesis, resulting in higher susceptibility to the infection by *Sclerotinia sclerotiorum* (Bourdenx et al., 2011), highlighting that the wax alkanes also play significant signaling roles. Correspondingly, the transgenic cucumber (*Cucumis sativus*) fruit with lower expression of CsWAX2, a homolog of the Arabidopsis WAX2 gene involved in the biosynthesis of VLC wax alkanes, resulted in an overall reduction of 50% in the wax content of the fruit surface, owing to major reductions in C_{29} and C_{31} alkanes. Inoculation assays with *B. cinerea* demonstrated that its pathogenicity was dramatically impaired only at the fruit surface of this mutant, but not on the fruit surfaces of WT and WAX2-overexpression plants (Wang et al., 2015). WAX2 was shown to be allelic to *CER3/YORE-YORE (YRE)/FACELESS POLLEN1* (*FLP1*) and has a pleiotropic phenotype, including an altered wax composition (Rowland et al., 2007). Finally, polar wax-associated terpenoids on the avocado fruit surface were shown to induce appressorium formation (Kolattukudy et al., 1995).

The findings described above emphasize that different epicuticular wax components can affect various processes of pathogenic fungal infection, yet these effects are seemingly far more complex than assumed, as demonstrated by Uppalapati et al. (2012). The forward-genetics screen using Barrel clover (*Medicago truncatula*) *Tnt1* retrotransposon insertion lines followed by the authors found that the *inhibitor of rust germ tube differentiation 1* (*irg1*) mutant failed to promote the pre-infection structural differentiation of two rust pathogens, *Phakopsora pachyrhizi* and *Puccinia emaculata*, on the abaxial leaf surface. The chemical analysis of the epicuticular wax composition revealed a >90% reduction in C_{30} primary alcohols and overaccumulation of C_{29} and C_{31} alkanes in the leaves of the *irg1* mutant (Uppalapati et al., 2012). Further analyses validated that IRG1 encodes the Cys(2)His(2) zinc transcription factor, PALM1, which plays important role in regulating epicuticular wax metabolism and transport. Yet, the most intriguing observation was that the altered wax composition in leaves of this mutant had entirely dissimilar effects on the virulence of pathogenic fungi with different lifestyles. As mentioned above, the *irg1* mutant inhibited the pre-infection structural differentiation of the rust fungal species *Phakopsora pachyrhizi* and *Puccinia emaculata*, but had no effect on the pathogenicity of the necrotrophic fungus *Phoma medicaginis* (Uppalapati et al., 2012), suggesting that the changes in leaf wax composition might be limited to fungal species that form pre-infection appressoria structures in response to the surface signals, unlike *Phoma medicaginis*, which directly penetrates the cuticle without forming these structures.

Cutin Monomers Released During Infection Activate Fungal Cutinases and Initiate the Formation of Infection Organs

The cuticle is considered as the major protective barrier that fungi should overcome. During the earliest stages of infection, fungal cutinases secreted from spores landing on the plant cuticle surface release cutin monomers from the cuticle in a spatially localized manner (Köller et al., 1982; **Figure 2**). Many reports on pathogenic fungi with different life styles have established the importance of the signaling of these released cutin monomers for the continuation and progression of infection, as it leads to the elevated cutinase activity at later stages of the fungal development essential for the cuticle penetration (Woloshuk and Kolattukudy, 1986; Francis et al., 1996; Gilbert et al., 1996). These include *in vitro* studies of a vast range of pathogenic fungi demonstrating that the cutinase activity significantly increases upon the addition of typical cutin monomers into their growing media, mainly C_{16} and C_{18} *n*-aliphatic primary alcohols and 16-hydroxyhexadecanoic acid. Amongst the pathogenic fungi investigated are the hemibiotrophic fungal species of *Fusarium solani* (Purdy and Kolattukudy, 1975; Lin and Kolattukudy, 1978; Woloshuk and Kolattukudy, 1986), *Colletotrichum graminicola* (Pascholati et al., 1993), and *Colletotrichum gloeosporioides* (Wang et al., 2017), and also the necrotrophic fungal species of *B. cinerea* (van der Vlugt-Bergmans et al., 1997), *Ascochyta rabiei* (Tenhaken et al., 1997), *Pyrenopeziza brassicae* (Davies et al., 2000), *S. sclerotiorum* (Bashi et al., 2012), *Venturia inaequalis* (Köller et al., 1991), and *Monilinia fructicola* (Lee et al., 2010). Another set of reports demonstrated that, apart from activating fungal cutinases, released cutin monomers trigger the formation of spore germ tubes and specialized infection organs, such as appressoria. This was demonstrated in the biotrophic fungal pathogens *Erysiphe graminis* f. sp. *hordei* and hemibiotrophic *Magnaporthe grisea* (Francis et al., 1996; Gilbert et al., 1996; DeZwaan et al., 1999; Zhang et al., 2005).

The Significant Impact of Cuticle Imperfections on the Nature of Plant–Fungal Interactions

Cutin monomers that are released from the host plant cuticle during infection might shape plant–fungal interactions by

endorsing several fungal infection strategies. The question of how defects in cuticle structure, biochemistry, and permeability affect these interactions has puzzled researchers in recent years. Sadler et al. (2016) demonstrated that the physical structure and the precise molecular arrangement of wax molecules affect cuticular permeability, but not the thickness of wax and cutin depositions in the cuticle. In the current section, we elaborate on some of the key reports that inferred the significant impact of cuticle defects on various stages of fungal infection, from the adhesion of fungal spores to the plant surface, through the physical attachment of infection organs, to the capacity of the fungus to penetrate into the inner tissue of the host plant. These studies highlight how these defects might consequently lead to immunity or susceptibility of the host plant upon an attack by pathogenic fungi.

In an early study, Sieber et al. (2000) generated Arabidopsis plants with heterologous overexpression of a cell wall-targeted fungal cutinase from *Fusarium oxysporum*. These transgenic plants, termed CUTE, displayed a striking full immunity to *B. cinerea* despite dramatic modifications in their cuticle ultrastructure and enhanced permeability to solutes and strong postgenital organ fusions (Sieber et al., 2000; Chassot et al., 2007). These results paved the way to the notion that the cuticle is a key component of plant–fungal interactions, and that alterations to its structure and permeability might facilitate immunity to invading fungi. Some follow-up studies geared toward characterizing the interactions between cuticle-deficient mutants and pathogenic fungi further strengthened this notion. For example, the Arabidopsis *lacs2* mutant, deficient in the long-chain acyl-CoA synthetase 2 enzyme that catalyzes the synthesis of fatty acyl-CoA intermediates in the cutin pathway and unsubstituted fatty acids in wax biosynthesis, had a fivefold reduction in the total amount of ω-hydroxylated fatty acids and their derivatives as compared to the WT variant. These modifications led to a strong resistance of the *lacs2* mutant plant to the necrotrophic fungi *B. cinerea* and *S. sclerotiorum* (Schnurr et al., 2004; Bessire et al., 2007). In addition, the 70% reduction in the cutin content of the *cyp86a2/att1* mutant, which is deficient in the CYP86A2 P450-dependent monooxygenase that hydroxylates fatty acids, led to enhanced resistance to *B. cinerea* (Xiao et al., 2004). The *Arabidopsis thaliana* ATP-binding cassette (ABC) protein AtABCG32, an ABC transporter localized to the plasma membrane of epidermal cells, was suggested to export cutin precursors from these cells to the surface (Bessire et al., 2011). The mutation of this gene in the corresponding Arabidopsis *pec1/abcg32* mutant also led to resistance to *B. cinerea*. Fully expanded leaves of this mutant featured significantly lower levels of the cutin monomer C_{16} dicarboxylic and ω-hydroxy $C_{18:2}$ acids, apparently leading to a more permeable cuticle (Fabre et al., 2016). Similarly, rice (*Oryza sativa*) plants with silenced or mutated expression of *OsABCG31*, the homolog of the Arabidopsis ABCG32, displayed increased cuticle permeability and were more resistant to *M. oryzae* (Garroum et al., 2016).

Resistant phenotypes to *B. cinerea* were also detected in the Arabidopsis mutant lines *fiddlehead* (*kcs10*/*fdh*), *lacerata* (*cyp86a8/lcr*), and *bodyguard* (*bdg*), which surprisingly accumulate more cutin, even though they carry mutations in key cuticle biosynthetic genes (Voisin et al., 2009). *kcs10*/*fdh* is deficient in the 3-ketoacyl-CoA synthase 10 condensing enzyme that is part of the fatty acid elongation complex involved in the synthesis of VLCFAs, though its exact function in cuticle formation has yet to be determined (Lolle et al., 1992, 1997; Pruitt et al., 2000); *cyp86a8/lcr* is mutated in CYP86A8, which is involved in the fatty acid hydroxylation pathway (Wellesen et al., 2001); and *bdg* has a mutation in BODYGUARD, an extracellular α/β hydrolase suggested to be involved in cutin polyester assembly (Kurdyukov et al., 2006b; Jakobson et al., 2016).

However, not all plants that feature an increase in cuticle permeability display heightened resistance against pathogenic fungi. The Arabidopsis *hothead* (*hth*) mutant is deficient in its ability to oxidize long-chain ω-hydroxy fatty acids to ω-oxo fatty acids and, therefore, has less α,ω-dicaroxylic fatty acids and more ω-hydroxy fatty acids. This results in a disordered cuticle membrane structure and increased leaf cuticle permeability (Lolle et al., 1998; Kurdyukov et al., 2006a). Conversely, *hth* does not exhibit increased resistance to *B. cinerea* (Bessire et al., 2007). The Arabidopsis double mutant *gpat4/gpat8*, which features altered expression of two glycerol-3-phosphate *sn*-2-acetyltransferases essential for cuticle assembly, is more susceptible to infection by the necrotrophic fungus *A. brassicicola* (Li et al., 2007). Moreover, Arabidopsis mutants that are defective in acyl carrier protein4 (ACP4) and exhibit malformed leaf cuticle are also more susceptible to *B. cinerea* (Xia et al., 2009). Additional studies showed that mutations in SHINE1, a transcription factor of the ethylene response factor (ERF) family that regulates cutin biosynthesis, produce less cutin, and are more susceptible to *B. cinerea* (Kannangara et al., 2007; Sela et al., 2013). Likewise, lower cutin content in the cuticles of the tomato (*Solanum lycopersicum*) fruit skin due to reduced expression of cutin regulator SHINE3 leads to higher susceptibility to *B. cinerea* (Buxdorf et al., 2014). Finally, the cutin polymerization in the tomato fruit skin occurs *via* the transesterification of hydroxyacylglycerol precursors catalyzed by the Gly-Asp-Ser-Leu (GDSL)-motif lipase/hydrolase family protein cutin deficient1 (CD1; Yeats et al., 2012). The fruit skin cuticle of its corresponding mutant, *cd1*, has significantly less cutin, and its fruits are more susceptible to *B. cinerea* (Isaacson et al., 2009).

Possible Mechanisms by Which Host Plants Perceive Cutin Monomers and/or Cuticle Defects to Elicit Defense Responses

The impressive studies described above provide solid lines of evidence that mutants and transgenic lines with altered cuticular structure and increased permeability exhibit higher resistance to attacks by pathogenic fungi. This concept is still under debate, as other permeable cuticle mutants display an opposite trend, that is, heightened susceptibility to pathogenic fungi. In this section, we mention some of the possible mechanisms that have been raised to explain how host plants perceive

cutin monomers and/or changes in cuticle structure and permeability.

Earlier studies showed that the ectopic supplementation of synthetic analogs of typical cutin monomers can confer treated plants with higher resistance against attack by pathogenic fungi. For instance, Namai et al. (1993) treated *Sasanishiki* rice plants with C_{18} epoxy fatty acids and examined the ability of these compounds to inhibit the germination and germ tube elongation of the spores of the rice blast fungus *Pyricularia oryzae*. The authors were able to show that the rate of necrotic lesions formed on the treated leaves was significantly lower than leaves of nontreated control plants, indicating the induction of resistance to the pathogen by the epoxides in the plants. Additionally, uptake experiments using [1-^{14}C] derivatives validated that the supplemented epoxides were incorporated into the treated leaves (Namai et al., 1993). In the same way, the topical spray application of synthetic cutin monomers or of a cutin hydrolysate from apple fruit partially protected barley and rice leaves from infection by the fungal pathogens *E. graminis* f.sp. *tritici* and *M. grisea*, respectively. It was further demonstrated that *cis*-9,10-epoxy-18-OH stearic acid (HESA), the most abundant cutin monomer in barley, was amongst the most active com pounds. Interestingly, these substances did not seem to have any inhibitory effect on pathogenic fungi when added to their growing media, further suggesting that the resistance observed in these treated plants is associated with the induction of plant defense responses (Schweizer et al., 1994, 1996b). The hypothesis that free cutin monomers are perceived by plant cells as endogenous stress-associated signals were examined in a model system consisting of cultured potato (*Solanum tuberosum*) cells, where, again, HESA was the most active compound in the induction of transient alkalinization of the culture medium, implying an induced defense response. The authors also demonstrated that the application of cutin monomers stimulated the production of the plant stress hormone ethylene and activated the expression of defense-associated genes such as phenylalanine ammonia-lyase (PAL), glutathione S-transferase (GST), and 3-hydroxy-3-methylglutaryl-coenzyme A reductase (HMGR; Schweizer et al., 1996a). Finally, Fauth et al. (1998) showed that adding alkaline hydrolysates of cutin from cucumber (*Cucumber sativus*), tomato, and apple to the epidermal surface of gently abraded hypocotyls of etiolated cucumber seedlings resulted in the generation of H_2O_2. The authors concluded that the physiological significance of this might be that upon cuticle degradation by fungal cutinases, the cutin monomers may act as H_2O_2 elicitors to induce defense responses (Fauth et al., 1998). Altogether, these reports provide circumstantial evidence that free cutin monomers can be perceived by the host plant cells as chemical signals and endogenous elicitors of defense responses, though the mechanism by which the host plants sense cutin monomers and/or cuticle defects is yet to be fully determined.

Another mechanism raised to explain the link between a permeable cuticle and increased resistance of the host plants to attack by pathogenic fungi involves the accumulation of reactive oxygen species (ROS). A study performed by L'Haridon et al. (2011) proposed that the production of ROS like H_2O_2 and O_2^-, a permeable cuticle, and increased resistance to invading fungi are all tightly associated. The authors demonstrated that Arabidopsis plants with wounded leaves, plants treated with cutinase, and the cuticle-deficient mutants *bdg* and *lacs2.3*, all produce more ROS and exhibit increased resistance to *B. cinerea*. Remarkably, the authors were able to show that the ROS accumulation and induced resistance occurs under certain conditions only once the cuticle has been permeabilized, and that invading fungi circumvent this mechanism by generating effectors that interfere with the ROS production (L'Haridon et al., 2011). A follow-up study demonstrated that the soft mechanical stress applied to Arabidopsis leaf surfaces by gentle sweeping results in altered cuticle permeability, accompanied by strong resistance to *B. cinerea*, rapid changes in calcium concentrations, and the release of ROS. The authors concluded that Arabidopsis plants can convert gentle forms of mechanical stimuli into strong activation of defense mechanisms against *B. cinerea* (Benikhlef et al., 2013). Finally, the overexpression of DEWAX, an AP2/ERF-type transcription factor that negatively regulates cuticular wax biosynthesis, increases cuticle permeability (Ju et al., 2017). Even though this phenomenon has been attributed more to pronounced changes in cuticular wax deposition than to cutin deposition, both an *in situ* assay of hydrogen peroxide and fluorometric measurements showed that the levels of ROS are higher in DEWAX-overexpressing leaves as compared to the WT leaves. These plants displayed more tolerance to *B. cinerea* infection, accompanied by the upregulation of defense-related genes. Thus, the authors concluded that the increased ROS accumulation and DEWAX-mediated upregulation of defense-related genes are closely associated with enhanced resistance to *B. cinerea* (Ju et al., 2017). Unlike these studies, Dubey et al. (2020) found no difference in ROS levels between cotyledons of WT- and polyunsaturated fatty acid (PUFA)-deficient mutant *fad2-3* Arabidopsis plants, even though this mutant was characterized by cuticle permeability defects (Dubey et al., 2020). To summarize, the above studies suggest an exciting explanation for the increased resistance to *B. cinerea* of several mutants and transgenic plants with a more permeable cuticle and higher ROS production, yet the exact association between these two parameters is not fully understood and requires further examination.

An additional option by which a more permeable cuticle confers resistance relates to the production of fungitoxic substances on the cuticle surface. In fact, fungitoxic activity was measured in diffusates isolated from leaves of the cuticle-deficient mutants *lcr*, *lacs2*, and *pec1/abcg32*, and also the cutinase-expressing CUTE plants (Bessire et al., 2007, 2011; Chassot et al., 2007). Even though it was assumed that fungitoxic activity is associated with the same compound/s in all these cases, the chemical nature of such metabolite/s was not reported. A candidate for such a metabolite was recently raised by Dubey et al. (2020), who identified the over accumulation of 7-methylsulfonylheptyl glucosinolate (7MSOHG) at the cuticle surfaces of (PUFA)-deficient Arabidopsis mutants. Cuticle permeability defects accompanied by arrested hyphal growth were detected in *fad2-1* and *fad* triple mutants of *B. cinerea*.

Therefore, the authors linked the appearance of 7MSOHG to defects in cuticle composition and permeability, and resistance to fungi (Dubey et al., 2020). Based on these results, Dubey et al. (2021) investigated the fungi-toxic activity of natural isothiocyanate derivatives of glucosinolates together with semisynthetic glucosinolates and chemical fungicides. The study confirmed that 13 out of the 31 tested were efficient fungicides when applied alone, whereas some operated in a synergistic manner when used in combination against three plant pathogenic fungal species, *Alternaria radicina*, *Fusarium graminearum*, and *Plectosphaerella cucumerina* (Dubey et al., 2021). Altogether, it is reasonable to assume that not only glucosinolates but also fungitoxic metabolites from different biochemical groups play important defensive roles against pathogenic fungi and accumulate at the cuticle surface.

Lastly, defense-related transcriptional responses seem to be common amongst some of the permeable cuticle mutants, raising the possibility that these changes indirectly affect plant–pathogen interactions by conferring resistance against fungi and mounting systemic acquired resistance (SAR). Voisin et al. (2009) compared gene expression changes in young rosette leaves of *lcr*, *fdh*, and *bdg* mutants to that of WT leaves and found commonly upregulated genes that participate in the cuticle and cell wall remodeling and in defense responses upon abiotic stresses and pathogens. Hence, the increased resistant phenotype of these three cuticle-deficient mutants to *B. cinerea* might be the result of primed defense mechanisms that arise due to cuticular defects. To gain deeper insight into the core mechanism by which cuticular defects trigger these types of transcriptional responses, the authors performed an overlap meta-analysis of differentially expressed genes. Using this approach, the *SERRATE* (*SE*) gene was identified and shown to encode a nuclear protein of multiprotein RNA-processing complexes and to be epistatic to *lcr* and *bdg* (Voisin et al., 2009). A link between cuticular defects and defense mechanisms was also proposed for the Arabidopsis *acp4* mutants mentioned earlier. These mutants successfully generated the mobile signal, yet failed to induce SAR. It was demonstrated that the inactivation of SAR is associated with cuticle impairment in these mutants, rather than with alterations in the signaling pathways of the stress-related hormones salicylic and jasmonic acids (Xia et al., 2009).

CONCLUDING REMARKS

In this review, we delineate the multifaceted roles played by epicuticular waxes and released cutin monomers as chemical signaling molecules in the interactions between host plants and pathogenic fungi. The early and recent key reports we present in this fascinating field of research accentuate how these interactions are presumably far more complex than currently assumed. It is evident that these interactions are multifactorial, are regulated simultaneously by many components derived from both the pathogenic fungi and the host plant, and are highly influenced by the biochemical, structural, and permeability properties of the cuticle. Evidence shows that certain wax components affect pre-penetration and infection processes of fungi with different life styles, yet the mechanisms underlying these types of relationships are not fully known. Efforts to elucidate the roles of epicuticular waxes in plant–fungal interactions have thus far mostly utilized mutants with altered wax compositions. However, this approach is still challenging, as in most cases, compositional changes in one biochemical group of wax compounds are typically accompanied by changes in other groups of compounds.

How the cutin monomers released from the cuticle by fungal cutinases during the early stages of infection are recognized by the host plant to elicit defense responses and acquired resistance to pathogens remains a question to be explicated. Thus far, several possible mechanisms have been proposed involving the production of ROS, the accumulation of fungitoxic compounds at the cuticle surface and a primed defense-related transcriptional response, all of which were associated with cuticle defects. In their review, Serrano et al. (2014) suggested that a more permeable cuticle might facilitate the faster perception of signals derived from the cuticle that is being degraded by fungal cutinase during infection and/or that cutin monomers over accumulate in cuticle-deficient mutants due to incomplete cutin polymer assembly. The validity and nature of all these possible mechanisms would require further attention from the research community investigating the field of plant cuticle–pathogenic fungi interactions.

While the cuticle has been solely attributed to aboveground tissues, a recent pioneering study showed that a cuticle-like cell wall structure covers plant root caps and contributes to its protection against abiotic stresses (Berhin et al., 2019). The authors were able to demonstrate that this specialized polyester-rich cuticle is formed in early developing root caps of primary and lateral roots and lost upon the removal of the first root cap cell layer (Berhin et al., 2019). The discovery of cuticle in roots opens a whole new element in the research field of plant cuticle–pathogen interactions, which is of great significance due to the devastating diseases originating from soil-grown pathogenic fungi that attack root tissues. The varied subset of cuticle mutants available today offers an excellent platform with which to examine the possible interactions between root cap cuticles and pathogenic fungi. All in all, the outcome of such efforts is expected to aid the agricultural community to minimize economic and yield losses.

AUTHOR CONTRIBUTIONS

GCA, EM, SS, and HC drafted the manuscript. GCA and HC prepared the figures. AA and HC edited the manuscript. All authors contributed to the article and approved the submitted version.

ACKNOWLEDGMENTS

The authors would like to thank Natalie Page for proofreading the manuscript and for valuable comments.

REFERENCES

Aragón, W., Reina-Pinto, J. J., and Serrano, M. (2017). The intimate talk between plants and microorganisms at the leaf surface. *J. Exp. Bot.* 68, 5339–5350. doi: 10.1093/jxb/erx327

Bashi, Z. D., Roger Rimmer, S., Khachatourians, G. G., and Hegedus, D. D. (2012). Factors governing the regulation of *Sclerotinia sclerotiorum* cutinase A and polygalacturonase 1 during different stages of infection. *Can. J. Microbiol.* 58, 605–616. doi: 10.1139/w2012-031

Benikhlef, L., L'Haridon, F., Abou-Mansour, E., Serrano, M., Binda, M., Costa, A., et al. (2013). Perception of soft mechanical stress in *Arabidopsis* leaves activates disease resistance. *BMC Plant Biol.* 13:133. doi: 10.1186/1471-2229-13-133

Berhin, A., de Bellis, D., Franke, R. B., Buono, R. A., Nowack, M. K., and Nawrath, C. (2019). The root cap cuticle: a cell wall structure for seedling establishment and lateral root formation. *Cell* 176, 1367–1378.e8. doi: 10.1016/j.cell.2019.01.005

Berto, P., Comménil, P., Belingheri, L., and Dehorter, B. (1999). Occurrence of a lipase in spores of *Alternaria brassicicola* with a crucial role in the infection of cauliflower leaves. *FEMS Microbiol. Lett.* 180, 183–189. doi: 10.1111/j.1574-6968.1999.tb08794.x

Bessire, M., Borel, S., Fabre, G., Carrac, L., Efremova, N., Yephremov, A., et al. (2011). A member of the PLEIOTROPIC DRUG RESISTANCE family of ATP binding cassette transporters is required for the formation of a functional cuticle in *Arabidopsis*. *Plant Cell* 23, 1958–1970. doi: 10.1105/tpc.111.083121

Bessire, M., Chassot, C., Jacquat, A. C., Humphry, M., Borel, S., Petétot, J. M. D. C., et al. (2007). A permeable cuticle in *Arabidopsis* leads to a strong resistance to *Botrytis cinerea*. *EMBO J.* 26, 2158–2168. doi: 10.1038/sj.emboj.7601658

Bourdenx, B., Bernard, A., Domergue, F., Pascal, S., Léger, A., Roby, D., et al. (2011). Overexpression of Arabidopsis ECERIFERUM1 promotes wax very-long-chain alkane biosynthesis and influences plant response to biotic and abiotic stresses. *Plant Physiol.* 156, 29–45. doi: 10.1104/pp.111.172320

Burdon, J. J., and Thrall, P. H. (2009). Coevolution of plants and their pathogens in natural habitats. *Science* 324, 755–756. doi: 10.1126/science.1171663

Buschhaus, C., and Jetter, R. (2011). Composition differences between epicuticular and intracuticular wax substructures: how do plants seal their epidermal surfaces? *J. Exp. Bot.* 62, 841–853. doi: 10.1093/jxb/erq366

Buxdorf, K., Rubinsky, G., Barda, O., Burdman, S., Aharoni, A., and Levy, M. (2014). The transcription factor SlSHINE3 modulates defense responses in tomato plants. *Plant Mol. Biol.* 84, 37–47. doi: 10.1007/s11103-013-0117-1

Chassot, C., Nawrath, C., and Métraux, J. P. (2007). Cuticular defects lead to full immunity to a major plant pathogen. *Plant J.* 49, 972–980. doi: 10.1111/j.1365-313X.2006.03017.x

Chen, G., Komatsuda, T., Ma, J. F., Li, C., Yamaji, N., and Nevo, E. (2011). A functional cutin matrix is required for plant protection against water loss. *Plant Signal. Behav.* 6, 1297–1299. doi: 10.4161/psb.6.9.17507

Cohen, H., Dong, Y., Szymanski, J. J., Lashbrooke, J. G., Meir, S., Almekias-Siegel, E., et al. (2019). A multilevel study of melon fruit reticulation provides insight into skin lignosuberization hallmarks. *Plant Physiol.* 179, 1486–1501. doi: 10.1104/pp.18.01158

Cohen, H., Szymanski, J., and Aharoni, A. (2017). Assimilation of "omics" strategies to study the cuticle layer and suberin lamellae in plants. *J. Exp. Bot.* 68, 5389–5400. doi: 10.1093/jxb/erx348

Davies, K. A., De Lorono, I., Foster, S. J., Li, D., Johnstone, K., and Ashby, A. M. (2000). Evidence for a role of cutinase in pathogenicity of *Pyrenopeziza brassicae* on Brassicas. *Physiol. Mol. Plant Pathol.* 57, 63–75. doi: 10.1006/pmpp.2000.0282

DeZwaan, T. M., Carroll, A. M., Valent, B., and Sweigard, J. A. (1999). *Magnaporthe grisea* Pth11p is a novel plasma membrane protein that mediates appressorium differentiation in response to inductive substrate cues. *Plant Cell* 11, 2013–2030. doi: 10.1105/tpc.11.10.2013

Domínguez, E., Heredia-Guerrero, J. A., and Heredia, A. (2011). The biophysical design of plant cuticles: an overview. *New Phytol.* 189, 938–949. doi: 10.1111/j.1469-8137.2010.03553.x

Dubey, O., Dubey, S., Schnee, S., Glauser, G., Nawrath, C., Gindro, K., et al. (2020). Plant surface metabolites as potent antifungal agents. *Plant Physiol. Biochem.* 150, 39–48. doi: 10.1016/j.plaphy.2020.02.026

Dubey, S., Guignard, F., Pellaud, S., Pedrazzetti, M., van der Schuren, A., Gaume, A., et al. (2021). Isothiocyanate derivatives of glucosinolates as efficient natural fungicides. *PhytoFrontiers* 1, 40–50. doi: 10.1094/PHYTOFR-08-20-0010-R

Fabre, G., Garroum, I., Mazurek, S., Daraspe, J., Mucciolo, A., Sankar, M., et al. (2016). The ABCG transporter PEC1/ABCG32 is required for the formation of the developing leaf cuticle in *Arabidopsis*. *New Phytol.* 209, 192–201. doi: 10.1111/nph.13608

Fauth, M., Schweizer, P., Buchala, A., Markstadter, C., Riederer, M., Kato, T., et al. (1998). Cutin monomers and surface wax constituents elicit H_2O_2 in conditioned cucumber hypocotyl segments and enhance the activity of other H_2O_2 elicitors. *Plant Physiol.* 117, 1373–1380. doi: 10.1104/pp.117.4.1373

Feng, J., Wang, F., Liu, G., Greenshields, D., Shen, W., Kaminskyj, S., et al. (2009). Analysis of a *Blumeria graminis*-secreted lipase reveals the importance of host epicuticular wax components for fungal adhesion and development. *Mol. Plant-Microbe Interact.* 22, 1601–1610. doi: 10.1094/MPMI-22-12-1601

Fernández, V., Guzmán-Delgado, P., Graça, J., Santos, S., and Gil, L. (2016). Cuticle structure in relation to chemical composition: re-assessing the prevailing model. *Front. Plant Sci.* 7:427. doi: 10.3389/fpls.2016.00427

Ferreira, A. P. S., Pinho, D. B., Machado, A. R., and Pereira, O. L. (2014). First report of *Curvularia eragrostidis* causing postharvest rot on pineapple in Brazil. *Plant Dis.* 98, 1277–1277. doi: 10.1094/PDIS-03-14-0288-PDN

Francis, S. A., Dewey, F. M., and Gurr, S. J. (1996). The role of cutinase in germling development and infection by *Erysiphe graminis* f.sp. *hordei*. *Physiol. Mol. Plant Pathol.* 49, 201–211. doi: 10.1006/pmpp.1996.0049

Gabler, F. M., Smilanick, J. L., Mansour, M., Ramming, D. W., and Mackey, B. E. (2003). Correlations of morphological, anatomical, and chemical features of grape berries with resistance to *Botrytis cinerea*. *Phytopathology* 93, 1263–1273. doi: 10.1094/PHYTO.2003.93.10.1263

Garroum, I., Bidzinski, P., Daraspe, J., Mucciolo, A., Humbel, B. M., Morel, J. B., et al. (2016). Cuticular defects in *Oryza sativa* ATP-binding cassette transporter G31 mutant plants cause dwarfism, elevated defense responses and pathogen resistance. *Plant Cell Physiol.* 57, 1179–1188. doi: 10.1093/pcp/pcw066

Gilbert, R. D., Johnson, A. M., and Dean, R. A. (1996). Chemical signals responsible for appressorium formation in the rice blast fungus *Magnaporthe grisea*. *Physiol. Mol. Plant Pathol.* 48, 335–346. doi: 10.1006/pmpp.1996.0027

Gomes, S., Bacelar, E., Martins-Lopes, P., Carvalho, T., and Guedes-Pinto, H. (2012). Infection process of olive fruits by *Colletotrichum acutatum* and the protective role of the cuticle and epidermis. *J. Agric. Sci.* 4, 101–110. doi: 10.5539/jas.v4n2p101

Hansjakob, A., Bischof, S., Bringmann, G., Riederer, M., and Hildebrandt, U. (2010). Very-long-chain aldehydes promote in vitro prepenetration processes of *Blumeria graminis* in a dose- and chain length-dependent manner. *New Phytol.* 188, 1039–1054. doi: 10.1111/j.1469-8137.2010.03419.x

Hansjakob, A., Riederer, M., and Hildebrandt, U. (2011). Wax matters: absence of very-long-chain aldehydes from the leaf cuticular wax of the glossy11 mutant of maize compromises the prepenetration processes of *Blumeria graminis*. *Plant Pathol.* 60, 1151–1161. doi: 10.1111/j.1365-3059.2011.02467.x

Heckman, D. S., Geiser, D. M., Eidell, B. R., Stauffer, R. L., Kardos, N. L., and Hedges, S. B. (2001). Molecular evidence for the early colonization of land by fungi and plants. *Science* 293, 1129–1133. doi: 10.1126/science.1061457

Inada, N., and Savory, E. A. (2011). Inhibition of prepenetration processes of the powdery mildew *Golovinomyces orontii* on host inflorescence stems is reduced in the Arabidopsis cuticular mutant *cer3* but not in *cer1*. *J. Gen. Plant Pathol.* 77, 273–281. doi: 10.1007/s10327-011-0331-0

Isaacson, T., Kosma, D. K., Matas, A. J., Buda, G. J., He, Y., Yu, B., et al. (2009). Cutin deficiency in the tomato fruit cuticle consistently affects resistance to microbial infection and biomechanical properties, but not transpirational water loss. *Plant J.* 60, 363–377. doi: 10.1111/j.1365-313X.2009.03969.x

Jakobson, L., Lindgren, L. O., Verdier, G., Laanemets, K., Brosché, M., Beisson, F., et al. (2016). BODYGUARD is required for the biosynthesis of cutin in *Arabidopsis*. *New Phytol.* 211, 614–626. doi: 10.1111/nph.13924

Jeffree, C. H. (2006). "The fine structure of the plant cuticle," in *Biology of the Plant Cuticle*. eds. M. Riederer and C. Müller (Oxford, UK: Blackwell Publishing), 11–125.

Jenks, M. A., Tuttle, H. A., Eigenbrode, S. D., and Feldmann, K. A. (1995). Leaf Epicuticular waxes of the eceriferum mutants in *Arabidopsis*. *Plant Physiol.* 108, 369–377. doi: 10.1104/pp.108.1.369

Jetter, R., and Riederer, M. (2016). Localization of the transpiration barrier in the epi- and intracuticular waxes of eight plant species: water transport resistances are associated with fatty acyl rather than alicyclic components. *Plant Physiol.* 170, 921–934. doi: 10.1104/pp.15.01699

Ju, S., Go, Y. S., Choi, H. J., Park, J. M., and Suh, M. C. (2017). DEWAX transcription factor is involved in resistance to *Botrytis cinerea* in *Arabidopsis thaliana* and *Camelina sativa*. *Front. Plant Sci.* 8:1210. doi: 10.3389/fpls.2017.01210

Kannangara, R., Branigan, C., Liu, Y., Penfield, T., Rao, V., Mouille, G., et al. (2007). The transcription factor WIN1/SHN1 regulates cutin biosynthesis in *Arabidopsis thaliana*. *Plant Cell* 19, 1278–1294. doi: 10.1105/tpc.106.047076

Kolattukudy, P. E. (1985). Enzymatic penetration of the plant cuticle by fungal pathogens. *Annu. Rev. Phytopathol.* 23, 223–250. doi: 10.1146/annurev.py.23.090185.001255

Kolattukudy, P. E., Rogers, L. M., Li, D., Hwang, C. S., and Flaishman, M. A. (1995). Surface signaling in pathogenesis. *Proc. Natl. Acad. Sci. U. S. A.* 92, 4080–4087. doi: 10.1073/pnas.92.10.4080

Köller, W., Allan, C. R., and Kolattukudy, P. E. (1982). Protection of *Pisum sativum* from *Fusarium solani* f. sp. *pisi* by inhibition of cutinase with organophosphorus pesticides. *Phytopathology* 72, 1425–1430. doi: 10.1094/Phyto-72-1425

Köller, W., Smith, F. D., and Reynolds, K. L. (1991). Phenotypic instability of flusilazole sensitivity in *Venturia inaequalis*. *Plant Pathol.* 40, 608–611. doi: 10.1111/j.1365-3059.1991.tb02425.x

Kong, L., and Chang, C. (2018). Suppression of wheat TaCDK8/TaWIN1 interaction negatively affects germination of *Blumeria graminis* f.sp. *tritici* by interfering with very-long-chain aldehyde biosynthesis. *Plant Mol. Biol.* 96, 165–178. doi: 10.1007/s11103-017-0687-4

Kong, L., Zhi, P., Liu, J., Li, H., Zhang, X., Xu, J., et al. (2020). Epigenetic activation of Enoyl-CoA reductase by an acetyltransferase complex triggers wheat wax biosynthesis. *Plant Physiol.* 183, 1250–1267. doi: 10.1104/pp.20.00603

Kubicek, C. P., Starr, T. L., and Glass, N. L. (2014). Plant cell wall-degrading enzymes and their secretion in plant-pathogenic fungi. *Annu. Rev. Phytopathol.* 52, 427–451. doi: 10.1146/annurev-phyto-102313-045831

Kurdyukov, S., Faust, A., Nawrath, C., Bär, S., Voisin, D., Efremova, N., et al. (2006b). The epidermis-specific extracellular BODYGUARD controls cuticle development and morphogenesis in *Arabidopsis*. *Plant Cell* 18, 321–339. doi: 10.1105/tpc.105.036079

Kurdyukov, S., Faust, A., Trenkamp, S., Bär, S., Franke, R., Efremova, N., et al. (2006a). Genetic and biochemical evidence for involvement of HOTHEAD in the biosynthesis of long-chain α-,ω-dicarboxylic fatty acids and formation of extracellular matrix. *Planta* 224, 315–329. doi: 10.1007/s00425-005-0215-7

L'Haridon, F., Besson-Bard, A., Binda, M., Serrano, M., Abou-Mansour, E., Balet, F., et al. (2011). A permeable cuticle is associated with the release of reactive oxygen species and induction of innate immunity. *PLoS Pathog.* 7:e1002148. doi: 10.1371/journal.ppat.1002148

Laluk, K., and Mengiste, T. (2010). Necrotroph attacks on plants: wanton destruction or covert extortion? *Arabidopsis Book* 8:e0136. doi: 10.1199/tab.0136

Lee, M. H., Chlu, C. M., Roubtsova, T., Chou, C. M., and Bostock, R. M. (2010). Overexpression of a redox-regulated cutinase gene, MfCUTI, increases virulence of the brown rot pathogen *Monilinia fructicola* on *Prunus* spp. *Mol. Plant-Microbe Interact.* 23, 176–186. doi: 10.1094/MPMI-23-2-0176

Lewandowska, M., Keyl, A., and Feussner, I. (2020). Wax biosynthesis in response to danger: its regulation upon abiotic and biotic stress. *New Phytol.* 227, 698–713. doi: 10.1111/nph.16571

Li, Y., Beisson, F., Koo, A. J. K., Molina, I., Pollard, M., and Ohlrogge, J. (2007). Identification of acyltransferases required for cutin biosynthesis and production of cutin with suberin-like monomers. *Proc. Natl. Acad. Sci. U. S. A.* 104, 18339–18344. doi: 10.1073/pnas.0706984104

Lin, T. S., and Kolattukudy, P. E. (1978). Induction of a biopolyester hydrolase (Cutinase) by low levels of cutin monomers in *Fusarium solani* f. sp. *pisi*. *J. Bacteriol.* 133, 942–951. doi: 10.1128/jb.133.2.942-951.1978

Lolle, S. J., Berlyn, G. P., Engstrom, E. M., Krolikowski, K. A., Reiter, W. D., and Pruitt, R. E. (1997). Developmental regulation of cell interactions in the Arabidopsis fiddlehead-1 mutant: a role for the epidermal cell wall and cuticle. *Dev. Biol.* 189, 311–321. doi: 10.1006/dbio.1997.8671

Lolle, S. J., Cheung, A. Y., and Sussex, I. M. (1992). Fiddlehead: An *Arabidopsis* mutant constitutively expressing an organ fusion program that involves interactions between epidermal cells. *Dev. Biol.* 152, 383–392. doi: 10.1016/0012-1606(92)90145-7

Lolle, S. J., Hsu, W., and Pruitt, R. E. (1998). Genetic analysis of organ fusion in *Arabidopsis thaliana*. *Genetics* 149, 607–619. doi: 10.1093/genetics/149.2.607

Lo-Presti, L., Lanver, D., Schweizer, G., Tanaka, S., Liang, L., Tollot, M., et al. (2015). Fungal effectors and plant susceptibility. *Annu. Rev. Plant. Biol.* 66, 513–545. doi: 10.1146/annurev-arplant-043014-114623

Lutzoni, F., Nowak, M. D., Alfaro, M. E., Reeb, V., Miadlikowska, J., Krug, M., et al. (2018). Contemporaneous radiations of fungi and plants linked to symbiosis. *Nat. Commun.* 9:5451. doi: 10.1038/s41467-018-07849-9

Manandhar, J. B., and Hartman, G. L. (1995). Anthracnose development on pepper fruits inoculated with *Colletotrichum gloeosporioides*. *Plant Dis.* 79:380. doi: 10.1094/PD-79-0380

Martin, L. B. B., and Rose, J. K. C. (2014). There's more than one way to skin a fruit: formation and functions of fruit cuticles. *J. Exp. Bot.* 65, 4639–4651. doi: 10.1093/jxb/eru301

Namai, T., Kato, T., Yamaguchi, Y., and Hirukawa, T. (1993). Anti-rice blast activity and resistance induction of C-18 oxygenated fatty acids. *Biosci. Biotechnol. Biochem.* 57, 611–613. doi: 10.1271/bbb.57.611

Pascholati, S. F., Deising, H., Leiti, B., Anderson, D., and Nicholson, R. L. (1993). Cutinase and non-specific esterase activities in the conidial mucilage of *Colletotrichum graminicola*. *Physiol. Mol. Plant Pathol.* 42, 37–51. doi: 10.1006/pmpp.1993.1004

Philippe, G., Geneix, N., Petit, J., Guillon, F., Sandt, C., Rothan, C., et al. (2020). Assembly of tomato fruit cuticles: a cross-talk between the cutin polyester and cell wall polysaccharides. *New Phytol.* 226, 809–822. doi: 10.1111/nph.16402

Podila, G. K., Rogers, L. M., and Kolattukudy, P. E. (1993). Chemical signals from avocado surface wax trigger germination and appressorium formation in *Colletotrichum gloeosporioides*. *Plant Physiol.* 103, 267–272. doi: 10.1104/pp.103.1.267

Pruitt, R. E., Vielle-Calzada, J. P., Ploense, S. E., Grossniklaus, U., and Lolle, S. J. (2000). FIDDLEHEAD, a gene required to suppress epidermal cell interactions in *Arabidopsis*, encodes a putative lipid biosynthetic enzyme. *Proc. Natl. Acad. Sci. U. S. A.* 97, 1311–1316. doi: 10.1073/pnas.97.3.1311

Purdy, R. E., and Kolattukudy, P. E. (1975). Hydrolysis of plant cuticle by plant pathogens. Properties of cutinase I, cutinase II, and a nonspecific esterase isolated from *Fusarium solani pisi*. *Biochemistry* 14, 2832–2840. doi: 10.1021/bi00684a007

Reisige, K., Gorzelanny, C., Daniels, U., and Moerschbacher, B. M. (2006). The C28 aldehyde octacosanal is a morphogenetically active component involved in host plant recognition and infection structure differentiation in the wheat stem rust fungus. *Physiol. Mol. Plant Pathol.* 68, 33–40. doi: 10.1016/j.pmpp.2006.05.006

Ringelmann, A., Riedel, M., Riederer, M., and Hildebrandt, U. (2009). Two sides of a leaf blade: *Blumeria graminis* needs chemical cues in cuticular waxes of *Lolium perenne* for germination and differentiation. *Planta* 230, 95–105. doi: 10.1007/s00425-009-0924-4

Rowland, O., Lee, R., Franke, R., Schreiber, L., and Kunst, L. (2007). The CER3 wax biosynthetic gene from *Arabidopsis thaliana* is allelic to WAX2/YRE/FLP1. *FEBS Lett.* 581, 3538–3544. doi: 10.1016/j.febslet.2007.06.065

Sadler, C., Schroll, B., Zeisler, V., Waßmann, F., Franke, R., and Schreiber, L. (2016). Wax and cutin mutants of *Arabidopsis*: quantitative characterization of the cuticular transport barrier in relation to chemical composition. *Biochim. Biophys. Acta* 1861, 1336–1344. doi: 10.1016/j.bbalip.2016.03.002

Samuels, L., Kunst, L., and Jetter, R. (2008). Sealing plant surfaces: cuticular wax formation by epidermal cells. *Annu. Rev. Plant Biol.* 59, 683–707. doi: 10.1146/annurev.arplant.59.103006.093219

Schnurr, J., Shockey, J., and Browse, J. (2004). The acyl-CoA synthetase encoded by LACS2 is essential for normal cuticle development in Arabidopsis. *Plant Cell* 16, 629–642. doi: 10.1105/tpc.017608

Schulze-Lefert, P., and Panstruga, R. (2003). Establishment of biotrophy by parasitic fungi and reprogramming of host cells for disease resistance. *Annu. Rev. Phytopathol.* 41, 641–667. doi: 10.1146/annurev.phyto.41.061002.083300

Schweizer, P., Felix, G., Buchala, A., Müller, C., and Métraux, J. P. (1996a). Perception of free cutin monomers by plant cells. *Plant J.* 10, 31–341. doi: 10.1046/j.1365-313X.1996.10020331.x

Schweizer, P., Jeanguenat, A., Mösinger, E., and Métraux, J. P. (1994). "Plant protection by free cutin monomers in two cereal pathosystems," in *Advances*

in Molecular Genetics of Plant-Microbe Interactions. eds. M. J. Daniels, J. A. Downie and A. E. Osbourn (Dordrecht: Springer), 371–374.

Schweizer, P., Jeanguenat, A., Whitacre, D., Métraux, J. P., and Mösinger, E. (1996b). Induction of resistance in barley against *Erysiphe graminis* f.sp. *hordei* by free cutin monomers. *Physiol. Mol. Plant Pathol.* 49, 103–120. doi: 10.1006/pmpp.1996.0043

Sela, D., Buxdorf, K., Shi, J. X., Feldmesser, E., Schreiber, L., Aharoni, A., et al. (2013). Overexpression of AtSHN1/WIN1 provokes unique defense responses. *PLoS One* 8:e70146. doi: 10.1371/journal.pone.0070146

Serrano, M., Coluccia, F., Torres, M., L'Haridon, F., and Métraux, J. P. (2014). The cuticle and plant defense to pathogens. *Front. Plant Sci.* 5:274. doi: 10.3389/fpls.2014.00274

Shepherd, T., and Griffiths, D. W. (2006). The effects of stress on plant cuticular waxes. *New Phytol.* 71, 469–499. doi: 10.1111/j.1469–8137.2006.01826.x

Sieber, P., Schorderet, M., Ryser, U., Buchala, A., Kolattukudy, P., Métraux, J. P., et al. (2000). Transgenic Arabidopsis plants expressing a fungal cutinase show alterations in the structure and properties of the cuticle and postgenital organ fusions. *Plant Cell* 12, 721–737. doi: 10.1105/tpc.12.5.721

Tenhaken, R., Arnemann, M., Köhler, G., and Barz, W. (1997). Characterization and cloning of cutinase from *Ascochyta rabiei*. *Z. Naturforsch. C. J. Biosci.* 52, 197–208. doi: 10.1515/znc-1997-3-411

Uppalapati, S. R., Ishiga, Y., Doraiswamy, V., Bedair, M., Mittal, S., Chen, J., et al. (2012). Loss of abaxial leaf epicuticular wax in *Medicago truncatula* irg1/palm mutants results in reduced spore differentiation of anthracnose and nonhost rust pathogens. *Plant Cell* 24, 353–370. doi: 10.1105/tpc.111.093104

van der Vlugt-Bergmans, C. J. B., Wagemakers, C. A. M., and van Kan, J. A. L. (1997). Cloning and expression of the cutinase A gene of *Botrytis cinerea*. *Mol. Plant-Microbe Interact.* 10, 21–29. doi: 10.1094/MPMI.1997.10.1.21

Voisin, D., Nawrath, C., Kurdyukov, S., Franke, R. B., Reina-Pinto, J. J., Efremova, N., et al. (2009). Dissection of the complex phenotype in cuticular mutants of Arabidopsis reveals a role of SERRATE as a mediator. *PLoS Genet.* 5:e1000703. doi: 10.1371/journal.pgen.1000703

Wang, W., Liu, X., Gai, X., Ren, J., Liu, X., Cai, Y., et al. (2015). *Cucumis sativus* L. WAX2 plays a pivotal role in wax biosynthesis, influencing pollen fertility and plant biotic and abiotic stress responses. *Plant Cell Physiol.* 56, 1339–1354. doi: 10.1093/pcp/pcv052

Wang, F., Zhang, F., Chen, M., Liu, Z., Zhang, Z., Fu, J., et al. (2017). Comparative transcriptomics reveals differential gene expression related to *Colletotrichum gloeosporioides* resistance in the octoploid strawberry. *Front. Plant Sci.* 8:779. doi: 10.3389/fpls.2017.00779

Wang, F., Zhang, P., Qiang, S., Zhu, Y. Z., and Xu, L. L. (2008). Effects of epicuticular wax from *Digitaria sanguinalis* and *Festuca arundinacea* on infection by *Curvularia eragrostidis*. *Australas. Plant Pathol.* 37, 43–52. doi: 10.1071/AP07077

Wang, X., Zhi, P., Fan, Q., Zhang, M., and Chang, C. (2019). Wheat CHD3 protein TaCHR729 regulates the cuticular wax biosynthesis required for stimulating germination of *Blumeria graminis* f.sp. *tritici*. *J. Exp. Bot.* 70, 701–713. doi: 10.1093/jxb/ery377

Weidenbach, D., Jansen, M., Franke, R. B., Hensel, G., Weissgerber, W., Ulferts, S., et al. (2014). Evolutionary conserved function of barley and Arabidopsis 3-ketoacyl-CoA synthases in providing wax signals for germination of powdery mildew fungi. *Plant Physiol.* 166, 1621–1633. doi: 10.1104/pp.114.246348

Wellesen, K., Durst, F., Pinot, F., Benveniste, I., Nettesheim, K., Wisman, E., et al. (2001). Functional analysis of the LACERATA gene of Arabidopsis provides evidence for different roles of fatty acid omega-hydroxylation in development. *Proc. Natl. Acad. Sci. U. S. A.* 98, 9694–9699. doi: 10.1073/pnas.171285998

Woloshuk, C. P., and Kolattukudy, P. E. (1986). Mechanism by which contact with plant cuticle triggers cutinase gene expression in the spores of *Fusarium solani* f. sp. *pisi*. *Proc. Natl. Acad. Sci.* 83, 1704–1708. doi: 10.1073/pnas.83.6.1704

Xia, Y., Gao, Q. M., Yu, K., Lapchyk, L., Navarre, D. R., Hildebrand, D., et al. (2009). An intact cuticle in distal tissues is essential for the induction of systemic acquired resistance in plants. *Cell Host Microbe* 5, 151–165. doi: 10.1016/j.chom.2009.01.001

Xiao, F., Goodwin, S. M., Xiao, Y., Sun, Z., Baker, D., Tang, X., et al. (2004). *Arabidopsis* CYP86A2 represses *Pseudomonas syringae* type III genes and is required for cuticle development. *EMBO J.* 23, 2903–2913. doi: 10.1038/sj.emboj.7600290

Yeats, T. H., Martin, L. B. B., Viart, H. M. F., Isaacson, T., He, Y., Zhao, L., et al. (2012). The identification of cutin synthase: formation of the plant polyester cutin. *Nat. Chem. Biol.* 8, 609–611. doi: 10.1038/nchembio.960

Yeats, T. H., and Rose, J. K. C. (2013). The formation and function of plant cuticles. *Plant Physiol.* 163, 5–20. doi: 10.1104/pp.113.222737

Zhang, Z., Henderson, C., Perfect, E., Carver, T. L. W., Thomas, B. J., Skamnioti, P., et al. (2005). Of genes and genomes, needles and haystacks: *Blumeria graminis* and functionality. *Mol. Plant Pathol.* 6, 561–575. doi: 10.1111/j.1364-3703.2005.00303.x

Ziv, C., Zhao, Z., Gao, Y. G., and Xia, Y. (2018). Multifunctional roles of plant cuticle During plant-pathogen interactions. *Front. Plant Sci.* 9:1088. doi: 10.3389/fpls.2018.01088

Conflict of Interest: The authors declare that the research was conducted in the absence of any commercial or financial relationships that could be construed as a potential conflict of interest.

frontiers in Plant Science

ORIGINAL RESEARCH
published: 30 June 2021
doi: 10.3389/fpls.2021.655799

Leaf Cuticular Transpiration Barrier Organization in Tea Tree Under Normal Growth Conditions

Mingjie Chen[1†], Yi Zhang[2,3†], Xiangrui Kong[2,4†], Zhenghua Du[3], Huiwen Zhou[1], Zhaoxi Yu[1], Jianheng Qin[1] and Changsong Chen[2,4*]*

[1]College of Life Sciences, Key Laboratory of Tea Biology of Henan Province, Xinyang Normal University, Xinyang, China, [2]Tea Research Institute, Fujian Academy of Agricultural Sciences, Fuan, China, [3]Horticultural Plant Biology and Metabolomics Center, Haixia Institute of Science and Technology, Fujian Agriculture and Forestry University, Fuzhou, China, [4]The Fujian Research Branch of the National Tea Genetic Improvement Center, Fuzhou, China

OPEN ACCESS

Edited by:
Antonio Heredia,
University of Malaga, Spain

Reviewed by:
Aline Xavier De Souza,
Julius Maximilian University of Würzburg, Germany
Olfa Zarrouk,
Smart Farm CoLab (SFCOLAB), Portugal

***Correspondence:**
Mingjie Chen
mjchen@xynu.edu.cn
Changsong Chen
ccs6536597@163.com

[†]These authors have contributed equally to this work

Specialty section:
This article was submitted to Plant Physiology, a section of the journal Frontiers in Plant Science

Received: 19 January 2021
Accepted: 07 June 2021
Published: 30 June 2021

Citation:
Chen M, Zhang Y, Kong X, Du Z, Zhou H, Yu Z, Qin J and Chen C (2021) Leaf Cuticular Transpiration Barrier Organization in Tea Tree Under Normal Growth Conditions. Front. Plant Sci. 12:655799. doi: 10.3389/fpls.2021.655799

The cuticle plays a major role in restricting nonstomatal water transpiration in plants. There is therefore a long-standing interest to understand the structure and function of the plant cuticle. Although many efforts have been devoted, it remains controversial to what degree the various cuticular parameters contribute to the water transpiration barrier. In this study, eight tea germplasms were grown under normal conditions; cuticle thickness, wax coverage, and compositions were analyzed from the epicuticular waxes and the intracuticular waxes of both leaf surfaces. The cuticular transpiration rates were measured from the individual leaf surface as well as the intracuticular wax layer. Epicuticular wax resistances were also calculated from both leaf surfaces. The correlation analysis between the cuticular transpiration rates (or resistances) and various cuticle parameters was conducted. We found that the abaxial cuticular transpiration rates accounted for 64–78% of total cuticular transpiration and were the dominant factor in the variations for the total cuticular transpiration. On the adaxial surface, the major cuticular transpiration barrier was located on the intracuticular waxes; however, on the abaxial surface, the major cuticular transpiration barrier was located on the epicuticular waxes. Cuticle thickness was not a factor affecting cuticular transpiration. However, the abaxial epicuticular wax coverage was found to be significantly and positively correlated with the abaxial epicuticular resistance. Correlation analysis suggested that the very-long-chain aliphatic compounds and glycol esters play major roles in the cuticular transpiration barrier in tea trees grown under normal conditions. Our results provided novel insights about the complex structure–functional relationships in the tea cuticle.

Keywords: ***Camellia sinensis*, cuticular transpiration rate, epicuticular waxes, intracuticular waxes, wax coverage, cuticle thickness, substructure**

INTRODUCTION

The plant cuticle is an extracellular hydrophobic layer covering the outer epidermal surface of leaves and fruits and protects plants against biotic and abiotic stresses (Eigenbrode and Espelie, 1995; Krauss et al., 1997; Neinhuis and Barthlott, 1997; Yeats and Rose, 2013; Silva et al., 2017). The primary function of the cuticle is to regulate nonstomatal water loss,

thus facilitating the adaption of plants to a changing environment (Riederer and Schneider, 2001). The cuticle is composed principally of cutin polyester polymer and soluble cuticular waxes and also contains polysaccharides and proteins (Fernández et al., 2017). The cutin mainly consists of C16 and C18 hydroxyl fatty acids that are cross-linked by ester bonds to form a stable polymer matrix (Nawrath, 2006; Pollard et al., 2008; Fich et al., 2016). Cuticular waxes are mixtures of very-long-chain aliphatic compounds (acids, alkanes, aldehydes, ketones, alcohols, and esters) and cyclic compounds (triterpenoids, tocopherols, and sterols; Samuels et al., 2008). Part of the cuticular waxes is filled into the cutin framework as intracuticular waxes, and part of the waxes is deposited on the surface of the cutin matrix as epicuticular waxes (Jeffree, 2006). Previous studies have reported that the cyclic compounds are mainly located in intracuticular waxes. In contrast, the very-long-chain aliphatic compounds are widely distributed in the epicuticular and intracuticular waxes (Weissflog et al., 2010; Jetter and Riederer, 2016; Zeisler and Schreiber, 2016; Lino et al., 2020; Zhang et al., 2020). Cuticular wax components differ among plant species, developmental stages, tissue types, and even between both sides of the same leaf (Jetter and Riederer, 2016; Zhu et al., 2018; Cheng et al., 2019; Romero and Rose, 2019; Diarte et al., 2020; Lino et al., 2020; Zhang et al., 2020).

There is a long-standing interest to understand the structure–function relationships of the cuticle. Previous studies established that the cuticular transpiration barriers are mainly constituted by cuticular waxes rather than the cutin polymer matrix (Riederer and Schreiber, 1995; Richardson et al., 2007). The cuticular transpiration barrier is mainly contributed by aliphatic compounds, which are located on the intracuticular waxes (Jetter and Riederer, 2016; Zeisler-Diehl et al., 2018; Cheng et al., 2019; Zhang et al., 2020). Recently, there were controversial reports suggesting that cyclic compounds are negatively correlated with cuticular transpiration rates of developing fruits or under drought stress (Schuster et al., 2016; Romero and Rose, 2019; Lino et al., 2020; Zhang et al., 2020); however, other studies found that the cyclic compounds do not contribute to the transpiration barrier or even are positively correlated with the cuticular transpiration rate (Buschhaus and Jetter, 2012; Jetter and Riederer, 2016; Staiger et al., 2019).

Jetter and Riederer (2016) chose eight different plant species of which cuticles belong to two major groups based on the presence and contents of alicyclic compounds of the adaxial leaf surface. Correlation analysis suggests that cuticular transpiration resistance is associated with aliphatic compounds. By now, there are a few studies about the abaxial cuticle, but it remains unclear whether the abaxial cuticle possesses a similar structural arrangement as the adaxial surface. In addition, most previous studies only concentrated on one species or multiple different plant species under the assumption that they may share similar cuticular characteristics. Few studies focus on multiple germplasms of the same plant species, which has the advantage to exploit the variations to boost the power of correlation analysis. In this study, eight different tea germplasms were selected, their cuticles essentially belong to the same type (in terms of the contents and compositions of VLCFA derivatives and alicyclic compounds), but various degrees of variations in cuticular parameters were found. The wax compositions from the adaxial and the abaxial leaf surfaces were analyzed, along with the cuticular transpiration rates (or resistance) from cuticle substructures. This study is trying to address the following questions: (1) To what degree the abaxial cuticular transpiration contributes to the total leaf cuticular transpiration? (2) How the transpiration barrier is organized on the abaxial surface? (3) Which are the wax compounds that contribute to the cuticular transpiration barriers at individual cuticle substructure?

MATERIALS AND METHODS

Eight *Camellia sinensis* germplasms, namely, *Jinguanyin*, *0316B*, *Wuniuzao*, *0306A*, *0306H*, *Fuyun 20*, *0202-10*, and *Hongyafoshou*, were clonally propagated and planted in the tea garden at the Tea Research Institute of Fujian Academy of Agricultural Sciences (Fuan, China; 119.3° E, 27.1° N). They were managed by the regular agricultural practice. In May 2019, they had been growing for 12 years since planting. When the growing twigs reached the stage of one bud and seven leaves, the fifth leaf was used for the investigation.

Transmission Electron Microscopy

For transmission electron microscopy (TEM) analysis, the sample was prepared in accordance with the method described in the study by Zhu et al. (2018). The central part of the fifth leaf was cut into small pieces (2 mm × 4 mm) and fixed in 5% (v/v) glutaraldehyde solution overnight in a freezer at 4°C. Samples were rinsed with 0.1 M PBS buffer (pH 7.2), post-fixed in 1% (w/v) osmium tetroxide, then dehydrated through 30% (v/v) and 50% (v/v) ethanol. Samples were stained with saturated uranyl acetate in 70% (v/v) ethanol overnight, and then rinsed with 70% (v/v) ethanol several times to remove unbound dye. Samples were dehydrated in 90% (v/v) and 100% ethanol; then the ratio of acetone to ethanol was increased in sequential treatments. Samples were embedded in a graded acetone/Epon/Spurr's epoxy resin and polymerized, then sectioned, and observed under a TEM (HT7700, Hitachi, Japan).

Scanning Electron Microscopy and Stomata Parameter Measurement

The fifth leaf was collected from the eight germplasms. Samples were air-dried at room temperature. Before scanning electron microscopy (SEM) observation, small pieces of samples were fixed to aluminum sample holders, freeze-dried (HCP-2 critical point dryer, Hitachi, Japan), sputtered (IB5 ion coater, Eiko, Japan) with a thin layer of gold, then observed under a SEM (JEM-6380LV, JEOL, Japan). Leaf stomatal density was determined from 10 SEM images with different fields of view. Guard cell length and guard cell pair width were calculated by using the ImageJ software.

Cuticle Thickness Measurement

The cuticle thickness was measured from TEM images. Three biological replicates were used. For each biological replicate,

at least six measurements were taken from different cuticle positions, and the results were expressed as average ± SE.

Wax Sampling

The epicuticular waxes were isolated by the method described in the study by Zhang et al. (2020). Delipidated gum arabic in 90% (w/w) aqueous solution was evenly applied to the leaf surface by a soft paintbrush; dry polymer film was peeled off and collected into a glass tube containing 21 ml of chloroform: water (2:1, v/v) and 75 μg of internal standard n-tetracosane (Sigma-Aldrich, St. Louis, United States). After vigorous vortexing and phase separation, the organic phase was transferred into a new glass tube. The extraction was repeated once, and the organic phases were combined and evaporated under the CentriVap Console (Labconco, KS, United States) to obtain epicuticular waxes. The adaxial epicuticular waxes were isolated first, followed by the isolation of abaxial epicuticular waxes.

After the removal of epicuticular waxes, the leaves were used to extract the intracuticular waxes by rinsing with chloroform (Zhang et al., 2020). The adaxial intracuticular waxes were rinsed first, followed by rinsing with the abaxial intracuticular waxes. The collected chloroform solution was evaporated dry to get the adaxial or the abaxial intracuticular waxes, respectively.

Wax Analysis

Before gas chromatography–mass spectrometry (GC–MS) and GC-flame ionization detector (FID) analysis, wax samples were derivatized by *N,O*-bis(trimethylsilyl)-trifluoroacetamide (BSTFA, Aldrich, GC grade) containing 1% trimethylchlorosilane (Aldrich) in pyridine (Aldrich, 99.8%, anhydrous). Individual wax components were identified from MS data by comparing their mass spectra with the National Institute of Standard Database (NIST 14). Waxes were quantified from the FID data by normalizing peak area to the internal standard. DB-1 column (30 m × 0.25 mm × 0.25 μm, Agilent, CA, United States) was used. The constant flow rates of helium carrier gas for GC–MS and GC-FID were 1.2 and 1.7 ml min^{-1}, respectively. The flow rates for hydrogen, nitrogen, and zero air were 40, 30, and 400 ml min^{-1}, respectively. Oven temperature program was initiated at 70°C, raised by 10°C min^{-1} to 200°C, held for 2 min, then raised by 3°C min^{-1} to 320°C, held for 20 min before return to 70°C. The MS detector setting was as follows: EI-70 eV, ionization source temperature: 230°C.

Cuticular Transpiration Rate Measurement

The cuticular transpiration rate was measured by following the method described in the study by Zhang et al. (2020). Growing twigs at the stage of one bud and seven leaves were harvested and kept in water overnight under dark. The next day, the abaxial surface of the fifth leaf was sprayed with 50 mM ABA to promote stomata closure. For each germplasm, six different treatments were performed to the fifth leaf, namely, (1) control, no additional treatments were applied (T); (2) the adaxial surface was sealed with vaseline (Ad/Vas); (3) the abaxial surface was sealed with vaseline (Ab/Vas); (4) both leaf surfaces were sealed with vaseline (Ad/Vas::Ab/Vas); (5) the adaxial epicuticular waxes were removed by gum arabic, while the abaxial surface was sealed with vaseline ($-Ew_{Ad}$::Ab/Vas); and (6) the abaxial epicuticular waxes were removed by gum arabic, while the adaxial surface was sealed with vaseline ($-Ew_{Ab}$::Ad/Vas). After completing these pretreatments, the fifth leaf was removed and photographed, and the projected leaf area (A) was calculated by ImageJ software. The initial, water-saturated fresh leaf weight (W_i) was recorded. Leaves were then placed in a controlled dark room (25°C, 50% humidity), and the leaf weight was recorded hourly by balance; the measurement lasted for 8 h ($W_{t1,\ 2...8}$). Each treatment group included five leaves representing five biological replicates. The cuticular transpiration rates from the total leaf surface (T_{Total_C}), the adaxial surface (T_{Ad}), the abaxial surface (T_{Ab_C}), the adaxial intracuticular waxes ($T_{Ad/intra}$), and the abaxial intracuticular waxes ($T_{Ab/intra\_C}$) were calculated by the formula described before (Zhang et al., 2020). The transpiration rate from the epicuticular waxes cannot be directly measured by the method described in the study by Zhang et al. (2020). After the removal of epicuticular wax, the higher the ratio increase of the intracuticular transpiration rate, the higher the epicuticular resistance would be. By using this relationship, here, we define the epicuticular resistance as the relative ratio increase of the intracuticular transpiration rate after the epicuticular wax removal. Thus, in this study, the cuticular transpiration rate and the resistance represent two different terminologies. The adaxial epicuticular resistance ($R_{Ad/epi}$) was calculated by the formula (I):

$$R_{Ad/epi}(\%) = \left[\left(T_{Ad/intra} - T_{Ad}\right) / T_{Ad/intra}\right] \times 100 \quad (I)$$

T_{Ad} and $T_{Ad/intra}$ represent the adaxial cuticular transpiration rates before and after epicuticular wax removal, respectively;

The abaxial epicuticular resistance (R_{Ab/epi_C}) was calculated by the formula (II):

$$R_{Ab/epi\_C}(\%) = \left[\left(T_{Ab/intra\_C} - T_{Ab\_C}\right) / T_{Ab/intra\_C}\right] \times 100 \quad (II)$$

T_{Ab} and $T_{Ab/intra\_C}$ represent the abaxial cuticular transpiration rates before and after abaxial epicuticular wax removal, respectively.

It is worth mentioning that Jetter and Riederer (2016) defined resistance as the inverse of permeance and different from the definition here.

Statistical Analysis

The mean and SE were calculated by ANOVA. Significance was determined by one-way ANOVA based on Duncan's multiple range tests. Regression analysis between cuticular transpiration rate and wax composition was performed by SPSS (V17.0; SPSS, IBM, Armonk, United States). Bivariate correlations based on Pearson's correlation (two-tailed) were used to determine the significance of correlations between different parameters.

RESULTS

The Cuticle Thickness of the Eight Tea Germplasms

To measure the cuticle thickness, the fifth leaf of the eight tea germplasms was prepared for TEM observation. Under our sample preparation method, the cuticle showed a whitish appearance, and the cell wall was stained dark (**Supplementary Figure S1**). Thus, the cuticle was clearly discerned from TEM imaging. Among the eight tea germplasms, the average thickness of the adaxial cuticle ranged from 2.12 to 2.99 μm, with *Wuniuzao* and *Jinguanyin* ranked as the thinnest and the thickest adaxial cuticle, respectively. The abaxial cuticle thickness showed relatively smaller variations and ranged from 1.24 to 1.46 μm, with *0306H* and *Jinguanyin* ranked as the thinnest and the thickest abaxial cuticle, respectively. For individual germplasms, the adaxial cuticle generally was thicker than the abaxial cuticle (**Figure 1**; **Supplementary Figure S1**).

The Epi- and Intracuticular Wax Coverage of the Eight Tea Germplasms

To compare the compositional characteristics of the cuticle from the eight tea germplasms, waxes were isolated from the epi- and intracuticular compartments of both leaf surfaces, and then analyzed by GC–MS and GC-FID. For individual germplasm, the wax coverages from the adaxial and abaxial surfaces did not correlate with their respective cuticle thickness. Although the adaxial cuticle was thicker than the abaxial cuticle (**Figure 1**; **Supplementary Figure S1**), the wax coverage from the adaxial surface and the abaxial surface was similar (**Figure 2**). This suggests that the wax density from the adaxial surface was lower than that of the abaxial surface. In addition, the epicuticular waxes and the intracuticular waxes from the adaxial surface and the abaxial surface showed different wax distribution patterns. On the adaxial surface, the waxes were almost equally distributed between the epicuticular waxes and the intracuticular waxes; in contrast, the intracuticular waxes coverage on the abaxial surface was about 1.45–3.33 times higher than that of the epicuticular waxes. For individual germplasm, the coverage of adaxial the epicuticular waxes generally was higher than that of the abaxial the epicuticular waxes. Among the four cuticular compartments of each germplasm, the coverage of the abaxial intracuticular waxes ranked as the highest except *Wuniuzao* (**Figure 2**). *Hongyafoshou* showed the lowest total wax coverage (0.73 μg cm^{-2}) among the eight tea germplasms. Accordingly, its wax coverage from each cuticular compartment was also the lowest.

The Epi- and Intracuticular Wax Compositions of the Eight Tea Germplasms

At the chemical class level, tea leaf waxes include glycols, caffeine, VLCFAs, and their primary alcohols, alkyl esters,

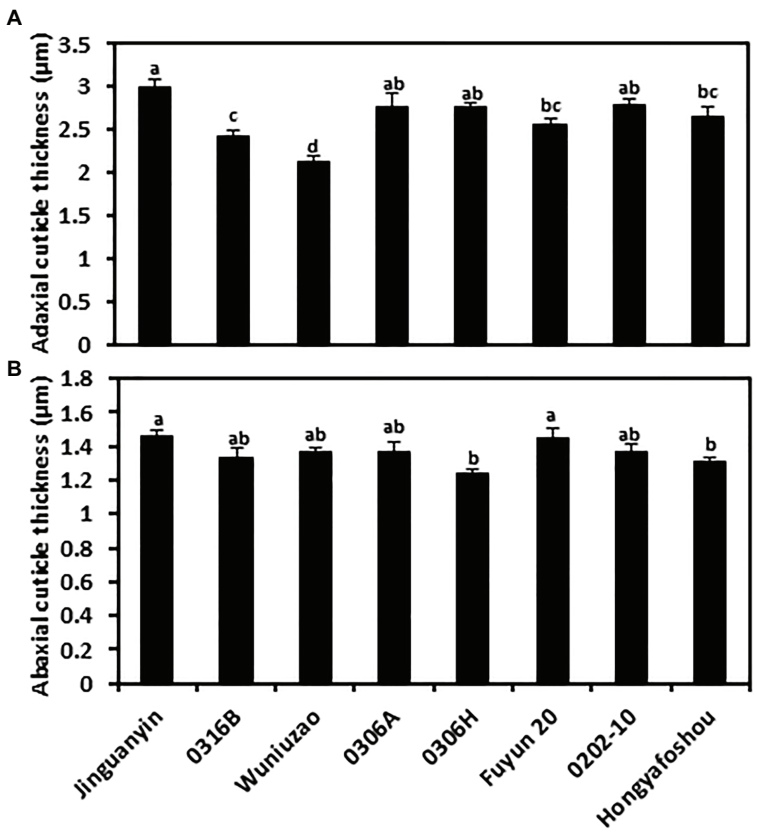

FIGURE 1 | Cuticle thickness from the adaxial and the abaxial cuticle of the eight tea germplasms. **(A)** The adaxial surface; **(B)** the abaxial surface. Different lowercase letters represent the statistical significance ($p < 0.05$).

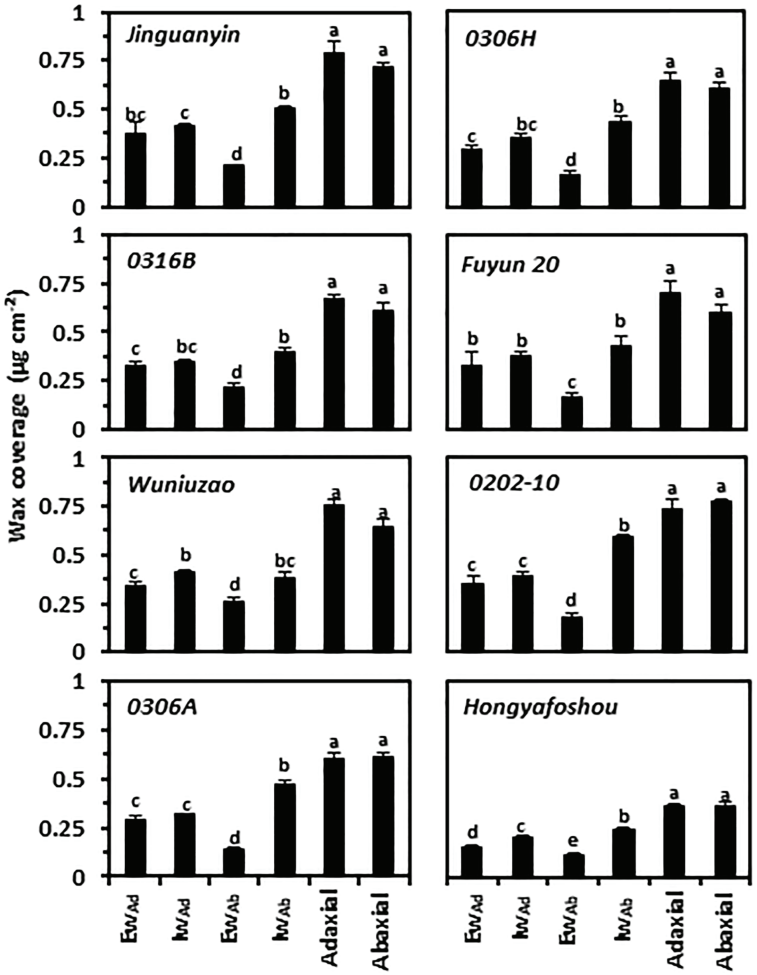

FIGURE 2 | Cuticular wax coverage from the epi- and the intracuticular compartments of both leaf surfaces. Ew: the epicuticular waxes; Iw: the intracuticular waxes; Ad: the adaxial surface; Ab: the abaxial surface. Different lowercase letters represent the statistical significance ($p < 0.05$).

aldehydes, and alkane derivatives; mature tea leaves also contained considerable amounts of pentacyclic triterpenoids, steroids, and tocopherols (Zhu et al., 2018; Chen et al., 2020; Zhang et al., 2020). The adaxial epicuticular and intracuticular waxes were dominated by VLCFA compounds (acids, aldehydes, 1-alcohols, and alkanes) in all germplasms, which accounted for 46–67% of the total epicuticular wax coverage and 41–54% of the total intracuticular wax coverage (**Figure 3**). Compared to the abaxial epicuticular waxes, the adaxial epicuticular waxes showed higher coverage of aldehydes, 1-alkanols, alkanes, and β-tocopherol. Compared to the abaxial intracuticular waxes, the adaxial intracuticular waxes showed higher coverage of 1-alkanols, alkanes, and β-tocopherol, but showed lower coverage of triterpenoids, steroids, and caffeine (**Figure 3**). Due to these biased distributions of individual wax components on both leaf surfaces, the adaxial coverages of 1-alkanols, alkanes, and β-tocopherol were higher than those of the abaxial surface; in contrast, the adaxial coverage of triterpenoids, steroids, and caffeine was lower than that of the abaxial surface.

The Cuticular Transpiration Rates From Different Leaf Surfaces and Cuticular Compartments

The water transpiration rates from the fifth leaf were measured. On the leaf drying curve, *Hongyafoshou* and *Fuyun 20* reached a constant level 4th h post-excision; however, the remaining six germplasms reached constant levels at the 5th h post-excision (**Supplementary Figure S2**). The observed leaf transpiration rates for the control and various treatments were recorded; the values at the 1st h and the 5th h post-excision are presented in **Supplementary Table S1**. The residual stomata transpiration rate was obtained by using the difference in the total transpiration rate between the 1st h and the 5th h of the control leaves (T_1–T_5). *Hongyafoshou* and *Fuyun 20* showed higher residual stomata transpiration rates compared to other six tea germplasms. Accordingly, they reached a constant level 1 h earlier than others. The total leaf transpiration rate at the 5th h post-excision was used as proxy of the total cuticular transpiration rate since at this time point the stomata was fully closed. The cuticular transpiration rates from the adaxial

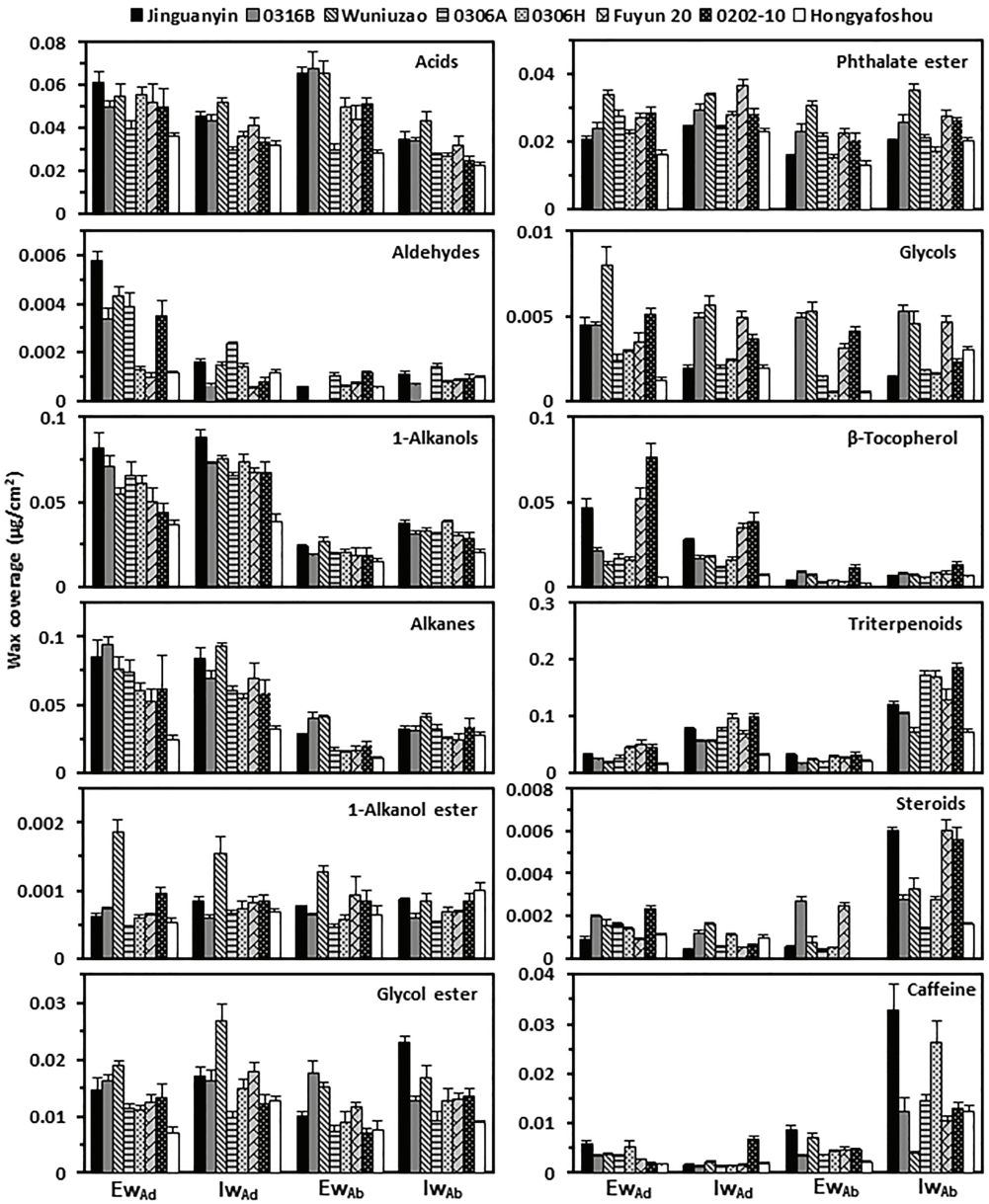

FIGURE 3 | The wax compositional comparison from the epi- and intracuticular compartments among the eight tea germplasms. Ew_{Ad}: the adaxial eipcuticular waxes; Iw_{Ad}: the adaxial intracuticular waxes; Ew_{Ab}: the abaxial eipcuticular waxes; Iw_{Ab}: the abaxial intracuticular waxes.

surface and the abaxial surface were obtained from the observed data by applying the established formula (Zhang et al., 2020; **Figure 4**; **Supplementary Table S1**).

The total cuticular transpiration rate (T_{Total_C}) ranged from 0.090 $mg.h^{-1}.cm^{-2}$ for *Jinguanyin* to 0.216 $mg.h^{-1}.cm^{-2}$ for *Hongyafoshou* (**Figure 4A**, top panel). Accordingly, *Hongyafoshou* showed higher cuticular transpiration rates from all its cuticular compartments and also lower abaxial epicuticular resistance (R_{Ab/epi_C}; **Figures 4A**,**B**). The adaxial cuticular transpiration rates showed small variations among these eight tea germplasms; in contrast, the abaxial cuticular transpiration rates showed much larger variations. The abaxial cuticular transpiration rate (T_{Ab_C}) was about 1.8–3.3-fold high of the adaxial surface (T_{Ad}) in all the eight tea germplasms (**Figure 4A**). The abaxial intracuticular transpiration rates ($T_{Ab/intra\_C}$) were about 4.6–6.5-fold higher than the adaxial intracuticular waxes ($T_{Ad/intra}$). The resistance of the abaxial epicuticular waxes (R_{Ab/epi_C}) was about 2.8–6.4-fold higher than that of the adaxial epicuticular waxes ($R_{Ad/epi}$; **Figure 4B**). Overall, the water loss from the adaxial surface (T_{Ad}) accounted for 22–36% of the total leaf water loss (T_{Total_C}), while the water loss from the abaxial surface (T_{Ab_C}) accounted for 64–78% of the total leaf water loss (**Figure 4**). It is clear that the adaxial leaf surface showed a better cuticular transpiration barrier compared to its abaxial surface.

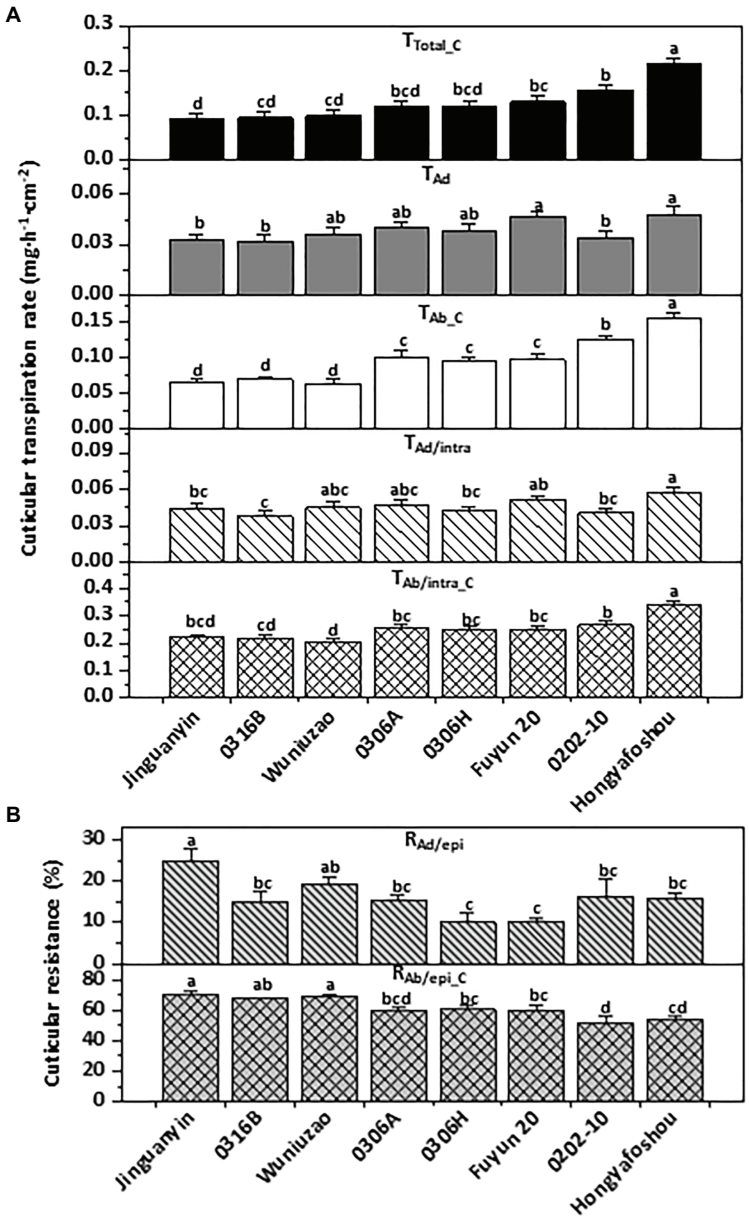

FIGURE 4 | Cuticular transpiration rate **(A)** and epicuticular resistance **(B)** of the eight tea germplasms. Different lowercase letters represent the statistical significance ($p < 0.05$). T_{Total_C}: the total cuticular transpiration rate; T_{Ad}: the adaxial cuticular transpiration rate; T_{Ab_C}: the abaxial cuticular transpiration rate; $T_{Ad/intra}$: the adaxial intracuticular transpiration rate; $T_{Ab/intra\_C}$: the abaxial intracuticular transpiration rate; $R_{Ad/epi}$: the adaxial epicuticular resistance; R_{Ab/epi_C}: the abaxial epicuticular resistance.

Machado et al. (2020) studied 30 different native tree species, including drought deciduous and evergreen, and found that residual stomatal transpiration had a significant impact on the minimum conductance; the stomata distribution pattern in the epidermis was a key factor determining the variation in minimum conductance. To exclude the stomatal effects on the cuticular transpiration rate measurement, in this study the stomata density, guard cell length, and guard cell pair width were measured from SEM images (**Supplementary Figure S3A**). The average stomata density from these eight tea germplasms ranged from 225 to 240 mm^{-2}; no significant difference was observed among them (**Supplementary Figure S3B**). Significant differences in guard cell length and guard cell pair width were observed among some pairs of germplasm (**Supplementary Figures S3C,D**). However, no significant correlations were found between these three stomata parameters and the abaxial cuticular transpiration rates. Machado et al. (2020) also observed that for evergreens there is no significant association between stomatal properties and leaf water leaks. Our data suggest that the variations in the abaxial cuticular transpiration rates from these eight tea germplasms likely resulted from other factors rather than stomatal characteristics (**Figure 4A**; **Supplementary Figure S3**).

To uncover the relationships among the cuticular transpiration rates (or resistance), Pearson's correlation analysis was carried out (**Figure 5**). The total cuticular transpiration rate (T_{Total_C}) was significantly and positively correlated with the abaxial cuticular transpiration rate (T_{Ab_C}; R^2 = 0.94) and the abaxial intracuticular transpiration rate ($T_{Ab/intra\_C}$; R^2 = 0.94), and significantly and negatively correlated with the abaxial epicuticular resistance (R_{Ab/epi_C}; R^2 = −0.73). On the adaxial surface, the adaxial cuticular transpiration rate (T_{Ad}) was significantly and positively correlated with the adaxial intracuticular transpiration rate ($T_{Ad/intra}$; R^2 = 0.86); however, T_{Ad} was not correlated with the adaxial epicuticular resistance ($R_{Ad/epi}$). On the abaxial surface, the abaxial cuticular transpiration rate (T_{Ab_C}) was significantly and positively correlated with the abaxial intracuticular transpiration rate ($T_{Ab/intra\_C}$; R^2 = 0.93) and negatively correlated with the abaxial epicuticular resistance (R_{Ab/epi_C}; R^2 = −0.89). The abaxial intracuticular transpiration rate ($T_{Ab/intra\_C}$) was significantly and negatively correlated with the abaxial epicuticular resistance (R_{Ab/epi_C}; R^2 = −0.67; **Figure 5**).

Correlation Analysis Between Cuticular Transpiration Rates and Cuticle Structural Parameters

Pearson's correlation analyses were carried out to identify the associations of cuticular transpiration rates with wax chemical classes from individual cuticular compartments. We found that the total leaf cuticular transpiration rates (T_{Total_C}) were significantly and negatively correlated with the total wax coverage (Ad + Ab; R^2 = −0.56; **Table 1**). In addition, the abaxial epicuticular resistance (R_{Ab/epi_C}) was significantly and positively correlated with the abaxial epicuticular wax coverage (Ab_{Ew}; R^2 = +0.56). No significant correlations were found from other cuticular compartments (**Table 1**).

Among the total leaf wax coverage (Ad + Ab), acids, 1-alkanols, alkanes, and glycol esters were found to be significantly and negatively correlated with the total leaf cuticular transpiration rates (T_{Total_C}). Consistent with the total leaf wax coverage (Ad + Ab), these same waxes from the abaxial surface ($Ab_{Ew + Iw}$) were also significantly and negatively correlated with the abaxial cuticular transpiration rates (T_{Ab_C}); furthermore, these wax classes from the abaxial epicuticular layer (Ab_{Ew}) were significantly and positively correlated with the abaxial epicuticular resistance (R_{Ab/epi_C}). In abaxial intracuticular waxes (Ab_{Iw}), acids and 1-alkanols were significantly and negatively correlated with the abaxial intracuticular transpiration rates ($T_{Ab/intra\_C}$).

Among the adaxial cuticular waxes ($Ad_{Ew + Iw}$), 1-alkanols and alkanes were significantly and negatively correlated with the adaxial cuticular transpiration (T_{Ad}). Aldehydes from the adaxial epicuticular waxes (Ad_{Ew}) were significantly and positively correlated with the adaxial epicuticular resistance ($R_{Ad/epi}$). In adaxial intracuticular waxes (Ad_{Iw}), 1-alkanols were significantly and negatively correlated with the adaxial intracuticular transpiration rate ($T_{Ad/intra}$; **Table 1**).

The correlations of cuticular transpiration rates or resistance with individual wax components from each cuticular substructure were also analyzed (**Table 2**). Seven wax components from the total wax coverage (Ad + Ab) were found to be significantly and negatively correlated with total leaf cuticular transpiration rates (T_{Total_C}); they were two acids (C16 and C18), three 1-alkanols (C26, C28, and C32), and two alkanes (C25 and C29; **Table 2**). Four of them, namely, two acids (C16, C18) and two 1-alkanol (C28, C32), from the total abaxial wax coverage ($Ab_{Ew + Iw}$) showed similar correlations with the abaxial cuticular transpiration rate. Such correlations were not found from the adaxial surface ($Ad_{Ew + Iw}$). C25 alkane from the total leaf wax coverage showed a significant and negative correlation

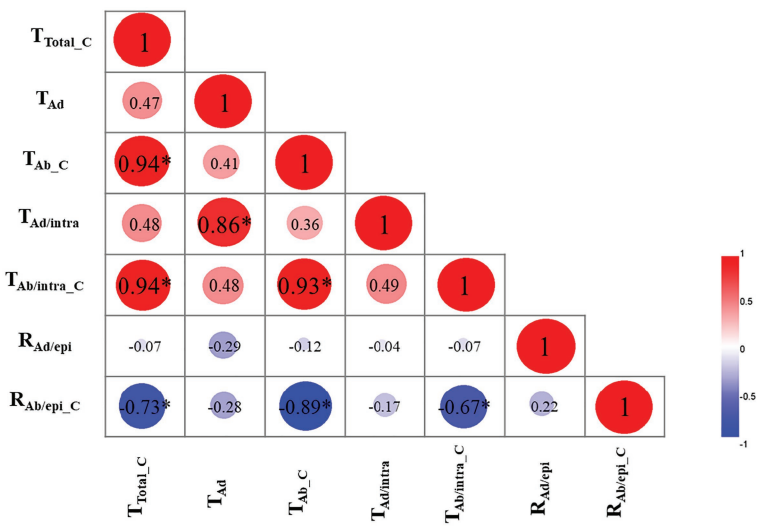

FIGURE 5 | Correlation analysis of cuticular transpiration rate (or resistance; R^2). T_{Total_C}: the total cuticular transpiration rate; T_{Ad}: the adaxial cuticular transpiration rate; T_{Ab_C}: the abaxial cuticular transpiration rate; $T_{Ad/intra}$: the adaxial intracuticular transpiration rate; $T_{Ab/intra\_C}$: the abaxial intracuticular transpiration rate; $R_{Ad/epi}$: the adaxial epicuticular resistance; R_{Ab/epi_C}: the abaxial epicuticular resistance. $^*p < 0.05$.

TABLE 1 | Correlation analysis between cuticular transpiration rate (or resistance) and cuticular wax chemical classes (R^2).

	Ad + Ab	$Ad_{Ew + Iw}$	$Ab_{Ew + Iw}$	Ad_{Iw}	Ab_{Iw}	Ad_{Ew}	Ab_{Ew}
Acids	−0.62*	−0.29	−0.77*	−0.09	−0.70*	+0.08	+0.57*
Aldehydes	−0.17	−0.42	+0.28	+0.00	+0.21	+0.75*	−0.50
1-Alkanols	−0.88*	−0.53*	−0.76*	−0.51*	−0.62*	+0.18	+0.62*
Alkanes	−0.80*	−0.58*	−0.50*	−0.21	−0.22	+0.15	+0.60*
1-Alkanol esters	−0.03	−0.06	−0.00	−0.00	+0.20	+0.08	+0.08
Glycol esters	−0.51*	−0.18	−0.74*	−0.01	−0.37	+0.16	+0.53*
Phthalate esters	−0.19	−0.02	−0.21	−0.01	−0.22	−0.00	+0.15
Glycols	−0.15	−0.20	−0.10	−0.06	−0.07	+0.17	+0.03
β-Tocopherol	−0.01	−0.06	+0.00	−0.07	+0.00	+0.01	−0.01
Triterpenoids	−0.03	−0.06	+0.02	−0.31	−0.00	−0.27	−0.04
Steroids	−0.21	−0.22	−0.17	−0.04	−0.10	−0.01	+0.18
Caffeine	−0.13	−0.44	−0.09	−0.07	−0.00	+0.11	+0.45
Coverage	−0.56*	−0.46	−0.28	−0.38	−0.18	+0.10	+0.56*

*Ad: adaxial; Ab: abaxial; Ew: epicuticular waxes; Iw: intracuticular waxes. *$p < 0.05$.*

TABLE 2 | Correlation analysis between cuticular transpiration rate (or resistance) and cuticular wax components (R^2).

	Ad + Ab	$Ad_{Ew + Iw}$	$Ab_{Ew + Iw}$	Ad_{Iw}	Ab_{Iw}	Ad_{Ew}	Ab_{Ew}
C16 Acid	−0.58*	−0.15	−0.78*	−0.14	−0.64*	+0.00	+0.53*
C18 Acid	−0.60*	−0.24	−0.74*	−0.18	−0.69*	+0.21	+0.49*
C26 1-Alkanol	−0.80*	−0.23	−0.30	−0.56*	−0.40	−0.01	+0.03
C28 1-Alkanol	−0.78*	−0.52	−0.59*	−0.42	−0.60*	+0.32	+0.51*
C32 1-Alkanol	−0.64*	−0.43	−0.65*	−0.43	−0.39	+0.01	+0.25
C26 Aldehyde	−0.28	−0.34	ND	+0.00	ND	+0.59*	ND
C28 Aldehyde	−0.42	−0.49	ND	−0.03	ND	+0.53*	ND
C30 Aldehyde	−0.02	−0.31	+0.28	+0.06	+0.21	+0.83*	−0.50
C21 Alkane	−0.18	−0.13	−0.31	−0.03	−0.07	+0.00	+0.55*
C25 Alkane	−0.55*	−0.41	−0.33	−0.10	−0.09	+0.35	+0.61*
C29 Alkane	−0.85*	−0.53*	−0.64*	−0.19	−0.22	+0.09	+0.50*
C18 Glycol ester	−0.16	+0.00	−0.32	+0.06	−0.11	+0.20	+0.61*
C19 Glycol ester	−0.40	−0.19	−0.69*	−0.04	−0.43	+0.04	+0.35
C20 Glycol	−0.11	−0.29	−0.05	+0.00	−0.10	+0.59*	−0.00
Betulin	−0.36	−0.03	−0.52*	−0.00	−0.39	ND	ND

*Ad: adaxial; Ab: abaxial; Ew: epicuticular waxes; Iw: intracuticular waxes. *$p < 0.05$.*

with the total leaf cuticular transpiration rate; such correlations were not found from the adaxial or the abaxial surfaces; instead, a significant and positive correlation was found on the abaxial epicuticular waxes between wax coverage and the abaxial epicuticular resistance (**Table 2**). In contrast, C29 alkane showed similar significant and negative correlations from the total leaf wax coverage (Ad + Ab), total adaxial wax coverage ($Ad_{Ew + Iw}$), and total abaxial wax coverage ($Ab_{Ew + Iw}$). C19 glycol ester and betulin from the abaxial surface ($Ab_{Ew + Iw}$) showed significant and negative correlations with the abaxial cuticular transpiration rates; such correlations were not found from the total leaf wax coverage and the total adaxial wax coverage.

On the adaxial surface, one wax component (C29 alkane) showed a significant and negative correlation with the adaxial cuticular transpiration rate; such correlations were not found from the adaxial epicuticular waxes or intracuticular waxes. Instead, another wax component (C26 1-alkanol) from the adaxial intracuticular waxes showed a significant and negative correlation with the adaxial intracuticular transpiration rate, although such correlation was not found from the total adaxial wax coverage. Four more wax components from the adaxial epicuticular waxes, namely, three aldehydes (C26, C28, and C30) and one glycol (C20), showed significant and positive correlations with the adaxial epicuticular resistance.

On the abaxial surface, seven wax components from the total abaxial coverage ($Ab_{Ew + Iw}$) showed significant and negative correlations with the abaxial cuticular transpiration rates; they were two acids (C16 and C18), two 1-alkanols (C28 and C32), one alkane (C29), one glycol ester (C19), and one triterpenoid (betulin). Three of them (C16 acid, C18 acid, and C28 1-alkanol) from the abaxial intracuticular wax showed similar correlations with the abaxial intracuticular transpiration rates; a significant and positive correlation with the abaxial epicuticular resistance was also observed. The other three wax components (C32 1-alkanol, C19 glycol ester, and betulin) did not show correlations from neither the abaxial epicuticular waxes nor the intracuticular waxes.

The correlation analysis of the adaxial epicuticular waxes identified four more wax components showing significant and positive correlations with the adaxial epicuticular resistance ($R_{Ad/epi}$), namely, three aldehydes (C26, C28, and C30) and one glycol (C20). These four components did not show correlations from neither the total adaxial waxes nor the adaxial

intracuticular waxes. The correlation analysis from the abaxial epicuticular waxes identified seven wax components showing significant and positive correlations with the abaxial epicuticular resistance (R_{Ab/epi_C}), namely, two acids (C16 and C18), one 1-alkanol (C28), three alkanes (C21, C25, and C29), and one glycol ester (C18). Four of them, namely, two acids (C16 and C18), one 1-alkanol (C28), and one alkane (C29), have been identified from the total abaxial waxes and the abaxial intracuticular waxes. The other three wax components (C21 alkane, C25 alkane, and C18 glycol ester) were found only from the abaxial epicuticular waxes to show such a significant and positive correlation.

DISCUSSION

The principal goal of this study was to quantify to which degree the epicuticular waxes and the intracuticular waxes contribute to the barrier against nonstomatal water loss in mature tea leaves. To address this question, cuticular transpiration rates from eight tea germplasms were measured from each leaf side and individual cuticular substructures. In addition, the epicuticular and intracuticular wax coverage and compositions from both leaf surfaces were determined.

The Adaxial and the Abaxial Leaf Surfaces Showed Different Structures of Cuticular Transpiration Barrier

Cuticular transpiration takes place on both the adaxial and the abaxial leaf surfaces. The nonstomatal adaxial cuticle has been extensively studied, and it has been demonstrated that the adaxial intracuticular waxes constitute the major transpiration barrier, while the adaxial epicuticular waxes are not (Jetter and Riederer, 2016; Zeisler and Schreiber, 2016; Zeisler-Diehl et al., 2018). In contrast, there are few studies about the transpiration barriers from the abaxial leaf surface, largely due to the presence of stomata on this surface. Under normal growth conditions, stomatal transpiration is much higher than cuticular transpiration, which makes the measurement of the abaxial cuticular transpiration technically challenging. The recently established new method enables us to measure cuticular transpiration from different leaf surfaces and cuticular substructures simultaneously (Lino et al., 2020; Zhang et al., 2020). By applying this method, the cuticular transpiration rates from the eight tea germplasms were measured. On the adaxial surface, adaxial epicuticular resistance ($R_{Ad/epi}$) was in the range of 10–25% (**Figure 4B**, upper panel); the total adaxial transpiration rate (T_{Ad}) was significantly and positively correlated with the adaxial intracuticular transpiration rate ($T_{Ad/intra}$; **Figure 5**). Therefore, our data in tea leaves were in accordance with previous conclusions (Jetter and Riederer, 2016; Zeisler and Schreiber, 2016; Zeisler-Diehl et al., 2018; Zhang et al., 2020). The cuticular transpiration rates from the abaxial surface were about 1.8–3.3 times higher than those of the adaxial surface (**Figure 4**). Thus, in addition to *Hedera helix* leaves (Šantrůček et al., 2004), tea leaves also showed higher abaxial cuticular transpiration compared with its adaxial surface. Correlation analysis showed that the total cuticular transpiration rate was significantly correlated with the abaxial cuticular transpiration rate rather than the adaxial cuticular transpiration rate (**Figure 5**).

The abaxial cuticular transpiration rate (T_{Ab_C}) was positively correlated with the abaxial intracuticular transpiration ($T_{Ab/intra\_C}$) and negatively correlated with the abaxial epicuticular resistance (R_{Ab/epi_C}). Our data suggest that the abaxial epicuticular waxes constituted another major transpiration barrier, while the abaxial intracuticular waxes were not (**Figure 5**).

It remains unclear why the adaxial and abaxial surfaces showed different structural organizations in the cuticular transpiration barrier, and what are the underlying mechanisms. Considering that the adaxial and the abaxial leaf surfaces have different niches such as light irradiance, insects, pathogen infestation patterns, etc., we speculate that the adaxial surface is optimized to restrict water loss, while the abaxial surface could be evolved to cope with other environmental stresses, which could compromise its potency as an efficient transpiration barrier. The different environmental niches could provide essential signals to differentially regulate wax biosynthesis or transport, which takes place within the adaxial epidermal cells and the abaxial epidermal cells, respectively. As a result, cuticle structural characteristics on the respective leaf surface could be affected. For crop breeding to improve drought tolerance traits or other related traits, more attention should be paid to germplasms with lower abaxial cuticular transpiration rates.

Plant Growth Conditions Affected the Contribution of Structural Parameters to Tea Cuticular Transpiration Barriers

Most previous studies did not differentiate the epicuticular waxes and the intracuticular waxes, and bulk wax data were used to establish the cuticle structure–function relationship. Under this scenario, the important effects of substructures could be averaged out (Jetter and Riederer, 2016). This may explain the contradicting results from the literature regarding the cuticle thickness and wax coverage for the contributions to the cuticular transpiration barrier. Although no correlations have been reported between cuticular transpiration rate and cuticular wax coverage under normal growth conditions, the specific wax components, rather than wax coverage, have been found to affect cuticular transpiration (Riederer and Schneider, 2001; Jetter and Riederer, 2016). Water deficit induces the increase in cuticle thickness, which associates with the reduction in transpiration rate (Kosma et al., 2009; Jäger et al., 2014); similar observations were also found in tea following water deprivation treatments (Chen et al., 2020; Zhang et al., 2020). However, in other studies, cuticle thickness was not correlated with cuticular transpiration (Schreiber and Riederer, 1996; Jetter and Riederer, 2016; Bi et al., 2017). In this study, the eight germplasms were grown under normal conditions, cuticle thickness from the adaxial and the abaxial surfaces was measured, and no correlations were found between the cuticular transpiration rates and the cuticle thickness from both leaf surfaces. These data suggest that under normal growth conditions, cuticle thickness may not be a major structural parameter affecting the cuticular transpiration barrier.

However, the total leaf cuticular transpiration rates were found to be significantly and negatively correlated with the total leaf wax coverage (**Table 1**), which are consistent with the results from *Arabidopsis*, barley, tomato, and nectarine (Seo et al., 2011; Hasanuzzaman et al., 2017; Romero and Rose, 2019; Lino et al., 2020). In addition, the abaxial epicuticular resistance was significantly and positively correlated with the abaxial epicuticular wax coverage. Meanwhile, no significant correlations were found from individual leaf surfaces, neither the adaxial epicuticular and intracuticular waxes nor the abaxial intracuticular waxes (**Table 1**). Thus, the correlation between wax coverage and cuticular transpiration barrier could be species-specific or cuticle substructure-specific. This work highlights the importance of analyzing the wax coverage from cuticle substructure rather than using bulked data. Previously, we found that following drought treatment, the cuticular transpiration rates are significantly and negatively correlated with the adaxial and the abaxial intracuticular waxes; but no correlations were found between cuticular transpiration rates and the adaxial or the abaxial wax coverage (Zhang et al., 2020). These discrepancies suggest that wax coverage is not the only factor that affects the cuticular transpiration barrier. Instead, cuticle structural changes induced by other drought stress could play larger roles in affecting cuticular transpiration barrier properties. This notion was supported by the significant wax compositional changes following drought treatments (Chen et al., 2020; Zhang et al., 2020).

Aliphatic Compounds and Glycol Esters Contributed to the Cuticular Transpiration Barrier in Tea Under Normal Growth Conditions

In this study, correlation analysis revealed that acids, 1-alkanols, alkanes, and glycol esters from the total leaf wax coverage (Ad + Ab) were associated with T_{Total_C} (**Table 1**). These data were in accordance with previous reports that the major cuticular transpiration barrier was formed by very-long-chain aliphatic compounds (Vogg et al., 2004; Jetter and Riederer, 2016). These same wax chemical groups (except acids and glycol esters) also showed similar roles on the adaxial and the abaxial surfaces as well as on the abaxial epicuticular waxes (**Table 1**). 1-Alkanols contributed to the transpiration barrier from the adaxial and the abaxial intracuticular waxes, while glycol esters specifically function on the abaxial epicuticular waxes layer (**Table 1**).

At the individual wax chemical level, there was no overlap of the contributing wax components between the adaxial and abaxial surfaces except C29 alkane, which contributed to the transpiration barrier on both leaf surfaces. The adaxial intracuticular waxes constituted a major leaf transpiration barrier, and 1-alkanol (C26) appeared to be the major contributor affecting its transpiration barrier properties. Although the adaxial epicuticular waxes were not a major transpiration barrier, three aldehydes (C26, C28, and C30) and one glycol (C20) were identified to affect its barrier properties (**Table 2**). The abaxial epicuticular waxes were another major transpiration barrier, and more wax components were identified as a contributor to their barrier formation (**Table 2**). Similar to the adaxial epicuticular waxes, the abaxial intracuticular waxes were not the major transpiration barrier. However, three wax components (C16 acid, C18 acid, and C28 1-alkanol) were identified to contribute to their transpiration barrier properties. These data suggest that for the individual wax component, its cuticular substructure localization affects its potency as a contributor to the transpiration barrier. This may explain the contradicting results from different plant species studied by different researchers (Riederer and Schneider, 2001; Seo et al., 2011; Jetter and Riederer, 2016; Hasanuzzaman et al., 2017; Romero and Rose, 2019; Lino et al., 2020). This also suggests that each cuticular compartment may have different microstructures, but a comparable transpiration barrier still can be formed.

The coverage of 1-alkanols and alkanes from the adaxial surface ($Ad_{Ew + Iw}$) was higher than that of the abaxial surface ($Ab_{Ew + Iw}$; **Figure 3**; **Supplemental Data 1**). Accordingly, compared with the abaxial surface, the adaxial surface showed a lower water transpiration rate and thus better barrier properties against water loss (**Figure 4**). On both leaf surfaces, 1-alkanols and alkanes were significantly and negatively correlated with the cuticular transpiration rate (**Table 1**). This suggests that differential distributions of specific aliphatic wax components on the adaxial and the abaxial surfaces could be one important factor to shape their barrier characteristics.

Generally, the adaxial leaf surface is densely covered with wax crystal, which deflects solar irradiance (Zhu et al., 2018; Zhang et al., 2020). 1-Alkanols and alkanes are the major components of wax crystal (Riederer and Schneider, 1990; Jetter et al., 2000; Cameron et al., 2006; Dragota and Riederer, 2007), which may explain why the adaxial epicuticular waxes were enriched with 1-alkanols and alkanes (**Figure 3**). Interestingly, both wax components did not contribute to the adaxial epicuticular resistance (**Tables 1** and **2**). Under field conditions, the adaxial surface is exposed to solar light directly; the deposition of wax compounds, especially 1-alkanols and alkanes, could increase the size and density of wax crystal and deflect solar radiation more efficiently, resulting in reduced leaf surface temperature and water loss (Long et al., 2003; Fukuda et al., 2008). However, the *in vitro* transpiration measurement in this study was performed under dark conditions; thus, it may miss out their true roles *in planta* under field conditions.

As a chemical group, triterpenoids did not show a significant correlation with the cuticular transpiration rate or resistance (**Table 1**), which is in accordance with previous studies (Jetter and Riederer, 2016; Staiger et al., 2019). However, at the individual chemical level, betulin, a triterpenoid from the abaxial surface, showed significant and negative correlations with the abaxial cuticular transpiration rate (**Table 2**). Previously, we found that triterpenoids play an important role in the formation of the cuticular transpiration barrier following drought stress (Zhang et al., 2020). The cuticular waxes from a desert plant are composed of mainly triterpenoids, which are deposited within the cutin matrix, and play a critical role in protecting the polymer against thermal expansion (Schuster et al., 2016). The studies of tomatoes and nectarines showed that triterpenoid deposition plays a major role in regulating

fruit permeability during fruit development and water stress (Romero and Rose, 2019; Lino et al., 2020). Based on these findings, we speculate that triterpenoid deposition could modify cuticle transpiration barrier properties in response to stresses or specific developmental stages.

In summary, here, we conducted a comprehensive analysis of all cuticular substructures from eight tea germplasms. The adaxial intracuticular waxes and the abaxial epicuticular waxes constitute the major cuticular transpiration barriers; the abaxial cuticular transpiration rates were higher than the adaxial cuticular transpiration rates and significantly and positively correlated with the total leaf cuticular transpiration. The very-long-chain aliphatic compounds and glycol esters were important contributors to the overall cuticular transpiration barrier as well as in specific cuticle substructure of tea leaves. This work offered novel insights about the cuticular substructure–function relationship in tea plants.

DATA AVAILABILITY STATEMENT

The original contributions presented in the study are included in the article/**Supplementary Material**, further inquiries can be directed to the corresponding authors.

AUTHOR CONTRIBUTIONS

MC, CC, and YZ conceived the original research plans. MC and CC supervised the experiments. YZ, XK, ZD, HZ, ZY, and JQ performed the experiments. ZD provided technical assistance to YZ. MC and YZ designed the experiments and analyzed the data, and wrote the article with contributions from all the authors. MC agrees to serve as the author responsible for contact and ensures communication. All authors contributed to the article and approved the submitted version.

FUNDING

This work was supported by the National Science Foundation of China (grant no. 31870803) and the Ministry of Agriculture of P. R. China (CARS-19).

ACKNOWLEDGMENTS

The authors thank Mr. Zijian Chen (zijian.chen@hitachi-powergrids.com) from Hitachi ABB Power Grids Co., for English language editing, and the metabolomics core from the Horticultural Plant Biology and Metabolomics Center at the Fujian Agriculture and Forestry University for helping with wax lipid analysis.

SUPPLEMENTARY MATERIAL

The Supplementary Material for this article can be found online at: https://www.frontiersin.org/articles/10.3389/fpls.2021.655799/full#supplementary-material

REFERENCES

Bi, H., Kovalchuk, N., Langridge, P., Tricker, P. J., Lopato, S., and Borisjuk, N. (2017). The impact of drought on wheat leaf cuticle properties. *BMC Plant Biol.* 17:85. doi: 10.1186/s12870-017-1033-3

Buschhaus, C., and Jetter, R. (2012). Composition and physiological function of the wax layers coating arabidopsis leaves: β-amyrin negatively affects the intracuticular water barrier. *Plant Physiol.* 160, 1120–1129. doi: 10.1104/pp.112.198473

Cameron, K. D., Teece, M. A., and Smart, L. B. (2006). Increased accumulation of cuticular wax and expression of lipid transfer protein in response to periodic drying events in leaves of tree tobacco. *Plant Physiol.* 140, 176–183. doi: 10.1104/pp.105.069724

Chen, M., Zhu, X., Zhang, Y., Du, Z., Chen, X., Kong, X., et al (2020). Drought stress modify cuticle of tender tea leaf and mature leaf for transpiration barrier enhancement through common and distinct modes. *Sci. Rep.* 10:6696. doi: 10.1038/s41598-020-63683-4

Cheng, G., Huang, H., Zhou, L., He, S., Zhang, Y., and Cheng, X. (2019). Chemical composition and water permeability of the cuticular wax barrier in rose leaf and petal: a comparative investigation. *Plant Physiol. Biochem.* 135, 404–410. doi: 10.1016/j.plaphy.2019.01.006

Diarte, C., de Souza, A. X., Staiger, S., Deininger, A. C., Bueno, A., Burghardt, M., et al. (2020). Compositional, structural and functional cuticle analysis of *Prunus laurocerasus* L. sheds light on cuticular barrier plasticity. *Plant Physiol. Biochem.* 158, 434–445. doi: 10.1016/j.plaphy.2020.11.028

Dragota, S., and Riederer, M. (2007). Epicuticular wax crystals of Wollemia nobilis: morphology and chemical composition. *Ann. Bot.* 100, 225–231. doi: 10.1093/aob/mcm120

Eigenbrode, S. D., and Espelie, K. E. (1995). Effects of plant epicuticular lipids on insect herbivores. *Annu. Rev. Entomol.* 40, 171–194. doi: 10.1146/annurev.en.40.010195.001131

Fernández, V., Bahamonde, H. A., Peguero-Pina, J. J., Gil-Pelegrín, E., Sancho-Knapik, D., Gil, L., et al. (2017). Physico-chemical properties of plant cuticles and their functional and ecological significance. *J. Exp. Bot.* 68, 5293–5306. doi: 10.1093/jxb/erx302

Fich, E. A., Segerson, N. A., and Rose, J. K. (2016). The plant polyester cutin: biosynthesis, structure, and biological roles. *Annu. Rev. Plant Biol.* 67, 207–233. doi: 10.1146/annurev-arplant-043015-111929

Fukuda, S., Satoh, A., and Kasahara, H., Matsuyama, H., Takeuchi, Y. (2008). Effects of ultraviolet-B irradiation on the cuticular wax of cucumber (*Cucumis sativus*) cotyledons. *J. Plant Res.* 121, 179–189. doi: 10.1007/s10265-007-0143-7

Hasanuzzaman, M., Davies, N. W., Shabala, L., Zhou, M., Brodribb, T. J., and Shabala, S. (2017). Residual transpiration as a component of salinity stress tolerance mechanism: a case study for barley. *BMC Plant Biol.* 17:107. doi: 10.1186/s12870-017-1054-y

Jäger, K., Fábián, A., Eitel, G., Szabó, L., Deák, C., Barnabás, B., et al. (2014). A morphophysiological approach differentiates bread wheat cultivars of contrasting tolerance under cyclic water stress. *J. Plant Physiol.* 171, 1256–1266. doi: 10.1016/j.jplph.2014.04.013

Jeffree, C. E. (2006). "The fine structure of the plant cuticle," in *Biology of the Plant Cuticle. Vol. 23.* eds. M. Riederer and C. Müller (Oxford: Blackwell), 11–144.

Jetter, R., and Riederer, M. (2016). Localization of the transpiration barrier in the epi- and intracuticular waxes of eight plant species: water transport resistances are associated with fatty acyl rather than alicyclic components. *Plant Physiol.* 170, 921–934. doi: 10.1104/pp.15.01699

Jetter, R., Schäffer, S., and Riederer, M. (2000). Leaf cuticular waxes are arranged in chemically and mechanically distinct layers: evidence from *Prunus laurocerasus* L. *Plant Cell Environ.* 23, 619–628. doi: 10.1046/j.1365-3040.2000.00581.x

Kosma, D. K., Bourdenx, B., Bernard, A., Parsons, E. P., Lü, S., Joubés, J., et al. (2009). The impact of water deficiency on leaf cuticle lipids of *Arabidopsis*. *Plant Physiol.* 151, 1918–1929. doi: 10.1104/pp.109.141911

Krauss, P., Markstädter, C., and Riederer, M. (1997). Attenuation of UV radiation by plant cuticles from woody species. *Plant Cell Environ.* 20, 1079–1085. doi: 10.1111/j.1365-3040.1997.tb00684.x

Lino, L., Quilot-Turion, B., Dufour, C., Corre, M., Lessire, R., Génard, M., et al. (2020). Cuticular waxes of nectarines during fruit development in relation to surface conductance and susceptibility to *Monilinia laxa*. *J. Exp. Bot.* 71, 5521–5537. doi: 10.1093/jxb/eraa284

Long, L. M., Patel, H. P., Cory, W. C., and Stapleton, A. E. (2003). The maize epicuticular wax layer provides UV protection. *Funct. Plant Biol.* 30, 75–81. doi: 10.1071/FP02159

Machado, R., Loram-Lourenço, L., Farnese, F. S., Alves, R. D. F. B., de Sousa, L. F., Silva, F. G., et al. (2020). Where do leaf water leaks come from? Trade-offs underlying the variability in minimum conductance across tropical savanna species with contrasting growth strategies. *New Phytol.* 229, 1415–1430. doi: 10.1111/NPH.16941

Nawrath, C. (2006). Unraveling the complex network of cuticular structure and function. *Curr. Opin. Plant Biol.* 9, 281–287. doi: 10.1016/j.pbi.2006.03.001

Neinhuis, C., and Barthlott, W. (1997). Characterization and distribution of water-repellent, self-cleaning plant surfaces. *Ann. Bot.* 79, 667–677. doi: 10.1006/anbo.1997.0400

Pollard, M., Beisson, F., Li, Y. H., and Ohlrogge, J. B. (2008). Building lipid barriers: biosynthesis of cutin and suberin. *Trends Plant Sci.* 13, 236–246. doi: 10.1016/j.tplants.2008.03.003

Richardson, A., Wojciechowski, T., Franke, R., Schreiber, L., Kerstiens, G., Jarvis, M., et al. (2007). Cuticular permeance in relation to wax and cutin development along the growing barley (*Hordeum vulgare*) leaf. *Planta* 225, 1471–1481. doi: 10.1007/s00425-006-0456-0

Riederer, M., and Schneider, G. (1990). The effect of the environment on the permeability and composition of Citrus leaf cuticles. II. Composition of soluble cuticular lipids and correlation with transport properties. *Planta* 180, 54–165. doi: 10.1007/BF00193990

Riederer, M., and Schneider, L. (2001). Protecting against water loss: analysis of the barrier properties of plant cuticles. *J. Exp. Bot.* 52, 2023–2032. doi: 10.1093/jexbot/52.363.2023

Riederer, M., and Schreiber, L. (1995). "Waxes: transport barriers of plant cuticles," in *Waxes: Chemistry, Molecular Biology and Functions*. ed. R. J. Hamilton (Dundee: Oily), 131–156.

Romero, P., and Rose, J. K. C. (2019). A relationship between tomato fruit softening, cuticle properties and water availability. *Food Chem.* 295, 300–310. doi: 10.1016/j.foodchem.2019.05.118

Samuels, L., Kunst, L., and Jetter, R. (2008). Sealing plant surfaces: cuticular wax formation by epidermal cells. *Annu. Rev. Plant Biol.* 59, 683–707. doi: 10.1146/annurev.arplant.59.103006.093219

Šantrůček, J., Šimáňová, E., Karbulková, J., Šimková, M., and Schreiber, L. (2004). A new technique for measurement of water permeability of stomatous cuticular membranes isolated from *Hedera helix* leaves. *J. Exp. Bot.* 55, 1411–1422. doi: 10.1093/jxb/erh150

Schreiber, L., and Riederer, M. (1996). Ecophysiology of cuticular transpiration: comparative investigation of cuticular water permeability of plant species from different habitats. *Oecologia* 107, 426–432. doi: 10.1007/BF00333931

Schuster, A., Burghardt, M., Alfarhan, A., Bueno, A., Hedrich, R., Leide, J., et al. (2016). Effectiveness of cuticular transpiration barriers in a desert plant at controlling water loss at high temperatures. *AoB Plants* 8, 1–14. doi: 10.1093/aobpla/plw027

Seo, P. J., Lee, S. B., Suh, M. C., Park, M. J., Go, Y. S., and Park, C. M. (2011). The MYB96 transcription factor regulates cuticular wax biosynthesis under drought conditions in *Arabidopsis*. *Plant Cell* 23, 1138–1152. doi: 10.1105/tpc.111.083485

Silva, G. A., Pereira, R. M., Rodrigues-Silva, N., Souza, T. C., Ferreira, D. O., Queiroz, E. A., et al. (2017). Wax removal and diamondback moth performance in collards cultivars. *Neotrop. Entomol.* 46, 1–7. doi: 10.1007/s13744-017-0493-3

Staiger, S., Seufert, P., Arand, K., Burghardt, M., Popp, C., and Riederer, M. (2019). The permeation barrier of plant cuticles: uptake of active ingredients is limited by very long-chain aliphatic rather than cyclic wax compounds. *Pest Manag. Sci.* 75, 3405–3412. doi: 10.1002/ps.5589

Vogg, G., Fischer, S., Leide, J., Emmanuel, E., Jetter, R., Levy, A. A., et al. (2004). Tomato fruit cuticular waxes and their effects on transpiration barrier properties: functional characterization of a mutant deficient in a very-long-chain fatty acid beta-ketoacyl-CoA synthase. *J. Exp. Bot.* 55, 1401–1410. doi: 10.1093/jxb/erh149

Weissflog, I., Vogler, N., Akimov, D., Dellith, A., Schachtschabel, D., Svatos, A., et al. (2010). Toward in vivo chemical imaging of epicuticular waxes. *Plant Physiol.* 154, 604–610. doi: 10.1104/pp.110.161786

Yeats, T. H., and Rose, J. K. C. (2013). The formation and function of plant cuticles. *Plant Physiol.* 163, 5–20. doi: 10.1104/pp.113.222737

Zeisler, V., and Schreiber, L. (2016). Epicuticular wax on cherry laurel (*Prunus laurocerasus*) leaves does not constitute the cuticular transpiration barrier. *Planta* 243, 65–81. doi: 10.1007/s00425-015-2397-y

Zeisler-Diehl, V., Müller, Y., and Schreiber, L. (2018). Epicuticular wax on leaf cuticles does not establish the transpiration barrier, which is essentially formed by intracuticular wax. *J. Plant Physiol.* 227, 66–74. doi: 10.1016/j.jplph.2018.03.018

Zhang, Y., Chen, X., Du, Z., Zhang, W., Devkota, A. R., Chen, Z., et al. (2020). A proposed method for simultaneous measurement of cuticular transpiration from different leaf surfaces in *Camellia sinensis*. *Front. Plant Sci.* 11:420. doi: 10.3389/fpls.2020.00420

Zhu, X. F., Zhang, Y., Du, Z. H., Chen, X. B., Zhou, X., Kong, X. R., et al. (2018). Tender leaf and fully-expanded leaf exhibited distinct cuticle structure and wax lipid composition in *Camellia sinensis cv Fuyun 6*. *Sci. Rep.* 8:14944. doi: 10.1038/s41598-018-33344-8

Conflict of Interest: The authors declare that the research was conducted in the absence of any commercial or financial relationships that could be construed as a potential conflict of interest.

frontiers in Plant Science

ORIGINAL RESEARCH
published: 20 July 2021
doi: 10.3389/fpls.2021.694123

Water Soaking Disorder in Strawberries: Triggers, Factors, and Mechanisms

*Grecia Hurtado and Moritz Knoche**

Institute for Horticultural Production Systems, Leibniz University Hannover, Hannover, Germany

Water soaking is an important surface disorder of strawberries that limits unprotected field production. The objective was to identify the mechanism(s) of water soaking. Symptomatic fruit show pale, deliquescent patches of skin. This damage extends into the flesh. Numerous cuticular microcracks occurred in water-soaked areas. Water soaking occurred only if the skin was exposed to liquid water. Water soaking was more rapid when the cuticle had been abraded. Water soaking, anthocyanin leakage, and water uptake all increased with incubation time. There was a lag phase for water soaking and anthocyanin leakage, but not for water uptake. Susceptibility to water soaking increased with fruit ripening and mass. Incubation in isotonic PEG 6000 increased cuticular microcracking but decreased water soaking and water uptake. Incubation in hypotonic fruit juice (natural and artificial) increased water soaking incidence and severity but reduced water uptake. Incubation in dilute citric and malic acids increased plasma membrane permeability as indexed by anthocyanin leakage and increased water soaking. Thus, water soaking involves cuticular microcracking, localized water uptake, bursting of cells, and the release of organic acids into the apoplast. The damage propagates from cell to cell.

Keywords: rain damage, water soaking, *Fragaria* × *ananassa* Duch, cracking, leakage, cuticle, microcrack

OPEN ACCESS

Edited by:
Eva Domínguez,
Institute of Subtropical and Mediterranean Horticulture La Mayora UMA-CSIC, Spain

Reviewed by:
Jesús Cuartero,
Institute of Subtropical and Mediterranean Horticulture La Mayora UMA-CSIC, Spain
Adam Solti,
Eötvös Loránd University, Hungary

***Correspondence:**
Moritz Knoche
moritz.knoche@obst.uni-hannover.de

Specialty section:
This article was submitted to Plant Physiology, a section of the journal Frontiers in Plant Science

Received: *12 April 2021*
Accepted: *11 June 2021*
Published: *20 July 2021*

Citation:
Hurtado G and Knoche M (2021) Water Soaking Disorder in Strawberries: Triggers, Factors, and Mechanisms. Front. Plant Sci. 12:694123. doi: 10.3389/fpls.2021.694123

INTRODUCTION

Strawberry is a soft fleshy fruit of global importance (Hummer and Hancock, 2009). It is highly perishable, but nevertheless grown mainly in the open field where fruit quality is often severely compromised by rain. The main disorders arising from rain are water soaking and cracking (Herrington et al., 2009). With water soaking, the appearance of the fruit surface is compromised, with the skin looking lighter-colored and deliquescent (Herrington et al., 2009). With cracking, easily visible, gaping cracks occur that often extend deep into the flesh. Both disorders may be observed on different regions of the fruit surface, the calyx, neck, shoulder, or tip (Herrington et al., 2011). Both water soaking and cracking increase the incidence of fruit rots pre- and post-harvest. Together, these disorders result in significant economic loss due not only to the lost opportunity (reduced yield) but also to the additional labor involved in harvesting, grading, and packing a fruit population high in individuals suffering compromised quality (Herrington et al., 2009). In addition, the loss at the consumer level increases.

As a result of these limitations, strawberry production is slowly shifting from open field, to semi- or fully protected cultivation in plastic tunnels or greenhouses. This shift is occurring particularly in areas where the incidence of rainfall is high during the later stages of fruit growth and harvest. However, the additional costs of the protection structures and of energy increase the

production costs (Khoshnevisan et al., 2013). Furthermore, not all strawberry cultivars are suitable for production in tunnels where, in susceptible cultivars, protected cultivation sometimes increases the incidence of powdery mildew, spider mites, and calcium deficiency disorders (Grijalba et al., 2015).

The mechanistic bases of water soaking and cracking in strawberries have not yet been properly determined. However, such understanding is the obvious prerequisite to the development of effective countermeasures that mitigate water soaking and cracking through the introduction of innovative cultural methods and/or breeding. The objective of this study was to identify the triggers, factors, and mechanisms underlying the water soaking disorder in strawberry fruit.

MATERIALS AND METHODS

Plant Material

Strawberry fruit (*Fragaria* × *ananassa* Duch., cultivars Clery, Faith, Florentina, Malwina) were harvested from commercial plantings at Gleidingen (lat. 52°16′ N, long. 9°50′ E) and Bad Nenndorf (lat. 52°21′ N, long. 9°20′ E). The change in cultivars was necessary, because in strawberry a given cultivar is available at the optimum stage of ripeness only for a limited period of time. Unless otherwise specified, fruits were harvested randomly at commercial ripeness (>80% of the fruit surface red), placed in a foam tray, and selected for uniformity of size, shape, and color and for freedom from visual defects. Care was taken to not touch the fruit surface. The pedicel was cut to a maximum length of 5 mm. Fruits were processed fresh on the day of sampling or held at 2°C and 80% RH for no longer than 1 day. Previous studies showed that holding fruit for up to 2 days under these conditions had no effect on rates of water uptake or transpiration (data not shown). Unless otherwise specified, the calyx was removed from the fruit by carefully pulling the tip of the calyx toward the pedicel. This occasionally required the fruit to be held down by holding on to the pedicel. In most instances, gravity was sufficient for the fruit to remain in the foam tray during the removal of the calyx. The fruit surface was not touched by hand during the entire procedure. The pedicel stump and the attachment zones of the calyx represent openings that are accessible for water uptake. To exclude artifacts, these holes were sealed using a fast-curing, non-phytotoxic silicone rubber (SE 9186 Clear; Dow Corning Corp., Midland, United States). This procedure is illustrated in **Supplementary Figure 1**.

General Procedure

The water soaking damage was induced by incubating fruit in deionized water (one fruit per 100 mL) at room temperature. The fruits were forced under water using a soft plastic-foam plug. After a period of immersion, the fruits were carefully blotted using the soft tissue paper. The extent of water soaking was quantified using a 5-point rating scale or by direct measurement using image analysis. The 5-point rating scale was as follows: score 0 = no water soaking; score 1 = <10% of the surface water-soaked; score 2 = 10–35%; score 3 = 35–60%; and score 4 = >60% of the fruit surface area water-soaked.

The water-soaked fruit surface was inspected by light and fluorescence microscopy. Fruit were incubated in 0.1% acridine orange (Carl Roth, Karlsruhe, Germany) for 3 min, then rinsed with deionized water, and carefully blotted. The fluorescent tracer acridine orange penetrates any microscopic cracks in the cuticle, but not an intact cuticle (Peschel and Knoche, 2005; Becker and Knoche, 2012b; Khanal et al., 2021). The fruit surface was then inspected under incident white and incident fluorescent light using a binocular microscope (Leica MZ10F with filter GFP plus 480–440 nm excitation, ≥510 nm emission; Leica Microsystems GmbH, Wetzlar, Germany). Furthermore, surface scans of water-soaked regions and non-water-soaked control regions were prepared at ×500 using a digital microscope (VHX-7000; Keyence, Osaka, Japan) and coaxial illumination.

Water uptake into submerged fruit was quantified gravimetrically. Fruits were incubated individually in deionized water. Before each weighing, a fruit was carefully blotted dry using a soft paper tissue, then weighed (CPA225D; Sartorius, Göttingen, Germany), and thereafter immediately returned to the incubation solution for a further period. Unless specified otherwise, the number of replicates was 15.

Experiments

The **effect of partial immersion in water on water soaking** was investigated in "Florentina" fruit. Fruits were incubated for 24 h in deionized water such that (a) one half of the fruit was submerged (longitudinal axis horizontal), or (b) just the fruit tip (longitudinal axis vertical), or (c) just the calyx end (longitudinal axis vertical).

The **effect of wounding on water soaking** was investigated in "Florentina" fruit. The treatments were (a) an incision 5 mm long, 3 mm deep using a razor blade; (b) a hole 1.6 mm diameter and 5 mm deep; and (c) abrasion of the cuticle with carborundum powder (grain size 1,200; Schriever, Hamburg, Germany) of about 10 mm^2. Treated fruits were then incubated in deionized water for 3 h, and calibrated photographs were taken immediately thereafter. The soaked areas around the wounds were quantified by image analysis (cellSens Dimension 1.7.1; Olympus Soft Imaging Solutions, Münster, Germany). The numbers of replicates were 10.

Different procedures to quantify water soaking were compared using "Florentina" fruit. These procedures included the comparison of the rating scheme (above) with direct measurement of water-soaked areas using image analysis. In designs involving repeated measures, to exclude artifacts resulting from repeated blotting, the experiment was run twice: First, using independent measurements and ratings (destructive sampling), and second, using repeated observations (measurements and ratings) on the same fruit (non-destructive sampling). For the repeated measurements, the fruit was rotated and photographed from opposite sides at each time interval. Only when the area of water soaking exceeded 60% of the total fruit surface was the fruit peeled and the peel flattened on a glass plate. A calibrated photograph was taken (Canon DS126271; Canon Inc., Tokyo, Japan). The water-soaked area was quantified using image analysis (cellSens Dimension 1.7.1; Olympus Soft

Imaging Solutions, Münster, Germany). The minimum number of replicates was 60.

The **time courses** of change in the water-soaked area, in the absorbance of the incubation solution, and in the mass of water uptake were determined over a 10-h incubation period. The water-soaked area was quantified using image analysis (cellSens Dimension 1.7.1; Olympus Soft Imaging Solutions), and the water uptake was measured gravimetrically as described above. The leakage of anthocyanin into the incubation medium was determined by measuring the absorbance of the incubation medium at 520 nm using a spectrophotometer (Specord 210; Analytik Jena, Jena, Germany). Since the absorbance of an anthocyanin solution depends on pH, the pH was first adjusted to pH 2.3 using citric acid at a final concentration of 37 mM.

Relationships between water soaking, microcracking, and water uptake were studied by incubating "Clery" fruit for 0, 2, 4, 8, 16, and 24 h in deionized water. Water soaking was quantified using the rating scheme described above. Microcracking of the cuticle was indexed by quantifying the area infiltrated with acridine orange using fluorescence microscopy. The fruits were dipped in 0.1% (w/w) aqueous acridine orange (Carl Roth, Karlsruhe, Germany) for 5 min. Thereafter, fruits were rinsed, blotted dry, and viewed at ×6.3 under a fluorescence binocular microscope (MZ10F; Leica Microsystems, Wetzlar, Germany). Four calibrated images within randomly selected microscope "windows" were taken (Camera DP71; GFP-plus filter, 480–440 nm excitation, ≥510 nm emission wavelength) per fruit on a total of 10 fruit. The area infiltrated by acridine orange was quantified using image analysis (cellSens Dimension 1.7.1; Olympus Soft Imaging Solutions, Münster, Germany). A tissue infiltrated with acridine orange exhibits orange, yellow, and green fluorescence (Peschel and Knoche, 2005). To quantify the infiltrated areas, the appropriate color thresholds were selected, and all images were batch-processed using the same settings for these thresholds. The infiltrated areas were expressed as a percentage of the area of the microscope window. Water uptake was determined gravimetrically.

The **site on the fruit surface** where water soaking first appeared was identified in "Florentina" strawberries. Fruits were immersed in deionized water and continually inspected for symptoms of water soaking. When a fruit exhibited water soaking, it was cut into four slices of equal thickness and perpendicular to its longitudinal axis. The slice in which symptoms first appeared was recorded. Two batches of fruit were inspected: (a) one with the calyx present and (b) one with the calyx removed. The total number of replicates was 92 per treatment. The osmotic potentials of the juice expressed from the different slices from the same batch were measured. A fruit was cut into two halves along its longitudinal axis. One half was used to express the juice to determine the mean osmotic potential of the fruit. The other half was cut transversally into four slices of equal thickness. The osmotic potential of the expressed juices was determined by water vapor pressure osmometry (VAPRO 5600; Wescor, Utah, United States).

A "gaping assay" was carried out to **evaluate the strain relaxation** in the different regions of the fruit surface. A cut 5 mm long and 2 mm deep was made using a razor blade. Calibrated photographs (Lumix DMC-G80; Panasonic Corporation, Osaka, Japan) were taken on a macrostand immediately after the cut had been made and again 24 h later. Gape width was measured by image analysis. Fruits was maintained at 100% RH during the assay to minimize transpiration. The experiments were carried out using "Florentina" fruit. The number of replicates was 10.

The **effect of ripeness on water soaking** was studied in the fruit of "Florentina." Fruit were selected at six stages of ripeness as indexed by color, ranging from white to dark red (CM-2600 d, orifice 3 mm diameter; Konica Minolta, Tokyo, Japan). All fruit were incubated for 6 h to induce water soaking. Water soaking was quantified using the rating scheme described above. Water uptake was measured gravimetrically (CPA225D; Sartorius, Göttingen, Germany). The osmotic potentials (VAPRO 5600; Wescor, Utah, United States) of the expressed juices were analyzed from the fruit of the same batch.

The **effect of fruit size on water soaking** was investigated by incubating fruit of five different size classes in water for 6 h. The size classes were <15, 15–20, 20–25, 25–30, and 30–40 g. Water soaking was rated as indicated above. Color (CM-2600 d, orifice 3 mm diameter; Konica Minolta, Tokyo, Japan) and soluble solids (°Brix) using a refractometer (DR6200-T; A. Kruess Optronic, Hamburg, Germany) were determined. This experiment was carried out using "Malwina" fruit. The total number of replicates was 92.

The **effect of water uptake on water soaking** was studied by incubating "Clery" strawberries in solutions of polyethylene glycol 6000 (PEG 6000) or in deionized water. The PEG 6000 solution was prepared to be isotonic to the juice expressed from the fruit of the same batch. The time courses of change in water-soaked area and in water uptake were established by sampling fruit at 0, 1, 2, 4, 6, 8, 11, and 24 h. In addition, the fruit surface was inspected for microcracks as described above.

The role of the osmolytes contained in expressed strawberry juice in the phenomenon of water soaking was addressed in two different experiments.

We analyzed the **effect on water soaking of expressed strawberry juice (natural) and of a synthetic juice** prepared by combining pure solutions of the five major strawberry osmolytes (artificial). Natural juice was expressed from the fruit of the same batch as used in the experiment. The osmolytes in the artificial juice and their relative amounts were glucose (30.3%), fructose (33.2%), sucrose (7.6%), citric acid (9.7%), malic acid (5.7%), and potassium applied as KOH (9.6%) (Herrmann, 2001). Natural and artificial juice was used at "full" (isotonic with the fruit) or "half strength" (half isotonic). Osmotic potentials of the solutions were measured by water vapor pressure osmometry (VAPRO 5600; Wescor, Utah, United States). Deionized water served as control. Fruits were incubated for 4 h, and the water-soaked area was then quantified. The rates of water uptake were determined gravimetrically on fruit from the same batch at 0.5-h intervals for up to 1.5 h. The rates of water uptake were calculated (mg h^{-1}) on an individual fruit basis, from the slope of a linear regression fitted through a plot of increasing fruit mass vs. time. The experiment was carried out using "Faith" fruit.

In the second experiment, the **effect of the individual major osmolytes** of "Florentina" strawberry, i.e., of glucose (121.0 mM),

fructose (132.7 mM), sucrose (30.4 mM), citric acid (38.9 mM), and malic acid (22.6 mM), on water soaking and the rate of water uptake was established. The solution's concentrations were derived from the composition of the isotonic artificial juice of fruit from the same batch. Deionized water and the isotonic artificial juice were used as controls. The water-soaked area and the rate of water uptake were determined as described above.

The **role of malic and citric acid** in water soaking was studied using a leakage assay and anthocyanin as an indicator of cell membrane damage in "Florentina" (Winkler et al., 2015). Cell walls were stressed to varying extents by incubating fruit in solutions of PEG 6000 of different osmotic potentials, and a time course of anthocyanin leakage was established. Cylinders of the outer flesh and fruit skin were excised using a biopsy punch (8 mm diameter), and these were cut to 2 mm length, rejecting the skin, using parallel razor blades. Flesh disks were blotted and rinsed, and then incubated in isotonic PEG 6000 solution, with and without (control) 39 mM citric and 23 mM malic acid. Disks were removed from solution after 1, 2, 4, 8, and 24 h. The absorbance of the incubation medium was quantified at 520 nm using a spectrophotometer (Specord 210; Analytik Jena, Jena, Germany). Before measuring, the pH of the solution used as a control was adjusted by adding the same volume of acids (after incubation was terminated) as that present in the treatment solution. In this way, the control and treatment solutions had the same pH (pH 2.5), and there was no confounding in anthocyanin detection due to variable pH. In a subsequent experiment, disks were incubated in PEG 6000 solutions of osmotic potential 0, −0.6, −1.2, −1.8, or −2.4 MPa with and without the two acids. Disks were removed from the solutions after 4 h, and the anthocyanin content of the incubation medium was measured as described above. Six disks were excised per fruit and used as paired observations. Three disks represent one replicate. The experiment was carried out using 10 replicates.

Data Analyses

All experiments were conducted and analyzed using completely randomized designs. Data were analyzed by analysis of variance and linear regression. Means were compared using Tukey's studentized range tests ($p < 0.05$) and the statistical software R (version 3.5.1; R Foundation for Statistical Computing, Vienna, Austria). Unless individual observations are shown (e.g., **Figure 3C**-inset, **Figures 4A,B**-insets, and **Figure 4D**), data are presented as means ± standard errors.

RESULTS

Water soaking in strawberries appeared as irregular patches of skin that are pale, deliquescent, and sometimes pinkish. At times, they looked slightly translucent compared to the shiny, dark-red controls (**Figure 1A**). The symptoms usually started on the margin between the depressions of adjacent achenes. When severe, the patches covered a major portion of the fruit surface (**Figures 1A,B**). Water soaking was not limited to the fruit skin but extended several mm below the surface into the flesh (**Figure 1C**). Scans of the fruit surface and fluorescence microscopy of water-soaked fruit revealed the presence of numerous microcracks in the water-soaked areas (**Figures 1E–G**). There were no or only few microcracks in non-treated control fruit (no water soaking) (**Figure 1D**). Water soaking was never associated with fungal development during the short incubation periods of our experiments.

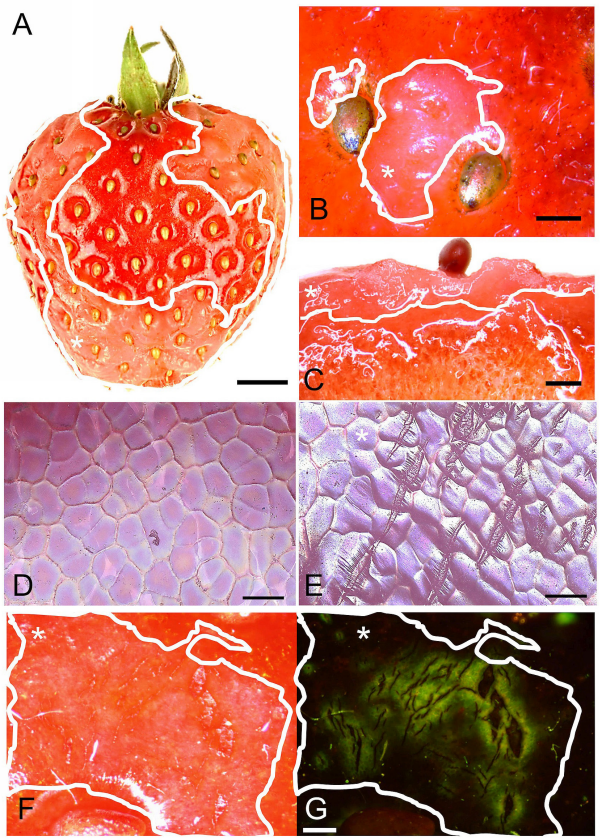

FIGURE 1 | (A) Macroscopic view of fruit with water soaking symptoms; **(B)** Detail of achenes with surrounding water-soaked area viewed under a light microscope; **(C)** Micrograph of cross-section of tissue with water soaking. **(D,E)** Scans of the surface in a digital microscope of non-treated and water-soaked fruit with numerous microcracks. **(F,G)** Micrographs of developing symptoms of water soaking viewed under incident **(F)** and fluorescent light **(G)**. Microcracks were infiltrated with acridine orange. The penetrated fluorescent tracer appears as a green fluorescence around a microcrack in the cuticle. Water soaking symptoms are marked by a solid white line. White asterisks in **A**, **B**, **C**, **E**, **F** and **G** identify the water-soaked area. Scale bar in **(A)** = 5 mm, **(B,C)** = 1 mm, **(D,E)** = 0.1 mm and in **(F,G)** = 0.5 mm.

Water soaking was always localized and limited to the regions in direct contact with the incubation solution. It never occurred in regions above the water surface when fruit was partially submerged (**Figures 2A–C**). Water soaking rapidly developed at a wound. Abrading the cuticle using carborundum powder was highly effective in inducing water soaking (**Figures 2E–I**). Incisions made using a razor blade or puncturing the fruit skin were markedly less effective in inducing water soaking.

When completely submerging fruit, the surface area affected by water soaking increased primarily because the water-soaked area expanded, and not because the number of water-soaked

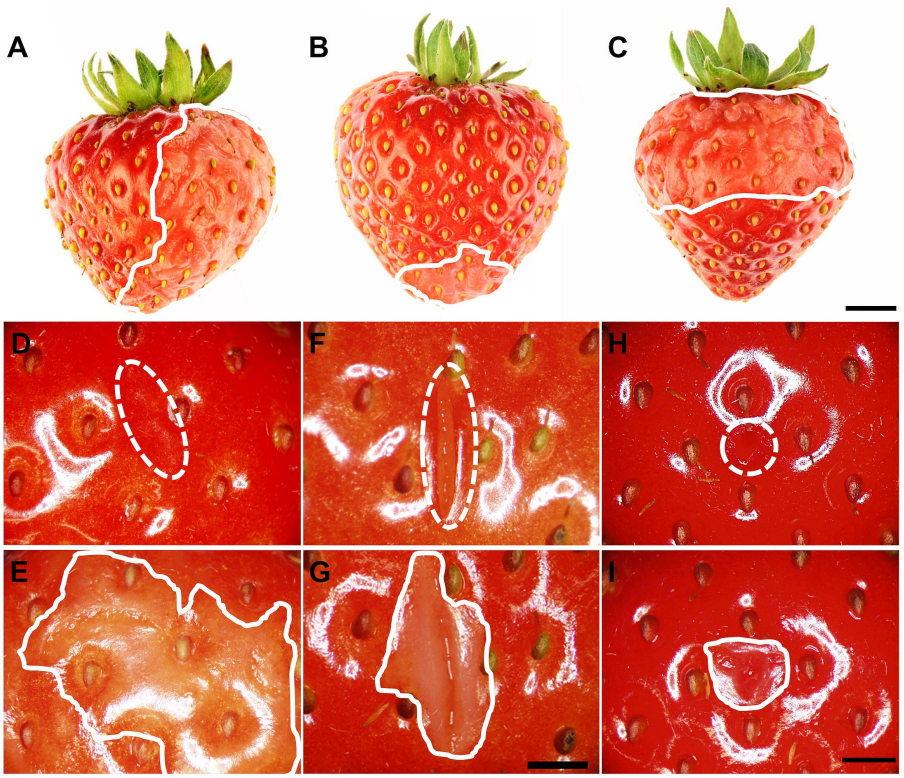

FIGURE 2 | (A–C) Induction of local water soaking symptoms by partial immersion of a strawberry fruit in water. **(A)** Half of the fruit (long axis horizontal), **(B)** tip or **(C)** calyx end of the fruit (long axis vertical). Water soaking following abrasion of the cuticle (~10 mm^2), **(D,E)** incision of the skin using a razor blade (5 mm length × 3 mm depth), **(F,G)** and puncture of the skin using a dissection needle (1.6 mm diameter and 5 mm depth) **(H,I)**. **(D,F,H)** images taken immediately after wounding ($t = 0$ h); **(E,G,I)** images of same area taken after a 3-h incubation in deionized water. The fruit was submerged completely. The water-soaked area around the wound averaged 179.4 ± 48.8 mm^2 **(E)**, 37.5 ± 5.7 mm^2 **(G)**, and 20.7 ± 4.2 mm^2 **(H)**. Scale bar in **(A–C)** = 5 mm and **(D–I)** = 2.5 mm. The dashed white line indicates the wound area, and the solid white line indicates the margin of the water-soaked area. The area outside of the solid white line was also in contact with deionized water and serves as control for a non-water-soaked surface.

patches increased (**Figure 3A**). The surface area affected, increased sigmoidally with time until a major portion of the skin was affected (**Figure 3B**). There was no difference in the area affected or the rating score for water soaking between fruit that was sampled destructively and fruit that was monitored in a repeated-measures design (**Figures 3B,C**). Water soaking as indexed by the rating scheme was closely and significantly correlated with the water-soaked area as measured directly by image analysis (**Figure 3C**, inset).

The sigmoidal time course of the increase in water-soaked area had an initial lag phase where no symptoms appeared before water soaking began. Thereafter, the affected area increased (**Figure 4**). Similarly, following an initial lag phase, the leakage of anthocyanin increased. The leakage increased at a constant rate. However, for water uptake, there was no lag phase—water uptake began at the time of submersion and also accumulated at a constant rate (**Figure 4C**). When the water-soaked area or the leakage of anthocyanin (relative absorbance) was plotted vs. water uptake, a lag phase without water soaking and without anthocyanin leakage was present (**Figures 4A,B**, insets). These results indicate that water uptake increases up to some critical threshold beyond which water soaking and anthocyanin leakage begin. Water-soaked area and anthocyanin leakage were positively related until about 60% of the area was water-soaked. Above this value, anthocyanin leakage continued to increase, but water-soaked area remained largely constant (**Figure 4D**).

The water-soaked area, the infiltrated area, and the water uptake all increased nearly linearly with time (**Figure 5**). The water-soaked area and the area infiltrated by the fluorescence tracer were significantly and positively related ($r^2 = 0.95^{***}$; **Figure 5D**). It is worth noting that the rate of water uptake and the rate of water soaking were both markedly lower in "Clery" than in the cultivars used in other experiments.

Most water soaking began at the tip of the fruit, followed by the calyx end, the calyx equator zone, and the equator tip zone (**Figure 6A**). There was no difference between fruit with or without the calyx. Within the fruit, osmotic potential decreased and became more negative from the calyx, toward the tip of the fruit (**Figure 6B**). There was no significant difference in stress relaxation between different regions of the fruit as indexed by a lack of difference in gaping following skin incision (data not shown). In all regions, the gap produced by the incision averaged about 0.95 ± 0.03 mm ($n = 78$) (Hurtado, unpublished data).

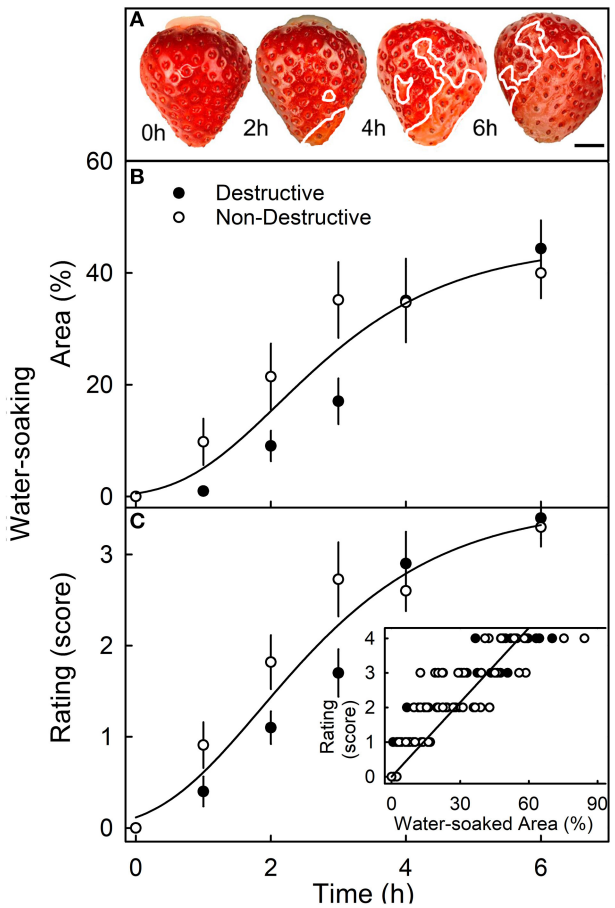

FIGURE 3 | Time course of water soaking. **(A)** Macroscopic view of change in water-soaked area with time. The symptomatic area is indicated by a solid white line. Scale bar, 5 mm. **(B,C)** Change in water soaking as indexed by the measurement of the water-soaked area **(B)** or as assessed by a 5-point rating scale **(C)**. (**C**, inset): Relationship between the water-soaked score and the water-soaked area. For the destructive sampling depicted in **(B)**, an independent set of fruit was assessed at any one time. For the non-destructive sampling in **(B)**, repeated observations were made on the same fruit that was photographed repeatedly. The water-soaked area was quantified by digital analysis. The 5-point rating scale: score 0, no water soaking; score 1, <10% of the surface area water-soaked; score 2, 10–35%; score 3, 35–60%; score 4 > 60%.

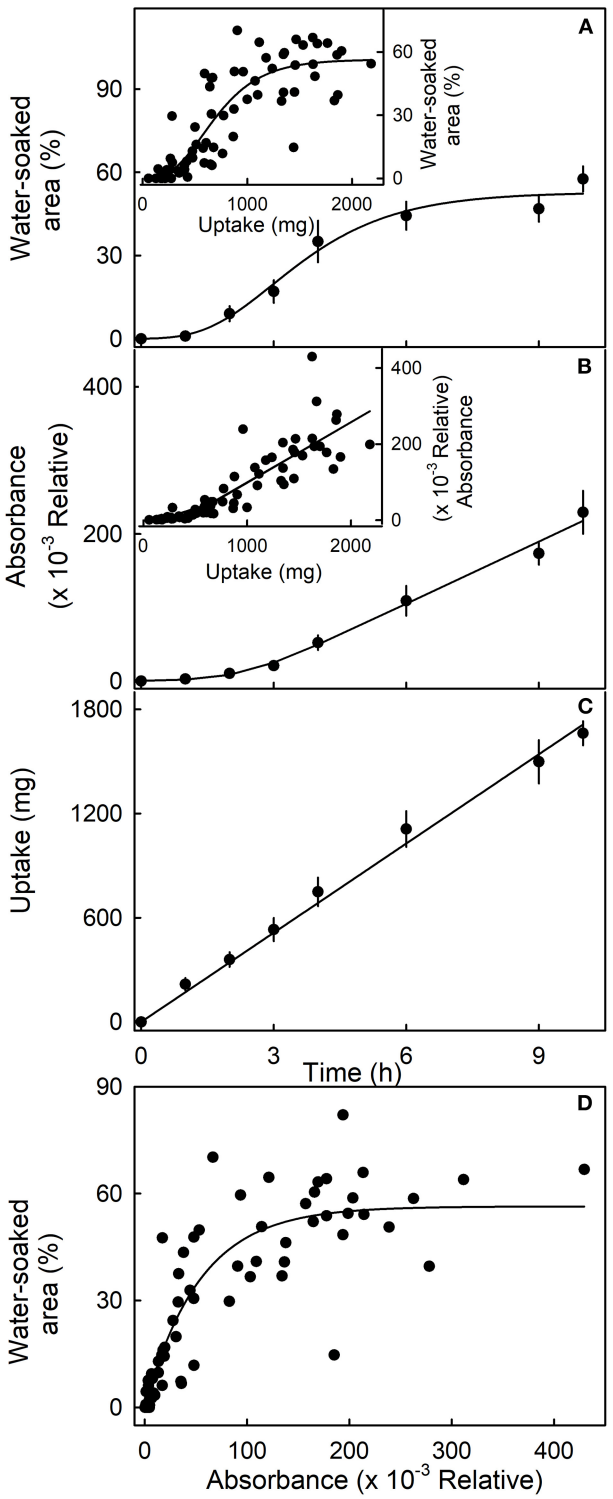

FIGURE 4 | Time course of **(A)** change in water-soaked area, **(B)** change in anthocyanin leakage as indexed by absorbance of the incubation solution at 520 nm, and **(C)** water uptake of strawberries incubated in deionized water. Insets. Relationship between the water-soaked area (inset in **A**), the change in absorbance (inset in **B**), and water uptake. **(D)** Relationship between the water-soaked area and the leakage of anthocyanins as indexed by the change in absorbance.

The susceptibility to water soaking increased sigmoidally with ripening as indexed by the change in fruit color from white to dark red (**Figure 7A**). Across the different ripeness stages, the water-soaked area and water uptake rate were linearly related (**Figure 7B**, main graph). Unripe fruit (white) had the lowest values of both uptake and water soaking, while fully ripe fruit (dark red) showed the highest values. Accordingly, the relationship between osmotic potential and water uptake was linear and positive. The fully ripe, dark-red fruit also had the most negative osmotic potentials and the highest rates of water uptake (**Figure 7B**, inset).

Water soaking increased as fruit mass increased (**Figure 8**, main graph). The largest fruit also had the highest rating

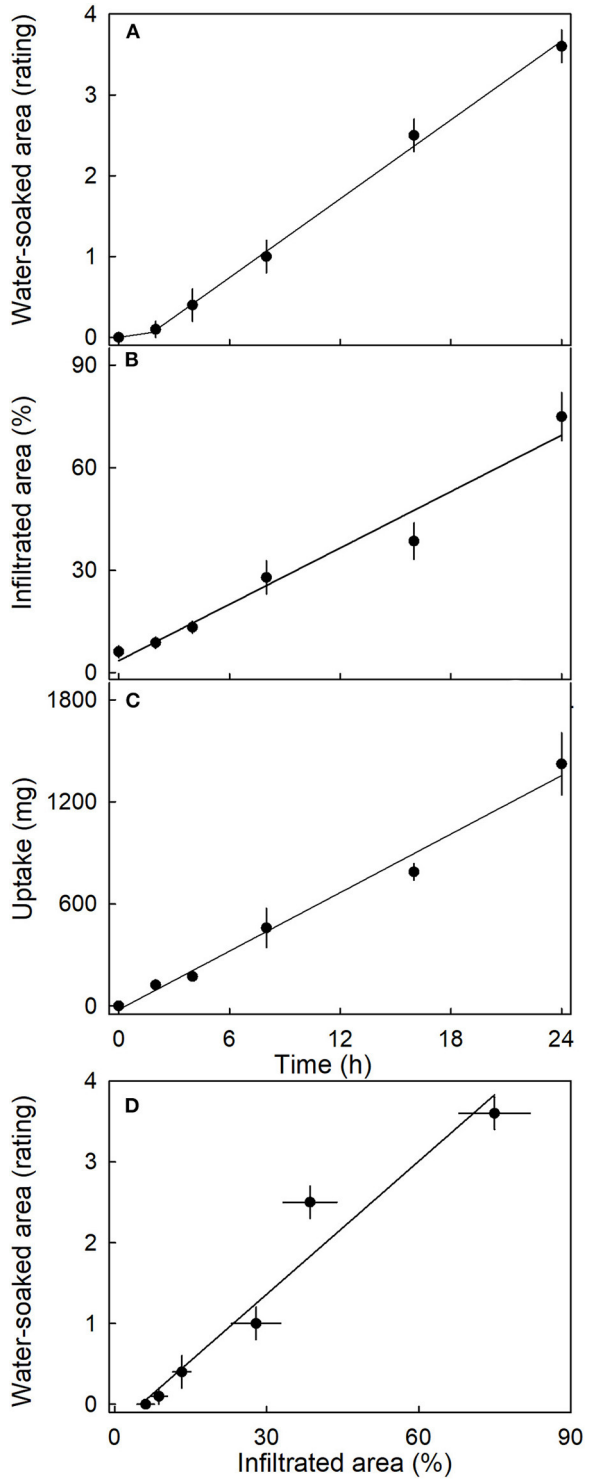

FIGURE 5 | Time course of **(A)** change in water-soaked area, **(B)** change in the area infiltrated by acridine orange, and **(C)** water uptake of strawberries incubated in deionized water. **(D)** Relationship between the water-soaked area and the area infiltrated by acridine orange. Acridine orange penetrates the strawberry fruit skin *via* microcracks in the cuticle. Water soaking was indexed using a 5-point rating scale: score 0, no water soaking; score 1, <10% of the surface area water-soaked; score 2, 10–35%; score 3, 35–60%; score 4 > 60%.

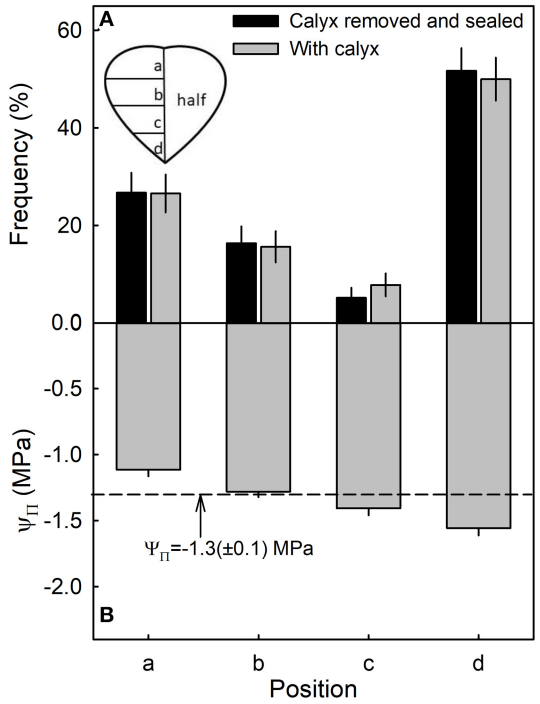

FIGURE 6 | Frequency of symptoms of water soaking **(A)** and the osmotic potential (Ψ_Π) of the juice **(B)** in different regions of a strawberry. The dashed line represents the mean osmotic potential of the fruit.

scores and hence the largest portions of their surfaces water-soaked. Fruit mass was independent of the soluble solids content (**Figure 8**, inset).

Incubating strawberries in isotonic PEG 6000 resulted in less water soaking and negligible water uptake compared to the control incubated in water (**Figure 9**). Interestingly, there was little difference in microcracking between fruit incubated in isotonic PEG 6000 or in water as indexed by the areas infiltrated by acridine orange (**Figure 9B**). The water-soaked area and the area infiltrated by acridine orange were positively related (**Figure 9D**).

Incubating strawberries in natural juice or artificial juice prepared at hypotonic, but not at isotonic concentrations, significantly increased water soaking. In contrast, water uptake decreased in both juices at hypotonic and even more so at isotonic concentrations as compared to the water control (**Table 1**). There were no differences either in water-soaked area or in water uptake between natural and artificial juice (data not shown). Interestingly, the rates of water uptake were consistently greater than zero, even though the incubation solution was isotonic to the fruit's expressed juice.

Studying the effects of the individual components of strawberry juice on water soaking and water uptake revealed that citric and malic acids markedly increased water soaking compared to the water control. The rates of water uptake were higher compared to the other osmolytes or the water control.

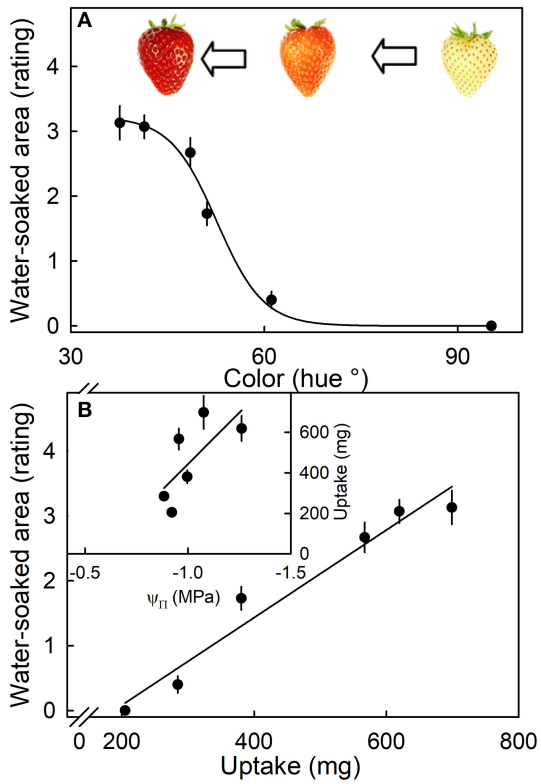

FIGURE 7 | (A) Effect of ripening stage (as indexed by hue angle) on the water-soaked area when strawberries are incubated in deionized water. **(B)** Relationship between the water-soaked area and water uptake. Inset: Uptake vs. osmotic potential. Water soaking was indexed using a 5-point rating scale: score 0, no water soaking; score 1, <10% of the surface area water-soaked; score 2, 10–35%; score 3, 35–60%; score 4 > 60%.

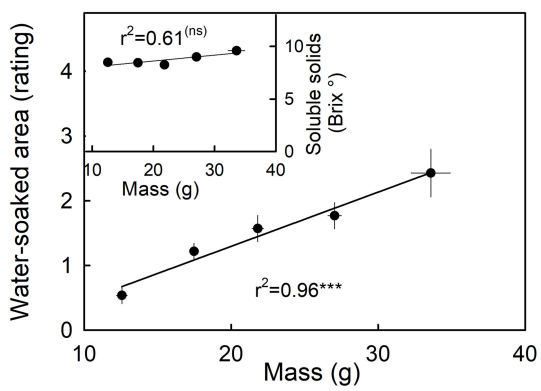

FIGURE 8 | Relationship between water soaking and fruit mass. Inset: Relationship between the soluble solids as indicated by °Brix and water soaking. Water soaking was indexed using a 5-point rating scale: score 0, no water soaking; score 1, <10% of the surface area water-soaked; score 2, 10–35%; score 3, 35–60%; score 4 > 60%.

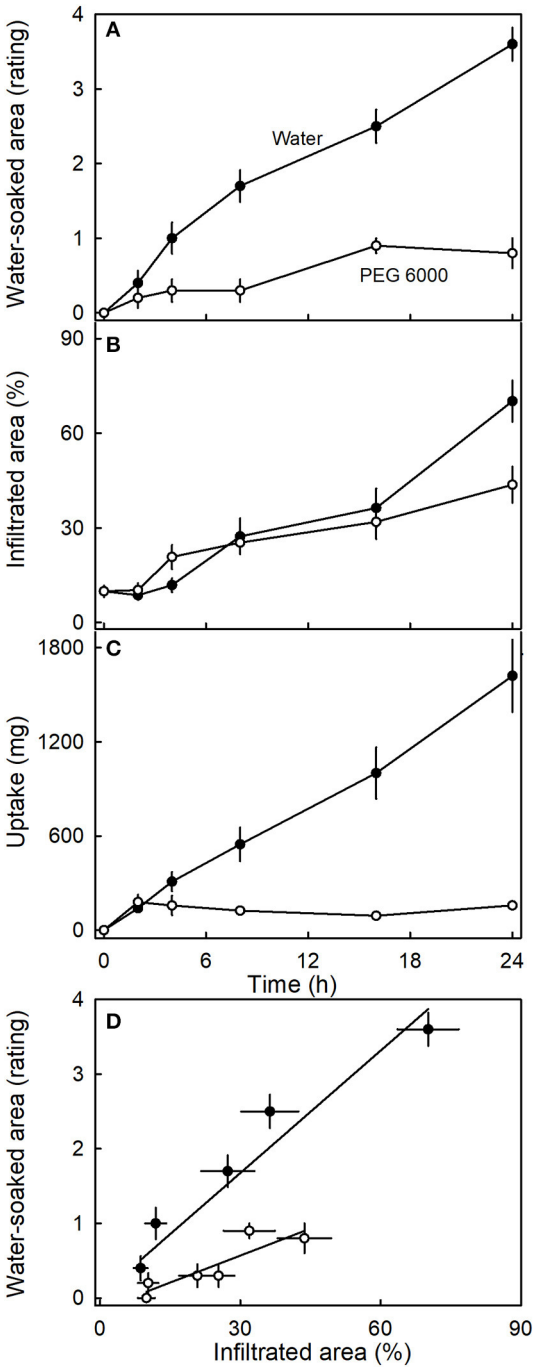

FIGURE 9 | Time course of **(A)** change in water-soaked area, **(B)** change in the area infiltrated by acridine orange, and **(C)** water uptake of strawberries incubated in deionized water or in isotonic polyethylene glycol 6000 (PEG 6000). **(D)** Relationship between the water-soaked area and the area infiltrated by acridine orange. Acridine orange penetrates the strawberry fruit skin *via* microcracks in the cuticle. Water soaking was indexed using a 5-point rating scale: score 0, no water soaking; score 1, <10% of the surface area water-soaked; score 2, 10–35%; score 3, 35–60%; score 4 > 60%.

The carbohydrates that accounted for most of the osmolarity in strawberry juice decreased both water soaking and rates of water uptake to levels below the water control (**Table 2**).

Anthocyanin leakage from flesh disks increased with time and was higher in the presence of citric and malic acid, than in the control (deionized water) (**Figure 10A**). The amounts of leakage

were also higher from hypotonic than from hypertonic solutions. Again, leakage in the presence of the acids exceeded that in their absence. A two-factorial analysis of variance revealed the significant main effects for osmotic potential and the acids; there was no significant interaction term between these two factors (**Figure 10B**).

DISCUSSION

The main findings are as follows:

1) Water soaking involves microcracking of the cuticle, water uptake, bursting of cells, and leakage of cell contents
2) The behavior of water soaking in strawberry bears many similarities to the zipper model used to explain rain cracking in sweet cherries.

Water Soaking Requires Microcracking of the Cuticle, Water Uptake, and the Bursting of Cells

This hypothesis is based on the following evidence.

(1) Surface wetness induced microcracking in the cuticle of the strawberry fruit when incubated in water in this and our earlier study (Hurtado et al., 2021) or in isotonic solutions (PEG 6000) (**Figure 9**). This is consistent with the literature reports of other fleshy fruit crops, including sweet cherry (Knoche and Peschel, 2006), apples (Knoche and Grimm, 2008; Khanal et al., 2021), *Ribes* berries (Khanal et al., 2011), and grapes (Becker and Knoche, 2012a). Microcracks impair the barrier properties of the cuticle. They represent a pathway for a rapid and localized water uptake by viscous flow through the strawberry fruit surface (Hurtado et al., 2021). Microcracking is an essential, but not the only requirement, in water soaking. For example, incubation in isotonic PEG 6000 induced microcracking, but markedly reduced water uptake and hence water soaking. Simulating microcracking by abrading the cuticle from the fruit surface induced water soaking like symptoms. After puncturing the fruit skin, the water-soaked area was much smaller. This is also consistent with the above hypothesis. It is important to note that microcracking of the cuticle due to moisture exposure also accounts for the localized nature of water soaking. Microcracks impair the cuticle's barrier function and allow a rapid, localized water uptake (Hurtado et al., 2021). This also explains why partial incubation of fruit resulted in water soaking only in the exposed regions.

(2) Water uptake markedly increased water soaking. Manipulations such as incubation in isotonic PEG 6000 that resulted in reduced water uptake also reduced water soaking. The only exceptions were treatments where the incubation solutions contained organic acids. The effect of organic acids is addressed in detail below. Also, more mature fruit, with more negative osmotic potentials and hence, higher rates of water uptake, also showed more water soaking. A more negative osmotic potential and hence, a higher rate of water uptake, is also consistent with a higher incidence of water soaking at the tip of the fruit. These results indicate that mature, ripe fruit is more susceptible to water soaking, particularly at the tip. The relatively high frequency of water soaking in the calyx end of the fruit (regions a, b) may have resulted from growth stress and strain that will be maximal in these regions. Additional evidence for a water uptake requirement comes from experiments where the fruit was incubated in artificial or natural juices. Here, water soaking was more severe in the hypotonic juices treatments, which had higher rates of water uptake, compared with the isotonic juices.

(3) Finally, bursting of cells is involved in water soaking. Evidence for this comes from the experiment on anthocyanin leakage. Here, up to some critical threshold, water uptake did not induce water soaking. However, beyond this threshold, water soaking began. The timing of the critical threshold for water uptake coincided with that for the onset of leakage. The latter indicates the onset of cell bursting. It is interesting to note that the release of organic acids that accompanies cell bursting seems to exacerbate water soaking. Experiments using natural or artificial juices and the major components thereof clearly identified citric and malic acids as the critical constituents that accelerate the development of water soaking. Both acids are released into the apoplast when a cell bursts. Here, they increase the permeability of the plasma membrane of neighboring cells. This causes cell leakage to propagate. Similar observations have been made for malic acid in sweet cherry, and these led to the development of the "Zipper model" where the acids "unzip" the skin (Winkler et al., 2015). In contrast to sweet cherry, in strawberry, citric and malic acids had no effect on the strength of the cell walls. This conclusion is inferred from the lack of a significant interaction between the osmotic potential of the incubation solution and the presence of the acids. At low (more negative) osmotic potentials, the incubation solutions were isotonic or hypertonic. A gradient for osmotic water uptake into the cells, and hence increased stress on the cell walls, must be absent. In contrast, at higher (less negative) osmotic potentials, the incubation solution was hypotonic, and hence, osmotic water uptake by the cells occurred. This imposes increased stress on the cell walls. However, the effect of the acids was independent of the applied stress on the cell walls. Hence, the acid effect must have been on the plasma membrane and not on the cell walls. This conclusion is also consistent with the wounding effect. Cuticle abrasion was more effective in inducing water soaking than either incisions or punctures. With abrasion, relatively large areas of the skin are damaged. It is the skin cells that contain most citric and malic acids (in the skin, the summed masses of both acids was 10.6 mg g^{-1}) compared with about half this amount in the flesh (in the flesh, the summed masses of both acids were 5.5 mg g^{-1}) (Holcroft and Kader, 1999).

The bursting of cells also offers a convincing explanation for the characteristic translucency of a water-soaked tissue. Water-soaked tissue typically results from the flooding of the gas-filled intercellular spaces (Sideris and Krauss, 1933). In addition, the leakage of both the tonoplast and the plasma membranes results in a general mixing of apoplastic and symplastic components (the anthocyanins are naturally contained within the tonoplast—vacuole). The apoplast pH is likely to increase, compared to that of the vacuole. As a result, the anthocyanins will likely react with water, to form colorless pseudobases (Brouillard et al., 1997; Holcroft and Kader, 1999). This explains the lighter color of a water-soaked tissue.

TABLE 1 | Effect of natural (expressed) juice and artificial (compounded) juice on development of water soaking in "Faith" strawberry.

Treatment	Water uptake (rate, mg h^{-1}) Osmotic potential (MPa)			Water soaking (score, arbitrary) Osmotic potential (MPa)		
	0.5	1.0	Mean	0.5	1.0	Mean
Artificial juice	104.3 ± 18.6	53.8 ± 12.4	78.9 ± 12.2$^{(ns)}$	2.2 ± 0.2	1.6 ± 0.3	1.9 ± 0.2$^{(ns)}$
Natural juice	83.2 ± 31.9	58.1 ± 13.0	70.7 ± 17.0	1.8 ± 0.2	1.5 ± 0.2	1.7 ± 0.1
Mean	93.8 ± 18.2a^{a}	55.8 ± 8.8 b	74.8 ± 10.4	2.0 ± 0.1 a	1.5 ± 0 b	1.8 ± 0.1

Water soaking was indexed using a 5-point rating scale: score 0, no water soaking; score 1, <10% of the surface area water-soaked; score 2, 10–35%; score 3, 35–60%; score 4 > 60%. In the deionized water control, the rate of water uptake was 122.8 ± 18.7 mg h^{-1}, and the score for water soaking was 1.6 ± 0.2.
Analysis of variance revealed no significant interaction term but a significant main effect for osmotic potential. $^{(ns)}$Non-significant effect for treatment.
^{a}Means followed by the same letter are not significantly different, Tukey's test at p = 0.05. ns, non-significant effect.

TABLE 2 | Effect of major osmolytes on the rate of water uptake and the development of water soaking in strawberries of cultivar "Florentina."

Component	Concentration (mM)	$-\Psi_{\Pi}$ (Mpa)	pH	Rate of uptake (mg h^{-1})	Rating (score)
Water	0.0	0.0	6.4	117.3 ± 13.8 b^{a}	1.9 ± 0.2 b
Malic acid	25.2	0.1	2.6	207.6 ± 27.1 a	3.7 ± 0.1 a
Citric acid	43.4	0.1	2.3	176.4 ± 16.8 a	3.5 ± 0.2 a
Carbohydrates	316.6	0.8	6.5	63.0 ± 7.4 c	1.0 ± 0.2 c
Artificial juice	428	1.1	3.2	50.2 ± 5.2 c	1.6 ± 0.2 b

Water soaking was indexed using a 5-point rating scale: score 0, no water soaking; score 1, < 10% of the surface area water-soaked; score 2, 10–35%; score 3, 35–60%; score 4 > 60%. The artificial juice was compounded from the major osmolytes found in strawberries (together these account for 96.1% of the osmolarity of a strawberry) (Herrmann, 2001). The artificial juice was isotonic with the expressed natural juice.
^{a}Means followed by the same letter are not significantly different, Tukey's test at p = 0.05.

The Mechanism of Water Soaking Is Similar to That of Cracking in Sweet Cherry Fruit

Water soaking in strawberry can be substantially explained in terms of the zipper model that accounts for sweet cherry fruit cracking during/following rainfall (Winkler et al., 2016). Based on this model, a series of sequential events leads to water soaking. First, the barrier function of the cuticle is impaired by the formation of microcracks in response to surface wetness (**Figure 2**). Because the cuticle of a strawberry is very thin (Hurtado et al., 2021), microcracks allow a rapid, localized water uptake into the subtending tissues. This uptake occurs by viscous flow and is more rapid than that by diffusion through an intact cuticle (Hurtado et al., 2021). Unlike in apple, there is no evidence of any repair processes in strawberry: wax deposition in a microcrack (Curry, 2009) or the formation of a periderm (Evert, 2006; Macnee et al., 2020). Second, water uptake causes cells to burst, as indicated by the leakage of anthocyanin. Because strawberries contain large amounts of citric and malic acid, particularly in the skin cells, and because these acids increase the permeability of plasma membranes, the neighboring cells also begin to leak. This propagation process causes the water-soaked area to spread both laterally and down into the fruit.

Unlike in sweet cherry, there is no evidence in strawberry that these organic acids cause a weakening of cell walls. Nevertheless, future evidence for a weakening would not be surprising, as both citric and malic acids are likely to extract Ca from the cell walls, and this loss will decrease cell-to-cell adhesion (Winkler et al., 2015). However, at this stage, there is no support for such effects in strawberry.

CONCLUSIONS

Our results demonstrate that water soaking in strawberry results from a series of events that involves microcracking of the cuticle, water uptake, a cell bursting, and the release of organic acids into the apoplast. In many ways, it is similar to rain cracking in fleshy fruit, such as sweet cherry. Based on our findings, a reliable strategy to prevent water soaking would be to limit a direct contact between water and the fruit surface. This may be achieved preharvest by protected cultivation, either in a greenhouse or in a plastic tunnel. Important measures postharvest include the use of appropriate packaging materials and handling practices that avoid the occurrence of liquid water on the surface, for example, due to condensation of water vapor. In the long run, the susceptibility of commercial strawberry genotypes to water soaking may be decreased by breeding. Our results and those by Herrington et al. (2009) demonstrate that susceptibility to water soaking differs among cultivars. Water soaking occurred in all cultivars used in our study, but at a markedly lower rate in "Clery" as compared to "Faith" and "Florentina." The basis of these differences has not yet been identified. Among the three cultivars, "Clery" also had the lowest rate of water uptake, which probably contributed to the lower rate of water soaking. Based on the findings presented herein and their similarity to the

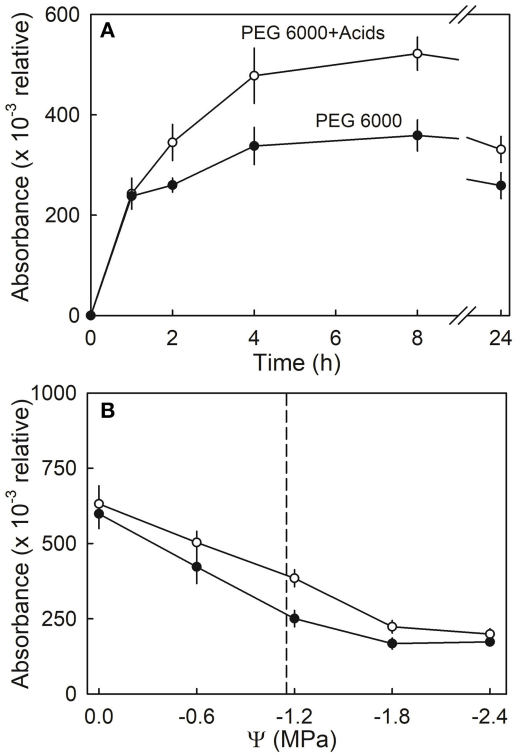

FIGURE 10 | (A) Time course of anthocyanin leakage from flesh disks excised from ripe strawberries in the presence or absence of citric or malic acids. Flesh disks were incubated in isotonic polyethylene 6000 (PEG 6000) solutions. **(B)** Effect of osmotic potential (Ψ) of the incubation solution on anthocyanin leakage in the presence or absence of citric or malic acids. The vertical dashed line indicates the osmotic potential of juice expressed from the fruit of the same batch.

phenomenon of rain cracking in sweet cherry, potentially useful aims for further research in water soaking are to determine (a) the pattern of cuticle deposition in developing strawberry fruit, (b) the water uptake characteristics, (c) the mechanical strength of their cell walls, and (d) the strength of their cell-to-cell adhesion. A better understanding of the phenomenon of microcracking would also be beneficial in reducing the incidence of fruit rots. Pathogens like *Botrytis cinerea* benefit from microcracks in the cuticle because of the impaired barrier functions (Jarvis, 1962).

DATA AVAILABILITY STATEMENT

The raw data supporting the conclusions of this article will be made available by the authors, without undue reservation.

AUTHOR CONTRIBUTIONS

MK obtained the funds to support the study. GH and MK planned the experiments, analyzed the data, wrote, revised, and edited the manuscript. GH conducted the experiments. All authors contributed to the article and approved the submitted version.

FUNDING

This research was funded by a grant from the Deutsche Forschungsgemeinschaft (KN 402/19-1).

ACKNOWLEDGMENTS

We thank Dr. Alexander Lang and Dr. Andreas Winkler for helpful comments on an earlier version of this manuscript, and Heike, Karl Walter, and Martin Brüggenwirth and Bendix Meyer for the gift of fruit.

SUPPLEMENTARY MATERIAL

The Supplementary Material for this article can be found online at: https://www.frontiersin.org/articles/10.3389/fpls.2021.694123/full#supplementary-material

REFERENCES

Becker, T., and Knoche, M. (2012a). Deposition, strain, and microcracking of the cuticle in developing 'Riesling' grape berries. *Vitis* 51, 1–6. doi: 10.5073/vitis.2012.51.1-6

Becker, T., and Knoche, M. (2012b). Water induces microcracks in the grape berry cuticle. *Vitis* 51, 141–142. doi: 10.5073/vitis.2012.51.141-142

Brouillard, R., Figueiredo, P., Elhabiri, M., and Dangles, O. (1997). Molecular interactions of phenolic compounds in relation to the colour of fruit and vegetables. *Proc. Phytochem. Soc. Euro.* 41, 29–49. doi: 10.1016/0031-9422(95)00530-7

Curry, E. (2009). "Growth-induced microcracking and repair mechanisms of fruit cuticles," in *Proceedings of the SEM Annual Conference*. (Albuquerque, NM).

Evert, R. F. (2006). *Esau's Plant Anatomy: Meristems, Cells, and Tissues of the Plant Body: Their Structure, Function, and Development*. Hoboken, NJ: John Wiley & Sons.

Grijalba, C. M., Pérez-Trujillo, M. M., Ruiz, D., and Ferrucho, A. M. (2015). Strawberry yields with high-tunnel and open-field cultivations and the relationship with vegetative and reproductive plant characteristics. *Agron. Colomb.* 33, 147–154. doi: 10.15446/agron.colomb.v33n2.52000

Herrington, M., Hardner, C., Wegener, M., Woolcock, L. L., and Dieters, M. J. (2011). Rain damage to strawberries grown in southeast Queensland: evaluation and genetic control. *HortScience* 46, 832–837. doi: 10.21273/HORTSCI.46.6.832

Herrington, M. E., Woolcock, L., Wegener, M., Dieters, M., and Moisander, J. (2009). Cultivar differences in tolerance to damages by rainfall. *Acta Hortic* 842, 483–486. doi: 10.17660/ActaHortic.2009.842.98

Herrmann, K. (2001). *Inhaltsstoffe von Obst und Gemüse*. Stuttgart: Ulmer.

Holcroft, D. M., and Kader, A. A. (1999). Controlled atmosphere-induced changes in pH and organic acid metabolism may affect color of stored strawberry fruit. *Postharvest Biol. Technol.* 17, 19–32. doi: 10.1016/S0925-5214(99)00023-X

Hummer, K. E., and Hancock, J. (2009). "Strawberry genomics: botanical history, cultivation, traditional breeding, and new technologies," in *Genetics and Genomics of Rosaceae*, eds S. E. Gardiner and K. M. Folta (New York, NY: Springer), 413–435.

Hurtado, G., Grimm, E., Brüggenwirth, M., and Knoche, M. (2021). Strawberry fruit skins are far more permeable to osmotic water

uptake than to transpirational water loss. *PLoS ONE* 16: e0251351. doi: 10.1371/journal.pone.0251351

Jarvis, W. R. (1962). The infection of strawberry and raspberry fruits by *Botrytis cinerea* Fr. *Ann. Appl. Biol.* 50, 569–575. doi: 10.1111/j.1744-7348.1962.tb06049.x

Khanal, B. P., Grimm, E., and Knoche, M. (2011). Fruit growth, cuticle deposition, water uptake, and fruit cracking in jostaberry, gooseberry, and black currant. *Sci. Hortic.* 128, 289–296. doi: 10.1016/j.scienta.2011.02.002

Khanal, B. P., Imoro, Y., Chen, Y. H., Straube, J., and Knoche, M. (2021). Surface moisture increases microcracking and water vapour permeance of apple fruit skin. *Plant Biol.* 23, 74–82. doi: 10.1111/plb.13178

Khoshnevisan, B., Rafiee, S., and Mousazadeh, H. (2013). Environmental impact assessment of open field and greenhouse strawberry production. *Eur. J. Agron.* 50, 29–37. doi: 10.1016/j.eja.2013.05.003

Knoche, M., and Grimm, E. (2008). Surface moisture induces microcracks in the cuticle of 'Golden Delicious' apple. *HortScience* 43, 1929–1931. doi: 10.21273/HORTSCI.43.6.1929

Knoche, M., and Peschel, S. (2006). Water on the surface aggravates microscopic cracking of the sweet cherry fruit cuticle. *J. Am. Soc. Hortic. Sci.* 131, 192–200. doi: 10.21273/JASHS.131.2.192

Macnee, N. C., Rebstock, R., Hallett, I. C., Schaffer, R. J., and Bulley, S. M. (2020). A review of current knowledge about the formation of native peridermal exocarp in fruit. *Funct. Plant Biol.* 47, 1019–1031. doi: 10.1071/FP19135

Peschel, S., and Knoche, M. (2005). Characterization of microcracks in the cuticle of developing sweet cherry fruit. *J. Am. Soc. Hortic. Sci.* 130, 487–495. doi: 10.21273/JASHS.130.4.487

Sideris, C. P., and Krauss, B. H. (1933). Physiological studies on the factors influencing the quality of pineapple fruits. I. *Pineapple Q.* 3, 82–114.

Winkler, A., Ossenbrink, M., and Knoche, M. (2015). Malic acid promotes cracking of sweet cherry fruit. *J. Am. Soc. Hortic. Sci.* 140, 280–287. doi: 10.21273/JASHS.140.3.280

Winkler, A., Peschel, S., Kohrs, K., and Knoche, M. (2016). Rain cracking in sweet cherries is not due to excess water uptake but to localized skin phenomena. *J. Am. Soc. Hortic. Sci.* 141, 653–660. doi: 10.21273/JASHS03937-16

Conflict of Interest: The authors declare that the research was conducted in the absence of any commercial or financial relationships that could be construed as a potential conflict of interest.

frontiers in Plant Science

ORIGINAL RESEARCH
published: 16 August 2021
doi: 10.3389/fpls.2021.696955

Impaired Cuticle Functionality and Robust Resistance to *Botrytis cinerea* in *Arabidopsis thaliana* Plants With Altered Homogalacturonan Integrity Are Dependent on the Class III Peroxidase AtPRX71

Riccardo Lorrai[1], Fedra Francocci[1†], Kay Gully[2], Helle J. Martens[3], Giulia De Lorenzo[1], Christiane Nawrath[2] and Simone Ferrari[1]*

[1]Dipartimento di Biologia e Biotecnologie "Charles Darwin", Sapienza Università di Roma, Rome, Italy, [2]Department of Plant Molecular Biology, University of Lausanne, Lausanne, Switzerland, [3]Section for Forest, Nature and Biomass, Department of Geosciences and Natural Resource Management, University of Copenhagen, Frederiksberg, Denmark

Pectin is a major cell wall component that plays important roles in plant development and response to environmental stresses. *Arabidopsis thaliana* plants expressing a fungal polygalacturonase (PG plants) that degrades homogalacturonan (HG), a major pectin component, as well as loss-of-function mutants for *QUASIMODO2* (*QUA2*), encoding a putative pectin methyltransferase important for HG biosynthesis, show accumulation of reactive oxygen species (ROS), reduced growth and almost complete resistance to the fungal pathogen *Botrytis cinerea*. Both PG and *qua2* plants show increased expression of the class III peroxidase AtPRX71 that contributes to their elevated ROS levels and reduced growth. In this work, we show that leaves of PG and *qua2* plants display greatly increased cuticle permeability. Both increased cuticle permeability and resistance to *B. cinerea* in *qua2* are suppressed by loss of *AtPRX71*. Increased cuticle permeability in *qua2*, rather than on defects in cuticle ultrastructure or cutin composition, appears to be dependent on reduced epidermal cell adhesion, which is exacerbated by *AtPRX71*, and is suppressed by the *esmeralda1* mutation, which also reverts the adhesion defect and the resistant phenotype. Increased cuticle permeability, accumulation of ROS, and resistance to *B. cinerea* are also observed in mutants lacking a functional FERONIA, a receptor-like kinase thought to monitor pectin integrity. In contrast, mutants with defects in other structural components of primary cell wall do not have a defective cuticle and are normally susceptible to the fungus. Our results suggest that disrupted cuticle integrity, mediated by peroxidase-dependent ROS accumulation, plays a major role in the robust resistance to *B. cinerea* of plants with altered HG integrity.

Keywords: cuticle, cell wall, plant immunity, *Botrytis cinerea*, peroxidase, plant-microbe interactions, pectin

OPEN ACCESS

Edited by:
Eva Domínguez, Institute of Subtropical and Mediterranean Horticulture La Mayora, Spain

Reviewed by:
Franco Rossi, CONICET Institute of Biotechnological Research (IIB-INTECH), Argentina
Shiyou Lu, Hubei University, China

***Correspondence:**
Simone Ferrari
simone.ferrari@uniroma1.it

***Present address:**
Fedra Francocci, Institute of Anthropic Impacts and Sustainability in marine environment (IAS), National Research Council (CNR), Rome, Italy

Specialty section:
This article was submitted to Plant Physiology, a section of the journal Frontiers in Plant Science

Received: *18 April 2021*
Accepted: *26 July 2021*
Published: *16 August 2021*

Citation:
Lorrai R, Francocci F, Gully K, Martens HJ, De Lorenzo G, Nawrath C and Ferrari S (2021) Impaired Cuticle Functionality and Robust Resistance to Botrytis cinerea in Arabidopsis thaliana Plants With Altered Homogalacturonan Integrity Are Dependent on the Class III Peroxidase AtPRX71. Front. Plant Sci. 12:696955. doi: 10.3389/fpls.2021.696955

INTRODUCTION

The cell wall (CW) is crucial for various important aspects of plant biology, providing mechanical support to the protoplast, modulating cell growth and shape, and mediating cell adhesion and cell-to-cell communication (McCann and Roberts, 1991; Carpita and Gibeaut, 1993; Somerville et al., 2004; Humphrey et al., 2007). The composition and relative abundance of the major CW structural components, namely, polysaccharides [cellulose (the major load-bearing component), hemicelluloses, and pectins], glycoproteins, and phenolic compounds (including lignin) widely change during cell growth and differentiation (Anderson and Kieber, 2020). Moreover, the CW is a barrier against the attack of pathogenic microorganisms and herbivores (Albersheim et al., 2010). In the epidermal cells of the aerial parts of the plant, the outermost surface of the CW is in continuation with the cuticle, a multi-layered hydrophobic structure that limits the diffusion of water, regulates the exchange of gases with the environment, and provides protection against pathogens (Yeats and Rose, 2013). The major components of the cuticle are cutin, a polyester rich in C16-C18 oxygenated and interesterified fatty acids (FA) derivatives, such as hydroxy and hydroxy-epoxy substituted FAs, and glycerol (Holloway, 1982; Pollard et al., 2008). The cuticle also contains waxes, mixtures of hydrophobic material containing very long-chain fatty acids, and other secondary metabolites (Kunst and Samuels, 2009; Yeats and Rose, 2013). As for the CW components, the wax and cutin compositions of the plant cuticle widely vary among plant species, organs, and during development (Yeats and Rose, 2013).

Since the cuticle-CW continuum represents the first site of contact with the plant, microbial pathogens have evolved an array of enzymes that degrade the cuticle and CW structural components to assist penetration and colonization, obtain carbon sources, and promote leakage of nutrients from the protoplast (Ziv et al., 2018; Lorrai and Ferrari, 2021). In particular, at early stages of infection, several phytopathogenic fungi synthesize cuticle-degrading enzymes (cutinases, esterases, and lipases) that are thought to prepare the infection site both for adhesion and penetration (Deising et al., 1992; Berto et al., 1999; Nielsen et al., 2000; Garrido et al., 2012). Later, tissue penetration and invasion are assisted by microbial CW-degrading enzymes, most notably pectinases, which are among the first to be secreted by many phytopathogens (De Lorenzo et al., 1997; Lorrai and Ferrari, 2021) and are important pathogenicity factors, in particular for those microbes causing soft rot symptoms (Reignault et al., 2008). For instance, the necrotrophic fungus *Botrytis cinerea*, the causal agent of gray mold in several plant species, secretes large amounts of pectinolytic enzymes, most notably polygalacturonases (PGs), that degrade homogalacturonan (HG), a major pectic component, during the early phases of infection and are crucial for plant invasion, host adaptability, and to determine the type of symptoms caused by this pathogen (Have et al., 1998; Kars et al., 2005).

The vulnerability that follows CW injury caused by pathogen infection and other stresses can be compensated in the plant by the activation of an array of defense responses, including the strengthening of the altered CW itself (Vaahtera et al., 2019; Gigli-Bisceglia et al., 2020; Lorrai and Ferrari, 2021). Activation of defense responses occurs upon perception of exogenous microbe-associated molecular patterns (MAMPs) and/or CW-derived molecules and fragments that are released in the apoplast by microbial enzymes during infection and are recognized as endogenous damage-associated molecular patterns (DAMPs), thereby activating the so-called pattern-triggered immunity (PTI; Gust et al., 2017; Bacete et al., 2018; De Lorenzo et al., 2018). DAMPs include fragments of HG [oligogalacturonides (OGs)], released by PGs, and fragments released from cellulose and hemicellulose (de Azevedo Souza et al., 2017; Locci et al., 2019; Rebaque et al., 2021). Pre-treatment with exogenous OGs can protect *Arabidopsis* against subsequent infection with *B. cinerea* (Ferrari et al., 2007). *In vivo*, the accumulation of OGs during infection can be favored by the presence of PG-inhibiting proteins (PGIPs) that inhibit the activity of specific isoforms of pathogen PGs (Ferrari et al., 2013; De Lorenzo et al., 2018). The role of PGIPs in plant defense against *B. cinerea* and other pathogens has been extensively demonstrated (Kalunke et al., 2015). Moreover, the expression of a PG-PGIP fusion protein leads to the apoplastic accumulation of elicitor-active OGs and increased resistance to *B. cinerea* and bacterial pathogens (Benedetti et al., 2015). Cutin monomers and wax components released upon degradation of the cuticle during pathogen penetration also act as DAMPs and elicit defense responses (Serrano et al., 2014).

Alterations of CW integrity (CWI) triggered, for example, by genetically or chemically induced changes in the CW cellulose content can also be perceived by the plant through a dedicated surveillance system that leads to a set of responses that include accumulation of reactive oxygen species (ROS), ectopic lignin deposition, production of jasmonate (JA), and activation of defense responses (Ellis et al., 2002; Caño-Delgado et al., 2003; Manfield et al., 2004; Hamann et al., 2009). Changes in CWI can be perceived by *Catharanthus roseus* Receptor-Like Kinase 1-like proteins characterized by the presence of extracellular malectin-like domains (Franck et al., 2018). Among these proteins, FERONIA (FER) is capable of binding pectin *in vitro* (Feng et al., 2018) and has been proposed to act as a pectin integrity sensor, monitoring the HG status, and triggering compensatory responses (Lin et al., 2018). The alteration of CWI *per se* affects the ability of pathogens to successfully penetrate and/or colonize their host (Miedes et al., 2014; Nafisi et al., 2015a; Houston et al., 2016; Bacete et al., 2018). *Arabidopsis* mutants with defects in the cellulose synthase subunits CESA4/IRREGULAR XYLEM5 (IRX5) and CESA8/IRX1, necessary for secondary CW formation (Taylor et al., 2000, 2003), and CESA3/ISOXABEN RESISTANT1 (IXR1)/CONSTITUTIVE EXPRESSION OF VSP1, required for cellulose deposition in primary CW (Desprez et al., 2007; Persson et al., 2007), show a strong resistance to *B. cinerea* (Ellis and Turner, 2001; Ellis et al., 2002; Hernández-Blanco et al., 2007). Alterations in cuticle integrity also strongly enhance *Arabidopsis* resistance to *B. cinerea*, as observed in plants overexpressing a fungal cutinase (CUTE plants)

or mutated in genes involved in cuticle biogenesis, including *LONG-CHAIN ACYL-COA SYNTHETASE2* (*LACS2*), *LACERATA* (*LCR*), and *BODYGUARD* (*BDG*; Bessire et al., 2007; Chassot et al., 2007; Tang et al., 2007).

The hormones jasmonate and ethylene play a major positive role for the resistance against *Botrytis*, whereas abscisic acid (ABA) is generally considered to act negatively (Mengiste, 2012; AbuQamar et al., 2017), since exogenous ABA enhances *Botrytis* pathogenicity, whereas mutations in genes involved in ABA biosynthesis or signaling reduce susceptibility to this fungus (Audenaert et al., 2002; Anderson et al., 2004; Asselbergh et al., 2007; L'Haridon et al., 2011). Because ABA biosynthesis and signaling are required for a normal cuticle structure and functionality (Curvers et al., 2010; Cui et al., 2016), it is possible that the role of this hormone in resistance to *B. cinerea* is mediated by its effects on the cuticle. Interestingly, *Botrytis* resistance associated with increased cuticle permeability can be genetically uncoupled from ABA sensitivity but requires a negative regulation of an ABA-dependent wound-inducible runaway cell death pathway (Cui et al., 2016).

We have previously reported that *Arabidopsis* and tobacco transgenic plants expressing an *Aspergillus niger* PG (henceforth, PG plants) have reduced de-esterified HG levels in the CW and reduced growth (Capodicasa et al., 2004; Lionetti et al., 2010; Francocci et al., 2013) and display a robust resistance to *B. cinerea* (Ferrari et al., 2008). PG plants do not show constitutive expression of typical marker genes for salicylic- (SA-), ethylene-, or JA-dependent defense responses (Raggi et al., 2015) but accumulate high levels of ROS and peroxidase activity in their tissues (Ferrari et al., 2008). Accumulation of ROS in PG plants is associated to an increased expression of the class III peroxidase gene *AtPRX71* (Raggi et al., 2015), whose overexpression was previously shown to confer resistance to *B. cinerea* (Chassot et al., 2007). Robust resistance to *B. cinerea* was also previously reported in the *quasimodo2-1* (*qua2-1*, henceforth *qua2*) mutant, defective in the *QUASIMODO2*/*TUMOROUS SHOOT DEVELOPMENT2* (QUA2/TSD2) gene, which encodes a putative pectin methyltransferase required for the biosynthesis of de-esterified HG (Mouille et al., 2007; Verger, 2014). Notably, like PG plants, *qua2* shows upregulation of *AtPRX71* expression and accumulates high peroxidase activity and ROS levels (Raggi et al., 2015). Loss of *AtPRX71* partially suppresses the accumulation of ROS and the defect in cell expansion of *qua2*, whereas its overexpression in the WT results in high levels of ROS and reduced cell expansion (Raggi et al., 2015), indicating that AtPRX71-mediated ROS production contributes to the growth defects observed in *qua2*, whereas its role in the resistance to *B. cinerea* of this mutant is unknown. In this work, we show that PG and *qua2* plants, but not other unrelated CW mutants, display increased leaf cuticle permeability and that exogenous ABA suppresses both cuticle permeability and *Botrytis* resistance of these plants. Notably, loss of *AtPRX71* restores cuticle functionality and fungal susceptibility in *qua2*, suggesting that a peroxidase-mediated increase in cuticle permeability is a major determinant of the robust resistance to *B. cinerea* observed in plants with a defective HG.

MATERIALS AND METHODS

Plant Material and Growth Conditions

All *Arabidopsis thaliana* plants used in this work belong to Columbia (Col-0) ecotype. The following mutants were obtained from the Nottingham *Arabidopsis* Stock Center: *prc1-1* (Desnos et al., 1996), *ixr1-2* (Scheible et al., 2001), *mur1-1* (Reiter et al., 1993), *mur4-1* (Reiter et al., 1997), and *fer-4* (Duan et al., 2010). Isolation of *atprx71-1* and the *qua2-1 atprx71-1* double mutant was previously described (Raggi et al., 2015), as well as generation of transgenic plants overexpressing the *A. niger pga* gene (PG plants; Lionetti et al., 2010) or *AtPRX71* (35S::PRX71 plants; Raggi et al., 2015). Seeds of *qua2* (Mouille et al., 2007) and *tsd2-1* (Krupková et al., 2007) were kind gifts of Gregory Mouille (Institut National de la Recherche Agronomique, Versailles, France) and Thomas Schmülling (Freie Universität Berlin, Berlin, Germany), respectively. Plants were grown in a growth chamber with a light intensity of 110–120 $\mu mol\, m^{-2}\, s^{-1}$ with a 12 h/12 h (dark/light) photoperiod, 70–75% humidity, and 20–22°C temperature. Before sowing, seeds were surface sterilized and stratified for 3 days in the dark at 4°C. ABA treatments on adult plants were performed spraying rosette leaves of five-week-old plants with a solution of 100 µm ABA (Duchefa) dissolved in ethanol [final ethanol concentration: 0.1% (v/v)].

Fungal Infections

Botrytis cinerea growth and inoculation were performed as previously described (Ferrari et al., 2007; Galletti et al., 2008). Briefly, 5 µl droplets of a spore suspension (5×10^5 conidia ml^{-1}) in 24 g L^{-1} potato dextrose broth were inoculated on rosette leaves of five-week-old plants grown in soil (two droplets per leaf, three or four fully expanded leaves per plant). Inoculated plants were covered with a transparent plastic dome to maintain high humidity and returned to the growth chamber. Lesions were photographed at 3 days post-infection and their area was measured using ImageJ software.[1]

Germination and Pathogenicity Assays in the Presence of Leaf Diffusates

Leaf diffusates were isolated as previously described (Bessire et al., 2007) with minor modifications. Briefly, potato dextrose broth (Duchefa) droplets (5 µl) were placed on the adaxial face of rosette leaves of five-week-old plants in 100% humidity. After 44 h of incubation, the diffusates were recovered and inoculated with *B. cinerea* spores to a final concentration of $5 \times 10^5\, ml^{-1}$. *In vitro* germination was calculated after 8 h of incubation. *In vivo* infections were performed using the same mixtures of leaf diffusates and spore, and lesion area was measured at 72 h after infection.

Gene Expression Analysis

To analyze gene expression, leaves were frozen in liquid nitrogen and homogenized with an MM301 Ball Mill (Retsch) for about

[1]http://rsb.info.nih.gov/ij/

1 min at 25 Hz. Total RNA was extracted with EUROGOLD TriFast-Nucleic Acids Isolation Reagent according to the manufacturer's instructions. 1 µg of total RNA was retrotranscribed into cDNA with Improm II Reverse Transcriptase (Promega). cDNA mixed with iTaq Universal SYBR Green Supermix (Bio-Rad) and primers specific for genes of interest was loaded on a 96-well plate and run on CFX96 Real-time System (Bio-Rad). Gene expression, relative to *UBIQUITIN5* (*UBQ5*), was calculated according to the ΔΔCT method (Livak and Schmittgen, 2001). Primer sequences were the following: *UBQ5* (At3g62250), GGAAGAAGAAGACTTACACC and AGTCCACACTTACCAC AGTA; *PAD3* (At3g26830), TCGCTGGCATAACACTATGG and TTGGGAGCAAGAGTGGAGT; *PR-1* (At2g14610), GGGAAAA CTTAGCCTGGGGT and GCACATCCGAGTCTCACTGA; *PDF1.2* (At5g44420), TCTCTTTGCTGCTTTCGACG and ACTTG TGTGCTGGGAAGACA; *MYB96* (At5g62470), TGCTATGGCTG CCCATCTGTT and AGCTGCAGATTGAGATGGACTA; *CER1* (At1g02205), TCCACTCCTGTGAGAACTGGT and TACTTGG TCCAAATCCGAGAGA; *LTP3* (At5g59320), TGCGAAGAG CATTTCTGGTCTC and TGATGTTGTTGCAGTTAGTGCTC; *LTP4* (At5g59310), AGTCCGCTGCAAAAGGGGTTA and TTGATGGTGGCGCAGTTGGT; *KCS2* (At1g04220), GCTAAA CAGCTTCTTCAGGTTCA and TCGGAAGATGCAGTTTGAG AGA; *BDG1* (At1g64670), AGAAACAGGATGCGAACGTACT and ACATGGTCCAAATAAGCCTCTAC; and *LACS2* (At1g 49430), GTAGAGGAGTTCTTGAGAATCATT and AACTCTCA GTCAATCCATAACCTT. The primers utilized for the amplification of the *B. cinerea BcAct* actin gene (accession no. AJ000335) were the following: AAGTGTGATGTTGATGTCC and CTGTTGGAAA GTAGACAAAG (Ferrari et al., 2008).

Cuticle Permeability Assays

Toluidine blue staining was performed as previously described (Tanaka et al., 2004) with minor modifications. 5 µl droplets of 0.05% (w/v) toluidine blue (Sigma-Aldrich) solution were incubated for 2 h on adaxial surface of fully expanded leaves from 35-day-old plants. After incubation, leaves were washed and photographed.

Chlorophyll extraction and quantification were performed as described previously (Sieber et al., 2000). Leaves were detached, weighed, and immersed in 10 ml of 80% (v/v) ethanol. Chlorophyll extraction occurred in the dark at room temperature with gentle shaking. Aliquots were taken at indicated time after immersion. Total chlorophyll content was quantified by measuring absorbance at 647 and 664 nm, and micromolar concentration of chlorophyll per gram of fresh weight was calculated with the following equation: $[19.536 \times (\text{Abs } 647\,\text{nm}) + 7.936 \times (\text{Abs } 664\,\text{nm})]\ g^{-1}$ (Sieber et al., 2000).

ROS and Cell Death Detection

ROS accumulation was revealed by diaminobenzidine tetrahydrochloride (DAB, Sigma-Aldrich) staining as described previously (Daudi and O'Brien, 2012). Briefly, detached leaves were vacuum infiltrated with 0.1% (w/v) DAB in 10 mm Na_2HPO_4 for 5 min and incubated for 8 h in the dark under gentle shaking. Chlorophyll was removed using a 3:1:1 ethanol:acetic acid:glycerol solution at 90–95°C for 15 min. Leaves were rinsed in distilled water and photographed.

Cell death was estimated with Evans blue staining as previously described (Dong et al., 2007) with minor modifications. Briefly, detached rosette leaves were vacuum infiltrated for 5 min with a 0.1% Evans blue (w/v) solution and stained at room temperature for 3–4 h. Samples were washed twice with phosphate buffer and chlorophyll was extracted overnight with 80% ethanol.

Microscopy

For gap area determination, leaves of five-week-old soil grown plants were harvested and cleared with 80% ethanol overnight. Leaves were stained with ruthenium red (0.05% w/v) for 10–60 min at room temperature and washed with water. Images were taken with a Nikon Digital Sight DS-Fi1c Camera and examined using a Nikon Eclipse E200 Microscope. Gap area was measured using ImageJ.[2] At least two leaves from each of four individual plants per genotype were analyzed.

Transmission electron microscopy (TEM) experiments were performed largely as previously described (Nafisi et al., 2015b). Leaf pieces (approximately 2 × 4 mm) were cut out from the middle part of mature rosette leaves, avoiding the larger veins. The samples were fixed for 2 h under vacuum with Karnovsky's fixative (2.5% v/v glutaraldehyde and 2% w/v formaldehyde in 0.1 M sodium cacodylate buffer, pH 7.2; all from Sigma-Aldrich). The fixative was replaced by a 0.1 M sodium cacodylate buffer, pH 7.2, and samples placed in a tissue rotator for 20 min, then washed with 0.1 M sodium cacodylate buffer, and incubated for additional 20 min. The buffer was removed and replaced by osmium fixative (1% w/v osmium tetroxide in 0.1 M sodium cacodylate buffer, pH 7.2; Sigma-Aldrich). The samples were left for post-fixation for 1 h in the rotator and thereafter rinsed in 0.1 M sodium cacodylate buffer and water for 20 min, respectively. Dehydration was performed by a series of 50 to 100% v/v acetone solutions, which were replaced every 20–30 min. Spurr's resin (Polysciences) was then added in a 1:3, 1:1, and 3:1 ratio with acetone and rotated for 30 min in each step. Pure Spurr's resin was applied, and samples were left without lids for 1 h so that any remaining acetone could vaporize. The samples were left overnight, and the resin was changed once before embedding in flat molds in the oven at 70°C for 8 h. An EM UC7 Ultramicrotome (Leica Microsystems) was used for making ultrathin sections of 40 nm thickness with a diamond knife. Sections were captured on carbon-coated grids, contrast stained with a 1% w/v uranyl acetate solution and a 0.5% w/v lead citrate solution, washed, and dried into filter paper. The images were taken with a CM100 Transmission Electron Microscope (Philips) with a side-mounted 11 MP camera (Morada) set to an acceleration voltage of 80 kV. Quantification of cuticle thickness was performed with ImageJ. A total of 75 individual measurements were made for the upper leaf epidermis in each genotype at the magnification of 64,000 ×.

[2] http://rsbweb.nih.gov/ij/index.html

Chemical Analysis of Cutin

For the chemical analysis of cutin, five-week-old rosettes were extracted in isopropanol/0.01% butylated hydroxytoluene and then delipidized twice (for 16 h and 8 h) with each of the following solvents: chloroform:methanol (2:1), chloroform:methanol (1:1), and methanol (with 0.01% butylated hydroxytoluene), under agitation, before being dried for 3 days under vacuum. Depolymerization was performed by base catalysis (Li-Beisson et al., 2013). In brief, dried plant samples were transesterified in 2 ml of reaction medium. 20 ml of reaction medium was composed of 3 ml methyl acetate, 5 ml of 25% sodium methoxide in dry methanol, and 12 ml dry methanol. 2 mg of methyl heptadecanoate and 4 mg of ω-pentadecalactone were added per sample as internal standards. After incubation of the samples at 60°C for 2 h, 3.5 ml dichloromethane, 0.7 ml glacial acetic acid, and 1 ml 0.9% NaCl (w/v) Tris 100 mM (pH 8.0) were added to each sample and subsequently vortexed for 20 s. After centrifugation (1,500 *g* for 2 min), the organic phase was collected, washed with 2 ml of 0.9% NaCl, and dried over sodium sulfate. The organic phase was then recovered and concentrated under a stream of nitrogen. The resulting cutin monomers were acetylated at 70°C for 2 h and injected out of hexane on a HP-5 MS column (J&W Scientific) in a gas chromatograph coupled to a mass spectrometer and a flame ionization detector (Agilent 6890 N GC Network systems). The temperature cycle of the oven was the following: 2 min at 50°C, increment of 20°C min^{-1} to 160°C, of 2°C min^{-1} to 250°C and 10°C min^{-1} to 310°C, and held for 15 min. Two independent experiments were performed with four replicates for each genotype and treatment, respectively, and a representative dataset is presented.

RESULTS

Arabidopsis Plants With Altered HG Display a Robust Resistance to *B. Cinerea* and Enhanced Cuticle Permeability That Are Both Suppressed by Exogenous ABA

It was previously reported that PG and *qua2* plants display a robust resistance to *B. cinerea* (Ferrari et al., 2008; Verger, 2014), that resembles that of *Arabidopsis* plants with altered cuticle (Bessire et al., 2007; Chassot et al., 2007; Tang et al., 2007). Moreover, ABA positively regulates cuticle structure and functionality (Curvers et al., 2010; Cui et al., 2016) while negatively affecting resistance to *B. cinerea* (Audenaert et al., 2002; Anderson et al., 2004; Asselbergh et al., 2007; L'Haridon et al., 2011). We therefore examined whether plants with HG defects show changes in cuticle permeability, and whether ABA affects this phenotype. Rosette leaves of WT, PG, and *qua2* plants were sprayed with a control solution or with ABA, and cuticle permeability was evaluated after 24 h using two different assays: toluidine blue staining of the leaf surface (**Figure 1A**) and measurement of chlorophyll leakage in ethanol (**Figure 1B**). The results of both assays clearly indicated that cuticle permeability is increased in PG and *qua2* plants, compared to the WT, and that pre-treatments with ABA significantly reduce permeability in both lines (**Figures 1A,B**). We then tested whether the strong resistant phenotype associated to HG alterations is also negatively affected by this hormone. PG plants and the two allelic mutants *qua2* and *tsd2-1* (Krupková et al., 2007) were sprayed with ABA and, after 24 h, inoculated with *B. cinerea*. Control-treated PG and mutant plants displayed, as expected, a strong resistance to the fungus (**Figure 2**). ABA pre-treatments did not significantly alter basal susceptibility in WT plants but restored WT-like levels of susceptibility in all transgenic and mutant lines (**Figure 2**). These data suggest that an increased cuticle permeability might be responsible for the enhanced resistance against *B. cinerea* caused by defects in HG composition. Since transgene expression in PG plants was observed to vary among generations, all subsequent experiments were conducted on *qua2* plants, which showed similar phenotypes in terms of resistance to *B. cinerea*, leaf permeability, and response to ABA.

Previous work indicates that on the surface of *Arabidopsis* leaves having an increased cuticle permeability antifungal compounds effective against *B. cinerea* are present, possibly contributing to their robust resistance to this pathogen (Bessire et al., 2007). Consistently, leaf diffusates from *qua2* plants reduced *in vitro B. cinerea* spore germination (**Supplementary Figure 1A**) and suppressed *in vivo* disease development (**Supplementary Figure 1B**). These results support the conclusion that the increased cuticle permeability of plants with altered HG has a major role in their enhanced resistance to *B. cinerea*.

Because alterations of cuticle permeability may be due to a defective cutin, its composition was investigated. Compared to the WT, several oxygenated ester-bound lipid compounds typical for cutin were increased in untreated *qua2* mutant leaves, including the main cutin component, *i.e.*, 18:2 dicarboxylic acid (18:2 DCA; **Figure 3**; Li-Beisson et al., 2013), leading to an overall increase of oxygenated cutin monomers by 36% (**Figure 3** insert), while unsubstituted ester-bound fatty acids were unchanged. ABA treatment increased unsubstituted and oxygenated ester-bound lipid compounds in WT by 46.1 and 44.5%, respectively. ABA treatment also increased unsubstituted ester-bound lipids in the *qua2* mutant by 20.9%, while oxygenated cutin monomers were however not further increased (**Figure 3A**). In addition, TEM analysis did not reveal major defects in the ultrastructure of the cuticle in the epidermal cells of *qua2* rosette leaves (**Figure 3B**), except for a slight but significant increase in cuticle thickness which might be due to the increased cutin monomer levels.

We also evaluated the expression of genes involved in the biosynthesis of cutin and waxes in fully expanded rosette leaves of *qua2* plants. In particular, we measured transcript levels for the following genes: *BDG*, required for proper cutin biosynthesis (Kurdyukov et al., 2006); *LACS2*, involved in the biosynthesis of cutin and wax monomers (Schnurr et al., 2004; Lü et al., 2009); *ECERIFERUM1* (*CER1*) and *3-KETOACYL-COENZYME A SYNTHASE 2* (*KCS2*), both implicated in cuticular wax biosynthesis

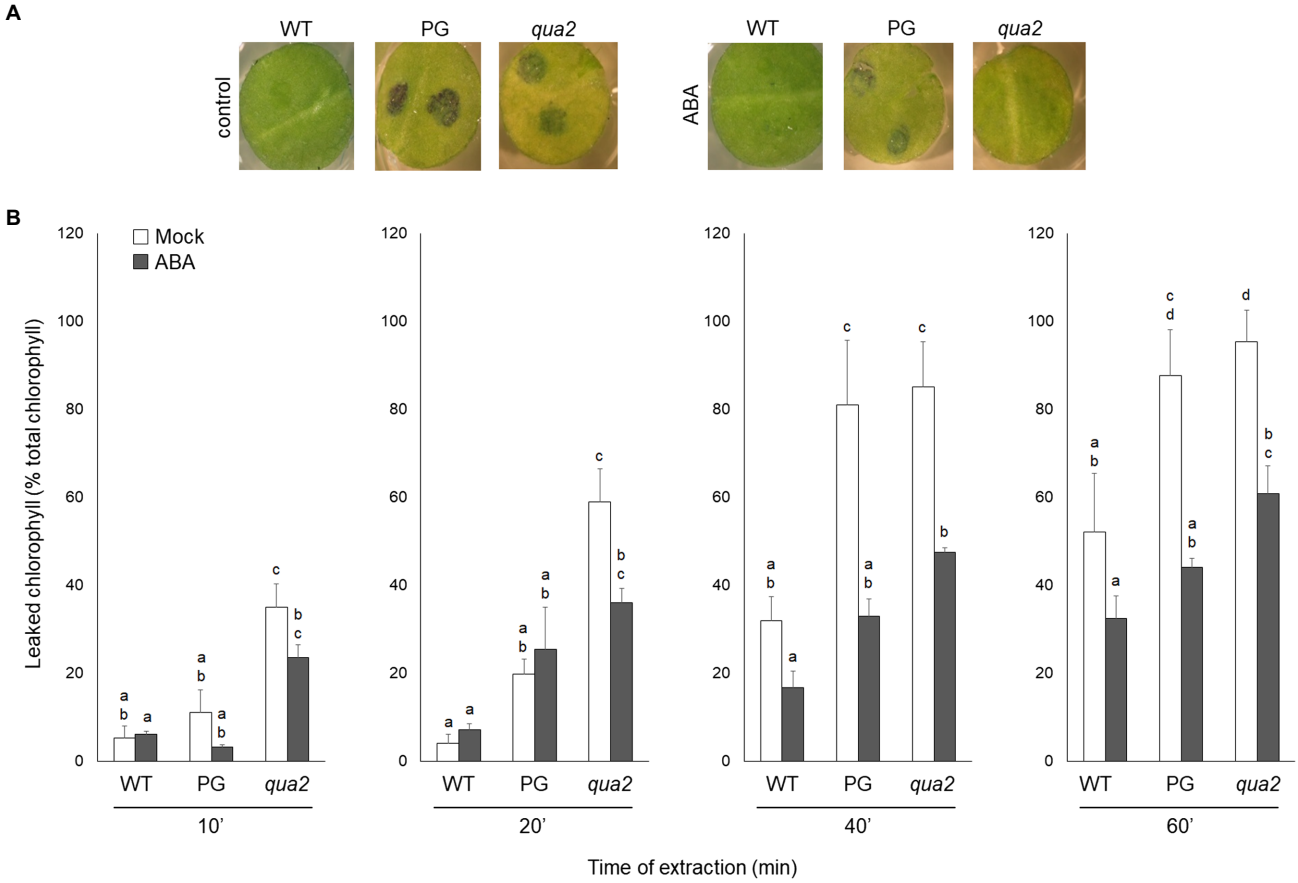

FIGURE 1 | Plants with altered HG have increased leaf cuticle permeability that is suppressed by exogenous ABA. **(A,B)**, WT, PG, and *qua2* five-week-old plants were sprayed with 0.01% MeOH or 100 μm ABA and, after 24 h, rosette leaves were collected. **(A)**, Leaf disks were stained with droplets of toluidine blue and washed with water. **(B)**, Leaves were incubated for the indicated times with 80% EtOH and the percentage of total chlorophyll released in the medium was spectrophotometrically measured. Bars indicate average percentage of total chlorophyll leaked at the indicated time of incubation ± *SD* ($n = 3$). For each time point, letters indicate statistically significant differences, according to two-way ANOVA followed by Tukey's significance test ($p < 0.05$). These experiments were repeated three times with similar results.

(Lee et al., 2009; Bourdenx et al., 2011; Bernard et al., 2012); and *MYB96*, encoding a transcription factor that positively regulates the expression of wax-related genes (Seo et al., 2011). We also evaluated the expression of *LIPID TRANSFER PROTEIN 3* (*LTP3*), a direct target of MYB96 (Guo et al., 2013), and its close homolog *LTP4*. This set of genes was selected because they all show altered expression in the *OG hypersensitive 1* (*ohy1*) mutant, that, like *qua2*, has a permeable cuticle, increased peroxidase levels and increased resistance to *B. cinerea* (Survila et al., 2016). Basal levels of expression of *LACS2* and *BDG* were not significantly different in WT and *qua2* rosette leaves, though they appeared more variable in the mutant (**Supplementary Figure 2**). Expression of *MYB96*, *LTP3*, and *LTP4* was significantly enhanced in *qua2*, compared to the WT, whereas *CER1* expression did not significantly change and *KCS2* expression was reduced in the mutant (**Supplementary Figure 2**). These data indicate that *qua2* does not show a major reduction of the expression of genes involved in cutin or wax biosynthesis that might explain its defect in permeability. Notably, ABA treatments induced the expression of all tested genes in both genotypes (**Supplementary Figure 2**), indicating that ABA-mediated regulation of genes involved in cuticle formation is not impaired in *qua2*.

AtPRX71 Contributes to Cuticle Permeability, Loss of Cell Adhesion, and Resistance to *B. Cinerea* in *qua2* Plants

Cuticle defects may lead to the expression of apoplastic peroxidases and accumulation of ROS (Chassot et al., 2007), as also observed in plants with defects in HG (Ferrari et al., 2008; Raggi et al., 2015). Moreover, overexpression of apoplastic peroxidases in WT plants also leads to ROS accumulation and enhanced cuticle permeability, responses that are both suppressed by ABA (Survila et al., 2016). It can be therefore hypothesized that the increased permeability of *qua2* might depend on its high levels of *AtPRX71* expression. To assess this, we analyzed cuticle permeability in fully expanded rosette leaves of WT, *qua2*, and *atprx71-1* (henceforth, *atprx71*) plants, in a *qua2*

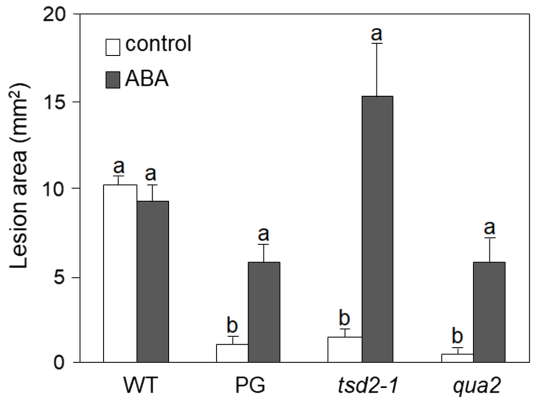

FIGURE 2 | Resistance to *Botrytis cinerea* conferred by altered HG is suppressed by exogenous ABA. Rosette leaves of five-week-old WT, PG, *qua2*, and *tsd2-1* plants were treated with 0.01% MeOH (white bars) or 100 µm ABA (grey bars) and, after 24 h, inoculated with a *B. cinerea* spore suspension. Lesion area was measured 2 days after inoculation ($n > 10$ lesions for each genotype). Bars indicate average lesion area ± *SE*. Different letters indicate statistically significant differences, according to two-way ANOVA followed by Tukey's significance test ($p < 0.05$). This experiment was repeated three times with similar results.

atprx71 double mutant, and in two transgenic lines overexpressing *AtPRX71* (*35S::PRX71* #22 and 24; Raggi et al., 2015). As expected, leaves of plants overexpressing *AtPRX71* showed greatly enhanced cuticle permeability, compared to untransformed plants, as determined by both toluidine blue staining and leaf chlorophyll leakage measurement (**Figures 4A,B**). Loss of *AtPRX71* did not affect cuticle permeability in the WT background but partially rescued the cuticle permeability defect of *qua2* (**Figures 4A,B**). Toluidine blue staining of whole rosettes showed that the cuticle of the entire lamina of mature (fully expanded) leaves of *qua2* plants is permeable, whereas younger leaves were not stained (**Figure 4C**). Mature leaves of the *qua2 atprx71* double mutant showed irregular patches of permeable cuticle, supporting the hypothesis that *AtPRX71* contributes to the increased cuticle permeability of *qua2* (**Figure 4C**). Plants overexpressing *AtPRX71* showed a very high cuticle permeability of the entire lamina of younger leaves, and an irregular distribution of permeable cuticle patches in older leaves (**Figure 4C**). Interestingly, ABA pre-treatments, which suppressed cuticle permeability in *qua2* (**Figures 1A,B**), also reduced ROS accumulation in this mutant, as determined by DAB staining (**Supplementary Figure 3**). These results suggest that accumulation of ROS mediated by *AtPRX71* is at least partially responsible for the increased cuticle permeability of *qua2* leaves. In addition, despite the high basal levels of ROS, no significant increase in Evans blue staining, indicative of cell death, was observed in *qua2* leaves, both in uninfected plants and at early stages of *B. cinerea* infection (16 h post-infection, hpi), though staining at 40 hpi was reduced in the mutant, possibly as a consequence of the reduced ability of the fungus to infect this mutant (**Supplementary Figure 4A**) and suggesting that, in *qua2*, the fungus is restricted at an early stage of infection. Consistently, expression of the fungal actin *BcAct* gene was comparable in WT and *qua2* plants at 24 hpi but increased at 36 hpi only in WT plants (**Supplementary Figure 4B**).

It was previously shown that *QUA2* is required for normal cell adhesion (Mouille et al., 2007). Since *qua2* plants do not show major changes in cuticle ultrastructure and do not display a reduction in ester-bound lipids or in the expression of most cuticle-related genes that we have analyzed, we speculated that a reduced adhesion of the epidermal cells might contribute to its increased permeability. Indeed, cracks between adjacent cells and opening of the cuticle at cell junctions were previously described in the hypocotyl of *qua1-1* (Verger et al., 2018), a mutant for a glycosyltransferase that is required for pectin synthesis and cell adhesion (Bouton et al., 2002; Mouille et al., 2007). Indeed, examination of the surface of *qua2* rosette leaves revealed the presence of gaps between adjacent epidermal cells (**Figure 5**). Notably, the area of these gaps was significantly reduced in the *qua2 atprx71* double mutant (**Figure 5**), indicating that increased peroxidase levels in plants with altered HG exacerbate the adhesion defect in *qua2* leaf epidermis. In contrast, overexpression of *AtPRX71* in a WT background did not result in any detectable loss of cell adhesion (**Figure 5**). Moreover, ABA treatments did not affect epidermal cell gap area in *qua2* (**Supplementary Figure 5**). Interestingly, a mutation in the *ESMERALDA1* gene, previously shown to suppress the cell adhesion defect in *qua2* without affecting its galacturonic acid content (Verger et al., 2016), also suppressed its increased cuticle permeability (**Supplementary Figure 6**), supporting the hypothesis that the defects in cell adhesion and in cuticle functionality in *qua2* are linked.

We next evaluated whether *AtPRX71* contributes to the resistance to *B. cinerea* observed in *qua2*. As previously reported (Raggi et al., 2015), symptoms caused by this pathogen in the *atprx71* mutant were comparable to those observed in the WT (**Figure 6**), confirming that *AtPRX71* is not necessary for basal resistance to this fungus in plants with normal pectin composition. *AtPRX71* overexpression was sufficient to significantly increase resistance to *B. cinerea* (**Figure 6**), a result also in agreement with previous observations (Chassot et al., 2007). Notably, the *qua2 atprx71* double mutant was significantly less resistant than *qua2*, though it was still more resistant than the WT (**Figure 6**). Taken together, these results suggest that *AtPRX71* is required for the strong resistance to *B. cinerea* of *qua2*, possibly because it contributes to increased cuticle permeability.

To further investigate the role of *AtPRX71* in *qua2* resistance, we examined the expression of three defense-related genes, *PHYTOALEXIN DEFICIENT 3* (*PAD3*), *PATHOGENESIS-RELATED 1* (*PR-1*), and *PLANT DEFENSIN 1.2* (*PDF1.2*), during fungal infection of WT, *qua2*, *atprx71*, and *qua2 atprx71* plants. These genes were selected since they are markers for different defense-related pathways: *PR-1* and *PDF1.2* are well-known markers for the activation of SA-dependent and JA/ethylene-dependent responses, respectively (Glazebrook, 2005), whereas *PAD3*, encoding a cytochrome P450 required

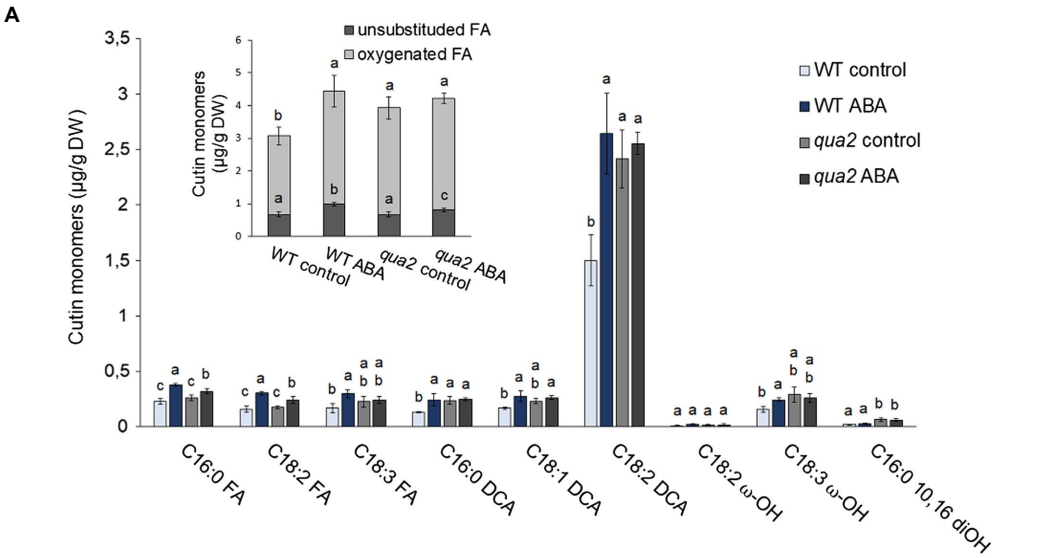

	number of images	number of measurements	cuticle thickness (nm) ± SD	Student's t-test significativity (P value)
WT	15	75	22.09 ± 5.96	< 0.01
qua2	13	72	26.76 ± 9.34	

FIGURE 3 | Cutin deposition and cuticle thickness are enhanced in *qua2* mutant leaves. **(A)**, Five-week-old plants were sprayed with 0.01% MeOH (control) or 100 µm ABA and leaves collected after 24 h. Quantification of transesterified aliphatic and aromatic cutin monomers reveals an increase of main cutin components in *qua2* which are not further increased after ABA treatment. The graph shows the analysis of the principal cutin monomers and the inset shows the sum of the indicated monomer classes per genotype and treatment. Data are mean ± *SD*; $n = 4$ replicates. Different letters indicate significant differences as determined by ANOVA followed by Tukey's significance test ($p < 0.05$). DW, dry weight; DCA, dicarboxylic acid; ω-OH, ω-hydroxy acid; and FA, fatty acid. **(B)**, TEM images of the cuticle of epidermal cells of the adaxial face of rosette leaves of five-week-old WT (top panel) and *qua2* (middle panel) plants. Pictures are representative of 15 (WT) and 13 (*qua2*) images. Bars, 125 nm. Bottom panel measurement of cuticle thickness from images taken as above described.

for the biosynthesis of camalexin (Schuhegger et al., 2006), is rapidly induced by *B. cinerea* and by DAMPs and MAMPs independently of SA, JA, and ethylene (Ferrari et al., 2007; Gravino et al., 2015) and is required for basal and elicitor-induced resistance to this fungus (Ferrari et al., 2003, 2007). At 8 hpi, *PAD3* transcript levels were significantly higher in *qua2* than in the WT (**Supplementary Figure 7A**), suggesting that plants with altered HG display an anticipated response to the pathogen. This early induction of *PAD3* expression also occurred in the *qua2 atprx71* double mutant (**Supplementary Figure 7A**), indicating that it does not depend on an increased peroxidase activity. At 24 hpi, levels of *PAD3* transcripts increased to a greater extent in the WT than in *qua2* and *qua2 atprx71* plants (**Supplementary Figure 7A**), possibly because fungal growth was reduced in both mutants. Expression of *PR-1* and *PDF1.2* during *B. cinerea* infection increased at later time points than *PAD3* and was similar in WT and *qua2* plants (**Supplementary Figures 7B,C**), suggesting that activation of SA- and JA/ET-mediated pathways does not significantly contribute to the resistance observed in the mutant.

Cuticle Permeability and Resistance to *B. Cinerea* in Mutants Affected in Different Primary CW Components

Since plants with altered HG show increased ROS accumulation, cuticle permeability and resistance to *B. cinerea*, we assessed whether mutants with defects in other CW polysaccharides also display these phenotypes. We tested *prc1* and *ixr1-2*, which have mutations in *CESA1* and *CESA3*, respectively (Fagard et al., 2000; Scheible et al., 2001), required for primary CW cellulose deposition (Fagard et al., 2000; Scheible et al., 2001;

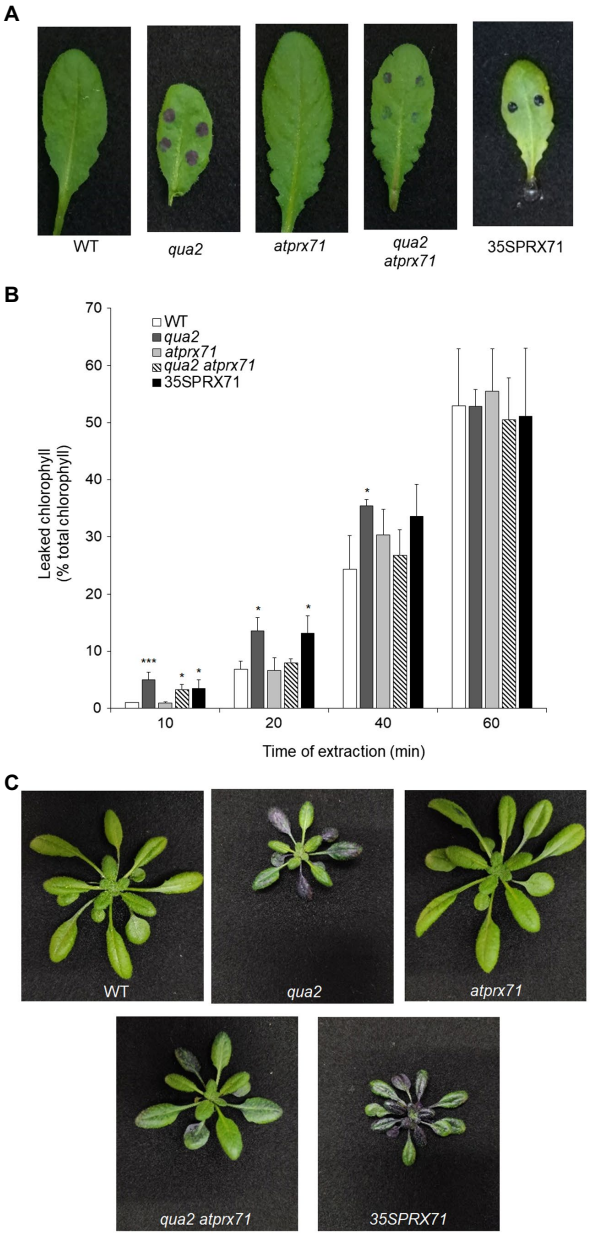

FIGURE 4 | Increased cuticle permeability of *qua2* leaves is partially dependent on *AtPRX71*. Permeability of the cuticle of fully expanded rosette leaves **(A)** of five-week-old Col-0 (WT), *qua2*, *atprx71*, *qua2 atprx71*, and 35S::AtPRX71 #22 (35SPRX71) plants was determined by toluidine blue staining. **(B)** The amount of chlorophyll leached from rosette leaves as in **(A)** was measured after incubation in 80% EtOH at the indicated times. Bars indicate average concentration ± *SD* (n = 3). For each time point, asterisks indicate significant differences, according to Student's t-test between WT and mutants (*$p < 0.05$; ***$p < 0.01$). These experiments were repeated three times with similar results. **(C)** Toluidine blue staining of the entire rosette of five-week-old plants. Representative images of at least five plants per genotype are shown.

Desprez et al., 2007; Persson et al., 2007), *murus1* (*mur1*), defective in a GDP-Man-4,6-dehydratase required for the synthesis of Fuc and therefore impaired in xyloglucan and RGII integrity (O'Neill et al., 2001), and *murus4* (*mur4*), defective in a UDP-D-Xylose epimerase required for Ara biosynthesis (Burget et al., 2003) and characterized by a 50% reduction in Ara, mainly representative of RG-I and arabinogalactan proteins (AGPs; Reiter et al., 1997; Burget and Reiter, 1999). In addition, we analyzed the *fer-4* mutant (Duan et al., 2010), which is defective in the *FER* gene, important for pectin integrity perception (Li et al., 2016; Feng et al., 2018). Cuticle permeability was unaffected in *prc1*, *mur4*, and *ixr1-2* leaves, and only moderately increased in *mur1*, but was extremely increased in *fer-4* (**Figures 7A,B**), suggesting that cuticle defects are caused by alterations of HG integrity and/or of its perception, but not by alterations of other primary CW components. DAB staining revealed accumulation of ROS in *mur1*, *ixr1-2*, and *fer-4* rosette leaves (**Figure 7C**), indicating that high ROS levels *per se* are not sufficient to impair cuticle functionality. Whole rosette toluidine blue staining showed that all leaves of *prc1*, *mur4*, and *ixr1-2* plants have normal cuticle permeability, whereas patches of increased permeability could be observed in the older leaves of *mur1* plants (**Supplementary Figure 8**). The pattern of cuticle permeability of *fer-4* and *qua2* was similar, with almost complete staining of the lamina of fully expanded leaves, but not of younger leaves (**Supplementary Figure 8**).

To test how changes in different primary CW polysaccharides affect susceptibility to *B. cinerea*, *prc1*, *ixr-2*, *mur1*, *mur4*, and *fer-4* plants were inoculated with the fungus and lesion area was measured after 48 h. Only *fer-4* showed an almost complete resistance, comparable to that of *qua2*, whereas *ixr1-2* showed slightly reduced lesion size (**Figure 8**), consistent with the moderate resistance previously observed in the allelic mutant *ixr1-1* (Hernández-Blanco et al., 2007). Fungal resistance in all the other tested mutants was not significantly altered (**Figure 8**). Overall, our results suggest that defects in HG composition and/or integrity maintenance specifically confer a robust resistance to *B. cinerea* that correlates with loss of cell adhesion and enhanced cuticle permeability.

DISCUSSION

Increased Cuticle Permeability Caused by Loss of HG Integrity Depends on AtPRX71 and Correlates With a Defective Epidermal Cell Adhesion

The traditional view of a cuticle separated from the underlying CW of epidermal cells is currently challenged by increasing evidence indicating that CW polysaccharides are entangled with cutin in the "cuticular layer" beneath the "cuticle proper" and that these polysaccharides affect cuticle deposition and functionality (Fernández et al., 2016). Indeed, some authors now prefer to consider the cuticle as an extreme modification of the outer CW (Domínguez et al., 2011), or a region of the CW extremely rich in lipids (Fernández et al., 2016). Here, we show that plants with defective HG, either caused by the *qua2* mutation or by expression of a fungal PG, and plants lacking a functional FER, supposed to act as a sensor of HG

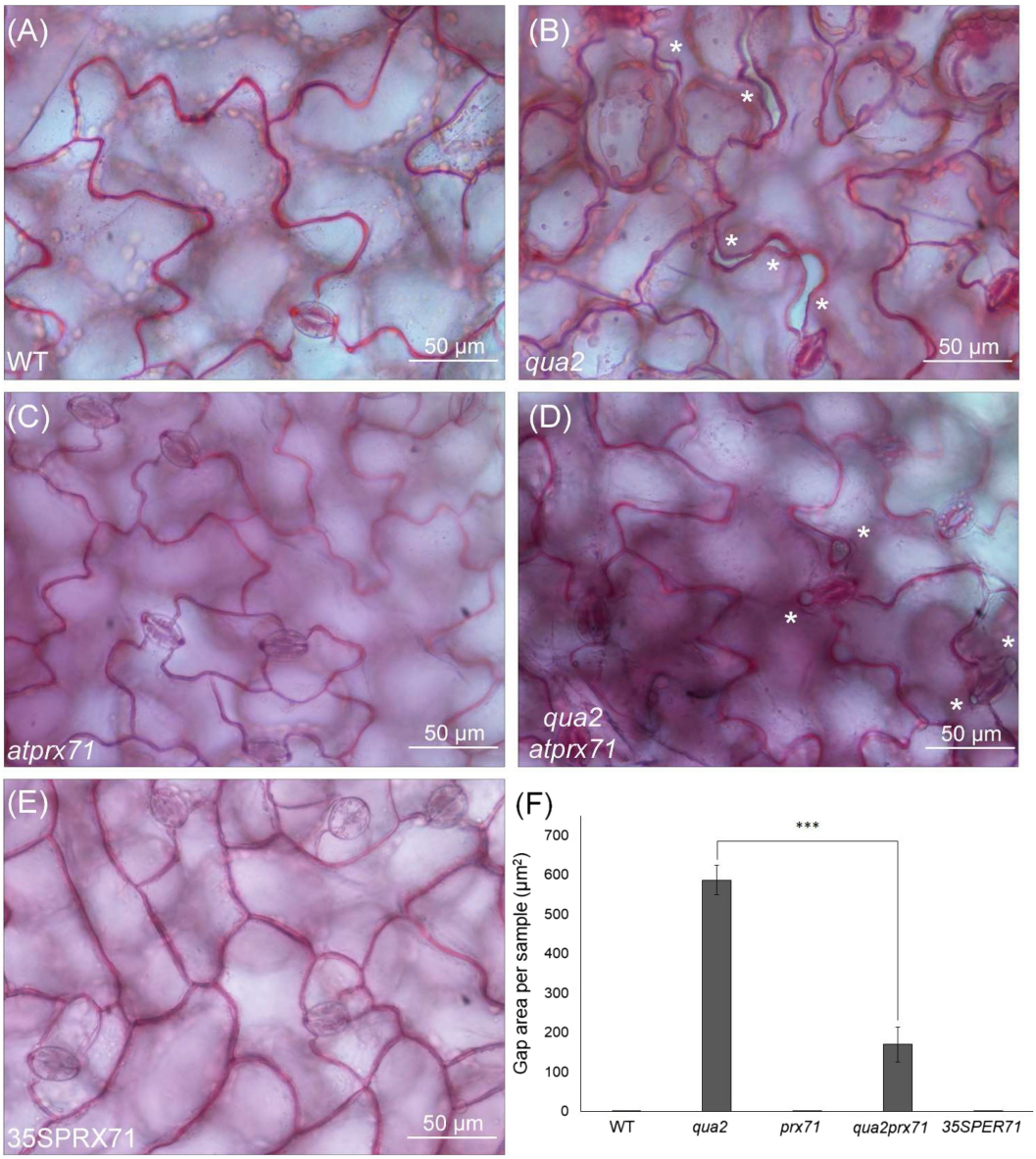

FIGURE 5 | Cell-adhesion defects in *qua2* leaves are suppressed by loss of *AtPRX71*. Rosette leaves of five-week-old Col-0 (WT) **(A)**, *qua2* **(B)**, *atprx71* **(C)**, *qua2 atprx71* **(D)**, and 35S::AtPRX71 #22 (35SPRX71) **(E)** plants were stained with ruthenium red and epidermal cells of the adaxial face were photographed. Asterisks indicate gaps between adjacent cells. **(A–E)**, Representative images of at least five images per genotype. **(F)**, For each experiment, total area of the gaps between adjacent cells per image was analyzed (total area of images = 60,000 µm^2). Bars indicate average gap area ± *SD* (n = 3). Asterisks indicate statistically significant difference between *qua2* and *qua2 atprx71*, according to Student's t-test ($^{***}p < 0.01$).

integrity (Lin et al., 2018), show increased cuticle permeability (**Figures 1 and 7**), supporting a strict interconnection between pectin composition and cuticle functionality. Indeed, pectin can be found in epidermal cells at the interface of the CW with the cuticle (Orgell, 1955; Jeffree, 2006), and the observation that the tomato mutant *sitiens*, defective in ABA biosynthesis, shows both altered cuticle and pectin composition (Curvers et al., 2010) further supports a link between these two structures. Overexpression of the *Arabidopsis* PME inhibitor PMEI5 leads to reduced permeability and organ fusion (Müller et al., 2013), suggesting that the degree of methylation of HG might be important for a functional cuticle. However, since *qua2* has a normal ratio between methylated and non-methylated HG (Mouille et al., 2007), total HG levels are probably more important in determining the defects in cuticle functionality of this mutant. It was previously reported that *qua2* is specifically affected in HG, without observable changes in other polysaccharides, including RG-I (Mouille et al., 2007). The recent observation that disrupted cellulose biosynthesis and orientation occurs in *qua2* mutants strongly indicates that an

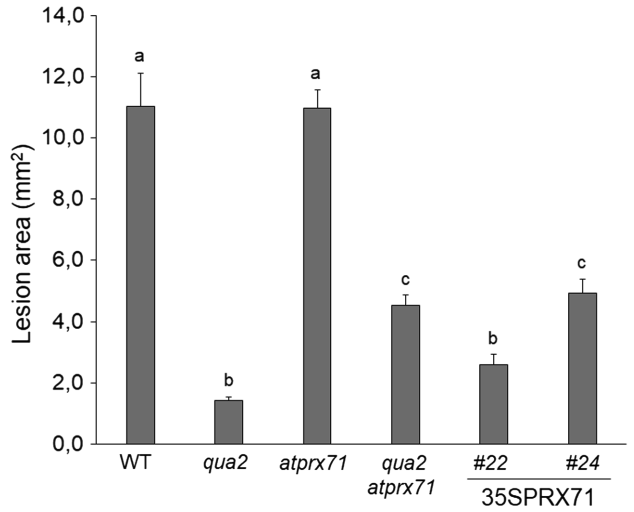

FIGURE 6 | Resistance to *B. cinerea* in *qua2* is partially dependent on *AtPRX71*. Rosette leaves of five-week-old WT plants, *qua2, atprx71*, and *qua2 atprx71* plants, and of two independent transgenic lines overexpressing *AtPRX71* (35SPRX71 #22 and #24) were inoculated with a *B. cinerea* spore suspension, and lesion area was measured 2 days after inoculation ($n > 10$ for each genotype). Bars indicate average lesion area ± *SE*. Different letters indicate statistically significant differences, according to one-way ANOVA followed by Tukey's significance test ($p < 0.01$).

intact HG is required for proper CESA functionality (Du et al., 2020). However, it is unlikely that the reduced cuticle permeability observed in *qua2* and PG plants is due to a defect in the cellulose network, since mutants impaired in primary CW cellulose deposition (*prc1* and *ixr1-2*) do not show major changes in cuticle permeability.

The mechanism(s) linking altered HG integrity to loss of cuticle functionality is not clear, but our data suggest that production of ROS mediated by apoplastic peroxidases might play a role. We have previously found that *qua2*, as well as PG plants, accumulates high levels of ROS as a consequence of an increased expression of *AtPRX71* (Raggi et al., 2015). We show here that cuticle functionality is lost in plants overexpressing *AtPRX71*, and a mutation in this gene partially complements cuticle permeability in *qua2* (**Figure 4**). This is consistent with the previous observation that the *Arabidopsis ohy1* mutant, overexpressing another peroxidase gene, *PER57*, displays increased cuticle permeability (Survila et al., 2016). The increased permeability of both *qua2* and *ohy1* cuticles is therefore likely mediated by peroxidase-generated ROS, as supported by the observation that ABA suppresses both ROS accumulation and cuticle permeability in *ohy1* plants (Survila et al., 2016) as well as in plants with altered HG (**Figure 1** and **Supplementary Figure 3**). How elevated peroxidase levels might influence cuticle functionality is still unclear. It was reported that expression of genes required for cutin biosynthesis is suppressed in the *ohy1* mutant (Survila et al., 2016), suggesting that elevated ROS produced by peroxidases negatively influence cutin production. Paradoxically, compared to the WT, *qua2* leaves display increased levels of ester-bound lipids, including 18:2 DCA, the main cutin component (Li-Beisson et al., 2013; **Figure 3A**), and a slight increase in cuticle thickness (**Figure 3B**), which might depend on increased cutin levels. Moreover, in contrast to *ohy1*, *qua2* plants do not display a reduction in the expression of *BDG* and indeed show increased basal transcript levels for *LACS2* (**Supplementary Figure 2**), consistent with the observed increase in residue-bound lipid content. An increased cutin monomer load was also previously observed in other mutants with altered permeability, namely, *lcr*, *fiddlehead* (*fdh*), *bdg*, *fatty acid desaturase2* (*fad2*), and the *fad3 fad7 fad8* triple (*fad* triple) mutant (Kurdyukov et al., 2006; Voisin et al., 2009; Dubey et al., 2020) and is suggestive of a compensatory response, possibly as a consequence of a more unstructured cutin and/or defects in wax-cutin associations, leading to the incorporation of more cutin-like material in the epidermal CWs of the mutant. Notably, *qua2* plants also display greatly increased basal levels of transcript levels of *MYB96, LTP3*, and its close homolog *LTP4* (**Supplementary Figure 2**). MYB96 is a transcription factor positively regulating genes involved in wax biosynthesis, and expression of *LTP3* was also previously shown to be upregulated in an activation-tagged *myb96-1D* mutant (Seo et al., 2011). These results suggest that the altered permeability caused by defects in HG is not due to a reduced expression of cuticle-related genes, at least in mature rosette leaves. Moreover, induction of the expression of cuticle-related genes by exogenous ABA was unaffected in *qua2* plants, ruling out a defect in ABA perception/signaling in this mutant.

The different expression pattern of cuticle-related genes in *ohy1* and *qua2* suggests that the impact of high peroxidase levels *per se* on cuticle formation is not completely overlapping with that of altered pectin composition, though they might contribute to increase cuticle permeability in the context of a defective pectin composition. Indeed, our results indicate that lack of *AtPRX71* partially suppresses the cell adhesion defect in *qua2* leaf epidermis (**Figure 5**). Moreover, the *esmd1* mutation completely suppressed in *qua2* both loss of epidermal cell adhesion (Verger et al., 2016) and cuticle permeability (**Supplementary Figure 6**), supporting the hypothesis of a link between a defective cell adhesion and an altered cuticle functionality in plants with reduced HG content. Cell separation in the hypocotyl and cotyledons of *qua1*, another mutant defective in HG (Bouton et al., 2002), can be restored by reducing water potential, indicating that adhesion defects relate to the tensile status of the tissue (Verger et al., 2018). It is conceivable that a similar correlation also occurs in *qua2*, and the observation that the *atprx71* mutation partially complements the cell adhesion defect in leaves of this mutant (**Figure 5**) points to a role of CW peroxidases in the ability to withstand tensile stress in the presence of a defective pectin, as *AtPRX71* also appears to negatively regulate cell expansion (Raggi et al., 2015). However, since peroxidase overexpression increases cuticle permeability also in the absence of HG defects (Survila et al., 2016; **Figure 4**), and plants overexpressing *AtPRX71* do not display

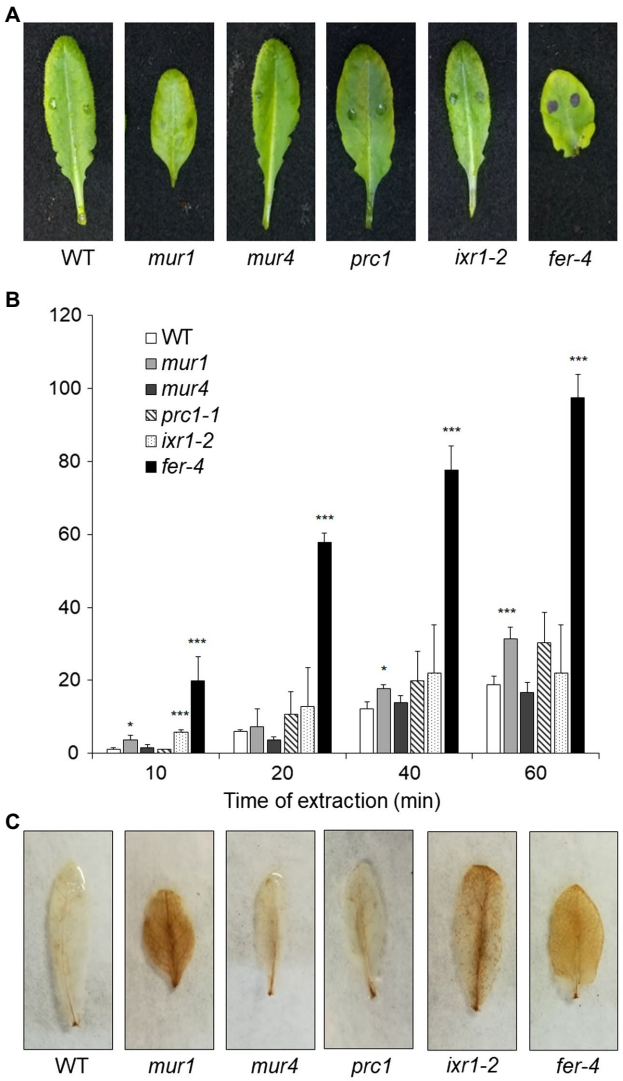

FIGURE 7 | Cuticle permeability and ROS accumulation in mutants with impaired cell wall integrity. **(A,B)**, Rosette leaves of five-week-old Col-0 (WT), *mur1*, *mur4*, *prc1*, *irx1-2*, and *fer-4* plants were stained with toluidine blue **(A)** to assay cuticle permeability or **(B)** incubated for the indicated times with 80% EtOH, and the concentration of chlorophyll leaked in the medium and of total chlorophyll was spectrophotometrically measured. Bars in **(B)** indicate average percentage of total chlorophyll leaked at the indicated time of incubation ± *SD* ($n = 3$). For each time point, asterisks indicate statistically significant differences with the control-treated WT samples, according to Student's t-test (***$p < 0.01$; *$p < 0.01$). **(C)**, rosette leaves as in **(A,B)** were stained with DAB for ROS accumulation. These experiments were repeated three times with similar results.

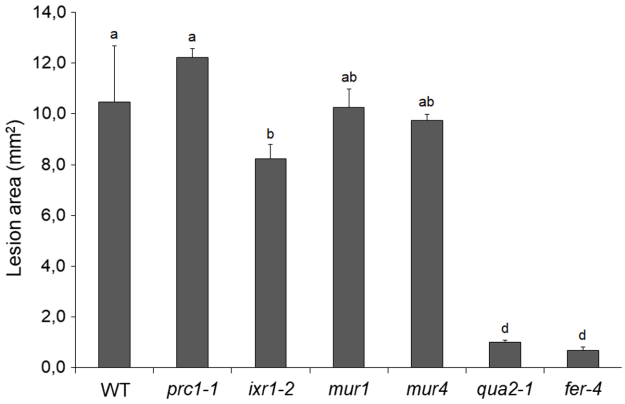

FIGURE 8 | Resistance to *B. cinerea* in cell wall mutants. Rosette leaves of five-week-old WT plants and of *prc1*, *ixr1-2*, *mur1*, *mur4*, *qua2*, and *fer-4* mutant plants were inoculated with a *B. cinerea* spore suspension, and lesion area was measured 2 days after inoculation ($n > 12$ lesions for each genotype). Bars indicate average lesion area ± *SE*. Different letters indicate statistically significant differences, according to one-way ANOVA followed by Tukey's significance test ($p < 0.01$).

loss of cell adhesion (**Figure 5**). cuticle functionality might be impaired by very high levels apoplastic peroxidases independently of its impact on cell adhesion. Moreover, as the *atprx71* mutation does not fully complement the permeability of *qua2*, peroxidase-independent mechanisms responsible for the impaired cuticle functionality of plants with defective HG can also be envisioned. It was recently proposed that, in tomato fruits, close association occurs between cutin and pectins, and the latter probably play a determinant role in the organization and formation of the cutin-polysaccharide continuum (Philippe et al., 2020), suggesting that alterations in HG content might directly impair proper assembly of cutin.

Loss of Cuticle Functionality Is a Major Determinant of the Robust Resistance to *B. Cinerea* Caused by Altered HG Integrity

The results presented in this work indicate that the dramatic increase in cuticle permeability of plants with altered HG integrity, as well as of *fer-4* plants, is a major determinant of their robust resistance to *B. cinerea*. These conclusion is supported by the observations that both cuticle permeability and resistance in *qua2* and PG plants are suppressed by ABA treatments (**Figures 1, 2**) and are partially complemented in the *qua2 atprx71* double mutant (**Figures 4, 6**). Moreover, suppression of the cell adhesion defect in *qua2* by the *esmd1* mutation fully restores both cuticle functionality and susceptibility to *B. cinerea* (**Supplementary Figure 6**). On the other hand, mutations that impair different structural polysaccharides of the primary CW beside HG have no or minor effects on cuticle permeability and fungal resistance (**Figures 7, 8**). Our results are consistent with previous reports indicating that defects in cuticle integrity caused by overexpression of a fungal cutinase (CUTE plants) or by mutations in *Arabidopsis* genes involved in cuticle biogenesis, including *LACS2*, *LCR*, *FDH*, and *BDG*, confer an almost complete resistance to *B. cinerea* in rosette leaves (Bessire et al., 2007; Chassot et al., 2007; Tang et al., 2007; Voisin et al., 2009). A similar observation has also been made in cotyledons of *fad2* and *fad* triple mutant (Dubey et al., 2020).

The mechanisms by which an altered cuticle leads to increased resistance to *B. cinerea* are not fully elucidated. Different explanations have been proposed, including deregulation of

cell death (Cui et al., 2019), enhanced diffusion of antifungal compounds (Bessire et al., 2007; Chassot et al., 2007), increased production and/or diffusion of DAMPs and MAMPs (Chassot et al., 2007; Curvers et al., 2010), hyperaccumulation of ROS (Asselbergh et al., 2007; L'Haridon et al., 2011), an altered leaf microbiome (Ritpitakphong et al., 2016), and over-accumulation of fungitoxic secondary metabolites on the plant surface (Dubey et al., 2020). These explanations are not mutually exclusive, and it is conceivable that multiple mechanisms contribute to the loss of susceptibility to *B. cinerea* in plants with a permeable cuticle. The results presented in this work indicate that diffusates from the *qua2* leaf surface inhibit *B. cinerea* germination and impair the ability of the fungus to successfully infect WT plants (**Supplementary Figure 1**), supporting the hypothesis that an enhanced accumulation and/or diffusion of antimicrobial compounds in *qua2* plants contributes to their robust resistance. Moreover, increased production and/or diffusion of elicitors are also possible, as expression of the elicitor-induced gene *PAD3* during infection occurs much earlier in *qua2* plants than in the WT (**Supplementary Figure 7**). It was previously shown that the ABA-hypersensitive *enhanced response to aba1-2* (*era1-2*) mutant also has a permeable cuticle and is resistant to *B. cinerea* (Cui et al., 2019). Notably, resistance in this mutant was suppressed by the *botrytis susceptible1* mutation that confers deregulated cell death (Cui et al., 2019). Since *qua2* plants show reduced Evans blue staining at late stages of fungal infection (**Supplementary Figure 4**), we cannot rule out that regulation of cell death might play a role in the resistance of this mutant, though it is also possible that the observed reduction in staining simply reflects the reduced extent of lesion development in the mutant.

Our results suggest that peroxidase-mediated ROS accumulation plays a major role in resistance of plants with altered HG content. Loss of *PRX71* in *qua2* reduces peroxidase activity and ROS levels (Raggi et al., 2015) and suppresses cuticle permeability and resistance (**Figures 4, 6**). This suggests that the resistant phenotype of plants with altered HG is due to their defective cuticle, which in turn is dependent on their enhanced peroxidase levels that increase the extent of loss of cell adhesion in the epidermis. Accumulation of high ROS levels was also observed in *Arabidopsis* plants with an altered cuticle caused by cutinase treatment or mutations in *LACS* and *BDG* and in the tomato *sitiens* mutant and linked to their resistance to *B. cinerea* (Asselbergh et al., 2007; L'Haridon et al., 2011). In cotyledons of *Arabidopsis*, enhanced ROS production could not be correlated to resistance to *Botrytis* and cuticle permeability (Dubey et al., 2020). It is however conceivable that in *Arabidopsis* and tomato leaves, a positive feedback mechanism exists between HG integrity, cuticle functionality, and peroxidase-mediated ROS production: loss of HG integrity results in elevated peroxidase levels and ROS accumulation, causing a defective cuticle that triggers further production of ROS. However, additional, cuticle-independent mechanisms by which elevated peroxidase levels may contribute to the enhanced resistance of plants with defective HG cannot be ruled out. Indeed, class III peroxidases play multiple roles in plant-pathogen interactions, mediating reinforcement of the CW, and contributing to the oxidative burst induced by DAMPs and MAMPs (Almagro et al., 2009). Antisense expression of the French bean peroxidase type 1 in *Arabidopsis* reduces the expression of two endogenous peroxidases (*PRX33* and *PRX34*) required for elicitor-induced oxidative burst and gene expression and for basal resistance to *B. cinerea* (Bindschedler et al., 2006; Daudi et al., 2012). Accumulation of ROS also mediates immunity to *B. cinerea* induced by wounding, and both wound-induced ROS accumulation and resistance are suppressed by ABA (L'Haridon et al., 2011). We indeed found that exogenous ABA in *qua2* plants reduces ROS levels (**Supplementary Figure 3**) and restores fungal susceptibility (**Figure 2**). Therefore, ROS generated by an increased expression of apoplastic peroxidases might lead, in plants with altered HG, to a robust resistance to *B. cinerea* not only because they affect cuticle integrity, but also because they might restrict fungal infection either directly or through the activation of other defense-related pathways. Notably, ROS are produced in the host apoplast by *B. cinerea* as a virulence factor, possibly mediating induction of cell death (Govrin and Levine, 2000). However, high levels of ROS *per se* do not induce cell death in *qua2* leaves (**Supplementary Figure 4**) and might indeed promote immunity to *B. cinerea* (Asselbergh et al., 2007; Serrano et al., 2014; Survila et al., 2016).

Previous work indicates that SA-, JA-, and ethylene-mediated responses all contribute to basal resistance of *Arabidopsis* to *B. cinerea* (Ferrari et al., 2003). Both basal- and fungal-induced expression of *PDF1.2* and *PR-1*, typical marker genes for these defense-related pathways, are comparable in WT and *qua2* plants. Similarly, microarray analysis previously failed to reveal constitutive expression of *PR-1* or *PDF1.2* in PG plants (Raggi et al., 2015). Therefore, the resistant phenotype of plants with impaired HG integrity does not appear to be dependent of the SA-, JA-, or ethylene-mediated pathways, as also previously observed for rosettes of CUTE plants (Chassot et al., 2007) and cotyledons of the *fad2* and *fad* triple mutant (Dubey et al., 2020). PAD3-mediated biosynthesis of camalexin is crucial for both basal- and elicitor-induced resistance of *Arabidopsis* to *B. cinerea* (Ferrari et al., 2003, 2007), and expression of *PAD3* in response to this pathogen and to OGs occurs independently of SA-, ethylene-, and JA-mediated signaling (Ferrari et al., 2007). Notably, basal- and pathogen-induced expression of *PAD3* is greatly enhanced in *qua2* (**Supplementary Figure 7**). Indeed, it was previously suggested that altered cuticle permeability in plants that overexpress class III peroxidases primes the expression of OG-responsive defense-related genes (Survila et al., 2016). However, in contrast to resistance, the enhanced expression of *PAD3* in *qua2* during early stages of infection is not suppressed by mutations in *AtPRX71* (**Supplementary Figure 7**). Consistently, resistance of CUTE plants to *B. cinerea* is also independent of *PAD3* (Chassot et al., 2007). Therefore, increased production of pectin-derived signals, like OGs, might promote, in plants with

altered HG, earlier expression of defense responses during infection, but this has a minor impact on resistance against *B. cinerea*, compared to the effects caused by a defective cuticle.

Cuticle Defects and Robust Resistance to *B. Cinerea* Are Specifically Associated to Loss of HG Integrity or of the Ability to Perceive it

It is now widely accepted that defects in CWI caused by a biotic or abiotic stress trigger responses aimed at restoring or compensating for the damage to ensure proper CW functionality (Gigli-Bisceglia et al., 2020; Rui and Dinneny, 2020). Increasing evidence indicates that loss of CWI also induces defenses effective against pathogens and that there is extensive crosstalk between the CWI maintenance system and PTI (Bacete et al., 2018; Bacete and Hamann, 2020; Gigli-Bisceglia et al., 2020). Indeed, mutants impaired in different CW structural components often display enhanced resistance to specific pathogens (Bacete et al., 2018; Molina et al., 2020), and increased resistance to necrotrophic fungi is often observed in mutants impaired in secondary CW components (Ellis and Turner, 2001; Hernández-Blanco et al., 2007; Molina et al., 2020). We found that neither cuticle permeability nor resistance to *B. cinerea* are significantly affected in a set of mutants impaired in different polysaccharidic components of the primary CW (**Figures 7, 8**), suggesting that loss of HG integrity can specifically confer a robust resistance to this pathogen, probably because of its impact on cuticle integrity. Notably, *fer-4* also shows increased cuticle permeability and strong resistance to *B. cinerea* (**Figures 7, 8**). This might be the consequence of a defect in HG content, like that observed in *qua2*, though a detailed analysis of pectin composition in *fer-4* leaves is required to support this conclusion. FER-dependent signaling is necessary to maintain pectin integrity during salt stress, which causes softening of the CW in roots, and cells in *fer-4* roots explode during growth recovery (Feng et al., 2018). Notably, similar defects are observed in the *mur1* mutant, which disrupts pectin cross-linking, and *fer-4* CWI defects can be rescued by calcium and borate, which facilitate HG and RGII cross-linking (Feng et al., 2018). Moreover, a significant reduction in de-esterified pectin was recently detected at the filiform apparatus of *fer-4* ovules (Duan et al., 2020). This indicates that FER might be required for sensing pectin integrity, and lack of it results in the inability of plants to adjust pectin composition in response to stress. It must be noted, however, that FER can also function as a scaffold for PAMP receptors, positively modulating immunity, and can also interact with endogenous RAPID ALKALINIZATION FACTOR propeptides to inhibit PTI (Stegmann et al., 2017). Induction of ROS and activation of MAP kinases in response to flg22 are also enhanced in *fer-4* (Keinath et al., 2010), supporting the notion that lack of FER induces the constitutive activation of signaling pathways normally activated during PTI. Further investigation will help determine if the increased resistance to *B. cinerea* of *fer-4* plants is caused by a defect in maintaining a proper pectin composition, and the consequent alteration of cuticle integrity or rather depends on the negative role of FER in modulating PTI.

CONCLUSION

We have shown that loss of HG integrity, or of the ability to monitor it, results in an increase cuticle permeability that correlates with a defective epidermal cell adhesion and leads to accumulation of antimicrobial compounds on the leaf surface. Increased permeability confers an almost complete resistance to *B. cinerea*, and both phenotypes are partially dependent on *AtPRX71* and completely suppressed by loss of *ESMERALDA1*. In addition, HG alterations also appear to enhance defense responses during fungal infection independently of cuticle permeability, but these responses do not seem to play a major role in the robust resistance to *B. cinerea* observed in *qua2*. These results indicate that HG has a crucial role in maintaining cuticle integrity and highlight the complexity of the interactions between CW composition and resistance to pathogens.

DATA AVAILABILITY STATEMENT

The raw data supporting the conclusions of this article will be made available by the authors, without undue reservation.

AUTHOR CONTRIBUTIONS

RL, FF, GDL, CN, HJM, and SF designed the experiments and analyzed the data. RL, FF, HJM, and KG performed the experiments. RL, CN, GDL, and SF wrote the manuscript. All authors contributed to the article and approved the submitted version.

FUNDING

This work was supported by the Ministero dell'Istruzione, dell'Università e della Ricerca (project "ORIGAMI" grant number ARS01_00881 to SF), the Sapienza Università di Roma (Progetti di Ricerca 2019 grant number RM11916B6F156C03 to SF), and the Swiss National Science Foundation, Switzerland (grant 31003A-170127 to CN).

ACKNOWLEDGMENTS

We thank Sara Raggi and Stephane Verger (Umeå University, Umeå, Sweden) for critical reading of the manuscript.

SUPPLEMENTARY MATERIAL

The Supplementary Material for this article can be found online at https://www.frontiersin.org/articles/10.3389/fpls.2021.696955/full#supplementary-material

REFERENCES

AbuQamar, S., Moustafa, K., and Tran, L. S. (2017). Mechanisms and strategies of plant defense against *Botrytis cinerea*. *Crit. Rev. Biotechnol.* 37, 262–274. doi: 10.1080/07388551.2016.1271767

Albersheim, P., Darvill, A., Roberts, K., Sederoff, R., and Staehelin, A. (2010). *Plant Cell Walls*. New York, NY:Garland Science.

Almagro, L., Gómez Ros, L. V., Belchi-Navarro, S., Bru, R., Ros Barceló, A., and Pedreno, M. A. (2009). Class III peroxidases in plant defence reactions. *J. Exp. Bot.* 60, 377–390. doi: 10.1093/jxb/ern277

Anderson, J. P., Badruzsaufari, E., Schenk, P. M., Manners, J. M., Desmond, O. J., Ehlert, C., et al. (2004). Antagonistic interaction between abscisic acid and jasmonate-ethylene signaling pathways modulates defense gene expression and disease resistance in *Arabidopsis*. *Plant Cell* 16, 3460–3479. doi: 10.1105/tpc.104.025833

Anderson, C. T., and Kieber, J. J. (2020). Dynamic construction, perception, and remodeling of plant cell walls. *Annu. Rev. Plant Biol.* 71, 39–69. doi: 10.1146/annurev-arplant-081519-035846

Asselbergh, B., Curvers, K., França, S. C., Audenaert, K., Vuylsteke, M., Van Breusegem, F., et al. (2007). Resistance to *Botrytis cinerea* in sitiens, an abscisic acid-deficient tomato mutant, involves timely production of hydrogen peroxide and cell wall modifications in the epidermis. *Plant Physiol.* 144, 1863–1877. doi: 10.1104/pp.107.099226

Audenaert, K., Pattery, T., Cornelis, P., and Höfte, M. (2002). Induction of systemic resistance to *Botrytis cinerea* in tomato by Pseudomonas aeruginosa 7NSK2: role of salicylic acid, pyochelin, and pyocyanin. *Mol. Plant Microbe. Interact.* 15, 1147–1156. doi: 10.1094/MPMI.2002.15.11.1147

Bacete, L., and Hamann, T. (2020). The role of mechanoperception in plant cell wall integrity maintenance. *Plants* 9:574. doi: 10.3390/plants9050574

Bacete, L., Mélida, H., Miedes, E., and Molina, A. (2018). Plant cell wall-mediated immunity: cell wall changes trigger disease resistance responses. *Plant J.* 93, 614–636. doi: 10.1111/tpj.13807

Benedetti, M., Pontiggia, D., Raggi, S., Cheng, Z., Scaloni, F., Ferrari, S., et al. (2015). Plant immunity triggered by engineered *in vivo* release of oligogalacturonides, damage-associated molecular patterns. *Proc. Natl. Acad. Sci. U. S. A.* 112, 5533–5538. doi: 10.1073/pnas.1504154112

Bernard, A., Domergue, F., Pascal, S., Jetter, R., Renne, C., Faure, J.-D., et al. (2012). Reconstitution of plant alkane biosynthesis in yeast demonstrates that *Arabidopsis* ECERIFERUM1 and ECERIFERUM3 are core components of a very-long-chain alkane synthesis complex. *Plant Cell* 24, 3106–3118. doi: 10.1105/tpc.112.099796

Berto, P., Comménil, P., Belingheri, L., and Dehorter, B. (1999). Occurrence of a lipase in spores of Alternaria brassicicola with a crucial role in the infection of cauliflower leaves. *FEMS Microbiol. Lett.* 180, 183–189. doi: 10.1111/j.1574-6968.1999.tb08794.x

Bessire, M., Chassot, C., Jacquat, A.-C., Humphry, M., Borel, S., Petétot, J. M.-C., et al. (2007). A permeable cuticle in *Arabidopsis* leads to a strong resistance to *Botrytis cinerea*. *EMBO J.* 26, 2158–2168. doi: 10.1038/sj.emboj.7601658

Bindschedler, L. V., Dewdney, J., Blee, K. A., Stone, J. M., Asai, T., Plotnikov, J., et al. (2006). Peroxidase-dependent apoplastic oxidative burst in *Arabidopsis* required for pathogen resistance. *Plant J.* 47, 851–863. doi: 10.1111/j.1365-313X.2006.02837.x

Bourdenx, B., Bernard, A., Domergue, F., Pascal, S., Léger, A., Roby, D., et al. (2011). Overexpression of *Arabidopsis* ECERIFERUM1 promotes wax very-long-chain alkane biosynthesis and influences plant response to biotic and abiotic stresses. *Plant Physiol.* 156, 29–45. doi: 10.1104/pp.111.172320

Bouton, S., Leboeuf, E., Mouille, G., Leydecker, M.-T., Talbotec, J., Granier, F., et al. (2002). QUASIMODO1 encodes a putative membrane-bound glycosyltransferase required for normal pectin synthesis and cell adhesion in *Arabidopsis*. *Plant Cell* 14, 2577–2590. doi: 10.1105/tpc.004259

Burget, E. G., and Reiter, W.-D. (1999). The mur4 mutant of *Arabidopsis* is partially defective in the de novo synthesis of uridine Diphosphol-arabinose. *Plant Physiol.* 121, 383–390. doi: 10.1104/pp.121.2.383

Burget, E. G., Verma, R., Molhoj, M., and Reiter, W. D. (2003). Molecular cloning and characterization of a golgi-localized UDP-d-xylose 4-epimerase encoded by the MUR4 gene of *Arabidopsis*. *Plant Cell* 15, 523–531. doi: 10.1105/tpc.008425

Caño-Delgado, A., Penfield, S., Smith, C., Catley, M., and Bevan, M. (2003). Reduced cellulose synthesis invokes lignification and defense responses in *Arabidopsis thaliana*. *Plant J.* 34, 351–362. doi: 10.1046/j.1365-313X.2003.01729.x

Capodicasa, C., Vairo, D., Zabotina, O., McCartney, L., Caprari, C., Mattei, B., et al. (2004). Targeted modification of homogalacturonan by transgenic expression of a fungal polygalacturonase alters plant growth. *Plant Physiol.* 135, 1294–1304. doi: 10.1104/pp.104.042788

Carpita, N. C., and Gibeaut, D. M. (1993). Structural models of primary cell walls in flowering plants: consistency of molecular structure with the physical properties of the walls during growth. *Plant J.* 3, 1–30. doi: 10.1111/j.1365-313X.1993.tb00007.x

Chassot, C., Nawrath, C., and Métraux, J.-P. (2007). Cuticular defects lead to full immunity to a major plant pathogen. *Plant J.* 49, 972–980. doi: 10.1111/j.1365-313X.2006.03017.x

Cui, F., Brosché, M., Lehtonen, M. T., Amiryousefi, A., Xu, E., Punkkinen, M., et al. (2016). Dissecting abscisic acid signaling pathways involved in cuticle formation. *Mol. Plant* 9, 926–938. doi: 10.1016/j.molp.2016.04.001

Cui, F., Wu, W., Wang, K., Zhang, Y., Hu, Z., Brosché, M., et al. (2019). Cell death regulation but not abscisic acid signaling is required for enhanced immunity to botrytis in *Arabidopsis* cuticle-permeable mutants. *J. Exp. Bot.* 70, 5971–5984. doi: 10.1093/jxb/erz345

Curvers, K., Seifi, H., Mouille, G., De Rycke, R., Asselbergh, B., Van Hecke, A., et al. (2010). Abscisic acid deficiency causes changes in cuticle permeability and pectin composition that influence tomato resistance to *Botrytis cinerea*. *Plant Physiol.* 154, 847–860. doi: 10.1104/pp.110.158972

Daudi, A., Cheng, Z., O'Brien, J. A., Mammarella, N., Khan, S., Ausubel, F. M., et al. (2012). The apoplastic oxidative burst peroxidase in *Arabidopsis* is a major component of pattern-triggered immunity. *Plant Cell* 24, 275–287. doi: 10.1105/tpc.111.093039

Daudi, A., and O'Brien, J. A. (2012). Detection of hydrogen peroxide by DAB staining in *Arabidopsis* leaves. *Bio. Protoc.* 2:e263. doi: 10.21769/BioProtoc.263

de Azevedo Souza, C., Li, S., Lin, A. Z., Boutrot, F., Grossmann, G., Zipfel, C., et al. (2017). Cellulose-derived oligomers act as damage-associated molecular patterns and trigger defense-like responses. *Plant Physiol.* 173, 2383–2398. doi: 10.1104/pp.16.01680

De Lorenzo, G., Castoria, R., Bellincampi, D., and Cervone, F. (1997). "Fungal invasion enzymes and their inhibition," in *Plant Relationships*. eds. G. C. Carroll and P. Tudzynski (Berlin, Heidelberg: Springer), 61–83.

De Lorenzo, G., Ferrari, S., Cervone, F., and Okun, E. (2018). Extracellular DAMPs in plants and mammals: immunity, tissue damage and repair. *Trends Immunol.* 39, 937–950. doi: 10.1016/j.it.2018.09.006

Deising, H., Nicholson, R. L., Haug, M., Howard, R. J., and Mendgen, K. (1992). Adhesion pad formation and the involvement of cutinase and esterases in the attachment of uredospores to the host cuticle. *Plant Cell* 4, 1101–1111. doi: 10.2307/3869478

Desnos, T., Orbovic, V., Bellini, C., Kronenberger, J., Caboche, M., Traas, J., et al. (1996). Procuste1 mutants identify two distinct genetic pathways controlling hypocotyl cell elongation, respectively in dark-and light-grown *Arabidopsis* seedlings. *Development* 122, 683–693. doi: 10.1242/dev.122.2.683

Desprez, T., Juraniec, M., Crowell, E. F., Jouy, H., Pochylova, Z., Parcy, F., et al. (2007). Organization of cellulose synthase complexes involved in primary cell wall synthesis in *Arabidopsis thaliana*. *Proc. Natl. Acad. Sci. U. S. A.* 104, 15572–15577. doi: 10.1073/pnas.0706569104

Domínguez, E., Heredia-Guerrero, J. A., and Heredia, A. (2011). The biophysical design of plant cuticles: an overview. *New Phytol.* 189, 938–949. doi: 10.1111/j.1469-8137.2010.03553.x

Dong, H., Deng, Y., Mu, J., Lu, Q., Wang, Y., Xu, Y., et al. (2007). The *Arabidopsis* spontaneous cell Death1 gene, encoding a ζ-carotene desaturase essential for carotenoid biosynthesis, is involved in chloroplast development, photoprotection and retrograde signalling. *Cell Res.* 17, 458–470. doi: 10.1038/cr.2007.37

Du, J., Kirui, A., Huang, S., Wang, L., Barnes, W. J., Kiemle, S. N., et al. (2020). Mutations in the pectin Methyltransferase QUASIMODO2 influence cellulose biosynthesis and wall integrity in *Arabidopsis*. *Plant Cell* 32, 3576–3597. doi: 10.1105/tpc.20.00252

Duan, Q., Kita, D., Li, C., Cheung, A. Y., and Wu, H.-M. (2010). FERONIA receptor-like kinase regulates RHO GTPase signaling of root hair development. *Proc. Natl. Acad. Sci. U. S. A.* 107, 17821–17826. doi: 10.1073/pnas.1005366107

Duan, Q., Liu, M.-C. J., Kita, D., Jordan, S. S., Yeh, F.-L. J., Yvon, R., et al. (2020). FERONIA controls pectin-and nitric oxide-mediated male–female interaction. *Nature* 579, 561–566. doi: 10.1038/s41586-020-2106-2

Dubey, O., Dubey, S., Schnee, S., Glauser, G., Nawrath, C., Gindro, K., et al. (2020). Plant surface metabolites as potent antifungal agents. *Plant Physiol. Biochem.* 150, 39–48. doi: 10.1016/j.plaphy.2020.02.026

Ellis, C., Karafyllidis, I., Wasternack, C., and Turner, J. G. (2002). The *Arabidopsis* mutant cev1 links cell wall signaling to jasmonate and ethylene responses. *Plant Cell* 14, 1557–1566. doi: 10.1105/tpc.002022

Ellis, C., and Turner, J. G. (2001). The *Arabidopsis* mutant cev1 has constitutively active jasmonate and ethylene signal pathways and enhanced resistance to pathogens. *Plant Cell* 13, 1025–1033. doi: 10.1105/tpc.13.5.1025

Fagard, M., Desnos, T., Desprez, T., Goubet, F., Refregier, G., Mouille, G., et al. (2000). PROCUSTE1 encodes a cellulose synthase required for normal cell elongation specifically in roots and dark-grown hypocotyls of *Arabidopsis*. *Plant Cell* 12, 2409–2423. doi: 10.1105/tpc.12.12.2409

Feng, W., Kita, D., Peaucelle, A., Cartwright, H. N., Doan, V., Duan, Q., et al. (2018). The FERONIA receptor kinase maintains cell-wall integrity during salt stress through Ca2+ signaling. *Curr. Biol.* 28, 666.e5–675.e5. doi: 10.1016/j.cub.2018.01.023

Fernández, V., Guzmán-Delgado, P., Graça, J., Santos, S., and Gil, L. (2016). Cuticle structure in relation to chemical composition: re-assessing the prevailing model. *Front. Plant Sci.* 7:427. doi: 10.3389/fpls.2016.00427

Ferrari, S., Galletti, R., Denoux, C., De Lorenzo, G., Ausubel, F. M., and Dewdney, J. (2007). Resistance to *Botrytis cinerea* induced in *Arabidopsis* by elicitors is independent of salicylic acid, ethylene, or jasmonate signaling but requires PHYTOALEXIN DEFICIENT3. *Plant Physiol.* 144, 367–379. doi: 10.1104/pp.107.095596

Ferrari, S., Galletti, R., Pontiggia, D., Manfredini, C., Lionetti, V., Bellincampi, D., et al. (2008). Transgenic expression of a fungal endo-polygalacturonase increases plant resistance to pathogens and reduces auxin sensitivity. *Plant Physiol.* 146, 669–681. doi: 10.1104/pp.107.109686

Ferrari, S., Plotnikova, J. M., De Lorenzo, G., and Ausubel, F. M. (2003). *Arabidopsis* local resistance to *Botrytis cinerea* involves salicylic acid and camalexin and requires EDS4 and PAD2, but not SID2, EDS5 or PAD4. *Plant J.* 35, 193–205. doi: 10.1046/j.1365-313X.2003.01794.x

Ferrari, S., Savatin, D. V., Sicilia, F., Gramegna, G., Cervone, F., and De Lorenzo, G. (2013). Oligogalacturonides: plant damage-associated molecular patterns and regulators of growth and development. *Front. Plant Sci.* 4:49. doi: 10.3389/fpls.2013.00049

Franck, C. M., Westermann, J., and Boisson-Dernier, A. (2018). Plant malectin-like receptor kinases: from cell wall integrity to immunity and beyond. *Annu. Rev. Plant Biol.* 69, 301–328. doi: 10.1146/annurev-arplant-042817-040557

Francocci, F., Bastianelli, E., Lionetti, V., Ferrari, S., De Lorenzo, G., Bellincampi, D., et al. (2013). Analysis of pectin mutants and natural accessions of *Arabidopsis* highlights the impact of de-methyl-esterified homogalacturonan on tissue saccharification. *Biotechnol. Biofuels* 6:163. doi: 10.1186/1754-6834-6-163

Galletti, R., Denoux, C., Gambetta, S., Dewdney, J., Ausubel, F. M., De Lorenzo, G., et al. (2008). The AtrbohD-mediated oxidative burst elicited by oligogalacturonides in *Arabidopsis* is dispensable for the activation of defense responses effective against *Botrytis cinerea*. *Plant Physiol.* 148, 1695–1706. doi: 10.1104/pp.108.127845

Garrido, S. M., Kitamoto, N., Watanabe, A., Shintani, T., and Gomi, K. (2012). Functional analysis of FarA transcription factor in the regulation of the genes encoding lipolytic enzymes and hydrophobic surface binding protein for the degradation of biodegradable plastics in aspergillus oryzae. *J. Biosci. Bioeng.* 113, 549–555. doi: 10.1016/j.jbiosc.2011.12.014

Gigli-Bisceglia, N., Engelsdorf, T., and Hamann, T. (2020). Plant cell wall integrity maintenance in model plants and crop species-relevant cell wall components and underlying guiding principles. *Cell. Mol. Life Sci.* 77, 2049–2077. doi: 10.1007/s00018-019-03388-8

Glazebrook, J. (2005). Contrasting mechanisms of defense against biotrophic and necrotrophic pathogens. *Annu. Rev. Phytopathol.* 43, 205–227. doi: 10.1146/annurev.phyto.43.040204.135923

Govrin, E. M., and Levine, A. (2000). The hypersensitive response facilitates plant infection by the necrotrophic pathogen *Botrytis cinerea*. *Curr. Biol.* 10, 751–757. doi: 10.1016/S0960-9822(00)00560-1

Gravino, M., Savatin, D. V., Macone, A., and De Lorenzo, G. (2015). Ethylene production in *B otrytis cinerea*-and oligogalacturonide-induced immunity requires calcium-dependent protein kinases. *Plant J.* 84, 1073–1086. doi: 10.1111/tpj.13057

Guo, L., Yang, H., Zhang, X., and Yang, S. (2013). Lipid transfer protein 3 as a target of MYB96 mediates freezing and drought stress in *Arabidopsis*. *J. Exp. Bot.* 64, 1755–1767. doi: 10.1093/jxb/ert040

Gust, A. A., Pruitt, R., and Nürnberger, T. (2017). Sensing danger: key to activating plant immunity. *Trends Plant Sci.* 22, 779–791. doi: 10.1016/j.tplants.2017.07.005

Hamann, T., Bennett, M., Mansfield, J., and Somerville, C. (2009). Identification of cell-wall stress as a hexose-dependent and osmosensitive regulator of plant responses. *Plant J.* 57, 1015–1026. doi: 10.1111/j.1365-313X.2008.03744.x

Hernández-Blanco, C., Feng, D. X., Hu, J., Sánchez-Vallet, A., Deslandes, L., Llorente, F., et al. (2007). Impairment of cellulose synthases required for *Arabidopsis* secondary cell wall formation enhances disease resistance. *Plant Cell* 19, 890–903. doi: 10.1105/tpc.106.048058

Holloway, P. J. (1982). "*Structure and Histochemistry of Plant Cuticular Membranes: An Overview*," in *The plant cuticle*. eds. D. F. Cutler, K. L. Alvin and C. E. Price (London: Academic Press).

Houston, K., Tucker, M. R., Chowdhury, J., Shirley, N., and Little, A. (2016). The plant cell wall: a complex and dynamic structure as revealed by the responses of genes under stress conditions. *Front. Plant Sci.* 7:984. doi: 10.3389/fpls.2016.00984

Humphrey, T. V., Bonetta, D. T., and Goring, D. R. (2007). Sentinels at the wall: cell wall receptors and sensors. *New Phytol.* 176, 7–21. doi: 10.1111/j.1469-8137.2007.02192.x

Jeffree, C. E. (2006). "The fine structure of the plant cuticle," in *Annual Plant Reviews, Vol. 23: Biology of the Plant Cuticle*. eds. M. Riederer and C. Müller (Blackwell Publishing), 11–125. doi: 10.1002/9780470988718.ch2

Kalunke, R. M., Tundo, S., Benedetti, M., Cervone, F., De Lorenzo, G., and D'Ovidio, R. (2015). An update on polygalacturonase-inhibiting protein (PGIP), a leucine-rich repeat protein that protects crop plants against pathogens. *Front. Plant Sci.* 6:146. doi: 10.3389/fpls.2015.00146

Kars, I., Krooshof, G. H., Wagemakers, L., Joosten, R., Benen, J. A., and Van Kan, J. A. (2005). Necrotizing activity of five *Botrytis cinerea* endopolygalacturonases produced in Pichia pastoris. *Plant J.* 43, 213–225. doi: 10.1111/j.1365-313X.2005.02436.x

Keinath, N. F., Kierszniowska, S., Lorek, J., Bourdais, G., Kessler, S. A., Shimosato-Asano, H., et al. (2010). PAMP (pathogen-associated molecular pattern)-induced changes in plasma membrane compartmentalization reveal novel components of plant immunity. *J. Biol. Chem.* 285, 39140–39149. doi: 10.1074/jbc.M110.160531

Krupková, E., Immerzeel, P., Pauly, M., and Schmülling, T. (2007). The TUMOROUS SHOOT DEVELOPMENT2 gene of *Arabidopsis* encoding a putative methyltransferase is required for cell adhesion and co-ordinated plant development. *Plant J.* 50, 735–750. doi: 10.1111/j.1365-313X.2007.03123.x

Kunst, L., and Samuels, L. (2009). Plant cuticles shine: advances in wax biosynthesis and export. *Curr. Opin. Plant Biol.* 12, 721–727. doi: 10.1016/j.pbi.2009.09.009

Kurdyukov, S., Faust, A., Nawrath, C., Bär, S., Voisin, D., Efremova, N., et al. (2006). The epidermis-specific extracellular BODYGUARD controls cuticle development and morphogenesis in *Arabidopsis*. *Plant Cell* 18, 321–339. doi: 10.1105/tpc.105.036079

L'Haridon, F., Besson-Bard, A., Binda, M., Serrano, M., Abou-Mansour, E., Balet, F., et al. (2011). A permeable cuticle is associated with the release of reactive oxygen species and induction of innate immunity. *PLoS Pathog.* 7:e1002148. doi: 10.1371/journal.ppat.1002148

Lee, S.-B., Jung, S.-J., Go, Y.-S., Kim, H.-U., Kim, J.-K., Cho, H.-J., et al. (2009). Two *Arabidopsis* 3-ketoacyl CoA synthase genes, KCS20 and KCS2/DAISY, are functionally redundant in cuticular wax and root suberin biosynthesis, but differentially controlled by osmotic stress. *Plant J.* 60, 462–475. doi: 10.1111/j.1365-313X.2009.03973.x

Li, C., Wu, H.-M., and Cheung, A. Y. (2016). FERONIA and her pals: functions and mechanisms. *Plant Physiol.* 171, 2379–2392. doi: 10.1104/pp.16.00667

Li-Beisson, Y., Shorrosh, B., Beisson, F., Andersson, M. X., Arondel, V., Bates, P. D., et al. (2013). Acyl-lipid metabolism. *Arabidopsis Book* 11:e0161. doi: 10.1199/tab.016

Lin, W., Tang, W., Anderson, C. T., and Yang, Z. (2018). FERONIA's sensing of cell wall pectin activates ROP GTPase signaling in *Arabidopsis*. bioRxiv [preprint]. doi: 10.1101/269647

Lionetti, V., Francocci, F., Ferrari, S., Volpi, C., Bellincampi, D., Galletti, R., et al. (2010). Engineering the cell wall by reducing de-methyl-esterified

homogalacturonan improves saccharification of plant tissues for bioconversion. *Proc. Natl. Acad. Sci. U. S. A.* 107, 616–621. doi: 10.1073/pnas.0907549107

Livak, K. J., and Schmittgen, T. D. (2001). Analysis of relative gene expression data using real-time quantitative PCR and the 2− ΔΔCT method. *Methods* 25, 402–408. doi: 10.1006/meth.2001.1262

Locci, F., Benedetti, M., Pontiggia, D., Citterico, M., Caprari, C., Mattei, B., et al. (2019). An *Arabidopsis* berberine bridge enzyme-like protein specifically oxidizes cellulose oligomers and plays a role in immunity. *Plant J.* 98, 540–554. doi: 10.1111/tpj.14237

Lorrai, R., and Ferrari, S. (2021). Host Cell Wall damage during pathogen infection: mechanisms of perception and role in plant-pathogen interactions. *Plan. Theory* 10:399. doi: 10.3390/plants10020399

Lü, S., Song, T., Kosma, D. K., Parsons, E. P., Rowland, O., and Jenks, M. A. (2009). *Arabidopsis* CER8 encodes LONG-CHAIN ACYL-COA SYNTHETASE 1 (LACS1) that has overlapping functions with LACS2 in plant wax and cutin synthesis. *Plant J.* 59, 553–564. doi: 10.1111/j.1365-313X.2009.03892.x

Manfield, I. W., Orfila, C., McCartney, L., Harholt, J., Bernal, A. J., Scheller, H. V., et al. (2004). Novel cell wall architecture of isoxaben-habituated *Arabidopsis* suspension-cultured cells: global transcript profiling and cellular analysis. *Plant J.* 40, 260–275. doi: 10.1111/j.1365-313X.2004.02208.x

McCann, M. C., and Roberts, K. (1991). "Architecture of the primary cell wall," in *The Cytoskeletal Basis of Plant Growth and Form*. ed. C. W. Lloyd. (London: Academic Press) 109–129.

Mengiste, T. (2012). Plant immunity to necrotrophs. *Annu. Rev. Phytopathol.* 50, 267–294. doi: 10.1146/annurev-phyto-081211-172955

Miedes, E., Vanholme, R., Boerjan, W., and Molina, A. (2014). The role of the secondary cell wall in plant resistance to pathogens. *Front. Plant Sci.* 5:358. doi: 10.3389/fpls.2014.00358

Molina, A., Miedes, E., Bacete, L., Rodríguez, T., Mélida, H., Denancé, N., et al. (2020). *Arabidopsis* cell wall composition determines disease resistance specificity and fitness. *Proc. Natl. Acad. Sci. U. S. A.* 118:e2010243118. doi: 10.1073/pnas.2010243118

Mouille, G., Ralet, M.-C., Cavelier, C., Eland, C., Effroy, D., Hématy, K., et al. (2007). Homogalacturonan synthesis in *Arabidopsis thaliana* requires a Golgi-localized protein with a putative methyltransferase domain. *Plant J.* 50, 605–614. doi: 10.1111/j.1365-313X.2007.03086.x

Müller, K., Levesque-Tremblay, G., Fernandes, A., Wormit, A., Bartels, S., Usadel, B., et al. (2013). Overexpression of a pectin methylesterase inhibitor in *Arabidopsis thaliana* leads to altered growth morphology of the stem and defective organ separation. *Plant Signal. Behav.* 8:e26464. doi: 10.4161/psb.26464

Nafisi, M., Fimognari, L., and Sakuragi, Y. (2015a). Interplays between the cell wall and phytohormones in interaction between plants and necrotrophic pathogens. *Phytochemistry* 112, 63–71. doi: 10.1016/j.phytochem.2014.11.008

Nafisi, M., Stranne, M., Fimognari, L., Atwell, S., Martens, H. J., Pedas, P. R., et al. (2015b). Acetylation of cell wall is required for structural integrity of the leaf surface and exerts a global impact on plant stress responses. *Front. Plant Sci.* 6:550. doi: 10.3389/fpls.2015.00550

Nielsen, K. A., Nicholson, R. L., Carver, T. L., Kunoh, H., and Oliver, R. P. (2000). First touch: an immediate response to surface recognition in conidia of Blumeria graminis. *Physiol. Mol. Plant Pathol.* 56, 63–70. doi: 10.1006/pmpp.1999.0241

O'Neill, M. A., Eberhard, S., Albersheim, P., and Darvill, A. G. (2001). Requirement of borate cross-linking of cell wall rhamnogalacturonan II for *Arabidopsis* growth. *Science* 294, 846–849. doi: 10.1126/science.1062319

Orgell, W. H. (1955). The isolation of plant cuticle with Pectic enzymes. *Plant Physiol.* 30:78. doi: 10.1104/pp.30.1.78

Persson, S., Paredez, A., Carroll, A., Palsdottir, H., Doblin, M., Poindexter, P., et al. (2007). Genetic evidence for three unique components in primary cell-wall cellulose synthase complexes in *Arabidopsis*. *Proc. Natl. Acad. Sci. U. S. A.* 104, 15566–15571. doi: 10.1073/pnas.0706592104

Philippe, G., Geneix, N., Petit, J., Guillon, F., Sandt, C., Rothan, C., et al. (2020). Assembly of tomato fruit cuticles: a cross-talk between the cutin polyester and cell wall polysaccharides. *New Phytol.* 226, 809–822. doi: 10.1111/nph.16402

Pollard, M., Beisson, F., Li, Y., and Ohlrogge, J. B. (2008). Building lipid barriers: biosynthesis of cutin and suberin. *Trends Plant Sci.* 13, 236–246. doi: 10.1016/j.tplants.2008.03.003

Raggi, S., Ferrarini, A., Delledonne, M., Dunand, C., Ranocha, P., De Lorenzo, G., et al. (2015). The *Arabidopsis* class III peroxidase AtPRX71 negatively regulates growth under physiological conditions and in response to cell wall damage. *Plant Physiol.* 169, 2513–2525. doi: 10.1104/pp.15.01464

Rebaque, D., Del Hierro, I., López, G., Bacete, L., Vilaplana, F., Dallabernardina, P., et al. (2021). Cell wall-derived mixed-linked β-1, 3/1, 4-glucans trigger immune responses and disease resistance in plants. *Plant J.* 106, 601–615. doi: 10.1111/tpj.15185

Reignault, P., Valette-Collet, O., and Boccara, M. (2008). The importance of fungal pectinolytic enzymes in plant invasion, host adaptability and symptom type. *Eur. J. Plant Pathol.* 120, 1–11. doi: 10.1007/s10658-007-9184-y

Reiter, W.-D., Chapple, C. C., and Somerville, C. R. (1993). Altered growth and cell walls in a fucose-deficient mutant of *Arabidopsis*. *Science* 261, 1032–1035. doi: 10.1126/science.261.5124.1032

Reiter, W.-D., Chapple, C., and Somerville, C. R. (1997). Mutants of *Arabidopsis thaliana* with altered cell wall polysaccharide composition. *Plant J.* 12, 335–345. doi: 10.1046/j.1365-313X.1997.12020335.x

Ritpitakphong, U., Falquet, L., Vimoltust, A., Berger, A., Métraux, J.-P., and L'Haridon, F. (2016). The microbiome of the leaf surface of *Arabidopsis* protects against a fungal pathogen. *New Phytol.* 210, 1033–1043. doi: 10.1111/nph.13808

Rui, Y., and Dinneny, J. R. (2020). A wall with integrity: surveillance and maintenance of the plant cell wall under stress. *New Phytol.* 225, 1428–1439. doi: 10.1111/nph.16166

Scheible, W.-R., Eshed, R., Richmond, T., Delmer, D., and Somerville, C. (2001). Modifications of cellulose synthase confer resistance to isoxaben and thiazolidinone herbicides in *Arabidopsis* Ixr1 mutants. *Proc. Natl. Acad. Sci.* 98, 10079–10084. doi: 10.1073/pnas.191361598

Schnurr, J., Shockey, J., and Browse, J. (2004). The acyl-CoA synthetase encoded by LACS2 is essential for normal cuticle development in *Arabidopsis*. *Plant Cell* 16, 629–642. doi: 10.1105/tpc.017608

Schuhegger, R., Nafisi, M., Mansourova, M., Petersen, B. L., Olsen, C. E., Svatoš, A., et al. (2006). CYP71B15 (PAD3) catalyzes the final step in camalexin biosynthesis. *Plant Physiol.* 141, 1248–1254. doi: 10.1104/pp.106.082024

Seo, P. J., Lee, S. B., Suh, M. C., Park, M.-J., Go, Y. S., and Park, C.-M. (2011). The MYB96 transcription factor regulates cuticular wax biosynthesis under drought conditions in *Arabidopsis*. *Plant Cell* 23, 1138–1152. doi: 10.1105/tpc.111.083485

Serrano, M., Coluccia, F., Torres, M., L'Haridon, F., and Métraux, J.-P. (2014). The cuticle and plant defense to pathogens. *Front. Plant Sci.* 5:274. doi: 10.3389/fpls.2014.00274

Sieber, P., Schorderet, M., Ryser, U., Buchala, A., Kolattukudy, P., Métraux, J.-P., et al. (2000). Transgenic *Arabidopsis* plants expressing a fungal cutinase show alterations in the structure and properties of the cuticle and postgenital organ fusions. *Plant Cell* 12, 721–737. doi: 10.1105/tpc.12.5.721

Somerville, C., Bauer, S., Brininstool, G., Facette, M., Hamann, T., Milne, J., et al. (2004). Toward a systems approach to understanding plant cell walls. *Science* 306, 2206–2211. doi: 10.1126/science.1102765

Stegmann, M., Monaghan, J., Smakowska-Luzan, E., Rovenich, H., Lehner, A., Holton, N., et al. (2017). The receptor kinase FER is a RALF-regulated scaffold controlling plant immune signaling. *Science* 355, 287–289. doi: 10.1126/science.aal2541

Survila, M., Davidsson, P. R., Pennanen, V., Kariola, T., Broberg, M., Sipari, N., et al. (2016). Peroxidase-generated apoplastic ROS impair cuticle integrity and contribute to DAMP-elicited defenses. *Front. Plant Sci.* 7:1945. doi: 10.3389/fpls.2016.01945

Tanaka, T., Tanaka, H., Machida, C., Watanabe, M., and Machida, Y. (2004). A new method for rapid visualization of defects in leaf cuticle reveals five intrinsic patterns of surface defects in *Arabidopsis*. *Plant J.* 37, 139–146. doi: 10.1046/j.1365-313X.2003.01946.x

Tang, D., Simonich, M. T., and Innes, R. W. (2007). Mutations in LACS2, a long-chain acyl-coenzyme A synthetase, enhance susceptibility to avirulent pseudomonas syringae but confer resistance to *Botrytis cinerea* in *Arabidopsis*. *Plant Physiol.* 144, 1093–1103. doi: 10.1104/pp.106.094318

Taylor, N. G., Howells, R. M., Huttly, A. K., Vickers, K., and Turner, S. R. (2003). Interactions among three distinct CesA proteins essential for cellulose synthesis. *Proc. Natl. Acad. Sci. U. S. A.* 100, 1450–1455. doi: 10.1073/pnas.0337628100

Taylor, N. G., Laurie, S., and Turner, S. R. (2000). Multiple cellulose synthase catalytic subunits are required for cellulose synthesis in *Arabidopsis*. *Plant Cell* 12, 2529–2539. doi: 10.1105/tpc.12.12.2529

Have, A.ten, Mulder, W., Visser, J., and van Kan, J. A. (1998). The endopolygalacturonase gene Bcpg1 is required for full virulence of *Botrytis cinerea*. *Mol. Plant Microbe. Interact.* 11, 1009–1016. doi:10.1094/MPMI.1998.11.10.1009

Vaahtera, L., Schulz, J., and Hamann, T. (2019). Cell wall integrity maintenance during plant development and interaction with the environment. *Nat. Plants* 5, 924–932. doi: 10.1038/s41477-019-0502-0

Verger, S. (2014). Genetic and chemical genomic dissection of the cell adhesion mechanisms in plants. Ph.D. dissertation (Paris).

Verger, S., Chabout, S., Gineau, E., and Mouille, G. (2016). Cell adhesion in plants is under the control of putative O-fucosyltransferases. *Development* 143, 2536–2540. doi: 10.1242/dev.132308

Verger, S., Long, Y., Boudaoud, A., and Hamant, O. (2018). A tension-adhesion feedback loop in plant epidermis. *Elife* 7:e34460. doi: 10.7554/eLife.34460

Voisin, D., Nawrath, C., Kurdyukov, S., Franke, R. B., Reina-Pinto, J. J., Efremova, N., et al. (2009). Dissection of the complex phenotype in cuticular mutants of *Arabidopsis* reveals a role of SERRATE as a mediator. *PLoS Genet.* 5:e1000703. doi: 10.1371/journal.pgen.1000703

Yeats, T. H., and Rose, J. K. C. (2013). The formation and function of plant cuticles. *Plant Physiol.* 163, 5–20. doi: 10.1104/pp.113.222737

Ziv, C., Zhao, Z., Gao, Y. G., and Xia, Y. (2018). Multifunctional roles of plant cuticle during plant-pathogen interactions. *Front. Plant Sci.* 9:1088. doi: 10.3389/fpls.2018.01088

Conflict of Interest: The authors declare that the research was conducted in the absence of any commercial or financial relationships that could be construed as a potential conflict of interest.

Publisher's Note: All claims expressed in this article are solely those of the authors and do not necessarily represent those of their affiliated organizations, or those of the publisher, the editors and the reviewers. Any product that may be evaluated in this article, or claim that may be made by its manufacturer, is not guaranteed or endorsed by the publisher.

frontiers in Plant Science

ORIGINAL RESEARCH
published: 22 September 2021
doi: 10.3389/fpls.2021.728627

Water Sorption and Desorption of Isolated Cuticles From Three Woody Species With Focus on *Ilex aquifolium*

Clara Vega, María Valbuena-Carabaña, Luis Gil and Victoria Fernández**

Departamento de Sistemas y Recursos Naturales, Universidad Politécnica de Madrid, Madrid, Spain

The cuticle is a lipid-rich layer that protects aerial plant organs against multiple stress factors such as dehydration. In this study, cuticle composition and structure in relation to water loss are examined in a broad ecophysiological context, taking into consideration leaf age and side from *Ilex aquifolium* (holly) in comparison with *Eucalyptus globulus* (eucalypt) and *Prunus laurocerasus* (cherry laurel). Enzymatically isolated cuticular membranes from holly leaves were studied under three treatment conditions: natural (no chemical treatment), after dewaxing, and after methanolysis, and the rate of water loss was assessed. Structural and chemical changes were evaluated using different microscopy techniques and by Fourier transform infrared (FTIR) spectroscopy. The potential mechanisms of solute absorption by holly leaves were additionally evaluated, also testing if its prickly leaf margin may facilitate uptake. The results indicate that the treatment conditions led to structural changes, and that chemical composition was hardly affected because of the occurrence of cutan. Structural changes led to more hydrophilic adaxial surfaces, which retained more water and were more efficient than natural cuticles, while changes were not significant for abaxial surfaces. Across natural cuticles, age was a significant factor for eucalypt but not for holly. Young eucalypt cuticles were the group that absorbed more water and had the lowest water loss rate. When comparing older leaf cuticles of the three species, cherry laurel was found to absorb more water, which was, however, lost more slowly, compared with the other species. Evidence was gained that holly leaves can absorb foliar-applied solutes (traced after calcium chloride application) through the adaxial and abaxial surfaces, the adaxial mid veins, and to a lower extent, the spines. In conclusion, for the species examined, the results show variations in leaf cuticle composition and structure in relation to leaf ontogeny, and water sorption and desorption capacity.

Keywords: cuticle, FTIR, holly, microscopy, leaf surfaces, water loss, cutan

OPEN ACCESS

Edited by:
Amauri Bueno, Julius Maximilian University of Würzburg, Germany

Reviewed by:
Aline Xavier De Souza, Julius Maximilian University of Würzburg, Germany
Shutang Tan, University of Science and Technology of China, China
Hua Huang, Chinese Academy of Sciences, China

****Correspondence:***
Clara Vega
clara.vega@upm.es
Victoria Fernández
v.fernandez@upm.es

Specialty section:
This article was submitted to Plant Physiology, a section of the journal Frontiers in Plant Science

Received: *21 June 2021*
Accepted: *19 August 2021*
Published: *22 September 2021*

Citation:
Vega C, Valbuena-Carabaña M, Gil L and Fernández V (2021) Water Sorption and Desorption of Isolated Cuticles From Three Woody Species With Focus on Ilex aquifolium. Front. Plant Sci. 12:728627. doi: 10.3389/fpls.2021.728627

INTRODUCTION

The cuticle is a protective epidermal layer of plants, located at the interface between plant organs and the surrounding environment (Kerstiens, 1996). The chemical and structural nature of the cuticle have been explained though different models over the years (Von Mohl, 1847; Holloway, 1982; Jeffree, 2006), but recent approaches have suggested to consider the cuticle as a lipidized part

of the epidermal cell wall (Domínguez et al., 2011; Guzmán et al., 2014a; Philippe et al., 2020). The cuticle is mainly composed of a cutin/cutan lipid polymer matrix, cell wall polysaccharides, and associated soluble lipids, also known as cuticular waxes (Holloway, 1982; Jeffree, 2006).

The two major components of the lipid polymer matrix are cutin [e.g., main compound in *Lycopersicon esculentum* (*Solanum lycopersicum*) fruit cuticles; Segado et al., 2016] and cutan (the most abundant lipid polymer in, e.g., *Beta vulgaris*; Nip et al., 1986a), or a mixture of both (e.g., *Prunus laurocerasus*; Tegelaar et al., 1991). Cutin is a biopolyester formed by polyhydroxy fatty acids, while cutan is thought to be an ether-linked network of methylene chains, double bonds, and carboxyl groups (McKinney et al., 1996; Villena et al., 1999; Jeffree, 2006). Recent studies suggest that cutan monomers are composed of very long aliphatic chains with different functional groups and a polymeric core of aromatic moieties (Leide et al., 2020). However, because of the high molecular weight and complexity of cutan, its chemical composition is still not fully characterized (Fich et al., 2016; Díaz et al., 2020). Cutan has also been described according to its resistance to degradation by increasingly harsh chemical treatments (Heredia-Guerrero et al., 2014; Leide et al., 2020).

Cutan presence was first reported in detail in *Agave americana* and *Clivia miniata* (Schmidt and Schönherr, 1982; Nip et al., 1986b; Villena et al., 1999), and since then, other species have been tested (Tegelaar et al., 1991; Mösle et al., 1998; Guzmán-Delgado et al., 2016). Cutan has been related to drought adaptation, as it enhances the hydrophobic nature of cuticles (Boom et al., 2005) and might be a target candidate to account for the rigid appearance of some cuticles (Bargel et al., 2006). Furthermore, cutan-containing species are thought to follow strategies such as CAM photosynthesis or a thicker cuticle, which would prevent water loss more effectively. However, thick evergreen leaves or succulence alone do not correlate with cutan presence (Boom et al., 2005; Gupta et al., 2006).

Plant cuticles are also composed of polysaccharides and additional non-polymer lipids, such as waxes (soluble cuticular lipids) (Jeffree, 2006). The inner side of the cuticle is rich in cellulose, hemicellulose, and pectin, which are the most abundant epidermal cell wall polysaccharides (Guzmán et al., 2014a,b; Segado et al., 2016; Philippe et al., 2020). Soluble lipids are located either on the cuticle surface (epicuticular waxes) or distributed within the cuticle (intracuticular waxes) (Jeffree, 2006). A mixture of different long-chain aliphatic molecules, such as alkanes, alcohols, aldehydes, fatty acids, and esters, are present in the cuticle, together with variable amounts of cyclic compounds (Jetter and Riederer, 2016). There is controversy about the role of intra- vs. epi-cuticular waxes as barrier to leaf transpiration (Jetter and Riederer, 2016; Zeisler-Diehl et al., 2018; Zhang et al., 2021), but recent evidence suggests that their importance may be specific to leaf side (Zhang et al., 2020) and species, which respond plastically to drought (Chen et al., 2020; Sanjari et al., 2021). Additionally, variable amounts of phenolic compounds have been recovered in the cuticle of different organs and plant species (Karabourniotis and Liakopoulos, 2005; España et al., 2014).

The genus *Ilex* is present throughout temperate and tropical regions worldwide (Galle, 1997). The only species present in Spain is *Ilex aquifolium* L. (English holly or holly), an evergreen broad-leaved, small dioecious tree. Holly inhabits northern areas as well as some locations in central mountain ranges where the conditions are more humid. This species has been described to have an all-reticulate thick leaf cuticle (Holloway and Baker, 1970), with fibrils reaching the outer surface without a distinct cuticle proper (CP) (Holloway, 1982; Jeffree, 2006). Cuticle morphological characteristics (Jeffree, 2006), cutin description (Holloway and Baker, 1970), cuticle water loss (Burghardt and Riederer, 2003), and cuticle mechanical properties (Khanal et al., 2013) have been examined in previous reports. However, various aspects related to holly leaf cuticle composition, structure, and permeability are not fully understood to date.

The cuticle can be considered a composite membrane made of hydrophobic lipids (chiefly cutin/cutan, waxes, and minor phenol amounts) and hydrophilic polysaccharides (Fernández et al., 2016). The bi-directional transport of water and solutes across the cuticle has been associated with the occurrence of polysaccharides (Chamel et al., 1991; Reina et al., 2001; Riederer, 2006). However, the nano-structural arrangement remains unclear (e.g., Philippe et al., 2020; Segado et al., 2020). Furthermore, environmental factors such as temperature and/or relative humidity (RH) will affect the physicochemical properties of cuticle components (Schönherr and Schmidt, 1979; Domínguez et al., 2011), affecting water transport (i.e., transpiration and water absorption) across the epidermal cell wall (Fernández et al., 2021).

Water deposited onto the leaves after rain, dew, or fog exposure will interact with the surface and condense as films or drops depending on wettability (Fernández et al., 2021). Leaf water condensation has great importance in arid and semiarid regions and can contribute to fog harvesting and water delivery to the roots (Fernández et al., 2021), helping plants cope with water shortage (Malek et al., 1999; Holanda et al., 2019). The site of study, Montejo forest, is located in a valley, which likely causes dew formation during nocturnal cooling (Merinero et al., 2015). Some studies have demonstrated that spines can direct dew from their tips to their bases to help moisturize the plant (Malik et al., 2016), so we aim to evaluate if holly spines may play a role in retaining dew moisture, thus helping the plant to cope with dry season environmental conditions.

The main objective of this study was to examine the potential link between cuticle composition and structure in relation to water loss in a broad ecophysiological context, taking into consideration leaf age and side from holly in comparison with other two species: *Eucalyptus globules* Labill. (blue gum eucalypt or eucalypt) and *P. laurocerasus* L. (cherry laurel). Both sides of young and old cuticles subjected to treatments were evaluated to estimate their water loss rate. Finally, the potential mechanisms of solute absorption by holly leaves were evaluated, also testing if its prickly leaf margin may facilitate foliar absorption.

MATERIALS AND METHODS

Plant Material and Experimental Conditions

Holly leaves were collected in "El Hayedo de Montejo" forest, approximately 90 km north of Madrid, in central Spain (3°30′W, 41°07′N). Montejo is a sub-Mediterranean beech-oak mixed forest, protected according to regional laws. As an average (1994–2019 record), mean annual temperatures correspond to 10°C and annual precipitations to 876 mm. Maximal rainfall occurs in spring (May) and autumn (November) and there is a dry summer season in June, July, and August, where the average precipitation and temperature values are 153.7 mm and 16.7°C (see González, 2015, for 1994–2013 period; 2013–2019 period is unpublished data).

Blue gum eucalypt and cherry laurel leaves were collected from the Forest Engineering School Arboretum (Technical University of Madrid, Spain). Young leaves (sprouted in the year of collection) and old leaves (sprouted in previous years) were collected and taken to the laboratory. Then, leaf margins and mid ribs were removed with a scalpel. For cuticle isolation, leaf sections were immersed in a solution of 5% cellulase, 5% pectinase (Novozymes, Bagsvaerd, Denmark), 1% polyvinylpyrrolidone (Sigma–Aldrich, Munich, Germany), and 2 mM sodium azide set to pH 5 with sodium citrate (Guzmán et al., 2014b) for 1 month. The adaxial and abaxial sides of the leaves were studied separately. Cuticular waxes were removed from the isolated cuticles (500 mg) using a 2:1-(v/v) chloroform: methanol mixture for 24 h at 23°C and 45 rpm speed in an orbital shaker. We used a fraction of the dewaxed cuticles (150 mg) for the methanolysis procedure, as described by Graça and Pereira (2000) for a combined dewaxing-methanolysis treatment.

Electron Microscopy

Adaxial and abaxial cuticles isolated from the old and young leaves were examined either naturally (i.e., directly after enzymatic isolation) or after chemical treatment (named as D: dewaxed; M: dewaxed and methanolysis). The spines occurring in the leaf margin were analyzed by different microscopy techniques. Scanning electron microscopy (SEM) was performed to explore surface features, while transmission electron microscopy (TEM) enabled us to observe cell wall ultrastructure in epidermal cross sections. For simplicity, cell walls were analyzed in terms of lipidic layer and polysaccharides layer (Fernández et al., 2016). Light optical microscopy (LM) was performed (Zeiss Axioplan II; Carl Zeiss, Jena, Germany) to examine the epidermal cell wall and leaf mesophyll cross sections, and to measure the thickness of different cell wall layers. Cuticle thickness was measured with a micrometer (4,000/F; Baxlo, Barcelona, Spain) (two repetitions per sample).

For SEM and TEM observations, the cuticles were cut into 4 mm^2 pieces and fixed in 2.5% glutaraldehyde-4% paraformaldehyde (both from Electron Microscopy Sciences [EMS], Inc. Hatfield, PA, United States) for 6 h at 4°C, rinsed in an ice-cold phosphate buffer, pH 7.2, four times within a period of 6 h, and left overnight. The samples for SEM analysis were then dehydrated in an increasing absolute ethanol (Sigma–Aldrich, Munich, Germany) series (30, 50, 70, 80, 90, and 100%; three times for each concentration). They were subsequently subjected to critical point drying (Leica EM CPD300; Leica Microsystems, Wetzlar, Germany). Prior to observation, the samples were gold-sputtered and then examined with a JEOL JSM-6400 microscope (JEOL Ltd., Tokyo, Japan).

For TEM, fixed tissues were also rinsed in the ice-cold phosphate buffer, pH 7.2, four times within a period of 6 h and left overnight. Next morning, the samples were post-fixed for 1.5 h in a 1:1 water and 2% osmium tetroxide (TAAB Laboratories, Berkshire, United Kingdom) solution containing 3% potassium ferrocyanide (Sigma-Aldrich, Munich, Germany). Then, they were washed with distilled water (three times), dehydrated in a graded series of acetone 30, 50, 70, 80, 90, 95, and 100% (twice, 15 min for each concentration) and embedded in acetone-Spurr's resin (TAAB Laboratories, Berkshire, United Kingdom) mixtures (3:1, 2 h; 1:1, 2 h; 1:3, 3 h) and in pure resin overnight (kept at 25°C). Pure resin sample embedding was carried out in blocks that were incubated at 70°C for 3 days. Finally, semi-thin sections were cut, mounted on nickel grids, and post-stained with Reynolds lead citrate (EMS, Inc., Hatfield, PA, United States) for 5 min prior to observation with a JEOL JEM 1010 electron microscope (JEOL Ltd., Tokyo, Japan) at 80 kV and equipped with a CCD camera (Megaview II, Olympus, Japan) (Bahamonde et al., 2018).

Image analysis was carried out with the ImageJ1.52a software (National Institutes of Health, Bethesda, MD, United States) to measure stomatal density and stomatal percentage in total abaxial surface and cuticle and epidermal cell wall thickness of all the groups. Measurements were carried out at periclinal areas on 10 micrographs per sample, with 20 repetitions.

Fourier Transform Infrared Spectroscopy

Fourier transform infrared spectroscopy is a technique that has proven to be useful for cutane valuation in plant cuticles (Johnson et al., 2007; Fernández et al., 2011; Leide et al., 2020); thus, we used it to study holly cuticle composition. Infrared spectra of all the groups were obtained with an attenuated total reflectance (ATR) accessory (MIRacle ATR; PIKE Technologies, Madison, WI, United States) coupled to an FTIR spectrometer (Nicolet Nexus 670/870; Thermo Fisher Scientific, Waltham, MA, United States). The spectra of the samples were recorded in transmission mode in the range 4,000–400 cm^{-1} (with 4 cm^{-1} resolution accumulating 64 scans) and were analyzed with the Omnicv4.1b (Thermo Fisher Scientific, Waltham, MA, United States) software (Guzmán-Delgado et al., 2016). Both sides of the young and old cuticles by the different treatments (isolated intact cuticles, dewaxed cuticles, and post-methanolysis cuticles) were analyzed.

The esterification index is an indicator of how esterified a cutin matrix is, calculated as the ratio between the ester functional group ν(C=O) and the asymmetric vibration of the methylene functional group reflecting the cross-linking of cutin monomers $\nu_a(CH_2)$. The index is directly related to the cross-linking of cutin, and high values of this ratio imply a higher esterification

degree (Benítez et al., 2004; Girard et al., 2012; Heredia-Guerrero et al., 2014).

Water Loss

The cuticles were weighed after dehydration and after immersion in distilled water for 1 h. Subsequently, the surface of the rehydrated cuticles was gently blotted with soft paper tissue to remove superficial water, and the cuticles were left to air dry, controlling RH and temperature throughout the measuring process. Re-hydrated cuticular water loss was gravimetrically monitored after surface water removal, every 2 min for the first 30 min, every 5 min for the next hour, and every 10 min during the last hour. Measurements were taken for the 12 different groups: young and old leaf cuticles, both adaxial and abaxial side cuticles, and cuticles subjected to different treatments: untreated, dewaxed, and combined dewaxed-methanolysis (two repetitions per group).

For analysis, we adjusted weight-time data to an exponential decay model. The variables studied were: coefficient beta (β), which represents the slope of the decay model, being lower when the water loss curve drops more quickly; Tseca, which is the time (in min) required to reach the asymptote in the decay model; and absorbed, which is the water absorbed in an hour of being submerged in relation to dry weight (%). We also evaluated if temperature or RH influenced the data.

First, we evaluated how the treatments affected water loss in the holly cuticles. Then, the rate of water loss in the natural holly cuticles was compared with that in the eucalypt and cherry laurel cuticles. Blue gum eucalypt lacks cutan (Guzmán et al., 2014a), while cherry laurel contains both cutin and cutan. Cutan is associated with the residue obtained after cuticle solvent extraction and acid-catalyzed transesterification (Tegelaar et al., 1991; Leide et al., 2020). The adaxial eucalypt cuticles were compared with the holly cuticles to study which aspects may vary in the absence of cutan, taking age into account. Furthermore, holly, cherry laurel, and eucalypt adaxial old cuticles were compared to assess species factor.

Foliar Solute Absorption

We aimed to determine if different holly leaf areas, such as spines, may contribute to the process of solute absorption. First, we used a contact angle meter (DSA 100; Krüss, Hamburg, Germany) to observe the wettability by the water of drops deposited onto different leaf areas, such as spines. Second, using Ca-chloride (Sigma-Aldrich, Munich, Germany) as tracer, we evaluated spine solute absorption in comparison with other leaf parts, namely, the adaxial lamina, abaxial lamina, and adaxial mid vein, by implementing the procedure described by Bahamonde et al. (2018). In brief, leaves were selected and marked in two adult individuals, also selecting a group of untreated control leaves. Early in the morning (around 8 a.m.), using a micro-syringe, drops of approximately 3–4 μl 150 mM $CaCl_2$ were applied on leaves still attached to the trees, carefully depositing them onto the mid nerves and spines, but using a brush for both lamina surfaces. After 24 h, the Ca-treated and untreated leaves were detached from the trees and were taken to the laboratory. They were thoroughly washed in an acidulated (0.1 N HCl) 0.1% detergent solution, followed by abundant tap water and two baths of distilled water. The washed leaves were then left to dry at ambient temperature for 1 h, and were subsequently dried in a stove at 50°C for 72 h. The dry leaves were ground to powder and analyzed by inductively coupled plasma-optical emission spectrometry (ICP-OES) to determine tissue Ca concentrations in the treated and untreated holly leaves.

Data Analysis

Statistical analyses were carried out using the R software (R Core Team, 2013). The data analysis included normality and homoscedasticity tests for the different traits evaluated. Normality was assessed by Shapiro–Wilk test (Razali and Wah, 2011) and homoscedasticity by Fligner–Kileen test. If data were normal and homoscedastic, an ANOVA and a *post-hoc* Tukey's HSD test would be conducted. Otherwise, a non-parametric Kruskal-Wallis test and a pairwise Willcoxon test would be carried out to evaluate differences among the groups.

RESULTS

Leaf Structure and Surface Topography

Leaf thickness had an average value of 442.29 ± 11.33 μm, spongy mesophyll was arranged in columns with large intercellular spaces, and there was a two-to-three-layer palisade parenchyma. A hypodermis is also present in the adaxial side under the epidermis (**Figure 1**). Regarding cell wall structure, the old leaves had a thicker lipidic layer, while the younger leaves had a thicker layer of polysaccharides (**Figure 2**). Furthermore, cell wall width values of the old leaves are more dispersed, with the adaxial side being higher than the abaxial side (**Table 1**). Stomatal leaf density did not significantly vary with age, having young leaves an average of 150.39 ± 20.77 while old leaves had 151.22 ± 15.74 stomata mm^{-2}.

The prickly part of the leaves (i.e., the spines) has an epidermis covered with a cuticle of similar appearance to the one of the leaf lamina (**Figure 1**). Spine epidermal cells are separated from a ring of stone cells (sclerenchyma, which surrounds the vascular bundle), by an area of intercellular space. Hence, the main fundamental tissue present in the spines is sclerenchyma in the form of stone cells surrounding the vascular bundle.

Cuticle Response to Treatments

The treatments significantly affected cuticle structure and composition. The thickness of the natural cuticles (0.032 ± 0.007 mm) decreased by half after dewaxing (0.018 ± 0.008 mm) and by approximately another half after methanolysis (0.008 ± 0.004 mm). Age also affected natural cuticle thickness, increasing adaxial side thickness (from 0.030 to 0.037 mm) but leading to a decrease in the thickness of the abaxial side (from 0.036 to 0.026 mm), which was more affected by dewaxing.

Furthermore, SEM images showed that adaxial cuticle dewaxing (i.e., wax removal, see the gray areas between white colored cell walls, **Supplementary Figure 1**) was more effective in the young leaves than in the older ones. Methanolysis caused a similar effect on cuticles isolated from both the old and young leaves, which acquired a hollow structure associated

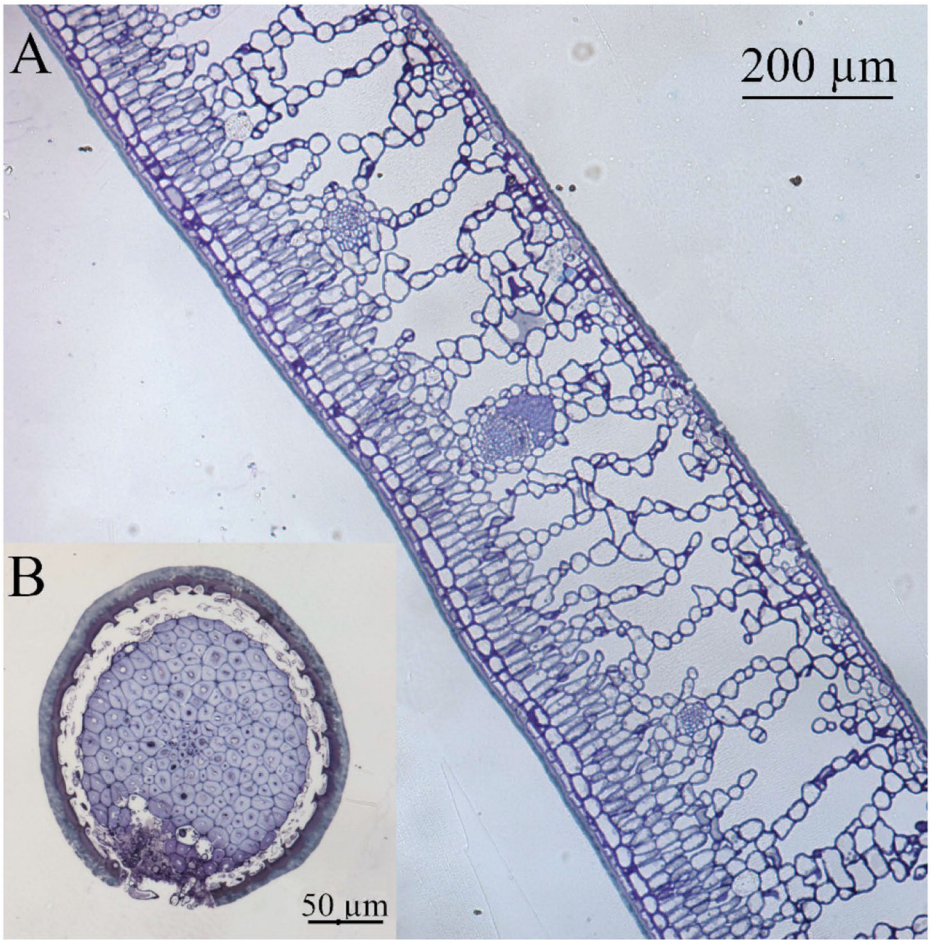

FIGURE 1 | Light microscopy cross section of **(A)** holly leaf and **(B)** spine, both showing a thick cuticle as interface with the surrounding environment. Tissues were stained with Toluidine blue.

with an epidermal cell contour (**Supplementary Figure 1**). The abaxial cuticle structure was also affected by chemical treatment, mainly by the removal of cuticle materials in patches and especially in areas around stomata. However, after dewaxing and methanolysis, waxes and ester links were not completely removed, as derived from the different colors observed in residual patches (**Supplementary Figure 2**).

Regarding cuticle composition, a higher proportion of material was extracted by dewaxing (from 24 to 29%) compared with the effect of methanolysis (from 3 to 8%), this proportion being higher for the abaxial leaf cuticles compared with the adaxial ones.

Spectroscopic Characterization

Absorbance values from the different FTIR bands are shown for the adaxial and abaxial (**Figure 3**) cuticles, comparing the effect of age and chemical treatments. The results showed that after dewaxing and methanolysis, cuticle composition still included the main groups belonging to cutin, waxes, polysaccharides, and esters. Only one band related to fatty acids (1,688 cm^{-1}) was strongly affected in all the groups, and there was a very small effect on glycosidic bonds typical of polysaccharides (1,000 and 1,030 cm^{-1}) for the old adaxial side leaves (**Figure 3**).

The cutin esterification index was significantly lower in the younger leaves (0.3418 ± 0.0899) compared with that in the older leaves (0.4609 ± 0.1791), where the ester bands (1,103, 1,167, and 1,733 cm^{-1}) were strongest (**Figure 3**). The highest index values were recorded for the dewaxed cuticles (0.529 ± 0.1155), and the lowest values were determined for the untreated cuticles (0.263 ± 0.035) and leaf side did not affect index values. Thus, dewaxing was more effective in the young cuticles, and the combined treatment was more effective for the old cuticles.

Water Loss

Water loss measurements showed that cuticle weight decreased according to an exponential decay model with the equation: $y = \alpha e^{\beta x} + \theta$, where α, β, and θ are coefficients, x is time, and y is weight. Neither temperature nor RH had a significant influence on the trials developed. Age and treatment only led to significant changes for the adaxial leaf cuticles (**Figure 4**).

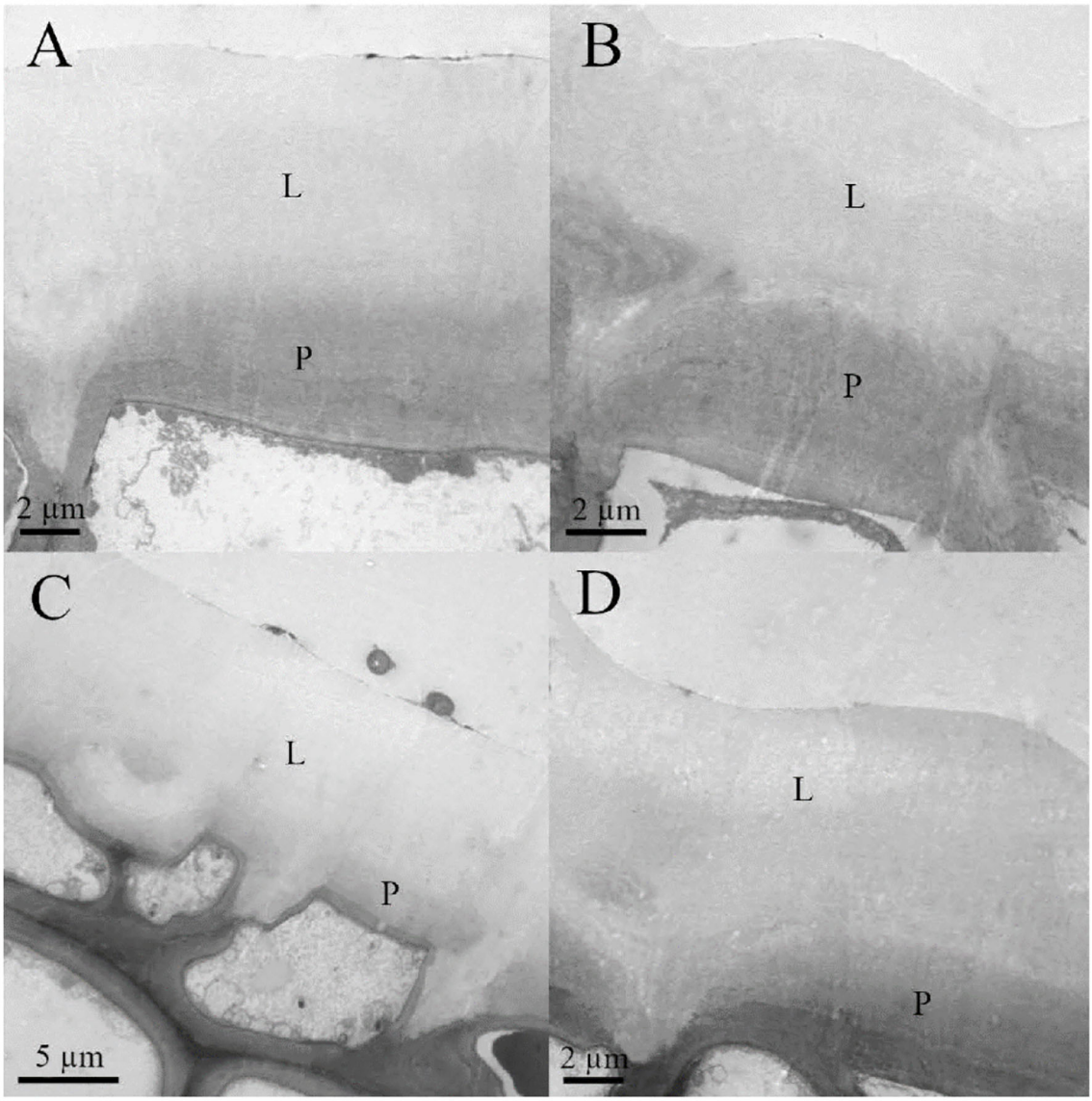

FIGURE 2 | Transmission electron microscopy (TEM) micrographs of **(A)** adaxial young, **(B)** abaxial young, **(C)** adaxial old, and **(D)** abaxial old English holly leaves. Lipidic fraction (L) and polysaccharides fraction (P) of the cell wall are shown.

TABLE 1 | Thickness of different external epidermal cell wall areas.

Side	Age	Lipidic fraction (μm)	Polysaccharide fraction (μm)	Total cell wall (μm)
Adaxial	Young	7.66 ± 0.39b	4.51 ± 0.40a	12.64 ± 0.37a
	Old	11.80 ± 1.41a	0.70 ± 0.20b	12.45 ± 1.47ac
Abaxial	Young	6.14 ± 0.78b	4.45 ± 0.60a	10.60 ± 0.50b
	Old	8.01 ± 0.84a	3.02 ± 1.36a	11.04 ± 1.21bc
Differences	Age	***	***	
	Side	**		***

*Data are means ± SD (n = 30). Within columns and for the same species, values marked with different letters are significantly different according to Tukey's HSD test (P ≤ 0.05). Significance codes: 0 "***" 0.001 "**" 0.01 "*" 0.05 "." 0.1 " " 1.*

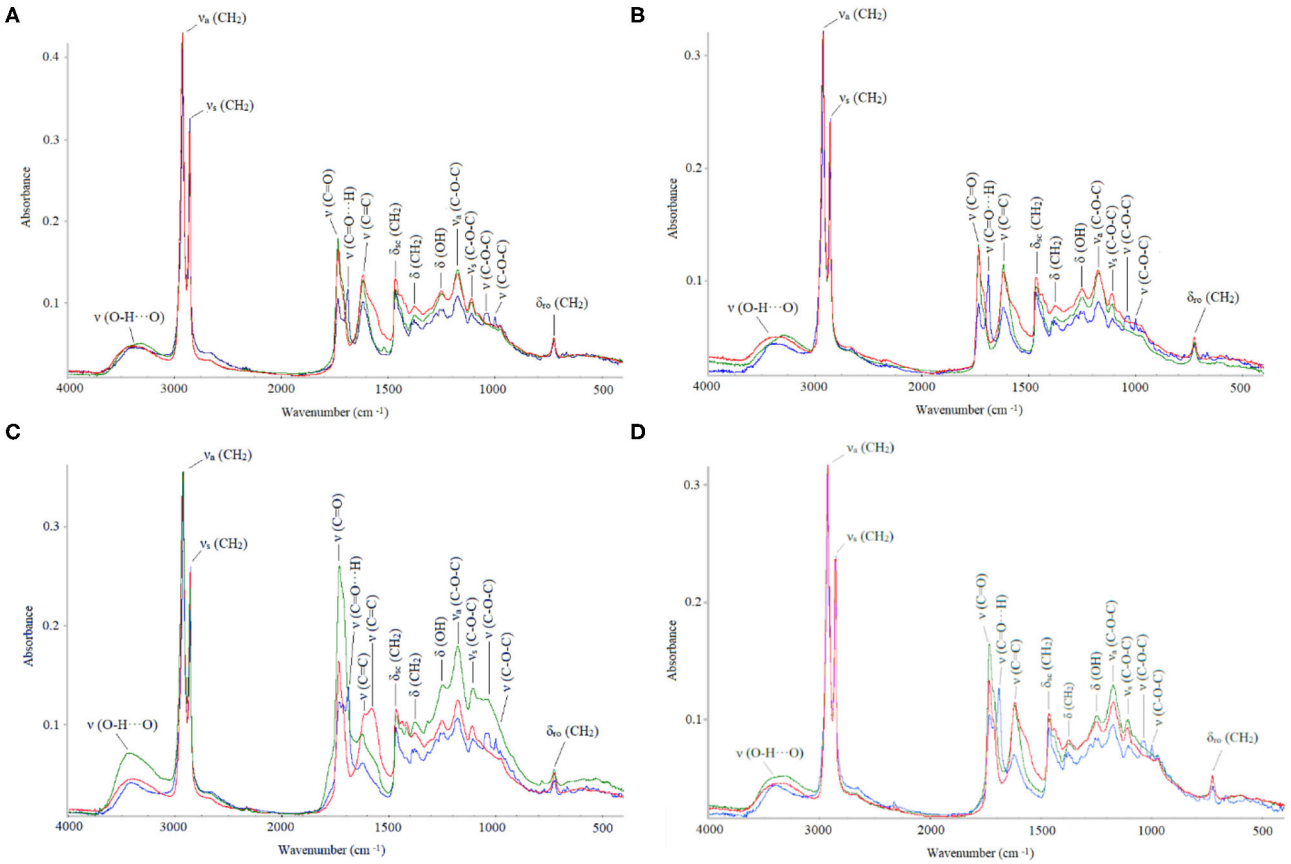

FIGURE 3 | Fourier transform infrared (FTIR) absorbance values (in cm^{-1}): natural (blue), dewaxed (green), and combined treatment (red). **(A)** Adaxial young, **(B)** abaxial young, **(C)** adaxial old, and **(D)** abaxial old cuticles.

Treatment increased the total dry time and decreased the water loss rate, while age increased the total dry time. Total absorbed water only varied slightly across the different groups (**Table 2**).

When comparing natural adaxial cuticles of the holly and eucalypt, we found that decrease rate varied with age in eucalypt but not in holly (**Figure 5**). The young Eucalypt cuticles had a steeper decay curve and a higher total dry time, but the total water absorbed was similar in both species (**Table 3**). We also compared the old natural adaxial cuticles of holly, eucalypt, and cherry laurel. The results showed that the cherry laurel cuticles were significantly different (**Figure 5**), losing water faster but also taking more time to fully dry than the other two species. Regarding the total water absorbed, holly and cherry laurel absorbed a greater amount of water than eucalypt (**Table 4**).

Foliar Solute Absorption

We found significant differences between the Ca concentration of the untreated leaves of holly and the other three groups supplied with Ca-chloride *via* different leaf parts (**Figure 6**). The spines were found to have adhesion for water and aqueous solution drops deposited with the syringe of the drop shape analysis system, subsequently, $CaCl_2$ drops, which had been carefully hanged to the spines attached leaves with a micro-syringe led to low tissue Ca increases, which were only slightly higher than those found in the untreated control leaves. The highest rate of Ca absorption was recorded after adaxial leaf surface treatment. Calcium solution drop deposition onto the central veins led to tissue Ca concentrations within the same range of leaves treated with Ca *via* the abaxial surface.

DISCUSSION

In this study, we attempted to establish a link between water loss, cuticular gross chemical composition, and inner structure by comparing the performance of three different species. As noted in previous studies (e.g., Chamel et al., 1991), it is not simple to establish a cause-effect relationship regarding cuticle composition, structure, and water transport, which is likely because of the limited understanding of nanoscale cuticle complexity and variability among the species. These aspects are not easy to trace, because there is an array of methodological and experimental constraints (Fernández et al., 2021). However, using selective chemical treatments and various methodologies can help us gain some ecophysiological insights into the topic (e.g., Chamel et al., 1991; Kerstiens, 2006; Leide et al., 2020). For example, for the adaxial leaf cuticles,

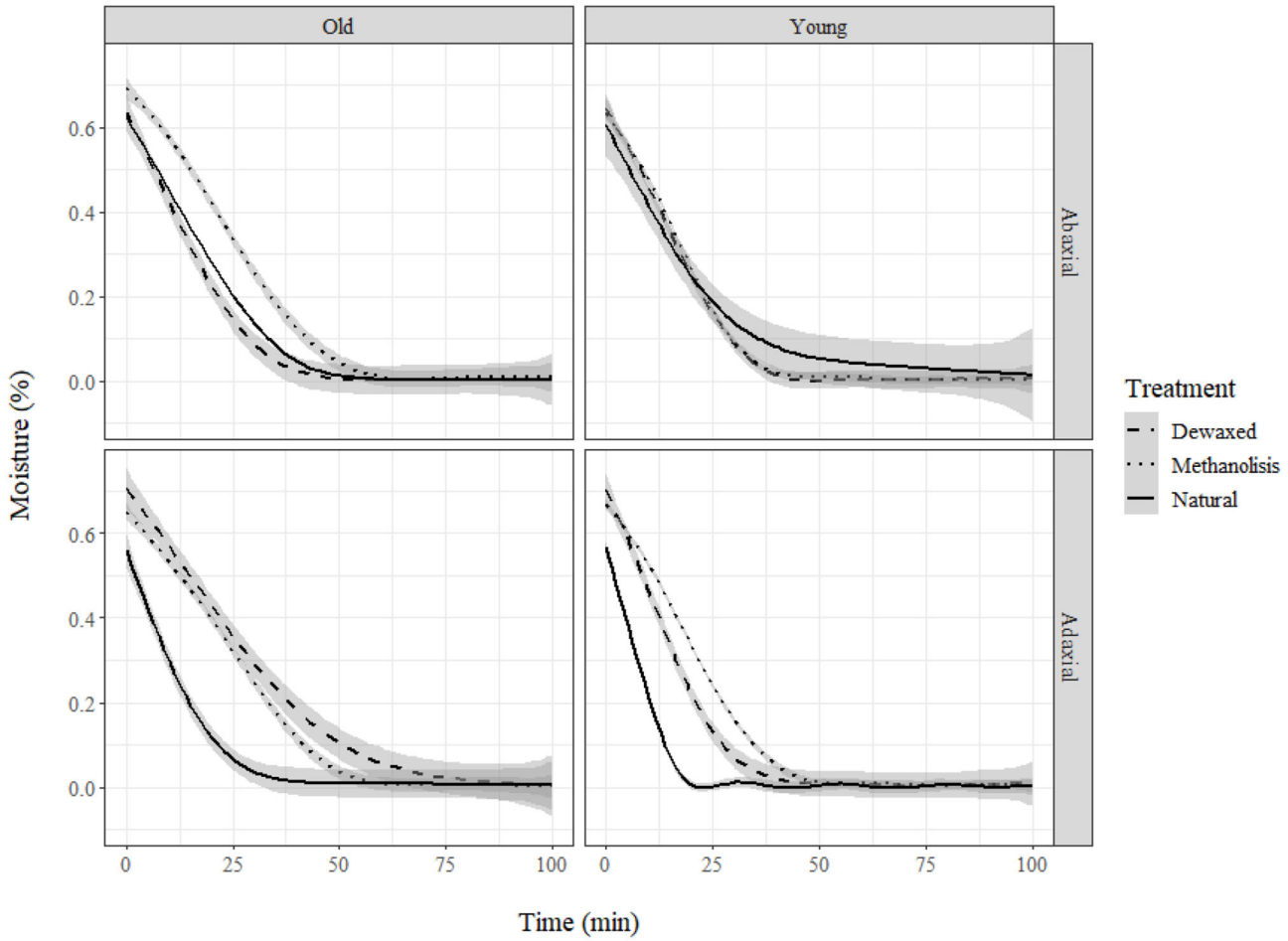

FIGURE 4 | Moisture loss (%) in holly cuticles depending on age, side, and treatment.

TABLE 2 | Transpiration parameters of holly leaf adaxial cuticles, as affected by chemical treatment and age.

Age	Treatment	Beta (β)	tseca (min)	Absorbed (%)
Young	Natural	−1.76 ± 0.08a	21 ± 1.4a	124.4 ± 8.4a
	Dewaxed	−2.25 ± 0.11ab	42.5 ± 3.5ab	176.0 ± 20.9a
	D–Methanolysis	−2.65 ± 0.01b	50 ± 0.0b	184.8 ± 16.2a
Old	Natural	−2.06 ± 0.36a	29.5 ± 7.8a	130.2 ± 9.3a
	Dewaxed	−2.91 ± 0.31b	60.0 ± 14.1b	196.0 ± 60.8a
	D–Methanolysis	−2.91 ± 0.07b	57.5 ± 3.5b	170.5 ± 8.8a
Differences	Age	.	*	
	Treatment	**	**	*

*Data are means ± SD (n = 30). Within columns and for the same age, values marked with different letters are significantly different according to Tukey's HSD test (P ≤ 0.05). Significance codes: 0 "***" 0.001 "**" 0.01 "*" 0.05 "." 0.1 " " 1.*

we observed no effect of leaf age on the water absorption capacity of holly, while the upper cuticle of the younger eucalypt leaves absorbed more water than the older ones. For both species and leaf age, we observed chemical and structural changes before and after chemical treatment, but the scenario is so complex that we cannot clearly associate cuticular water transport with cuticular chemical composition and ultrastructure. In the following paragraphs, the results obtained will be discussed in light of existing information on cuticle composition and structure in an ecophysiological background, considering also their relevance for foliar water absorption and leaf transpiration.

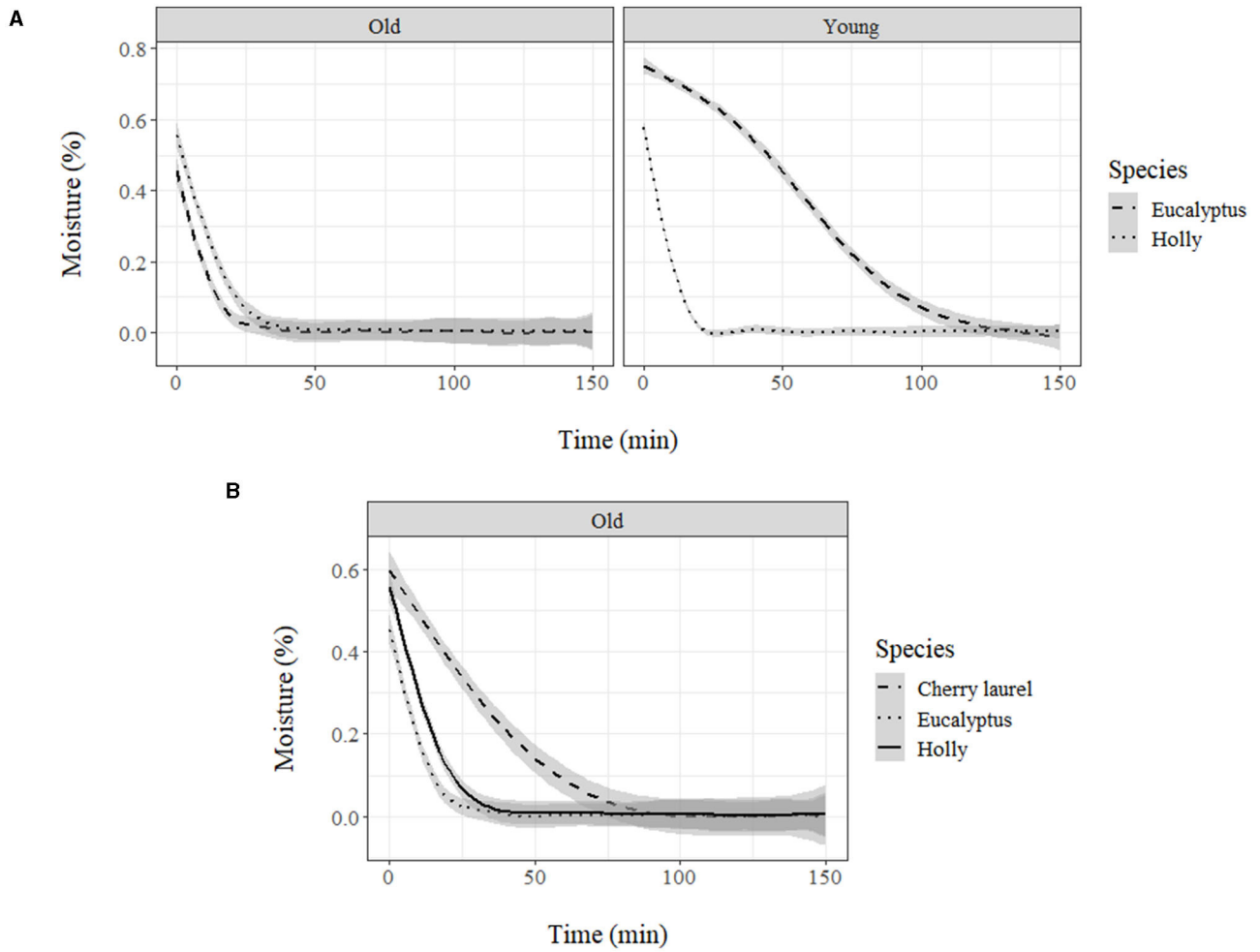

FIGURE 5 | (A) Moisture loss (%) of holly and eucalyptus young and old adaxial side cuticles and **(B)** moisture loss (%) of holly, eucalyptus, and cherry laurel old adaxial side cuticles.

TABLE 3 | Transpiration parameters of natural adaxial cuticles isolated from holly and blue gum eucalypt leaves.

Species	Age	Beta (β)	tseca (min)	Absorbed (%)
Holly	Young	−1.75 ± 0.08a	21.0 ± 1.4a	124.4 ± 8.4a
	Old	−2.06 ± 0.36a	29.5 ± 7.8a	130.2 ± 9.3a
Eucalypt	Young	−3.83 ± 0.07a	105.0 ± 7.1a	152.2 ± 22.1a
	Old	−1.90 ± 0.43b	26.5 ± 12.0b	91.1 ± 10.1b

Data are means ± SD (n = 30). Within columns for the same species, values marked with different letters are significantly different according to Tukey's HSD test (P ≤ 0.05).

Holly Leaf Characterization

Holly leaves have a thick cuticle, which is richer in lipids in older leaves and more abundant in polysaccharides in younger ones. Total cell wall and cuticle thickness were significantly higher in the adaxial side, as previously observed for other species (Gratani et al., 2006; Verdaguer et al., 2012; Vega et al., 2020), and age did not significantly affect thickness, which is in accordance with previous reports (Riederer and Schönherr, 1988; Viougeas et al., 1995; Guzmán-Delgado et al., 2016).

After dewaxing, cuticle thickness decreased, indicating that we had at least altered the composition and structure of some cuticle areas. We extracted 24% of soluble lipids, an amount comparable with other cutan-containing species (Guzmán-Delgado et al., 2016). Age was not a significant factor in terms of soluble lipid extraction, possibly because wax production ceases when the leaf becomes fully expanded, and in the present study, the leaves were sampled well after this developmental stage (Chamel et al., 1992).

Methanolysis was not as effective as expected, because ester bands were identified after this de-esterification treatment, with the occurrence of FTIR bands of similar or higher intensity in natural, dewaxes and de-esterified cuticles. The increase in ester bands could be related to the exposure of internal layers with

higher presence of ester bonds. Cutin esterification index was higher in old leaves as part of the cutin polymerization process (Heredia-Guerrero et al., 2020). Cutin esterification index might be related to biomechanical properties of the cuticle, allowing cell enlargement during development according to studies on tomato fruit (España et al., 2014).

Effect of Cuticle Chemical Treatment

Age and chemical treatment only led to significant changes in the thickness of the adaxial leaf cuticles of holly. Dewaxing affected adaxial side structure (as observed in SEM images) and thickness, resulting in a thinner cuticle but with a better capacity to retain water after a preliminary step of water sorption. A possible explanation for this can be that the extraction of lipids can lead to a more hydrophilic cuticle, hence favoring the retention of water.

Dewaxing and methanolysis affected the adaxial cuticle of the old leaves by reducing fatty acids interacting *via* strong hydrogen bonds (Heredia-Guerrero et al., 2014). Hydroxy fatty acids are highly present in holly cutin (Baker, 1970) but other bands related to cutin and waxes still occurred (720, 1,103, 1,167, 1,244, 1,377, 1,466, 1,688, 1,733, 2,844, and 2,930 cm^{-1}) after chemical treatment. The 720-cm^{-1} band is associated with CH_2 rocking vibration in long chain aliphatic substances (Guo and Bustin, 1998; Heredia-Guerrero et al., 2014) and the 1,377- and 1,466-cm^{-1} bands are bending vibrations of the methyl and methylene groups of fatty acids (Oleszko et al., 2015). Besides, the 1,244- and 1,103-cm^{-1} peaks can be related to C–O modes in secondary alcohols present in cutin (Marechal and Chamel, 1996), while 1,167-cm^{-1} peak can be assignedd to C–O (stretching) vibrations of ester groups, since they contain the majority of C–O groups. The simultaneous presence of aliphatic $\nu(CH_2)$ stretching bands at 2,930 and 2,844 cm^{-1} and $\delta(CH_2)$ bands at 1,466, 1,377, and 720 cm^{-1} can be related to esterified aliphatics (Zeier and Schreiber, 1999). Cutin bands were stronger in the adaxial side of both young and old leaves, as also reported by España et al. (2014).

Regarding waxes, Van Genderen et al. (1988) claimed that young leaves of holly were mainly composed of alkanes and esters of long-chain fatty acids. The smaller ester peak observed in older leaves could be a result of fatty acid-esters being used to synthesize alkanes. Furthermore, Niemann and Baas (1985) argued that old leaves have a more polar composition as saturated long-chain hydrocarbons start to accumulate during leaf extension.

Glycosidic bonds ν(C–O–C) were also affected by both treatments but only in the adaxial side of old leaves. Johnson et al. (2007) and Mazurek et al. (2017) associated the 1,030-cm^{-1} peak with cuticular polysaccharides, while Türker-Kaya and Huck (2017) related the peak with O–H and C–OH stretch related to cell wall polysaccharides (arabinan, cellulose). Other bands related to polysaccharides were at 1,000 and 1,622 cm^{-1}. Some authors claimed that the peaks at 1,000 $cm^{-1}$are due to aliphatic CH_2 wagging vibrations in alkenes (Guo and Bustin, 1998), and

TABLE 4 | Transpiration parameters of natural adaxial cuticles isolated from old holly, blue gum eucalypt, and cherry laurel leaves.

Species	Beta (β)	tseca (min)	Absorbed (%)
Holly	−2.06 ± 0.36a	29.5 ± 7.8a	130.2 ± 9.3b
Eucalypt	−1.90 ± 0.43a	26.5 ± 12.0a	91.1 ± 10.1a
Cherry laurel	−3.17 ± 0.45b	75.0 ± 21.2b	152.16 ± 22.1b

Data are means ± SD (n = 30). Within columns for the same species, values marked with different letters are significantly different according to Tukey's HSD test (P ≤ 0.05).

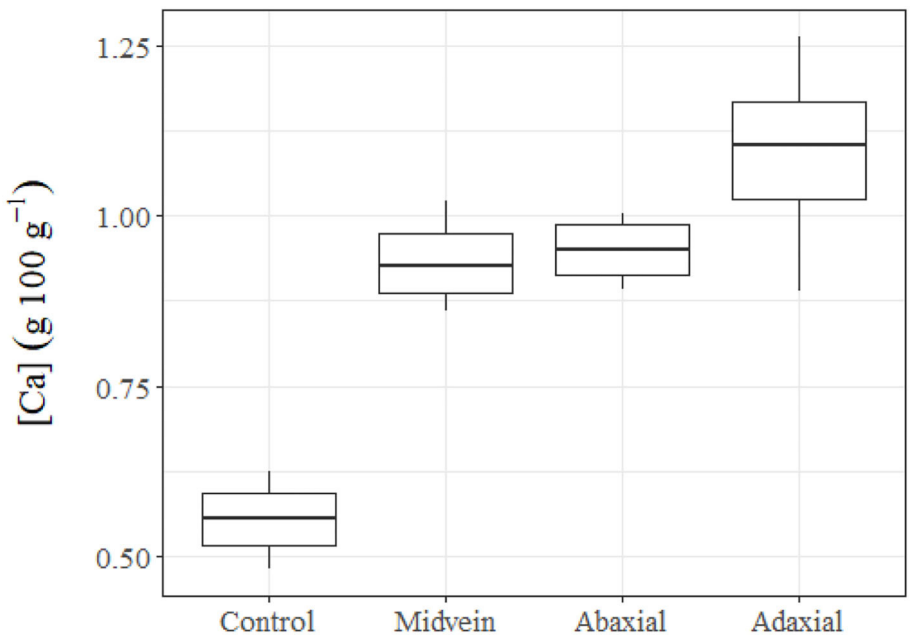

FIGURE 6 | Tissue Ca concentrations of untreated (control) holly leaves compared with leaves treated with 150 mM $CaCl_2$ *via* the mid vein, or the adaxial or abaxial leaf side. Holly leaves were sampled 24 h after foliar Ca application.

other reports described the 1,030- and 1,000-cm^{-1} peaks as heavy atoms (CC and CO) of low strength (Adapa et al., 2009) or as aliphatic ethers or alcohols (Chen et al., 2015). Following Stuart (2000), the polysaccharides present in holly are in line with the bands typical for hemicellulose and cellulose. Besides, the peak at 1,622 cm^{-1} may indicate the presence of pectin. We also detected a low-intensity 3,370-cm^{-1} band, which is associated with cutin and polysaccharides, according to Marechal and Chamel (1996), and may indicate the presence of a small number of H-bonds (Heredia-Guerrero et al., 2014).

Overall, the chemical treatments did not lead to major holly cuticle composition changes, as neither dewaxing nor methanolysis significantly affected cuticle ultrastructure. The results point toward the occurrence of cuticular compounds that were highly resistant to chemical treatments, i.e., the so-called cutan. To evaluate this, we compared the results with two species: *Ficus elastica* (rubber tree) and eucalypt, the first with cutan in its cuticle and the second without it. In the case of eucalyptus (Guzmán et al., 2014a), there is a high peak in polysaccharides (3,332 cm^{-1} band), and in non-solubilized long-chain compounds (1,029 cm^{-1}) where holly has a much lower band. Besides, there is a decrease in eucalyptus peaks after the treatments. We observed that the spectrum of holly is similar to the spectrum of rubber tree (Guzmán-Delgado et al., 2016), as both species have strong peaks in long chain aliphatics (2,918 and 2,850 cm^{-1}) even after being subjected to different treatments. Holly also follows the pattern of cutin polymer described for rubber tree. There are, nonetheless, some differences between them: holly does not have a peak at 468 cm^{-1} and does not decrease esters changing them to the spectral region of the ionized carboxylic groups (Guzmán-Delgado et al., 2016). Furthermore, comparing the absorbance pattern of holly with other two species containing cutan described in the literature (i.e., *A. americana* and *C. miniata*; Heredia-Guerrero et al., 2014), we observed that band distribution adjusted to the pattern of a leaf having cutan. Some studies have described an increase in cutan content as leaves age, improving its mechanical properties (Takahashi et al., 2012; Khanal and Knoche, 2017), and here we aimed to evaluate its potential contribution for dehydration resistance.

Transport of Water and Solutes

When comparing the rate of cuticular water absorption, we observed that for the holly leaves, age did not significantly affect the percentage of water absorbed or how fast water was subsequently lost. However, in the case of the blue gum eucalypt leaves (a species only having cutin polymer and lacking cutan), age was found to be a main factor, with the young cuticles absorbing more water than the older ones. When comparing between cuticles of older leaves of the three species, we found that both holly and cherry laurel, which contain cutan, absorbed more water than eucalypt. Consequently, the results point toward a potential relationship between cutan and an increased cuticular water sorption capacity. However, more research efforts are required to clarify the effect of cuticle composition and structure on water transport and, ultimately, on plant water economy (Forrester et al., 2010; Fernández et al., 2021).

Evidence was gained that holly leaves can absorb solutes (in this case, modeled with Ca ion) through the adaxial and abaxial surfaces, as well as *via* the mid veins. The amount of Ca absorbed after Ca drop deposit onto the mid veins was within a similar range of leaves treated with Ca through the abaxial and adaxial surfaces. Hence, veins can significantly contribute to the foliar absorption process, as also reported for beech leaves (Bahamonde et al., 2018). Furthermore, we found that the spines also absorbed Ca, but at lower rates than the rest of foliar Ca treatments.

CONCLUSIONS

In this study, we evaluated the effect of chemical treatment on isolated cuticles of young and old holly, cherry laurel, and blue gum eucalypt leaves by analyzing potential ultrastructural and chemical changes. The water sorption and desorption capacity of intact vs. chemically extracted cuticles was also evaluated, and species having cutan (i.e., holly and cherry laurel) were found to sorb more water than eucalypt (only having cutin as lipid polymer). Chemical treatments were not always successful in removing cuticular material, and only minor ultra-structural and chemical changes were recorded for holly leaves. Different solute absorption pathways were tested by the application of a 150-mM $CaCl_2$ solution to different leaf areas. Evidence of foliar Ca absorption was gained after Ca-chloride application to both leaf lamina surfaces, the mid veins, and to a lower extent, the spines present in leaf margins. It is concluded that more research is required for the characterization of chemicals and structural features of plant cuticles, and in relation to water and solute transport phenomena.

DATA AVAILABILITY STATEMENT

The original contributions presented in the study are included in the article/**Supplementary Material**, further inquiries can be directed to the corresponding author/s.

AUTHOR CONTRIBUTIONS

CV collected and analyzed the samples, performed the analysis, wrote the main draft, and edited and revised the article. VF conceived and designed the analysis, analyzed the samples and contributed to the writing, editing, and revision of the article. MV-C and LG contributed to experimental design and revised the draft. All authors accepted the final version of the manuscript.

FUNDING

This study was supported by the project S2013/MAE-2760 funded by Comunidad de Madrid. The funding source did not participate in study design, collection, analysis, or interpretation of data, in the writing of the report, or in the decision to submit the article for publication. CV is supported by an FPU predoctoral contract (Ministry of Science and Innovation, Spain).

ACKNOWLEDGMENTS

We want to thank Natalie Aguirre and Guillermo González Gordaliza for helping in holly leaf shoot collection in El Hayedo de Montejo forest.

SUPPLEMENTARY MATERIAL

The Supplementary Material for this article can be found online at: https://www.frontiersin.org/articles/10.3389/fpls.2021.728627/full#supplementary-material

REFERENCES

Adapa, P. K., Karunakaran, C., Tabil, L. G., and Schoenau, G. J. (2009). Potential applications of infrared and Raman spectromicroscopy for agricultural biomass. *Agric. Eng. Int. CIGR J.* 11, 1–25.

Bahamonde, H. A., Fernández, V., and Gil, L. (2018). Surface properties and permeability to calcium chloride of *Fagus sylvatica* and *Quercus petraea* leaves of different canopy heights. *Front. Plant Sci.* 9, 494. doi: 10.3389/fpls.2018.00494

Baker, E. A. (1970). The morphology and composition of isolated plant cuticles. *New phytol.* 69, 1053–1058. doi: 10.1111/j.1469-8137.1970.tb02485.x

Bargel, H., Koch, K., Cerman, Z., and Neinhuis, C. (2006). Evans Review No. 3: Structure–function relationships of the plant cuticle and cuticular waxes—a smart material? *Funct. Plant Biol.* 33, 893–910. doi: 10.1071/fp06139

Benítez, J., Matas, A., and Heredia, A. (2004). Molecular characterization of the plant biopolyester cutin by AFM and spectroscopic techniques. *J. Struct. Biol.* 147, 179–184. doi: 10.1016/j.jsb.2004.03.006

Boom, A., Damsté, J. S., and De Leeuw, J. W. (2005). Cutan, a common aliphatic biopolymer in cuticles of drought-adapted plants. *Org. Geochem.* 36, 595–601. doi: 10.1016/j.orggeochem.2004.10.017

Burghardt, M., and Riederer, M. (2003). Ecophysiological relevance of cuticular transpiration of deciduous and evergreen plants in relation to stomatal closure and leaf water potential. *J. Exp. Bot.* 54, 1941–1949. doi: 10.1093/jxb/erg195

Chamel, A., Escoubes, M., Baudrand, G., and Girard, G. (1992). Determination of water sorption by cuticles isolated from fir tree needles. *Trees* 6, 109–114. doi: 10.1007/bf00226589

Chamel, A., Pineri, M., and Escoubes, M. (1991). Quantitative determination of water sorption by plant cuticles. *Plant Cell Environ.* 14, 87–95. doi: 10.1111/j.1365-3040.1991.tb01374.x

Chen, M., Zhu, X., Zhang, Y., Du, Z., Chen, X., Kong, X., et al. (2020). Drought stress modify cuticle of tender tea leaf and mature leaf for transpiration barrier enhancement through common and distinct modes. *Sci. Rep.* 10, 1–12. doi: 10.1038/s41598-020-63683-4

Chen, Y., Zou, C., Mastalerz, M., Hu, S., Gasaway, C., and Tao, X. (2015). Applications of micro-fourier transform infrared spectroscopy (FTIR) in the geological sciences—a review. *Int. J. Mol. Sci.* 16, 30223–30250. doi: 10.3390/ijms161226227

Díaz, M. A. L., D'Angelo, J. A., Del Fueyo, G. M., and Carrizo, M. A. (2020). FTIR spectroscopic features of the pteridosperm *Rufloriniaorlandoi* and host rock (Springhill Formation, Lower Cretaceous, Argentina). *J. South Amer. Earth Sci.* 99, 102520. doi: 10.1016/j.jsames.2020.102520

Domínguez, E., Heredia-Guerrero, J. A., and Heredia, A. (2011). The biophysical design of plant cuticles: an overview. *New Phytol.* 189, 938–949. doi: 10.1111/j.1469-8137.2010.03553.x

España, L., Heredia-Guerrero, J. A., Segado, P., Benítez, J. J., Heredia, A., and Domínguez, E. (2014). Biomechanical properties of the tomato (*Solanum lycopersicum*) fruit cuticle during development are modulated by changes in the relative amounts of its components. *New Phytol.* 202, 790–802. doi: 10.1111/nph.12727

Fernández, V., Gil-Pelegrín, E., and Eichert, T. (2021). Foliar water and solute absorption: an update. *Plant J.* 105, 870–883. doi: 10.1111/tpj.15090

Fernández, V., Guzmán-Delgado, P., Graça, J., Santos, S., and Gil, L. (2016). Cuticle structure in relation to chemical composition: re-assessing the prevailing model. *Front. Plant Sci.* 7, 427. doi: 10.3389/fpls.2016.00427

Fernández, V., Khayet, M., Montero-Prado, P., Heredia-Guerrero, J. A., Liakopoulos, G., Karabourniotis, G., et al. (2011). New insights into the properties of pubescent surfaces: peach fruit as a model. *Plant Physiology*, 156, 2098–2108. doi: 10.1104/pp.111.176305

Fich, E. A., Segerson, N. A., and Rose, J. K. (2016). The plant polyester cutin: biosynthesis, structure, and biological roles. *Annu. Rev. Plant Biol.* 67, 207–233. doi: 10.1146/annurev-arplant-043015-111929

Forrester, D. I., Collopy, J. J., and Morris, J. D. (2010). Transpiration along an age series of *Eucalyptus globulus* plantations in southeastern Australia. *For. Ecol. Manage.* 259, 1754–1760. doi: 10.1016/j.foreco.2009.04.023

Galle, F. C. (1997). *Hollies: the Genus Ilex.* Portland, OR: Timber Press. doi: 10.1046/j.1469-8137.1998.21294.x

Girard, A. L., Mounet, F., Lemaire-Chamley, M., Gaillard, C., Elmorjani, K., Vivancos, J., et al. (2012). Tomato GDSL1 is required for cutin deposition in the fruit cuticle. *Plant Cell* 24, 3119–3134. doi: 10.1105/tpc.112.101055

González, G. (2015). *Estudio de la Regeneración en un Antiguo Hayedo Adehesado y su Influencia en el Crecimiento de Hayas Centenarias*. Hayedo de Montejo (Madrid). Madrid: Technical University of Madrid.

Graça, J., and Pereira, H. (2000). Methanolysis of bark suberins: analysis of glycerol and acid monomers. *Phytochem. Anal.* 11, 45–51. doi: 10.1002/(SICI)1099-1565(200001/02)11:1<45::AID-PCA481>3.0.CO;2-8

Gratani, L., Covone, F., and Larcher, W. (2006). Leaf plasticity in response to light of three evergreen species of the Mediterranean maquis. *Trees* 20, 549–558. doi: 10.1007/s00468-006-0070-6

Guo, Y., and Bustin, R. M. (1998). Micro-FTIR spectroscopy of liptinite macerals in coal. *Int. J. Coal. Geol.* 36, 259–275. doi: 10.1016/s0166-5162(97)00044-x

Gupta, N. S., Collinson, M. E., Briggs, D. E., Evershed, R. P., and Pancost, R. D. (2006). Reinvestigation of the occurrence of cutan in plants: implications for the leaf fossil record. *Paleobiology* 32, 432–449. doi: 10.1666/05038.1

Guzmán, P., Fernández, V., Graça, J., Cabral, V., Kayali, N., Khayet, M., et al. (2014a). Chemical and structural analysis of *Eucalyptus globulus* and *E. camaldulensis* leaf cuticles: a lipidized cell wall region. *Front. Plant Sci.* 5, 481. doi: 10.3389/fpls.2014.00481

Guzmán, P., Fernández, V., Khayet, M., García, M. L., Fernández, A., and Gil, L. (2014b). Ultrastructure of plant leaf cuticles in relation to sample preparation as observed by transmission electron microscopy. *Scient. World J.* 2014, 1–9. doi: 10.1155/2014/963921

Guzmán-Delgado, P., Graça, J., Cabral, V., Gil, L., and Fernández, V. (2016). The presence of cutan limits the interpretation of cuticular chemistry and structure: *Ficus elastica* leaf as an example. *Physiol. Plant.* 157, 205–220. doi: 10.1111/ppl.12414

Heredia-Guerrero, J. A., Benítez, J. J., Domínguez, E., Bayer, I. S., Cingolani, R., Athanassiou, A., et al. (2014). Infrared and Raman spectroscopic features of plant cuticles: a review. *Front. Plant Sci.* 5, 305. doi: 10.3389/fpls.2014.00305

Heredia-Guerrero, J. A., Williams, C. A., Guidetti, G., Cataldi, P., Ceseracciu, L., Debellis, D., et al. (2020). Plant-inspired polyaleuritate–nanocellulose composite photonic films. *ACS Appl. Polym. Mater.* 2, 1528–1534. doi: 10.1021/acsapm.9b01205

Holanda, A. E. R., Souza, B. C., Carvalho, E. C. D., Oliveira, R. S., Martins, F. R., Muniz, C. R., et al. (2019). How do leaf wetting events affect gas exchange and leaf lifespan of plants from seasonally dry tropical vegetation? *Plant Biol.* 21, 1097–1109. doi: 10.1111/plb.13023

Holloway, P. J. (1982). "Structure and histochemistry of plant cuticular membranes: an overview," in *The Plant Cuticle* (London: Academic Press), 1–32.

Holloway, P. J., and Baker, E. A. (1970). The cuticles of some angiosperm leaves and fruits. *Ann. Appl. Biol.* 66, 145–154. doi: 10.1111/j.1744-7348.1970.tb04612.x

Jeffree, C. E. (2006). The fine structure of the plant cuticle. *Biol. Plant Cutic.* 23, 11–125. doi: 10.1002/9780470988718.ch2

Jetter, R., and Riederer, M. (2016). Localization of the transpiration barrier in the epi-and intracuticular waxes of eight plant species: water transport resistances are associated with fatty acyl rather than alicyclic components. *Plant Physiol.* 170, 921–934. doi: 10.1104/pp.15.01699

Johnson, E. J., Dorot, O., Liu, J., Chefetz, B., and Xing, B. (2007). Spectroscopic characterization of aliphatic moieties in four plant cuticles. *Commun. Soil Sci. Plant Anal.* 38, 2461–2478. doi: 10.1080/00103620701588841

Karabourniotis, G., and Liakopoulos, G. (2005). "Phenolic compounds in plant cuticles: physiological and ecological aspects," in *Advances in Plant Physiology*, Vol. 8, ed A. Hemantaranjan (Jodhpur: Scientific Publishers), 33–47.

Kerstiens, G. (1996). Cuticular water permeability and its physiological significance. *J. Exp. Bot.* 47, 1813–1832. doi: 10.1093/jxb/47.12.1813

Kerstiens, G. (2006). Water transport in plant cuticles: an update. *J. Exp. Bot.* 57, 2493–2499. doi: 10.1093/jxb/erl017

Khanal, B. P., Grimm, E., Finger, S., Blume, A., and Knoche, M. (2013). Intracuticular wax fixes and restricts strain in leaf and fruit cuticles. *New Phytol.* 200, 134–143. doi: 10.1111/nph.12355

Khanal, B. P., and Knoche, M. (2017). Mechanical properties of cuticles and their primary determinants. *J. Exp. Bot.* 68, 5351–5367. doi: 10.1093/jxb/erx265

Leide, J., Nierop, K. G., Deininger, A. C., Staiger, S., Riederer, M., and De Leeuw, J. W. (2020). Leaf cuticle analyses: implications for the existence of cutan/non-ester cutin and its biosynthetic origin. *Ann. Bot.* 126, 141–162. doi: 10.1093/aob/mcaa056

Malek, E., McCurdy, G., and Giles, B. (1999). Dew contribution to the annual water balances in semi-arid desert valleys. *J. Arid Environ.* 42, 71–80. doi: 10.1006/jare.1999.0506

Malik, F. T., Clement, R. M., Gethin, D. T., Kiernan, M., Goral, T., Griffiths, P., et al. (2016). Hierarchical structures of cactus spines that aid in the directional movement of dew droplets. *Philos. Trans. A Math. Phys. Eng. Sci.* 374, 20160110. doi: 10.1098/rsta.2016.0110

Marechal, Y., and Chamel, A. (1996). Water in a biomembrane by infrared spectrometry. *J. Phys. Chem.* 100, 8551–8555. doi: 10.1021/jp951981i

Mazurek, S., Garroum, I., Daraspe, J., De Bellis, D., Olsson, V., A., et al. (2017). Connecting the molecular structure of cutin to ultrastructure and physical properties of the cuticle in petals of Arabidopsis. *Plant Physiol.* 173, 1146–1163. doi: 10.1104/pp.16.01637

McKinney, D. E., Bortiatynski, J. M., Carson, D. M., Clifford, D. J., De Leeuw, J. W., and Hatcher, P. G. (1996). Tetramethylammonium hydroxide (TMAH) thermochemolysis of the aliphatic biopolymer cutan: insights into the chemical structure. *Org. Geochem.* 24, 641–650. doi: 10.1016/0146-6380(96)00055-1

Merinero, S., Martínez, I., Rubio-Salcedo, M., and Gauslaa, Y. (2015). Epiphytic lichen growth in Mediterranean forests: effects of proximity to the ground and reproductive stage. *Basic Appl. Ecol.* 16, 220–230. doi: 10.1016/j.baae.2015.01.007

Mösle, B., Collinson, M. E., Finch, P., Stankiewicz, B. A., Scott, A. C., and Wilson, R. (1998). Factors influencing the preservation of plant cuticles: a comparison of morphology and chemical composition of modern and fossil examples. *Org. Geochem.* 29, 1369–1380. doi: 10.1016/s0146-6380(98)00080-1

Niemann, G. J., and Baas, W. J. (1985). The Composition of the Lipid Constituents of *Ilex aquifolium* L. (Aquifoliaceae) in relation to the age of the leaf. I. The leaf wax. *J. Plant Physiol.* 118, 219–226. doi: 10.1016/s0176-1617(85)80223-6

Nip, M., Tegelaar, E. W., Brinkhuis, H., De Leeuw, J. W., Schenck, P. A., and Holloway, P. J. (1986b). Analysis of modern and fossil plant cuticles by Curie point Py-GC and Curie point Py-GC-MS: recognition of a new, highly aliphatic and resistant biopolymer. *Org. Geochem.* 10, 769–778. doi: 10.1016/s0146-6380(86)80014-6

Nip, M., Tegelaar, E. W., De Leeuw, J. W., Schenck, P. A., and Holloway, P. J. (1986a). A new non-saponifiable highly aliphatic and resistant biopolymer in plant cuticles. *Naturwissenschaften* 73, 579–585. doi: 10.1007/bf00368768

Oleszko, A., Olsztyńska-Janus, S., Walski, T., Grzeszczuk-Ku,ć, K., Bujok, J., Gałecka, K., et al. (2015). Application of FTIR-ATR spectroscopy to determine the extent of lipid peroxidation in plasma during haemodialysis. *Biomed Res. Int.* 2015, 1–8. doi: 10.1155/2015/245607

Philippe, G., Geneix, N., Petit, J., Guillon, F., Sandt, C., Rothan, C., et al. (2020). Assembly of tomato fruit cuticles: a cross-talk between the cutin polyester and cell wall polysaccharides. *New Phytol.* 226, 809–822. doi: 10.1111/nph.16402

R Core Team (2013). *R: A Language and Environment for Statistical Computing*. R Foundation for Statistical Computing, Vienna. Available online at: http://www.R-project.org/

Razali, N. M., and Wah, Y. B. (2011). Power comparisons of shapiro-wilk, kolmogorov-smirnov, lilliefors and anderson-darling tests. *J. Stat. Model. Anal.* 2, 21–33.

Reina, J. J., Dominguez, E., and Heredia, A. (2001). Water sorption–desorption in conifer cuticles: the role of lignin. *Physiol. Plant.* 112, 372–378. doi: 10.1034/j.1399-3054.2001.1120310.x

Riederer, M. (2006). Thermodynamics of the water permeability of plant cuticles: characterization of the polar pathway. *J. Exp. Bot.* 57, 2937–2942. doi: 10.1093/jxb/erl053

Riederer, M., and Schönherr, J. (1988). Development of plant cuticles: fine structure and cutin composition of *Clivia miniata* Reg. leaves. *Planta* 174, 127–138. doi: 10.1007/bf00394885

Sanjari, S., Shobbar, Z. S., Ghanati, F., Afshari-Behbahanizadeh, S., Farajpour, M., Jowkar, M., et al. (2021). Molecular, chemical, and physiological analyses of sorghum leaf wax under post-flowering drought stress. *Plant Physiol. Biochem.* 159, 383–391. doi: 10.1016/j.plaphy.2021.01.001

Schmidt, H. W., and Schönherr, J. (1982). Development of plant cuticles: occurrence and role of non-ester bonds in cutin of *Clivia miniata* Reg. leaves. *Planta* 156, 380–384. doi: 10.1007/bf00397478

Schönherr, J., and Schmidt, H. W. (1979). Water permeability of plant cuticles. *Planta* 144, 391–400. doi: 10.1007/bf00391583

Segado, P., Domínguez, E., and Heredia, A. (2016). Ultrastructure of the epidermal cell wall and cuticle of tomato fruit (*Solanum lycopersicum* L.) during development. *Plant Physiol.* 170, 935–946. doi: 10.1104/pp.15.01725

Segado, P., Heredia-Guerrero, J. A., Heredia, A., and Domínguez, E. (2020). Cutinsomes and CUTIN SYNTHASE1 function sequentially in tomato fruit cutin deposition. *Plant Physiol.* 183, 1622–1637. doi: 10.1104/pp.20.00516

Stuart, B. (2000). *Infrared Spectroscopy: Fundamentals and Applications*. West Sussex: John Wiley and Sons. doi: 10.1002/0470011149

Takahashi, Y., Tsubaki, S., Sakamoto, M., Watanabe, S., and Azuma, J. I. (2012). Growth-dependent chemical and mechanical properties of cuticular membranes from leaves of *Sonneratia alba*. *Plant Cell Environ.* 35, 1201–1210. doi: 10.1111/j.1365-3040.2012.02482.x

Tegelaar, E. W., Kerp, H., Visscher, H., Schenck, P. A., and De Leeuw, J. W. (1991). Bias of the paleobotanical record as a consequence of variations in the chemical composition of higher vascular plant cuticles. *Paleobiology* 17, 133–144. doi: 10.1017/s0094837300010459

Türker-Kaya, S., and Huck, C. (2017). A review of mid-infrared and near-infrared imaging: principles, concepts and applications in plant tissue analysis. *Molecules* 22, 168. doi: 10.3390/molecules22010168

Van Genderen, H. H., Jaarsma, J., and Versluis, C. (1988). Long chain pentyl- and hexyl-esters and other lipoids in leaf wax of *Ilex aquifolium* L. (Aquifoliaceae). *Plant Sci.* 55, 231–238. doi: 10.1016/0168-9452(88)90066-0

Vega, C., González, G., Bahamonde, H. A., Valbuena-Carabaña, M., Gil, L., and Fernández, V. (2020). Effect of irradiation and canopy position on anatomical and physiological features of *Fagus sylvatica* and *Quercus petraea* leaves. *Plant Physiol. Biochem.* 152, 232–242. doi: 10.1016/j.plaphy.2020.05.007

Verdaguer, D., Llorens, L., Bernal, M., and Badosa, J. (2012). Photomorphogenic effects of UVB and UVA radiation on leaves of six Mediterranean sclerophyllous woody species subjected to two different watering regimes at the seedling stage. *Environ. Exp. Bot.* 79, 66–75. doi: 10.1016/j.envexpbot.2012.01.008

Villena, J. F., Domínguez, E., Stewart, D., and Heredia, A. (1999). Characterization and biosynthesis of non-degradable polymers in plant cuticles. *Planta* 208, 181–187. doi: 10.1007/s004250050548

Viougeas, M. A., Rohr, R., and Chamel, A. (1995). Structural changes and permeability of ivy (*Hedera helix* L.) leaf cuticles in relation to leaf development and after selective chemical treatments. *New Phytol.* 130, 337–348. doi: 10.1111/j.1469-8137.1995.tb01828.x

Von Mohl, H. (1847). Untersuchungen der Frage: bildet die cellulose die grundlage sammtlicher vegetabilischen membranen. *Botan. Z.* 5, 497–505.

Zeier, J., and Schreiber, L. (1999). Fourier transform infrared-spectroscopic characterisation of isolated endodermal cell walls from plant roots: chemical nature in relation to anatomical development. *Planta* 209, 537–542. doi: 10.1007/s004250050758

Zeisler-Diehl, V., Müller, Y., and Schreiber, L. (2018). Epicuticular wax on leaf cuticles does not establish the transpiration barrier, which is essentially formed by intracuticular wax. *J. Plant Physiol.* 227, 66–74. doi: 10.1016/j.jplph.2018.03.018

Zhang, Y., Chen, X., Du, Z., Zhang, W., Devkota, A. R., Chen, Z., et al. (2020). A proposed method for simultaneous measurement of cuticular transpiration from different leaf surfaces in *Camellia sinensis*. *Front. Plant Sci.* 11, 420. doi: 10.3389/fpls.2020.00420

Zhang, Y., Du, Z., Han, Y., Chen, X., Kong, X., Sun, W., et al. (2021). Plasticity of the cuticular transpiration barrier in response to water shortage and resupply in Camellia sinensis: a role of cuticular waxes. *Front. Plant Sci.* 11, 2051. doi: 10.3389/fpls.2020.600069

Conflict of Interest: The authors declare that the research was conducted in the absence of any commercial or financial relationships that could be construed as a potential conflict of interest.

Publisher's Note: All claims expressed in this article are solely those of the authors and do not necessarily represent those of their affiliated organizations, or those of the publisher, the editors and the reviewers. Any product that may be evaluated in this article, or claim that may be made by its manufacturer, is not guaranteed or endorsed by the publisher.

frontiers in Plant Science

ORIGINAL RESEARCH
published: 21 October 2021
doi: 10.3389/fpls.2021.730837

Direct Evidence for a Radial Gradient in Age of the Apple Fruit Cuticle

Yiru Si[1], *Bishnu P. Khanal*[1], *Oliver K. Schlüter*[2] *and Moritz Knoche*[1]*

[1] *Fruit Science Section, Institute of Horticultural Production Systems, Leibniz University Hannover, Hannover, Germany,*
[2] *Department of Horticultural Engineering, Leibniz Institute for Agricultural Engineering and Bioeconomy (ATB), Potsdam, Germany*

The pattern of cuticle deposition plays an important role in managing strain buildup in fruit cuticles. Cuticular strain is the primary trigger for numerous fruit-surface disorders in many fruit crop species. Recent evidence indicates a strain gradient may exist within the apple fruit cuticle. The outer layers of the cuticle are more strained and thus more susceptible to microcracking than the inner layers. A radial gradient in cuticle age is the most likely explanation. Our study aimed to establish whether (or not) deposition of new cutin in a developing apple fruit occurs on the inner surface of the cuticle, i.e., immediately abutting the outward-facing epidermal cell wall. Developing apples were fed with ^{13}C oleic acid through the skin. Following a 14-d period for incorporation, the fruit was harvested and the cuticular membranes (CMs) isolated enzymatically. The CMs were then ablated to varying extents from the inner or the outer surfaces, using a cold atmospheric pressure plasma (CAPP). Afterwards, the ablated CMs were dewaxed and the ^{13}C contents were determined by mass spectrometry. The incorporation of ^{13}C in the cutin fraction was higher than in the wax fraction. The ^{13}C content was highest in non-ablated, dewaxed CM (DCM) and decreased as ablation depth from the inner surface increased. There was no change in ^{13}C content when ablation was carried out from the outer surface. As fruit development proceeded, more ^{13}C label was found towards the middle of the DCM. These results offered direct evidence for deposition of cutin being on the inner surface of the cuticle, resulting in a radial gradient in cuticular age—the most recent deposition (youngest) being on the inner cuticle surface (abutting the epidermal cell wall) and the earliest deposition (oldest) being on the outer surface (abutting the atmosphere).

Keywords: ***Malus* × *domestica*, cuticle, cutin, wax, strain, stress**

OPEN ACCESS

Edited by:
Antonio Heredia,
University of Malaga, Spain

Reviewed by:
Benedicte Bakan,
Institut National de recherche pour l'agriculture, l'alimentation et l'environnement (INRAE), France
Lucas Busta,
University of Minnesota Duluth, United States

***Correspondence:**
Moritz Knoche
moritz.knoche@obst.uni-hannover.de

Specialty section:
This article was submitted to Plant Physiology, a section of the journal Frontiers in Plant Science

Received: *25 June 2021*
Accepted: *21 September 2021*
Published: *21 October 2021*

Citation:
Si Y, Khanal BP, Schlüter OK and Knoche M (2021) Direct Evidence for a Radial Gradient in Age of the Apple Fruit Cuticle. Front. Plant Sci. 12:730837. doi: 10.3389/fpls.2021.730837

INTRODUCTION

A cuticular membrane covers the outside of all primary-skin surfaces of all organs of terrestrial plants, specifically all leaves, many stems, and fruit. The cuticular membrane (CM) is a non-living extracellular polymer, deposited on the outer surface of the cell walls of the epidermis. It comprises an insoluble polymer matrix "cutin," solvent-soluble lipids "waxes," and cell wall polysaccharides (Schreiber and Schönherr, 1990; Dominguez et al., 2011; Yeats and Rose, 2013). The waxes are deposited within the CM as intracuticular waxes and also on the CM surface as epicuticular waxes. The primary function of the cuticle is to present a barrier against uncontrolled exchanges of respiratory gases (Jeffree, 2006) and water (Riederer and Schreiber, 2001; Kerstiens, 2006) and

invasion by pathogens (Huang, 2001; Heredia, 2003; Serrano et al., 2014). To continue its barrier functions, the cuticle must maintain its functional integrity throughout the life of a leaf or a fruit.

Maintenance of functional integrity presents a particular challenge to the cuticles of fruit. In contrast to leaves, a fruit skin is subject to an extended period of strain, as a fruit surface usually continues to extend from flowering through to fruit maturity, commonly a period of about five months. The epidermal and hypodermal cells beneath the cuticle cope with these growth strains by a combination of cell division, cell expansion, and, in some fruit skins, by a change in epidermal cell aspect ratio (Maguire, 1998; Knoche and Lang, 2017). However, the polymeric CM cannot grow or divide but is simply stretched out by the ongoing area growth of the underlying epidermis (Knoche et al., 2004). This ongoing strain can result in the formation of cuticular microcracks that compromise its barrier functions. Microcracking is aggravated by surface wetness (Khanal et al., 2021). Moreover, microcracks are the first visible symptoms of several important fruit-surface disorders, including russet, skin spots, neck shrivel, and macrocracks (Skene, 1980; Knoche and Lang, 2017). Throughout fruit development, the cuticle of an apple copes with the ongoing strain by the ongoing deposition of new cutin and wax (Lai et al., 2016)—else the stretched CM would become thinner and thinner. The continuing addition of new cutin to the extending cuticle and its impregnation with intracuticular waxes "fix" the strain, converting the elastic strain component into a plastic component (Khanal et al., 2013a).

Previous studies have shown that these processes result in the development of a radial gradient of strain across the CM, with the material on the inner side (abutting the cell walls) being less strained and that on the outer side (abutting the atmosphere) being more strained (Khanal et al., 2014). In this way, it is most common for a microcrack to appear first on the outer side of the CM and for this crack gradually to propagate deeper into the cuticle as straining continues, so as eventually to traverse the CM through to the inner (cell) side (Knoche et al., 2018). The most likely explanation for the observed radial gradient in strain is a corresponding gradient in the deposition and thus the age of the cuticle. Additional factors that may contribute to a radial gradient in strain are the presence of polysaccharides on the inner side of the cuticle (Dominguez et al., 2011), a compositional gradient of C16/C18 cutin monomers within the cuticle with C18 fatty acids having a higher impact on cuticle integrity (Kolattukudy and Walton, 1972; Walton and Kolattukudy, 1972; Kolattukudy et al., 1974; Kolattukudy, 1980; Straube et al., 2021) and/or changing status of cutin polymerization (Espana et al., 2014; Martin and Rose, 2014).

It was hypothesised that with cutin being added preferentially to the inner side of the CM, this region will be younger, and so it will have suffered a shorter history of expansion, and so it will be less strained than the outer side. Taking the opposite view, the cutin on the outer side of the CM will have been deposited earlier on in the life of the fruit, and so be older, and so have suffered a longer history of expansion, and so be more strained. This hypothesis would explain why microcracking usually begins on

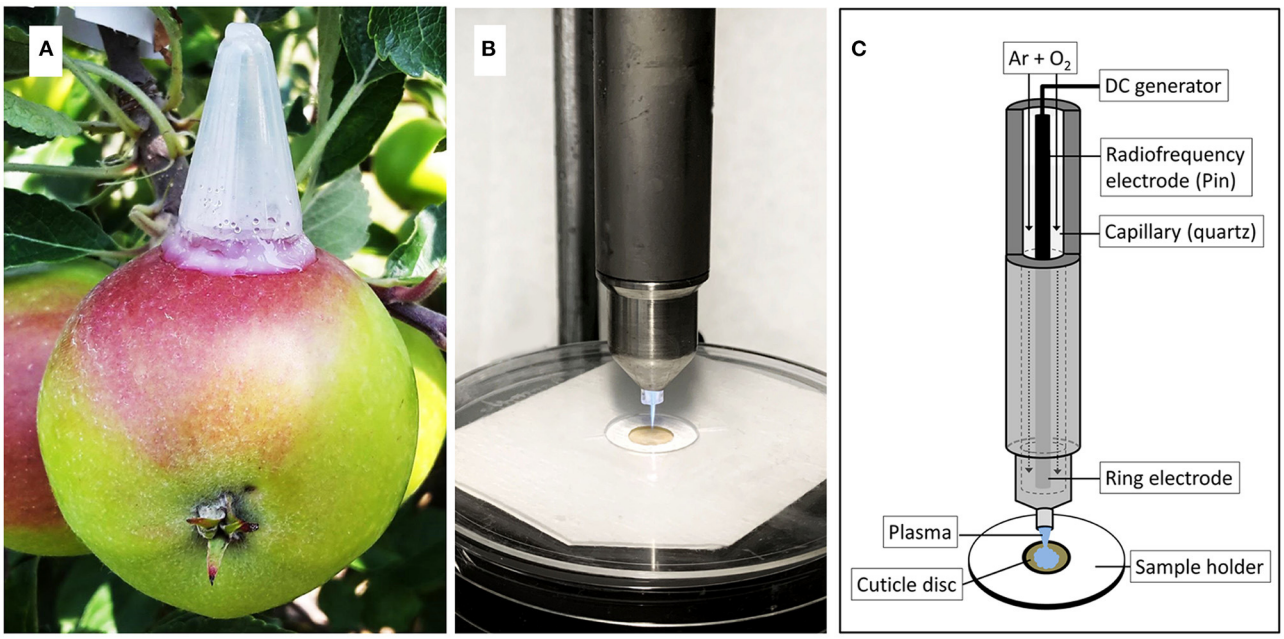

FIGURE 1 | Apple fruit with mounted polyethylene tube for feeding ^{13}C labelled oleic acid under field conditions **(A)**. Cold atmospheric pressure plasma (CAPP) is generated by a plasma jet during ablation of the cuticular membrane (CM) **(B)**. Sketch of plasma jet and CM sample holder illustrating the various parts of the plasma jet and the experimental setup **(C)**. The sketch was adapted from Bußler (2017).

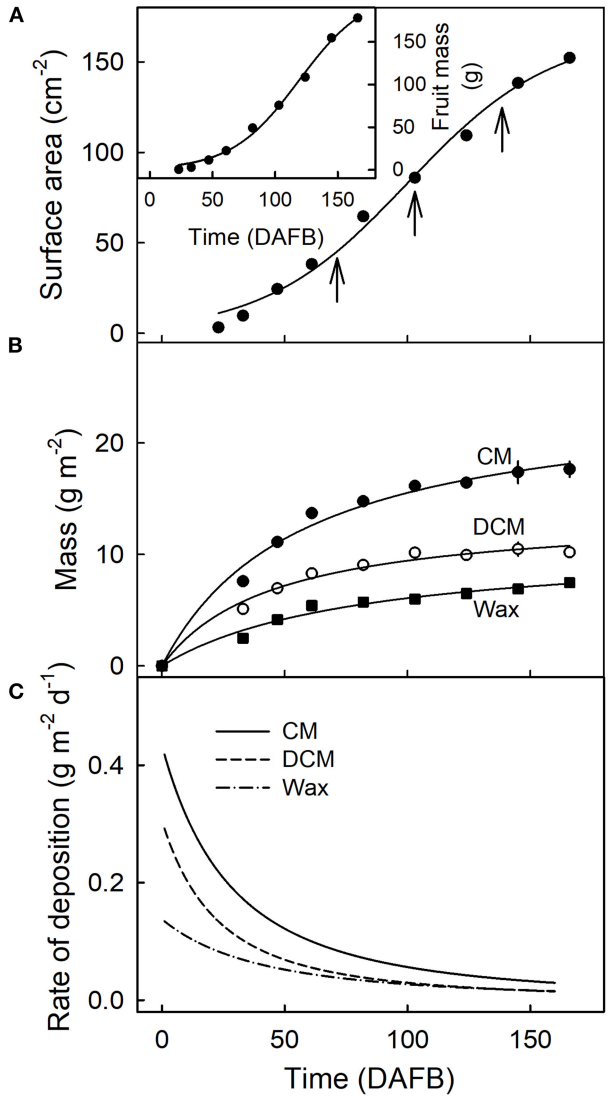

FIGURE 2 | Fruit surface area **(A)**, fruit mass [**(A)**, inset]and mass per unit area of the cuticular membrane (CM), the dewaxed CM, and the wax **(B)** during the development of apple fruit. **(C)** Rates of deposition of CM, DCM, and wax. The x-axis scale is in days after full bloom. The vertical arrows in A indicate the beginning of the feeding periods of ^{13}C oleic acid to the outer surface of developing apple fruit. Data points represent means ± SE, n = 15–60.

the outer side of the CM. It would also explain why dewaxed CMs (DCM) usually "curl" following extraction of wax. Unfortunately, direct evidence for the deposition and age gradients in the cuticle is lacking, i.e., that deposition occurs on the inner surface of the cuticle.

Therefore, the objective of this study was to provide direct evidence for a radial gradient in cuticle deposition and age. We first fed ^{13}C labelled oleic acid to the fruit surface. This was incorporated into the CM (Si et al., 2021a,b). Following feeding and incorporation, the cuticle was enzymatically isolated and then ablated from its inner surface, or its outer surface, using a cold atmospheric pressure plasma (CAPP). Thereafter, the ^{13}C content of the ablated CM was determined. We focused on the cutin fraction, since an association of ^{13}C with the wax fraction may have simply resulted from partitioning (Si et al., 2021a). We chose the 'Idared' apple for our study because 'Idared' is a russet non-susceptible cultivar where surface wetness during feeding does not trigger russet formation (Khanal et al., 2013b, 2021; Chen et al., 2020).

MATERIALS AND METHODS

Plant Material

'Idared' apple (*Malus* × *domestica* Borkh.) trees grafted on M9 rootstocks were cultivated in the Horticultural Research Station of the Leibniz University Hannover at Ruthe, Germany (lat. 52°14′N, long. 9°49′E) according to current EU regulations for integrated fruit production. Representative fruits of normal growth and free from visible blemishes were selected for the experiments.

Methods

Fruit Growth and Cuticle Deposition

Fruits were harvested at different stages of development and the mass of each was recorded. The surface area was calculated assuming sphericity and a mean density of 1 kg dm^{-3}. A sigmoid regression line was fitted through plots of fruit surface area vs. time in days after full bloom (DAFB) and fruit mass vs. DAFB. The number of replicates at each time was 60.

Cutin and wax deposition was quantified using enzymatically isolated CM using standard procedures. Briefly, epidermal skin segments (ES) were excised from the equatorial plane of fruit using a biopsy punch (8 mm, Acuderm Inc., FL, USA). The ES was incubated at ambient laboratory temperature in an isolation medium containing pectinase (90 ml L^{-1}, Panzym Super E flüssig, Novozymes A/S, Krogshoejvej, Bagsvaerd, Denmark) and cellulase (5 mL L^{-1}, Cellubrix L, Novozymes A/S). The enzyme solution was buffered in 50 mM citric acid and the pH adjusted to 4 using sodium hydroxide (NaOH). To avoid microbial growth, sodium azide (NaN_3) was added at a final concentration of 30 mM. The enzyme solution was periodically refreshed until the CMs separated from the underlying tissue. The CMs were cleaned using a soft camel-hair brush and thoroughly rinsed with deionized water.

To determine the mass per unit area, CMs were dried overnight at 40°C and then weighed on a microbalance (CPA2P; Sartorius, Göttingen, Germany). Subsequently, the CMs were Soxhlet extracted using a chloroform:methanol mixture (1:1 v/v) for 2.5 h. Dewaxed CMs (DCM) were again dried overnight and weighed.

Dosing Procedure and Cuticle Preparation

Feeding ^{13}C Labelled Oleic Acid

The solutions were prepared by dissolving uniformly ^{13}C labelled oleic acid (> 95% purity, Larodan AB, Solna, Sweden) in 0.05% surfactant solution (Glucopon 215 UP/Mb; BASF, Ludwigshafen, Germany) at a final concentration of 167 µM (equiv. to 50 mg L^{-1}). Solutions were vortexed for at least 3 min immediately after

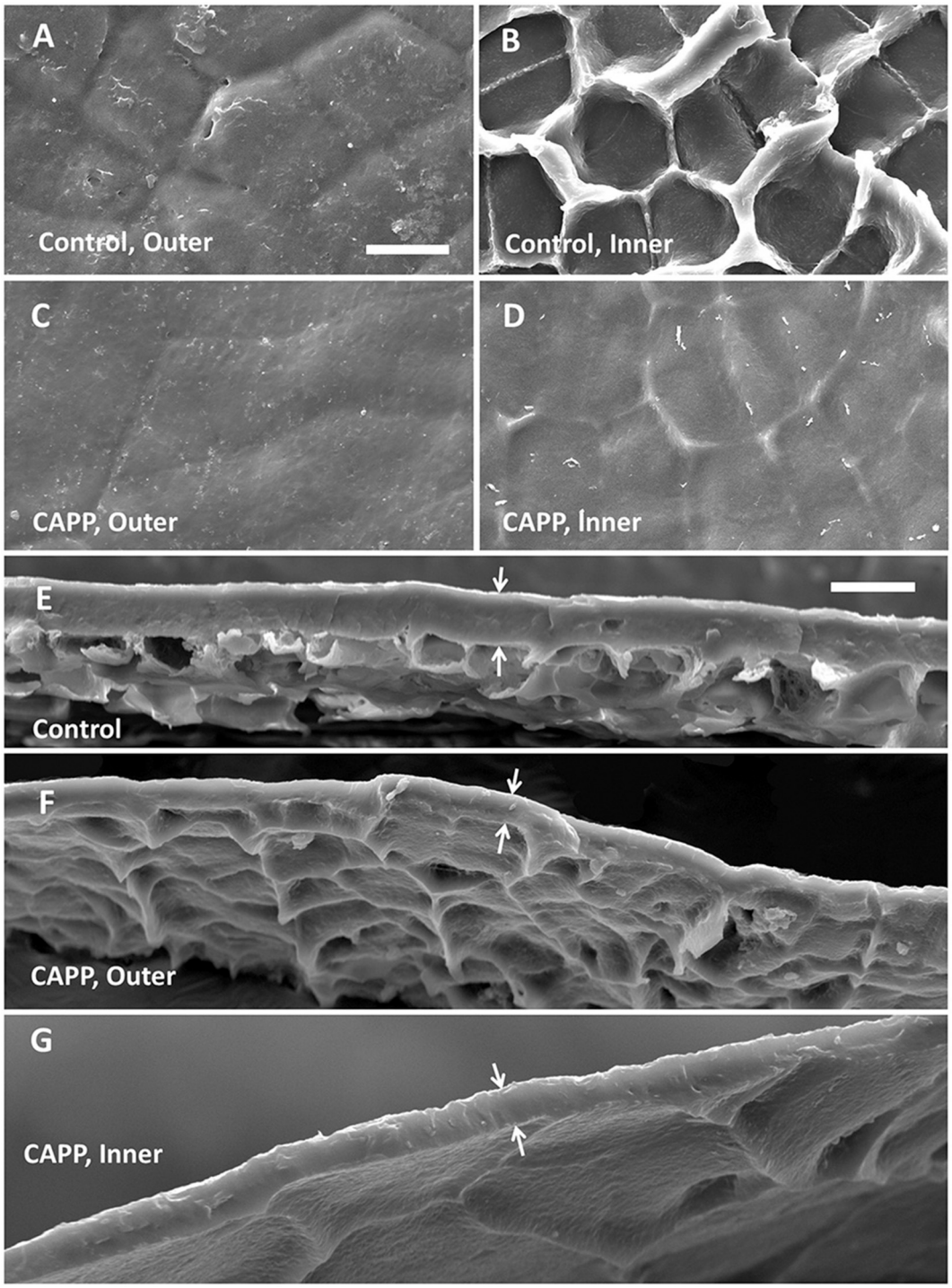

FIGURE 3 | Scanning electron micrographs of outer surfaces **(A,C)**, inner surfaces **(B,D)**, and cross-sections **(E–G)** of cuticular membranes (CMs) of apple fruit (fed with ^{13}C oleic acid at 69 days after full bloom [DAFB] and harvested at 178 DAFB) with ablation **(C,D,F,G)** and without ablation using a cold atmospheric pressure plasma (CAPP) **(A,B,E)** following wax extraction. The white arrows indicate the outer and inner surfaces of the CMs. The thickness of the CM differed significantly and was 11.0 ± 0.3 μm for the control, 7.4 ± 0.7 μm for the CAPP treatment of the outer side, and 5.5 ± 0.4 μm for the CAPP treatment of the inner side. Data on thickness represent means ± SE, $n = 3$–5.

preparation and again for 3 min immediately before application to the fruit surface. Donor solutions were always prepared fresh on the day of use.

The solution was applied as described earlier (Si et al., 2021a,b). Briefly, polyethylene tubes (25 mm height, 14 mm diameter) with a tapered tip and a minute hole in the tip were mounted in the equatorial region of the apple fruit using a non-phytotoxic silicon rubber (SE 9186 RTV; Dow Toray, Tokyo, Japan). A volume of 400 μL of donor solution was injected through the hole in the tip of the tube, and the hole was sealed using silicone rubber to prevent drying of the donor solution (**Figure 1A**). Feeding was terminated after 7 d when the tubes were removed. The original footprint of the tube was then marked with a permanent marker and the marked area was rinsed with deionized water. Fruits were sampled either 14 d after the termination of feeding or at commercial maturity.

Cuticle Isolation

After harvest, the marked area of the fruit surface was rinsed with 1% surfactant solution (Glucopon 215 UP/Mb; BASF) and blotted dry. A 12 mm diameter ES was excised from the central region of the marked area using a biopsy punch (Acuderm Inc., FL, USA). The CMs were isolated from the ES as described above. Isolated and cleaned CMs were stored in deionized water at ambient temperature until use.

Cold Atmospheric Pressure Plasma (CAPP) Treatment

The CMs were dried overnight at 40°C and weighed on a microbalance. The CM discs were mounted between two discs of thick paper. The upper paper disc had an 8 mm diameter hole in the centre. The paper/CM/paper "sandwich" was then positioned on a custom-made sample holder such that the CM surface was exposed to the plasma jet (**Figures 1B,C**). This setup prevented any movement of the CM during exposure to CAPP. The CAPP was generated from a mixture of 99.9% argon and 0.1 % oxygen (Air Liquide, Düsseldorf, Germany) using an 8 W plasma jet (kINPen 09; Neoplas tools, Greifswald, Germany) at ambient temperature and pressure (Weltmann et al., 2009). When the mixture of gases passed through the electrode operated at a high-frequency voltage (1.1 MHz; 2–6 kV peak-to-peak voltage), the CAPP was generated at the tip of the electrode (**Figures 1B,C**). The flow rate of the gas mixture was set at 5.4 L min^{-1} (Multigas controller, 647C; MKS Instruments, Andover, MA, USA). The power supplied to the plasma jet was 65 V at a resonance balancing of 0.05 A.

The CM discs mounted on the sample holder were subjected to CAPP treatment of the inner or outer side for durations of 0-, 5-, 10-, 15-, 20-, or 25-min. Earlier studies established that increasing exposure times to CAPP results in increasing ablation of synthetic polymers (Clouet and Shi, 1992) and isolated cuticles irrespective of the orientation of the cuticle (Khanal et al., 2014).

The distance between the CM and the tip of the plasma jet was set to 8 mm. This setup produced a CAPP treated area of about 8 mm diameter in the centre of the CM disc. Using these settings, the temperature of the CM disc always remained below 40°C (Khanal et al., 2014).

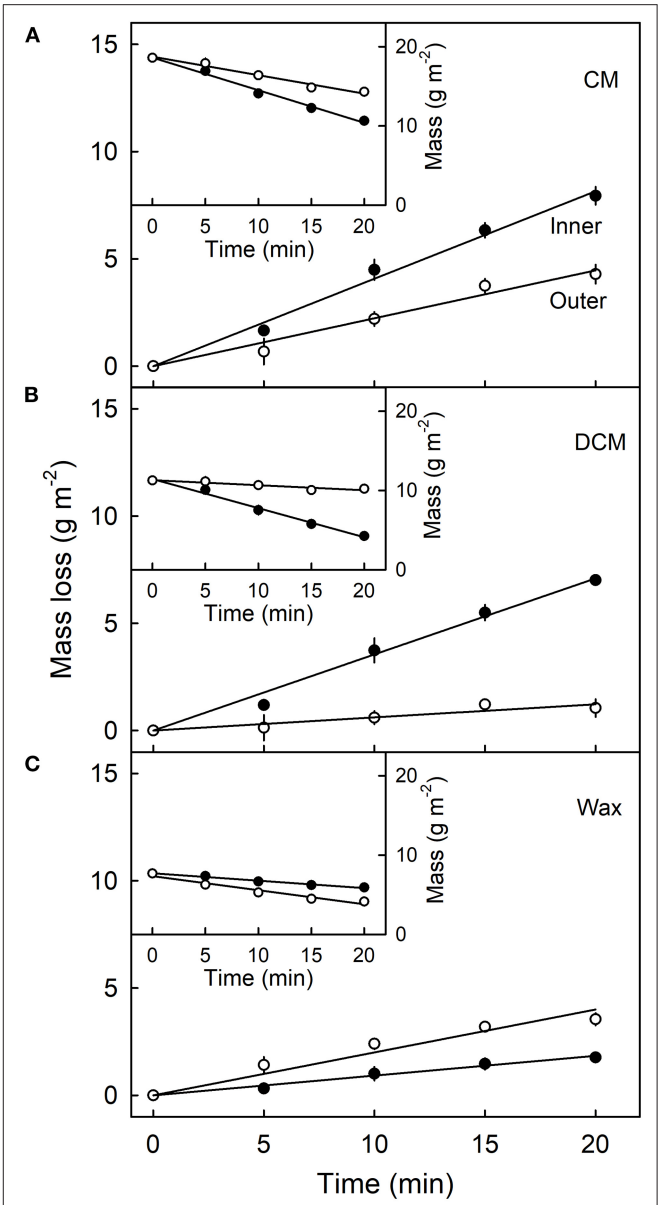

FIGURE 4 | Effect of duration of ablation of the cuticular membrane (CM) of apple fruit using cold atmospheric pressure plasma (CAPP) on the mass loss (main figures) and absolute mass (inset figures) of the CM **(A)**, the dewaxed CM (DCM) **(B)** and the wax **(C)**. The inner or the outer surface of the CM was ablated using CAPP and the mass loss of the CM, the cutin and wax fraction determined. The fruit was fed 138 days after full bloom and harvested 14 days after the termination of the feeding. Data points represent means ± SE, n = 6–16.

Scanning Electron Microscopy (SEM)

The effect of CAPP treatment on the outer and inner surfaces of the CMs was established using SEM. Non-ablated control CMs and CAPP treated CMs following wax extraction were observed in a Quanta 200 SEM (FEI Europe Main Office, Eindhoven, The Netherlands). Cross-sections were viewed following freeze fracturing in liquid nitrogen. Specimens were mounted on

TABLE 1 | Parameters of linear regression equations describing the relationships between mass loss (g m^{-2}) and the duration of ablation using a cold atmospheric pressure plasma (CAPP) on the morphological inner and outer sides of isolated cuticular membranes (CM) of 'Idared' apple.

Stage (DAFB)	Fraction	Morphological side	Slope ± SE	Coefficient of determination
69	CM	Inner	0.33 ± 0.01	0.999***
		Outer	0.23 ± 0.02	0.956***
	DCM	Inner	0.36 ± 0.02	0.992***
		Outer	0.10 ± 0.01	0.932**
	Wax	Inner	0.08 ± 0.00	0.990***
		Outer	0.13 ± 0.02	0.916**
103	CM	Inner	0.41 ± 0.01	0.999***
		Outer	0.32 ± 0.01	0.994***
	DCM	Inner	0.32 ± 0.02	0.979***
		Outer	0.12 ± 0.01	0.983***
	Wax	Inner	0.04 ± 0.00	0.941**
		Outer	0.22 ± 0.02	0.975***
138	CM	Inner	0.42 ± 0.01	0.995***
		Outer	0.21 ± 0.01	0.986***
	DCM	Inner	0.33 ± 0.02	0.985***
		Outer	0.08 ± 0.01	0.949**
	Wax	Inner	0.10 ± 0.00	0.995***
		Outer	0.20 ± 0.01	0.983***

The fruit was fed using ^{13}C oleic acid for 7 d beginning at 69, 103, and 138 days after full bloom (DAFB). After 7 d, feeding was terminated. The fruit was harvested 14 d after terminating feeding and the CMs were isolated. Wax was extracted after CAPP treatment. Dewaxed CMs are referred to as DCMs. Since the intercept term was not significantly different from zero, all regression lines were forced through the origin.

SE standard error of the estimate.

*Significance of the coefficients of determination at the 1 and 0.1% levels are indicated by ** and ***, respectively.*

aluminium stubs using conducting carbon tape and sputter-coated with gold. Calibrated images of the inner and outer surfaces were prepared at 1,000 x, those of cross-sections at 500 x. The acceleration potential was 15 kV.

Measurement of CM and DCM Mass

The mass loss during ablation of the CM by the CAPP treatment was quantified on a core disc excised from the ablated CMs. The core disc was of 4 mm diameter and was excised using a biopsy punch. The CMs were dried overnight at 40°C and weighed on a microbalance. The mass per unit area was calculated. Thereafter, the CMs were extracted in 2.0 ml chloroform:methanol (1:1, v/v) per disc for 24 h at ambient temperature. The dewaxed CMs were removed from the chloroform:methanol extraction mixture, rinsed once with fresh 0.5 ml chloroform:methanol, then dried overnight at 40°C. The DCM discs were then weighed and their mass per unit area calculated.

^{13}C Quantification Using Isotope Ratio Mass Spectrometry (IRMS)

The amount of unlabelled (^{12}C) and labelled carbon (^{13}C) in the 4 mm diameter CMs and DCMs (after CAPP treatment of the CMs) were measured on an elemental analyser (Isotope Cube; Elementar, Hanau, Germany) coupled with an isotope ratio mass spectrometer (Isoprime precisION; Isoprime-Elementar, Manchester, UK). We followed the procedure used by Si et al. (2021a,b). The labelled CM and DCM discs were crimped in aluminium boats (one disc per boat) (6 × 6 × 12 mm; LabNeed GmbH, Nidderau, Germany). The samples were combusted at 1,080°C under a pulse of oxygen. Cerium dioxide was supplied to catalyse the combustion. The resulting CO_2 was passed to an isotope ratio mass spectrometer where the standard and isotopic C contents were quantified by a heat conductivity detector. For each measurement, the detector was calibrated using a commercial sediment standard.

The C isotope ratio was calibrated online by injecting one pulse of the reference gas. The isotopic composition of C was calculated in the delta notation (at%) and referenced against Vienna Pee Dee Belemnite (VPDB). Further, C (at%) was referenced using international standards supplied by the International Atomic Energy Agency (IAEA, Vienna, Austria).

Sucrose (IAEA-CH-6), cellulose (IAEA-CH-3), and caffeine (IAEA-600) were used as standards for isotopic composition, and an in-house standard made from the spruce litter was used as an internal standard for quality control of C composition and the referenced isotopic composition.

The relative amount of tracer-derived C (R_{Tracer}) (new carbon) to the total carbon pool (old plus new carbon) was calculated using equation (1) (Gearing, 1991).

$$R_{Tracer} = \frac{at\%\ L - at\%\ C}{at\%\ C - at\%\ T} \times 100 \quad (1)$$

In this equation, at% represents the at% value of tracer (T) and labelled (L) or unlabelled control (C) CM or DCM sample. The total mass of tracer in the whole CM or DCM sample (M_{Tracer}) was calculated using equation (2).

$$M_{Tracer} = \frac{R_{Tracer} \times M_{Sample} \times \%C}{m_{sample}} \quad (2)$$

where M_{Sample} represents the total mass of the 4 mm diameter CM or DCM disc combusted in the elemental analyser, %C represents the carbon content of the respective sample, and m_{sample} represents the molar mass of carbon in the sample. All % values used in the above equations were divided by 100 prior to calculation.

Data Analyses

All experiments were conducted and analysed using completely randomised designs. Data were analysed by linear regression analysis using the statistical software package SAS version 9.1.3 (SAS Institute, Cary, NC). Data are presented as means ± standard errors. Where not shown, the error bars were smaller than data symbols.

RESULTS

Fruit surface area and fruit mass increased sigmoidally with time (**Figure 2A**). The masses of CM, DCM, and wax per unit fruit surface area, all increased during fruit development (**Figure 2B**). The rates of deposition of cutin and wax were highest in the early stages of fruit development, decreasing steadily until maturity (**Figures 2B,C**).

Untreated CMs revealed a typical pattern of imprints of epidermal cell walls with slight depressions above the anticlinal cell walls when viewed from the outer surface (**Figure 3A**). On the inner surface, there were cuticular ridges above the anticlinal cell walls (**Figure 3B**). Exposure of outer or inner surfaces of CMs to CAPP resulted in significant ablations of the CM as indexed by significant decreases in CM thickness (**Figures 3C–F**). The cuticular ridges present on the inner surface of the CM above the anticlinal epidermal cell walls had almost disappeared after CAPP treatment for 20 min (**Figures 3B,D,G**).

Mass loss per unit area of the CM (**Figure 4A**), DCM (**Figure 4B**) and wax (**Figure 4C**) increased linearly as the duration of CAPP treatment of the CM increased. The mass loss of the CM and the DCM was lower when the morphological outer surface was ablated, as compared with the ablation of the morphological inner surface. The reverse applied for wax mass. Here, ablation of the outer surface induced a larger loss in wax mass as compared with ablation of the inner surface. This is not surprising considering the presence of epicuticular wax on the outer surface of the CM. Similar results were obtained with CM ablated after feeding at 103 or 138 DAFB (**Table 1**). When treating the outer surface, CAPP treatment ablated the entire epicuticular wax layer plus some amount of the cutin and cuticular wax, whereas CAPP treatment of the inner surface ablated cutin plus any cuticular wax only.

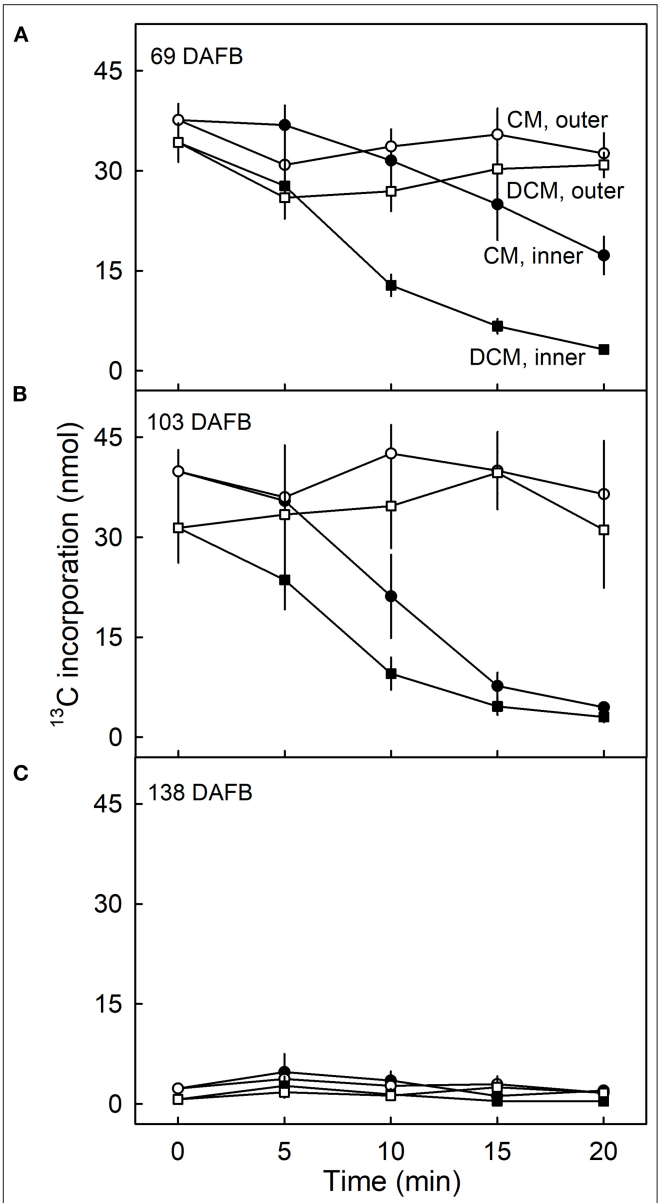

FIGURE 5 | Effect of duration of ablation of cuticular membranes (CM) of developing apple fruit using cold atmospheric pressure plasma (CAPP) on the amount of ^{13}C in the CM and the dewaxed CM (DCM). The inner or the outer surface of the CM was ablated using CAPP. Developing apple fruit were fed for 7 d using ^{13}C labelled oleic acid at 69 **(A)**, 103 **(B)**, 138 **(C)** days after full bloom (DAFB). The fruit was sampled 14 d after the termination of the feeding and the CMs were isolated. Data points represent means ± SE, n = 6–8.

The amount of ^{13}C in the CM and the DCM of fruit fed at 69 DAFB remained constant following ablation of the outer surface but decreased continuously when the inner surface was ablated (**Figure 5A**). Regardless of the duration of CAPP treatment of the inner side, the decrease in the amount of ^{13}C in the DCM was always higher than that in the CM indicating that incorporation was in the cutin matrix and not or less in the wax.

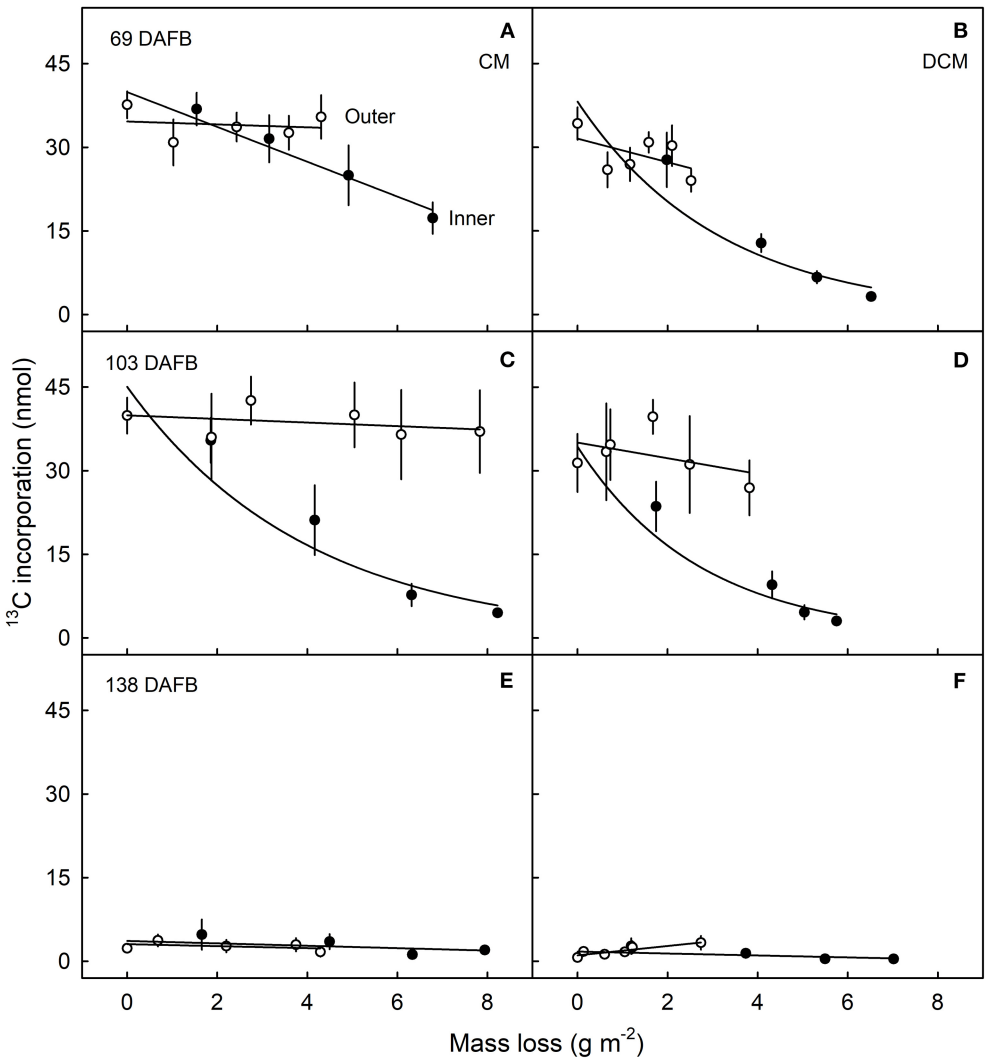

FIGURE 6 | Relationship between the amount of ^{13}C in the cuticular membrane (CM) **(A,C,E)** or in the dewaxed CM (DCM) **(B,D,F)** and the mass loss of the CM or DCM that resulted from ablation of the inner or outer surface of the CM using a cold atmospheric pressure plasma (CAPP). Developing apple fruit were fed for 7 d using ^{13}C labelled oleic acid at 69 **(A,B)**, 103 **(C,D)**, and 138 **(E,F)** days after full bloom (DAFB). The fruit was sampled 14 d after the termination of feeding and the CMs were isolated. Data points represent means ± SE, $n = 6$–8. For data on the relationships between mass loss and duration of ablation of the CM by CAPP see **Table 1**.

Qualitatively and quantitatively similar results were obtained when analysing CMs and DCMs of fruit fed at 103 DAFB (**Figure 5B**). At 138 DAFB, the amounts of incorporation of ^{13}C oleic acid in the CM and the DCM were low compared with those incorporated at 69 and 103 DAFB. There was no effect of CAPP treatment on ^{13}C content at 138 DAFB (**Figure 5C**).

Plotting the ^{13}C content of the CM or the DCM as a function of the amount of mass loss following CAPP treatment revealed that increasing mass loss resulted in decreasing ^{13}C content of CM and DCM when ablating their inner surfaces, but not when ablating their outer surfaces. With ablation of the outer surface of the CM, there was no relationship between the ^{13}C amounts in the CM or DCM and the mass losses of the CM or DCM following ablation. Similar results were obtained for CMs and DCMs of fruit fed at 69 and 103 DAFB (**Figures 6A–D**). There were no effects of ablation on the ^{13}C content of the CM or DCM for fruit fed at 138 DAFB (**Figures 6E,F**). At this stage of development, the deposition of CM has nearly ceased (**Figures 2B,C**).

Comparison of the ^{13}C contents of the DCM of fruit harvested 14 d after feeding at 69 DAFB with those from fruit harvested at maturity revealed significant differences (**Figure 7**). CAPP ablation of the CM of the fruit 14 d after feeding yielded an immediate decrease in ^{13}C content of the DCMs when carried out on the inner surface. However, when fruit was allowed to grow until maturity after feeding, ablation had no effects on the ^{13}C content up to a mass loss of about 4 g m^{-2}. Beyond this threshold, further ablation decreased the ^{13}C content as mass loss increased (**Figure 7A**). For DCMs of fruit fed at 103 DAFB and harvested at maturity, the ^{13}C contents began

to decrease for a mass loss of about 2 g m^{-2} (**Figure 7B**). In DCMs of fruit harvested 14 d after the termination of feeding, the ^{13}C content decreased continuously as mass loss increased. The fruit fed at 138 DAFB had very low ^{13}C contents in the DCM. Consequently, ablation by CAPP had little effect on the ^{13}C contents of the DCM (**Figure 7C**). This is consistent with the cessation of CM deposition at 138 DAFB (**Figures 2B,C**).

DISCUSSION

Our results evidence a radial gradient in the deposition and hence in the age of the cuticle of developing apple fruit. Feeding apple fruit with ^{13}C oleic acid resulted in the incorporation and the deposition of labelled material on the inner surface of the CM. Consequently, the inner surface of the CM is younger, whereas the outer surface was deposited early on in fruit development, and so is older. The evidence for this conclusion is two-fold.

First, we obtained a gradient in ^{13}C content of the DCM of fruit that (1) incorporated ^{13}C oleic acid in the cuticle (69 and 103 DAFB) and that (2) was harvested 14 d after the termination of the feeding period. The rate of this decrease was initially rapid but slowed as the duration of CAPP treatment increased and as the mass-loss increased.

Second, when the fruit was fed with ^{13}C oleic acid at 69 or 103 DAFB and then remained on the tree until maturity, the label was incorporated during the feeding period and immediately thereafter. However, un-labelled monomers were later incorporated in the cuticle on the inner surface. As cuticle deposition continued during development, the layer of the label was progressively overlaid and so "retreated" deeper into the cuticle as indicated in the sketch in **Figure 8**. Support for this view comes from the following observation. When the inner surface of the CM was ablated, short periods of ablation removed only the un-labelled portion of the cuticle, whereas longer ablations began to remove the labelled cuticle in ever deeper layers, and closer to the outer surface (**Figure 8**). The duration of the initial period without a decrease in ^{13}C and the magnitude of the mass loss before the removal of the ^{13}C labelled layer began depended on the thickness of the un-labelled layer, deposited after the termination of the feeding period. The duration of ablation before progressing into the labelled layer was longer for the feeding at 69 DAFB than for that at 103 DAFB. This interpretation is also consistent with the observation that treatment from the outer surface did not affect the ^{13}C content of the polymer matrix. The above conclusions also account for the radial gradient in strain in apple fruit CM that has been reported previously (Khanal et al., 2014). Due to the earlier deposition, the outer CM has a longer history of strain and is, therefore, more strained, whereas the inner layer was deposited later and, hence, will have experienced less strain. This conclusion is also consistent with the structural characteristics of the apple cuticle (de Vries, 1968; Konarska, 2013). A cuticle proper (CP) that is rich in wax is distinguished from the underlying cuticular layer (CL) (Jeffree, 1996; Yeats and Rose, 2013). The CL was rich in cutin and contains embedded polysaccharides. The development of the CP precedes that of the CL (Jeffree, 2006).

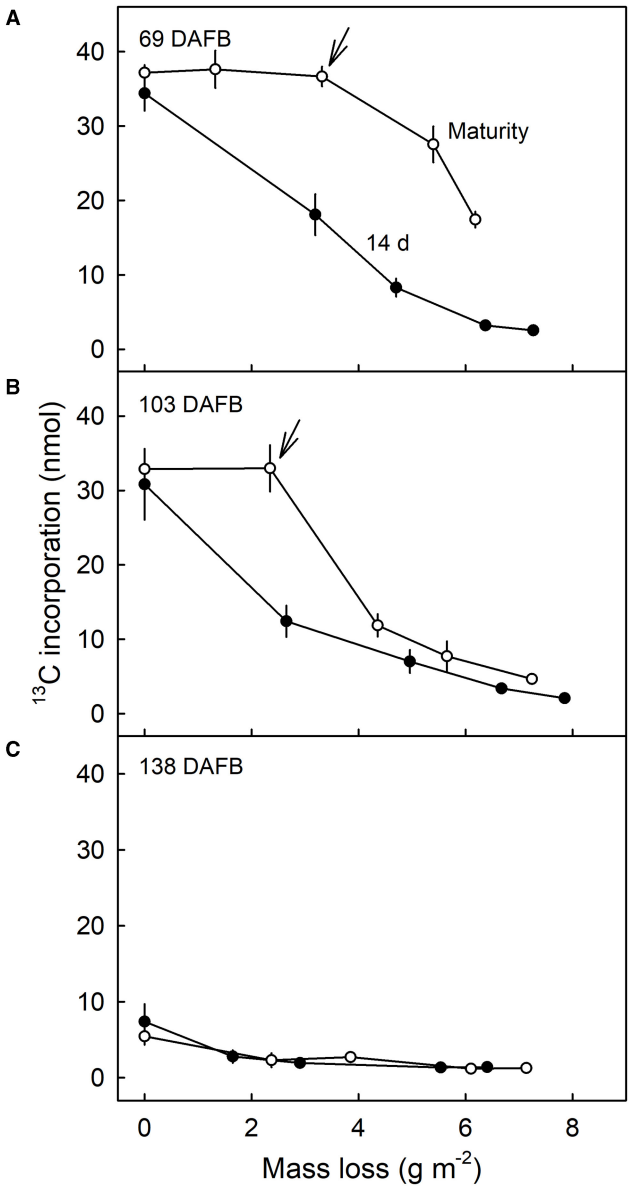

FIGURE 7 | Relationship between the amount of ^{13}C in the dewaxed cuticular membrane (DCM) and the mass loss of the DCM that resulted from ablation of the inner surface of the CM using a cold atmospheric pressure plasma (CAPP). Developing apple fruit were fed for 7 d using ^{13}C labelled oleic acid at 69 **(A)**, 103 **(B)**, and 138 **(C)** days after full bloom (DAFB). The fruit was sampled either 14 d after the termination of the feeding or at maturity and the CMs isolated. Data points represent means ± SE, $n = 8$–10. For data on the relationships between mass loss and duration of ablation of the CM by CAPP see **Supplementary Table 1**.

The question arose as to what the chemical nature of the label might be incorporated in the cuticle. Since there was very

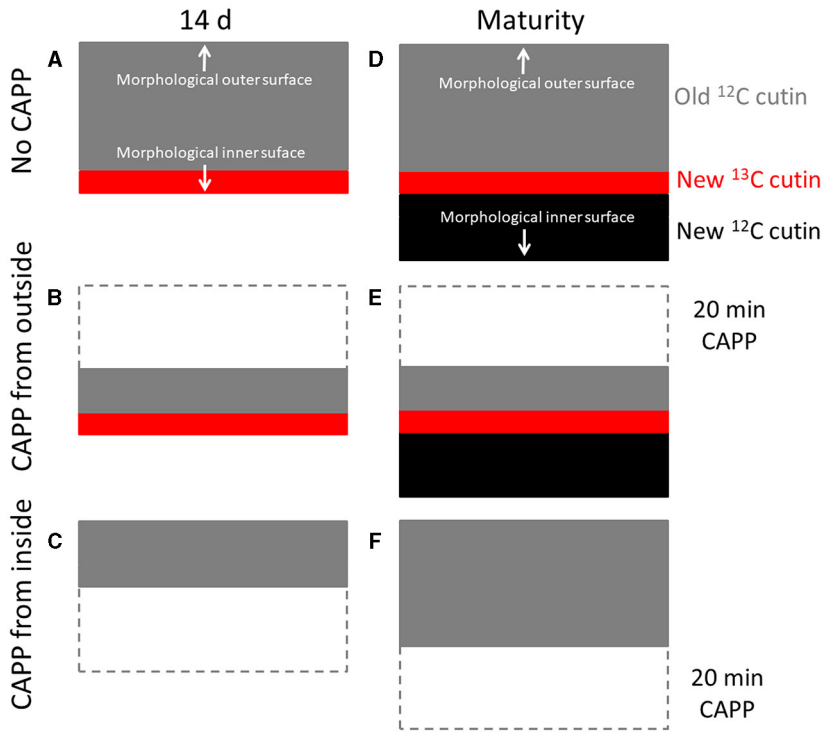

FIGURE 8 | Sketch illustrating the location of the ^{13}C labelled layer within the cuticular membrane (CM) that resulted from feeding the developing apple fruit using ^{13}C labelled oleic acid for 7 d. The ^{13}C labelled precursor is incorporated in the inner side of the CM **(A)**. Isolation of the CM at this stage and ablation from its outer side has no effect on the ^{13}C content until the ^{13}C labelled layer of the CM is ablated **(B)**, ablation from the inner side decreases the ^{13}C content of the CM as mass loss increases **(C)**. In contrast, when fruit remains on the tree until maturity, CM deposition continues on the inner side. The layer resulting from feeding ^{13}C oleic acid now "moves" into the CM **(D)**. Ablation from the outer side still has no effect on the ^{13}C content until the ^{13}C labelled layer of the CM is ablated **(E)**. When ablation from the inner side, ablation will not affect the ^{13}C content of the CM until the labelled layer is reached **(F)**. Further ablation then will decrease the ^{13}C content.

little label associated with the wax, most of the incorporation was in the dewaxed CM. This indicates chemical binding, not simply partitioning into the CM (Si et al., 2021a). The two major constituents of the dewaxed CM are cutin and polysaccharides (Schreiber and Schönherr, 1990). Several arguments suggest this incorporation occurred in the cutin fraction.

First, the incorporation pattern was similar to that of CM deposition—i.e., it was higher during the early developmental stages, but lower in the late-stage close to maturity. This is consistent with the deposition pattern of cutin during the development of the apple fruit (Lai et al., 2016). Second, feeding ^{14}C labelled oleic acids to apple skin discs resulted in the incorporation of the label in hydroxy C18 acids such as 18-hydroxyoctadecenoic acid, 10,18-dihydroxyoctadecanoic acid, and 9,10,18-trihydroxyoctadecanoic acid (Kolattukudy et al., 1971, 1973). These are major monomers of the apple fruit cutin (Walton and Kolattukudy, 1972; Straube et al., 2021). Also, until now the composition of apple cutin has been found to be consistent among all cultivars investigated (Holloway, 1973; Legay et al., 2017; Straube et al., 2021). Third, the cutin of apple fruit has been classified as a "mixed-type cutin" comprising C16 and C18 monomers (Holloway, 1982). This is in line with earlier observations from our laboratory, that when developing apple fruit were fed with ^{14}C palmitic acid and ^{14}C oleic acid incorporation in the CM of ^{14}C palmitic acid was very much lower than of ^{14}C oleic acid (Si et al., 2021a). This incorporation occurs in all apple cultivars investigated and at a rate that is significantly correlated with the mass of the CM per unit fruit surface area (Si et al., 2021b).

It may be argued that oleic acid is also a precursor for suberin and that the exposure of the apple fruit surface to the feeding solution may have resulted in microcracking and then periderm formation (Chen et al., 2020; Khanal et al., 2021). However, we considered this possibility extremely unlikely. First, 'Idared' is a cultivar that is known not to be susceptible to russeting (Khanal et al., 2013b). Russeting involves the formation of a periderm where the phellem typically has heavily suberized cell walls. Second, the feeding treatments in our study were done long after the period of greatest russet susceptibility was over (Chen et al., 2020; Khanal et al., 2021). Apple fruit is most susceptible to russet during the first 28 days after full bloom. Third, the apple fruit fed with oleic acid all had intact cuticles. There were no indications of either microcracking or russeting either to the naked eye or under SEM regardless of whether the fruit was harvested after a 7-day feeding plus the 14-d incorporation period or later at maturity. By this time, any russeting would have been visible on the fruit surface. Fourth, suberin is deposited inside the cell wall (Franke and Schreiber, 2007; Pollard et al., 2008). We obtained clean CMs after enzymatic isolation (see also **Figure 3**).

Furthermore, a 5-min CAPP treatment of the inner surface decreased CM mass by about 8% (Khanal et al., 2014). This would have been sufficient to remove any hypothetical suberized cell walls that might have been present. This would have left no label in the dewaxed CM. However, in the fruit harvested at maturity the label from the early feeding was incorporated deep into the CM.

These arguments demonstrated that both, the label detected in the inner surface of the dewaxed CM from fruit harvested after the feeding and the incorporation period, and the label found deeper in the dewaxed CM of fruit harvested at maturity, most likely represent hydroxy C18 monomers polymerized in the cutin.

Practical Implications

The deposition pattern of cutin on the inner side of the cuticle represents an important and critical mechanism that delays or prevents the formation of deep microcracks. A high rate of cutin deposition also maintains a minimum thickness of the CM during phases of rapid fruit expansion. Because the deposition occurs on the inner surface of the CM, the likelihood of the formation of microcracks that traverse the cuticle decreases. Microcracks that traverse the cuticle dramatically impair the barrier functions of the cuticle and trigger the formation of periderm, which led to russeting.

The results obtained in apple are thought likely to apply also to other fruit crop species that deposit cuticles throughout development. Further study should explore the possibility of stimulating the deposition of cutin during periods of rapid fruit growth, to help prevent deep propagation of microcracks.

DATA AVAILABILITY STATEMENT

The raw data supporting the conclusions of this article will be made available by the authors, without undue reservation.

AUTHOR CONTRIBUTIONS

BK and MK obtained the funds to support the study. YS, BK, and MK planned the experiments, wrote, revised, and edited the manuscript. YS and OS conducted the experiments. YS and BK analysed the data. All authors contributed to the article and approved the submitted version.

FUNDING

This research was funded by a grant from the Deutsche Forschungsgemeinschaft (KH 374/2-1).

ACKNOWLEDGMENTS

We thank Mr. Roger-Michael Klatt for operating the scanning electron microscope, Dr. Leopold Sauheitl for operating the mass spectrometer, and Dr. Alexander Lang for helpful comments on an earlier version of this manuscript.

SUPPLEMENTARY MATERIAL

The Supplementary Material for this article can be found online at: https://www.frontiersin.org/articles/10.3389/fpls.2021.730837/full#supplementary-material

REFERENCES

Bußler, S. (2017). *Cold atmospheric pressure plasma treatment of food matrices: tailored modification of product properties along value-added chains of plant and animal related products* (dissertation). Technische Universität Berlin, Berlin, Germany.

Chen, Y.-H., Straube, J.,Khanal, B. P., Knoche, M., and Debener, T. (2020). Russeting in apple is initiated after exposure to moisture ends. *I. Histological evidence. Plants* 9:1293. doi: 10.3390/plants9101293

Clouet, F., and Shi, M. K. (1992). Interactions of polymer model surfaces with cold plasmas: hexatriacontane as a model molecule of high-density polyethylene and octadecyl octadecanoate as a model of polyester. I. Degradation rate versus time and power. *J. Appl. Polym. Sci.* 46, 1955–1966. doi: 10.1002/app.1992.070461108

de Vries, H. A. M. A. (1968). Development of the structure of the normal, smooth cuticle of the apple 'Golden delicious', *Acta Bot. Neerlandica* 17, 229–241. doi: 10.1111/j.1438-8677.1968.tb00120.x

Dominguez, E., Cuartero, J., and Heredia, A. (2011). An overview on plant cuticle biomechanics. *Plant Sci.* 181, 77–84. doi: 10.1016/j.plantsci.2011.04.016

Espana, L., Heredia-Guerrero, J. A., Segado, P., Benitez, J. J., Heredia, A., and Dominguez, E. (2014). Biomechanical properties of the tomato (*Solanum lycopersicum*) fruit cuticle during development are modulated by changes in the relative amounts of its components. *New Phytol.* 202, 790–802. doi: 10.1111/nph.12727

Franke, R., and Schreiber, L. (2007). Suberin - a biopolyester forming apoplastic plant interfaces. *Curr. Opinion Plant Biol.* 10, 252–259. doi: 10.1016/j.pbi.2007.04.004

Gearing, J. N. (1991). "The study of diet and trophic relationships through natural abundance ^{13}C," in *Carbon Isotope Techniques*, eds D. C. Coleman and B. Fry (London: Academic Press), 201–208. doi: 10.1016/B978-0-12-179730-0.50018-7

Heredia, A. (2003). Biophysical and biochemical characteristics of cutin, a plant barrier biopolymer. *Biochim. Biophys. Acta* 1620, 1–7. doi: 10.1016/S0304-4165(02)00510-X

Holloway, P. J. (1973). Cutins of *Malus Pumila* fruits and leaves. *Phytochemistry* 12, 2913–2920. doi: 10.1016/0031-9422(73)80506-0

Holloway, P. J. (1982). "The chemical constitution of plant cutins," in *The Plant Cuticle*, eds D. F. Cutler, K. L. Alvin, and C. E. *Price* (New York, NY; London: Academic Press), 45–85.

Huang, J. S. (2001). Penetration of cuticles by plant pathogens. *Plant Pathogenesis and Resistance*. Dordrecht: Springer. 3–48. doi: 10.1007/978-94-017-2687-0_1

Jeffree, C. E. (1996). "Structure and ontogeny of plant cuticle," in *Plant Cuticle: An Integrated Functional Approach*, ed G. Kerstiens (Oxford: Bios Scientific Publishers), 33–82.

Jeffree, C. E. (2006). The fine structure of the plant cuticle. *Annu. Plant Rev.* 23, 11–125. doi: 10.1002/9780470988718.ch2

Kerstiens, G. (2006). Water transport in plant cuticles: an update. *J. Exp. Bot.* 57, 2493–2499. doi: 10.1093/jxb/erl017

Khanal, B.P., Grimm, E., Finger, S., Blume, A., and Knoche, M. (2013a). Intracuticular wax fixes and restricts strain in leaf and fruit cuticles. *New Phytol.* 200, 134–143. doi: 10.1111/nph.12355

Khanal, B. P., Imoro, Y., Chen, Y. H., Straube, J., and Knoche, M. (2021). Surface moisture increases microcracking and water vapor permeance of apple fruit skin. *Plant Biol.* 23:74–82. doi: 10.1111/plb.13178

Khanal, B. P., Knoche, M., Bußler, S., and Schlüter, O. (2014). Evidence for a radial strain gradient in apple fruit cuticles. *Planta* 240, 891–897. doi: 10.1007/s00425-014-2132-0

Khanal, B. P., Shrestha, R., Hückstädt, L., and Knoche, M. (2013b). Russeting in apple seems unrelated to the mechanical properties of the cuticle at maturity. *HortScience* 48, 1135–1138. doi: 10.21273/HORTSCI.48.9.1135

Knoche, M., Beyer, M., Peschel, S., Oparlakov, B., and Bukovac, M. J. (2004). Changes in strain and deposition of cuticle in developing sweet cherry fruit. *Physiol. Plant.* 120, 667–677. doi: 10.1111/j.0031-9317.2004.0285.x

Knoche, M., Khanal, B. P., Brüggenwirth, M., and Thapa, S. (2018). Patterns of microcracking in apple fruit skin reflect those of the cuticular ridges and of the epidermal cell walls. *Planta* 248, 293–306. doi: 10.1007/s00425-018-2904-z

Knoche, M., and Lang, A. (2017). Ongoing growth challenges fruit skin integrity. *CRC. Crit. Rev. Plant Sci.* 36, 190–215. doi: 10.1080/07352689.2017.1369333

Kolattukudy, P. E. (1980). Biopolyester membranes of plants: cutin and suberin. *Science* 208, 990–1000. doi: 10.1126/science.208.4447.990

Kolattukudy, P. E., Croteau, R., and Brown, L. (1974). Structure and biosynthesis of cuticular lipids: hydroxylation of palmitic acid and decarboxylation of C(28), C(30), and C(32) acids in *Vicia faba* flowers. *Plant Physiol.* 54, 670–677. doi: 10.1104/pp.54.5.670

Kolattukudy, P. E., and Walton, T. J. (1972). Structure and biosynthesis of the hydroxy fatty acids of cutin in *Vicia faba* leaves. *Biochem.* 11, 1897–1907. doi: 10.1021/bi00760a026

Kolattukudy, P. E., Walton, T. J., and Kushwaha, R. P. S. (1971). Epoxy acids in the lipid polymer, cutin and their role in the biosynthesis of cutin. *Biochem. Biophys. Res. Commun.* 42, 739–744.

Kolattukudy, P. E., Walton, T. J., and Kushwaha, R. P. S. (1973). Biosynthesis of the C18 family of cutin acids: ω-hydroxyoleic acid, ω-hydroxy-9,10-epoxystearic acid, 9,10,18-trihydroxystearic acid, and their 12-unsaturated analogs. *Biochemistry* 12, 4488–4497. doi: 10.1021/bi00746a029

Konarska, A. (2013). The structure of the fruit peel in two varieties of *Malus domestica* Borkh. (*Rosaceae*) before and after storage. *Protoplasma* 250, 701–714. doi: 10.1007/s00709-012-0454-y

Lai, X., Khanal, B. P., and Knoche, M. (2016). Mismatch between cuticle deposition and area expansion in fruit skins allows potentially catastrophic buildup of elastic strain. *Planta* 244, 1145–1156. doi: 10.1007/s00425-016-2572-9

Legay, S., Cocco, E., André, C. M., Guignard, C., Hausman, J. F., and Guerriero, G. (2017). Differential lipid composition and gene expression in the semi-russeted "Cox Orange Pippin" apple variety. *Front. Plant Sci.* 8:1656. doi: 10.3389/fpls.2017.01656

Maguire, K. M. (1998). *Factors affecting mass loss of apples* (dissertation). Massey University, Palmerston North, New Zealand.

Martin, L. B., and Rose, J. K. (2014). There's more than one way to skin a fruit: formation and functions of fruit cuticles. *J. Exp. Bot.* 65, 4639–4651. doi: 10.1093/jxb/eru301

Pollard, M., Beisson, F., Li, Y., and Ohlrogge, J. B. (2008). Building lipid barriers: biosynthesis of cutin and suberin. *Trends Plant Sci.* 13, 236–246. doi: 10.1016/j.tplants.2008.03.003

Riederer, M., and Schreiber, L. (2001). Protecting against water loss: analysis of the barrier properties of plant cuticles. *J. Exp. Bot.* 52, 2023–2032. doi: 10.1093/jexbot/52.363.2023

Schreiber, L., and Schönherr, J. (1990). Phase transitions and thermal expansion coefficients of plant cuticles: the effects of temperature on structure and function. *Planta* 182, 186–193. doi: 10.1007/BF00197109

Serrano, M., Coluccia, F., Torres, M., L'Haridon, F., and Métraux, J.-P. (2014). The cuticle and plant defense to pathogens. *Front. Plant Sci.* 5, 1–8. doi: 10.3389/fpls.2014.00274

Si, Y., Khanal, B. P., and Knoche, M. (2021b). Factors affecting cuticle synthesis in apple fruit identified under field conditions. *Sci. Hortic.* 290:110512. doi: 10.1016/j.scienta.2021.110512

Si, Y., Khanal, B. P., Sauheitl, L., and Knoche, M. (2021a). Cutin synthesis in developing, field-grown apple fruit examined by external feeding of labelled precursors. *Plants* 10, 1–14. doi: 10.3390/plants10030497

Skene, D. S. (1980). Growth stresses during fruit development in Cox's Orange Pippin apples. *J. Hort. Sci.* 55, 27–32. doi: 10.1080/00221589.1980.11514897

Straube, J., Chen, Y.-H., Khanal, B.P., Shumbusho, A., Zeisler-Diehl, V., Suresh, K., et al. (2021). Russeting in apple is initiated after exposure to moisture ends: molecular and biochemical Evidence. *Plants* 10:65. doi: 10.3390/plants10010065

Walton, T. J., and Kolattukudy, P. E. (1972). Determination of the structures of cutin monomers by a novel depolymerization procedure and combined gas chromatography and mass spectrometry. *Biochemistry* 11, 1885–1897. doi: 10.1021/bi00760a025

Weltmann, K.D., Kindel, E., Brandenburg, R., Meyer, C., Bussiahn, R., Wilke, C., et al. (2009). Atmospheric pressure plasma jet for medical therapy: plasma parameters and risk estimation. *Contrib. Plasma Phys.* 49, 631–640. doi: 10.1002/ctpp.200910067

Yeats, T. H., and Rose, J. K. C. (2013). The formation and function of plant cuticles. *Plant Physiol.* 163, 5–20. doi: 10.1104/pp.113.222737

Conflict of Interest: The authors declare that the research was conducted in the absence of any commercial or financial relationships that could be construed as a potential conflict of interest.

Publisher's Note: All claims expressed in this article are solely those of the authors and do not necessarily represent those of their affiliated organizations, or those of the publisher, the editors and the reviewers. Any product that may be evaluated in this article, or claim that may be made by its manufacturer, is not guaranteed or endorsed by the publisher.

frontiers in Plant Science

ORIGINAL RESEARCH
published: 26 October 2021
doi: 10.3389/fpls.2021.752309

The ARRE RING-Type E3 Ubiquitin Ligase Negatively Regulates Cuticular Wax Biosynthesis in *Arabidopsis thaliana* by Controlling ECERIFERUM1 and ECERIFERUM3 Protein Levels

*Shuang Liu[1], Meixuezi Tong[1,2], Lifang Zhao[1], Xin Li[1,2] and Ljerka Kunst[1]**

[1]*Department of Botany, University of British Columbia, Vancouver, BC, Canada,* [2]*Michael Smith Laboratories, University of British Columbia, Vancouver, BC, Canada*

OPEN ACCESS

Edited by:
Isabel Molina,
Algoma University, Canada

Reviewed by:
Mi Chung Suh,
Sogang University,
South Korea
Shiu Cheung Lung,
The University of Hong Kong,
Hong Kong, SAR China

***Correspondence:**
Ljerka Kunst
ljerka.kunst@ubc.ca

Specialty section:
This article was submitted to Plant Physiology, a section of the journal Frontiers in Plant Science

Received: *02 August 2021*
Accepted: *28 September 2021*
Published: *26 October 2021*

Citation:
Liu S, Tong M, Zhao L, Li X and Kunst L (2021) The ARRE RING-Type E3 Ubiquitin Ligase Negatively Regulates Cuticular Wax Biosynthesis in Arabidopsis thaliana by Controlling ECERIFERUM1 and ECERIFERUM3 Protein Levels. Front. Plant Sci. 12:752309. doi: 10.3389/fpls.2021.752309

The outer epidermal cell walls of plant shoots are covered with a cuticle, a continuous lipid structure that provides protection from desiccation, UV light, pathogens, and insects. The cuticle is mostly composed of cutin and cuticular wax. Cuticular wax synthesis is synchronized with surface area expansion during plant development and is associated with plant responses to biotic and abiotic stresses. Cuticular wax deposition is tightly regulated by well-established transcriptional and post-transcriptional regulatory mechanisms, as well as post-translationally *via* the ubiquitin-26S proteasome system (UPS). The UPS is highly conserved in eukaryotes and involves the covalent attachment of polyubiquitin chains to the target protein by an E3 ligase, followed by the degradation of the modified protein by the 26S proteasome. A large number of E3 ligases are encoded in the Arabidopsis genome, but only a few have been implicated in the regulation of cuticular wax deposition. In this study, we have conducted an E3 ligase reverse genetic screen and identified a novel RING-type E3 ubiquitin ligase, AtARRE, which negatively regulates wax biosynthesis in Arabidopsis. Arabidopsis plants overexpressing AtARRE exhibit glossy stems and siliques, reduced fertility and fusion between aerial organs. Wax load and wax compositional analyses of AtARRE overexpressors showed that the alkane-forming branch of the wax biosynthetic pathway is affected. Co-expression of AtARRE and candidate target proteins involved in alkane formation in both *Nicotiana benthamiana* and stable Arabidopsis transgenic lines demonstrated that AtARRE controls the levels of wax biosynthetic enzymes ECERIFERUM1 (CER1) and ECERIFERUM3 (CER3). CER1 has also been confirmed to be a ubiquitination substrate of the AtARRE E3 ligase by an *in vivo* ubiquitination assay using a reconstituted *Escherichia coli* system. The *AtARRE* gene is expressed throughout the plant, with the highest expression detected in fully expanded rosette leaves and oldest stem internodes. *AtARRE* gene expression can also be induced by exposure to pathogens. These findings reveal that wax biosynthesis in

mature plant tissues and in response to pathogen infection is controlled post-translationally.

Keywords: Arabidopsis, cuticle, cuticular wax biosynthesis, AtARRE, E3 ligase, CER1, CER3

INTRODUCTION

The primary aerial surfaces of land plants are covered with a cuticle, a continuous lipidic layer that restricts transpirational water loss, reflects harmful UV light, and prevents organ fusions during development (Reicosky and Hanover, 1978; Sieber et al., 2000; Riederer and Schreiber, 2001; Riederer, 2006). The cuticle also serves as a protective barrier against pathogens and insects (Müller, 2018; Ziv et al., 2018) and is involved in drought-stress signaling (Wang et al., 2011).

The cuticle is mostly composed of cutin and cuticular wax (Samuels et al., 2008). Cutin is a polymer of oxidized 16- and 18-carbon (C16 and C18) fatty acids and glycerol (Beisson et al., 2012), which forms the structural scaffold of the cuticle. Cuticular wax embeds and overlays this cutin matrix and is composed of very long-chain fatty acids (VLCFAs; C20-C38) and their derivatives, including alkanes, aldehydes, primary and secondary alcohols, ketones, and esters. Small amounts of triterpenoids, flavonoids, or sterols may also be present (Jetter et al., 2006; Buschhaus and Jetter, 2011). Wax composition varies among plant species, as well as between different organs, tissues, and developmental stages of the same plant species. These variations in wax composition affect the biochemical and physical properties of the plant surface, which helps the plant adapt to different environments.

Cuticular wax is synthesized by epidermal cells. C16 and C18 fatty acids are made in the plastid and activated to acyl-CoA thioesters, which are translocated to the endoplasmic reticulum (ER) for further elongation to VLC acyl-CoA wax precursors by a fatty acid elongase (FAE) complex (Haslam and Kunst, 2013a). In addition, the ECERIFERUM2-LIKE (CER2-LIKE) family of proteins is required for the formation of C30 to C34 VLC acyl-CoAs (Haslam et al., 2017). Following elongation, VLC acyl-CoAs are modified by one of two pathways, either the acyl reduction pathway, which generates primary alcohols and wax esters, or the alkane-forming pathway, which produces aldehydes, alkanes, secondary alcohols, and ketones (Samuels et al., 2008). In Arabidopsis (*Arabidopsis thaliana*) leaves and stems, cuticular wax is predominantly derived from the alkane-forming pathway. As the major wax component, alkanes represent over 70 and 50% of the total wax load in leaves and stems, respectively (Bourdenx et al., 2011). It has been proposed that the formation of alkanes is catalyzed by a multiprotein complex comprising CER1, CER3, and a cytochrome B5 protein (CYTB5) that converts VLC acyl-CoAs to alkanes with aldehydes as intermediates (Rowland et al., 2007; Bourdenx et al., 2011; Bernard et al., 2012). CYTB5 isoforms interact with CER1 and provide the electron(s) required for this redox-dependent reaction. The CER1 and CER3 proteins are integral membrane proteins with 35% amino acid identity that contain eight conserved His clusters in their N-terminal domain and an uncharacterized WAX2 domain at their C-terminus (Aarts et al., 1995; Chen et al., 2003; Bernard et al., 2012). In Arabidopsis stems, alkanes can be further oxidized to secondary alcohols and ketones by a cytochrome P450 enzyme, the MID-CHAIN ALKANE HYDROXYLASE1 (MAH1; Greer et al., 2007).

Wax biosynthesis is tightly controlled throughout plant development and in response to biotic and abiotic stresses. Forward and reverse genetic studies in Arabidopsis, barley (*Hordeum vulgare*), maize (*Zea mays*), rice (*Oryza sativa*), and tomato (*Solanum lycopersicum*) have significantly improved our understanding of cuticular wax deposition and regulatory pathways controlling this process (Samuels et al., 2008; Yeats and Rose, 2013). Production of cuticular waxes is primarily under transcriptional regulation. Several independent studies have demonstrated that the WAX INDUCER1/SHINE1 (WIN1/SHN1) transcription factor, known to predominantly regulate cutin production, also indirectly affects wax synthesis (Aharoni et al., 2004; Broun et al., 2004; Kannangara et al., 2007). Other transcription factors, including MYB16, MYB30, MYB94, MYB96, MYB106, and WRINKLED4, have been reported to positively regulate wax synthesis in Arabidopsis stems and leaves (Raffaele et al., 2008; Seo et al., 2011; Oshima et al., 2013; Lee et al., 2014; Lee and Suh, 2015b; Park et al., 2016). Conversely, the DEWAX and DEWAX2 transcription factors act as repressors of wax production in Arabidopsis (Go et al., 2014; Kim et al., 2018).

In addition to the transcriptional regulation described above, characterization of the Arabidopsis *CER7* gene and suppressors of the *cer7* mutant resulted in the discovery of a post-transcriptional regulatory mechanism that affects stem wax deposition during inflorescence development. It involves CER7-mediated *CER3* gene silencing by trans-acting small interfering RNAs (tasiRNAs; Hooker et al., 2007; Lam et al., 2012, 2015). Recently, another type of small RNAs, microRNAs (miRNAs), were also shown to participate in the regulation of wax synthesis. Specifically, miR156 targets the SQUAMOSA PROMOTER BINDING PROTEIN-LIKE 9 (SPL9) transcription factor that positively regulates the expression of the alkane-forming enzyme CER1 through direct binding to the *CER1* promoter. Furthermore, SPL9 was shown to be involved in the optimization of diurnal wax production in Arabidopsis stems and leaves by direct protein–protein interaction with a negative regulator of wax synthesis DEWAX (Li et al., 2019).

Work by several groups demonstrated that wax biosynthesis in Arabidopsis is also post-translationally controlled by the ubiquitin-proteasome system (UPS). The UPS involves two distinct steps: the covalent attachment of a polyubiquitin chain consisting of at least four ubiquitin residues to the protein target, followed by the degradation of the modified protein by the 26S proteasome. Ubiquitination is catalyzed by three enzymes: a ubiquitin-activating enzyme (E1), a ubiquitin-conjugating

enzyme (E2), and a ubiquitin ligase (E3). Among these proteins, E3 ligases play key roles in determining substrate specificity (Hershko and Ciechanover, 1998; Vierstra, 2009). Several Arabidopsis E3 ligases have been shown to be involved in regulating cuticular wax deposition. Characterization of the wax-deficient *cer9* mutant and isolation of the *CER9* gene revealed that it encodes a putative E3 ligase, although its enzyme activity and ubiquitination substrate have not been determined (Lü et al., 2012). More recently, MYB30-INTERACTING E3 LIGASE 1 (MIEL1) has been shown to negatively regulate cuticular wax biosynthesis in Arabidopsis stems by targeting MYB30 and MYB96 transcription factors for degradation (Lee and Seo, 2016; Gil et al., 2017). Additionally, F-box protein SAGL1 targets wax biosynthetic enzyme CER3 for degradation thereby negatively regulating cuticular wax production in response to changes in ambient humidity (Kim et al., 2019). In rice, the DROUGHT HYPERSENSITIVE E3 ligase negatively regulates wax production by targeting the RICE OUTERMOST CELL-SPECIFIC GENE4 (ROC4) transcription factor involved in drought-stress response for degradation by the UPS (Wang et al., 2018b).

Based on the presence of over 1,400 putative E3 ligases encoded in the Arabidopsis genome (Kraft et al., 2005) and their importance in the regulation of plant responses to environmental stress, we reasoned that additional E3 ligases may be involved in the control of cuticular wax deposition. Here, we report the identification of a RING-type E3 ubiquitin ligase named ABA-related RING-type E3 ligase (AtARRE) that negatively regulates wax production by promoting the degradation of wax biosynthetic enzymes CER1 and CER3. This E3 ligase was previously reported to be involved in abscisic acid (ABA) signaling, but its ubiquitination target has not been identified (Wang et al., 2018a). Our results demonstrate that Arabidopsis plants overexpressing AtARRE display glossy stems and siliques, markedly reduced wax loads, and often aerial organ fusions and reduced fertility. Co-expression of AtARRE and candidate substrates in both *Nicotiana benthamiana* and stable Arabidopsis transgenic lines indicates that CER1 and CER3 wax biosynthetic enzymes are targeted by the AtARRE for degradation *via* the 26S proteasome. The *AtARRE* gene is highly expressed in tissues that exhibit no or low wax production, such as roots and cotyledons in older developing seedlings, as well as fully expanded rosette leaves and older internodes at the bottom of the stem in mature plants. *AtARRE* expression can also be induced by pathogen infection. Taken together, our results suggest that AtARRE acts as a quick and efficient switch for turning off wax biosynthesis in tissues where it is no longer needed and upon exposure to pathogens.

MATERIALS AND METHODS

Plant Material and Growth Conditions

Arabidopsis thaliana ecotype Columbia-0 (Col-0) wild type was used in this study. Arabidopsis T-DNA insertion lines *atarre-1* (SALK_094303), *atarre-2* (SALK_034426C; Alonso et al., 2003), and the *cer1-4* and *cer4-4* mutants were obtained from the Arabidopsis Biological Resource Center (ABRC).[1] GABI-KAT T-DNA line *atarre-3* (GABI_383G01) was obtained from gabi-kat.de (Kleinboelting et al., 2012). *cer3-6* was a gift from Dr. Takuji Wada (RIKEN, Japan). AtARRE overexpression lines in Col-0 background were identified from the *snc1*-influencing plant E3 ligase reverse (SNIPER) genetic screen (Tong et al., 2017).

Arabidopsis seeds were germinated on *Arabidopsis thaliana* (AT) medium (Haughn and Somerville, 1986) supplemented with 1% (w/v) agar and appropriate antibiotics for transgene selection. Seven-day-old seedlings were transplanted to soil (Sunshine Mix 4 or 5, SunGro, Canada) supplemented with liquid AT medium and grown in a plant growth chamber at 20°C under continuous light [100 μmol m^{-2} s^{-1} of photosynthetically active radiation (PAR)]. Arabidopsis seeds grown for Agrobacterium-mediated transformation were directly spread on the soil supplemented with liquid AT medium at a density of 100 seeds/6″ pot and grown as described above.

Nicotiana benthamiana seeds were sown directly on soil (Sunshine Mix 4 or 5, SunGro, Canada) supplemented with liquid AT medium at a density of 1 seed/3.5″ square pot. Plants were grown under a 14-h light (25°C with 100 μmol m^{-2} s^{-1} PAR) and 10-h dark (20°C) cycle. For the transient expression assay, 4- to 5-week-old plants were taken out of the growth chamber and left at room temperature for 3 to 4 h before infiltration.

RNA Isolation, RT-PCR, and qPCR

Plant tissues were collected and immediately frozen in liquid nitrogen. RNA was extracted from Arabidopsis leaves, stems, flowers, seedlings, and roots using TRIzol (Thermo Fisher Scientific) according to the manufacturer's protocol. RNA was isolated from Arabidopsis siliques using a phenol:chloroform:isoamyl extraction and precipitated by lithium chloride and sodium acetate (Wilkins and Smart, 1996). RNA integrity was examined on a 1% standard agarose gel, and RNA was quantified using a NanoDrop 8000 (Thermo Scientific). Genomic DNA was removed by DNase I treatment (New England Biolabs) following the manufacturer's protocol, and single-stranded cDNA was synthesized from equal amounts of purified RNA using iScript RT Supermix (Bio-Rad). *ACTIN1* was used as an internal control. The iQ SYBR Green Supermix (Bio-Rad) was used in 20 μl reactions to perform qPCR in an iQ5 Multicolor Real-Time PCR Detection System (Bio-Rad) as specified by the manufacturer. Four technical replicates were performed for each sample, and gene expression levels were analyzed using the Pfaffl method (Pfaffl, 2001).

Cloning of Genes in Plant Expression Vectors

Standard methods were used for cloning, and all primer sequences are given in **Supplementary Table 1**. All constructs were confirmed by sequencing.

[1] arabidopsis.org/

The *pGreenST/35S:HA-AtARRE* construct, which was prepared for the SNIPER screen (Tong et al., 2017), was used as the site-directed mutagenesis template. Of the five splice variants known for the *AtARRE* gene (AT5G66070), AT5G66070.1 was used for the work described here. The *35S:HA-AtARRE*$^{(H197Y,H200Y)}$ site-directed mutagenesis construct was generated using primers H197200Y_F and H197200Y_R designed using the one-step site-directed mutagenesis method (Zheng et al., 2004). The PCR amplification was carried out using Phusion High Fidelity Polymerase (Thermo Fisher Scientific). The PCR products were separated by gel electrophoresis, purified using a PCR Purification Kit (BioBasic), and were further treated with restriction enzyme DpnI (New England Biolabs). The mutations in the *35S:HA-AtARRE*$^{(H197Y,H200Y)}$ construct were confirmed by sequencing.

The *35S:GFP-CER3* construct was prepared using Gateway cloning (Thermo Fisher) and destination vectors from Nakagawa et al. (2007). The coding sequence of the *CER3* gene was amplified from WT cDNA using CER3cDNA_attbF and CER3cDNA_attbR_WSTOP primers and recombined into the entry vector pDONR221. The insert was then transferred into the destination vector pGWB6 to generate pGWB6/*35S:GFP-CER3* and into pGWB15 to generate pGWB15/*35S:HA-CER3*. The *CER3* coding sequence without stop codon was also amplified using CER3cDNA_attbF and CER3cDNA_attbR_NoSTOP primers, recombined to pDONR221, and then transferred to the destination vector pGWB5 to generate pGWB5/*35S:CER3-GFP*.

The *35S:CER1-GFP* construct was made and provided by Dr. Hugo Zheng (McGill University, Canada). The coding region of the *CER1* gene was subcloned into the vector *pVKH18/35S:GFPC* (Dean et al., 2007) to produce the C-terminal CER1-GFP fusion under the control of the enhanced *35S* promoter. The *35S* promoter fragment was then removed from the vector *pVKH18/35S:CER1-GFP* and replaced with the *CER6* promoter using HindIII and XbaI to generate *pVKH18/CER6p:CER1-GFP*. The construct *pBIN/35S:HDEL-mCherry* was provided by Dr. Mathias Schuetz (Nelson et al., 2007), and the construct *pGreenST/35S:HA-SNIPER2* was described previously (Wu et al., 2020).

To generate the construct *AtARREp:GUS*, a fragment of 808 bp immediately upstream of the putative AtARRE start codon, which includes the 5′ UTR of *AtARRE*, as well as 3′ UTR and the last intron of the previous gene, was amplified from WT genomic DNA using LP_attb1_AtARRE and RP1_attb2_AtARRE and recombined into pDONR221 before being introduced into pGWB3 (Nakagawa et al., 2007; Vincent et al., 2018) using GATEWAY cloning (Thermo Fisher).

Cloning of Genes in Bacterial Expression Vectors

Standard methods were used for cloning, and all primer sequences are given in **Supplementary Table 1**. All constructs were confirmed by sequencing.

To generate the construct *pET28b/AtARRE-HIS* for the *in vitro* ubiquitination assay, a 326 bp fragment of coding sequence downstream of the transmembrane domains and upstream of the stop codon of *AtARRE* was amplified from WT cDNA using AtARRETMdel_F_EcoRI_28b and AtARRETMdel_R_SalI. This PCR product was ligated into the *pET28b* vector using EcoRI and SalI restriction sites to generate *pET28b/AtARRE-HIS*.

To reconstitute the plant ubiquitination cascade in *Escherichia coli*, Duet expression vectors (kindly provided by Dr. Dongping Lu, Chinese Academy of Science, China) *pCDFDuet/MBP-ABI3-HA-AtUBA1-S*, *pCDFDuet/AtUBA1-S*, *pACYCDue/AIP2-Myc-UBC8-S*, and *pET28a/FLAG-UBQ* were used to generate target co-expression constructs (Han et al., 2017). A 326 bp fragment of coding sequence downstream of the transmembrane domains and upstream of the stop codon of *AtARRE* was amplified from WT cDNA and ligated into the BamHI and StuI-digested *pACYCDue/AIP2-Myc-UBC8-S* vector to generate *pACYCDue/AtARRE-Myc-UBC8-S*. An 837 bp fragment of coding sequence downstream of the transmembrane domains and upstream of the stop codon of *CER1* was amplified from WT cDNA was ligated into the EcoRI and StuI-digested *pCDFDuet/MBP-ABI3-HA-AtUBA1-S* vector to generate *pCDFDuet/MBP-CER1-HA-AtUBA1-S*.

Agrobacterium-Mediated Plant Transformation

To produce transgenic lines for E3 ubiquitin ligase activity test, degradation assay, and GUS assay, *35S:HA-AtARRE*$^{(H197Y,H200Y)}$, *CER6p:CER1-GFP*, *AtARREp:GUS*, and *AtARREp:AtARRE-GUS* were introduced into *Agrobacterium tumefaciens* GV3101 cells carrying the pMP90 Ti plasmid. The pGreenST plasmid *35S:HA-AtARRE*$^{(H197Y,H200Y)}$ was co-transformed with the helper plasmid pSOUP (Hellens et al., 2000). Transformation of WT or *cer1-4* plants was carried out using the floral spray method (Chung et al., 2000). T1 transgenic seeds were harvested and screened on AT medium supplemented with 1% (w/v) agar and appropriate antibiotics.

Transient Expression in *Nicotiana benthamiana*

Transient expression in *N. benthamiana* was carried out using 4- to 5-week-old plants. Agrobacterium cultures were grown overnight in 3 ml of LB medium under antibiotic selection and diluted 1/20 in LB medium with antibiotics and 50 µm acetosyringone and incubated for a further 3–5 h. During this time, plants were taken out of the growth chamber and left at room temperature before infiltration. Cultures were centrifuged and resuspended in resuspension medium (4.43 g/L MS, 10 mm MES, and 150 µm acetosyringone) at an optical density of 0.6 at A_{600}. For co-expression of multiple constructs, suspensions were mixed in equal ratios. Agrobacterium suspension mixtures were infiltrated using a 1-ml syringe into the abaxial side of the *N. benthamiana* leaves. A permanent marker was used to mark the infiltrated area on the leaf. Infiltrated plants were incubated at room temperature for 48 h, and then, leaf samples were collected for microscopic imaging and/or protein extraction.

Cuticular Wax Extraction and Analysis by GC-FID

Cuticular wax extraction was performed using the method described by Haslam and Kunst (2013b). Briefly, the top 10 cm of 4- to 6-week-old inflorescence stems were cut and photographed to allow stem surface area to be calculated by measuring the number of pixels of the two-dimensional area in Photoshop (Adobe), converting the values to cm^2, and multiplying by π. After imaging, stems were submerged for 30 s in chloroform containing 10 μg tetracosane as an internal standard. After wax extraction, chloroform was evaporated under a stream of nitrogen gas and wax components were silylated in 10 μl N, *O*-Bis (trimethylsilyl) trifluoroacetamide (BSTFA; Sigma), and 10 μl pyridine for 1 h at 80°C. After derivatization, the solvent was evaporated under nitrogen gas and waxes were re-dissolved in 30 μl of chloroform for GC analysis. Samples were analyzed on an Agilent 7890A gas chromatograph equipped with a flame ionization detector (GC-FID) using an HP1 column (Agilent) in a 2.7:1 split mode with H_2 as the carrier gas at a flow rate of 30 ml/min. The gas chromatography program used was as follows: oven temperature was set at 50°C for 2 min, raised by 40°C/min to 200°C and held for 1 min, and then raised by 3°C/min to 320°C and held for 15 min. Wax components were identified by comparing their retention times with those of the internal standards. Four biological replicates were processed for each line.

Microscopy

Fluorescence signals of transiently expressed constructs in *N. benthamiana* were detected using a Perkin Elmer Ultraview VoX Spinning Disk Confocal Microscope. *N. benthamiana* leaf discs were mounted in distilled water and immediately imaged using a glycerol immersion lens. GFP was excited using a 488 nm laser with an 515/30 nm emission filter, and mCherry was excited using a 561 nm laser with an 595/50 nm emission filter. Confocal images were processed using the Volocity software (Perkin Elmer). GFP signal in infiltrated *N. benthamiana* leaf was also observed using a Nikon Eclipse 80i Scanning Laser Confocal Microscope excited with a 488 nm laser with an 515/30 nm emission filter.

For scanning electron microscopy (SEM), segments from the apical 1 cm of dry stems were mounted onto stubs and sputter-coated with gold particles for 10 min at 40 mA in an SEM Prep 2 sputter coater (Nanotech). The coated samples were viewed using an S4700 field emission SEM (Hitachi) with an accelerating voltage of 5 kV and a working distance of 12 mm.

GUS Histochemical Assay

Tissues at different developmental stages from transgenic lines expressing *AtARREp:GUS* constructs were immersed in GUS staining buffer {100 mM Na-phosphate, 10 mM EDTA, pH 7.0, 0.5 mM $K_3[Fe(CN)_6]$, 0.5 mM $K_4[Fe(CN)_6]$, 0.1% (v/v) Triton X-100, and 1 mM 5-bromo-4-chloro-3-indolyl-β-D-glucuronide (X-gluc)} and incubated for 1 to 3 h or overnight. The reaction was stopped by removing the GUS buffer and adding the 70% (v/v) ethanol. Chlorophyll was removed by incubating samples in 70–90% (v/v) ethanol before samples were examined under a Nikon SMZ18 Digital Microscope (Nikon, Japan).

Protein Extraction and Immunoblotting

Plant tissues were ground in liquid nitrogen, and total proteins were extracted in buffer containing 50 mM Tris-HCl, pH 7.5, 150 mM NaCl, 1 mM EDTA, 10% (v/v) glycerol, 1% Triton X-100, 1 mM PMSF, and 1X Halt™ protease inhibitor cocktail (Thermo Fisher Scientific). After centrifugation at 18,000 g for 20 min at 4°C, the supernatant was transferred to a new tube and the concentration of protein extract was determined using the Bradford reagent (Bio-Rad).

For SDS-polyacrylamide gel electrophoresis (SDS-PAGE), 4X SDS loading buffer (200 mM Tris-HCl, pH 6.8, 8% (w/v) SDS, 0.4% (w/v) bromophenol blue, 40% glycerol, and 400 mM DTT) was added to solubilized protein samples, and 10–35 μl of each protein sample was separated on a 10% acrylamide gel with 1% SDS at 200 V constant voltage for 50–60 min before being transferred to nitrocellulose membrane using a semi-dry blotting system (Bio-Rad) with Bjerrum Schafer-Nielsen buffer (Bio-Rad). Transfer was carried out at a constant voltage of 15 V for 50 min before the membrane was stained with Ponceau S, imaged, washed, and then blocked with 5% skim milk powder in Tris-buffered saline with 0.1% tween 20 (TBS-T). For immunoblotting, membranes were incubated with primary antibody for 1 h at room temperature. Primary antibodies used were anti-GFP (dilution 1:5,000; mouse IgG; Roche), anti-HA (dilution 1:2,500; rat IgG; Roche), anti-HIS (dilution 1:1,000; mouse IgG; Santa Cruz Biotechnology), anti-FLAG (dilution 1:5,000; mouse IgG; Sigma), anti-GST (dilution 1:1,000; rabbit IgG; Sigma), anti-Myc (dilution 1:1,000; Invitrogen), and anti-Ub (dilution 1:1,000; mouse IgG; Sigma). Membranes were then washed three times for 10 min each wash with TBS-T and then incubated with appropriate secondary antibodies, including anti-rabbit (dilution 1:10,000; Santa Cruz Biotechnology), anti-mouse (dilution 1:25,000; Santa Cruz Biotechnology), and anti-rat (dilution 1:10,000; Santa Cruz Biotechnology), for 1 h at room temperature. The membrane was washed three times as above with TBS-T before horseradish peroxidase was detected with the ECL Prime western blotting detection kit (GE).

Cell-Free Degradation Assay

Plant-derived protein degradation assays were performed as described in Wang et al. (2009), with modifications as follows. Total proteins were extracted from 8-day-old *CER6pro:CER1-GFP/cer1-4* transgenic seedlings and quantified. 80 μl protein extracts were then incubated with or without 40 μM MG132 (Sigma) at 30°C. Samples were taken at select time points, and the reaction was stopped by adding 5 μl 4X SDS loading buffer. CER1-GFP protein abundance in each sample was determined by immunoblotting using anti-GFP antibody.

In vitro Ubiquitination Assay

In vitro ubiquitination assays were performed as described in Zhao et al. (2013), with modifications as follows. The

plasmid *pET28b/AtARRE-HIS* was transformed into *E. coli* strain Rosetta™2 (DE3) for protein production. A 500 ml culture was grown in Terrific Broth (TB) medium [1.2% (w/v) tryptone, 2.4% (w/v) yeast extract, 0.4% (v/v) glycerol, 100 mM K-PO_4] until the exponential phase (OD_{600} = 0.6–1.0) before protein production was induced by adding 0.5 mM Isopropyl β-D-1-thiogalactopyranoside (IPTG). After growth overnight at 16–18°C, cells were collected by centrifugation at 6,000 g for 5 min and frozen in liquid nitrogen and stored at −80°C. Lysis buffer [50 mM $NaPO_4$, pH 7.5, 200 mM NaCl, 0.1% (v/v) Triton X, 5% glycerol, 1 mM PMSF, 1X Halt™ protease inhibitor cocktail, and 1 mg/ml lysozyme] was added to the frozen sample pellets, thawed at 37°C for 1 min, and resuspended. Lysate was cleared by centrifugation at 14,000 g for 15 min at 4°C followed by filtration through a 0.45 μm filter. The AtARRE-HIS recombinant proteins were purified using HisPur Ni-NTA Resin (Thermo Fisher) according to the manufacturer's protocol. Purified recombinant proteins AtUBA2-His and GST-AtUBC8 were kindly provided by Dr. Oliver Xiaoʼou Dong (Dong et al., 2018).

In vivo Ubiquitination Assay in Bacteria

In vivo ubiquitination assays in bacteria were carried out using the system described by Han et al. (2017). *E. coli* strain BL21 (DE3) containing different combinations of the expression vectors were grown in 2 ml of TB liquid medium with appropriate antibiotics at 37°C. When the culture A_{600} nm reached 0.4–0.6, 0.5 mM IPTG was added to induce the recombinant protein expression. After induction, bacteria were further grown at 28°C for 10–12 h, stored at 4°C overnight, and then harvested from 300 μl of culture by centrifugation at 12,000 g for 5 min. The pellets were resuspended in 100 μl 1x SDS loading buffer and boiled at 95°C for 5 min followed by immunoblotting.

RESULTS

Overexpression of *AtARRE* Results in Reduced Wax Accumulation on Arabidopsis Stems and Leaves

To identify novel E3 ligases involved in plant immunity, a SNIPER genetic screen has been carried out (Tong et al., 2017). In this screen, E3-ligase encoding genes induced during plant defense were overexpressed in the wild-type background. Unexpectedly, a number of independent transgenic plants with glossy bright green stems were uncovered among the T1 progeny, suggestive of altered cuticular wax accumulation (**Figure 1A**). In these plants, the *AtARRE/At5g66070* gene encoding a RING-type E3 ubiquitin ligase was expressed under the control of the cauliflower mosaic virus (CaMV) 35S promoter (**Supplementary Figures S1A,B**). Wax analysis of three representative AtARRE overexpression (AtARREOX) lines by gas chromatography demonstrated that they accumulated only 10–50% of the WT inflorescence stem wax and only ~65% of the WT leaf wax (**Figures 1B**,**C**). The stem wax phenotype was further evaluated by scanning electron microscopy (SEM); wild-type stem surface was densely and uniformly covered with column-, vertical plate-, and rod-shaped wax crystals, whereas AtARREOX lines displayed considerably lower density of all types of wax structures (**Figure 1D**).

The wax deficiency uncovered in the AtARREOX lines prompted us to examine the wax phenotypes of *atarre* mutants. We obtained three T-DNA insertion lines of *AtARRE* in the Col-0 ecotype and determined *AtARRE* gene expression in mutant alleles by qPCR. Even though we detected reduced levels of *AtARRE* transcript in all three T-DNA lines (**Supplementary Figures S1A,B**), we found no major differences in the total stem wax load or composition with respect to the wild type (**Supplementary Figures S1C,D**).

AtARREOX Lines Exhibit Altered Wax Composition and Abnormal Organ Morphogenesis

To further investigate the role of AtARRE in cuticular wax biosynthesis, we carried out a detailed analysis of wax composition of AtARREOX lines. We found that amounts of all stem wax components were altered in AtARREOX plants in comparison with the wild type, and detected considerable changes in their relative proportions. In particular, there was a prominent decrease in absolute amounts of alkane pathway-derived compounds that could be attributed primarily to C29 alkanes (68–98.7% decrease), C29 ketones (50–97.6% decrease), and C29 secondary alcohols (56–97% decrease). Conversely, the amounts of fatty acids on AtARREOX stems were higher than in the wild type (115–167% increase) and so was the relative proportion of fatty acids, aldehydes, and primary alcohols (**Figure 1E, Supplementary Figure S1E**). We also examined the wax composition of AtARREOX rosette leaves. As observed with stem wax, leaf wax also contained significantly reduced amounts of C29 and C31 alkanes relative to the wild type, but also increased amounts of C33 alkanes (**Figure 1F**). In addition, we detected a major increase in C24 and C26 fatty acids, as well as C26 primary alcohols (**Figure 1F**). Collectively, these data suggest that wax production by the alkane-forming pathway is impaired in AtARRE overexpressors.

AtARREOX lines with the most severe wax deficiency displayed additional phenotypes including abnormal organ morphogenesis, dwarfism, organ fusions, and reduced fertility over multiple generations (**Figure 2**). For example, the inflorescence stems of AtARRE overexpressors were considerably shorter than the wild type. Additionally, these plants also exhibited organ fusions between flower buds, flowers, and siliques, as well as between flowers and leaves (**Figures 2C**,**D**). Reduced fertility was also often detected. In most cases, fertility could be restored by growing plants under high humidity, except in individuals with severe floral organ fusions (**Supplementary Figure S2**). Similar phenotypes have previously been reported for several Arabidopsis wax-deficient *eceriferum* mutants (Koornneef et al., 1989).

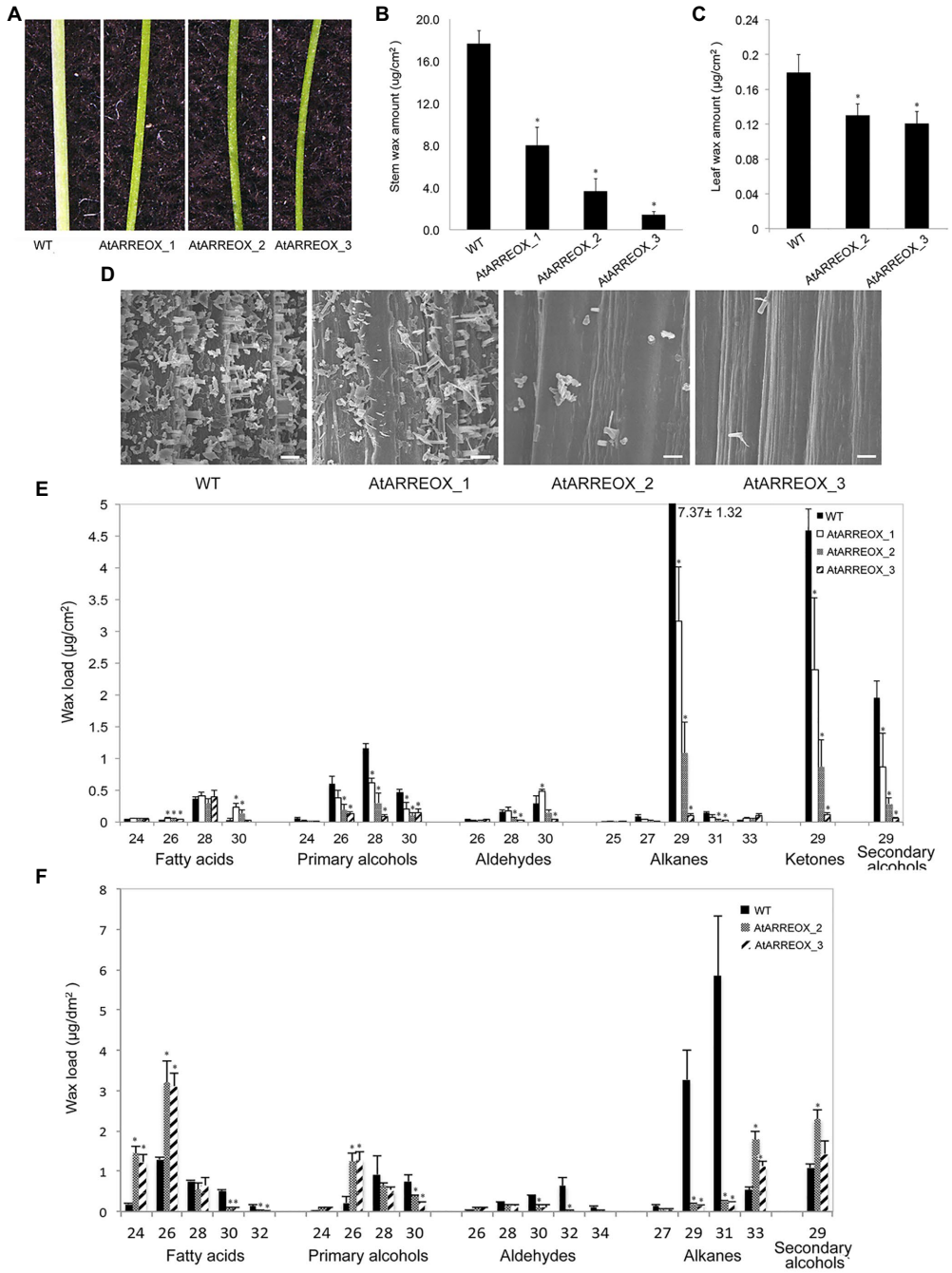

FIGURE 1 | Characterization of the wax-deficient phenotypes of AtARREOX lines. **(A)** Stems of 6-week-old wild type (WT) and three representative AtARREOX lines. Total stem **(B)** and leaf **(C)** wax load of WT and AtARREOX lines as determined by GC-FID. Error bars represent means ± SD ($n = 4$). **(D)** SEM images of WT and AtARREOX inflorescence stem surfaces. Scale bar = 20 μm. The stem **(E)** and rosette leaf **(F)** wax composition of WT and AtARREOX lines as measured by GC-FID. Error bars represent means ± SD ($n = 4$). Statistically significant differences between the WT and each AtARREOX line were determined by Student's *t* test and are indicated by asterisks ($p < 0.05$).

AtARRE E3 Ubiquitin Ligase Activity Is Required for Its Function in Wax Deposition

AtARRE (*AT5G66070*) encodes a predicted polypeptide of 221 amino acids with a molecular mass of 27 kDa containing three transmembrane domains located at the N-terminus and a RING domain located at the C-terminus (**Figure 3A**). RING domain proteins act as E3 ligases by binding to an E2-ubiquitin thioester and catalyzing ubiquitin transfer (Deshaies and Joazeiro, 2009). Whether the RING domain-related E3 ubiquitin

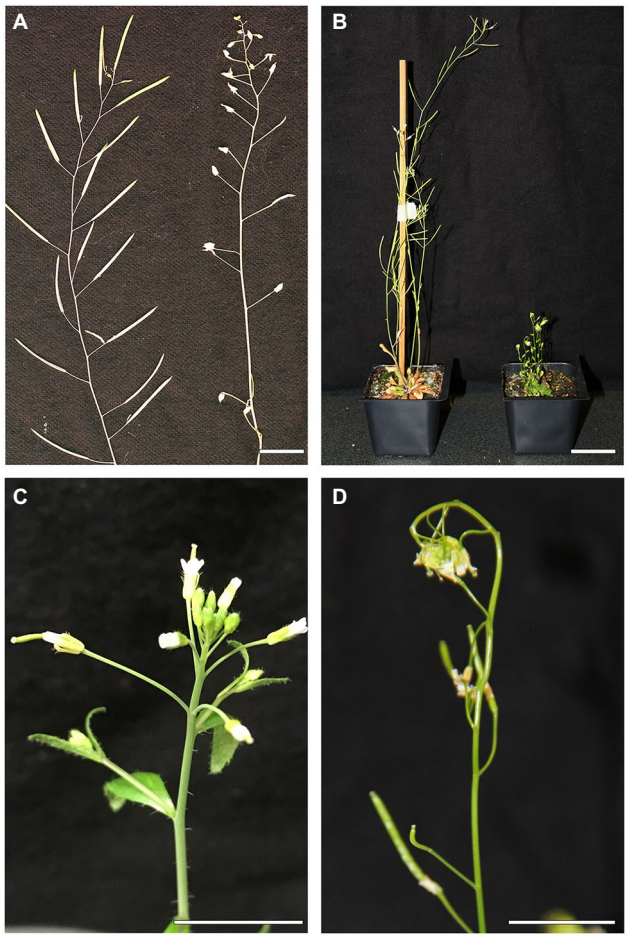

FIGURE 2 | Abnormal organ morphogenesis in the AtARREOX lines. **(A)** Dry stems of WT (left) and a T3 AtARREOX_2 individual (right). **(B)** 6-week-old WT plant (left) and a T3 AtARREOX_3 plant (right). **(C)** Flowers of WT (Col-0). **(D)** Organ fusions between flower buds of a T3 AtARREOX_3 individual. Scale bars = 2 cm.

ligase activity of the AtARRE protein is required for its function in cuticular wax metabolism is not known. RING domain E3 ligases are known to undergo self-ubiquitination in the absence of their native substrate (Lorick et al., 1999). We used this feature of RING E3 ligases to determine whether AtARRE has E3 ligase activity. Unfortunately, the insolubility of the full-length AtARRE protein upon expression in *E. coli* prohibited purification of enough protein for the self-ubiquitination assay. Therefore, an AtARRE protein fragment without the N-terminal transmembrane domains was used to produce the recombinant AtARRE-HIS protein. Incubation of the purified AtARRE-HIS recombinant protein with E1, E2, ubiquitin, and ATP resulted in a laddering pattern characteristic of ubiquitination on a protein blot when anti-HIS antibodies were used for AtARRE-HIS detection. This laddering is indicative of a range of molecular weights for AtARRE-HIS as it carries ubiquitin chains of different lengths (**Figure 3B**). Such a laddering pattern was also detected when anti-Flag antibodies that were used for FLAG-Ub detection of Ub chains bound to AtARRE-HIS. Thus, AtARRE exhibits E3 ligase activity and undergoes self-ubiquitination *in vitro*. The self-ubiquitination of AtARRE was not observed when E1, E2, or ubiquitin were omitted from the assays.

Conserved Cys and His residues in the RING domain are critical for the E3 ligase activity (Deshaies and Joazeiro, 2009). Their substitution disrupts the RING domain and results in a dominant-negative form of E3 ligase predicted to confer the same phenotype as the loss of E3 ligase function. To further verify whether AtARRE E3 ligase activity is required for its function, we replaced the conserved AtARRE RING domain His-197 and His-200 with Tyr residues by site-directed mutagenesis and expressed the modified protein in wild-type plants. In contrast to AtARRE overexpression which caused wax deficiency, overexpression of the double mutant AtARRE$^{(H197YH200Y)}$ protein had no effect on the stem wax load (**Figure 3C**). Thus, the E3 ligase activity of AtARRE is required for its function in stem wax deposition.

AtARRE Overexpression Phenotypes Mimic *cer1* and *cer3* Wax-Deficient Mutants

E3 ligase-mediated ubiquitination of proteins in most cases results in their degradation by the 26S proteasome. Because the most conspicuous result of AtARRE overexpression was reduced cuticular wax accumulation on Arabidopsis inflorescence stems, we hypothesized that AtARRE may act as a negative regulator of wax deposition by ubiquitinating, and thus targeting for degradation, a key player involved in wax biosynthesis. If this is the case, identifying the ubiquitination substrate of AtARRE is critical for determining its biological function. As a first step in uncovering potential candidate ubiquitination substrates, we compared stem wax compositional changes of AtARRE overexpressors with those of *ecerifierum* (*cer*) Arabidopsis mutants caused by loss-of-function mutations in wax biosynthetic genes (**Figure 4, Supplementary Figure S3**). AtARRE overexpressors displayed dramatically reduced alkane, secondary alcohols, and ketone levels on their stem surfaces, similar to null mutants disrupted in *CER1* and *CER3* genes required for the production of waxes by the alkane-forming branch of wax biosynthesis, but not the mutants with lesions in the *CER4* gene required for the production of waxes by the acyl reduction pathway. The distinguishing feature between *cer1* and *cer3* is that *cer1* has slightly increased amounts of aldehydes and reduced primary alcohol levels, whereas *cer3* exhibits a major reduction in aldehydes and similar amounts of primary alcohols to the wild type. Thus, the wax profile of AtARREOX lines is most similar to that of the *cer1* mutant. Besides cuticular wax changes, some AtARREOX lines additionally display reduced plant height and reduced fertility previously described for the *cer1-1* and *cer3-1* mutant alleles (Koornneef et al., 1989), and organ fusion phenotypes characteristic of *cer3*, but not *cer1* mutants (Aarts et al., 1995; Chen et al., 2003; Bourdenx et al., 2011).

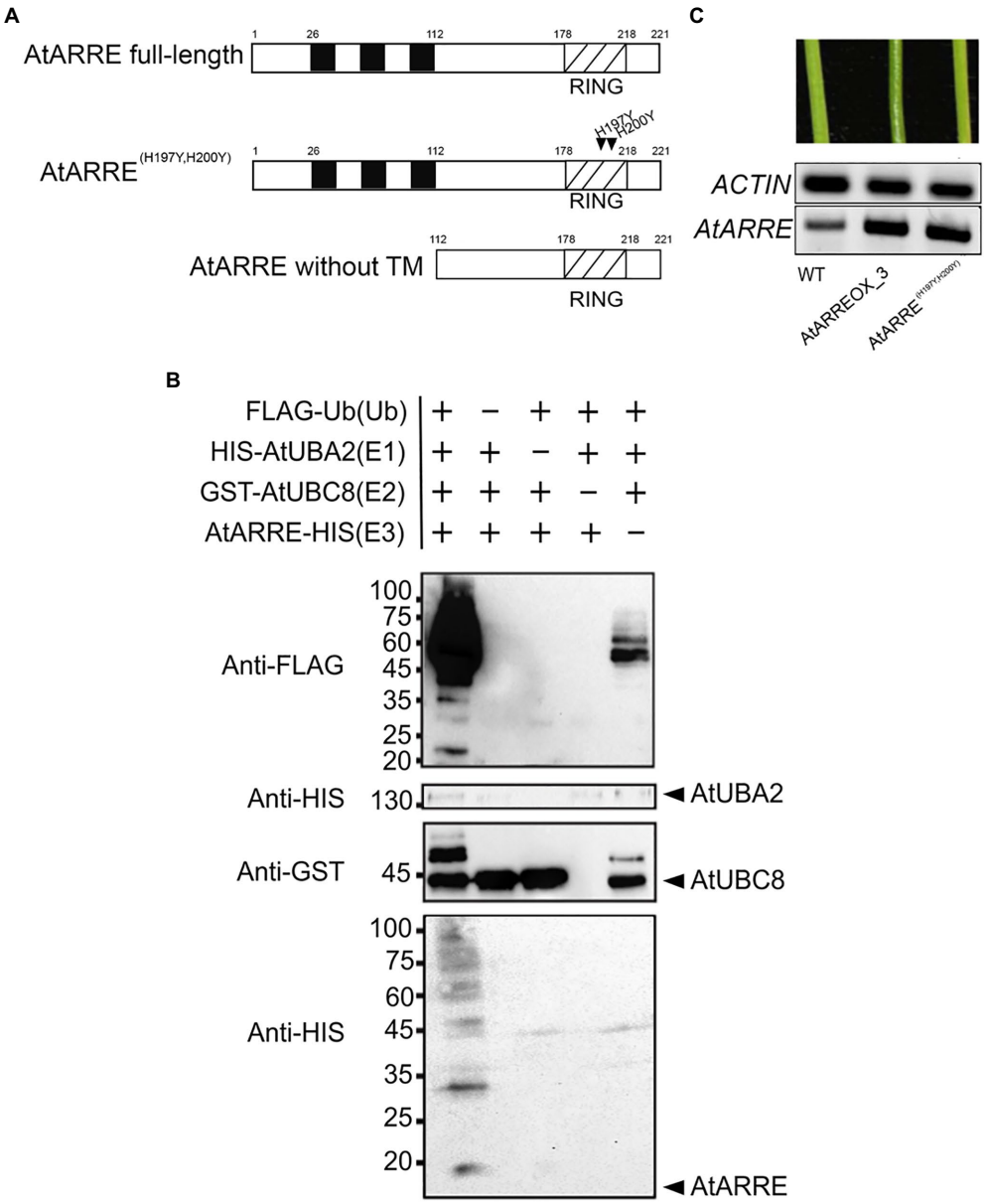

FIGURE 3 | AtARRE exhibits E3 ubiquitin ligase activity. **(A)** Schematic representations of the full-length AtARRE protein (top), AtARRE protein with mutated RING domain (middle) and truncated AtARRE protein without transmembrane domains used for self-ubiquitination assay (bottom). Arrows show the point mutations in the RING domain. **(B)** *In vitro* ubiquitination assays were performed in the presence (+) or absence (–) of AtUBA2 (E1; 140 kDa), AtUBC8 (E2; 44 kDa), AtARRE (E3; 14.4 kDa), and ubiquitin (Ub; 9.5 kDa). Ubiquitination of AtARRE was detected by immunoblotting using an anti-FLAG antibody or anti-HIS antibody. AtUBC8 and AtUBA2 were detected by immunoblotting using anti-GST and anti-HIS antibody, respectively. Molecular mass markers are indicated on the left. **(C)** Stems of 6-week-old WT, AtARREOX_3 (T3 generation), and representative AtARRE$^{(H197YH200Y)}$. *AtARRE* transcript accumulation in each sample was measured by RT-PCR. *ACTIN* was used as an internal control.

AtARRE Promotes CER1 Degradation by the 26S Proteasome

To determine whether CER1 is subjected to 26S proteasome-dependent degradation, we performed a modified cell-free degradation assay. For this purpose, we made *CER6pro:CER1-GFP/cer1-4* transgenic lines in which the *CER6pro:CER1-GFP* transgene complemented the *cer1-4* wax deficiency (**Supplementary Figure S4A**). Total proteins extracted from 8-day-old *CER6pro:CER1-GFP/cer1-4* seedlings were incubated with or without the 26S proteasome inhibitor MG132 for 90 min and protein levels determined by immunoblotting. The CER1-GFP amounts decreased rapidly in the absence of MG132, but in the presence of MG132, the levels of CER1-GFP remained notably higher over time, suggesting that the 26S proteasome is involved in CER1 proteolysis (**Figure 5A**).

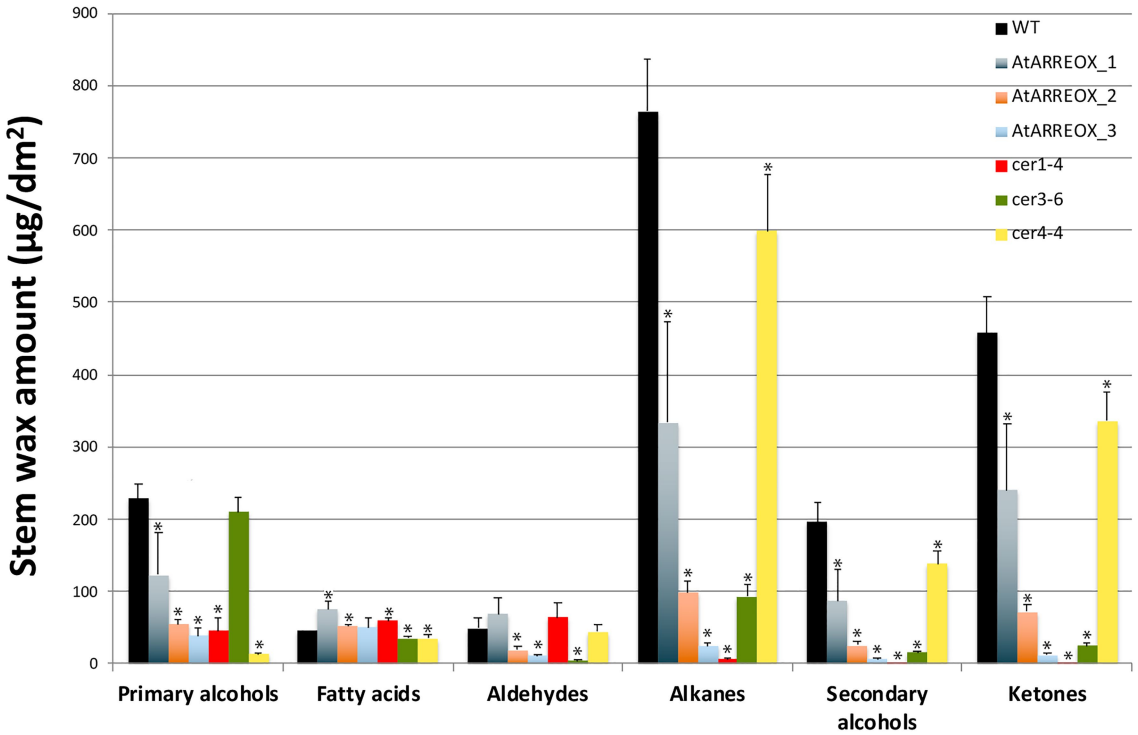

FIGURE 4 | A comparison of stem wax load and composition of AtARRE overexpression lines, and *cer1-4*, *cer3-6*, and *cer4-4* mutants. Stem wax load and composition of 6-week-old WT, AtARREOX lines, *cer1-4*, *cer3-6*, and *cer4-4* were determined by GC-FID. Values are means of four biological replicates, and error bars represent SD. Statistically significant differences of wax component amounts between the WT and different genotypes ($p < 0.05$) were determined by Student's *t* test and are indicated by asterisks.

We next carried out an Agrobacterium-mediated transient expression assay in *N. benthamiana* leaves. Agrobacterium cell cultures expressing *35Spro:CER1-GFP* and *35Spro:HA-AtARRE* were co-infiltrated on one half of a *N. benthamiana* leaf. Cell cultures expressing *35Spro:CER1-GFP* and *35Spro:HA* empty vector or *35Spro:CER1-GFP* and the *35pro:HA-SNIPER2* vector containing the *SNIPER2* E3 ligase gene not involved in wax deposition were co-infiltrated symmetrically on the other half of the same leaf as negative controls (**Supplementary Figure S4B**). *35Spro:HDEL-mCherry* was also included in each sample as a marker for ER visualization. In *N. benthamiana* cells transformed with CER1-GFP and *35Spro:HA* empty vector, the GFP signal could be easily detected after 48 h, persisted past 72 h and was undetectable 96 h after infiltration (**Supplementary Figure S4C**). Bright GFP fluorescence was also detected in cells co-expressing CER1-GFP and the SNIPER2 E3 ligase control 3 days post-infiltration, but not in those cells co-expressing CER1-GFP and AtARRE (**Figure 5B**). In contrast, similar intensity of mCherry fluorescence from the ER-localized HDEL-mCherry marker was detected in all infiltrated regions on both sides of the leaf (**Figure 5B**). Immunoblot analysis confirmed that CER1-GFP protein level was much lower in the presence of AtARRE than in the negative control sample expressing SNIPER2 E3 ligase (**Figure 5D**). Unlike the native AtARRE protein, co-expression of CER1-GFP and the AtARRE$^{(H197YH200Y)}$ protein with mutated RING domain did not affect CER1 protein levels, indicating that catalytic activity of AtARRE is required for CER1 degradation (**Figures 5C,D**). When the substrate CER1 was replaced with CER2, a component of VLCFAs elongation machinery (Haslam et al., 2012), GFP tagged CER2 fluorescence signal intensity was found to be indistinguishable in the presence and absence of AtARRE. Immunoblot results were consistent with microscopy data (**Supplementary Figures S4D,E**) and demonstrate that AtARRE specifically targets CER1 for degradation by the 26S proteasome.

The AtARRE-dependent degradation of CER1 was further verified in stable transgenic lines of Arabidopsis. Plants harboring the CER1-GFP transgene were crossed with the wild type, AtARREOX, and AtARREOX$^{(H197YH200Y)}$ lines, and the abundance of the CER1-GFP in F1 progeny was examined by immunoblotting. Whereas CER1-GFP transcript accumulation was similar in the F1 progeny from all the crosses, the CER1-GFP protein level in the AtARREOX lines was much lower than observed in the wild type and AtARREOX$^{(H197YH200Y)}$ lines (**Figure 5E**). Collectively, these results confirm that AtARRE promotes the degradation of CER1, suggesting that CER1 is the ubiquitination substrate of AtARRE.

CER1 Is Ubiquitinated by AtARRE in a Reconstituted *E. coli* System

To directly test whether CER1 is a ubiquitination substrate of the AtARRE E3 ligase, we performed an *in vivo*

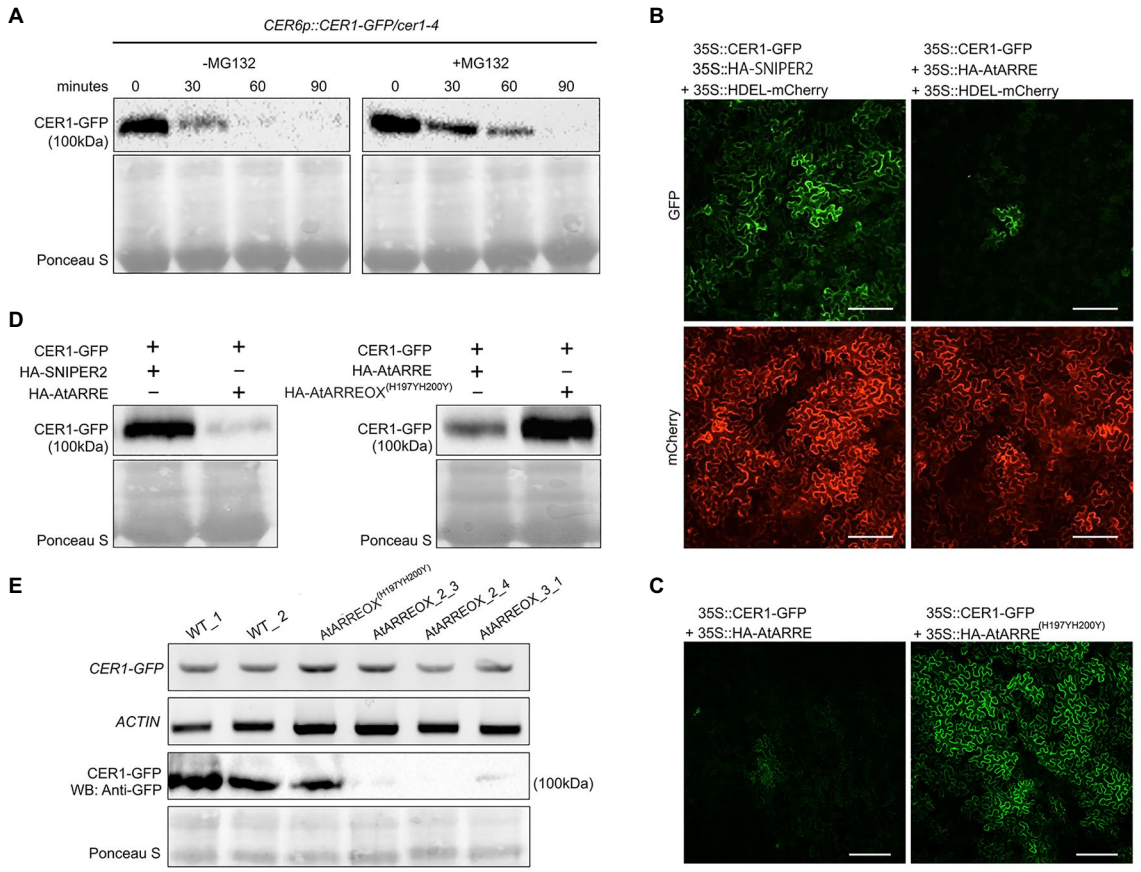

FIGURE 5 | AtARRE promotes CER1 degradation in the *Nicotiana benthamiana* transient expression system and in stable transgenic lines of Arabidopsis. **(A)** CER1 is turned over by the 26S proteasome *in planta*. Total proteins were extracted from 8-day-old *CER6pro:CER1-GFP/cer1-4* transgenic plants and incubated with (+) or without (–) 40 μM MG132. CER1-GFP protein levels were detected over time by immunoblotting using anti-GFP antibody. **(B,C)** Transient expression in *N. benthamiana* leaf epidermal cells. CER1-GFP and an internal control HDEL-mCherry were co-expressed with HA-SNIPER2 E3 ligase or HA-AtARRE E3 ligase. CER1-GFP was co-expressed with HA-AtARRE or HA-AtARRE$^{(H197YH200Y)}$ with mutated RING domain. GFP fluorescence and mCherry fluorescence were examined by confocal microscopy. Scale bars = 100 μm. 4 technical replicates and 16 biological replicates have been performed. **(D)** Amounts of CER1-GFP protein were determined by immunoblotting using anti-GFP in the same leaves assayed for fluorescence in **(B,C)**. **(E)** The AtARRE-dependent CER1 degradation in stable transgenic lines of Arabidopsis. RNA was extracted from 4-week-old Arabidopsis leaves. The *CER1-GFP* steady-state transcript levels were determined by RT-PCR, and *ACTIN* was used as an internal control (top two rows). Total protein was extracted from the 4-week-old plant leaves. The CER1-GFP protein level was determined by immunoblotting using anti-GFP antibody; Ponceau S staining shows equal protein loading (bottom two rows).

ubiquitination assay in a heterologous *E. coli* system that expresses the Arabidopsis ubiquitination cascade (Han et al., 2017). In this experiment, recombinant ubiquitination components E1 (AtUBA1-S), E2 (AtUBC8-S), E3 (AtARRE-Myc), ubiquitin (His-Flag-AtUBQ10), and the presumed ubiquitination substrate (MBP-CER1-HA) were co-expressed in *E. coli* (**Figure 6A**), and bacterial lysates were analyzed by immunoblotting. Our results show that in the presence of all ubiquitination components, a smear indicative of CER1 ubiquitination can be detected by an anti-HA antibody (**Figure 6B**). Using an anti-Myc antibody, AtARRE-Myc recombinant protein also shows a laddering pattern indicative of AtARRE self-ubiquitination. These data support the *in vitro* ubiquitination assay results that AtARRE is an active E3 ligase and demonstrate that it can ubiquitinate CER1 *in vivo*.

AtARRE Promotes CER3-GFP Degradation

Even though stem wax profiles of AtARRE overexpressors are more similar to the *cer1* than the *cer3* mutant, the overexpression lines also exhibit organ fusions previously detected in *cer3*, but not in *cer1* mutants. Because CER1 and CER3 proteins are highly related and share 35% sequence identity (Bernard et al., 2012), it is tempting to speculate that in addition to CER1, CER3 may also be a target of the AtARRE-mediated ubiquitination and UPS proteolysis resulting in the dual *cer1*- and *cer3*-like phenotypic features of AtARRE overexpression lines. To investigate whether this is the case, we tested whether AtARRE affects the protein levels of CER3-GFP in *N. benthamiana* leaf epidermal cells. Agrobacterium cells expressing *35Spro:CER3-GFP*, the *35Spro:HA-AtARRE*, and the *35Spro:HDEL-mCherry* transgenes were co-infiltrated on one half of a *N. benthamiana* leaf, while Agrobacterium cells

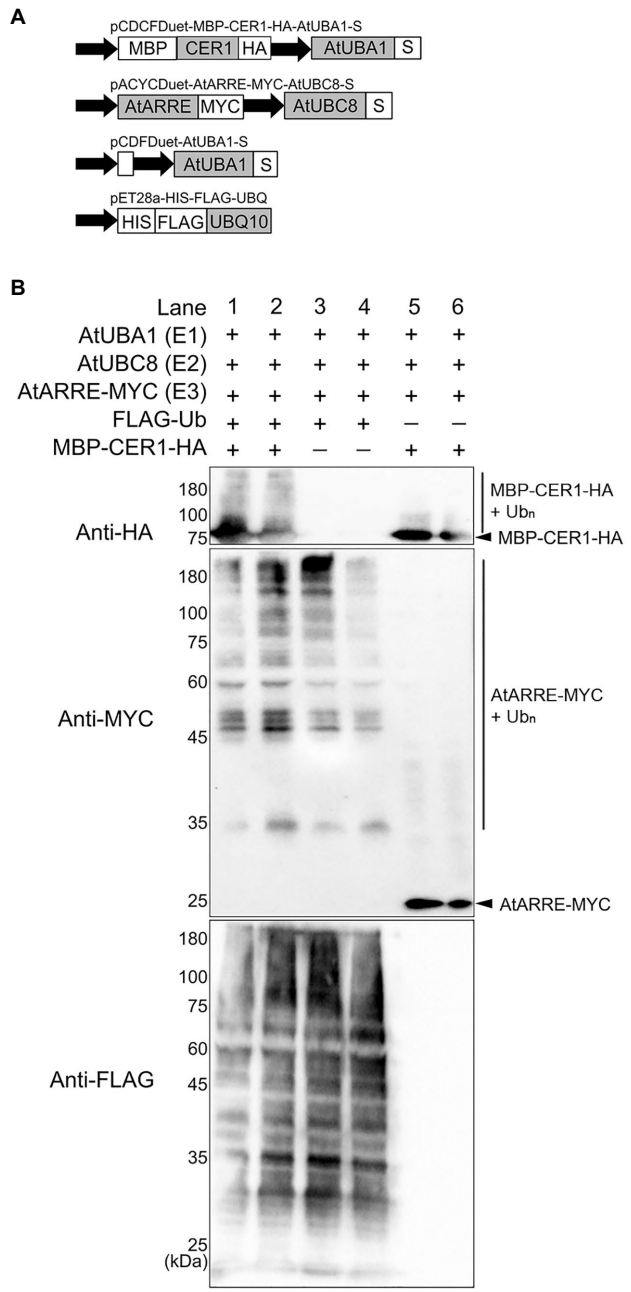

FIGURE 6 | Ubiquitination of CER1 by AtARRE in a heterologous *Escherichia coli* system. **(A)** Schematic representation of the plasmids used in the assay. MBP, maltose-binding protein; HA, hemagglutinin. These constructs were transformed into the *E. coli* Rosetta (DE3) strain to reconstitute the ubiquitination cascade. **(B)** Bacterial lysates from *E. coli* strains expressing (+) or missing (–) combinations of AtUBA1-S (E1), AtUBC8-S (E2), AtARRE-MYC (E3), His-FLAG-UBQ10 (Ub), and MBP-CER1-HA (substrate) (+), and strains missing Ub or CER1 (–) were analyzed by immunoblotting. Anti-HA and anti-MYC antibodies were used to detect ubiquitinated CER1 and self-ubiquitinated AtARRE, respectively. Anti-FLAG antibody was used to detect all Ub conjugates. Two replicates for each combination of constructs are shown.

harboring *35Spro:CER3-GFP*, *35Spro:HA-SNIPER2*, and *35Spro:HDEL-mCherry* were co-infiltrated on the other side of the same leaf as a negative control. Similar to CER1-GFP,

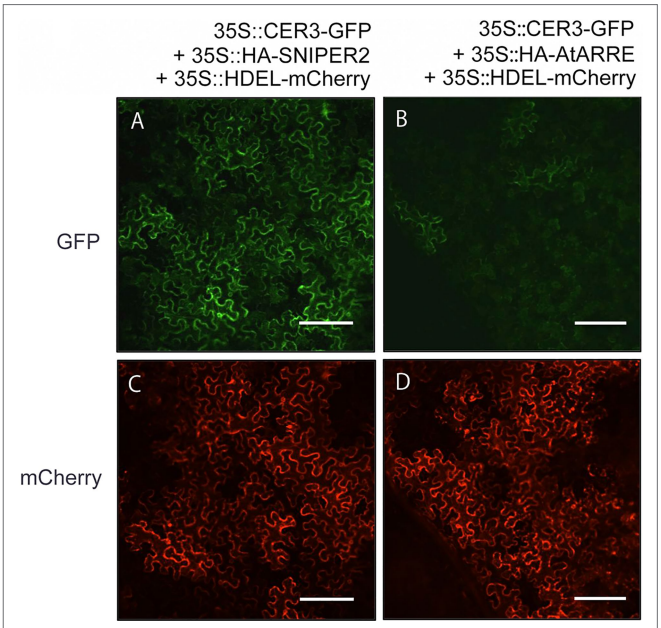

FIGURE 7 | AtARRE promotes CER3 degradation in the *N. benthamiana* transient expression system. **(A,C)** *35Spro:CER3-GFP* was co-expressed with *35Spro:HA-SNIPER2* or **(B,D)** *35Spro:HA-AtARRE*. *35Spro:HDEL-mCherry* was included as an internal control and ER marker. GFP fluorescence **(A,B)** and mCherry fluorescence **(C,D)** signals of leaf epidermal cells were examined by confocal microscopy 72 h post-infiltration. 12 biological replicates were performed. Scale bars = 100 μm.

AtARRE promoted CER3-GFP degradation as indicated by considerably reduced CER3-GFP fluorescence in the presence of transiently co-expressed AtARRE in comparison with the control co-expressing CER3-GFP with HA-SNIPER2 E3 ligase. By contrast, the signal of the internal control HDEL-mCherry was prominent and indistinguishable on both halves of the leaf (**Figure 7**). These results demonstrate that CER3 is likely also the AtARRE ubiquitination target. We tried to confirm that AtARRE controls the levels of CER3 in transgenic lines of Arabidopsis, but consistently failed to detect CER3-GFP protein on immunoblots.

AtARRE Gene Is Expressed in Tissues That Exhibit Low Wax Production and Upon Exposure to Pathogens

To obtain clues regarding the functional significance of the AtARRE-mediated protein degradation of wax biosynthetic enzymes, we investigated the transcription profile of *AtARRE* gene in different plant tissues using qRT-PCR (**Figure 8A**). The *AtARRE* gene was expressed in all tissues examined, with higher expression in rosette leaves and lower expression in flowers and siliques. To further determine the *AtARRE* expression pattern in different cell types and at different Arabidopsis developmental stages, an 808 bp fragment of genomic sequence immediately upstream of the *AtARRE* coding region was fused to the β-glucuronidase (GUS) reporter gene, and this *AtARREpro:GUS* reporter was transformed into wild-type

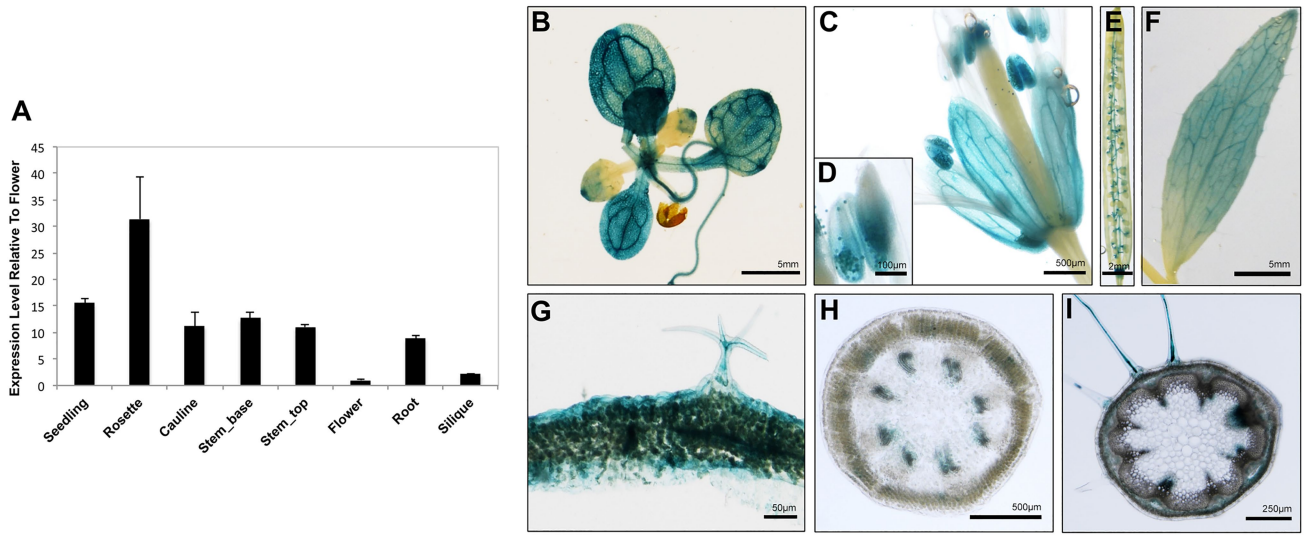

FIGURE 8 | Expression pattern of *AtARRE* gene in different plant tissues and cell types. **(A)** qRT-PCR analysis of *AtARRE* gene expression in the WT relative to flowers and normalized to *ACTIN*. Seedling and root tissue samples were derived from 10-day-old WT seedlings, and all other aerial tissues samples were derived from 6-week-old WT. Error bars represent means ± SD ($n = 4$). **(B–I)** Putative *AtARRE* promoter activity determined by GUS assay in transgenic lines expressing the *AtARREpro:GUS* reporter. Promoter activity was examined after GUS staining in 14-day-old seedlings **(B)**, flowers **(C)**, anthers containing pollen grains **(D)**, siliques **(E)**, cauline leaves **(F)**, cross section of rosette leaf from a 6-week-old plant **(G)**, cross section of the top 3 cm **(H)** and the bottom 3 cm **(I)** of the inflorescence stem of a 6-week-old plant.

Arabidopsis. GUS activity was examined in tissue samples from mature plants and in developing seedlings of ten independent transgenic lines.

In mature plants, high GUS activity was detected in the fully expanded rosette leaves, sepals, pollen grains, and cauline leaves (**Figures 8B–F**). These results are consistent with the published RNA-seq data showing high *AtARRE* expression in mature leaves and sepals (Klepikova et al., 2016). Strong GUS signal was also detected in, but not specific to, the epidermal cells of rosette leaves, as well as trichomes, which are specialized epidermal cells (**Figure 8G**). Surprisingly, no expression of *AtARRE* was detected in the epidermal cell layer of the stem (**Figures 8H,I**). This may be due to the fact that the 5′ promoter fragment used in the *AtARREpro:GUS* construct does not contain the regulatory element required for the *AtARRE* expression in stem epidermal cell layer. In fact, according to published RNA-seq and microarray data, *AtARRE* shows the highest expression level in the senescent first internode of the stem, and higher expression was detected in the epidermal cell layer at the bottom of the inflorescence stem compared to the top of the stem (Suh et al., 2005; Klepikova et al., 2016). During seedling development, GUS activity was first detected in roots in 3-day-old seedlings and cotyledons at 4 days after imbibition (**Supplementary Figure S5**), but the GUS staining was much more pronounced in both organs in 5-day-old seedlings.

The observed expression profile fits the role of AtARRE as a negative regulator of wax biosynthesis in tissues that exhibit no or low wax production, such as mature cotyledons in older developing seedlings, as well as fully expanded rosette leaves and older internodes at the bottom of the stem in mature plants. Unexpectedly, *AtARRE* was also found to be expressed in roots, even though *CER1* and *CER3* genes encoding AtARRE ubiquitination substrates are not expressed in roots or are expressed at a very low level, respectively (Bourdenx et al., 2011).

Because AtARRE was discovered in a reverse genetic screen conducted to identify novel plant immunity-related E3 ligases, we were interested in determining whether AtARRE is induced upon exposure to pathogens. An earlier study has shown that *AtARRE* is upregulated after treatment with chitin, a potent elicitor of plant defense responses (Libault et al., 2007). Our qRT-PCR analysis revealed that elicitation with flg22, a peptide derived from bacterial flagellin, also results in a major increase in *AtARRE* expression (**Figure 9A**). In addition, infiltration of plants with the type III secretion deficient bacterial strain *Pseudomonas syringae* pv. *tomato* (*P.s.t.*) DC3000 *hrcC*$^{-}$ and the virulent bacterial strain *P. syringae* pv. *maculicola* (*P.s.m.*) ES4326 (**Figures 9B,C**) strongly upregulated *AtARRE* expression. Collectively, these data suggest that AtARRE may be involved in regulating cuticular wax biosynthesis in response to pathogen attack.

DISCUSSION

As an integral part of the cuticle, wax protects plants against diverse biotic and abiotic stress factors present in their environment. To fulfill this protective role, wax composition and wax load need to be continuously adjusted in response to changing environmental conditions (Shepherd and Wynne Griffiths, 2006; Bernard and Joubès, 2013). This is accomplished by extensive transcriptional, post-transcriptional,

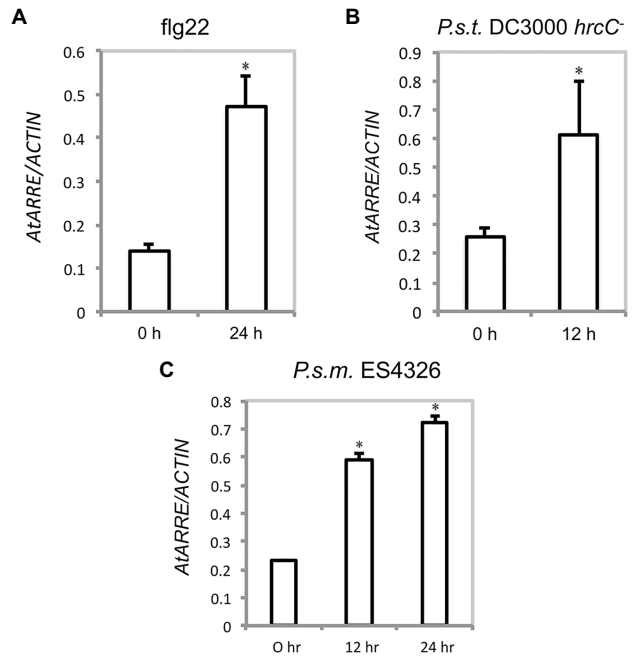

FIGURE 9 | *AtARRE* gene expression is induced by flg22 and pathogen treatment. **(A)** Four-week-old WT plants were infiltrated with 100 nM flg22, **(B)** *P.s.t.* DC3000 *hrcC*– at a dose of $OD_{600} = 0.002$, or **(C)** *P.s.m.* ES4326 at a dose of $OD_{600} = 0.0002$. Samples were collected 0, 12, or 24 h after treatment. Expression level of *AtARRE* was measured by qRT-PCR, and values were normalized to the level of *ACTIN*. Error bars represent means ± SD ($n = 4$). Significant difference compared with WT was determined by Student's *t* test and indicated by an asterisk ($p < 0.01$).

and post-translational regulation of cuticular wax metabolism (Lee and Suh, 2015a).

VLC alkanes are the major cuticular wax component in many plant species including Arabidopsis, where they comprise more than 70% of the total wax amount in leaves and 50% in stems (Bourdenx et al., 2011). VLC alkane production is catalyzed by CER1 and CER3 enzymes, which together with the cytochrome B5 form a multiprotein ER-membrane-associated complex (Bourdenx et al., 2011; Bernard et al., 2012) Not surprisingly, both enzymes act as key control points for wax biosynthesis. Several transcription factors including MYB30, MYB94, MYB96, DEWAX, and DEWAX2 regulate the expression of *CER1* and/or *CER3* in specific organs of Arabidopsis or in response to environmental stress (Raffaele et al., 2008; Seo et al., 2011; Go et al., 2014; Lee and Suh, 2015b). Components involved in chromatin remodeling are also required for the transcriptional regulation of *CER1* or *CER3*. HISTONE MONOUBIQUITINATION 1 and 2 (HUB1 and HUB2) are two E3 ligases that are involved in histone monoubiquitination and active chromatin formation, which leads to the transcriptional activation of wax biosynthetic genes, such as *CER1* (Ménard et al., 2014). GENERAL CONTROL NON-REPRESSED PROTEIN5 (GCN5) is a histone acetyltransferase that positively modulates *CER3* expression *via* histone acetylation (Wang et al., 2018c). In addition to transcriptional regulation, two classes of small RNAs, tasiRNA and miRNA, post-transcriptionally control *CER3* and *CER1* transcript levels, respectively (Lam et al., 2012, 2015; Li et al., 2019). Finally, studies on the E3 ligase MIEL1 have shown that it negatively regulates wax accumulation in aerial plant organs (Gil et al., 2017). MIEL1 controls the stability of wax-associated transcription factors MYB96 and MYB30 and thereby indirectly affects the expression of their downstream targets *CER1* and *CER3* (Marino et al., 2013; Lee and Seo, 2016; Gil et al., 2017). Even though the regulatory framework governing wax accumulation has been established, the intricacies of this process remain poorly understood.

Here, we demonstrate that CER1 and CER3 protein levels, and thus alkane formation, are also controlled directly by the AtARRE RING-type E3 ubiquitin ligase that we identified in our SNIPER genetic screen (Tong et al., 2017). We found that AtARRE overexpression in wild-type Arabidopsis results in phenotypes characteristic of cuticular wax deficiency, including glossy stems and siliques, reduced fertility and fusions between aerial organs, suggesting that AtARRE is a negative regulator of wax biosynthesis (**Figures 1A**, **2**). The wax analysis of AtARRE overexpression lines confirmed that they have reduced stem and leaf wax loads (**Figures 1B**–**F**) and revealed that their wax profile most closely resembled that of the *cer1* mutant (**Figure 4**). Functional characterization of AtARRE showed that this protein has E3 ubiquitin ligase activity and that this activity depends on the integrity of the key amino acid residues in its RING domain. When these conserved residues in the RING domain were mutated, the AtARRE protein no longer had any effect on the stem wax accumulation when it was overexpressed in Arabidopsis (**Figure 3**). These results demonstrate that E3 ligase activity of AtARRE is essential for its function in wax biosynthesis.

Because wax composition of the AtARRE overexpressors was most similar to the *cer1* mutant, we tested whether CER1 was the AtARRE ubiquitination substrate. An *in vivo* ubiquitination assay in a heterologous *E. coli* system expressing the Arabidopsis ubiquitination cascade confirmed AtARRE-mediated CER1 ubiquitination (**Figure 6**). Furthermore, transient co-expression of AtARRE and CER1 in both *N. benthamiana* leaves and in stable transgenic lines of Arabidopsis resulted in AtARRE-dependent degradation of CER1. Thus, AtARRE E3 ligase negatively regulates cuticular wax accumulation by ubiquitinating VLC alkane biosynthetic enzyme CER1 and targeting it for degradation by the 26S proteasome (**Figure 5**).

It is well-established that the UPS is redundant and that individual proteins may be targeted by multiple E3 ligases. Conversely, a single E3 ligase may have the ability to target multiple substrates for degradation (Iconomou and Saunders, 2016). CER1 and CER3, two key VLC alkane biosynthetic enzymes, share 35% amino acid identity, and both are integral membrane proteins with eight conserved His clusters at their N-terminus and an uncharacterized WAX2 domain at their C-terminus (Bernard et al., 2012). Due to their sequence similarity, it was possible that both of these proteins were substrates of the AtARRE E3 ligase. This fact, together with the observation that AtARRE overexpressors exhibit organ fusions similar to those detected in *cer3*, but not in *cer1* mutants, prompted us to investigate whether AtARRE additionally controls CER3 levels. As previously demonstrated for

CER1, AtARRE co-expression with CER3 in the *N. benthamiana* leaf indeed stimulated CER3 degradation (**Figure 7**). Thus, CER3 is also likely an AtARRE ubiquitination substrate.

The expression analysis of *AtARRE* gene revealed that it is preferentially expressed in tissues that exhibit no or low wax production such as roots and cotyledons in the later stages of seedling development, as well as older rosette leaves and inflorescence stem sections (**Figure 8**). These data suggest that the primary role of AtARRE may be to target CER1 and CER3 proteins for degradation in order to terminate wax production *via* the alkane pathway in tissues where it is no longer needed. Additionally, *AtARRE* gene transcription is upregulated upon exposure to bacterial pathogen *P. syringae* (**Figure 9**). Previous analysis of the *cer1* mutant showed that reduced VLC alkane levels in cuticular wax are associated with increased cuticle permeability, but have no major effect on plant immunity. In contrast, *CER1* overexpression resulted in alkane overproduction and decreased cuticle permeability, but surprisingly also in greater susceptibility to *P. syringae* (Bourdenx et al., 2011). Similarly, cucumber (*Cucumis sativus*) lines overexpressing *CER3* exhibited enhanced susceptibility to the fungal pathogen *Botrytis cinerea* (Wang et al., 2015). Thus, induction of *AtARRE* upon exposure to pathogens and the resulting degradation of CER1 and CER3 may serve as a regulatory mechanism aimed at decreasing VLC alkane levels and optimizing cuticular wax composition to enhance plant resistance to bacterial pathogens. However, further work is needed to clearly define the role of AtARRE in plant immunity.

Recently, *AtARRE* was also reported to be induced by sodium chloride and ABA treatments (Wang et al., 2018a). Analyses of seed germination, stomatal closure, root elongation, and expression of ABA-responsive genes in *atarre* mutants showed that all these processes were hypersensitive to ABA, whereas AtARRE overexpressors exhibited reduced ABA sensitivity, leading the authors to propose that AtARRE is a negative regulator of ABA-dependent abiotic stress responses in plants (Wang et al., 2018a). This study did not identify the AtARRE ubiquitination target or propose the molecular mechanism governing these ABA stress responses, but it is unlikely that the AtARRE-mediated CER1 degradation by the proteasome that controls attenuation of cuticular wax biosynthesis in the shoot described here is involved. On the contrary, water deficit, salt, and ABA treatment have been shown to cause a large increase in wax amount in the leaf cuticle, predominantly due to an increase in VLC alkane content (Kosma et al., 2009). A huge induction of the *CER1* alkane biosynthetic gene consistent with the elevated alkane amounts was also observed, presumably resulting in greater CER1 protein levels. Thus, even though the ABA signaling would not be expected to rely on the AtARRE-CER1 module, it is conceivable that AtARRE function in ABA-dependent signal transduction requires destruction of a different and as yet undiscovered protein target. A good example of an E3 ligase with multiple physiological roles that depend on proteasomal degradation of different protein substrates is MIEL1. MIEL1 controls seed germination and cuticular wax accumulation in Arabidopsis stems by primarily targeting MYB96 transcription factor for degradation, but in addition attenuates pathogen defense responses by promoting degradation of MYB30 (Marino et al., 2013; Lee and Seo, 2016).

CONCLUSION

Our findings indicate that AtARRE E3 ubiquitin ligase negatively regulates cuticular wax accumulation in Arabidopsis shoots by promoting degradation of CER1 and CER3 VLC alkane biosynthetic enzymes. Based on its expression in mature and senescing tissues and its induction upon plant exposure to pathogens, we propose that AtARRE serves as an efficient regulatory switch that terminates wax biosynthesis *via* the alkane-forming pathway when it is no longer required, or to optimize wax composition in response to pathogen infection.

DATA AVAILABILITY STATEMENT

The raw data supporting the conclusions of this article will be made available by the authors, without undue reservation.

AUTHOR CONTRIBUTIONS

LK and XL planned and designed research. SL, MT, and LZ performed the experiments. SL, LZ, XL, and LK analyzed and discussed the data. SL and LK wrote the manuscript. All authors contributed to the article and approved the submitted version.

FUNDING

This work was supported by Natural Sciences and Engineering Research Council of Canada Discovery Grants to XL and LK, and scholarships from the China Scholarship Council to SL and MT.

ACKNOWLEDGMENTS

We thank the Arabidopsis Biological Resource Center for providing *cer 1-4* and *cer4-4* mutants and T-DNA insertion alleles, Dr. Takuji Wada (RIKEN, Japan) for the *cer3-6* mutant, and the BioImaging Facility at the University of British Columbia for assistance with microscopy. We are grateful to Dr. Oliver Xiaoʾou Dong (UBC) for advice on ubiquitination assays, Dr. Yuli Ding (UBC) for help with pathogen treatment, and Drs. Tegan Haslam and Gillian Dean (UBC) for thoughtful comments on our manuscript.

SUPPLEMENTARY MATERIAL

The Supplementary Material for this article can be found online at: https://www.frontiersin.org/articles/10.3389/fpls.2021.752309/full#supplementary-material

REFERENCES

Aarts, M. G., Keijzer, C. J., Stiekema, W. J., and Pereira, A. (1995). Molecular characterization of the *CER1* gene of Arabidopsis involved in epicuticular wax biosynthesis and pollen fertility. *Plant Cell* 7, 2115–2127. doi: 10.1105/tpc.7.12.2115

Aharoni, A., Dixit, S., Jetter, R., Thoenes, E., van Arkel, G., and Pereira, A. (2004). The SHINE clade of AP2 domain transcription factors activates wax biosynthesis, alters cuticle properties, and confers drought tolerance when overexpressed in Arabidopsis. *Plant Cell* 16, 2463–2480. doi: 10.1105/tpc.104.022897

Alonso, J. M., Stepanova, A. N., Leisse, T. J., Kim, C. J., Chen, H., Shinn, P., et al. (2003). Genome-wide insertional mutagenesis of *Arabidopsis thaliana*. *Science* 301, 653–657. doi: 10.1126/science.1086391

Beisson, F., Li-Beisson, Y., and Pollard, M. (2012). Solving the puzzles of cutin and suberin polymer biosynthesis. *Curr. Opin. Plant Biol.* 15, 329–337. doi: 10.1016/j.pbi.2012.03.003

Bernard, A., Domergue, F., Pascal, S., Jetter, R., Renne, C., Faure, J.-D., et al. (2012). Reconstitution of plant alkane biosynthesis in yeast demonstrates that Arabidopsis ECERIFERUM1 and ECERIFERUM3 are core components of a very-long-chain alkane synthesis complex. *Plant Cell* 24, 3106–3118. doi: 10.1105/tpc.112.099796

Bernard, A., and Joubès, J. (2013). Arabidopsis cuticular waxes: advances in synthesis, export and regulation. *Prog. Lipid Res.* 52, 110–129. doi: 10.1016/j.plipres.2012.10.002

Bourdenx, B., Bernard, A., Domergue, F., Pascal, S., Leger, A., Roby, D., et al. (2011). Overexpression of Arabidopsis *ECERIFERUM1* promotes wax very-long-chain alkane biosynthesis and influences plant response to biotic and abiotic stresses. *Plant Physiol.* 156, 29–45. doi: 10.1104/pp.111.172320

Broun, P., Poindexter, P., Osborne, E., Jiang, C. Z., and Reichmann, J. L. (2004). WIN1, a transcriptional activator of epidermal wax accumulation in Arabidopsis. *Proc. Natl. Acad. Sci. U. S. A.* 101, 4706–4711. doi: 10.1073/pnas.0305574101

Buschhaus, C., and Jetter, R. (2011). Composition differences between epicuticular and intracuticular wax substructures: how do plants seal their epidermal surfaces? *J. Exp. Bot.* 62, 841–853. doi: 10.1093/jxb/erq366

Chen, X., Goodwin, S. M., Boroff, V. L., Liu, X., and Jenks, M. A. (2003). Cloning and characterization of the *WAX2* gene of Arabidopsis involved in cuticle membrane and wax production. *Plant Cell* 15, 1170–1185. doi: 10.1105/tpc.010926

Chung, M. H., Chen, M. K., and Pan, S. M. (2000). Floral spray transformation can efficiently generate Arabidopsis. *Transgenic Res.* 9, 471–486. doi: 10.1023/A:1026522104478

Dean, G. H., Zheng, H., Tewari, J., Huang, J., Young, D. S., Hwang, Y. T., et al. (2007). The Arabidopsis *MUM2* gene encodes a β-galactosidase required for the production of seed coat mucilage with correct hydration properties. *Plant Cell* 19, 4007–4021. doi: 10.1105/tpc.107.050609

Deshaies, R. J., and Joazeiro, C. A. P. (2009). RING domain E3 ubiquitin ligases. *Annu. Rev. Biochem.* 78, 399–434. doi: 10.1146/annurev.biochem.78.101807.093809

Dong, O. X., Ao, K., Xu, F., Johnson, K. C. M., Wu, Y., Li, L., et al. (2018). Individual components of paired typical NLR immune receptors are regulated by distinct E3 ligases. *Nat. Plants* 4, 699–710. doi: 10.1038/s41477-018-0216-8

Gil, H. L., Kim, J., Suh, M. C., and Seo, P. J. (2017). The MIEL1 E3 ubiquitin ligase negatively regulates cuticular wax biosynthesis in Arabidopsis stems. *Plant Cell Physiol.* 58, 1249–1259. doi: 10.1093/pcp/pcx065

Go, Y. S., Kim, H., Kim, H. J., and Suh, M. C. (2014). Arabidopsis cuticular wax biosynthesis is negatively regulated by the *DEWAX* gene encoding an AP2/ERF-type transcription factor. *Plant Cell* 26, 1666–1680. doi: 10.1105/tpc.114.123307

Greer, S., Wen, M., Bird, D., Wu, X., Samuels, L., Kunst, L., et al. (2007). The cytochrome P450 enzyme CYP96A15 is the midchain alkane hydroxylase responsible for formation of secondary alcohols and ketones in stem cuticular wax of Arabidopsis. *Plant Physiol.* 145, 653–667. doi: 10.1104/pp.107.107300

Han, Y., Sun, J., Yang, J., Tan, Z., Luo, J., and Lu, D. (2017). Reconstitution of the plant ubiquitination cascade in bacteria using a synthetic biology approach. *Plant J.* 91, 766–776. doi: 10.1111/tpj.13603

Haslam, T. M., Gerelle, W. K., Graham, S. W., and Kunst, L. (2017). The unique role of the ECERIFERUM2-LIKE clade of the BAHD acyltransferase superfamily in cuticular wax metabolism. *Plan. Theory* 6:23. doi: 10.3390/plants6020023

Haslam, T. M., and Kunst, L. (2013a). Extending the story of very-long-chain fatty acid elongation. *Plant Sci.* 210, 93–107. doi: 10.1016/j.plantsci.2013.05.008

Haslam, T. M., and Kunst, L. (2013b). Wax analysis of stem and rosette leaves in *Arabidopsis thaliana*. *Bioprotocols* 3:e782. doi: 10.21769/BioProtoc.782

Haslam, T. M., Mañas-Fernández, A., Zhao, L., and Kunst, L. (2012). Arabidopsis ECERIFERUM2 is a component of the fatty acid elongation machinery required for fatty acid extension to exceptional lengths. *Plant Physiol.* 160, 1164–1174. doi: 10.1104/pp.112.201640

Haughn, G. W., and Somerville, C. R. (1986). Sulfonylurea-resistant mutants of *Arabidopsis thaliana*. *Mol. Gen. Genet.* 204, 430–434. doi: 10.1007/BF00331020

Hellens, R. P., Edwards, E. A., Leyland, N. R., Bean, S., and Mullineaux, P. M. (2000). pGreen: a versatile and flexible binary Ti vector for Agrobacterium-mediated plant transformation. *Plant Mol. Biol.* 42, 819–832. doi: 10.1023/A:1006496308160

Hershko, A., and Ciechanover, A. (1998). The ubiquitin system. *Annu. Rev. Biochem.* 67, 425–479. doi: 10.1146/annurev.biochem.67.1.425

Hooker, T. S., Lam, P., Zheng, H., and Kunst, L. (2007). A core subunit of the RNA-processing/degrading exosome specifically influences cuticular wax biosynthesis in Arabidopsis. *Plant Cell* 19, 904–913. doi: 10.1105/tpc.106.049304

Iconomou, M., and Saunders, D. N. (2016). Systematic approaches to identify E3 ligase substrates. *Biochem. J.* 473, 4083–4101. doi: 10.1042/BCJ20160719

Jetter, R., Kunst, L., and Samuels, A. L. (2006). "Composition of plant cuticular waxes," in *Annual Plant Reviews*. eds. M. Riederer and C. Müller (Oxford, UK: Blackwell Publishing Ltd), 145–181.

Kannangara, R., Branigan, C., Liu, Y., Penfield, T., Rao, V., Mouille, G., et al. (2007). The transcription factor WIN1/SHN1 regulates cutin biosynthesis in *Arabidopsis thaliana*. *Plant Cell* 19, 1278–1294. doi: 10.1105/tpc.106.047076

Kim, H., Go, Y. S., and Suh, M. C. (2018). DEWAX2 transcription factor negatively regulates cuticular wax biosynthesis in Arabidopsis leaves. *Plant Cell Physiol.* 59, 966–977. doi: 10.1093/pcp/pcy033

Kim, H., Yu, S., Jung, S. H., Lee, B., and Suh, M. C. (2019). The F-box protein SAGL1 and ECERIFERUM3 regulate cuticular wax biosynthesis in response to changes in humidity in Arabidopsis. *Plant Cell* 31, 2223–2240. doi: 10.1105/tpc.19.00152

Kleinboelting, N., Huep, G., Kloetgen, A., Viehoever, P., and Weisshaar, B. (2012). GABI-Kat SimpleSearch: new features of the *Arabidopsis thaliana* T-DNA mutant database. *Nucleic Acids Res.* 40, D1211–D1215. doi: 10.1093/nar/gkr1047

Klepikova, A. V., Kasianov, A. S., Gerasimov, E. S., Logacheva, M. D., and Penin, A. A. (2016). A high resolution map of the *Arabidopsis thaliana* developmental transcriptome based on RNA-seq profiling. *Plant J.* 88, 1058–1070. doi: 10.1111/tpj.13312

Koornneef, M., Hanhart, C. J., and Thiel, F. (1989). A genetic and phenotypic description of *Eceriferum (cer)* mutants in *Arabidopsis thaliana*. *J. Hered.* 80, 118–122. doi: 10.1093/oxfordjournals.jhered.a110808

Kosma, D. K., Bourdenx, B., Bernard, A., Parsons, E. P., Lü, S., Joubès, J., et al. (2009). The impact of water deficiency on leaf cuticle lipids of Arabidopsis. *Plant Physiol.* 151, 1918–1929. doi: 10.1104/pp.109.141911

Kraft, E., Stone, S. L., Ma, L., Su, N., Gao, Y., Lau, O. S., et al. (2005). Genome analysis and functional characterization of the E2 and RING-type E3 ligase ubiquitination enzymes of Arabidopsis. *Plant Physiol.* 139, 1597–1611. doi: 10.1104/pp.105.067983

Lam, P., Zhao, L., Eveleigh, N., Yu, Y., Chen, X., and Kunst, L. (2015). The exosome and trans-acting small interfering RNAs regulate cuticular wax biosynthesis during Arabidopsis inflorescence stem development. *Plant Physiol.* 167, 323–336. doi: 10.1104/pp.114.252825

Lam, P., Zhao, L., McFarlane, H. E., Aiga, M., Lam, V., Hooker, T. S., et al. (2012). RDR1 and SGS3, components of RNA-mediated gene silencing, are required for the regulation of cuticular wax biosynthesis in developing inflorescence stems of Arabidopsis. *Plant Physiol.* 159, 1385–1395. doi: 10.1104/pp.112.199646

Lee, S. B., Kim, H., Kim, R. J., and Suh, M. C. (2014). Overexpression of Arabidopsis MYB96 confers drought resistance in *Camelina sativa* via cuticular wax accumulation. *Plant Cell Rep.* 33, 1535–1546. doi: 10.1007/s00299-014-1636-1

Lee, H. G., and Seo, P. J. (2016). The Arabidopsis MIEL1 E3 ligase negatively regulates ABA signalling by promoting protein turnover of MYB96. *Nat. Commun.* 7:12525. doi: 10.1038/ncomms12525

Lee, S. B., and Suh, M. C. (2015a). Advances in the understanding of cuticular waxes in *Arabidopsis thaliana* and crop species. *Plant Cell Rep.* 34, 557–572. doi: 10.1007/s00299-015-1772-2

Lee, S. B., and Suh, M. C. (2015b). Cuticular wax biosynthesis is up-regulated by the MYB94 transcription factor in Arabidopsis. *Plant Cell Physiol.* 56, 48–60. doi: 10.1093/pcp/pcu142

Li, R.-J., Li, L.-M., Liu, X.-L., Kim, J.-C., Jenks, M. A., and Lü, S. (2019). Diurnal regulation of plant epidermal wax synthesis through antagonistic roles of the transcription factors SPL9 and DEWAX. *Plant Cell* 31, 2711–2733. doi: 10.1105/tpc.19.00233

Libault, M., Wan, J., Czechowski, T., Udvardi, M., and Stacey, G. (2007). Identification of 118 Arabidopsis transcription factor and 30 ubiquitin-ligase genes responding to chitin, a plant-defense elicitor. *Mol. Plant-Microbe Interact.* 20, 900–911. doi: 10.1094/MPMI-20-8-0900

Lorick, K. L., Jensen, J. P., Fang, S., Ong, A. M., Hatakeyama, S., and Weissman, A. M. (1999). RING fingers mediate ubiquitin-conjugating enzyme (E2)-dependent ubiquitination. *Proc. Natl. Acad. Sci. U. S. A.* 96, 11364–11369. doi: 10.1073/pnas.96.20.11364

Lü, S., Zhao, H., Des Marais, D. L., Parsons, E. P., Wen, X., Xu, X., et al. (2012). Arabidopsis *ECERIFERUM9* involvement in cuticle formation and maintenance of plant water satus. *Plant Physiol.* 159, 930–944. doi: 10.1104/pp.112.198697

Marino, D., Froidure, S., Canonne, J., Ben Khaled, S., Khafif, M., Pouzet, C., et al. (2013). Arabidopsis ubiquitin ligase MIEL1 mediates degradation of the transcription factor MYB30 weakening plant defence. *Nat. Commun.* 4:1476. doi: 10.1038/ncomms2479

Ménard, R., Verdier, G., Ors, M., Erhardt, M., Beisson, F., and Shen, W. H. (2014). Histone H2B monoubiquitination is involved in the regulation of cutin and wax composition in *Arabidopsis thaliana*. *Plant Cell Physiol.* 55, 455–466. doi: 10.1093/pcp/pct182

Müller, C. (2018). Plant–insect interactions on cuticular surfaces. *Annu. Plant. Rev.* 23, 398–422. doi: 10.1002/9781119312994.apr0241

Nakagawa, T., Kurose, T., Hino, T., Tanaka, K., Kawamukai, M., Niwa, Y., et al. (2007). Development of series of gateway binary vectors, pGWBs, for realizing efficient construction of fusion genes for plant transformation. *J. Biosci. Bioeng.* 104, 34–41. doi: 10.1263/jbb.104.34

Nelson, B. K., Cai, X., and Nebenführ, A. (2007). A multicolored set of in vivo organelle markers for co-localization studies in Arabidopsis and other plants. *Plant J.* 51, 1126–1136. doi: 10.1111/j.1365-313X.2007.03212.x

Oshima, Y., Shikata, M., Koyama, T., Ohtsubo, N., Mitsuda, N., and Ohme-Takagi, M. (2013). MIXTA-like transcription factors and WAX INDUCER1/SHINE1 coordinately regulate cuticle development in Arabidopsis and *Torenia fournieri*. *Plant Cell* 25, 1609–1624. doi: 10.1105/tpc.113.110783

Park, C. S., Go, Y. S., and Suh, M. C. (2016). Cuticular wax biosynthesis is positively regulated by WRINKLED4, an AP2/ERF-type transcription factor, in Arabidopsis stems. *Plant J.* 88, 257–270. doi: 10.1111/tpj.13248

Pfaffl, M. W. (2001). A new mathematical model for relative quantification in real-time RT-PCR. *Nucleic Acids Res.* 29:e45. doi: 10.1093/nar/29.9.e45

Raffaele, S., Vailleau, F., Leger, A., Joubès, J., Miersch, O., Huard, C., et al. (2008). A MYB transcription factor regulates very-long-chain fatty acid biosynthesis for activation of the hypersensitive cell death response in Arabidopsis. *Plant Cell* 20, 752–767. doi: 10.1105/tpc.107.054858

Reicosky, D. A., and Hanover, J. W. (1978). Physiological effects of surface waxes. *Plant Physiol.* 62, 101–104. doi: 10.1104/pp.62.1.101

Riederer, M. (2006). "Introduction: biology of the plant cuticle" in *Biology of the Pant Cuticle*. eds. M. Riederer and C. Müller (Oxford, UK: Blackwell), 4–5.

Riederer, M., and Schreiber, L. (2001). Protecting against water loss: analysis of the barrier properties of plant cuticles. *J. Exp. Bot.* 52, 2023–2032. doi: 10.1093/jexbot/52.363.2023

Rowland, O., Lee, R., Franke, R., Schreiber, L., and Kunst, L. (2007). The *CER3* wax biosynthetic gene from *Arabidopsis thaliana* is allelic to WAX2/YRE/FLP1. *FEBS Lett.* 581, 3538–3544. doi: 10.1016/j.febslet.2007.06.065

Samuels, L., Kunst, L., and Jetter, R. (2008). Sealing plant surfaces: cuticular wax formation by epidermal cells. *Annu. Rev. Plant Biol.* 59, 683–707. doi: 10.1146/annurev.arplant.59.103006.093219

Seo, P. J., Lee, S. B., Suh, M. C., Park, M. J., Go, Y. S., and Park, C. M. (2011). The MYB96 transcription factor regulates cuticular wax biosynthesis under drought conditions in Arabidopsis. *Plant Cell* 23, 1138–1152. doi: 10.1105/tpc.111.083485

Shepherd, T., and Wynne Griffiths, D. (2006). The effects of stress on plant cuticular waxes. *New Phytol.* 171, 469–499. doi: 10.1111/j.1469-8137.2006.01826.x

Sieber, P., Schorderet, M., Ryser, U., Buchala, A., Kolattukudy, P., Métraux, J.-P., et al. (2000). Transgenic Arabidopsis plants expressing a fungal cutinase show alterations in the structure and properties of the cuticle and postgenital organ fusions. *Plant Cell* 12, 721–737. doi: 10.1105/tpc.12.5.721

Suh, M. C., Samuels, A. L., Jetter, R., Kunst, L., Pollard, M., Ohlrogge, J., et al. (2005). Cuticular lipid composition, surface structure, and gene expression in Arabidopsis stem epidermis. *Plant Physiol.* 139, 1649–1665. doi: 10.1104/pp.105.070805

Tong, M., Kotur, T., Liang, W., Vogelmann, K., Kleine, T., Leister, D., et al. (2017). E3 ligase SAUL1 serves as a positive regulator of PAMP-triggered immunity and its homeostasis is monitored by immune receptor SOC3. *New Phytol.* 215, 1516–1532. doi: 10.1111/nph.14678

Vierstra, R. D. (2009). The ubiquitin-26S proteasome system at the nexus of plant biology. *Nat. Rev.* 10, 385–397. doi: 10.1038/nrm2688

Vincent, N. G., Charette, J. M., and Baserga, S. J. (2018). The SSU processome interactome in *Saccharomyces cerevisiae* reveals novel protein subcomplexes. *RNA* 24, 77–89. doi: 10.1261/rna.062927.117

Wang, B., Li, C., Kong, X., Li, Y., Liu, Z., Wang, J., et al. (2018a). AtARRE, an E3 ubiquitin ligase, negatively regulates ABA signaling in *Arabidopsis thaliana*. *Plant Cell Rep.* 37, 1269–1278. doi: 10.1007/s00299-018-2311-8

Wang, W., Liu, X., Gai, X., Ren, J., Liu, X., Cai, Y., et al. (2015). *Cucumis sativus* L. *WAX2* plays a pivotal role in wax biosynthesis, influencing pollen fertility and plant biotic and abiotic stress responses. *Plant Cell Physiol.* 56, 1339–1354. doi: 10.1093/pcp/pcv052

Wang, Z., Tian, X., Zhao, Q., Liu, Z., Li, X., Ren, Y., et al. (2018b). The E3 ligase DROUGHT HYPERSENSITIVE negatively regulates cuticular wax biosynthesis by promoting the degradation of transcription factor ROC4 in rice. *Plant Cell* 30, 228–244. doi: 10.1105/tpc.17.00823

Wang, T., Xing, J., Liu, X., Yao, Y., Hu, Z., Peng, H., et al. (2018c). GCN5 contributes to stem cuticular wax biosynthesis by histone acetylation of CER3 in Arabidopsis. *J. Exp. Bot.* 69, 2911–2922. doi: 10.1093/jxb/ery077

Wang, Z.-Y., Xiong, L., Li, W., Zhu, J.-K., and Zhu, J. (2011). The plant cuticle is required for osmotic stress regulation of abscisic acid biosynthesis and osmotic stress tolerance in Arabidopsis. *Plant Cell* 23, 1971–1984. doi: 10.1105/tpc.110.081943

Wang, F., Zhu, D., Huang, X., Li, S., Gong, Y., Yao, Q., et al. (2009). Biochemicali insights on degradation of Arabidopsis DELLA proteins gained from a cell-free assay system. *Plant Cell* 21, 2378–2390. doi: 10.1105/tpc.108.065433

Wilkins, T. A., and Smart, L. B. (1996). "Isolation of RNA from plant tissue," in *A Laboratory Guide to RNA*. ed. P. A. Krieg (New York: Wiley-Liss), 21–41.

Wu, Z., Tong, M., Tian, L., Zhu, C., Liu, X., Zhang, Y., et al. (2020). Plant E3 ligases SNIPER1 and SNIPER2 broadly regulate the homeostasis of sensor NLR immune receptors. *EMBO J.* 39:e104915. doi: 10.15252/embj.2020104915

Yeats, T. H., and Rose, J. K. C. (2013). The formation and function of plant cuticles. *Plant Physiol.* 163, 5–20. doi: 10.1104/pp.113.222737

Zhao, Q., Tian, M., Li, Q., Cui, F., Liu, L., Yin, B., et al. (2013). A plant-specific *in vitro* ubiquitination analysis system. *Plant J.* 74, 524–533. doi: 10.1111/tpj.12127

Zheng, L., Baumann, U., and Reymond, J.-L. (2004). An efficient one-step site-directed and site-saturation mutagenesis protocol. *Nucleic Acids Res.* 32:e115. doi: 10.1093/nar/gnh110

Ziv, C., Zhao, Z., Gao, Y. G., and Xia, Y. (2018). Multifunctional roles of plant cuticle during plant-pathogen interactions. *Front. Plant Sci.* 9:1088. doi: 10.3389/fpls.2018.01088

Conflict of Interest: The authors declare that the research was conducted in the absence of any commercial or financial relationships that could be construed as a potential conflict of interest.

Publisher's Note: All claims expressed in this article are solely those of the authors and do not necessarily represent those of their affiliated organizations, or those of the publisher, the editors and the reviewers. Any product that may be evaluated in this article, or claim that may be made by its manufacturer, is not guaranteed or endorsed by the publisher.

frontiers in Plant Science

ORIGINAL RESEARCH
published: 05 November 2021
doi: 10.3389/fpls.2021.738949

Arabidopsis thaliana Cuticle Composition Contributes to Differential Defense Response to *Botrytis cinerea*

Wendy Aragón[1,2], Damien Formey[1], Norma Yaniri Aviles-Baltazar[1], Martha Torres[1] and Mario Serrano[1]**

[1] Centro de Ciencias Genómicas, Universidad Nacional Autónoma de México, Cuernavaca, Mexico, [2] Programa de Doctorado en Ciencias Biomédicas, Centro de Ciencias Genómicas, Universidad Nacional Autónoma de México, Cuernavaca, Mexico

The chemical composition of a plant cuticle can change in response to various abiotic or biotic stresses and plays essential functions in disease resistance responses. *Arabidopsis thaliana* mutants altered in cutin content are resistant to *Botrytis cinerea*, presumably because of increased cuticular water and solute permeability, allowing for faster induction of defense responses. Within this context, our knowledge of wax mutants is limited against this pathogen. We tested the contribution of cuticular components to immunity to *B. cinerea* using mutants altered in either cutin or wax alone, or in both cutin and wax contents. We found that even all the tested mutants showed increased permeability and reactive oxygen species (ROS) accumulation in comparison with wild-type plants and that only cutin mutants showed resistance. To elucidate the early molecular mechanisms underlying cuticle-related immunity, we performed a transcriptomic analysis. A set of upregulated genes involved in cell wall integrity and accumulation of ROS were shared by the cutin mutants *bdg*, *lacs2-3*, and *eca2*, but not by the wax mutants *cer1-4* and *cer3-6*. Interestingly, these genes have recently been shown to be required in *B. cinerea* resistance. In contrast, we found the induction of genes involved in abiotic stress shared by the two wax mutants. Our study reveals new insight that the faster recognition of a pathogen by changes in cuticular permeability is not enough to induce resistance to *B. cinerea,* as has previously been hypothesized. In addition, our data suggest that mutants with resistant phenotype can activate other defense pathways, different from those canonical immune ones.

Keywords: cuticle, cuticular mutants, *B. cinerea*, permeability, ROS, cell wall

OPEN ACCESS

Edited by:
Isabel Molina,
Algoma University, Canada

Reviewed by:
Ye Xia,
The Ohio State University, United States
Lucas Busta,
University of Minnesota Duluth, United States

****Correspondence:***
Wendy Aragón
waragon@ccg.unam.mx
Mario Serrano
serrano@ccg.unam.mx

Specialty section:
This article was submitted to Plant Physiology, a section of the journal Frontiers in Plant Science

Received: *09 July 2021*
Accepted: *06 October 2021*
Published: *05 November 2021*

Citation:
Aragón W, Formey D, Aviles-Baltazar NY, Torres M and Serrano M (2021) Arabidopsis thaliana Cuticle Composition Contributes to Differential Defense Response to Botrytis cinerea. Front. Plant Sci. 12:738949. doi: 10.3389/fpls.2021.738949

INTRODUCTION

A cuticle is a hydrophobic structure that covers the surface of the epidermal cells of the aerial parts of plants, such as leaves, stems, flowers, seeds, and fruits; and represents one of the evolutionary adaptations that has allowed plants to counteract the adverse effects produced by biotic and abiotic factors (Jeffree, 2006; Jetter et al., 2006; Riederer, 2006; Nawrath et al., 2013). The structure and chemical composition of a cuticle vary widely among different plant species, and even between

organs and stages of its development (Jeffree, 2006; Nawrath et al., 2013; Ingram and Nawrath, 2017). Despite this variability, all cuticles are mainly made up of two types of lipid compounds: cutin and waxes. Cutin is a polymer layer formed by a network of esterified ω-hydroxylated fatty acids *via* intermolecular ester bonds, leading to a three-dimensional structure that is produced and secreted by epidermal cells. Waxes comprise a mixture of very long-chain fatty acids (VLCFAs, 24–36 carbon atoms) and their derivatives, including alkanes, alcohols, and aldehydes, together with secondary metabolites, such as flavonoids and triterpenoids (Li-Beisson et al., 2013; Nawrath et al., 2013; Fernández et al., 2016).

Genetic approaches that use mutagenized populations of *Arabidopsis thaliana* (Bernard and Joubès, 2013; Yeats and Rose, 2013; Borisjuk et al., 2014; Domínguez et al., 2015; Fich et al., 2016), tomato, and maize (Isaacson et al., 2009; Javelle et al., 2010; Girard et al., 2012) have allowed for the identification of many key enzymes involved in cuticle biosynthesis and deposition. Some of these mutants, such as the cutin mutants *bodyguard* (*bdg*), *lacs2*, *lacerata* (*lcr*/*cyp86a8), cyp86a2*/*att1, abcg32*/*pec1,* and *myb96* (Wellesen et al., 2001; Schnurr et al., 2004; Xiao et al., 2004; Kurdyukov et al., 2006; Seo and Park, 2010; Benikhlef et al., 2013; Fabre et al., 2016; Zhao et al., 2019), and the wax mutants *fiddlehead* (*fdh*/*kcs10*), *cer1*, *cer3*/*wax2,* and *dewax* (Yephremov et al., 1999; Chen et al., 2003; Kurata et al., 2003; Rowland et al., 2007; Voisin et al., 2009; Sakuradani et al., 2013; Go et al., 2014; Liu et al., 2020) show a strong reduction in cutin and wax contents. Despite the loss of its cuticular structure, which might be thought to be detrimental to the plant, these mutants can accumulate significantly either more cutin monomers or more wax components when the other is reduced relative to wild type as a compensatory mechanism to maintain the integrity of cuticle (Voisin et al., 2009; Nawrath et al., 2013; Serrano et al., 2014).

To date, studies have identified the role of cuticular components during interaction with pathogens, showing that a cuticle is a physical and chemical barrier and that its components may act as signaling and defense molecules for both fungi and plants (Serrano et al., 2014; Aragón et al., 2017; Ziv et al., 2018). For instance, cutin monomers induce the germination of *Magnaporthe grisea* during the infection process of rice (*Oryza sativa*) (Gilbert et al., 1996), appressorium formation of the powdery mildew *Erysiphe graminis*in barley (*Hordeum vulgare)* (Francis et al., 1996), and induction of a protein kinase-mediated pathway required for the pathogenic development of *Colletotrichum trifolii* (Dickman et al., 2003). Besides the cutin monomers, specific wax components, such as very-long-chain (VLC) aldehydes, induce the pre-penetration process of *Blumeria graminis* both *in vitro* (Hansjakob et al., 2010) and *in planta* (Hansjakob et al., 2011). Additionally, other wax components, such as VLC primary alcohols of avocado (*Persea americana*), induce germination and appressorium formation of *Colletotrichum gloeosporioides* (Podila et al., 1993). In contrast, plants might perceive cutin monomers released by the action of fungal cutinase as elicitors. This hypothesis was evaluated when rice and barley plants were treated with synthetic cutin monomers (C18 fatty acids) and showed resistance to *E. graminis* and *M. grisea,* respectively (Schweizer et al., 1996). In the same way, cucumber seedlings respond to hydrolyzates of cutin by producing H_2O_2, which has been associated with early defense responses against pathogens (Fauth et al., 1998).

Cuticular mutants and transgenic lines have contributed to the advancement of our knowledge of how defects in cuticle structure might lead to immunity of plants upon the attack by pathogenic fungi. Fungal cutinase-expressing (CUTE) plants and *A. thaliana* cutin mutants with an altered ultrastructure and increased permeability of the cuticle, such as *lacs2* (deficient in the long-chain acyl-CoA synthetase 2 enzyme that catalyzes the synthesis of intermediates in the cutin pathway and in wax biosynthesis), *bdg* (mutated in BODYGUARD, an extracellular α/β hydrolase suggested to be involved in cutin polyester assembly), and *lcr* (mutated in *CYP86A8*, which is involved in the biosynthesis of cutin pathway), displayed increased resistance to the necrotrophic fungus *Botrytis cinerea* (Sieber et al., 2000; Bessire et al., 2007; Chassot et al., 2007; Tang et al., 2007; Voisin et al., 2009). Likewise, we have recently described that a mutant with a strong reduction in both cutin and wax contents, *eca2* (expression constitutiva del gen*ATL2)*, is resistant to *B. cinerea* and to the hemibiotrophic bacterial pathogen *Pseudomonas syringae* pv tomato strain DC3000 (*Pst* DC3000), but susceptible to *Phytophthora brassicae* compared with WT plants (Blanc et al., 2018). In contrast, the mutants *lacs2,acp4,* and *myb96* with altered cutin content exhibited enhanced susceptibility against *Pst* DC3000 (Tang et al., 2007; Xia et al., 2009; Seo and Park, 2010). Besides these cutin mutants, only a few *A. thaliana* mutants with defects in wax biosynthesis or regulation have been screened for their responses to different pathogens. For instance, *cer1-1* mutants affected in *CER1* (wax biosynthetic gene fora VLC-aldehyde decarbonylase) have a significantly reduced wax load, showed susceptibility to the necrotrophic fungus *Sclerotinia sclerotiorum* (Aarts et al., 1995; Bourdenx et al., 2011), and enhanced resistance to the biotrophic fungus *Golovinomyces orontii*, whereas, in *cer3-6* and *cer3-8* mutants affected in *CER3/WAX2/YRE* (a wax biosynthetic gene for VLC-acyl-CoA reductase), the growth and reproduction of these fungi were slightly inhibited (Rowland et al., 2007; Inada and Savory, 2011). An evaluation of *in planta* bacterial growth in *cer1-1* confirmed susceptibility to bacterium *Pst* DC3000 (Xia et al., 2009; Bourdenx et al., 2011), as well as in the mutant *cer3-6* (Lee et al., 2016). The *dewax* mutant (knockout in *DEWAX* that codified to the transcription factor DEWAX, which represses cuticular wax biosynthesis) has been reported to be more susceptible to *B. cinerea* (Go et al., 2014; Ju et al., 2017). In order to explain the resistance against *B. cinerea* observed on mutants with altered cutin composition, several reports have characterized physiological changes and the induction of defense responses. These reports include analysis on cuticular water and solute permeability (hereafter referred to as cuticular permeability), the production of reactive oxygen species (ROS), expression of genes implicated in plant defense signaling pathways (Bessire et al., 2007; Chassot et al., 2007; Voisin et al., 2009; L'Haridon et al., 2011; Blanc et al., 2018), and analysis of the abscisic acid (ABA) signaling pathway (L'Haridon et al., 2011; Cui et al., 2016). Based on these reports, a model to explain the cuticle-derived resistance to *B. cinerea* was proposed. In the

cutin mutants, changes in cuticular structure and permeability allow pathogen- and/or damage-associated molecular patterns (PAMPs or DAMPs), released from both the pathogen and the plant cuticle or cell wall, respectively, to be more rapidly recognized by plant pattern recognition receptors, triggering immune responses (Serrano et al., 2014). Nevertheless, we are far away from fully understanding the early mechanisms and role(s) that cuticular components might play during the plant-fungal pathogen interaction, especially against *B. cinerea*, which leads to resistance.

In this report, we characterized mutants altered in either cutin (*bdg*, *lacs2-3*) or wax (*cer1-4* and *cer3-6*) alone, or altered in both cutin and wax (*eca2*) contents during the interaction with *B. cinerea*. We determined that while all the mutants have an increased permeability, only the cutin mutants were resistant to this pathogen. Additionally, in order to identify the molecular elements that lead to this resistance or susceptibility, we performed a genome-wide transcriptional characterization before and after the challenge with the fungus. This analysis allowed us to identify a set of genes, expressed only in mutants altered in cutin content, that have recently been described as part of resistance mechanisms against *B. cinerea* (Lionetti et al., 2017; Bacete et al., 2018; Del Corpo et al., 2020). Our study allows us to understand how modification in cuticular components activates defense responses against this agronomical important phytopathogen.

MATERIALS AND METHODS

Plant Material and Growth Conditions

Arabidopsis thaliana plants were grown in a greenhouse at 22 to 23°C and 60% humidity under a long day photo period (16-h light) for 4 weeks. The following plants were used: C24 ecotype as wild-type (WT) for the *eca2* mutant altered in both cutin and wax components (Salinas-Mondragón et al., 1999; Serrano and Guzmán, 2004; Blanc et al., 2018) and Columbia-0 (Col-0) as WT for mutants altered in cutin content: *bdg* (Kurdyukov et al., 2006; Voisin et al., 2009) and *lacs2-3* (CS65776 (obtained from the Arabidopsis Biological Resource Center, ABRC) (Bessire et al., 2007). The mutants altered in wax content were *cer1-4* (SALK_008544C) (Bourdenx et al., 2011) and *cer3-6* (*yre-1*) (Rowland et al., 2007), and were kindly provided by Professor Ljerka Kunst, Department of Botany, University of British Columbia, Vancouver, BC, Canada. All the selected mutants have been genetically (confirmed homozygous lines) and chemically characterized in detail (**Supplementary Table 1**).

Pathogen Infection Assays

Botrytis cinerea strain B05.10 was cultured on potato dextrose agar (PDA, 39 g L^{-1}) plates. Spores were harvested in distilled water and filtered to remove hyphae. For inoculations, spore concentration was adjusted to 5×10^4 spores ml^{-1} in 1/4 -strength potato dextrose broth (PDB, 6 g L^{-1}; Sigma-Aldrich, United States). For the analysis of lesion development, six fully expanded leaves per 4-week-old soil-grown plant were inoculated with a single drop of 6 μl of a spore suspension over each leaf, and at least 30 lesions were evaluated in each experiment. The inoculated plants were covered with plastic lids to maintain moisture level and transferred to a growth chamber at 22°C and a 24-h dark cycle. After 72 hpi, symptoms were evaluated. The level of resistance (disease incidence) was expressed by the percentage of plants showing disease symptoms extending beyond the inoculation site in each mutant. The developed lesions were quantified using the Image J analysis software (Fiji Is Just Image J[1]) (Schindelin et al., 2012). The experiments were repeated with at least three individual biological replicates, each with 10 technical replicates.

Cuticular Permeability Assays

The toluidine blue staining performed was from a previously described method (Tanaka et al., 2004; Bessire et al., 2007). Rosette leaves of 4-week-old plants were detached and immersed for 2 h in 0.025% TB (Sigma-Aldrich, United States) solution in 1/4 PDB (Sigma-Aldrich, United States) and were rinsed with tap water. Photos were used to measure the stained area (mm^2) using imageJ see text footnote 1. For staining with calcofluor white (Sigma-Aldrich, United States), the leaves were bleached in absolute ethanol overnight, incubated in 0.2 M sodium phosphate buffer (pH 9) for 1 h, and for 5 min in 0.5% calcofluor white in 0.2 M sodium phosphate buffer (pH 9). Then, the leaves were rinsed in sodium phosphate buffer to remove excess calcofluor solution, and photographed under UV light (L'Haridon et al., 2011). Chlorophyll leakage from the rosette leaves was determined by a previously described protocol (Schnurr et al., 2004). For chlorophyll measurement, the fresh weight of detached leaves of mutants and wild-type plants was measured, and they were immersed in 80% ethanol. After 1 h, 1-ml aliquots were removed, and absorbance was measured at 664 and 647 nm. The micromolar concentration of total chlorophyll per gram of fresh weight of leaves was calculated using the equation: total micromoles chlorophyll = 7.93 (A_{664}) + 19.53 (A_{647}) (Lolle et al., 1997; Voisin et al., 2009). The experiments were repeated with at least three biological replicates, each with six technical replicates.

Detection of Reactive Oxygen Species

3, 3′-Diaminobenzidine and NBT staining were performed to determine the presence of hydrogen peroxide (H_2O_2) and superoxide (O_2^-), respectively. The presence of H_2O_2 was visualized with 3, 3′-diaminobenzidine (Sigma-Aldrich, United States) (Thordal-Christensen et al., 1997; L'Haridon et al., 2011). Detached leaves were immersed in 1 mg ml^{-1} DAB-HCl, pH 3.8, by gentle vacuum infiltration. For superoxide (O_2^-) staining, detached leaves were immersed for 30 min in 0.1% nitroblue tetrazolium (NBT) chloride (Sigma-Aldrich, United States) in 50 mM potassium phosphate buffer pH 7.5 (L'Haridon et al., 2011; Lehmann et al., 2015). Following incubation, the DAB and NBT staining solutions were removed and replaced with a bleaching solution (ethanol: acetic acid: = 3:1). H_2O_2 was visualized as a reddish-brown stain formed by the reaction of DAB with endogenous H_2O_2. The O_2^- content was detected as a dark blue stain of a formazan compound formed as a result of

[1]https://imagej.net/Fiji

NBT reacting with endogenous O^{2-}. The reactive oxygen species (ROS) production in detached rosette leaves unchallenged and challenged with the pathogen was detected using 5-(6) carboxy-2′, 7′-dichlorofluorescein diacetate (DCF-DA; Sigma-Aldrich, United States). The leaves were immersed in 60 μM of DCF-DA in a standard medium (1 mM KCl, 1 mM $MgCl_2$, 1 mM $CaCl_2$, 5 mM 2-morpholinoethanesulfonic acid adjusted to pH 6.1 with NaOH) (L'Haridon et al., 2011; Benikhlef et al., 2013). The leaves were then observed using a Carl Zeiss Axioplan 2 epifluorescence microscope with a GFP filter set (excitation 480/40 nm, emission 527/30 nm). Microscope images were saved as TIFF files, and the accumulation of fluorescence was quantified as pixels using imageJ see text footnote 1.

RNA Extraction, RNA Sequencing, and Analysis

For RNA-seq, rosette leaves of the Col-0, C24, *eca2*, *bdg*, *lacs2-3*, *cer1-4,* and *cer3-6* plants were inoculated by spraying the entire leaves with spore suspension (5×10^4 spores ml^{-1}) of *B. cinerea.* At least eight whole rosettes of each plant were collected at 6 hpi and as well under non-infected conditions. Total RNA for RNA-seq was isolated from two different biological replicates for each mutant and WT using a Spectrum™ Total RNA kit (Sigma-Aldrich, United States). Total RNA concentration and purity were measured using NanoDrop™ 2000 (Thermo Fisher Scientific, Inc., Waltham, MA, United States). Library construction and sequencing were performed by Beijing Genomics Institute (BGI) Americas[2] using DNBSeq™ technology. The sequencing was performed using paired end generating 100-bp size reading. The sequences are publicly available in the following link: https://dataview.ncbi.nlm.nih.gov/object/PRJNA761130?reviewer=jgq29l4gjk5tenf7e4q3755opm.
Approximately 20 million reads per sample were aligned to the *A. thaliana* transcriptome ([3]TAIR version 10) using Bowtie2 (v2.3.5) (Langmead and Salzberg, 2012). The bioinformatics data processing summary for each mutant is shown in **Supplementary Table 2**. We calculated gene expression levels using the RNA-seq by expectation maximization (RSEM) method (v1.3.3) (Li and Dewey, 2011). Differentially expressed genes (DEGs) were identified using the software DESeq2 in the *Integrated Differential Expression Analysis MultiEXperiment* (IDEAMEX) (Jiménez-Jacinto et al., 2019), with a FoldChange ≥ 2, and adjusted *p*-value ≤ 0.05. Additionally, the DEGs were functionally annotated with Gene Ontology (GO) terms extracted with PANTHER (v16.0) (GO term enrichment analysis) and Database for Annotation, Visualization, and Integrated Discovery (DAVID) (v6.8), by using Fisher's exact test and correction with an FDR. Plots were created with the ggplot2 library using RStudio (v1.4.1106). To further identify DEGs common among the cutin and wax mutants, we drew Venn diagrams using the VennDiagram package in R (v4.0.3), and the webtool Venn Diagram[4]. Figures showing heatmaps were generated using the webtool Heatmapper[5] (Babicki et al., 2016).

[2]https://www.bgi.com/us

[3]https://www.arabidopsis.org/

[4]http://bioinformatics.psb.ugent.be/webtools/Venn/

[5]http://www.heatmapper.ca/expression/

Quantitative RT-PCR Analysis

Total RNA was isolated from the frozen rosette leaves of WT and the mutants infected and non-infected with *B. cinerea* (6 hpi) collected directly into liquid nitrogen and stored at −80°C. Wet weight of 100 mg was used for RNA isolation from a pool of leaves from six plants of each genotype using TRI Reagent® (Sigma-Aldrich, United States), following the instructions of the manufacturer. Sample quality was assessed by using denaturing gel electrophoresis and measured using NanoDrop 1000 Spectrophotometer (Thermo Fisher Scientific, Inc., Waltham, MA, United States). A 1-μg sample of total RNA was treated with DNase I, RNAse-free (Thermo Fisher Scientific, Inc., Waltham, MA, United States), and then used as the template for cDNA synthesis with a RevertAid H Minus RevertAid First Strand cDNA Synthesis kit (Thermo Fisher Scientific, Inc., Waltham, MA, United States). Quantitative RT-PCR (RT-qPCR) reactions contained cDNA (diluted 1/40) in Maxima SYBR Green/ROX qPCR Master Mix (2×) (Thermo Fisher Scientific, Inc., Waltham, MA, United States) and 0.5 μM of specific primers. Primers for the RT-qPCR gene expression analysis have been previously described: *AtPME17* (Del Corpo et al., 2020), *AtPME41* (Choi B. et al., 2017), *RAP2.6/ERF108* (Imran et al., 2018), and *CAT3* (Zou et al., 2015). All the reactions were performed in 96-well plates using the 7300 Real-Time PCR System and 7300 System Software (Applied Biosystems, Foster City, CA, United States). PCR conditions were 95°C initial denaturations for 15 min, 40 cycles of 15 s/95°C, 30 s/60°C, and 30 s/72°C, after each run, a dissociation curve was acquired to check for amplification specificity by heating the samples from 60 to 95°C. The relative gene expression level for each sample was calculated using the comparative Ct method (Schmittgen and Livak, 2008) and normalized with the geometrical mean of two housekeeping genes, *CF150* (AT1G72150) and *ACT2* (AT3G18780) (Serrano and Guzmán, 2004; Czechowski et al., 2005). One-way ANOVA followed by Tukey comparisons was performed to evaluate the significance of the differential gene expression using the mean values from three biological replicates for each sample.

Statistical Analysis

One-way analysis of variance, followed by Tukey's (honestly significant difference (HSD) comparisons, was performed to determine statistical significance. GraphPad Prism8 v 8.0.1 (GraphPad Software, San Diego CA, United States) was used. Data represent the mean ± SE. Differences at $p < 0.001$ were considered significant.

RESULTS

Mutants With Alteration in Cuticular Wax or Cutin Composition Confer Differential Resistance to *Botrytis cinerea*

In recent years, a number of *Arabidopsis* mutants with defects in different steps of cutin biosynthesis, transgenic plants expressing a fungal cutinase and/or direct application of cutinase on wild type rosette leaves, have shown resistance to *B. cinerea*. These

results has been interpreted as evidence of the participation of the cutin monomers in the resistance against this pathogen (Sieber et al., 2000; Chassot et al., 2007; Voisin et al., 2009). Despite the previous data from several mutants involved in the synthesis and regulation of cuticular waxes, in interaction with pathogens (Bourdenx et al., 2011; Lee et al., 2016; Ju et al., 2017), the link between wax composition/structure and the resistance or susceptibility of mutants against *B. cinerea* have not been described in detail. In addition, molecular defense mechanisms underlying the phenotypes of both the wax and cutin mutant lines mainly affected in cuticular biosynthesis are still unknown. To determine if changes in wax composition lead to resistance to this phytopathogen, we confronted the *eca2* mutant (with modified cutin and wax components), cutin mutants *lacs2-3* and *bdg,* and two mutants with reduced wax content, *cer1-4* and *cer3-6,* with *B. cinerea* and compared them with their corresponding wild-type plants. After inoculation (3 dpi), we observed that only *eca2*, *bdg,* and *lacs2-3* showed resistance to this pathogen (**Figure 1A**). These cutin-altered mutants exhibited less than 20 and 35% of disease incidence, respectively, while their corresponding WT plants showed an incidence of 100% (**Figure 1B**). However, in the *cer1-4* and *cer3-6* mutants affected only in wax composition, susceptibility similar to that of Col-0 was observed (**Figures 1A,B**). Additionally, the lesion average area was significantly smaller in the cutin mutants *eca2,bdg,* and *lacs2-3* compared with the wax mutants *cer1-4* and *cer3-6* (**Figure 1C**). One interesting observation is that under our experimental conditions, the majority of leaves from *eca*2 remained free of disease symptoms 7 dpi compared with their corresponding WT plants (C24), whereas only some of the leaves from *bdg* and *lacs2-3* remained free of disease symptoms at this time. In contrast, all the inoculated leaves of *cer1-4* and *cer3-6* already showed signs of fungal infection at 3 dpi, similar to the WT plants (data not shown). These results indicated that an altered wax composition does not correlate with resistance against the necrotrophic fungi *B. cinerea*, as previously observed in cutin mutants.

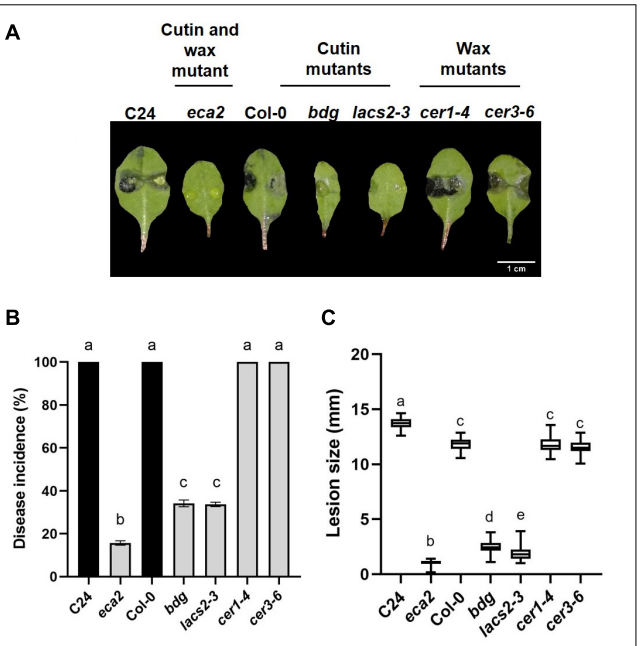

FIGURE 1 | Differential phenotypic response of cuticular mutants to *B. cinerea.* Leaves of WT plants C24 and Col-0 and the cuticular mutants *eca2*, *bdg*, *lacs2-3*, *cer1-4*, and *cer3-6* were infected with *B. cinerea*. Disease symptoms on rosette leaves after 72 hpi **(A)**, disease incidence **(B)**, and lesion size **(C)** were evaluated. Three independent experiments were done (n = 60 ±SD). Different lowercase letter columns indicate significant difference, according to one-way analysis of variance (ANOVA) (p-value < 0.001) followed by Tukey test. Representative pictures are shown.

Changes in Cutin or Wax Content Lead to Increased Leaf Permeability

Previous reports on the *bdg*, *lacs2-3,* and *eca2* mutants have shown that they have a permeable cuticle (Bessire et al., 2007; Chassot et al., 2007; Voisin et al., 2009; L'Haridon et al., 2011; Blanc et al., 2018). To determine if the wax mutants present similar permeability, we assessed it by toluidine blue (TB) and calcofluor staining and measuring the increased efflux of chlorophyll, as previously described (Tanaka et al., 2004; L'Haridon et al., 2011; Cui et al., 2016). The *eca2*, *bdg,* and *lacs2-3* leaves showed the characteristic dark blue and bright patterns correlated with the TB and calcofluor stain, respectively, while *cer1-4* and *cer3-6* had weaker calcofluor staining and smaller TB-stained area compared with the cutin mutants (**Figures 2A,B**). Nevertheless, the quantification of the TB-stained area shows that all the mutants (such as *cer1-4* and *cer3-6*) present statistically significant increased permeability compared with their corresponding WT plants (**Figure 2B**). Next, we analyzed cuticular permeability by chlorophyll leaching. When non-infected rosette leaves are immersed in 80% ethanol, mutants defective either in cutin and/or wax composition lose chlorophyll more rapidly than their corresponding WT plants (**Figure 2C**). We observed that the cutin mutants *lacs2-3* and *eca2* had similar chlorophyll-leaching rates of approximately 4-fold more than their corresponding WT plants. The *bdg*, *cer1-4* and *cer3-6* mutants show 3- and 2-fold greater chlorophyll leaching, respectively, compared with Col-0 (**Figure 2C**), thus corroborating the results of the toluidine blue and calcofluor tests. Taken together, these results indicate that modification of the content of cutin and/or wax leads to a more permeable cuticle.

Cuticle-Related Mutants Show Basal Reactive Oxygen Species Accumulation

Previous reports on *Arabidopsis* mutants with defects in cuticle structure associated with alterations in the composition of cutin monomers showed increased reactive oxygen species (ROS) levels, even when leaves were not challenged with a pathogen (Chassot et al., 2007; L'Haridon et al., 2011; Blanc et al., 2018). To test if the production of ROS, one of the most early and rapid defense reactions to pathogen attack, is present in mutants with alterations in the composition of cuticular wax, we evaluated the accumulation of ROS in uninfected leaves of *eca2, bdg*, *lacs2-3, cer1-4,* and *cer3-6* using three different dyes: 5-(and-6)-carboxy-2,7-dichlorodihydrofluorescein diacetate (DCF-DA) that detects a broad range of oxidizing reagents (L'Haridon et al., 2011); 3, 3′-diaminobenzidine (DAB), which

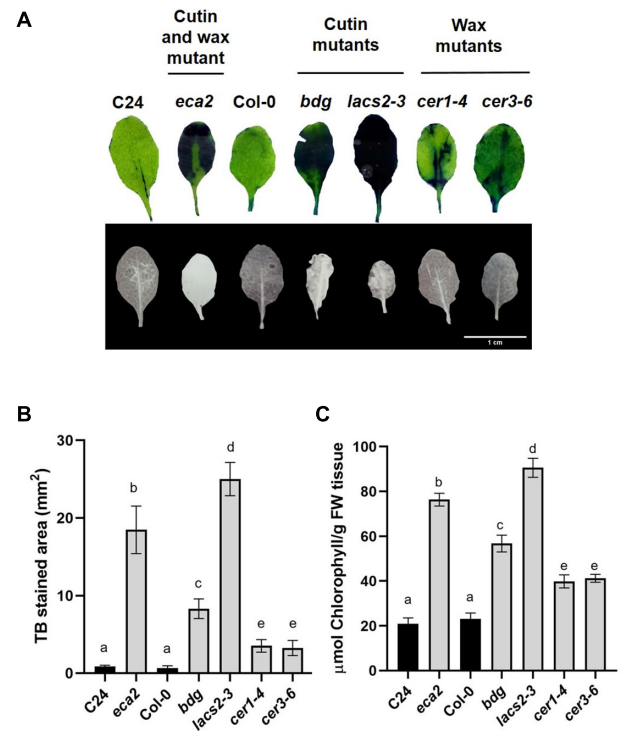

FIGURE 2 | Cuticular mutants present increased leaf permeability. **(A)** Upper panel: leaves of 4-week-old WT plants and the cuticular mutants were stained with toluidine blue. Lower panel: leaves were stained with calcofluor white and viewed under UV light. **(B)** Toluidine blue-stained areas were quantified using the Fiji software. **(C)** Chlorophyll leaching 60 min after immersion of the leaves on 80% EtOH was spectrophotometrically measured as previously described (L'Haridon et al., 2011). Different lowercase letter columns indicate significant differences according to one-way analysis of variance (ANOVA) (p-value < 0.001) followed by Tukey's test. Representative pictures are shown.

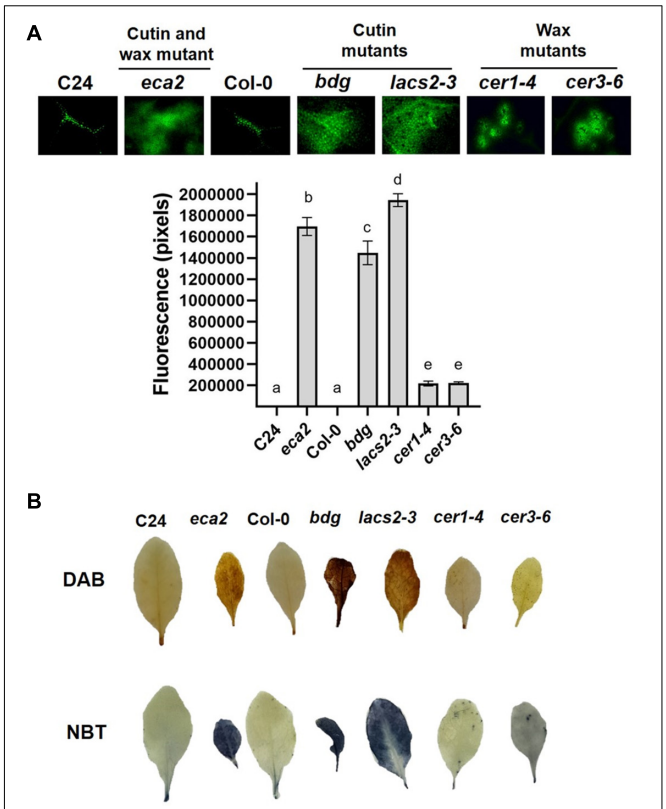

FIGURE 3 | Reactive oxygen species (ROS) accumulation in the cuticular mutants and WT plants. **(A)** DCF-DA staining was observed on leaves by using epifluorescence microscopy. **(B)** 3, 3′-diaminobenzidine (DAB) and nitroblue tetrazolium (NBT) were used to detect the accumulation of hydrogen peroxide (H_2O_2) and superoxide (O_2^-), respectively. Six independent experiments were carried out with similar results ($n = 6 \pm$ SD). Scale bar = 100 µm. Different lowercase letter columns indicate significant differences, according to one-way analysis of variance (ANOVA) (p-value < 0.001) followed by Tukey's test. Representative pictures are shown.

detects H_2O_2; and nitroblue tetrazolium (NBT), which detects O_2^-(Thordal-Christensen et al., 1997; Mengiste et al., 2003). Stronger DCF-DA fluorescence was observed in *eca2*, *bdg,* and *lacs2-3* compared with the mutants with altered wax content, *cer1-4* and *cer3-6* (**Figure 3A**). Nevertheless, ROS accumulation in the latter mutants was stronger than in Col-0 (**Figure 3A**). The DAB and NBT staining showed that coloration in the mutants with altered cutin (*eca2, bdg,* and *lacs2*) was much darker than in *cer1-4* and *cer3-6*, indicating higher ROS accumulation (**Figure 3B**). To further study this immune response, we analyzed ROS accumulation in leaves at 6 hpi with *B. cinerea*. We observed that all the mutants, such as *cer1-4* and *cer3-6,* showed stronger accumulation than their corresponding WT plants in all the staining methodologies (DCF-DA, DAB, and NBT) (**Supplementary Figure 1**). At this point, our data illustrate a possible correlation between cuticle permeability, ROS production, and *B. cinerea* resistance associated with alterations in the composition of cutin monomers, as previously described. However, although cuticle permeability and ROS accumulation are observed in the wax mutants, their susceptibility suggests that these changes might not only be associated with the resistance against *B. cinerea*, as we have previously hypothesized.

Reduction in Cutin and Wax Contents Induced Differential Transcriptional Changes

To investigate the molecular basis that might contribute to the differential response against *B. cinerea* among the cuticular mutants, RNA transcriptome sequencing (RNA-seq) and analysis were performed on non-infected plants. We identified that the number of differentially expressed genes (DEGs) was different in each mutant, compared with their corresponding WT plant, as follows: 2,386 in *eca2*, 3,506 in *bdg*, 1,688 in *lacs2-3*, 2,819 in *cer1-4,* and 611 in *cer3-6* (**Figure 4A** and **Supplementary Data 1**). Additionally, we studied if these DEGs were shared among the mutants (**Figure 4B**). Interestingly, a large proportion of the DEGs (up- and down-regulated genes) was unique in most of the mutants, except for *lacs2-3* and *cer3-6*. For instance, 68, 51, and 69% of the DEGs were only detected in *eca2*, *bdg,* and *cer1-4,* respectively, while 35 and 23% of the DEGs were only identified in *lacs2-3* and *cer3-6* (**Figure 4B**). We also looked at DEGs shared only

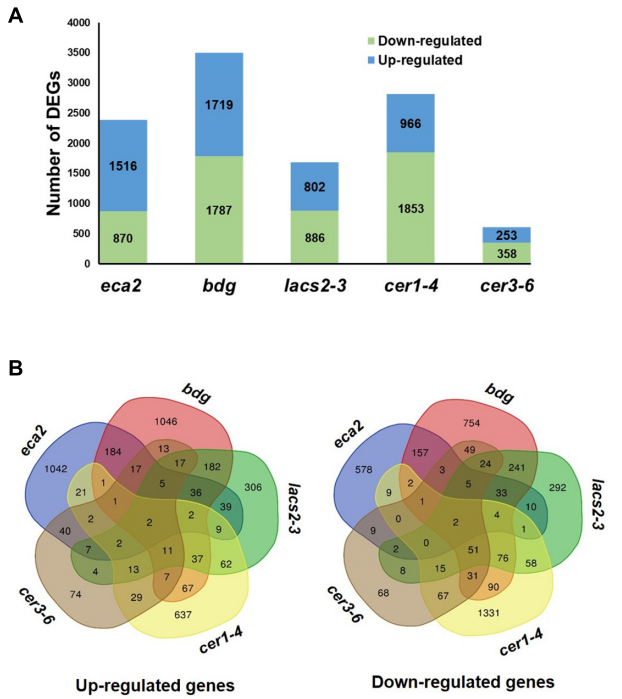

FIGURE 4 | Transcriptome analysis of non-infected cuticular mutants. **(A)** Number of differentially expressed genes (DEGs) (Log2FC ≥ 1 or ≤ −1 with an adjusted *p*-value ≤ 0.05) identified in the cutin and wax mutants. **(B)** Venn diagrams show the overlap of upregulated and downregulated genes among the cutin or wax mutants.

in *B. cinerea*-resistant or susceptible mutants (**Supplementary Data 2**). The Gene Ontology (GO) analysis of these DEGs from the cutin and wax mutants showed substantial differences. Among the 36 induced genes identified in the three cutin mutants, there is enrichment in the transmembrane receptor protein tyrosine kinase signaling pathway, wax biosynthetic process, and cuticle development. Among the 29 induced genes in the wax mutants, there is enrichment in the regulation of response to stress, regulation of response to external stimulus, and developmental process involved in reproduction (**Supplementary Data 3**). On the other hand, for 67 genes that are downregulated in the wax mutants, the DEG biological process categories were associated with photosynthesis and response to abiotic stress, while the 33 downregulated genes identified in the cutin mutants were classified as regulation of metabolic process (**Supplementary Data 3**). Finally, we identified that only two genes were upregulated in all five mutants. They were *GRP3* (AT2G05520), which encodes an Arabidopsis Glycine Rich Protein, and the AT3G14470, which encodes an NB-ARC domain-containing disease resistance protein. Similarly, only two genes were downregulated in all the five mutants: *CBF3* (AT4G25480), which encodes a member of the ERF/AP2 transcription factor family, and a gene that encodes a xyloglucan endotransglycosylase/hydrolase (AT3G44990) (**Figure 4B**). These results suggest a differential transcriptional regulation in all the cuticular mutants.

Under Non-challenged Conditions, Cutin Mutants Transcriptionally Induced Differential Defense Responses

A transcriptional modification of plant defense response genes in non-infected cutin mutants has been previously described (Voisin et al., 2009; Nawrath et al., 2013). However, to our knowledge, it has not been shown in wax mutants. The GO analysis on the identified DEGs for each mutant reveals that only *eca2*, *bdg*, and *lacs2-3* show the modification of expression of genes classified as part of the response to biotic stresses (**Figure 5** and **Supplementary Data 4**). These GO processes included: response to biotic stimulus and response to other organisms, involved in interspecies interaction between organisms and defense responses, while in the mutants *cer1-4* and *cer3-6*, statistically significant GO processes were classified into the response to abiotic stresses (**Figure 5** and **Supplementary Data 4**). In order to further characterize these results in cutin mutants, we analyzed the transcriptome profile of selected marker genes related to the jasmonic acid/ethylene- (JA/ET), salicylic acid (SA), and abscisic acid (ABA) pathways that have been described to be induced during the interaction with this necrotrophic pathogen (AbuQamar et al., 2006; Windram et al., 2012) (**Supplementary Figure 2**, **Supplementary Data 1**). Interestingly, under non-infected conditions, most of these genes were actually downregulated and only a few were induced. These results suggest that while the basal transcriptomic response to biotic stresses is activated in the cutin mutants, canonical defense responses against this pathogen are not induced before the interaction occurs.

Plant Defense Response Genes Are Induced Only in Cutin Mutants During the Interaction With the Pathogen

To further study the modification of the plant transcriptome in cutin and wax mutants, we performed RNA-seq analysis of *B. cinerea*-infected *Arabidopsis* leaves at 6 hpi. Interestingly, we observed a clear difference in the number of genes that are induced or repressed in the cutin mutants compared with the wax mutants. For instance, the number of DEGs in *eca2*, *bdg*, and *lacs2-3* was 2,595, 4,823, and 4,865; while in *cer1-4* and *cer3-6*, the number was only 241 and 411, respectively (**Figure 6A**, **Supplementary Data 5**). This represents approximately 10- to 8-fold more DEGs in the cutin mutants than in the mutants with reduced content of wax. To determine the processes that are transcriptionally induced, we performed a GO analysis of upregulated genes (**Figure 6C**). This analysis reveals a clear enrichment of GO terms related to response to a biotic stimulus only in the mutants with a reduced level of cutin. These terms include the biological process involved in interspecies interaction between organisms, defense response, response to biotic stimulus, response to fungus, and defense response to other organisms, among others (**Figure 6C**, **Supplementary Data 6**), while the GO analysis of upregulated genes in *cer1-4* and *cer3-6* reveals enrichment in response to abiotic stimuli, such as response to an organic substance, cytokinin-activated

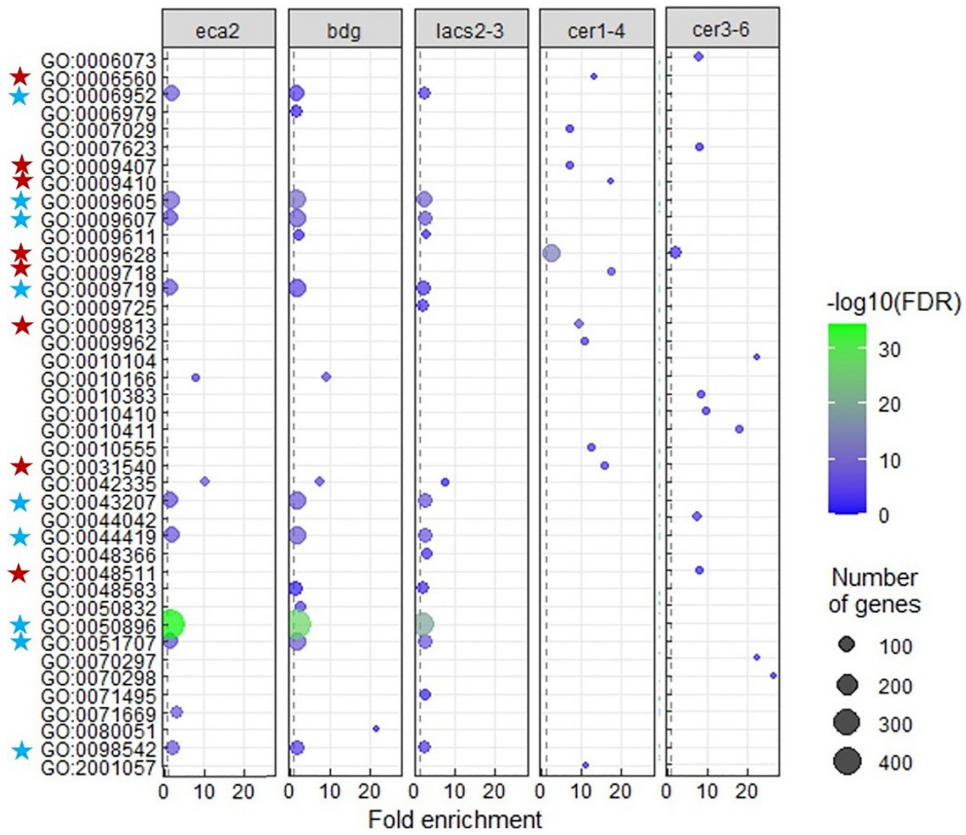

FIGURE 5 | Gene ontology (GO) enrichment among upregulated genes in each cutin or wax mutant. Terms that were largely redundant were removed. Enrichment of "Biological process" GO-terms (FDR < 0.01). The color of the circles indicates the significance of the term (–log FDR), and dot size indicates the number of genes that are associated with that term. The blue stars indicate the GO terms common and mainly related to response to biotic stress, and the red stars indicate the GO terms related to response to abiotic stress, in the cutin and wax mutants, respectively.

signaling pathway, response to chemical, and response to stimulus (**Figure 6C**, **Supplementary Data 7**). Additionally, we found that 214 and 11 DEGs were commonly induced in the cutin and wax mutants, respectively (**Figure 6B**, **Supplementary Data 7**). Additionally, 240 common downregulated genes were identified in *eca2*, *bdg,* and *lacs2-3* (**Figure 6B**, **Supplementary Data 7**), which were classified into the following GO terms: response to salt stress, response to oxidative stress, response to water deprivation, and response to cold. The seven repressed genes common between *cer3-6* and *cer1-4* belong to response to stimulus, single organism process, and response to external stimulus (**Supplementary Data 8**). Taken together, these data indicate that the enhanced resistance against *B. cinerea* observed in *eca2*, *bdg,* and *lac2-3* could be explained by the expression of defense-related genes, which are not induced in the wax mutants.

Canonical Defense Response Genes Are Differentially Induced in Cutin Mutants

We further characterized the defense mechanisms in the mutants with reduced levels of cutin that might participate in the resistance against *B. cinerea*. We were interested in identifying if JA/ ET-, SA-, ABA- and/or other defense-related genes were differentially expressed in the cutin and wax mutants (**Figure 7**). Remarkably, even though many of the hormone- and defense-related genes were induced in all the cutin mutants, we did not detect genes that were expressed simultaneously in all of them, except for the LRR receptor-like protein kinase (*BAK1*) and its interactor *Botrytis-induced kinase 1* (*BIK1*), which are involved in the early stages of recognition of pathogens (Veronese et al., 2005; Liu et al., 2017; van der Burgh et al., 2019). This result suggests that resistance against *B. cinerea* might not be exclusively mediated by these well-described genes.

A Set of Genes Related to Cell Wall Remodeling Is Induced in Mutants With Altered Cutin Monomer Content

Based on the expression profile of *BAK1* and *BIK1*, we identified all the genes that are commonly upregulated among the three cutin resistant mutants, *eca2*, *bdg,* and *lacs2-3,* but downregulated in *cer1-4* and *cer3-6* (**Figures 6B**, **8A**). We identified 214 genes that share this expression pattern (**Supplementary Data 7**). From this set of genes, we performed a GO analysis and the genes were classified into the response to biotic stimulus, response to fungus, innate immune response, and defense response to other

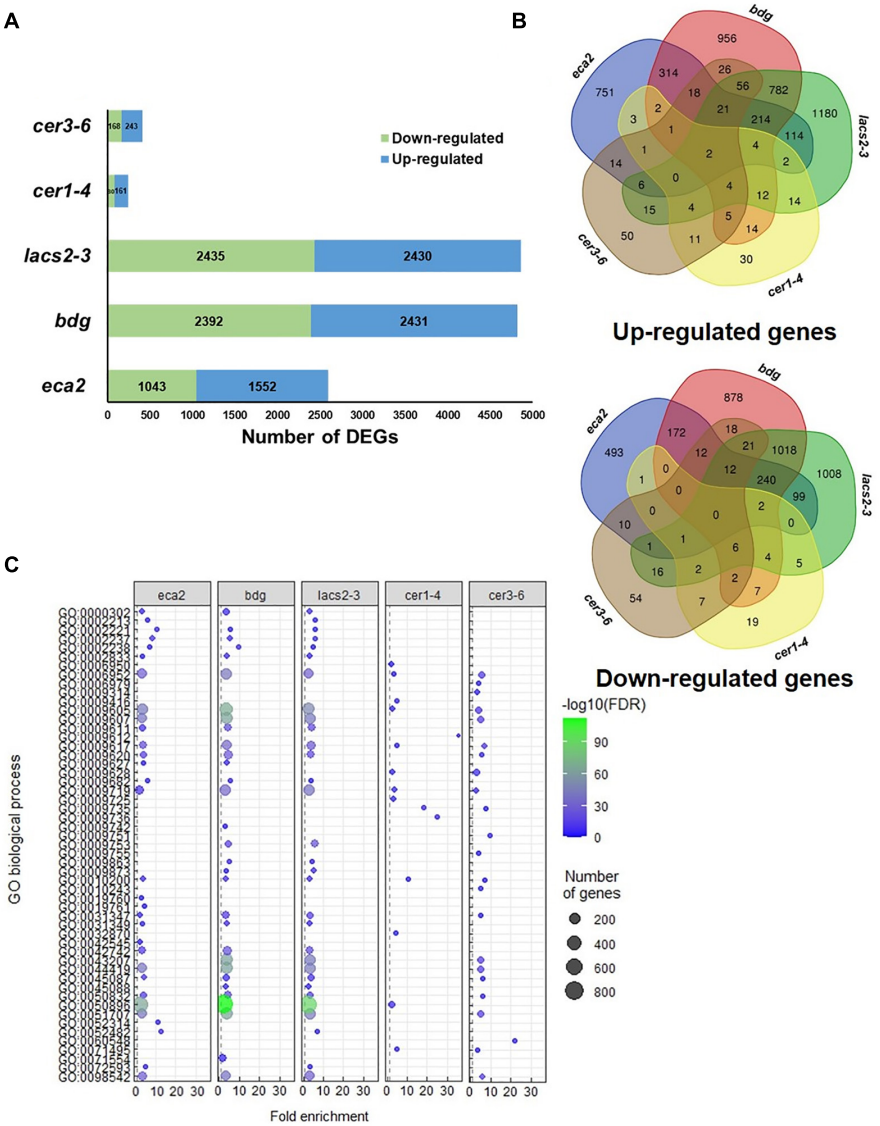

FIGURE 6 | Transcriptome analysis of cuticular mutants infected with *Botrytis cinerea* (6 hpi). **(A)** Number of DEGs (Log2FC ≥ 1 or ≤ −1 with an adjusted *p*-value ≤ 0.05) identified in the cutin and wax mutants. **(B)** Venn diagrams show the overlap of upregulated and downregulated genes among the cutin or wax mutants. **(C)** GO analysis for upregulated genes in each cuticular mutant. Dot plot shows fold enrichment (FDR < 0.01) of the top 25 most significant enrichment terms of biological process.

organisms (**Table 1**). Interestingly, among these DEGs, we found genes that are involved in cell wall remodelings, such as *AtPME17* (AT2G45220) and *AtPME41* (AT4G02330), and encoding pectin methylesterases (PMEs), which have been recently identified in response to *B. cinerea* (Lionetti et al., 2012; Bellincampi et al., 2014; Bethke et al., 2014, 2016). Likewise, two members of the APETALA2/ETHYLENE RESPONSIVE FACTOR (AP2/ERF) family, transcription factors *RAP2.6/ERF108* and *RAP2.6L/ERF113*, catalase *CAT3*, peroxidases *AtPRX71* [recently identified in resistance to *B. cinerea* (Lorrai et al., 2021)], and Sugar Transporter Protein *STP13,* and genes related to pattern-recognition receptors (PRRs), such as *RLK7*, *RLK5,* and *RLP30,* were identified as DEGs (**Figure 8A**). In order to confirm these expression patterns and to validate our RNA-seq analysis, we analyzed the expression of *AtPME17*, *AtPME41*, *RAP2.6/ERF108,* and *CAT3* by RT-qPCR (**Figure 8B**). As expected, we found that all these selected genes were induced 6 hpi in *eca2*, *bdg,* and *lacs2-3*, and that they were downregulated in *cer1-4* and *cer3-6* (**Figure 8B**).

DISCUSSION

Plants have developed sophisticated responses, such as effects of abiotic and biotic stimuli, to survive in a challenging environment. One of these mechanisms includes preformed

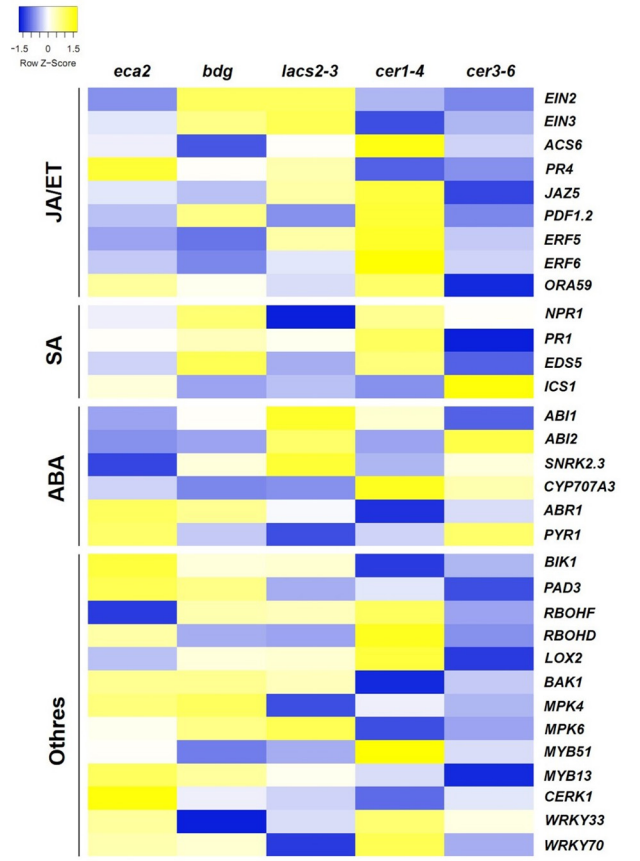

FIGURE 7 | Expression pattern of the jasmonic acid (JA)/ethylene (ET), salicylic acid (SA), and abscisic acid (ABA) signaling pathways and other defense-related genes in response to *B. cinerea* (6 hpi). The colors of the heat map represent the *z*-score of each gene expression calculated between the expression of the mutant compared with its corresponding WT, ranging from blue (–1.5) to yellow (1.5).

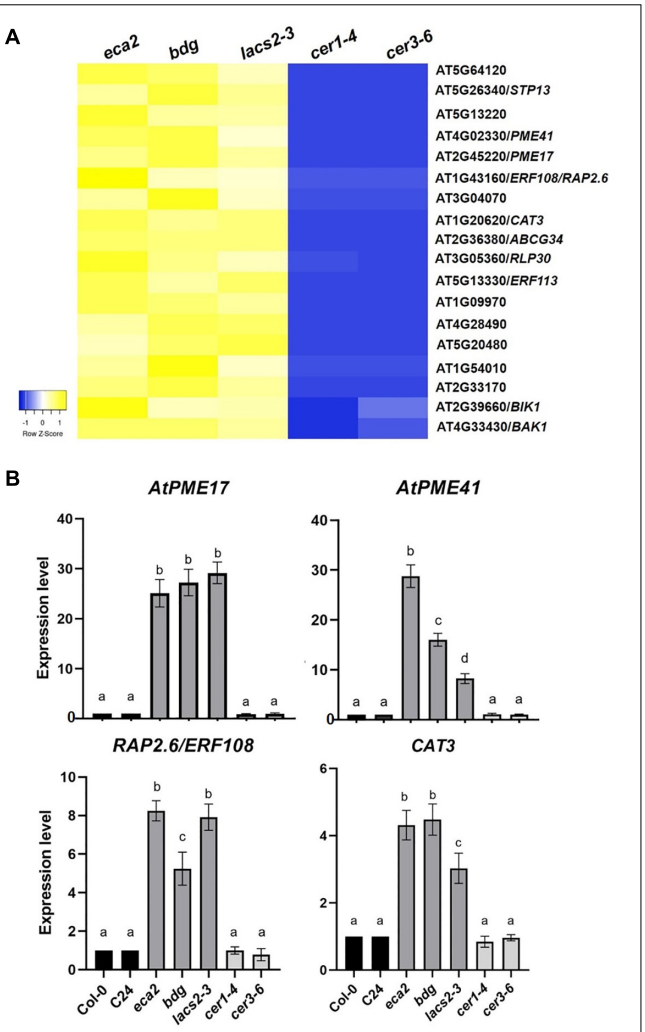

FIGURE 8 | Commonly expressed genes induced in mutants with a reduced level of cutin monomers. **(A)** Heatmap shows the expression levels of upregulated genes shared by the cutin mutants in response to *B. cinerea* (6 hpi). The colors of the heat map represent the z-score of the log2FC of each gene ranging from blue (–1) to yellow (1). **(B)** Expression analysis of some shared up-regulated genes between cutin mutants infected with *B. cinerea*. Expression levels were determined by RT-qPCR in rosette leaves harvested 6 hpi, based on Ct values, normalized with the expression of the two housekeeping genes. The data represent the means of three independent biological replicates with their respective technical replicates, for each sample. Error bars indicate ±SD. Different letters indicate significance differences among samples according to one-way ANOVA followed by Tukey test ($p \leq 0.001$).

physical barriers on the plant surface, such as the cuticle (Chassot et al., 2007; Serrano et al., 2014; Aragón et al., 2017; Bacete et al., 2018; Engelsdorf et al., 2018; Molina et al., 2021). The cuticle, mainly formed by cutin and waxes, also serves as a source of signaling molecules that coordinate the dialog between plants and microorganisms (Aragón et al., 2017; Ziv et al., 2018). In *A. thaliana* and *Solanum lycopersicum*, changes in permeability, associated with modifications in cutin composition, have been linked to resistance against the necrotrophic fungus *B. cinerea* (Bessire et al., 2007; Chassot et al., 2007; Isaacson et al., 2009; Voisin et al., 2009; Martin et al., 2017; Blanc et al., 2018). This resistance has been attributed to faster recognition of pathogens due to a permeable cuticle, accumulation of ROS, and induction of plant defense responses. However, plants with reduced content of waxes, which also have a modified cuticle structure, have not been characterized in detail with respect to this phenotype. In this study, we determined that the wax mutants have a more permeable cuticle but are as susceptible as the wild-type plants. This is in line with the fact that not all cuticle mutants show resistance to *B. cinerea*. For instance, the cuticle mutants *acp4* and *gl1* showed susceptibility to both bacterial pathogens *Pseudomonas syringae* and *B. cinerea* (Xia et al., 2009, 2010; Benikhlef et al., 2013; Lim et al., 2020). Similarly, *shn1*, with cutin monomer content altered, has a more permeable cuticle but is more susceptible to three necrotrophic fungal pathogens, *B. cinerea*, *S. sclerotiorum,* and *Alternaria brassicicola* (Sela et al., 2013; Buxdorf et al., 2014). These results suggest that, as expected, cuticle structural integrity is an important physical barrier against

TABLE 1 | GO enrichment analysis of Biological process of the 214 common upregulated genes in *eca2*, *bdg* and *lacs2-3* infected with *Botrytis cinerea* (genes are listed in **Supplementary Data 6**).

GO_ID	GO description	Gene number	Fold enrichment	*p-value*
GO:0002237	response to molecule of bacterial origin	5	18.3	3.76E-02
GO:0045087	innate immune response	9	8.71	4.46E-03
GO:0002376	immune system process	10	6.82	9.56E-03
GO:0010038	response to metal ion	18	6.28	3.62E-06
GO:0009620	response to fungus	12	5.15	1.65E-02
GO:0033993	response to lipid	24	4.44	4.83E-06
GO:0010035	response to inorganic substance	27	4.43	4.33E-07
GO:0098542	defense response to other organism	23	4.28	2.10E-05
GO:0043207	response to external biotic stimulus	29	3.97	1.01E-06
GO:0051707	response to other organism	29	3.97	1.01E-06
GO:0009607	response to biotic stimulus	29	3.97	1.03E-06
GO:0044419	biological process involved in interspecies interaction between organisms	29	3.88	1.70E-06
GO:0006952	defense response	24	3.79	9.29E-05
GO:0009605	response to external stimulus	35	3.47	4.23E-07
GO:0048583	regulation of response to stimulus	17	3.42	4.03E-02
GO:0042221	response to chemical	61	3.41	1.19E-14
GO:0019752	carboxylic acid metabolic process	19	3.38	1.43E-02
GO:1901700	response to oxygen-containing compound	34	3.37	1.72E-06
GO:0006082	organic acid metabolic process	22	3.36	2.72E-03
GO:0043436	oxoacid metabolic process	21	3.33	5.46E-03
GO:0009725	response to hormone	27	3.25	2.58E-04
GO:0009719	response to endogenous stimulus	27	3.18	4.12E-04
GO:0010033	response to organic substance	35	3.07	1.02E-05
GO:0044281	small molecule metabolic process	29	2.92	7.32E-04
GO:0006950	response to stress	59	2.84	1.60E-10
GO:0050896	response to stimulus	91	2.47	1.89E-15
GO:0009987	cellular process	126	1.59	1.69E-08
GO:0008152	metabolic process	84	1.51	3.41E-02

multiple pathogens (such as *B. cinerea*), and that mutants *sma4, lcr*, *bdg, lacs2,* and *eca2,* which possess a low content of cutin, a permeable cuticle, and are resistant to *B. cinerea,* are exceptions to the rule. Additionally, our results indicate that faster recognition of the pathogen by changing cuticle permeability is not enough to induce plant innate immunity responses and resistance to *B. cinerea,* as previously hypothesized (Bessire et al., 2007; Serrano et al., 2014). Nevertheless, these cutin mutants can be used as models to investigate the molecular mechanisms behind the successful induction of defense responses against this agronomically important pathogen.

Plant development and responses to the environment are induced and regulated by signaling networks of "*trio signaling*" messengers: ROS, electrical signals, and calcium (Choi W.G. et al., 2017). In particular, ROS are induced by activating various oxidases and peroxidases in response to abiotic and biotic conditions (Torres and Dangl, 2005; O'Brien et al., 2012; Baxter et al., 2014; Saini et al., 2018). During host-pathogen interactions, the production of ROS is important for plants and for necrotrophic fungi, such as *B. cinerea* and *S. sclerotiorum*. For instance, one of the earliest defense responses to a pathogen attack is the so-called "oxidative burst," the production of ROS at the site of invasion. A plant releases high amounts of reactive oxygen species (ROS) to counteract the pathogen. On the other hand, *Botrytis cinerea* also takes advantage of this plant defense to kill host cells before they are invaded by hyphae and is able to cope with external oxidative stress in order to survive in the necrotic tissue (Siegmund and Viefhues, 2016). We have described a direct relationship between the accumulation of ROS and resistance to *B. cinerea* after mechanical stimulus or by triggering defense responses through elicitors (Benikhlef et al., 2013; Narváez-Barragán et al., 2020; Batista-Oliveira et al., 2021). Additionally, the resistance against this pathogen observed in the cutin mutants has been also linked to increased levels of ROS under non-infected conditions (reviewed in Serrano et al., 2014). Here, we show that under non-challenged conditions, although all the mutants accumulated more ROS than the WT plants, the cutin mutants *eca2*, *bdg,* and *lacs2-3* have higher levels of superoxide and hydrogen peroxide than the wax mutants *cer1-4* and *cer3-6* (**Figure 3**). Interestingly, at 6 hpi, all the cuticular mutants have higher levels of superoxide and hydrogen peroxide than the WT plants (**Supplementary Figure 1**). Despite the *B. cinerea*-induced ROS burst observed in the wax mutants, they showed susceptibility. Two possibilities can be explored to explain this phenotype based on ROS accumulation. First, since a moderate level of ROS is detected in the susceptible mutants *cer1-4* and *cer3-6*, the level of ROS during the initial interaction with the pathogen could be important in triggering resistance against this pathogen. In agreement with this, it has been described that the inhibition of the size of lesions caused by *B. cinerea* is directly proportional to the level of ROS induced by soft mechanical stress (Benikhlef et al., 2013). On the other hand, during biotic interactions, ROS have been characterized to participate in multiple processes, such as reinforcement of the cell wall, regulation of hormone-induced signaling pathways, and triggering of hypersensitive response (Lehmann et al., 2015). Since we observed an increase of ROS in the wax mutants only after the interaction with the pathogen, it is possible that timing, not only the activation of the oxidative burst, is important to efficiently build up a defense response. Either way, our results suggest that besides ROS-dependent resistance, it is probable

that other(s) mechanism(s) may be involved to trigger the plant response and, therefore, induce resistance against *B. cinerea*.

To further characterize the molecular mechanisms underlying the resistance or susceptibility in the cuticular mutants, we performed a transcriptomic analysis on the non-infected plants. Up-regulated genes identified in the cutin mutants were classified into the response to biotic stimulus, while GO terms in *cer1-4* and *cer3-6* were mainly associated with response to abiotic stimulus (**Figure 5**), suggesting that the identified DEGs in cutin mutants could be part of a primed defense response mechanism. These results are in line with previous reports, where a defense priming mechanism has been observed in plants treated with cutin monomers, as well as in other cuticular mutants, leading to expression of a suite of faster and stronger defense responses upon challenge with *B. cinerea* (Schweizer et al., 1996; Fauth et al., 1998; Bessire et al., 2007; Chassot et al., 2007; Conrath, 2011; Conrath et al., 2015; Mauch-Mani et al., 2017). Notably, our data also identified genes related to PRRs, highlighting the leucine-rich repeat receptor kinase (LRR-RK) (**Figure 4**). Previous studies have reported the importance of PRRs in the priming state. The plant receptor FLS2 and its co-receptor BAK1 were associated with the enhanced responsiveness of *Arabidopsis* plants to the bacterial flagellin peptide flg22 (Tateda et al., 2014), as well as the malectin-like LRR receptor-like kinase IOS1, which is associated with FLS2 and the bacterial receptor EF-Tu (Yeh et al., 2016). Taken together, our results suggest that before the interaction with the pathogen occurs, the cutin mutants are in a priming state compared with the wax mutants or WT plants and that once the infection takes place, they might respond in a faster and more efficient manner, stopping the infection.

Previous reports have characterized secondary responses transcriptionally induced during the interaction with *B. cinerea*. Among these defense responses, SA-, ET-, ABA- and JA-related pathways are induced (AbuQamar et al., 2006; Mengiste, 2012; Windram et al., 2012). To determine if a similar set of genes was present in the cutin and wax mutants, we performed a transcriptome analysis at 6 hpi. In *cer1-4* and *cer3-6* the defense responses are not induced, and most of the DEGs were classified into the response to abiotic stimulus, while in the cutin mutants, enrichment of defense-related genes was identified (**Figure 6**). However, in *eca2*, *bdg,* and *lacs2-3,* a similar profile of these defense marker genes, which could explain the resistance phenotype for all these mutants based on these hormone-induced responses, was not observed (**Figure 7**). From this set of genes, only two, involved in the early stages of recognition of pathogen, were identified to be induced in all the cutin mutants: the LRR receptor-like protein kinase (*BAK1*) and its interactor *Botrytis-induced kinase 1* (*BIK1*). This result is in accordance with previous reports showing that the *Arabidopsis* mutant *sma4* with a defective cuticle displayed increased resistance to *B. cinerea*, and that this process was

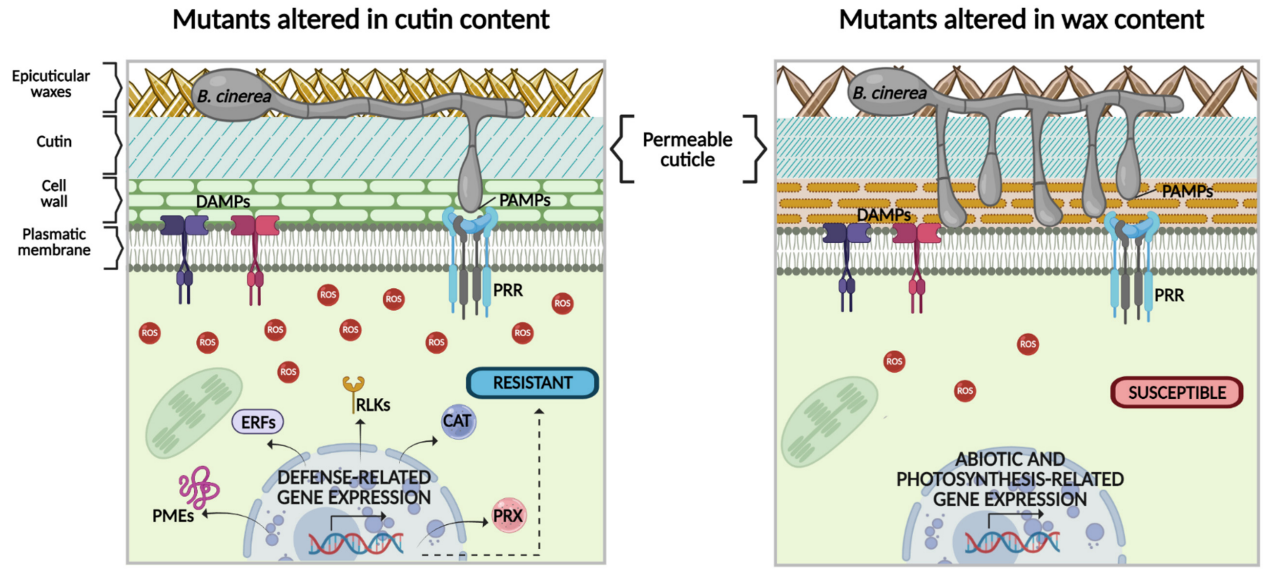

FIGURE 9 | Hypothetical model of the role of cuticular components cutin and wax in differential response to the necrotrophic fungus *B. cinerea*. In previous studies, a direct relationship between increased permeability in cutin mutants and resistance to *B. cinerea* has been proposed. However, our data show that despite both cuticular mutants having enhanced cuticular permeability, compared with the WT plants, only mutants with altered cutin content show resistance to *B. cinerea*. This phenotype could be explained as follows: (1) in the cutin mutants, once plant plasma membrane-localized receptors recognize pathogen-/damage-associated molecular patterns (PAMPs/DAMPs) a more intense ROS production is observed, compared with mutants with altered wax content. (2) During cutin mutant-*B. cinerea* interaction, defense-related signaling pathways are triggered, which are different from canonical immune ones, such as expression genes encoding catalases (*CAT3*) and peroxidases (*PRX*), as well as LRR-receptor-like kinases (*RLK5, RLK7, RLP30*), transcription factors (*ERF108* and *ERF113*), and genes involved in the remodeling of the cell wall, such as *PMEs*. (3) In contrast, according to our data, in the mutants with altered wax content, ROS production is not enough to effectively prevent *B. cinerea* colonization. In these mutants, other secondary signals might be activated to control the expression of genes related to abiotic stimuli, instead of the expression of defense-related genes (the image was designed using bioRENDER application, https://biorender.com/).

independent of the JA and ET signaling pathways (Tang et al., 2007; Wang et al., 2020). Similarly, in CUTE plants, resistance to *B. cinerea* was not found to correlate with the induction of genes associated with the SA, ET, or JA signaling pathways (Chassot et al., 2007). In sum, these results suggest that the resistance to *B. cinerea* observed in *eca2*, *bdg,* and *lacs2-3* might not only be driven by the induction of canonical defense responses, previously identified to be important in stopping the infection.

Since the stronger difference between cutin and wax mutants was resistance and susceptibility to *B. cinerea,* respectively, we hypothesized that a set of genes should be induced only in *eca2*, *bdg,* and *lacs2-3* but repressed in *cer1-4* and *cer3-6* (**Supplementary Data 7**). Among these DEGs, we identified genes previously characterized to be involved in ROS regulation and cell wall biosynthesis, and are discussed next. The peroxidase (At*PRX71*) and catalases (*CAT3* andAT4G37530) genes were identified as DEGs in the cutin mutants. These genes have been described as part of ROS-scavenging systems to maintain ROS homeostasis in different compartments of the cell, and could, thus, restrict the ROS-dependent damage or finely coordinate the ROS-dependent signal transduction in the presence of a pathogen (Torres et al., 2006; O'Brien et al., 2012). However, necrotrophic pathogens also produce ROS to kill host cells triggering a hypersensitive reaction (HR), thereby facilitating the infection (Govrin and Levine, 2000; Torres et al., 2006; van Kan, 2006). Based on this evidence, it is possible that the expression of these scavengers might help either the plant to inhibit the proper ROS-induced infection process of *B. cinerea*, or regulate ROS-dependent plant defense responses. Clearly, this hypothesis should be tested in future studies.

Additionally, we identified the induction of pectin methylesterases (PMEs) *AtPME41* and *AtPME17* (**Figure 8**) in the cutin mutants in response to *B. cinerea*. Importantly, these genes have not been reported before as a part of the defense genes against *B. cinerea* in any cuticular mutants. Our data are in accordance with previous results showing that plants activate a local and strong PME activity in response to pathogens with different lifestyles (Lionetti et al., 2012; Bethke et al., 2014; Lionetti, 2015). Once the pathogen overcomes the cuticle, the pectin matrix, which is the major fraction of the cell wall of dicots and non-aminaceous monocots, is the next target for fungal necrotrophs (van Kan, 2006; Laluk and Mengiste, 2010; Lionetti et al., 2012; Bellincampi et al., 2014). PME activity was proposed to be involved in the release and perception of defense of endogenous signals with elicitor activities from cellular components during infection, such as oligogalacturonides (OGs) considered as DAMPs (Lionetti et al., 2012; Ferrari et al., 2013; De Lorenzo et al., 2019). *AtPME41* synthesizes a member of PMEs that has an important role in activating the immune response when *Arabidopsis* is challenged with the necrotroph *A. brassicicola* (Lionetti et al., 2012; Bethke et al., 2014). Additionally, Del Corpo et al. demonstrated the functional role of AtPME17 in triggering PME activity by the JA/ET-dependent pathway and in resistance against pectinolytic necrotrophic fungi, such as *B. cinerea* (Del Corpo et al., 2020).

Finally, this study illustrates that *B. cinerea* resistance in the cutin mutants *eca2*, *bdg,* and *lacs2-3,* compared with *cer1-4* and *cer3-6*, clearly consists of a multitude of signaling events, from pre-activated defense or priming as initial resistance, production of ROS, and increased expression of non-canonical defense-related genes (**Figure 9**).

CONCLUSION

We have shown that while *cer1-4* and *cer3-6* have altered cuticle permeability, they present a susceptible phenotype, suggesting that the faster recognition of the pathogenic fungus *B. cinerea* is not enough to induce plant innate immune responses and resistance as previously hypothesized. In the cutin mutants *eca2*, *bdg,* and *lacs2-3* responding to *B. cinerea,* a profile of previously characterized defense-response gene markers was not observed, suggesting that mutants with resistant phenotypes can activate other defense pathways, different from these canonical immune ones. Nevertheless, we identified the induction of genes involved in cell wall remodeling in the cutin mutants, which have not been previously reported as part of the defense genes against *B. cinerea* in any cuticular mutants. Based on these results, our study can be used as a starting point to understand the molecular basis involved in early defense mechanisms related to cuticular components against this agronomically important necrotrophic pathogen.

DATA AVAILABILITY STATEMENT

The datasets presented in this study can be found in online repositories. The names of the repository/repositories and accession number(s) can be found below: NCBI BioProject; PRJNA761130.

AUTHOR CONTRIBUTIONS

WA, DF, and MS conceived and designed the experiments. WA, DF, NA-B, and MT performed the experiments. WA, DF, and MS wrote and revised the manuscript. All authors contributed to the article and approved the submitted version.

FUNDING

This study was supported by funds from Dirección General de Asuntos del Personal Académico-UNAM (PAPIIT), grants IA202620 and IN203720 to DF and MS, respectively, as well as the Ciencias Básicas grant from CONACYT No. A1-S-16129 to DF and UC MEXUS-CONACYT Grant No. CN-10-109 to MS. WA is a doctoral student from Programa de Doctoradoen Ciencias Biomédicas, UNAM, and she received the fellowship No. 240087 from Consejo Nacional de Ciencia y Tecnología (CONACYT).

ACKNOWLEDGMENTS

We thank Michael F. Dunn and Antony Buchala for the critical reading and comments on the manuscript. Thank you is also extended to Daniel Tapia Maruri from CEPROBI-IPN and MC Yordan Jhovani Romero-Contreras from CCG-UNAM for the technical help. NA-B acknowledges the fellowship, No. 929445, from CONACYT, Mexico.

SUPPLEMENTARY MATERIAL

The Supplementary Material for this article can be found online at: https://www.frontiersin.org/articles/10.3389/fpls.2021.738949/full#supplementary-material

Supplementary Figure 1 | Reactive oxygen species (ROS) production at 6 hpi with *Botrytis cinerea* in leaves from 4-week-old plants of *Arabidopsis thaliana* cuticular mutants and wild-type (WT) Columbia-0 (Col-0) and C24 plants. Fluorescence after DCF-DA staining was observed on leaves by using epifluorescence microscopy. 3, 3′-Diaminobenzidine (DAB) and nitroblue tetrazolium (NBT) were used to detect the accumulation of hydrogen peroxide (H_2O_2) and superoxide (O_2^-), respectively. The experiment was carried out six times, with similar results ($n = 6 \pm$ SD). Scale bar = 100 μm. Different lowercase letter columns indicate significant differences, according to one-way analysis of variance (ANOVA) (p-value < 0.001) followed by Tukey's test. Representative pictures are shown.

Supplementary Figure 2 | The heat map shows the expression pattern in non-infected cutin and wax mutants, as well as the WT plants of the jasmonic acid (JA)/ethylene (ET), salicylic acid (SA), and abscisic acid (ABA) signaling pathways, and other defense-related genes selected from the literature. The colors of the heat map represent the z-score of each gene ranging from blue (−2) to yellow (2).

Supplementary Table 1 | Cuticular wax and cutin composition of rosette leaves of Arabidopsis Col-0 (wt), *cer1-4*, *cer3-6* (yre), *bdg*, *lacs2-3*, C24 (wt), and *eca2*.

Supplementary Table 2 | Summary of bioinformatics data and mapped reads of *Arabidopsis thaliana* cutin and wax mutants in the RNA-seq libraries in non-infected and infected with *Botrytis cinerea* (6 hpi).

Supplementary Data 1 | List of significantly differentially expressed genes (DEGs) in non-infected cutin and wax mutants, related to **Figure 4A**. List of defense-related genes abundant in the non-infected mutants and wild-type (WT) plants, related to **Supplementary Figure 2**.

Supplementary Data 2 | List of up- and down-regulated genes shared by non-infected cutin or wax mutants, related to **Figure 4B**.

Supplementary Data 3 | Gene Ontology (GO) term enrichment of up- and down-regulated genes shared by non-infected cutin or wax mutants, related to **Figure 4B**.

Supplementary Data 4 | GO term enrichment of up- and downregulated genes in each non-infected cutin or wax mutant, related to **Figure 5**.

Supplementary Data 5 | List of significantly DEGs in cutin and wax mutants infected with *B. cinerea* (6 hpi), related to **Figure 6A**. List of defense-related genes abundant in the infected mutants and WT plants, related to **Figure 7**.

Supplementary Data 6 | List of up- and downregulated genes shared by cutin or wax mutants infected with *B. cinerea* (6 hpi), related to **Figure 6B**.

Supplementary Data 7 | GO term enrichment of up- and downregulated genes shared by infected cutin or wax mutants, related to **Figure 6C**.

Supplementary Data 8 | GO term enrichment of up- and downregulated genes shared by infected cutin or wax mutants, related to **Figure 6B**.

REFERENCES

Aarts, M. G., Keijzer, C. J., Stiekema, W. J., and Pereira, A. (1995). Molecular characterization of the CER1 gene of *Arabidopsis* involved in epicuticular wax biosynthesis and pollen fertility. *Plant Cell* 7, 2115–2127. doi: 10.1105/tpc.7.12.2115

AbuQamar, S., Chen, X., Dhawan, R., Bluhm, B., Salmeron, J., Lam, S., et al. (2006). Expression profiling and mutant analysis reveals complex regulatory networks involved in *Arabidopsis* response to *Botrytis* infection. *Plant J.* 48, 28–44. doi: 10.1111/j.1365-313X.2006.02849.x

Aragón, W., Reina-Pinto, J. J., and Serrano, M. (2017). The intimate talk between plants and microorganisms at the leaf surface. *J. Exp. Bot.* 68, 5339–5350. doi: 10.1093/jxb/erx327

Babicki, S., Arndt, D., Marcu, A., Liang, Y., Grant, J. R., Maciejewski, A., et al. (2016). Heatmapper: web-enabled heat mapping for all. *Nucleic Acids Res.* 44, W147–W153. doi: 10.1093/nar/gkw419

Bacete, L., Mélida, H., Miedes, E., and Molina, A. (2018). Plant cell wall-mediated immunity: cell wall changes trigger disease resistance responses. *Plant J.* 93, 614–636. doi: 10.1111/tpj.13807

Batista-Oliveira, J. S., Formey, D., Torres, M., Aragón, W., Romero-Contreras, Y. J., Maruri-López, I., et al. (2021). Gadolinium protects *Arabidopsis thaliana* against *Botrytis cinerea* through the activation of JA/ET-induced defense responses. *Int. J. Mol. Sci.* 22:4938. doi: 10.3390/ijms22094938

Baxter, A., Mittler, R., and Suzuki, N. (2014). ROS as key players in plant stress signalling. *J. Exp. Bot.* 65, 1229–1240. doi: 10.1093/jxb/ert375

Lionetti, V. (2014). Plant cell wall dynamics and wall-related susceptibility in plant-pathogen interactions. *Front. Plant Sci.* 5: 228. doi: 10.3389/fpls.2014.00228

Benikhlef, L., L'Haridon, F., Abou-Mansour, E., Serrano, M., Binda, M., Costa, A., et al. (2013). Perception of soft mechanical stress in *Arabidopsis* leaves activates disease resistance. *BMC Plant Biol.* 13: 133. doi: 10.1186/1471-2229-13-133

Bernard, A., and Joubès, J. (2013). *Arabidopsis cuticular* waxes: advances in synthesis, export and regulation. *Prog. Lipid Res.* 52, 110–129. doi: 10.1016/j.plipres.2012.10.002

Bessire, M., Chassot, C., Jacquat, A.-C., Humphry, M., Borel, S., Petétot, J. M.-C., et al. (2007). A permeable cuticle in *Arabidopsis* leads to a strong resistance to *Botrytis cinerea*. *EMBO J.* 26, 2158–2168. doi: 10.1038/sj.emboj.7601658

Bethke, G., Grundman, R. E., Sreekanta, S., Truman, W., Katagiri, F., and Glazebrook, J. (2014). Arabidopsis PECTIN METHYLESTERASEs contribute to immunity against *Pseudomonas* syringae. *Plant Physiol.* 164, 1093–1107. doi: 10.1104/pp.113.227637

Bethke, G., Thao, A., Xiong, G., Li, B., Soltis, N. E., Hatsugai, N., et al. (2016). Pectin biosynthesis is critical for cell wall integrity and immunity in *Arabidopsis thaliana*. *Plant Cell* 28, 537–556. doi: 10.1105/tpc.15.00404

Blanc, C., Coluccia, F., L'Haridon, F., Torres, M., Ortiz-Berrocal, M., Stahl, E., et al. (2018). The cuticle mutant eca2 modifies plant defense responses to biotrophic and necrotrophic pathogens and herbivory insects. *Mol. Plant Microbe Interact.* 31, 344–355. doi: 10.1094/MPMI-07-17-0181-R

Borisjuk, N., Hrmova, M., and Lopato, S. (2014). Transcriptional regulation of cuticle biosynthesis. *Biotechnol. Adv.* 32, 526–540. doi: 10.1016/j.biotechadv.2014.01.005

Bourdenx, B., Bernard, A., Domergue, F., Pascal, S., Léger, A., Roby, D., et al. (2011). Overexpression of *Arabidopsis* ECERIFERUM1 promotes wax very-long-chain alkane biosynthesis and influences plant response to biotic and abiotic stresses. *Plant Physiol.* 156, 29–45. doi: 10.1104/pp.111.172320

Buxdorf, K., Rubinsky, G., Barda, O., Burdman, S., Aharoni, A., and Levy, M. (2014). The transcription factor SlSHINE3 modulates defense responses in tomato plants. *Plant Mol. Biol.* 84, 37–47. doi: 10.1007/s11103-013-0117-1

Chassot, C., Nawrath, C., and Métraux, J.-P. (2007). Cuticular defects lead to full immunity to a major plant pathogen. *Plant J.* 49, 972–980. doi: 10.1111/j.1365-313X.2006.03017.x

Chen, X., Goodwin, S. M., Boroff, V. L., Liu, X., and Jenks, M. A. (2003). Cloning and characterization of the WAX2 gene of *Arabidopsis* involved in cuticle

membrane and wax production. *Plant Cell* 15, 1170–1185. doi: 10.1105/tpc.010926

Choi, B., Ghosh, R., Gururani, M. A., Shanmugam, G., Jeon, J., Kim, J., et al. (2017). Positive regulatory role of sound vibration treatment in *Arabidopsis thaliana* against *Botrytis cinerea* infection. *Sci. Rep.* 7:2527. doi: 10.1038/s41598-017-02556-9

Choi, W. G., Miller, G., Wallace, I., Harper, J., Mittler, R., and Gilroy, S. (2017). Orchestrating rapid long-distance signaling in plants with Ca(2+), ROS and electrical signals. *Plant J.* 90, 698–707. doi: 10.1111/tpj.13492

Conrath, U. (2011). Molecular aspects of defence priming. *Trends Plant Sci.* 16, 524–531. doi: 10.1016/j.tplants.2011.06.004

Conrath, U., Beckers, G. J. M., Langenbach, C. J. G., and Jaskiewicz, M. R. (2015). Priming for enhanced defense. *Annu. Rev. Phytopathol.* 53, 97–119. doi: 10.1146/annurev-phyto-080614-120132

Cui, F., Brosché, M., Lehtonen, M. T., Amiryousefi, A., Xu, E., Punkkinen, M., et al. (2016). Dissecting abscisic acid signaling pathways involved in cuticle formation. *Mol. Plant* 9, 926–938. doi: 10.1016/j.molp.2016.04.001

Czechowski, T., Stitt, M., Altmann, T., Udvardi, M. K., and Scheible, W. R. (2005). Genome-wide identification and testing of superior reference genes for transcript normalization in *Arabidopsis*. *Plant Physiol.* 139, 5–17. doi: 10.1104/pp.105.063743

De Lorenzo, G., Ferrari, S., Giovannoni, M., Mattei, B., and Cervone, F. (2019). Cell wall traits that influence plant development, immunity, and bioconversion. *Plant J.* 97, 134–147. doi: 10.1111/tpj.14196

Del Corpo, D., Fullone, M. R., Miele, R., Lafond, M., Pontiggia, D., Grisel, S., et al. (2020). AtPME17 is a functional *Arabidopsis thaliana* pectin methylesterase regulated by its PRO region that triggers PME activity in the resistance to *Botrytis cinerea*. *Mol. Plant Pathol.* 21, 1620–1633. doi: 10.1111/mpp.13002

Dickman, M. B., Ha, Y. S., Yang, Z., Adams, B., and Huang, C. (2003). A protein kinase from *Colletotrichum trifolii* is induced by plant cutin and is required for appressorium formation. *Mol. Plant Microbe Interact.* 16, 411–421. doi: 10.1094/MPMI.2003.16.5.411

Domínguez, E., Heredia-Guerrero, J. A., and Heredia, A. (2015). Plant cutin genesis: unanswered questions. *Trends Plant Sci.* 20, 551–558. doi: 10.1016/j.tplants.2015.05.009

Engelsdorf, T., Gigli-Bisceglia, N., Veerabagu, M., Mckenna, J. F., Vaahtera, L., Augstein, F., et al. (2018). The plant cell wall integrity maintenance and immune signaling systems cooperate to control stress responses in *Arabidopsis thaliana*. *Sci. Signal.* 11:eaao3070. doi: 10.1126/scisignal.aao3070

Fabre, G., Garroum, I., Mazurek, S., Daraspe, J., Mucciolo, A., Sankar, M., et al. (2016). The ABCG transporter PEC1/ABCG32 is required for the formation of the developing leaf cuticle in *Arabidopsis*. *New Phytol.* 209, 192–201. doi: 10.1111/nph.13608

Fauth, M., Schweizer, P., Buchala, A., Markstadter, C., Riederer, M., Kato, T., et al. (1998). Cutin monomers and surface wax constituents elicit H2O2 in conditioned cucumber hypocotyl segments and enhance the activity of other H2O2 elicitors. *Plant Physiol.* 117, 1373–1380. doi: 10.1104/pp.117.4.1373

Fernández, V., Guzmán-Delgado, P., Graça, J., Santos, S., and Gil, L. (1998). Cuticle structure in relation to chemical composition: re-assessing the prevailing model. *Front. Plant Sci.* 7: 427. doi: 10.3389/fpls.2016.00427

Ferrari, S., Savatin, D., Sicilia, F., Gramegna, G., Cervone, F., and De Lorenzo, G. (2013). Oligogalacturonides: plant damage-associated molecular patterns and regulators of growth and development. *FrFront. Plant Sci.* 4: 49. doi: 10.3389/fpls.2013.00049

Fich, E. A., Segerson, N. A., and Rose, J. K. (2016). The plant polyester cutin: biosynthesis, structure, and biological roles. *Annu. Rev. Plant Biol.* 67, 207–233. doi: 10.1146/annurev-arplant-043015-111929

Francis, S. A., Dewey, F. M., and Gurr, S. J. (1996). The role of cutinase in germling development and infection byErysiphe graminisf.sp.hordei. *Physiol. Mol. Plant Pathol.* 49, 201–211. doi: 10.1006/pmpp.1996.0049

Gilbert, R. D., Johnson, A. M., and Dean, R. A. (1996). Chemical signals responsible for appressorium formation in the rice blast fungus*Magnaporthe grisea*. *Physiol. Mol. Plant Pathol.* 48, 335–346. doi: 10.1006/pmpp.1996.0027

Girard, A.-L., Mounet, F., Lemaire-Chamley, M., Gaillard, C., Elmorjani, K., Vivancos, J., et al. (2012). Tomato GDSL1 is required for cutin deposition in the fruit cuticle. *Plant Cell* 24, 3119–3134. doi: 10.1105/tpc.112.101055

Go, Y. S., Kim, H., Kim, H. J., and Suh, M. C. (2014). *Arabidopsis* cuticular wax biosynthesis is negatively regulated by the DEWAX gene encoding an AP2/ERF-type transcription factor. *Plant Cell* 26, 1666–1680. doi: 10.1105/tpc.114.123307

Govrin, E. M., and Levine, A. (2000). The hypersensitive response facilitates plant infection by the necrotrophic pathogen *Botrytis cinerea*. *Curr. Biol.* 10, 751–757. doi: 10.1016/s0960-9822(00)00560-1

Hansjakob, A., Bischof, S., Bringmann, G., Riederer, M., and Hildebrandt, U. (2010). Very-long-chain aldehydes promote in vitro prepenetration processes of *Blumeria graminis* in a dose- and chain length-dependent manner. *New Phytol.* 188, 1039–1054. doi: 10.1111/j.1469-8137.2010.03419.x

Hansjakob, A., Riederer, M., and Hildebrandt, U. (2011). Wax matters: absence of very-long-chain aldehydes from the leaf cuticular wax of the glossy11 mutant of maize compromises the prepenetration processes of *Blumeria graminis*. *Plant Pathol.* 60, 1151–1161. doi: 10.1111/j.1365-3059.2011.02467.x

Imran, Q. M., Hussain, A., Lee, S.-U., Mun, B.-G., Falak, N., Loake, G. J., et al. (2018). Transcriptome profile of NO-induced *Arabidopsis* transcription factor genes suggests their putative regulatory role in multiple biological processes. *Sci. Rep.* 8:771. doi: 10.1038/s41598-017-18850-5

Inada, N., and Savory, E. A. (2011). Inhibition of prepenetration processes of the powdery mildew *Golovinomyces orontii* on host inflorescence stems is reduced in the *Arabidopsis cuticular* mutant cer3 but not in cer1. *J. Gen. Plant Pathol.* 77:273. doi: 10.1007/s10327-011-0331-0

Ingram, G., and Nawrath, C. (2017). The roles of the cuticle in plant development: organ adhesions and beyond. *J. Exp. Bot.* 68, 5307–5321. doi: 10.1093/jxb/erx313

Isaacson, T., Kosma, D. K., Matas, A. J., Buda, G. J., He, Y., Yu, B., et al. (2009). Cutin deficiency in the tomato fruit cuticle consistently affects resistance to microbial infection and biomechanical properties, but not transpirational water loss. *Plant J.* 60, 363–377. doi: 10.1111/j.1365-313X.2009.03969.x

Javelle, M., Vernoud, V., Depège-Fargeix, N., Arnould, C., Oursel, D., Domergue, F., et al. (2010). Overexpression of the epidermis-specific homeodomain-leucine zipper IV transcription factor Outer Cell Layer1 in maize identifies target genes involved in lipid metabolism and cuticle biosynthesis. *Plant Physiol.* 154, 273–286. doi: 10.1104/pp.109.150540

Jeffree, C. E. (2006). "The fine structure of the plant cuticle," in *Annual Plant Reviews Volume 23: Biology of the Plant Cuticle*, eds M. Riederer and C. Muller (Hoboken, NJ: Blackwell Publishing Ltd), 11–125. doi: 10.1002/9780470988718.ch2

Jetter, R., Kunst, L., and Samuels, A. L. (2006). "Composition of plant cuticular waxes," in *Annual Plant Reviews Volume 23: Biology of the Plant Cuticle*, eds M. Riederer and C. Muller (Hoboken, NJ: Blackwell Publishing Ltd), 145–181. doi: 10.1002/9781119312994.apr0232

Jiménez-Jacinto, V., Sanchez-Flores, A., and Vega-Alvarado, L. (2019). Integrative differential expression analysis for multiple experiments (IDEAMEX): a web server tool for integrated RNA-Seq data analysis. *Front. Genet.* 10: 279. doi: 10.3389/fgene.2019.00279

Ju, S., Go, Y. S., Choi, H. J., Park, J. M., and Suh, M. C. (2017). DEWAX transcription factor is involved in resistance to *Botrytis cinerea* in *Arabidopsis thaliana* and *Camelina sativa*. *Front. Plant Sci.* 8: 1210. doi: 10.3389/fpls.2017.01210

Kurata, T., Kawabata-Awai, C., Sakuradani, E., Shimizu, S., Okada, K., and Wada, T. (2003). The YORE-YORE gene regulates multiple aspects of epidermal cell differentiation in *Arabidopsis*. *Plant J.* 36, 55–66. doi: 10.1046/j.1365-313x.2003.01854.x

Kurdyukov, S., Faust, A., Nawrath, C., Bär, S., Voisin, D., Efremova, N., et al. (2006). The epidermis-specific extracellular BODYGUARD controls cuticle development and morphogenesis in *Arabidopsis*. *Plant Cell* 18, 321–339. doi: 10.1105/tpc.105.036079

Laluk, K., and Mengiste, T. (2010). Necrotroph attacks on plants: wanton destruction or covert extortion? *Arabidopsis Book* 8:e0136. doi: 10.1199/tab.0136

Langmead, B., and Salzberg, S. L. (2012). Fast gapped-read alignment with Bowtie 2. *Nat. Methods* 9, 357–359. doi: 10.1038/nmeth.1923

Lee, S., Fu, F., Xu, S., Lee, S. Y., Yun, D.-J., and Mengiste, T. (2016). Global regulation of plant immunity by histone lysine methyl transferases. *Plant Cell* 28, 1640–1661.

Lehmann, S., Serrano, M., L'Haridon, F., Tjamos, S. E., and Metraux, J.-P. (2015). Reactive oxygen species and plant resistance to fungal pathogens. *Phytochemistry* 112, 54–62. doi: 10.1016/j.phytochem.2014.08.027

L'Haridon, F., Besson-Bard, A., Binda, M., Serrano, M., Abou-Mansour, E., Balet, F., et al. (2011). A permeable cuticle is associated with the release of reactive oxygen species and induction of innate immunity. *PLoS Pathog.* 7, e1002148. doi: 10.1371/journal.ppat.1002148

Li, B., and Dewey, C. N. (2011). RSEM: accurate transcript quantification from RNA-Seq data with or without a reference genome. *BMC Bioinform.* 12: 323. doi: 10.1186/1471-2105-12-323

Li-Beisson, Y., Shorrosh, B., Beisson, F., Andersson, M. X., Arondel, V., Bates, P. D., et al. (2013). Acyl-lipid metabolism. *Arabidopsis Book* 11: e0161.

Lim, G.-H., Liu, H., Yu, K., Liu, R., Shine, M. B., Fernandez, J., et al. (2020). The plant cuticle regulates apoplastic transport of salicylic acid during systemic acquired resistance. *Sci. Adv.* 6:eaaz0478.

Lionetti, V. (2015). PECTOPLATE: the simultaneous phenotyping of pectin methylesterases, pectinases, and oligogalacturonides in plants during biotic stresses. *Front. Plant Sci.* 6:331. doi: 10.3389/fpls.2015.00331

Lionetti, V., Cervone, F., and Bellincampi, D. (2012). Methyl esterification of pectin plays a role during plant-pathogen interactions and affects plant resistance to diseases. *J. Plant Physiol.* 169, 1623–1630. doi: 10.1016/j.jplph.2012.05.006

Lionetti, V., Fabri, E., De Caroli, M., Hansen, A. R., Willats, W. G. T., Piro, G., et al. (2017). Three pectin methylesterase inhibitors protect cell wall integrity for *Arabidopsis* immunity to *Botrytis*. *Plant Physiol.* 173, 1844–1863. doi: 10.1104/pp.16.01185

Liu, J., Chen, S., Chen, L., Zhou, Q., Wang, M., Feng, D., et al. (2017). BIK1 cooperates with BAK1 to regulate constitutive immunity and cell death in *Arabidopsis*. *J. Integr. Plant Biol.* 59, 234–239. doi: 10.1111/jipb.12529

Liu, N., Zhao, L., Tang, L., Stobbs, J., Parkin, I., Kunst, L., et al. (2020). Mid-infrared spectroscopy is a fast screening method for selecting *Arabidopsis genotypes* with altered leaf cuticular wax. *Plant Cell Environ.* 43, 662–674. doi: 10.1111/pce.13691

Lolle, S. J., Berlyn, G. P., Engstrom, E. M., Krolikowski, K. A., Reiter, W. D., and Pruitt, R. E. (1997). Developmental regulation of cell interactions in the *Arabidopsis* fiddlehead-1 mutant: a role for the epidermal cell wall and cuticle. *Dev. Biol.* 189, 311–321. doi: 10.1006/dbio.1997.8671

Lorrai, R., Francocci, F., Gully, K., Martens, H. J., De Lorenzo, G., Nawrath, C., et al. (2021). Impaired cuticle functionality and robust resistance to *Botrytis cinerea* in *Arabidopsis thaliana* plants with altered homogalacturonan integrity are dependent on the class III peroxidase AtPRX71. *Front. Plant Sci.* 12:696955. doi: 10.3389/fpls.2021.696955

Martin, L. B. B., Romero, P., Fich, E. A., Domozych, D. S., and Rose, J. K. C. (2017). Cuticle biosynthesis in tomato leaves is developmentally regulated by abscisic acid. *Plant Physiol.* 174, 1384–1398. doi: 10.1104/pp.17.00387

Mauch-Mani, B., Baccelli, I., Luna, E., and Flors, V. (2017). Defense priming: an adaptive part of induced resistance. *Annu. Rev. Plant Biol.* 68, 485–512. doi: 10.1146/annurev-arplant-042916-041132

Mengiste, T. (2012). Plant immunity to necrotrophs. *Annu. Rev. Phytopathol.* 50, 267–294. doi: 10.1146/annurev-phyto-081211-172955

Mengiste, T., Chen, X., Salmeron, J., and Dietrich, R. (2003). The *Botrytis* susceptible1 gene encodes an R2R3MYB transcription factor protein that is required for biotic and abiotic stress responses in *Arabidopsis*. *Plant Cell* 15, 2551–2565. doi: 10.1105/tpc.014167

Molina, A., Miedes, E., Bacete, L., Rodríguez, T., Mélida, H., Denancé, N., et al. (2021). *Arabidopsis* cell wall composition determines disease resistance specificity and fitness. *Proc. Natl. Acad. Sci. U.S.A.* 118:e2010243118. doi: 10.1073/pnas.2010243118

Narváez-Barragán, D. A., Tovar-Herrera, O. E., Torres, M., Rodríguez, M., Humphris, S., Toth, I. K., et al. (2020). Expansin-like Exl1 from *Pectobacterium* is a virulence factor required for host infection, and induces a defence plant response involving ROS, and jasmonate, ethylene and salicylic acid signalling pathways in *Arabidopsis thaliana*. *Sci. Rep.* 10:7747. doi: 10.1038/s41598-020-64529-9

Nawrath, C., Schreiber, L., Franke, R. B., Geldner, N., Reina-Pinto, J. J., and Kunst, L. (2013). Apoplastic diffusion barriers in *Arabidopsis*. *Am. Soc. Plant Biol.* 11:e0167. doi: 10.1199/tab.0167

O'Brien, J. A., Daudi, A., Butt, V. S., and Paul Bolwell, G. (2012). Reactive oxygen species and their role in plant defence and cell wall metabolism. *Planta* 236, 765–779. doi: 10.1007/s00425-012-1696-9

Podila, G. K., Rogers, L. M., and Kolattukudy, P. E. (1993). Chemical signals from avocado surface wax trigger germination and appressorium formation in *Colletotrichum gloeosporioides*. *Plant Physiol.* 103, 267–272. doi: 10.1104/pp.103.1.267

Riederer, M. (2006). "Introduction: biology of the plant cuticle," in *Annual Plant Reviews Volume 23: Biology of the Plant Cuticle*, eds M. Riederer and C. Muller (Hoboken, NJ: Blackwell Publishing Ltd), 1–10. doi: 10.1002/9780470988718.ch1

Rowland, O., Lee, R., Franke, R., Schreiber, L., and Kunst, L. (2007). The CER3 wax biosynthetic gene from *Arabidopsis thaliana* is allelic to WAX2/YRE/FLP1. *FEBS Lett.* 581, 3538–3544. doi: 10.1016/j.febslet.2007.06.065

Saini, P., Gani, M., Kaur, J. J., Godara, L. C., Singh, C., Chauhan, S. S., et al. (2018). "Reactive oxygen species (ROS): a way to stress survival in plants," in *Abiotic Stress-Mediated Sensing and Signaling in Plants: An Omics Perspective*, eds S. M. Zargar and M. Y. Zargar (Singapore: Springer), 127–153. doi: 10.1007/978-981-10-7479-0_4

Sakuradani, E., Zhao, L., Haslam, T. M., and Kunst, L. (2013). The CER22 gene required for the synthesis of cuticular wax alkanes in *Arabidopsis thaliana* is allelic to CER1. *Planta* 237, 731–738. doi: 10.1007/s00425-012-1791-y

Salinas-Mondragón, R. E., Garcidueñas-Piña, C., and Guzmán, P. (1999). Early elicitor induction in members of a novel multigene family coding for highly related RING-H2 proteins in Arabidopsis thaliana. *Plant Mol. Biol.* 40, 579–590. doi: 10.1023/a:1006267201855

Schindelin, J., Arganda-Carreras, I., Frise, E., Kaynig, V., Longair, M., Pietzsch, T., et al. (2012). Fiji: an open-source platform for biological-image analysis. *Nat. Methods* 9, 676–682. doi: 10.1038/nmeth.2019

Schmittgen, T. D., and Livak, K. J. (2008). Analyzing real-time PCR data by the comparative C(T) method. *Nat. Protoc.* 3, 1101–1108. doi: 10.1038/nprot.2008.73

Schnurr, J., Shockey, J., and Browse, J. (2004). The Acyl-CoA synthetase encoded by LACS2 is essential for normal cuticle development in *Arabidopsis*. *Plant Cell* 16, 629–642. doi: 10.1105/tpc.017608

Schweizer, P., Felix, G., Buchala, A., Müller, C., and Métraux, J.-P. (1996). Perception of free cutin monomers by plant cells. *Plant J.* 10, 331–341. doi: 10.1046/j.1365-313x.1996.10020331.x

Sela, D., Buxdorf, K., Shi, J. X., Feldmesser, E., Schreiber, L., Aharoni, A., et al. (2013). Overexpression of AtSHN1/WIN1 provokes unique defense responses. *PLoS One* 8:e70146. doi: 10.1371/journal.pone.0070146.g006

Seo, P. J., and Park, C.-M. (2010). MYB96-mediated abscisic acid signals induce pathogen resistance response by promoting salicylic acid biosynthesis in *Arabidopsis*. *New Phytol.* 186, 471–483. doi: 10.1111/j.1469-8137.2010.03183.x

Serrano, M., Coluccia, F., Torres, M., L'Haridon, F., and Métraux, J. P. (2014). The cuticle and plant defense to pathogens. *Front. Plant Sci.* 5:274. doi: 10.3389/fpls.2014.00274

Serrano, M., and Guzmán, P. (2004). Isolation and gene expression analysis of *Arabidopsis thaliana* mutants with constitutive expression of ATL2, an early elicitor-response RING-H2 zinc-finger gene. *Genetics* 167, 919–929. doi: 10.1534/genetics.104.028043

Sieber, P., Schorderet, M., Ryser, U., Buchala, A., Kolattukudy, P., Métraux, J.-P., et al. (2000). Transgenic *Arabidopsis* plants expressing a fungal cutinase show alterations in the structure and properties of the cuticle and postgenital organ fusions. *Plant Cell* 12, 721–738. doi: 10.1105/tpc.12.5.721

Siegmund, U., and Viefhues, A. (2016). "Reactive oxygen species in the *Botrytis* - host interaction," in *Botrytis - the Fungus, the Pathogen and its Management in Agricultural Systems*, eds S. Fillinger and Y. Elad (Cham: Springer International Publishing), 269–289. doi: 10.1007/978-3-319-23371-0_14

Tanaka, T., Tanaka, H., Machida, C., Watanabe, M., and Machida, Y. (2004). A new method for rapid visualization of defects in leaf cuticle reveals five intrinsic patterns of surface defects in *Arabidopsis*. *Plant J.* 37, 139–146. doi: 10.1046/j.1365-313x.2003.01946.x

Tang, D., Simonich, M. T., and Innes, R. W. (2007). Mutations in LACS2, a long-chain Acyl-Coenzyme a synthetase, enhance susceptibility to avirulent *Pseudomonas syringae* but confer resistance to *Botrytis cinerea* in *Arabidopsis*. *Plant Physiol.* 144, 1093–1103. doi: 10.1104/pp.106.094318

Tateda, C., Zhang, Z., Shrestha, J., Jelenska, J., Chinchilla, D., and Greenberg, J. T. (2014). Salicylic acid regulates *Arabidopsis* microbial pattern receptor kinase levels and signaling. *Plant Cell* 26, 4171–4187. doi: 10.1105/tpc.114.131938

Thordal-Christensen, H., Zhang, Z., Wei, Y., and Collinge, D. B. (1997). Subcellular localization of H2O2 in plants. H2O2 accumulation in papillae and

hypersensitive response during the barley—powdery mildew interaction. *Plant J.* 11, 1187–1194. doi: 10.1046/j.1365-313x.1997.11061187.x

Torres, M. A., and Dangl, J. L. (2005). Functions of the respiratory burst oxidase in biotic interactions, abiotic stress and development. *Curr. Opin. Plant Biol.* 8, 397–403. doi: 10.1016/j.pbi.2005.05.014

Torres, M. A., Jones, J. D. G., and Dangl, J. L. (2006). Reactive oxygen species signaling in response to pathogens. *Plant Physiol.* 141, 373–378. doi: 10.1104/pp.106.079467

van der Burgh, A. M., Postma, J., Robatzek, S., and Joosten, M. H. A. J. (2019). Kinase activity of SOBIR1 and BAK1 is required for immune signalling. *Mol. Plant Pathol.* 20, 410–422. doi: 10.1111/mpp.12767

van Kan, J. A. (2006). Licensed to kill: the lifestyle of a necrotrophic plant pathogen. *Trends Plant Sci.* 11, 247–253. doi: 10.1016/j.tplants.2006.03.005

Veronese, P., Nakagami, H., Bluhm, B., Abuqamar, S., Chen, X., Salmeron, J., et al. (2005). The membrane-anchored *Botrytis*-induced kinase1 plays distinct roles in *Arabidopsis* resistance to necrotrophic and biotrophic pathogens. *Plant Cell* 18, 257–273. doi: 10.1105/tpc.105.035576

Voisin, D., Nawrath, C., Kurdyukov, S., Franke, R. B., Reina-Pinto, J. J., Efremova, N., et al. (2009). Dissection of the complex phenotype in cuticular mutants of *Arabidopsis* reveals a role of SERRATE as a mediator. *PLoS Genet.* 5:e1000703. doi: 10.1371/journal.pgen.1000703

Wang, X., Kong, L., Zhi, P., and Chang, C. (2020). Update on cuticular wax biosynthesis and its roles in plant disease resistance. *Int. J. Mol. Sci.* 21:5514. doi: 10.3390/ijms21155514

Wellesen, K., Durst, F., Pinot, F., Benveniste, I., Nettesheim, K., Wisman, E., et al. (2001). Functional analysis of the LACERATA gene of *Arabidopsis* provides evidence for different roles of fatty acid ω-hydroxylation in development. *Proc. Natl. Acad. Sci. U.S.A.* 98, 9694–9699. doi: 10.1073/pnas.171285998

Windram, O., Madhou, P., Mchattie, S., Hill, C., Hickman, R., Cooke, E., et al. (2012). *Arabidopsis* defense against *Botrytis cinerea*: chronology and regulation deciphered by high-resolution temporal transcriptomic analysis. *Plant Cell* 24, 3530–3557. doi: 10.1105/tpc.112.102046

Xia, Y., Gao, Q.-M., Yu, K., Lapchyk, L., Navarre, D., Hildebrand, D., et al. (2009). An intact cuticle in distal tissues is essential for the induction of systemic acquired resistance in plants. *Cell Host Microbe* 5, 151–165. doi: 10.1016/j.chom.2009.01.001

Xia, Y., Yu, K., Navarre, D., Seebold, K., Kachroo, A., and Kachroo, P. (2010). The glabra1 mutation affects cuticle formation and plant responses to microbes. *Plant Physiol.* 154, 833–846. doi: 10.1104/pp.110.161646

Xiao, F., Mark Goodwin, S., Xiao, Y., Sun, Z., Baker, D., Tang, X., et al. (2004). *Arabidopsis* CYP86A2 represses *Pseudomonas* syringae type III genes and is required for cuticle development. *EMBO J.* 23, 2903–2913. doi: 10.1038/sj.emboj.7600290

Yeats, T. H., and Rose, J. K. (2013). The formation and function of plant cuticles. *Plant Physiol.* 163, 5–20. doi: 10.1104/pp.113.222737

Yeh, Y. H., Panzeri, D., Kadota, Y., Huang, Y. C., Huang, P. Y., Tao, C. N., et al. (2016). The *Arabidopsis* Malectin-Like/LRR-RLK IOS1 is critical for BAK1-dependent and BAK1-independent pattern-triggered immunity. *Plant Cell* 28, 1701–1721. doi: 10.1105/tpc.16.00313

Yephremov, A., Wisman, E., Huijser, P., Huijser, C., Wellesen, K., and Saedler, H. (1999). Characterization of the FIDDLEHEAD gene of *Arabidopsis* reveals a link between adhesion response and cell differentiation in the epidermis. *Plant Cell* 11, 2187–2201. doi: 10.1105/tpc.11.11.2187

Zhao, L., Haslam, T. M., Sonntag, A., Molina, I., and Kunst, L. (2019). Functional overlap of long-chain Acyl-CoA synthetases in *Arabidopsis*. *Plant Cell Physiol.* 60, 1041–1054. doi: 10.1093/pcp/pcz019

Ziv, C., Zhao, Z., Gao, Y. G., and Xia, Y. (2018). Multifunctional roles of plant cuticle during plant-pathogen interactions. *Front. Plant Sci.* 9:1088. doi: 10.3389/fpls.2018.01088

Zou, J.-J., Li, X.-D., Ratnasekera, D., Wang, C., Liu, W.-X., Song, L.-F., et al. (2015). *Arabidopsis* CALCIUM-DEPENDENT PROTEIN KINASE8 and CATALASE3 function in abscisic acid-mediated signaling and H2O2 homeostasis in stomatal guard cells under drought stress. *Plant Cell* 27, 1445–1460. doi: 10.1105/tpc.15.00144

Conflict of Interest: The authors declare that the research was conducted in the absence of any commercial or financial relationships that could be construed as a potential conflict of interest.

Publisher's Note: All claims expressed in this article are solely those of the authors and do not necessarily represent those of their affiliated organizations, or those of the publisher, the editors and the reviewers. Any product that may be evaluated in this article, or claim that may be made by its manufacturer, is not guaranteed or endorsed by the publisher.

frontiers in Plant Science

ORIGINAL RESEARCH
published: 24 November 2021
doi: 10.3389/fpls.2021.781987

Variation in Petal and Leaf Wax Deposition Affects Cuticular Transpiration in Cut Lily Flowers

*Guiping Cheng[1], Ling Wang[3], Hairong Wu[4], Xinfan Yu[1], Nan Zhang[2], Xiaorong Wan[1], Lihong He[1] and Hua Huang[2]**

[1]College of Agriculture and Biology, Zhongkai University of Agriculture and Engineering, Guangzhou, China, [2]Institute of Fruit Tree Research, Guangdong Academy of Agricultural Sciences/Key Laboratory of South Subtropical Fruit Biology and Genetic Resource Utilization, Ministry of Agriculture and Rural Affairs/Guangdong Provincial Key Laboratory of Tropical and Subtropical Fruit Tree Research, Guangzhou, China, [3]Sericultural & Agri-Food Research Institute, Guangdong Academy of Agricultural Sciences/Key Laboratory of Functional Foods, Ministry of Agriculture and Rural Affairs/Key Laboratory of Agricultural Products Processing, Guangzhou, China, [4]Customs Technology Center of Guangzhou Customs District, Guangzhou, China

The vase life of cut flowers is largely affected by post-harvest water loss. Cuticular wax is the primary barrier to uncontrolled water loss for aerial plant organs. Studies on leaf cuticular transpiration have been widely conducted; however, little is known about cuticular transpiration in flowers. Here, the cuticular transpiration rate and wax composition of three lily cultivars were determined. The minimum water conductance of tepal cuticles was higher at the green bud than open flower stage. Lily cuticular transpiration exhibited cultivar- and organ-specific differences, where transpiration from the tepals was higher than leaves and was higher in the 'Huang Tianba' than 'Tiber' cultivar. The overall wax coverage of the tepals was higher compared to that of the leaves. Very-long-chain aliphatics were the main wax constituents and were dominated by *n*-alkanes with carbon (C) chain lengths of C_{27} and C_{29}, and C_{29} and C_{31} in the tepal and leaf waxes, respectively. Primary alcohols and fatty acids as well as small amounts of alkyl esters, ketones, and branched or unsaturated *n*-alkanes were also detected in both tepal and leaf waxes, depending on the cultivar and organ. In addition, the chain-length distributions were similar between compound classes within cultivars, whereas the predominant C-chain lengths were substantially different between organs. This suggests that the less effective transpiration barrier provided by the tepal waxes may result from the shorter C-chain aliphatics in the tepal cuticle, compared to those in the leaf cuticle. These findings provide further insights to support the exploration of potential techniques for extending the shelf life of cut flowers based on cuticular transpiration barrier properties.

Keywords: lily flowers, cuticular wax, leaf, tepal, transpiration

OPEN ACCESS

Edited by:
Amauri Bueno, Julius Maximilian University of Würzburg, Germany

Reviewed by:
Dimitrios Fanourakis, Technological Educational Institute of Crete, Greece
Victoria Fernandez, Polytechnic University of Madrid, Spain

****Correspondence:***
Hua Huang
huangw0109@gmail.com

Specialty section:
This article was submitted to Plant Physiology, a section of the journal Frontiers in Plant Science

Received: *23 September 2021*
Accepted: *25 October 2021*
Published: *24 November 2021*

Citation:
Cheng G, Wang L, Wu H, Yu X, Zhang N, Wan X, He L and Huang H (2021) Variation in Petal and Leaf Wax Deposition Affects Cuticular Transpiration in Cut Lily Flowers. Front. Plant Sci. 12:781987. doi: 10.3389/fpls.2021.781987

INTRODUCTION

The surfaces of aerial plant organs are covered by cuticle, and its primary function is to prevent uncontrolled water loss (Riederer and Schreiber, 2001). Plant cuticle is predominantly a mixture of waxes, including very-long-chain fatty acids and their derivatives, cyclic terpenoids, with cutin polymers providing a scaffold matrix, mainly C_{16} and C_{18} with or without hydroxy groups

(Yeats and Rose, 2013). It is well known that the cuticular waxes, rather than the cutin matrix, are the barrier to non-stomatal water loss (Riederer and Schreiber, 1995; Jetter and Riederer, 2016). The diversity of cuticular wax components and their spatial arrangements results in a wide variety of cuticular transpiration barrier properties across species, organs, and developmental stages (Jetter and Riederer, 2016; Huang et al., 2017; Bourgault et al., 2020). Previous studies have focused on how the barrier properties of leaf or fruit cuticles affect water loss or chemical substrates (Riederer and Schreiber, 2001; Jetter and Riederer, 2016), whereas few studies have been conducted on the barrier properties of flower cuticles.

The thin cuticle covering the petal surface plays an important role in interactions with pollinators (Whitney et al., 2011). Previous studies reported that cuticular transpiration in fruit cuticular membranes was higher than that of leaf cuticles. It implied that it might not be necessary to form such efficient cuticular barriers to transpiration for fruit as the life time is usually shorter than leaf tissues (Schreiber and Riederer, 1996). Chemical analysis has indicated that the wax layer of *Cosmos bipinnatus* var. 'Sensation Pinkie' petals contains relatively high concentrations of C_{22} and C_{24} fatty acids and primary alcohols, which are much shorter than those in the wax layer of leaves. Therefore, the petal cuticle exhibits weaker transpiration barrier properties than the leaf cuticles (Buschhaus et al., 2015). Similarly, C-chain lengths of waxes in petal cuticles of 'Movie star' and 'Tineke' roses were generally between C_{26} and C_{29}, but ranged from C_{29} to C_{33} in the leaf cuticles. The C-chain differences were thought to be one of the factors inducing higher transpiration rate for the petals compared to that for the leaves in roses (Cheng et al., 2019). A comparative study on cuticular wax chemical differences between flowers and other organs has also been conducted (Guo and Jetter, 2017). In addition, significant changes in the composition of the wax on snapdragon petals were found over 12 days from the opening stage to senescence (Goodwin et al., 2003). However, more information about the chemical composition of petal cuticles and its contribution to barrier properties during petal development are still awaiting to be explored.

Oriental lily, a *Lilium* spp., is one of the most popular ornamental plants. Lilies are widely grown in temperate, subtropical, and tropical regions, and blooming from spring to early autumn. Oriental lily cut flowers usually comprise the flower head and the stem and keep some leaves. The lily flower head has two whorls of tepals (floral leaves) and each of the inner and outer whorls normally has three tepals (van Doorn and Han, 2011). The inner tepals are covered by the outer tepals during flower development. Lilies are widely planted by consumers for their elegant look and wide open, brightly colored tepals. The vase life of lily flowers varies with cultivar, cultivation, and post-harvest conditions. In addition, the shelf life of the cut flowers is impacted by rapid water loss or the deterioration of stem tissues after harvest (Torre and Fjeld, 2001; Cheng et al., 2020).

The present study aimed to characterize and compare the chemical composition of the cuticular waxes of lily tepals and leaves as well as to determine their potential contributions to limit cuticular transpiration from the tepals and leaves of three lily cultivars. The transpiration rate and chemical composition of the cuticular waxes (1) on the tepals at the green bud and open stages of the *Lilium* spp. cultivar 'Casa Blanca', and (2) on the leaves and tepals of two *Lilium* spp. cultivars 'Huang Tianba' and 'Tiber' were determined. These findings enabled comparisons of the cuticular wax chemicals on tepals at different development stages and organs, as well as link the transpiration barrier differences.

MATERIALS AND METHODS

Plant Materials

Three *Lilium* spp. cultivars: 'Casa Blanca', 'Huang Tianba', and 'Tiber' were used to evaluate the water permeability and cuticular wax composition differences of the leaf and tepal cuticles. The lily seedlings of all three cultivars were grown in pots filled with soil in a climate chamber at Zhongkai University of Agriculture and Engineering, Guangzhou, China (include coordinates). For the duration of the experiment, the growth conditions were with an average daily light intensity of 100 μmol m^{-2} s^{-1} coming from LED lamps (Guangzhou Blueseatec Electronic Co. Ltd., Guangdong, China). The growing was set at a 12/12-h day/night light cycle with a temperature of 20 ± 2°C and a relative humidity of 60 ± 5% in greenhouse. The plants were watered daily to keep the soil moist and facilitate healthy growth. Lily flowers have open tepals and leaves on the stem when harvested (**Figure 1**). In this study, *Lilium* spp. 'Casa Blanca' was selected to comparatively analyse the cuticular transpiration rate and wax composition of the inner and outer tepals at the green bud and open stages (**Figure 2**), whereas the open tepals and leaves of the *Lilium* spp. 'Huang Tianba' and 'Tiber' cultivars were used to compare the cuticular transpiration rate and wax composition between different organs. The stem and flower samples for transpiration rate and wax chemical analyses were carefully harvested. Once the experimental plants had reached the appropriate flowering stages, samples were harvested. The flowering stems were cut at 60–80 cm in length and immediately placed in water at room ambient approximately 20°C in preparation for analysis.

Transpiration Rate Determination

The rate of cuticular transpiration from inner and outer tepals of green bud and open flowers of 'Casa Blanca' and from the whole tepals and leaves was determined gravimetrically (Cheng et al., 2019). Twelve fresh samples for tepals or leaves from green bud, open flowers or different cultivars without any defects were selected from plants of each cultivar. All samples were fully hydrated prior to evaluation. The petioles of the tepals and leaves were sealed with paraffin wax (melting point approximately 60°C) to avoid water loss from the cut wounds. The temperature (20 ± 2°C) and relative humidity (45 ± 5%) of the surrounding atmosphere were monitored using a digital thermometer (Anymetre, Guangzhou, China). The weight loss of the tepals and leaves was recorded automatically every 30 min

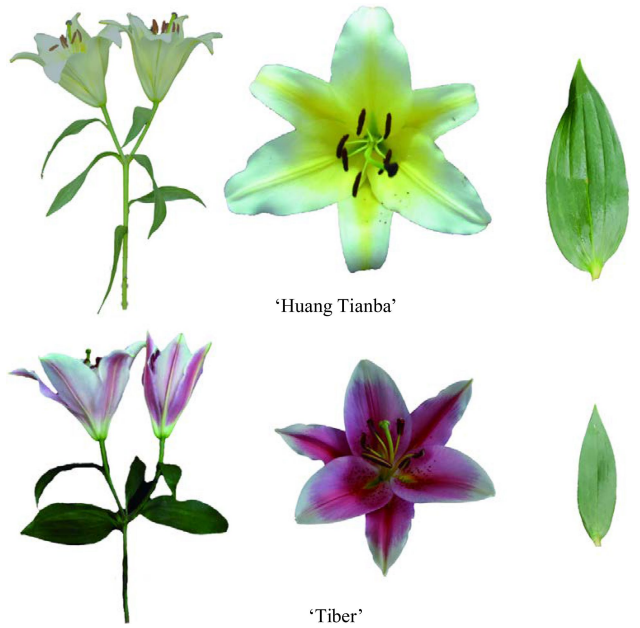

FIGURE 1 | *Lilium* spp. (lily) flowers of the cultivars 'Huang Tianba' and 'Tiber'. The cut flowers comprise open tepals, leaves, and stems.

for 8 h using a digital balance with a precision of 0.1 mg (BSA-224S; Sartorius, Beijing, China).

The dynamic transpiration changes of leaf and tepal tissues were inflected by the weight loss under different time points. Relative water content (RWC), as an important indicator of water status in plants, was calculated firstly based on full saturation fresh weight (FWs), actual fresh weight (FW) at each measured point, dry weight (DW) and surface area of the measured tissues. RWC was calculated as:

$$RWC = \frac{FW - DW}{FWs - DW}$$

and the RWD was calculated according to the changes of RWC:

$$RWD = 1 - RWC$$

The transpiration rate (flux of water vapor; F in g m^{-2} s^{-1}) was calculated from the changes in the fresh weight of the samples (W in g) over time (Δt in s) and surface area (A in m^2), as follows:

$$F = \frac{\Delta W}{\Delta t \times A}$$

The surface area of the tepals and leaves (A) was determined by digital scanning (LaserJet Pro MFP M126nw; HP, Shanghai, China). The water permeance (P in m s^{-1}) was calculated from the transpiration rate (F) divided by the driving force, as follows:

$$P = \frac{F}{c^*_{WV}\left(a_{petal} - a_{air}\right)}$$

where the water vapor saturation concentration at the actual tepal or leaf temperature (water vapor content of air at saturation;) was obtained from tabulated values (Nobel, 2009), the water activity in the air (a_{air}) was the recorded relative humidity, and the water activity in the tepals or leaves (a_{tepal}) or (a_{leaf}), respectively, was assumed to be unity (Burghardt and Riederer, 2003). The minimum water conductance based the drying curve of P *via* RWD was obtained.

Cuticular Wax Extraction

To extract the surface wax chemicals, tepals of different developmental stages, and from inner and outer positions of 'Casa Blanca', inner tepals and leaves of 'Huang Tianba' and 'Tiber' were harvested. Samples of petals and leaves of intact without defects and cracks were carefully selected, and sample surfaces were genteelly cleaned using a paint brush. Using tweezers to hold the petioles, the tepal and leaf samples were dipped vertically into chloroform (the extract solution). To fully extract the cuticular waxes, each sample was dipped in chloroform three times for 30 s each, and the extracts were combined. Then, approximately 5 µg *n*-tetracosane was added to the extracts as an internal standard. The solvent was evaporated under a gentle stream of nitrogen and collected for further analysis.

Wax Composition Analyses

Dried samples were derivatized with *N, O*-bis (trimethylsilyl) trifluoroacetamide in pyridine at 70°C for 30 min. To determine the quantity of wax components, samples were analyzed using a capillary gas chromatograph (7820A, GC System; Agilent Technologies, Santa Clara, CA, USA) equipped with a capillary column (30 m × 0.32 mm, DB-1 ms, and 0.1-µm-thick film; J&W Scientific, Agilent Technologies). The GC oven was held at 50°C for 2 min, raised by 40°C min^{-1} to 200°C, held at 200°C for 2 min, and then raised by 3°C min^{-1} to 320°C, and held at 320°C for 30 min. The carrier gas was hydrogen. The area of the peaks was compared to that of the internal standard to determine the quantity of wax components.

Wax components were analyzed using a temperature-controlled capillary gas chromatograph equipped with a mass spectrometric detector (m/z 50–750, MSD 5975; Agilent Technologies) under the same GC conditions as described above but with helium as the carrier gas. Single compounds were identified based on their electron ionization mass spectra using authentic standards, the Wiley 10th/NIST 2014 mass spectral library (W10N14; John Wiley & Sons, 2014), or by interpretation of the spectra according to their retention times, or by comparison with published data.

Statistical Analysis

Statistical analyses were performed using SPSS (version 23; IBM Corp., Armonk, NY, United States) and SigmaPlot 10 (Systat software, Inc., San Jose, CA, United States). The normal distribution of data was tested *via* a Shapiro–Wilk or Kolmogorov–Smirnov normality test (significance level: $p < 0.05$). Comparisons were analyzed using one-way analysis of variance. SigmaPlot 10 was used for graphing.

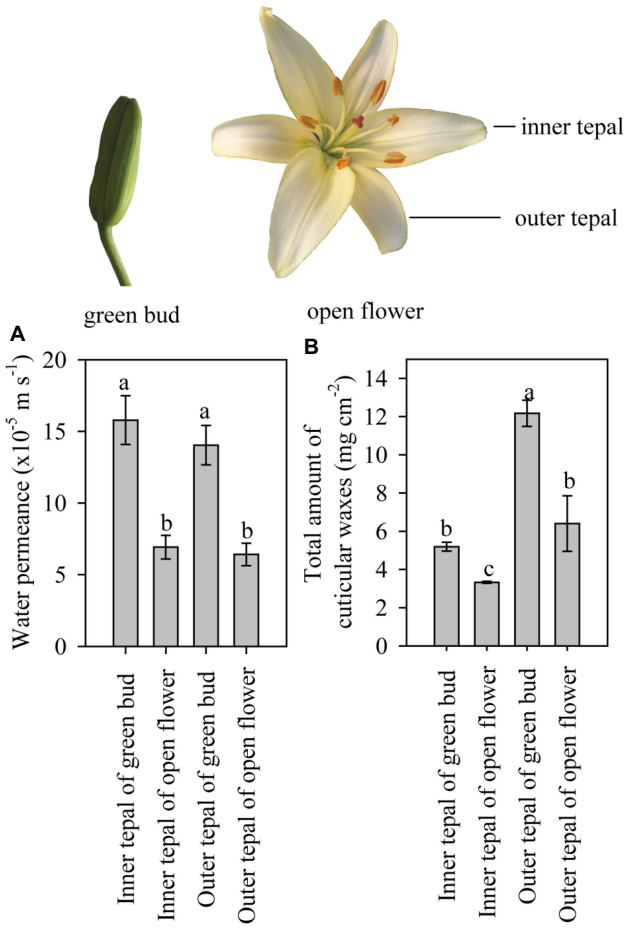

FIGURE 2 | Cuticular transpiration rate and wax coverage of tepals of lily flowers at the green bud and open stages. **(A)** Minimum water conductance and **(B)** total amount of cuticular waxes on the inner and outer tepals of green buds and open flowers of the *Lilium* cultivar 'Casa Blanca'. Data are presented as the mean ± standard deviation ($n = 12$ for transpiration, $n = 5$ for cuticular wax). The different letters on the bars indicate significant differences ($p < 0.05$).

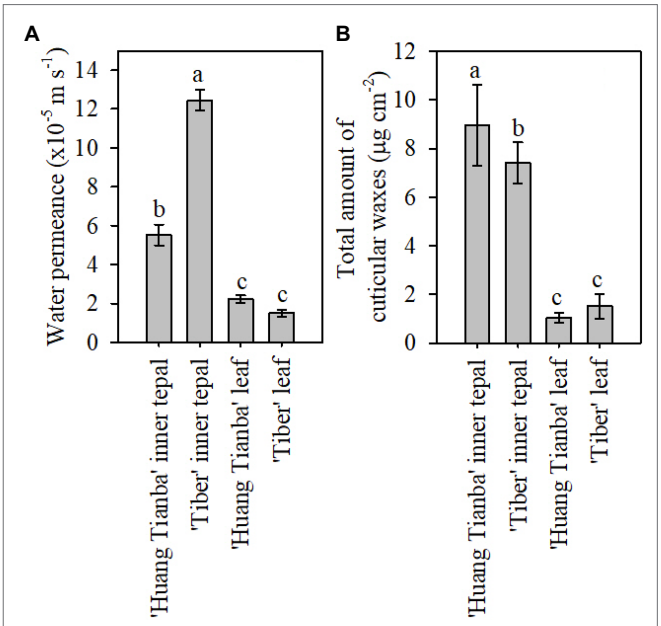

FIGURE 3 | Cuticular transpiration rate and wax coverage of leaves and tepals of lily flowers at the open stage. **(A)** Minimum water conductance, and **(B)** total amount of cuticular waxes on inner tepals and intact leaves of the *Lilium* cultivars 'Huang Tianba' and 'Tiber'. Data are presented as the mean ± standard deviation ($n = 12$ for transpiration, $n = 5$ for cuticular wax). The different lowercase letters on the bars indicate significant differences ($p < 0.05$).

RESULTS

Water Permeance

Tepals of the 'Casa Blanca' cultivar at the green bud stage exhibited higher transpiration rate than tepals at the open stage (**Figure 2A**), and the mean minimum conductance for the green buds was 1.6×10^{-4} m s^{-1} (inner tepals) and 1.4×10^{-4} m s^{-1} (outer tepals), whereas a lower minimum water conductance of 6.9×10^{-5} m s^{-1} and 6.4×10^{-5} m s^{-1} was recorded for inner and outer tepals in open flower, respectively (**Figure 2A**). Overall, the tepal minimum water conductance was significantly higher compared to that of the leaves (**Figure 3A**). The water permeance of the inner tepals of the 'Huang Tianba' and 'Tiber' cultivars was 5.5×10^{-5} m s^{-1} and 1.3×10^{-4} m s^{-1}, respectively. In comparison with tepals, the minimum water conductance of the leaves was much lower, being 2.2×10^{-5} m s^{-1} for the 'Huang tianba' cultivar and 1.5×10^{-5} m s^{-1} for the 'Tiber' cultivar (**Figure 3A**).

Wax Load and Chemical Composition at Different Tepal Development Stages

As the primary barrier to non-stomatal transpiration is determined by the wax pattern in the cuticle (Riederer and Schreiber, 2001), the composition of the wax on the leaves and tepals at the green bud and open flower stages was analyzed. The overall wax coverage was 12.17 ± 0.69 μg cm^{-2} and 6.40 ± 1.45 μg cm^{-2} on the outer tepals of the green bud and open flowers, respectively (**Figure 2B**). Lower amounts of wax were detected on the inner tepals of the green buds and open flowers at 5.19 ± 0.23 μg cm^{-2} and 3.33 ± 0.05 μg cm^{-2}, respectively (**Figure 2B**).

The waxes on the tepals of the green buds and open flowers were composed of very-long-chain fatty acids, primary alcohols, and *n*-alkanes (**Figure 4**). The most abundant wax components were *n*-alkanes, which comprised 73.28% (of the total wax) on the outer tepals and 70.27% on the inner tepals at the green bud stage, and 76.68% on the outer tepals and 77.34% on the inner tepals of the open flowers (**Figure 4**). Primary alcohols occurred also in relatively higher proportions in the cuticle on the green bud tepals (4.09% outer and 8.30% inner) compared to that on the tepals of the open flowers (1.29% outer and 6.07% inner, **Figure 4**). There were no obvious differences in the fatty acid content of the wax on the tepals at the green bud and open flower stages. Very-long-chain alkyl esters and cyclic sterols were detected only in the wax on the tepals of the open flowers (**Figure 4**; **Supplementary Table S1**).

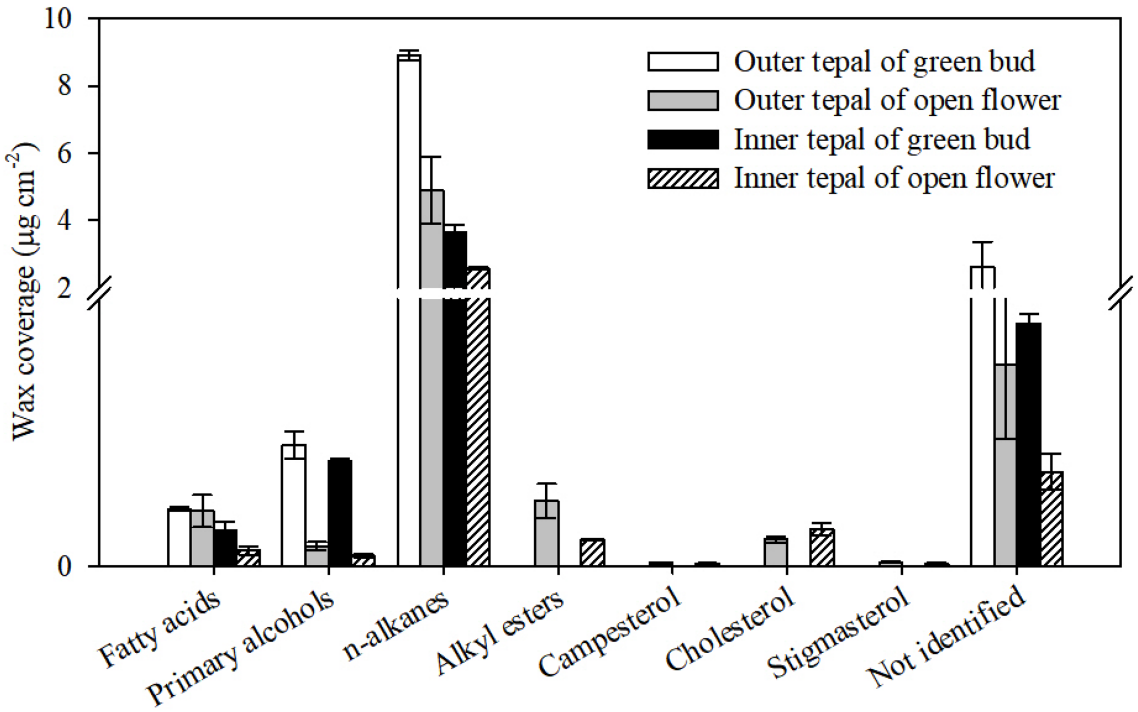

FIGURE 4 | Chemical composition of cuticular waxes on green bud and open flower tepals of *Lilium* cultivar 'Casa Blanca'. Data are presented as the mean ± standard deviation ($n = 5$).

Acyclic components dominated the wax mixtures on the tepals in green buds and open flowers. The prominent components of the *n*-alkanes had chain lengths ranged from C_{22} to C_{33}, with most abundant of C_{27} and C_{29}. The C_{33} *n*-alkane was detected only in the cuticle of tepals at the open flower stage (**Figure 5**; **Supplementary Table S1**). Chain length of primary alcohols ranged from C_{22} to C_{30}, with a dominant chain length of C_{26}. In addition, primary alcohols with chain lengths of C_{28} and C_{30} were more abundant in outer and inner tepals at the open flower stage (24.21 and 19.10%, respectively) compared to that of green bud tepals (25.04 and 18.00%, respectively). The fatty acid fraction in the green bud cuticles were dominated by C_{20} and C_{22}, whereas chain lengths ranged from C_{20} to C_{26} for fatty acid in the open flower cuticles. The alkyl esters, which were detected only in the cuticles of the open flower tepals, possessed chain lengths ranging from C_{40} to C_{48} (**Figure 5**; **Supplementary Table S1**).

Cuticular Waxes of Open Flower Tepals and Leaves in Different Cultivars

Comparative profiling of the cuticular waxes on the tepals and leaves of the 'Huang Tianba' and 'Tiber' cultivars was conducted. The overall amount of cuticular wax on the inner tepals was $8.95 \pm 1.68\,\mu g\,cm^{-2}$ for the 'Huang Tianba' cultivar, which was higher than that for the inner tepals of the 'Tiber' cultivar ($7.41 \pm 0.85\,\mu g\,cm^{-2}$; **Figure 3B**). Compared to the significant difference in wax quantity on the tepals of the two cultivars, the amount of wax on the leaves showed only a slight variation between cultivars at $1.04 \pm 0.20\,\mu g\,cm^{-2}$ for 'Huang Tianba', and $1.52 \pm 0.51\,\mu g\,cm^{-2}$ for 'Tiber' (**Figure 3B**).

The wax mixtures of both tepal and leaf cuticles were dominated by very-long-chain acyclic components such as fatty acids, primary alcohols, *n*-alkanes, alkyl esters, and small amounts of branched *n*-alkanes and *n*-alkenes (**Figure 6**; **Supplementary Table S2**). The most abundant aliphatic fraction in both the tepal and leaf waxes comprised *n*-alkanes, which contributed 72.49 and 65.27% for the 'Huang Tianba' cultivar, and 44.09 and 33.03% for the 'Tiber' cultivar, respectively. The coverage of *n*-alkanes was significantly higher on the surface of the tepals compared to that on the leaf surfaces for both cultivars (**Figure 6**; **Supplementary Table S2**). The primary alcohols contributed 4.93 and 7.07% ('Huang Tianba'), and 7.68 and 33.99% ('Tiber') of the tepal and leaf wax coverage, respectively. Compared to the relatively small concentrations of fatty acids in the tepal and leaf cuticles of the 'Huang Tianba' cultivar (1.16 and 7.31%, respectively), higher fatty acid levels were found in the 'Tiber' tepal and leaf cuticles (14.84 and 11.72%, respectively, **Figure 6**; **Supplementary Table S2**). Small amounts of *n*-alkenes and branched *n*-alkanes were detected in the tepal cuticles of both cultivars, and traces were found in the leaf cuticle of the 'Tiber' cultivar. Alkyl esters were not detected in the leaf waxes, but occurred in the tepal waxes of both cultivars. In addition, traces or no signals of cyclic compounds were detected in the tepal and leaf waxes of both the 'Huang Tianba' and 'Tiber' cultivars (**Figure 6**; **Supplementary Table S2**).

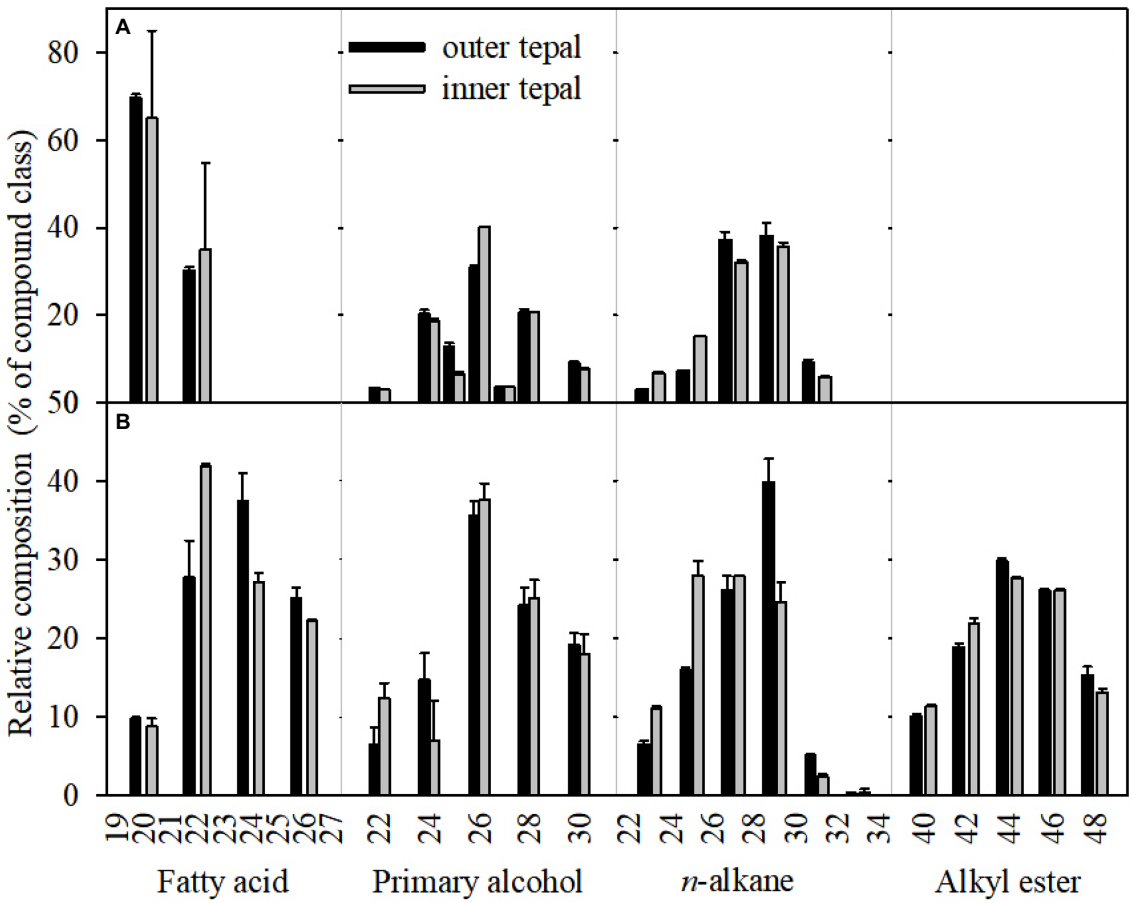

FIGURE 5 | Carbon chain-length distribution of the cuticular waxes on the tepals of green buds **(A)** and open flowers **(B)** of the *Lilium* cultivar 'Casa Blanca'. Data are presented as the mean ± standard deviation ($n = 5$).

The chain-length distributions were similar among the compound classes within cultivars, whereas the predominant carbon chain lengths were substantially different between organs. The chain lengths of the *n*-alkanes, which were predominantly odd-number carbon chains, ranged from C_{22} to C_{33}, with mostly C_{29} ('Huang Tianba') and C_{27} ('Tiber') in the tepal cuticles, and C_{31} ('Huang Tianba') and C_{29} ('Tiber') chain lengths in the leaf waxes (**Figure 7**; **Supplementary Table S2**).

A broad range of primary alcohol chain lengths (C_{23} to C_{34}) was found, with prominent of C_{30} and C_{26} in the tepal cuticles and leaf cuticles of both cultivars. In both cultivars, the chain lengths of the fatty acid fraction ranged from C_{20} to C_{30}, with the C_{24} chain length predominantly in the tepal cuticles. However, leaf cuticles contained fatty acids with chain lengths ranging from C_{20} to C_{32}, with a predominance of the C_{26}. The unbranched alkyl esters, which were detected only in the tepal waxes, ranged in chain length from C_{39} to C_{46} (**Figure 6**). In addition, *n*-alkenes ranged in chain length from C_{25} to C_{31}, with a dominant chain length of C_{29} in the tepal waxes. Ketones with chain lengths of C_{29} and C_{31} were detected in the leaf cuticles of the 'Tiber' cultivar (**Figure 7**; **Supplementary Table S2**).

DISCUSSION

The transpiration of cut flowers has been recently cared by researchers on different species and flower organs. As the occurrence of stomata, water loss occurred mainly through the leaf tissues in the intact cut flowers. When most of the stomata closed, leaves were still the main parts for water loss in roses, but not in carnation or chrysanthemum (Lin et al., 2020; Tsaniklidis et al., 2020; Fanourakis et al., 2021). These studies considered stomatal transpiration as the main pathway for water loss in cut flowers. However, the non-functional or non-stomatal transpiration, which has been widely reported to be the cuticular transpiration for leaves and fruit (Riederer and Schreiber, 2001), whereas relatively little is available for flowers. So far, only two studies reported the cuticular transpiration of flowers. The water permeability of intact petal of *C. bipinnatus* "Sensation" was 6.7×10^{-5} m s^{-1} (Buschhaus et al., 2015). Our previous study on rose petals found similar cuticular transpiration levels with 4.1×10^{-5} m s^{-1} for the 'Movie star' and 8.9×10^{-5} m s^{-1} for 'Tineke' (Cheng et al., 2019). Cut lily flowers contains flowering head with tepals, leaves, and stem (**Figure 1**; van Doorn and Han, 2011). Stomata occurred on the abaixal side of leaf and outer tepal surfaces of lily

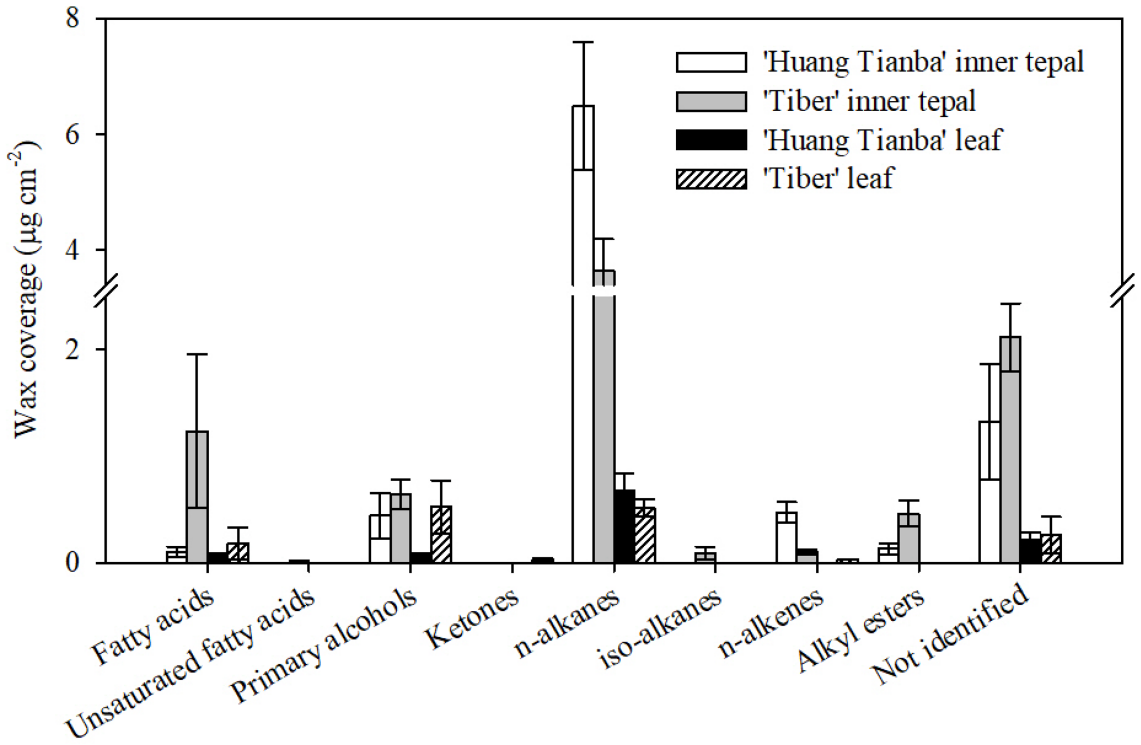

FIGURE 6 | Chemical composition of cuticular waxes on the tepals and leaves of the *Lilium* cultivars 'Huang Tianba' and 'Tiber'. Data are presented as the mean ± standard deviation ($n = 5$).

flowers (**Supplementary Figure S1**). The minimum conductance was used to indicate the cuticular transpiration or with non-functional stomata transpiration (Burghardt and Riederer, 2003). Leaf of lily flowers exhibited typical drying curves as reported previously (**Supplementary Figure S2**). The water loss of petals in lily flowers exhibited almost linearly following the time changes during the whole dehydration process (**Supplementary Figures S3**, **S4**). In addition, the stomata on lily tepals were shown covered by waxes or under closed status (**Supplementary Figure S1**). Therefore, the drying curve and water loss dynamic changes implied that the stomata of sepals might be non-functional.

The mean minimum conductance of the wax layer on the tepals of the green bud stage of the lily cultivar was higher than the tepals of the open flowers, which showed similar levels as reported results (Cheng et al., 2019). In a number of studies on leaf tissue transpiration, the reported water permeance ranges from 2.6×10^{-7} m s^{-1} for *Zamioculcas zamiifolia* (G.Lodd.) Engl. to 4×10^{-3} m s^{-1} for *Ipomoea batatas* (L.) Lam., with most values lower than 2×10^{-4} m s^{-1} (Schuster et al., 2017). The minimum water conductance of the cuticles on the green bud and open flower tepals and on the leaves of all three lily cultivars showed a similar level to that of most of the reported values. In addition, the minimum water conductance exhibited by the lily cuticles was higher in tepals than in leaves (**Figure 3A**). Taking water loss of petal and leaf cuticles in *C. bipinnatus* and rose cultivars (Buschhaus et al., 2015; Cheng et al., 2019) together, the wax layer on tepals and petals appears to be a less efficient barrier to transpiration compared to that on leaves. This might be related to the special functions of petals, which may have rapid cuticular transpiration together with volatilization of aroma to attract pollinators. On the other hand, flowers are relatively short-lived organs even when environmental conditions are favorable. Thus, it is probably not necessary for flowers to develop such a highly efficient transpiration barrier, compared to that needed on long-lived leaves. The cuticular wax loading on petals has been reported for only a few species, with values ranging from 2.7 μg cm^{-2} (*C. bipinnatus*; Buschhaus et al., 2015) to 37 μg cm^{-2} (*T. officinale*; Guo and Jetter, 2017). Only one study (on *Antirrhinum majus* L., the snapdragon) has examined the cuticular wax loading during petal development (Goodwin et al., 2003). By contrast, the accumulation of waxes on the tepals decreased substantially from the green bud to the open flower stage, for both the inner and outer tepals of the *Lilium* cultivar 'Casa Blanca'. The overall tepal wax coverage was not significantly different between the cultivars 'Huang Tianba' and 'Tiber'. However, wax coverage was higher on the tepals than on the leaves. As reported previously, wax coverage on the lily tepals exhibited cultivar-specific differences (Huang et al., 2017; Cheng et al., 2019). In addition, water permeance of the lily leaves was significantly lower than that of the tepals, supporting the assertion that there is no significant relationship between the cuticular water permeability and the total amount of wax (Riederer and Schreiber, 2001; Jetter and Riederer, 2016).

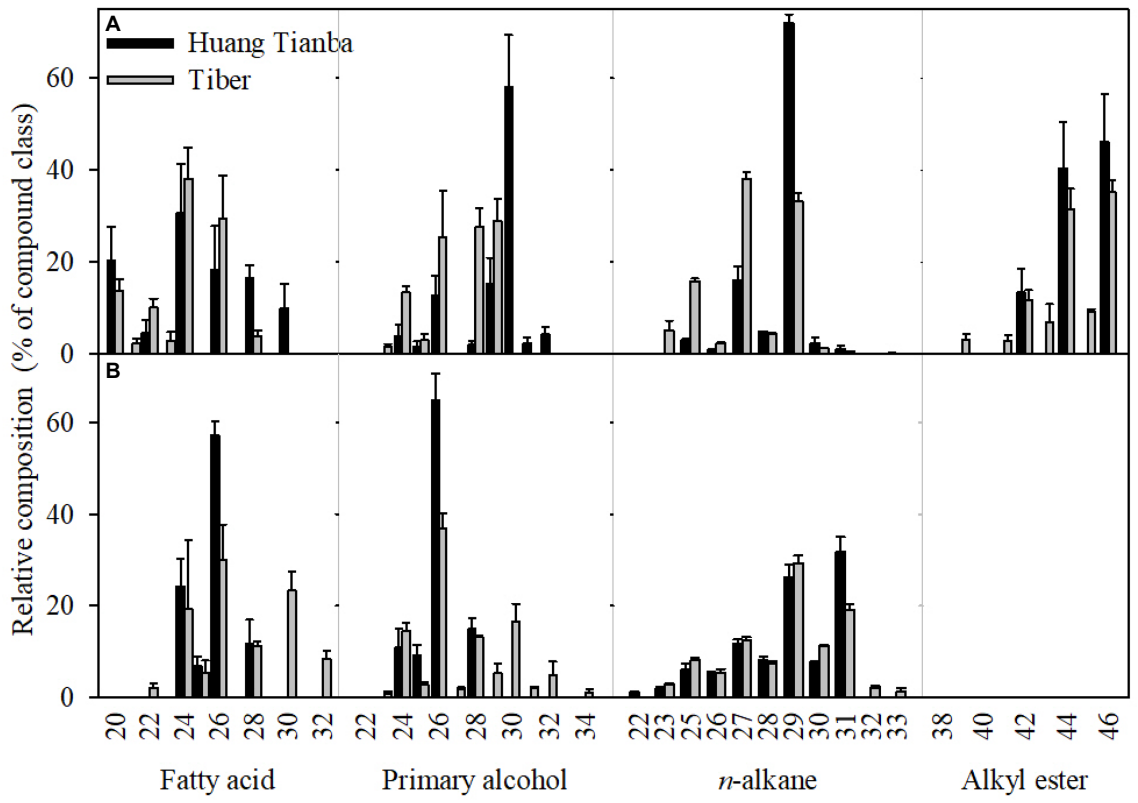

FIGURE 7 | Carbon chain-length distribution of the cuticular waxes on the inner tepals **(A)** and leaves **(B)** of the *Lilium* cultivars 'Huang Tianba' and 'Tiber'. Data are presented as the mean ± standard deviation ($n = 5$).

The chemical composition of petal cuticles differs among different flowers. The wax layers on the petals of *Solanum tuberosum* L. (potato) and *A. majus* (snapdragon) flowers contained relatively high concentrations of *n*-alkanes and methyl-branched alkanes (Goodwin et al., 2003; Guo and Jetter, 2017). Similarly, the major cuticular wax components of *Vicia faba* L. (faba bean) and *Rubus idaeus* L. (raspberry) petals were *n*-alkanes (Griffiths et al., 1999, 2000). Primary alcohols (21%) and *n*-alkanes (29%) were found in similar amounts in the wax layer of *T. officinale* (Guo et al., 2017). Our current study found that the waxes on petals of the rose cultivars 'Movie star' and 'Tineke' were dominated by *n*-alkanes (46.8 and 64.3%) and *n*-alkenes (47.3 and 20.2%; Cheng et al., 2019). Similarly, in the present study, *n*-alkanes were found to be the major components of the lily tepal waxes (**Figures 4, 6**). However, primary alcohols and alkyl esters were the predominant components in petal waxes of *C. bipinnatus* and *Petunia hybrida* Vilm. W115 (Petunia) flowers, whereas *n*-alkanes and triterpenoids occurred at low levels (King et al., 2007; Buschhaus et al., 2015). Minor amounts of branched *n*-alkanes or *n*-alkenes were found in the tepal waxes of the lily cultivars 'Huang Tianba' and 'Tiber', and sterols were found in the tepal waxes of open lily flowers (**Figures 4, 6**).

It has been proposed that the hydrophobic barrier of the cuticle is mainly determined by the chemical composition and chain-length distribution of the very-long-chain aliphatics and their structural arrangements (Riederer and Schreiber, 1995). The accumulation of very-long-chain components in the wax layer shift from C_{16} and C_{18} to longer than C_{20} carbon chains during the development of leaves in *Arabidopsis* (Jenks et al., 1995; Busta et al., 2017) and *Prunus laurocerasus* (Jetter and Schäffer, 2001). In maize, the predominant aliphatic components in the leaf cuticle were $C_{21,}$ C_{23}, and C_{25} *n*-alkanes at early stages of development but shifted to chain lengths over C_{28} in later development (Bourgault et al., 2020). Similarly, in the present study, the fatty acid fraction in the tepal waxes of the green bud stage mainly contained C_{20} and C_{22}, whereas they ranged from C_{20} to C_{26} in the open flower tepal cuticles (**Figure 5**; **Supplementary Tables S1** and **S2**). The *n*-alkanes with chain lengths over C_{31} and alkyl esters over C_{36} were detected only in the cuticles on the tepals of open flowers (**Figure 5**). A shift to longer hydrocarbon chain lengths is due to the bio-synthesis of waxes regulated by a series of genes and enzymes, as well as their functional properties during developmental stages (Busta et al., 2017).

Previous studies indicated that C-chains of cuticular waxes accumulating in petal waxes are shorter compared to those in leaf waxes. *C. bipinnatus* petal and leaf waxes are dominated by primary alcohols and fatty acids with carbon chain lengths of C_{22} and C_{24}, and C_{28} and C_{30}, respectively (Buschhaus et al., 2015). The waxes on the flowers and leaves of *T. officinale* contained branched C_{27} to C_{31}, and non-branched C_{27} to C_{33}

n-alkanes (Guo and Jetter, 2017). Alcohol esters with a predominance of C_{22} to C_{28}, and C_{28} to C_{32} were found in *P. hybrida* flower and leaf waxes, respectively (King et al., 2007). In *Arabidopsis*, *n*-alkanes with a chain length of C_{29} dominate the aliphatic pattern in petal waxes, whereas a chain length of C_{31} is dominant in the leaf waxes (Jenks et al., 1995; Shi et al., 2011). In rose cultivars 'Movie star' and 'Tineke', the predominant chain lengths are C_{31} and C_{33} *n*-alkanes in the leaf waxes, whereas C_{27} and C_{29} *n*-alkanes and *n*-alkenes dominate the petal waxes (Cheng et al., 2019). In the present study, the chain lengths of the *n*-alkanes ranged from C_{22} to C_{33}, with C_{27} and C_{29} chain lengths predominating in the tepal waxes, whereas chain lengths of C_{31} and C_{29} were dominant in the leaf waxes of the 'Huang Tianba' and 'Tiber' cultivars, respectively (**Figure 7**). These findings corroborated the typical chain-length distributions of the aliphatic component, being shorter in petal waxes compared to that in leaf waxes (Buschhaus et al., 2015; Jetter and Riederer, 2016).

In contrast to the chemical analysis of petal waxes, few studies have investigated the transpiration barrier properties of petal cuticles. A study on water permeability of petal waxes has been conducted for *C. bipinnatus* (Buschhaus et al., 2015). As mentioned above, the relatively high concentrations of C_{22} and C_{24} carbon chain components in *C. bipinnatus* petal waxes are thought to create a less efficient barrier to transpiration compared to that of the leaf cuticles. Similar results have been found for rose petal waxes in the 'Movie star' and 'Tineke' cultivars, which accumulated mainly C_{26} and C_{29}, resulting in higher cuticular transpiration compared to that in leaves with a predominance of C_{31} (Cheng et al., 2019). Patwari et al. (2019) found that the lack of very-long-chain wax esters induced a higher cuticular permeability in *wsd1* mutants in *Arabidopsis*. Taken previous results together with present study on lily, C-chain lengths distribution in cuticular wax might play a pivotal role in limiting non-stomatal transpiration in plant tissues. Flowers that accumulate very long chain of aliphatics might exhibit slower weight loss and longer shelf life during marketing.

In conclusion, cuticular transpiration of lily flower green bud tepals was significantly higher than that of the open flower tepals and was significantly higher in the tepals than in the leaves. The most abundant aliphatic compounds in the tepal waxes of the lily cultivars 'Casa Blanca' and 'Huang Tianba' were *n*-alkanes, whereas large amounts of primary alcohols were detected in the tepal waxes of the 'Tiber' cultivar. In addition, there was a predominance of relatively short carbon chain aliphatics in the tepal waxes of the green bud stage, compared to the chain lengths in tepal waxes of the open flower stage, and similar differences between the tepal and leaf waxes were found. These findings suggest that the less efficient transpiration barrier properties of the tepal waxes are probably related to the accumulation of relatively short-chain aliphatics. Furthermore, cuticular transpiration and the barrier properties of the cuticular waxes of lily cultivars exhibited organ- and cultivar-specific differences. These findings provide further insight to link the cuticular chemicals with functional properties as well as with the physiological adaptations of plant tissues. The findings of this study also contribute to the cultivar selection for flowers, in which accumulation of very long chain of aliphatics might exhibit slower weight loss and longer shelf life during marketing. The cuticular barrier properties are varied in organ-, cultivar-, and species differences, which are largely affected by the accumulation of chemical compositions and arrangement of cuticle (Riederer and Schreiber, 2001; Huang et al., 2017). In addition, the growing conditions have also been widely reported to be one of the most important factors in influencing the transpiration changes. Therefore, selecting appropriate cultivar, setting appropriate growing conditions including water and light availability, temperature and humidity control, etc., will largely influence the water loss of flowers. Combining post-harvest treatments such as nano-silver solution with sugars to spray on flowers forms thin aqueous membrane, slowing down the rapid post-harvest changes (Naing and Kim, 2020). Therefore, caring the transpiration barrier properties will be helpful for the development of techniques with the potential to extend the shelf life of cut flowers based on the transpiration barrier properties of the cuticular waxes after harvest.

DATA AVAILABILITY STATEMENT

The original contributions presented in the study are included in the article/**Supplementary Material**, further inquiries can be directed to the corresponding author.

AUTHOR CONTRIBUTIONS

HH and GC designed the project and prepared the manuscript. GC and LW performed most of the experiments. HW and XY took part in part of the experiments. NZ, XW, and LH helped to make interpretation of the results. All authors contributed to the article and approved the submitted version.

FUNDING

This work was supported by the Characteristic Innovation of Project of Education Department of Guangdong Province (Natural Science 2020KTSCX053), the Common Technical Innovation Team of Guangdong Province on Preservation and Logistics of Agricultural Products (2019KJ145), the Foundation of Guangxi Key Laboratory of Fruits and Vegetables Storage-Processing Technology (2021-01), and the special fund for scientific innovation strategy-construction of high level Academy of Agriculture Science of Guangdong Academy of Agricultural Sciences (R2019QD-012).

SUPPLEMENTARY MATERIAL

The Supplementary Material for this article can be found online at: https://www.frontiersin.org/articles/10.3389/fpls.2021.781987/full#supplementary-material

REFERENCES

Bourgault, R., Matschi, S., Vasquez, M., Qiao, P., Sonntag, A., Charlebois, C., et al. (2020). Constructing functional cuticles: analysis of relationships between cuticle lipid composition, ultrastructure, and water barrier function in developing adult maize leaves. *Ann. Bot.* 125, 79–91. doi: 10.1093/aob/mcz143

Burghardt, M., and Riederer, M. (2003). Ecophysiological relevance of cuticular transpiration of deciduous and evergreen plants in relation to stomatal closure and leaf water potential. *J. Exp. Bot.* 54, 1941–1949. doi: 10.1093/jxb/erg195

Buschhaus, C., Hager, D., and Jetter, R. (2015). Wax layers on *Cosmos bipinnatus* petals contribute unequally to total petal water resistance. *Plant Physiol.* 167, 80–88. doi: 10.1104/pp.114.249235

Busta, L., Hegebarth, D., Kroc, E., and Jetter, R. (2017). Changes in cuticular wax coverage and composition on developing Arabidopsis leaves are influenced by wax biosynthesis gene expression levels and trichome density. *Planta* 245, 297–311. doi: 10.1007/s00425-016-2603-6

Cheng, G. P., Huang, H., Zhou, L. Y., He, S. G., Zhang, Y. J., and Cheng, X. A. (2019). Chemical composition and water permeability of the cuticular wax barrier in rose leaf and petal: a comparative investigation. *Plant Physiol. Biochem.* 135, 404–410. doi: 10.1016/j.plaphy.2019.01.006

Cheng, G., Wang, L., He, S., Liu, J., and Huang, H. (2020). Involvement of pectin and hemicellulose depolymerization in cut gerbera flower stem bending during vase life. *Postharvest Biol. Technol.* 167:111231. doi: 10.1016/j.postharvbio.2020.111231

Fanourakis, D., Papadopoulou, E., Valla, A., Tzanakakis, V. A., and Nektarios, P. A. (2021). Partitioning of transpiration to cut flower organs and its mediating role on vase life response to dry handling: a case study in chrysanthemum. *Postharvest Biol. Technol.* 181:111636. doi: 10.1016/j.postharvbio.2021.111636

Goodwin, S. M., Kolosova, N., Kish, C. M., Wood, K. V., Dudareva, N., and Jenks, M. A. (2003). Cuticle characteristics and volatile emissions of petals in *Antirrhinum majus*. *Physiol. Plant.* 117, 435–443. doi: 10.1034/j.1399-3054.2003.00047.x

Griffiths, D. W., Robertson, G. W., Shepherd, T., Birch, A. N. E., Gordon, S. C., and Woodford, J. T. (2000). A comparison of the composition of epicuticular wax from red raspberry (*Rubus idaeus* L.) and hawthorn (*Crataegus monogyna* Jacq.) flowers. *Phytochemistry* 55, 111–116. doi: 10.1016/s0031-9422(00)00250-8

Griffiths, D. W., Robertson, G. W., Shepherd, T., and Ramsay, G. (1999). Epicuticular waxes and volatiles from faba bean (*Vicia faba*) flowers. *Phytochemistry* 52, 607–612. doi: 10.1016/S0031-9422(99)00298-8

Guo, Y., Busta, L., and Jetter, R. (2017). Cuticular wax coverage and composition differ among organs of *Taraxacum officinale*. *Plant Physiol. Biochem.* 115, 372–379. doi: 10.1016/j.plaphy.2017.04.004

Guo, Y., and Jetter, R. (2017). Comparative analyses of cuticular waxes on various organs of potato (*Solanum tuberosum* L.). *J. Agric. Food Chem.* 65, 3926–3933. doi: 10.1021/acs.jafc.7b00818

Huang, H., Burghardt, M., Schuster, A.-C., Leide, J., Lara, I., and Riederer, M. (2017). Chemical composition and water permeability of fruit and leaf cuticles of *Olea europaea* L. *J. Agric. Food Chem.* 65, 8790–8797. doi: 10.1021/acs.jafc.7b03049

Jenks, M. A., Tuttle, H. A., Eigenbrode, S. D., and Feldmann, K. A. (1995). Leaf epicuticular waxes of the eceriferum mutants in Arabidopsis. *Plant Physiol.* 108, 369–377. doi: 10.1104/pp.108.1.369

Jetter, R., and Riederer, M. (2016). Localization of the transpiration barrier in the epi- and intracuticular waxes of eight plant species: water transport resistances are associated with fatty acyl rather than alicyclic components. *Plant Physiol.* 170, 921–934. doi: 10.1104/pp.15.01699

Jetter, R., and Schäffer, S. (2001). Chemical composition of the Prunus laurocerasus leaf surface. Dynamic changes of the epicuticular wax film during leaf development. *Plant Physiol.* 126, 1725–1737. doi: 10.1104/pp.126.4.1725

King, A., Nam, J.-W., Han, J., Hilliard, J., and Jaworski, J. G. (2007). Cuticular wax biosynthesis in petunia petals: cloning and characterization of an alcohol-acyltransferase that synthesizes wax-esters. *Planta* 226, 381–394. doi: 10.1007/s00425-007-0489-z

Lin, X., Li, H., He, S., Pang, Z., Lin, S., and Li, H. (2020). Investigation of stomata in cut 'Master' carnations: organographic distribution, morphology, and contribution to water loss. *Hort Sci.* 55, 1144–1147. doi: 10.21273/HORTSCI14945-20

Naing, A. H., and Kim, C. K. (2020). Application of nano-silver particles to control the postharvest biology of cut flowers: A review. *Sci. Hort.* 270:109463. doi: 10.1016/j.scienta.2020.109463

Nobel, P. S. (2009). *Physicochemical and Environmental Plant Physiology*. *4th Edn*. San Diego: Academic Press.

Patwari, P., Salewski, V., Gutbrod, K., Kreszies, T., Dresen-Scholz, B., Peisker, H., et al. (2019). Surface wax esters contribute to drought tolerance in *Arabidopsis*. *Plant J.* 98, 727–744. doi: 10.1111/tpj.14269

Riederer, M., and Schreiber, L. (1995). "Waxes — the transport barriers of plant cuticles," in *Waxes: Chemistry, Molecular Biology and Functions*. *Vol. 6.* ed. R. J. Hamilton (West Ferry, Dundee: The Oily Press), 130–156.

Riederer, M., and Schreiber, L. (2001). Protecting against water loss: analysis of the barrier properties of plant cuticles. *J. Exp. Bot.* 52, 2023–2032. doi: 10.1093/jexbot/52.363.2023

Schreiber, L., and Riederer, M. (1996). Ecophysiology of cuticular transpiration: comparative investigation of cuticular water permeability of plant species from different habitats. *Oecologia* 107, 426–432. doi: 10.1007/BF00333931

Schuster, A.-C., Burghardt, M., and Riederer, M. (2017). The ecophysiology of leaf cuticular transpiration: are cuticular water permeabilities adapted to ecological conditions? *J. Exp. Bot.* 68, 5271–5279. doi: 10.1093/jxb/erx321

Shi, J. X., Malitsky, S., De Oliveira, S., Branigan, C., Franke, R. B., Schreiber, L., et al. (2011). SHINE transcription factors act redundantly to pattern the archetypal surface of *Arabidopsis* flower organs. *PLoS Genet.* 7:e1001388. doi: 10.1371/journal.pgen.1001388

Torre, S., and Fjeld, T. (2001). Water loss and postharvest characteristics of cut roses grown at high or moderate relative air humidity. *Sci. Hortic.* 89, 217–226. doi: 10.1016/S0304-4238(00)00229-6

Tsaniklidis, G., Rezaei Nejad, A., Ottosen, C.-O., and Woltering, E. J. (2020). Genotypic and phenotypic differences in fresh weight partitioning of cut rose stems: implications for water loss. *Acta Physiol. Plant* 42:48. doi: 10.1007/s11738-020-03044-w

van Doorn, W. G., and Han, S. S. (2011). Postharvest quality of cut lily flowers. *Postharvest Biol. Technol.* 62, 1–6. doi: 10.1016/j.postharvbio.2011.04.013

Whitney, H. M., Bennett, K. M. V., Dorling, M., Sandbach, L., Prince, D., Chittka, L., et al. (2011). Why do so many petals have conical epidermal cells? *Ann. Bot.* 108, 609–616. doi: 10.1093/aob/mcr065

Yeats, T. H., and Rose, J. K. C. (2013). The formation and function of plant cuticles. *Plant Physiol.* 163, 5–20. doi: 10.1104/pp.113.222737

Conflict of Interest: The authors declare that the research was conducted in the absence of any commercial or financial relationships that could be construed as a potential conflict of interest.

frontiers in Plant Science

MINI REVIEW
published: 29 November 2021
doi: 10.3389/fpls.2021.778131

Unraveling Cuticle Formation, Structure, and Properties by Using Tomato Genetic Diversity

*Johann Petit[1], Cécile Bres[1], Nicolas Reynoud[2], Marc Lahaye[2], Didier Marion[2], Bénédicte Bakan[2] and Christophe Rothan[1]**

[1]*INRAE, Univ. Bordeaux, UMR BFP, Villenave d'Ornon, France,* [2]*Unité Biopolymères, Interactions, Assemblages, INRAE, Nantes, France*

The tomato (*Solanum lycopersicum*) fruit has a thick, astomatous cuticle that has become a model for the study of cuticle formation, structure, and properties in plants. Tomato is also a major horticultural crop and a long-standing model for research in genetics, fruit development, and disease resistance. As a result, a wealth of genetic resources and genomic tools have been established, including collections of natural and artificially induced genetic diversity, introgression lines of genome fragments from wild relatives, high-quality genome sequences, phenotype and gene expression databases, and efficient methods for genetic transformation and editing of target genes. This mini-review reports the considerable progresses made in recent years in our understanding of cuticle by using and generating genetic diversity for cuticle-associated traits in tomato. These include the synthesis of the main cuticle components (cutin and waxes), their role in the structure and properties of the cuticle, their interaction with other cell wall polymers as well as the regulation of cuticle formation. It also addresses the opportunities offered by the untapped germplasm diversity available in tomato and the current strategies available to exploit them.

Keywords: tomato, cuticle, natural diversity, mutant, fruit, cutin, structure, property

OPEN ACCESS

Edited by:
Antonio Heredia, University of Malaga, Spain

Reviewed by:
Rafael Fernández-Muñoz, Consejo Superior de Investigaciones Científicas (CSIC), Spain
Federico Scossa, Council for Agricultural and Economics Research, Italy

****Correspondence:***
Christophe Rothan
christophe.rothan@inrae.fr

Specialty section:
This article was submitted to Plant Physiology, a section of the journal Frontiers in Plant Science

Received: *16 September 2021*
Accepted: *02 November 2021*
Published: *29 November 2021*

Citation:
Petit J, Bres C, Reynoud N, Lahaye M, Marion D, Bakan B and Rothan C (2021) Unraveling Cuticle Formation, Structure, and Properties by Using Tomato Genetic Diversity. Front. Plant Sci. 12:778131. doi: 10.3389/fpls.2021.778131

INTRODUCTION

Cultivated tomato (*Solanum lycopersicum* L.) is a major horticultural crop that has long been a model for the *Solanaceae* crop species (tomato, potato, eggplant, pepper …) and for fleshy fruit development and disease resistance (Rothan et al., 2019). Tomato is very suitable for laboratory studies (grown in greenhouse, miniature cultivars, short life cycle, autogamy, and easy genetic transformation) has extensive genetic resources, high-quality reference genome (Tomato Genome Consortium, 2012), sequences of hundreds of accessions (Zhu et al., 2018; Gao et al., 2019; Alonge et al., 2020), and available phenotype and gene expression databases.[1] Thanks to these resources and tools, genes underlying trait variations can be identified and their relationships with phenotypic variations can be established through *in planta* functional analysis.

In the last decades, the use of natural diversity available in tomato, such as the ripening mutants *ripening inhibitor* (*rin*) or *non-ripening* (*nor*), has been instrumental to decipher the

[1]https://solgenomics.net/

regulation of ripening (Klee and Giovannoni, 2011). These advances have been aided by the development of tools for functional analysis of target genes including RNA interference (RNAi) and CRISPR/Cas9 gene editing systems. The molecular determinants of fruit skin formation, which is an essential protective barrier against pests, pathogens, and water loss, have begun to be explored more recently (Vogg et al., 2004; Lemaire-Chamley et al., 2005; Hovav et al., 2007; Mintz-Oron et al., 2008).

Not surprisingly, since the cuticle is a major component of the fruit skin and is associated with a wide diversity of major breeding targets including fruit appearance (color, glossiness, regularity…) and properties (shelf-life, fungal resistance, and cracking; Bargel and Neinhuis, 2005; Petit et al., 2017; Lara et al., 2019), it has received considerable attention in recent years. In this field of study, tomato holds a prominent position among fleshy fruits because of its thick, astomatous, and easy-to-peel cuticle (Petit et al., 2017). Additionally, the wide diversity in cuticle architecture and composition found in wild tomato relatives (Yeats et al., 2012a; Halinski et al., 2015; Fernandez-Moreno et al., 2017) can be exploited for the discovery of novel cuticle-associated genes (Hovav et al., 2007; Zhang et al., 2021). Tomato has therefore become a model for the study of cuticle formation in plants. In the recent years, molecular determinants of cuticle have been identified and genetically altered lines have been produced, enabling the exploration of cuticle structure, properties, interactions with other cell wall components, and relationships with epidermal patterning. **Table 1** summarizes the major findings on known tomato cuticle-associated genes, the pathway, or biological process in which they are involved and the main alterations produced by their mutation or de-regulation. This mini-review focuses on the strategies, resources, and tools used to reveal their role, providing examples, and considers future goals and developments.

Linking gene to phenotype can be done using approaches known as (i) reverse genetics in which the function of a target gene is mainly determined by analyzing the phenotype of mutant or deregulated lines and (ii) forward genetics, in which tomato genetic diversity is first screened for phenotypes-of-interest and the underlying genes and their function are then identified.

EXPLORING THE FUNCTION OF CUTICLE-ASSOCIATED GENES THROUGH REVERSE GENETICS APPROACHES IN TOMATO

An obvious source of information on wax- and cutin-associated genes to study in tomato is the model plant Arabidopsis (Bernard and Joubes, 2013; Fich et al., 2016). Examples of the pertinence of this strategy are the conserved functions in Arabidopsis and tomato of the SHINE transcription factors (Shi et al., 2013; Al-Abdallat et al., 2014) and the recent demonstration that the SlABCG42 transporter, the tomato ortholog of the Arabidopsis ABCG PEC1 transporter, is functional and can transport various cutin precursors (Elejalde-Palmett et al., 2021).

For poorly characterized or unknown function genes, the information on where and when they are expressed provides the first cues on their possible role in cuticle formation. Gene expression has been explored in-depth in tomato fruit skin, a tissue which consists of the cuticle, the epidermis, and few layers of collenchyma cells underneath (Bargel and Neinhuis, 2005). Of special interest is the fruit expansion phase, before the onset of ripening, when rapid cuticle deposition occurs (Mintz-Oron et al., 2008; Petit et al., 2014). During the cell expansion phase, ploidy and volume of epidermal and sub-epidermal cells do not vary, whereas ploidy and cell volume undergo a dramatic increase in mesocarp cells (Joubès et al., 1999; Renaudin et al., 2017). In earlier studies, epidermis-expressed genes were identified *via* tissue-specific Expressed Sequence Tags (EST), microarrays (Lemaire-Chamley et al., 2005; Mintz-Oron et al., 2008), and proteome (Yeats et al., 2010). Several genes highlighted in these studies play prominent roles in cuticle formation, among which the *CUTIN SYNTHASE* (*CUS1*) catalyzing cutin polymerization (Girard et al., 2012; Yeats et al., 2012b) and the *SlMIXTA-like* regulating cuticle formation and epidermal patterning (Lashbrooke et al., 2015). Semi-quantitative RNA-seq coupled with laser microdissection (LMD) next allowed exhaustive inventory of gene transcripts expressed in plant tissues, including outer and inner fruit epidermis (Matas et al., 2011). Another original transcriptome-based approach used a chimera between two tomato species displaying genotype-specific E1 cell layer to provide a reference catalog of epidermis-specific genes (Filippis et al., 2013). Quantitative RNA-seq coupled with LMD later allowed the establishment of a quantitative tomato fruit gene atlas of developing fruit (Shinozaki et al., 2018). The resulting Tomato Expression Database (TEA) available at SGN[2] can be mined for clusters of genes co-expressed in specific developmental stages and cell types including inner and outer epidermis, which gives precious information on genes functionally linked to cuticle formation. Gene expression profiling can be further combined with various multi-omics technologies, typically metabolome (Fernandez-Moreno et al., 2016) and proteome (Szymanski et al., 2017), and with large scale sequencing of genetic diversity (Szymański et al., 2020) to assign putative functions to the genes and explore their role in cuticle formation. Novel functions revealed by biochemical approaches, e.g., the cutin:cutin-acid endo-transacylase (CCT) enzyme activity (Xin et al., 2021), may also ultimately lead to the isolation of the encoding gene.

Technologies used for the functional analysis of cuticle-associated genes (**Table 1**) include Virus-Induced Gene Silencing (VIGS; Ballester et al., 2010; España et al., 2014), stable gene overexpression (e.g., Shi et al., 2013) and silencing *via* RNA interference (RNAi; e.g., Girard et al., 2012; Lashbrooke et al., 2015) and artificial miRNA (Adato et al., 2009). More recently, the efficient CRISPR/Cas9 system, which allows genome editing of single or multiple target genes (Rothan et al., 2019), has been successfully used to validate the influence of a GA2-oxidase on cuticle formation and fruit firmness (Li et al., 2020). Recent development of genome editing technologies offers the possibility

[2]https://tea.solgenomics.net/

TABLE 1 | Genes involved in cuticle formation and properties studied in tomato.*

Gene-locus[a]	Solyc[b]	Type[c]	Function	Species[d]	Cultivar-accession[e]	Genetic variation origin/Allele[f]	Cuticle-associated traits	References
SlCYP86A69	08g081220	Enzyme	Cutin monomer biosynthesis	*Sl*	MT	EMS/*cd3/cyp86a69*	Fruit cuticle thickness and properties; cutin content; pathogen susceptibility	Isaacson et al., 2009; Shi et al., 2013; Buxdorf et al., 2014
SlGPAT6	09g014350	Enzyme	Cutin monomer biosynthesis	*Sl*	MT	EMS/*cud1/gpat6-a*	Fruit cuticle thickness and properties; cutin content; epidermal patterning; cell wall properties; pathogen interaction	Petit et al., 2016; Philippe et al., 2016; Fawke et al., 2019; Moreira et al., 2020
SlABCG36/42	05g018510 06g065670	Transporter	Cutin monomer transport	*Sl*	MT	RNAi silencing	Fruit cuticle thickness; cutin content and composition	Elejalde-Palmett et al., 2021
SlCUS1	11g006250	Enzyme	Cutin polymerization	*Sl*	MT	EMS/*gdsl2b/cus1-a*	Fruit cuticle thickness and properties; cutin content; epidermal patterning; susceptibility to pathogens	Petit et al., 2014; Moreira et al., 2020; Segado et al., 2020
				Sl	M82	EMS/*cd1/cus1*		Isaacson et al., 2009; Yeats et al., 2012b
				Slc	WVa106	RNAi silencing		Girard et al., 2012; Philippe et al., 2020a
SlDCR	03g025320	Enzyme	Cutin polymerization	*Sl*	M82	RNAi silencing	Flower and leaf fusion; fruit cracking and suberin formation	Lashbrooke et al., 2016
SlCER6/SlKCS6	02g085870	Enzyme	Wax biosynthesis	*Sl*	MT	*Ds*-insertion/*cer6*	Flower fusion; fruit dehydration; alkanes and terpenoids	Vogg et al., 2004; Leide et al., 2007; Smirnova et al., 2013
SlTTS1 *SlTTS2*	12g006530 12g006520	Enzyme	Triterpenoid biosynthesis	*Sh*	LA3917	Natural	Fruit cuticle wax triterpenoids; amyrin content and composition	Yeats et al., 2012a
SlCHS1 *SlCHS2*	09g091510 05g053550	Enzyme	Flavonoid biosynthesis	*Sl*	MT/MM/GD	VIGS	Cuticle composition and properties; flavonoid, polysaccharide, cutin content and esters linkage; epidermal patterning	España et al., 2014; Heredia et al., 2015
SlSHN1	03g116610	ERF	Regulation of wax biosynthesis	*Sl*	MM	OE	Leaf cuticular wax; plant drought resistance	Al-Abdallat et al., 2014
SlSHN3	06g053240	ERF	Regulation of cutin and wax biosynthesis	*Sl*	MT	OE	Fruit and leaf cutin and wax content; fruit epidermal patterning; pathogen susceptibility	Shi et al., 2013; Buxdorf et al., 2014

(Continued)

TABLE 1 | Continued

Gene-locus[a]	Solyc[b]	Type[c]	Function	Species[d]	Cultivar-accession[e]	Genetic variation origin/Allele[f]	Cuticle-associated traits	References
SlMIXTA-like	02g088190	MYB	Regulation of cutin and wax biosynthesis	*Sl*	MT	RNAi silencing	Fruit cuticle thickness and properties; cutin content; epidermal patterning	Lashbrooke et al., 2015
WOOLY	02g080260	HD-Zip IV	Regulation of wax biosynthesis	*Sl*	LA3186	Natural/*Wo*	Trichome initiation; leaf and fruit wax content	Xiong et al., 2020
SlMYB31	03g116100	MYB	Regulation of wax biosynthesis	*Sl*	AC	RNAi silencing/ OE	Fruit cuticle properties; wax content	Xiong et al., 2020
STICKY PEEL	01g091630	HD-Zip IV	Regulation of epiderm metabolism	*Sl*	M82	EMS/*cd2*	Fruit and leaf cuticle properties; cutin, wax, flavonoid, anthocyanin content and/or composition; glandular trichomes; pathogen susceptibility	Isaacson et al., 2009; Martin et al., 2016
HD-ZIP IV				*Sl*	LA0759	Natural/*pe*		Kimbara et al., 2012, 2013
				Sl	LA2467			Nadakuduti et al., 2012
YELLOW	01g079620	MYB	Regulation of flavonoid metabolism	*Sl*	LA3189	Natural/*y*	Fruit cuticle thickness and properties flavonoid accumulation in the cuticle; epidermal patterning	Adato et al., 2009
PINK FRUIT				*Sc*	LA1480	Natural/*y*		Ballester et al., 2010
SlMYB12				*Sl*	MT	EMS/*pf*		
LYCOPENE CYCLASE b		Enzyme	Carotenoid metabolism	*Sl*	MM	OE Arabidopsis AT3G10230	Extended shelf-life; fruit cuticle thickness and properties; ABA content; cutin and triterpenoid content	Diretto et al., 2020
SlPP2C3	06g076400	Enzyme	Regulation of ABA metabolism	*Sl*	MT	RNAi silencing/ OE	Fruit cuticle properties; epidermal patterning	Liang et al., 2021
GA2-OXIDASE	10g007570	Enzyme	GA catabolism	*Sl*	LA1310	Natural/*fis1*	Fruit firmness; cuticle thickness; cutin and wax content	Li et al., 2020
TAGL1	07g055920	MADS box	Regulation of fruit ripening	*Sl*	MM	RNAi silencing/ OE	Fruit cuticle thickness and properties; cutin, wax, cell wall and phenolics composition and content; epidermal patterning	Giménez et al., 2015
RIN	05g012020	MADS box	Regulation of fruit ripening	*Sl*	AC	Natural/*rin*	Long shelf-life; fruit cuticle composition and properties; cutin and wax composition	Kosma et al., 2010

(Continued)

TABLE 1 | Continued

Gene-locus[a]	Solyc[b]	Type[c]	Function	Species[d]	Cultivar-accession[e]	Genetic variation origin/Allele[f]	Cuticle-associated traits	References
NAC-NOR ALCOBACA	10g006880	NAC	Regulation of fruit ripening	*Sl*	DFD	Natural/*nor/alc*	Long shelf-life; cuticle composition and properties; cutin and wax content and composition	Saladié et al., 2007; Romero and Rose, 2019
				Sl	AC			Kosma et al., 2010
				Sl	de Penjar			Kumar et al., 2018
FUL1	06g069430	MADS box	Regulation of fruit ripening	*Sl*	MT	RNAi silencing	Cuticle properties	Bemer et al., 2012
FUL2	03g114830							
CWP1	04g082540		Unknown	*Sh*	LA1777	Natural/*cwp*	Cuticle fissures; fruit dehydration	Hovav et al., 2007; Chechanovsky et al., 2019
FNC				*Sp*	LA716	Natural		Zhang et al., 2021
SlEZ2	03g044380	Enzyme	Histone methylation	*Sl*	Wva106	RNAi silencing	Fruit brightness; cutin and wax content and composition	Boureau et al., 2016

**The table is focused on published studies in which the tomato cuticle was explicitly analyzed, as revealed by an extensive literature review.*

[a]Locus and/or gene names are indicated when available in the cited references. CYP, CYTOCHROME P450; GPAT, GLYCEROL-3-PHOSPHATE ACYLTRANSFERASE; ABCG, ATP-BINDING CASSETTE (ABC) G; CUS, CUTIN SYNTHASE; CER, ECERIFERUM; KCS, B-KETOACYL-COA-SYNTHASE; DCR, DEFECTIVE IN CUTICULAR RIDGES; TTS, TRITERPENE SYNTHASE; CHS, CHALCONE SYNTHASE; SHN, SHINE; HD-ZIP IV, HOMEODOMAIN-LEUCINE ZIPPER IV; PP2C, PROTEIN PHOSPHATASE 2C; TAGL1, TOMATO AGAMOUS-LIKE1; RIN, RIPENING INHIBITOR; NOR, NON-RIPENING; FUL, FRUITFULL; CWP, CUTICULAR WATER PERMEABILITY; AND FNC, FRUIT NETTED CRACKING.

[b]The SGN Solanum lycopersicum (Solyc) identifier is indicated.

[c]ERF, Ethylene Response Factor; MYB, HD-Zip, MADS box, and NAC are transcription factors.

[d]Sl, Solanum lycopersicum; Slc, Solanum lycopersicum var. cerasiformae; Sc, Solanum chmielewskii; Sh, Solanum habrochaites; and Sp, Solanum pennellii.

[e]For natural mutations, the original species and Tomato Genetics Resource Center (TGRC) accession number of the genotype carrying the allelic variant studied are indicated. When not available in the cited references, the background genotype in which the mutation has been introgressed is indicated. MT, Micro-Tom; MM, Moneymaker; AC, Ailsa Craig; and GD, Gardener's Delight.

[f]EMS, Ethyl methane sulfonate; RNAi, RNA interference; and OE, overexpression. The various names of the induced or natural alleles are indicated.

to specifically target cuticle genes in the fruit (Feder et al., 2020) when rapid cuticle deposition takes place (Mintz-Oron et al., 2008) by using the fruit- and expansion phase-specific promoter *proPPC2* (Fernandez et al., 2009; Guillet et al., 2012). This further opens the perspective to specifically edit a cuticle gene in fruit epidermis, for instance by employing the promoter from the wax biosynthesis *SlCER6* gene (Vogg et al., 2004) that drives reporter expression in both inner and outer fruit epidermis (Mintz-Oron et al., 2008).

DISCOVERING CUTICLE-ASSOCIATED GENES THROUGH FORWARD GENETICS APPROACHES IN TOMATO

Though the list of cuticle-associated genes can be considerably shortened by mining existing databases and literature, their systematic analysis in planta may remain problematic because of gene redundancy, pleiotropic effect, etc. This may restrict the focus to known gene families, thus impeding the discovery of original gene functions. An alternative approach is to screen natural or artificially induced genetic diversity for phenotypes-of-interest, e.g., fruit surface defects induced by cutin deficiency (Isaacson et al., 2009; Petit et al., 2014), and then identify causal genetic variation.

Using Natural Genetic Diversity for Linking Cuticle Phenotype to Gene

Wild tomato species are an important source of genes lost during domestication of tomato (Gao et al., 2019). The main tomato germplasm repository, from which seeds can be ordered, is the Tomato Genetics Resource Center (TGRC).[3] It includes the phenotypic description of wild tomato relatives and of thousands of cultivated tomato accessions carrying spontaneous or artificially induced mutations. Natural diversity can be screened for cuticle structure and composition (Yeats et al., 2012a; Halinski et al., 2015), transpirational water loss (Fich et al., 2020), and for mutations, such as *positional sterile* (*ps*), which causes organ fusion by affecting the wax decarboxylation pathway (Leide et al., 2011) or *yellow* (*y*) resulting from a *SlMYB12* mutation (Adato et al., 2009; Ballester et al., 2010).

Most wild tomato relatives are easily crossed with tomato to generate segregating populations, e.g., the *Solanum pimpinellifolium*-derived population (Barraj Barraj et al., 2021), thus allowing the detection of cuticle Quantitative Trait Locus (QTL) and candidate genes. Genomic regions of wild species can be further fixed in an uniform *S. lycopersicum* genetic background to produce Introgression Lines (Ils) or Backcross Inbred Lines (BIls; Bazakos

[3]https://tgrc.ucdavis.edu

et al., 2017; Petit et al., 2017). The most extensively used ILs, derived from *Solanum pennellii* (Eshed and Zamir, 1995), enabled the rapid mapping of cuticle-associated QTLs and genes for leaf waxes (Ofner et al., 2016), wax alkane and amyrin content (Fernandez-Moreno et al., 2017), epidermal reticulation of green fruit (Cui et al., 2017), and fruit skin microfissuring (Zhang et al., 2021). Large scale transcriptome and metabolome analysis of fruit skin from 580 inbred lines further identified genes involved in flavonoid biosynthesis and fungal resistance (Szymański et al., 2020). *Solanum habrochaites*-derived lines allowed the identification of candidate genes for wax triterpenoids (Yeats et al., 2012a) and the isolation of the *CWP1* gene of unknown function responsible for skin microfissuring (Hovav et al., 2007; Chechanovsky et al., 2019). *Solanum chmielewskii* ILs were used to identify a *y* mutant (Ballester et al., 2010).

The effects on cuticle formation of natural genetic variants found in cultivated tomato were also explored. *STICKY PEEL* encodes a HD-Zip IV protein that regulates epidermis metabolism and additional cuticle-associated traits (Kimbara et al., 2012; Nadakuduti et al., 2012) while *WOOLY*, a different HD-Zip IV protein, regulates trichome initiation and wax biosynthesis (Xiong et al., 2020). *GA2-OXIDASE*, which was identified through a fruit firmness QTL analysis, is unexpectedly related to a cuticle thickness QTL (Li et al., 2020) and connects cuticle formation with gibberellin (GA) signaling. In addition, because of the strong impact of cuticle properties on tomato postharvest storage (Saladié et al., 2007), lines harboring the well-studied non-ripening mutations *rin* and *nor* (Wang et al., 2020) as well as several long shelf-life tomato varieties ["Delayed Fruit Deterioration" (DFD) cultivar., de Penjar types] carrying allelic variants of *NAC-NOR* (e.g., *alcobaca*) have been characterized with respect to cuticle composition and properties (Saladié et al., 2007; Kosma et al., 2010; Kumar et al., 2018; Romero and Rose, 2019). The complex interplay between fruit development and ripening, epidermal patterning and metabolism, and cuticle formation and properties, which was revealed by these studies, was further supported by independent studies of the ripening regulators *FUL1/FUL2* (Bemer et al., 2012) and *TAGL1* (Giménez et al., 2015).

Using Artificially Induced Genetic Diversity for Linking Cuticle Phenotype to Gene

Several collections of artificially induced genetic diversity have been generated in cultivated tomato by transposon tagging (Meissner et al., 1997) or ethyl methanesulfonate (EMS) mutagenesis (Menda et al., 2004; Minoia et al., 2010; Saito et al., 2011; Just et al., 2013; Gupta et al., 2017). The two main mutagenized cultivars are the miniature Micro-Tom tomato (Meissner et al., 1997), which is well suited for laboratory use (Meissner et al., 1997; Just et al., 2013), and M82 (Menda et al., 2004), a processing tomato parent of the widely used *S. pennellii* ILs (Eshed and Zamir, 1995). Several *cutin-deficient* mutants were found in the M82 mutant collection (Isaacson et al., 2009) while more than 10 wax-altered and/or cutin-deficient *glossy* mutants were described in Micro-Tom (Petit et al., 2014). Many more mutants can be found by screening tomato mutant collections for obvious cuticle defects (Petit et al., 2014) and by browsing associated phenotypic databases (reviewed in Rothan et al., 2016), such as TOMATOMA[4] (Saito et al., 2011). EMS mutant collections can also be screened by TILLING (Targeting Induced Local Lesions IN Genomes; Okabe et al., 2011) though mutated alleles of target genes are now efficiently generated by gene editing (Rothan et al., 2019).

As detailed in **Table 1**, mutant collections have been instrumental for: (i) discovering novel gene functions (*SlCUS1*; Yeats et al., 2012b); (ii) isolating allelic variants of genes implicated in wax biosynthesis (*SlCER6*; Vogg et al., 2004; Smirnova et al., 2013), cutin biosynthesis (*SlCYP86A69*; Shi et al., 2013; *SlGPAT6*; Petit et al., 2016) and polymerization (*SlCUS1*; Petit et al., 2014), and regulation of flavonoid biosynthesis (*SlMYB12*; Fernandez-Moreno et al., 2016); and (iii) deciphering the regulation of epidermis (*HD-Zip IV*; Isaacson et al., 2009).

CONCLUDING REMARKS AND PERSPECTIVES

Thanks to its thick astomatous fruit cuticle that is easy to study and the wealth of mutants and lines with altered expression of cuticle-related genes already available, tomato provides an excellent model for deciphering the molecular determinants of cuticle formation, structure, and properties. As detailed in **Table 1**, reverse and forward genetics approaches led to the isolation of tomato genes involved in several cuticle-associated biosynthetic pathways including wax biosynthesis (*SlCER6*, *SLTTS1*, and *SlTTS2*); cutin biosynthesis (*SlCYP86A69* and *SlGPAT6*), transport (*SlABCG36/42*), and polymerization (*SlCUS1* and *SlDCR*); and flavonoid biosynthesis (*SlCHS1* and *SlCHS2*). Besides genes encoding various transcription factors (SlSHN1 and SlSHN3, SlMIXTA-like, two HD-Zip IV, SlMYB31, and SlMYB12) or related to ABA (*LYCOPENE CYCLASE b* and *SlPP2C3*) and GA (GA2-OXIDASE) hormonal pathways were shown to regulate cuticle formation and its coordination with epidermal patterning.

Altogether these studies demonstrated the interest of both reverse and forward genetic approaches for discovering novel cuticle gene functions and for generating new plant material to study in-depth cuticle architecture, properties, and interaction with other cell wall components. To face new challenges in cuticle studies, several research avenues can be envisaged in the next future. Analysis of key cuticle genes should be extended to additional family members not yet analyzed for their role in cuticle deposition. An example is that of the GDSL-domain family to which belongs the cutin synthase CUS1 enzyme, whose function was discovered and confirmed through convergent studies in tomato (**Table 1**). The expression of different *CUS1* homologs is deregulated, sometimes oppositely, in several cutin-deficient mutants (Lashbrooke et al., 2015; Petit et al., 2016). By analogy with the recently demonstrated role of GDSL-domain proteins in suberin formation (Ursache et al., 2021), CUS1 homologs (Yeats et al., 2014) may fulfill opposite functions of cutin polymerization and degradation in fruit skin, thereby adapting

[4]https://tomatoma.nbrp.jp/

cuticle formation to rapid fruit growth. Particular attention should also be given to enzymes from the poorly explored phenolic pathway in the epidermis which has evolutionary conserved roles in cuticle properties (Philippe et al., 2020b; Kriegshauser et al., 2021) and to proteins involved in the modification of cell wall polysaccharides (Philippe et al., 2020a). Cell wall enzymes and other proteins likely play central roles in cuticle structure and properties and in the coordination of cuticle deposition with organ development and epidermal patterning (Philippe et al., 2020b). So far, few studies have linked cuticle formation in tomato with hormones, except for ABA (Diretto et al., 2020; Liang et al., 2021) and GA (Li et al., 2020). The role of ABA is not surprising considering the importance of ABA signaling in the response to various stresses (Curvers et al., 2010; Liang et al., 2021), as established in tomato leaves (Martin et al., 2017). More unexpected is the role of GA, the effect of which on cuticle formation is far from being understood (Li et al., 2020). In view of its numerous roles in plant defense and development (Fenn and Giovannoni, 2021), ethylene is also a likely candidate for regulating cuticle formation in tomato fruit. The selection of new "guilt-by-association" target genes for these pathways and processes can be considerably aided by literature mining and/or exploitation of various genomic data (transcriptome, proteome, and metabolome) including co-expression analyses across various fruit cell types and developmental stages (Shinozaki et al., 2018) and across various plant species (Lashbrooke et al., 2016).

In addition to the approaches described above, which often requires previous knowledge of the gene, pathway or process to be targeted, the exploration of untapped genetic diversity, for example, tomato landraces (Conesa et al., 2020), is a way to get off the beaten tracks. This can be very rewarding but also lead to the isolation of challenging genes with no obvious or demonstrated link to the cuticle (Li et al., 2020), or even unknown function (Hovav et al., 2007). One bottleneck in such approach is the phenotyping of large collections (Petit et al., 2017). It can be easy for obvious cuticular defects (Hovav et al., 2007), more challenging for less evident changes (Petit et al., 2014), and complex when low or medium throughput technologies are required, e.g., for wax and cutin monomer analyses (Fernandez-Moreno et al., 2017). In the recent years, high resolution genotyping, whole genome sequencing-based strategies, such as mapping-by-sequencing (MBS) or QTL-seq (Garcia et al., 2016; Bazakos et al., 2017), accelerated gene isolation in tomato (Rothan et al., 2019). However, though identifying the causal mutation can be relatively straightforward in EMS mutants (Garcia et al., 2016), isolating causal genetic variations from natural diversity can be complex since it usually requires crossing the genotype-of-interest with a distant genotype. The subsequent co-segregation in the progeny of numerous cuticle traits unrelated to the trait-of-interest may make phenotyping very difficult and even prohibit high resolution mapping of the genetic variant (Rothan et al., 2016). Association mapping has emerged in the last decade as a powerful tool to discover linkages between gene polymorphism and variations in fruit traits by exploring natural genetic diversity. In tomato, sequencing of hundreds of accessions combined with fruit phenotyping pinpointed genetic variations associated with changes in fruit size, flavor, and color among which *SlMYB12* polymorphisms responsible for pink fruit color (Zhu et al., 2018). More recently, pan-genome analysis of hundreds of wild and cultivated tomato accessions further uncovered numerous unknown genes and genetic variations underlying fruit traits (Gao et al., 2019; Alonge et al., 2020). Phenotyping selected panels of sequenced accessions for cuticle-associated traits should yield numerous genetic variations controlling cuticle and skin formation and properties, and help identifying new functions involved in these processes. In addition to the genetic control of cuticle formation, the epigenetic regulation of wax and cutin biosynthesis will be worth exploring in the near future, as a preliminary study has shown that altering histone methylation status has a profound effect on the composition of tomato fruit cuticle (Boureau et al., 2016; **Table 1**).

ACCESSION NUMBERS

Sequence data from this article can be found in the SGN database under accession numbers found in **Table 1**.

AUTHOR CONTRIBUTIONS

CR wrote the manuscript. CB and DM revised and edited the manuscript. All authors contributed to the article and approved the submitted version.

REFERENCES

Adato, A., Mandel, T., Mintz-Oron, S., Venger, I., Levy, D., Yativ, M., et al. (2009). Fruit-surface flavonoid accumulation in tomato is controlled by a SlMYB12-regulated transcriptional network. *PLoS Genet.* 5:e1000777. doi: 10.1371/journal.pgen.1000777

Al-Abdallat, A. M., Al-Debei, H. S., Ayad, J. Y., and Hasan, S. (2014). Over-expression of SlSHN1 gene improves drought tolerance by increasing cuticular wax accumulation in tomato. *Int. J. Mol. Sci.* 15, 19499–19515. doi: 10.3390/ijms151119499

Alonge, M., Wang, X., Benoit, M., Soyk, S., Pereira, L., Zhang, L., et al. (2020). Major impacts of widespread structural variation on gene expression and crop improvement in tomato. *Cell* 182, 145.e23–161.e23. doi: 10.1016/j.cell.2020.05.021

Ballester, A. R., Molthoff, J., de Vos, R., Hekkert, B. L., Orzaez, D., Fernández-Moreno, J. P., et al. (2010). Biochemical and molecular analysis of pink tomatoes: deregulated expression of the gene encoding transcription factor SlMYB12 leads to pink tomato fruit color. *Plant Physiol.* 152, 71–84. doi: 10.1104/pp.109.147322

Bargel, H., and Neinhuis, C. (2005). Tomato (*Lycopersicon esculentum* mill.) fruit growth and ripening as related to the biomechanical properties of fruit skin and isolated cuticle. *J. Exp. Bot.* 56, 1049–1060. doi: 10.1093/jxb/eri098

Barraj Barraj, R., Segado, P., Moreno-González, R., Heredia, A., Fernández-Muñoz, R., and Domínguez, E. (2021). Genome-wide QTL analysis of tomato fruit cuticle deposition and composition. *Hortic. Res.* 8:113. doi: 10.1038/s41438-021-00548-5

Bazakos, C., Hanemian, M., Trontin, C., Jiménez-Gómez, J. M., and Loudet, O. (2017). New strategies and tools in quantitative genetics: how to go from the phenotype to the genotype. *Annu. Rev. Plant Biol.* 68, 435–455. doi: 10.1146/annurev-arplant-042916-040820

Bemer, M., Karlova, R., Ballester, A. R., Tikunov, Y. M., Bovy, A. G., Wolters-Arts, M., et al. (2012). The tomato FRUITFULL homologs TDR4/

FUL1 and BP7/FUL2 regulate ethylene-independent aspects of fruit ripening. *Plant Cell* 24, 4437–4451. doi: 10.1105/tpc.112.103283

Bernard, A., and Joubes, J. (2013). Arabidopsis cuticular waxes: advances in synthesis, export and regulation. *Prog. Lipid Res.* 52, 110–129. doi: 10.1016/j.plipres.2012.10.002

Boureau, L., How-Kit, A., Teyssier, E., Drevensek, S., Rainieri, M., Joubès, J., et al. (2016). A CURLY LEAF homologue controls both vegetative and reproductive development of tomato plants. *Plant Mol. Biol.* 90, 485–501. doi: 10.1007/s11103-016-0436-0

Buxdorf, K., Rubinsky, G., Barda, O., Burdman, S., Aharoni, A., and Levy, M. (2014). The transcription factor SlSHINE3 modulates defense responses in tomato plants. *Plant Mol. Biol.* 84, 37–47. doi: 10.1007/s11103-013-0117-1

Chechanovsky, N., Hovav, R., Frenkel, R., Faigenboim, A., Eselson, Y., Petreikov, M., et al. (2019). Low temperature upregulates *cwp* expression and modifies alternative splicing patterns, increasing the severity of *cwp*-induced tomato fruit cuticular microfissures. *Hortic. Res.* 6:122. doi: 10.1038/s41438-019-0204-9

Conesa, M. À., Fullana-Pericàs, M., Granell, A., and Galmés, J. (2020). Mediterranean long shelf-life landraces: an untapped genetic resource for tomato improvement. *Front. Plant Sci.* 10:1651. doi: 10.3389/fpls.2019.01651

Cui, L., Qiu, Z., Wang, Z., Gao, J., Guo, Y., Huang, Z., et al. (2017). Fine mapping of a gene (*ER4.1*) that causes epidermal reticulation of tomato fruit and characterization of the associated transcriptome. *Front. Plant Sci.* 8:1254. doi: 10.3389/fpls.2017.01254

Curvers, K., Seifi, H., Mouille, G., de Rycke, R., Asselbergh, B., and Van Hecke, A. (2010). Abscisic acid deficiency causes changes in cuticle permeability and pectin composition that influence tomato resistance to *Botrytis cinerea*. *Plant Physiol.* 154, 847–860. doi: 10.1104/pp.110.158972

Diretto, G., Frusciante, S., Fabbri, C., Schauer, N., Busta, L., Wang, Z., et al. (2020). Manipulation of β-carotene levels in tomato fruits results in increased ABA content and extended shelf life. *Plant Biotechnol. J.* 18, 1185–1199. doi: 10.1111/pbi.13283

Elejalde-Palmett, C., Martinez San Segundo, I., Garroum, I., Charrier, L., De Bellis, D., Mucciolo, A., et al. (2021). ABCG transporters export cutin precursors for the formation of the plant cuticle. *Curr. Biol.* 31, 2111.e9–2123.e9. doi: 10.1016/j.cub.2021.02.056

Eshed, Y., and Zamir, D. (1995). An introgression line population of *Lycopersicon pennellii* in the cultivated tomato enables the identification and fine mapping of yield-associated QTL. *Genetics* 141, 1147–1162. doi: 10.1093/genetics/141.3.1147

España, L., Heredia-Guerrero, J. A., Reina-Pinto, J. J., Fernández-Muñoz, R., Heredia, A., and Domínguez, E. (2014). Transient silencing of CHALCONE SYNTHASE during fruit ripening modifies tomato epidermal cells and cuticle properties. *Plant Physiol.* 166, 1371–1386. doi: 10.1104/pp.114.246405

Fawke, S., Torode, T. A., Gogleva, A., Fich, E. A., Sørensen, I., Yunusov, T., et al. (2019). Glycerol-3-phosphate acyltransferase 6 controls filamentous pathogen interactions and cell wall properties of the tomato and *Nicotiana benthamiana* leaf epidermis. *New Phytol.* 223, 1547–1559. doi: 10.1111/nph.15846

Feder, A., Jensen, S., Wang, A., Courtney, L., Middleton, L., Van Eck, J., et al. (2020). Tomato fruit as a model for tissue-specific gene silencing in crop plants. *Hortic. Res.* 7:142. doi: 10.1038/s41438-020-00363-4

Fenn, M. A., and Giovannoni, J. J. (2021). Phytohormones in fruit development and maturation. *Plant J.* 105, 446–458. doi: 10.1111/tpj.15112

Fernandez, A. I., Viron, N., Alhagdow, M., Karimi, M., Jones, M., Amsellem, Z., et al. (2009). Flexible tools for gene expression and silencing in tomato. *Plant Physiol.* 151, 1729–1740. doi: 10.1104/pp.109.147546

Fernandez-Moreno, J. P., Levy-Samoha, D., Malitsky, S., Monforte, A. J., Orzaez, D., Aharoni, A., et al. (2017). Uncovering tomato quantitative trait loci and candidate genes for fruit cuticular lipid composition using the *Solanum pennellii* introgression line population. *J. Exp. Bot.* 68, 2703–2716. doi: 10.1093/jxb/erx134

Fernandez-Moreno, J. P., Tzfadia, O., Forment, J., Presa, S., Rogachev, I., Meir, S., et al. (2016). Characterization of a new pink-fruited tomato mutant results in the identification of a null allele of the SlMYB12 transcription factor. *Plant Physiol.* 171, 1821–1836. doi: 10.1104/pp.16.00282

Fich, E. A., Fisher, J., Zamir, D., and Rose, J. (2020). Transpiration from tomato fruit occurs primarily via trichome-associated transcuticular polar pores. *Plant Physiol.* 184, 1840–1852. doi: 10.1104/pp.20.01105

Fich, E. A., Segerson, N. A., and Rose, J. K. (2016). The plant polyester cutin: biosynthesis, structure, and biological roles. *Annu. Rev. Plant Biol.* 67, 207–233. doi: 10.1146/annurev-arplant-043015-111929

Filippis, I., Lopez-Cobollo, R., Abbott, J., Butcher, S., and Bishop, G. J. (2013). Using a periclinal chimera to unravel layer-specific gene expression in plants. *Plant J.* 75, 1039–1049. doi: 10.1111/tpj.12250

Gao, L., Gonda, I., Sun, H., Ma, Q., Bao, K., Tieman, D. M., et al. (2019). The tomato pan-genome uncovers new genes and a rare allele regulating fruit flavor. *Nat. Genet.* 51, 1044–1051. doi: 10.1038/s41588-019-0410-2

Garcia, V., Bres, C., Just, D., Fernandez, L., Tai, F. W. J., Mauxion, J. P., et al. (2016). Rapid identification of causal mutations in tomato EMS populations via mapping-by-sequencing. *Nat. Protoc.* 11, 2401–2418. doi: 10.1038/nprot.2016.143

Giménez, E., Dominguez, E., Pineda, B., Heredia, A., Moreno, V., Lozano, R., et al. (2015). Transcriptional activity of the MADS box ARLEQUIN/TOMATO AGAMOUS-LIKE1 gene is required for cuticle development of tomato fruit. *Plant Physiol.* 168, 1036–1048. doi: 10.1104/pp.15.00469

Girard, A. L., Mounet, F., Lemaire-Chamley, M., Gaillard, C., Elmorjani, K., Vivancos, J., et al. (2012). Tomato GDSL1 is required for cutin deposition in the fruit cuticle. *Plant Cell* 24, 3119–3134. doi: 10.1105/tpc.112.101055

Guillet, C., Aboul-Soud, M. A., Le Menn, A., Viron, N., Pribat, A., Germain, V., et al. (2012). Regulation of the fruit-specific PEP carboxylase SlPPC2 promoter at early stages of tomato fruit development. *PLoS One* 7:e36795. doi: 10.1371/journal.pone.0036795

Gupta, P., Reddaiah, B., Salava, H., Upadhyaya, P., Tyagi, K., Sarma, S., et al. (2017). Next-generation sequencing (NGS)-based identification of induced mutations in a doubly mutagenized tomato (*Solanum lycopersicum*) population. *Plant J.* 92, 495–508. doi: 10.1111/tpj.13654

Halinski, L. P., Kalkowska, M., Kalkowski, M., Piorunowska, J., Topolewska, A., and Stepnowski, P. (2015). Cuticular wax variation in the tomato (*Solanum lycopersicum* L.), related wild species and their interspecific hybrids. *Biochem. Syst. Ecol.* 60, 215–224. doi: 10.1016/j.bse.2015.04.030

Heredia, A., Heredia-Guerrero, J. A., and Domínguez, E. (2015). CHS silencing suggests a negative cross-talk between wax and flavonoid pathways in tomato fruit cuticle. *Plant Signal. Behav.* 10:e1019979. doi: 10.1080/15592324.2015.1019979

Hovav, R., Chehanovsky, N., Moy, M., Jetter, R., and Schaffer, A. A. (2007). The identification of a gene (Cwp1), silenced during Solanum evolution, which causes cuticle microfissuring and dehydration when expressed in tomato fruit. *Plant J.* 52, 627–639. doi: 10.1111/j.1365-313X.2007.03265.x

Isaacson, T., Kosma, D. K., Matas, A. J., Buda, G. J., He, Y., Yu, B., et al. (2009). Cutin deficiency in the tomato fruit cuticle consistently affects resistance to microbial infection and biomechanical properties, but not transpirational water loss. *Plant J.* 60, 363–377. doi: 10.1111/j.1365-313X.2009.03969.x

Joubès, J., Phan, T. H., Just, D., Rothan, C., Bergounioux, C., Raymond, P., et al. (1999). Molecular and biochemical characterization of the involvement of cyclin-dependent kinase A during the early development of tomato fruit. *Plant Physiol.* 121, 857–869. doi: 10.1104/pp.121.3.857

Just, D., Garcia, V., Fernandez, L., Bres, C., Mauxion, J. P., Petit, J., et al. (2013). Micro-tom mutants for functional analysis of target genes and discovery of new alleles in tomato. *Plant Biotechnol.* 30, 1–7. doi: 10.5511/plantbiotechnology.13.0622a

Kimbara, J., Yoshida, M., Ito, H., Hosoi, K., Kusano, M., Kobayashi, M., et al. (2012). A novel class of sticky peel and light green mutations causes cuticle deficiency in leaves and fruits of tomato (*Solanum lycopersicum*). *Planta* 236, 1559–1570. doi: 10.1007/s00425-012-1719-6

Kimbara, J., Yoshida, M., Ito, H., Kitagawa, M., Takada, W., Hayashi, K., et al. (2013). Inhibition of CUTIN DEFICIENT 2 causes defects in cuticle function and structure and metabolite changes in tomato fruit. *Plant Cell Physiol.* 54, 1535–1548. doi: 10.1093/pcp/pct100

Klee, H. J., and Giovannoni, J. J. (2011). Genetics and control of tomato fruit ripening and quality attributes. *Annu. Rev. Genet.* 45, 41–59. doi: 10.1146/annurev-genet-110410-132507

Kosma, D. K., Parsons, E. P., Isaacson, T., Lü, S., Rose, J. K., and Jenks, M. A. (2010). Fruit cuticle lipid composition during development in tomato ripening mutants. *Physiol. Plant.* 139, 107–117. doi: 10.1111/j.1399-3054.2009.01342.x

Kriegshauser, L., Knosp, S., Grienenberger, E., Tatsumi, K., Gütle, D. D., Sørensen, I., et al. (2021). Function of the HYDROXYCINNAMOYL-CoA:SHIKIMATE HYDROXYCINNAMOYL TRANSFERASE is evolutionarily conserved in embryophytes. *Plant Cell.* 33, 1472–1491. doi: 10.1093/plcell/koab044

Kumar, R., Tamboli, V., Sharma, R., and Sreelakshmi, Y. (2018). NAC-NOR mutations in tomato Penjar accessions attenuate multiple metabolic processes and prolong the fruit shelf life. *Food Chem.* 259, 234–244. doi: 10.1016/j.foodchem.2018.03.135

Lara, I., Heredia, A., and Domínguez, E. (2019). Shelf life potential and the fruit cuticle: the unexpected player. *Front. Plant Sci.* 10:770. doi: 10.3389/fpls.2019.00770

Lashbrooke, J., Adato, A., Lotan, O., Alkan, N., Tsimbalist, T., Rechav, K., et al. (2015). The tomato MIXTA-like transcription factor coordinates fruit epidermis conical cell development and cuticular lipid biosynthesis and assembly. *Plant Physiol.* 169, 2553–2571. doi: 10.1104/pp.15.01145

Lashbrooke, J., Cohen, H., Levy-Samocha, D., Tzfadia, O., Panizel, I., Zeisler, V., et al. (2016). MYB107 and MYB9 homologs regulate suberin deposition in angiosperms. *Plant Cell* 28, 2097–2116. doi: 10.1105/tpc.16.00490

Leide, J., Hildebrandt, U., Reussing, K., Riederer, M., and Vogg, G. (2007). The developmental pattern of tomato fruit wax accumulation and its impact on cuticular transpiration barrier properties: effects of a deficiency in a beta-ketoacyl-coenzyme A synthase (LeCER6). *Plant Physiol.* 144, 1667–1679. doi: 10.1104/pp.107.099481

Leide, J., Hildebrandt, U., Vogg, G., and Riederer, M. (2011). The positional sterile (ps) mutation affects cuticular transpiration and wax biosynthesis of tomato fruits. *J. Plant Physiol.* 168, 871–877. doi: 10.1016/j.jplph.2010.11.014

Lemaire-Chamley, M., Petit, J., Garcia, V., Just, D., Baldet, P., Germain, V., et al. (2005). Changes in transcriptional profiles are associated with early fruit tissue specialization in tomato. *Plant Physiol.* 139, 750–769. doi: 10.1104/pp.105.063719

Li, R., Sun, S., Wang, H., Wang, K., Yu, H., Zhou, Z., et al. (2020). FIS1 encodes a GA2-oxidase that regulates fruit firmness in tomato. *Nat. Commun.* 11:5844. doi: 10.1038/s41467-020-19705-w

Liang, B., Sun, Y., Wang, J., Zheng, Y., Zhang, W., Xu, Y., et al. (2021). Tomato protein phosphatase 2C influences the onset of fruit ripening and fruit glossiness. *J. Exp. Bot.* 72, 2403–2418. doi: 10.1093/jxb/eraa593

Martin, L., Romero, P., Fich, E. A., Domozych, D. S., and Rose, J. (2017). Cuticle biosynthesis in tomato leaves is developmentally regulated by abscisic acid. *Plant Physiol.* 174, 1384–1398. doi: 10.1104/pp.17.00387

Martin, L. B., Sherwood, R. W., Nicklay, J. J., Yang, Y., Muratore-Schroeder, T. L., Anderson, E. T., et al. (2016). Application of wide selected-ion monitoring data-independent acquisition to identify tomato fruit proteins regulated by the CUTIN DEFICIENT2 transcription factor. *Proteomics* 16, 2081–2094. doi: 10.1002/pmic.201500450

Matas, A. J., Yeats, T. H., Buda, G. J., Zheng, Y., Chatterjee, S., Tohge, T., et al. (2011). Tissue- and cell-type specific transcriptome profiling of expanding tomato fruit provides insights into metabolic and regulatory specialization and cuticle formation. *Plant Cell* 23, 3893–3910. doi: 10.1105/tpc.111.091173

Meissner, R., Jacobson, Y., Melamed, S., Levyatuv, S., Shalev, G., Ashri, A., et al. (1997). A new model system for tomato genetics. *Plant J.* 12, 1465–1472. doi: 10.1046/j.1365-313x.1997.12061465.x

Menda, N., Semel, Y., Peled, D., Eshed, Y., and Zamir, D. (2004). In silico screening of a saturated mutation library of tomato. *Plant J.* 38, 861–872. doi: 10.1111/j.1365-313X.2004.02088.x

Minoia, S., Petrozza, A., D'Onofrio, O., Piron, F., Mosca, G., Sozio, G., et al. (2010). A new mutant genetic resource for tomato crop improvement by TILLING technology. *BMC Res. Notes* 3:69. doi: 10.1186/1756-0500-3-69

Mintz-Oron, S., Mandel, T., Rogachev, I., Feldberg, L., Lotan, O., Yativ, M., et al. (2008). Gene expression and metabolism in tomato fruit surface tissues. *Plant Physiol.* 147, 823–851. doi: 10.1104/pp.108.116004

Moreira, C., Bento, A., Pais, J., Petit, J., Escórcio, R., Correia, V. G., et al. (2020). An ionic liquid extraction that preserves the molecular structure of cutin shown by nuclear magnetic resonance. *Plant Physiol.* 184, 592–606. doi: 10.1104/pp.20.01049

Nadakuduti, S. S., Pollard, M., Kosma, D. K., Allen, C. Jr., Ohlrogge, J. B., and Barry, C. S. (2012). Pleiotropic phenotypes of the sticky peel mutant provide new insight into the role of CUTIN DEFICIENT2 in epidermal cell function in tomato. *Plant Physiol.* 159, 945–960. doi: 10.1104/pp.112.198374

Ofner, I., Lashbrooke, J., Pleban, T., Aharoni, A., and Zamir, D. (2016). *Solanum pennellii* backcross inbred lines (BILs) link small genomic bins with tomato traits. *Plant J.* 87, 151–160. doi: 10.1111/tpj.13194

Okabe, Y., Asamizu, E., Saito, T., Matsukura, C., Ariizumi, T., Brès, C., et al. (2011). Tomato TILLING technology: development of a reverse genetics tool for the efficient isolation of mutants from micro-tom mutant libraries. *Plant Cell Physiol.* 52, 1994–2005. doi: 10.1093/pcp/pcr134

Petit, J., Bres, C., Just, D., Garcia, V., Mauxion, J. P., Marion, D., et al. (2014). Analyses of tomato fruit brightness mutants uncover both cutin-deficient and cutin-abundant mutants and a new hypomorphic allele of GDSL lipase. *Plant Physiol.* 164, 888–906. doi: 10.1104/pp.113.232645

Petit, J., Bres, C., Mauxion, J. P., Bakan, B., and Rothan, C. (2017). Breeding for cuticle-associated traits in crop species: traits, targets, and strategies. *J. Exp. Bot.* 68, 5369–5387. doi: 10.1093/jxb/erx341

Petit, J., Bres, C., Mauxion, J. P., Tai, F. W., Martin, L. B., Fich, E. A., et al. (2016). The glycerol-3-phosphate acyltransferase GPAT6 from tomato plays a central role in fruit cutin biosynthesis. *Plant Physiol.* 171, 894–913. doi: 10.1104/pp.16.00409

Philippe, G., Gaillard, C., Petit, J., Geneix, N., Dalgalarrondo, M., Bres, C., et al. (2016). Ester cross-link profiling of the cutin polymer of wild-type and cutin synthase tomato mutants highlights different mechanisms of polymerization. *Plant Physiol.* 170, 807–820. doi: 10.1104/pp.15.01620

Philippe, G., Geneix, N., Petit, J., Guillon, F., Sandt, C., Rothan, C., et al. (2020a). Assembly of tomato fruit cuticles: a cross-talk between the cutin polyester and cell wall polysaccharides. *New Phytol.* 226, 809–822. doi: 10.1111/nph.16402

Philippe, G., Sørensen, I., Jiao, C., Sun, X., Fei, Z., Domozych, D. S., et al. (2020b). Cutin and suberin: assembly and origins of specialized lipidic cell wall scaffolds. *Curr. Opin. Plant Biol.* 55, 11–20. doi: 10.1016/j.pbi.2020.01.008

Renaudin, J. P., Deluche, C., Cheniclet, C., Chevalier, C., and Frangne, N. (2017). Cell layer-specific patterns of cell division and cell expansion during fruit set and fruit growth in tomato pericarp. *J. Exp. Bot.* 68, 1613–1623. doi: 10.1093/jxb/erx058

Romero, P., and Rose, J. (2019). A relationship between tomato fruit softening, cuticle properties and water availability. *Food Chem.* 295, 300–310. doi: 10.1016/j.foodchem.2019.05.118

Rothan, C., Bres, C., Garcia, V., and Just, D. (2016) in *Tomato Resources for Functional Genomics*. eds. M. Causse, J. Giovannoni, M. Bouzayen and M. Zouine (Berlin Heidelberg: Springer), 75–94.

Rothan, C., Diouf, I., and Causse, M. (2019). Trait discovery and editing in tomato. *Plant J.* 97, 73–90. doi: 10.1111/tpj.14152

Saito, T., Ariizumi, T., Okabe, Y., Asamizu, E., Hiwasa-Tanase, K., and Fukuda, N. (2011). TOMATOMA: a novel tomato mutant database distributing micro-tom mutant collections. *Plant Cell Physiol.* 52, 283–296. doi: 10.1093/pcp/pcr004

Saladié, M., Matas, A. J., Isaacson, T., Jenks, M. A., Goodwin, S. M., Niklas, K. J., et al. (2007). A reevaluation of the key factors that influence tomato fruit softening and integrity. *Plant Physiol.* 144, 1012–1028. doi: 10.1104/pp.107.097477

Segado, P., Heredia-Guerrero, J. A., Heredia, A., and Domínguez, E. (2020). Cutinsomes and CUTIN SYNTHASE1 function sequentially in tomato fruit cutin deposition. *Plant Physiol.* 183, 1622–1637. doi: 10.1104/pp.20.00516

Shi, J. X., Adato, A., Alkan, N., He, Y., Lashbrooke, J., Matas, A. J., et al. (2013). The tomato SlSHINE3 transcription factor regulates fruit cuticle formation and epidermal patterning. *New Phytol.* 197, 468–480. doi: 10.1111/nph.12032

Shinozaki, Y., Nicolas, P., Fernandez-Pozo, N., Ma, Q., Evanich, D. J., Shi, Y., et al. (2018). High-resolution spatiotemporal transcriptome mapping of tomato fruit development and ripening. *Nat. Commun.* 9, 364. doi: 10.1038/s41467-017-02782-9

Smirnova, A., Leide, J., and Riederer, M. (2013). Deficiency in a very-long-chain fatty acid β-ketoacyl-coenzyme a synthase of tomato impairs microgametogenesis and causes floral organ fusion. *Plant Physiol.* 161, 196–209. doi: 10.1104/pp.112.206656

Szymański, J., Bocobza, S., Panda, S., Sonawane, P., Cárdenas, P. D., Lashbrooke, J., et al. (2020). Analysis of wild tomato introgression lines elucidates the genetic basis of transcriptome and metabolome variation underlying fruit traits and pathogen response. *Nat. Genet.* 52, 1111–1121. doi: 10.1038/s41588-020-0690-6

Szymanski, J., Levin, Y., Savidor, A., Breitel, D., Chappell-Maor, L., Heinig, U., et al. (2017). Label-free deep shotgun proteomics reveals protein dynamics during tomato fruit tissues development. *Plant J.* 90, 396–417. doi: 10.1111/tpj.13490

Tomato Genome Consortium (2012). The tomato genome sequence provides insights into fleshy fruit evolution. *Nature* 485, 635–641. doi: 10.1038/nature11119

Ursache, R., De Jesus Vieira Teixeira, C., Dénervaud Tendon, V., Gully, K., De Bellis, D., Schmid-Siegert, E., et al. (2021). GDSL-domain proteins have key roles in suberin polymerization and degradation. *Nat. Plants* 7, 353–364. doi: 10.1038/s41477-021-00862-9

Vogg, G., Fischer, S., Leide, J., Emmanuel, E., Jetter, R., Levy, A. A., et al. (2004). Tomato fruit cuticular waxes and their effects on transpiration barrier properties: functional characterization of a mutant deficient in a very-long-chain fatty acid beta-ketoacyl-CoA synthase. *J. Exp. Bot.* 55, 1401–1410. doi: 10.1093/jxb/erh149

Wang, R., Angenent, G. C., Seymour, G., and de Maagd, R. A. (2020). Revisiting the role of master regulators in tomato ripening. *Trends Plant Sci.* 25, 291–301. doi: 10.1016/j.tplants.2019.11.005

Xin, A., Fei, Y., Molnar, A., and Fry, S. C. (2021). Cutin:cutin-acid endo-transacylase (CCT), a cuticle-remodelling enzyme activity in the plant epidermis. *Biochem. J.* 478, 777–798. doi: 10.1042/BCJ20200835

Xiong, C., Xie, Q., Yang, Q., Sun, P., Gao, S., Li, H., et al. (2020). WOOLLY, interacting with MYB transcription factor MYB31, regulates cuticular wax biosynthesis by modulating CER6 expression in tomato. *Plant J.* 103, 323–337. doi: 10.1111/tpj.14733

Yeats, T. H., Buda, G. J., Wang, Z., Chehanovsky, N., Moyle, L. C., Jetter, R., et al. (2012a). The fruit cuticles of wild tomato species exhibit architectural and chemical diversity, providing a new model for studying the evolution of cuticle function. *Plant J.* 69, 655–666. doi: 10.1111/j.1365-313X.2011.04820.x

Yeats, T. H., Howe, K. J., Matas, A. J., Buda, G. J., Thannhauser, T. W., and Rose, J. K. (2010). Mining the surface proteome of tomato (*Solanum lycopersicum*) fruit for proteins associated with cuticle biogenesis. *J. Exp. Bot.* 61, 3759–3771. doi: 10.1093/jxb/erq194

Yeats, T. H., Huang, W., Chatterjee, S., Viart, H. M., Clausen, M. H., Stark, R. E., et al. (2014). Tomato cutin deficient 1 (CD1) and putative orthologs comprise an ancient family of cutin synthase-like (CUS) proteins that are conserved among land plants. *Plant J.* 77, 667–675. doi: 10.1111/tpj.12422

Yeats, T. H., Martin, L. B., Viart, H. M., Isaacson, T., He, Y., Zhao, L., et al. (2012b). The identification of cutin synthase: formation of the plant polyester cutin. *Nat. Chem. Biol.* 8, 609–611. doi: 10.1038/nchembio.960

Zhang, C., Wang, T., Li, J., Zhang, D., Xie, Q., Munir, S., et al. (2021). Functional gain of fruit netted-cracking in an introgression line of tomato with higher expression of the FNC gene. *Front. Agric. Sci. Eng.* 8, 280–291. doi: 10.15302/J-FASE-2020374

Zhu, G., Wang, S., Huang, Z., Zhang, S., Liao, Q., Zhang, C., et al. (2018). Rewiring of the fruit metabolome in tomato breeding. *Cell* 172, 249.e12–261.e12. doi: 10.1016/j.cell.2017.12.019

Conflict of Interest: The authors declare that the research was conducted in the absence of any commercial or financial relationships that could be construed as a potential conflict of interest.

Publisher's Note: All claims expressed in this article are solely those of the authors and do not necessarily represent those of their affiliated organizations, or those of the publisher, the editors and the reviewers. Any product that may be evaluated in this article, or claim that may be made by its manufacturer, is not guaranteed or endorsed by the publisher.

frontiers in Plant Science

ORIGINAL RESEARCH
published: 07 December 2021
doi: 10.3389/fpls.2021.778745

Changes in Morphology, Metabolism and Composition of Cuticular Wax in Zucchini Fruit During Postharvest Cold Storage

Fátima Carvajal[1], Alejandro Castro-Cegrí[1], Raquel Jiménez-Muñoz[1], Manuel Jamilena[2], Dolores Garrido[1] and Francisco Palma[1]**

[1]Department of Plant Physiology, Facultad de Ciencias, University of Granada, Granada, Spain, [2]Department of Biology and Geology, Agrifood Campus of International Excellence (CeiA3), University of Almería, Almería, Spain

Cuticle composition is an important economic trait in agriculture, as it is the first protective barrier of the plant against environmental conditions. The main goal of this work was to study the role of the cuticular wax in maintaining the postharvest quality of zucchini fruit, by comparing two commercial varieties with contrasting behavior against low temperatures; the cold-tolerant variety 'Natura', and the cold-sensitive 'Sinatra', as well as 'Sinatra' fruit with induced-chilling tolerance through a preconditioning treatment (15°C for 48 h). The freshly-harvested 'Natura' fruit had a well-detectable cuticle with a significant lower permeability and a subset of 15 up-regulated cuticle-related genes. SEM showed that zucchini epicuticular waxes mainly consisted of round-shaped crystals and clusters of them, and areas with more dense crystal deposition were found in fruit of 'Natura' and of preconditioned 'Sinatra'. The cuticular wax load per surface was higher in 'Natura' than in 'Sinatra' fruit at harvest and after 14 days at 4°C. In addition, total cuticular wax load only increased in 'Natura' and preconditioned 'Sinatra' fruit with cold storage. With respect to the chemical composition of the waxes, the most abundant components were alkanes, in both 'Natura' and 'Sinatra', with similar values at harvest. The total alkane content only increased in 'Natura' fruit and in the preconditioned 'Sinatra' fruit after cold storage, whereas the amount of total acids decreased, with the lowest values observed in the fruit that showed less chilling injury (CI) and weight loss. Two esters were detected, and their content also decreased with the storage in both varieties, with a greater reduction observed in the cold-tolerant variety in response to low temperature. Gene expression analysis showed significant differences between varieties, especially in *CpCER1-like* and *CpCER3-like* genes, involved in alkane production, as well as in the transcription factors *CpWIN1-like* and *CpFUL1-like*, associated with cuticle development and epidermal wax accumulation in other species. These results suggest an important role of the alkane biosynthetic pathway and cuticle morphology in maintaining the postharvest quality of zucchini fruit during the storage at low temperatures.

Keywords: *Cucurbita pepo*, postharvest, cold stress, cuticle, cuticular wax, alkanes

OPEN ACCESS

Edited by:
Amauri Bueno, Julius Maximilian University of Würzburg, Germany

Reviewed by:
Hua Huang, Chinese Academy of Sciences, China

***Correspondence:**
Dolores Garrido
dgarrido@ugr.es
Francisco Palma
fpalma@ugr.es

Specialty section:
This article was submitted to Plant Physiology, a section of the journal Frontiers in Plant Science

Received: *17 September 2021*
Accepted: *12 November 2021*
Published: *07 December 2021*

Citation:
Carvajal F, Castro-Cegrí A, Jiménez-Muñoz R, Jamilena M, Garrido D and Palma F (2021) Changes in Morphology, Metabolism and Composition of Cuticular Wax in Zucchini Fruit During Postharvest Cold Storage. Front. Plant Sci. 12:778745. doi: 10.3389/fpls.2021.778745

INTRODUCTION

The cuticle is a barrier that was first developed in plants during their colonization to dry land. Due to its lipidic composition, the cuticle not only prevents dehydration but it is also a protective barrier against biotic and abiotic stress, and plays a role in preventing damage from mechanical stress (Domínguez et al., 2011). The cuticle is synthesized by the epidermal cell layer and is composed of a cutin matrix, in contact with the cell wall, and a complex group of different cuticular waxes that embed and cover the cutin matrix, constituting intracuticular and epicuticular waxes, respectively, (Ensikat et al., 2006; Koch and Ensikat, 2008; Buschhaus and Jetter, 2011). Cuticular waxes consist of a mixture of very-long chain fatty acids (VLCFAs) and its derivatives, which are synthesized by two pathways: the alcohol-forming pathway, which generates primary alcohols and esters, and the alkane-forming pathway, which produces aldehydes, alkanes, secondary alcohols, and ketones (Yeats and Rose, 2013). The biosynthesis of cuticular wax by one metabolic pathway or another may be regulated by different compounds, such as abscisic acid (Wang et al., 2015a; Romero and Lafuente, 2020). The predominant components of the waxes in the cuticle of many fruits are VLC-alkanes, which account for 50–80% of total wax content, and nonacosane (C29) or hentriacontane (C31), which are the majority. In addition, fatty acid alcohols, aldehydes, ketones, and triterpenoids have also been detected (Bauer et al., 2004; Parsons et al., 2012; Wang et al., 2015a; Wu et al., 2018).

In fleshy fruits, cuticular waxes play a crucial role in minimizing water loss/uptake through the surface, providing mechanical support, preventing fruit softening, and increasing pathogen resistance (Martin and Rose, 2013; Tafolla-Arellano et al., 2017; Trivedi et al., 2019). In blueberry fruits, wax removal decreased postharvest fruit quality during cold storage, accelerating water loss and decay (Chu et al., 2018). The cuticle in fruits is usually thicker than in leaves, and the structure and composition of cuticular wax has been shown to be closely related to the postharvest quality of fruit (Lara Ayala et al., 2014, 2019). The composition of cuticular wax varies widely among fruit species and cultivars (Trivedi et al., 2019), and many of the cuticular properties are affected by wax composition. The presence of long-chain alkanes and aldehydes has been found to increase water impermeability of fruit cuticles. With regard to this, a positive correlation between cuticle composition and water loss has been reported, finding that the alkane content was a significant determinant of water permeability in pepper (Parsons et al., 2012).

With respect to the biosynthetic pathway of the cuticular wax, most of the studies have been conducted in *Arabidopsis thaliana*, and many of the genes involved in alkane biosynthesis have been identified from *eceriferum* mutants (McNevin et al., 1993). Among them, CER2, CER26, CER1, and CER3 have been found to be determinant genes for the proper development of the cuticle, and shown to be involved in alkane biosynthesis. CER2 mutants were shown to have a severe wax deficiency and accumulated 26C wax components, being deficient for components longer than 28C (Haslam et al., 2017). CER26 mutants were shown to have a similar behavior to CER2, being specifically affected in the VLC-fatty acid elongation process (Pascal et al., 2013). Mutants with a CER1 loss-of-function have cuticles with a reduced number of alkanes and its derivatives (Bourdenx et al., 2011). CER3/WAX2 is also involved in the production of wax, with the *wax2* mutants having a decreased wax content of about 80% compared to wild type plants (Chen et al., 2003). WAX2 catalyzes the reduction of VLC-acyl-CoAs to intermediate VLC-aldehydes, which are then converted to alkanes through decarbonylation by CER1 (Bernard et al., 2012). The most important genes belonging to the alkane-forming pathway that lead to the formation of VLC-alkanes are CER1 and CER3. They interact physically, and it has been proposed that they are the core components of a VLC-alkane synthesis complex (Bernard et al., 2012). CER3 catalyzes the reduction of VLC-acyl-CoAs, forming aldehydes that are decarbonylated by CER1 to VLC-alkanes (Bernard et al., 2012). Homologues to these genes have been characterized in other species; in cucumber, the importance of CER1 and CER3 in wax biosynthesis and its implication in stress and water permeability has been investigated. The *CsCER1* transcript was induced by abiotic stresses, and transgenic RNAi lines with a knock down of the transcript were altered in cuticular wax biosynthesis (Wang et al., 2015a). *CsWAX2* (CER3) also played a significant role in the plant's response to biotic and abiotic stresses (Wang et al., 2015b). Along with the genes encoding for enzymes responsible for the biosynthesis of wax components, several transcription factors have been identified as regulators of the cuticular wax biosynthesis (Hen-Avivi et al., 2014), such as members of the SHINE clade of AP2-domain transcription factors, which are responsible for cuticle formation and deposition in several fruits, such as tomato, sweet cherry, apple, and mango (Alkio et al., 2012; Shi et al., 2013; Lashbrooke et al., 2015; Tafolla-Arellano et al., 2017).

During the postharvest cold storage of *Cucurbita pepo*, the fruits experience chilling injury (CI), a disease triggered by low temperatures, which affects fruit quality and is responsible for economic losses, with the intensity of the damages dependent on the variety (Carvajal et al., 2011). The search for resistance and improvement of zucchini fruit quality during postharvest cold storage has resulted in the selection of varieties that are more resistant to CI, such as 'Natura', and this resistant variety has been compared to a 'Sinatra', a very sensitive variety. The biochemical and genetic differences that make these two varieties resistant and sensitive, respectively, have been thoroughly investigated (Palma et al., 2014a,b; Carvajal et al., 2017), and different treatments have been applied to search for improvements in the quality of the fruit during cold storage. Fruit from the cold sensitive 'Sinatra', when preconditioned at 15°C for 48 h before storage at 4°C (PCT) were able to resist cold storage and improved in quality during the postharvest period (Carvajal et al., 2015). In a transcriptomic study, several genes that were differentially expressed during cold storage were selected (Carvajal et al., 2018b), and among them genes related to cuticular wax deposition were found. Since one of the differences

between 'Natura' and 'Sinatra' was the lower weight loss in the resistant 'Natura', one of the possibilities for cold resistance was a difference in the cuticle between these varieties. Based on this hypothesis, in a first approach, we detected that long-term cold storage diminished the expression of genes belonging to the fatty acid elongation complex and the ECERIFERUM proteins 1 and 3 (CER1 and CER3; Carvajal et al., 2018a). To shed light on the involvement of the cuticle in the maintenance of postharvest quality of zucchini fruit, the aim of the present work was to analyze the cuticle properties and the differences in cuticular waxes between the varieties 'Natura' and 'Sinatra', as well as in PCT 'Sinatra' fruit. Changes in permeability, structure, composition, and expression of cuticle-related genes will be discussed in terms of cold resistance.

MATERIALS AND METHODS

Fruit Material

Zucchini fruit (*Cucurbita pepo* L. Morphotype *Zucchini*) from the commercial varieties 'Natura' (EnzaZaden) and 'Sinatra' (Clause-Tezier) were provided by "Hortofrutícola La Ñeca S.L." Freshly-harvested fruits, free of disease symptoms, mechanical damage and with uniform length, were randomly divided into replicates and stored in a temperature-controlled chamber in permanent darkness at 4°C and 85–90% RH for 14 d. In addition to the control fruit in the case of the 'Sinatra' variety, a group of fruits were also preconditioned at 15°C for 48 h before storage at 4°C (PCT), according to Carvajal et al. (2015). For microscopy and chlorophyll leaching assays, 10 fruits were analyzed per storage time, variety, and treatment, and the experiment was conducted twice. Two more experiments using 18 fruits (three replicates of six fruits each) per storage time, variety, and treatment were performed to analyze the cuticular wax load and composition and to sample exocarp tissue for RNA extraction. For the latter, the tissue was frozen in liquid N_2, ground, and stored at −80°C.

Chlorophyll Leaching Assay

Freshly-harvested 'Natura' and 'Sinatra' fruit were used to assess epidermal permeability through the chlorophyll efflux assay, according to Kosma et al. (2009) with some modifications. Three cylinders were taken from the proximal, equatorial, and distal zones of each fruit using a cork borer. Both cylinder sides were excised with a razor blade resulting in two 3 mm thick discs per cylinder. Discs were washed 3 times in distilled water for 5 min and, lastly, immersed in equal volumes of 80% ethanol and maintained at room temperature in the dark with a gentle shake. The absorbance at 647 and 664 nm of the solution was measured at 15, 30, 60, 120, 180 min, and after 24 h. The micromolar concentration of total chlorophyll was calculated by the equation: total chlorophyll = $7.93(A_{664}) + 19.53(A_{647})$ (Lolle et al., 1997). The amount of chlorophyll leached was expressed as a percentage of the total chlorophyll extracted after 24 h.

Microscopy

For light microscopy, exocarp tissue was fixed, embedded, and cryosectioned according to Buda et al. (2009). Briefly, 2–3 mm exocarp cubes were sliced with a scalpel from the equatorial region of ten fruits per condition. The cubes were transferred to FAA fixative (5% formaldehyde, 5% acetic acid, and 45% ethanol) and vacuum infiltrated for 20 min. The FAA was replaced with fresh fixative and the samples were kept overnight at 4°C. After this, a sucrose gradient (10 and 20% in PBS buffer) was used following the same conditions than for the fixation process. FSC 22 Frozen Section medium (Leica) was used to fill the cryo-molds. Cryosections (40 and 50 µm) were obtained using a Leica CM1950 cryostat, transferred to Superfrost® Plus (Thermo Fisher Scientific, MA, United States), and stained with a 0.2% (w/v) Oil Red solution in 60% (v/v) isopropanol (Fukumoto and Fujimoto, 2002). The stained slides were visualized using an Axioscope 5 microscope and captured with an Axiocamp 305 color camera.

For scanning electron microscopy (SEM), exocarp tissue was fixed in 2.5% (w/v) glutaraldehyde in 0.1 M cacodylate buffer pH 7. The samples were rinsed four times in cacodylate buffer, dehydrated in a graded ethanol series, and critical point dried in CO_2 in a Polaron CPD 7501 dryer. Afterwards, they were mounted onto steel plates, evaporated with charcoal in a Hitachi evaporator, and sputter-coated with gold palladium in a Polaron Unit SEM Coating E5000. The samples were visualized and recorded using a Zeiss SUPRA40VP scanning electron microscope.

Cuticular Wax Analysis

Before the extraction, the fruits were washed in distilled water for 5 s and air dried. Then, epicuticular and intracuticular compounds (cuticular wax) were extracted by organic extraction. The cuticular wax was extracted by dipping the fruit for 1 min at room temperature in a chloroform:methanol mixture (2:1, v/v) containing 60 µg of tetracosane, lignoceryl alcohol, and lignoceric acid as internal standards. After the extraction, the exocarp of each fruit was separated using a vegetable peeler and photographed to measured total fruit surface using the ImageJ software (Schneider et al., 2012). The extraction solution was evaporated under a stream of nitrogen, resuspended in chloroform:distilled water (2:1, v/v), and the chloroform phase separated (Yeats et al., 2010). The solution containing the waxes was evaporated under a stream of nitrogen, and after that, maintained under vacuum conditions at room temperature. The wax load was determined gravimetrically.

Cuticular wax (1 mg) was derivatized with N,O-Bis(trimethylsilyl)trifluoroacetamide:pyridine (1,2) for 40 min at 70°C. After evaporating to dryness under nitrogen flow, the samples were re-dissolved in chloroform and injected into a gas chromatograph (Bruker 456-GC), coupled with an EVOQ triple quadrupole (TQ) detector and a ZB-5MS capillary column (30 m × 0.250 mm i.d. × 0.25 µm). Helium was used as a carrier gas at a flow rate of 1.2 ml min^{-1}. The running program was set as follows: the temperature was set to 50°C

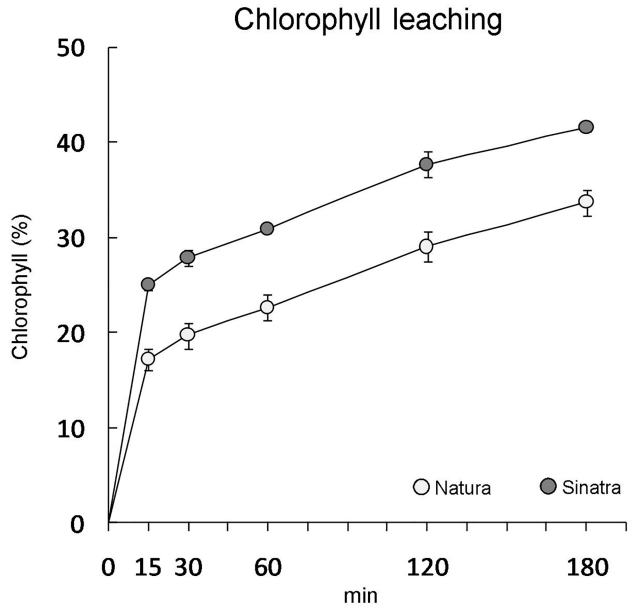

FIGURE 1 | Chlorophyll leaching of 'Natura' and 'Sinatra' fruit at harvest expressed as a percentage of total chlorophyll extracted after 24 h. Data presented are means ± SE of ten fruits. Differences between varieties were significant for every time assayed according to Duncan's test ($p < 0.05$).

for 2 min and then a ramping period was executed from the initial 50°C–200°C at a rate of 10°C min^{-1}, and finally increased to 320°C at a rate of 8°C min^{-1}, and held at this temperature for 20 min. The following parameters were employed: inlet, MS transfer line, ion source, quadrupole temperatures were 260°C, 260°C, 250°C, and 42°C, respectively. Electron impact (EI) ionization voltage was 70 eV, and the m/z range was set between 50 and 500.The identification of the main wax components was performed by comparing their mass spectra with the National Institute of Standards and Technology Version 2.3 library database, or from previously published data. Quantitative determination was achieved by comparing the peaks with the known value of an internal standard.

RNA Extraction and Gene Expression Analysis

Total RNA from the exocarp of each biological sample was extracted, treated with RNAse-Free DNAse, and purified using TRIsure™ reagent (Bioline) and the Direct-zol™ RNAMiniprep kit (Zymo Research). The quality and quantity of RNA was determined by agarose gel electrophoresis and a NanoDrop Lite spectrophotometer (Thermo Fisher Scientific). First-strand cDNA was synthesized from 1 µg total RNA using PrimeScript™ RT Master Mix (Takara). Primer pairs for the VLC-alkane biosynthesis genes *CpCER2-like* (*Cp4.1LG02g03940*), *CpCER26-like* (*Cp4.1LG17g02960*), *CpCER1-like* (*Cp4.1LG17g02820*), and *CpCER3-like* (*Cp4.1LG04g12660*), and the cuticle-related transcription factors *CpSHINE2* (*Cp4.1LG06g03420*), *CpWIN1-like* (*Cp4.1LG04g09380*), and *CpFUL1-like* (*Cp4.1LG03g15390*) were designed using the Primer3 web tool[1] and are listed in **Supplementary Table S1**. For qRT-PCR, the amplifications were run in an iCycler iQ thermal cycler (Bio-Rad). Quantification was performed with the iCycler iQTM associated software (Real Time Detection System Software, version 2.0). The relative gene expression was calculated using non-stored 'Natura' fruit as the calibration sample. *EF-1α* was used as the internal reference gene for normalizing the transcript profiles following the $2^{-\Delta\Delta Ct}$ method (Livak and Schmittgen, 2001).

Statistical Analysis

The experimental design was completely randomized. The data were subjected to an ANOVA using the SPSS 15.0 software (SPSS Inc.). The means were compared with Duncan's least significant difference test, and differences at $p < 0.05$ were considered significant.

RESULTS

Differences in Zucchini Fruit Cuticle Properties Between Varieties Before Storage

The outer surface of the epidermal cells was covered by a continuous bright-red structure in all the cryosections observed from the fruit of the cold-resistant variety 'Natura', indicating the presence of a well-detectable cuticle (**Supplementary Figure S1**). On the contrary, few cryosections showed a clearly distinguishable cuticle in fruit from the cold-sensitive variety 'Sinatra' (**Supplementary Figure S1**). Although in both varieties the cuticle was not thick enough to be measured, in 'Natura' it seemed thicker than in 'Sinatra'. The chlorophyll extraction rate was significantly higher in 'Sinatra' fruit (**Figure 1**), supporting the structural observations made with light microscopy.

In a previous study, we conducted a transcriptomic comparison of 'Natura' and 'Sinatra' exocarp before and after storage by RNA-Seq (Carvajal et al., 2018b). The result showed that the GO term 'fatty acid biosynthetic process' was overrepresented when comparing differentially expressed genes (DEGs) that were up-regulated in freshly-harvested 'Natura' versus 'Sinatra' fruit. In this work, we searched for possible cuticle-related DEGs between varieties at harvest and compared with their respective homologues in *Arabidopsis thaliana* or *Solanum lycopersicum* (**Supplementary Table S2**). From the 237 DEG annotated that were significantly up-regulated in 'Natura' with respect to 'Sinatra', a total of 15 were related to cuticle biosynthesis or its regulation, constituting 6.3% of the total. Among them, the transcript corresponding to the fatty acid hydroxylase homolog to the very-long-chain aldehyde decarbonylase CER1 from *Arabidopsis* had the highest differential accumulation. We found four DEGs encoding for 3-ketoacyl-CoA synthases; homologues to 3-ketoacyl-CoA synthase 6, 3-ketoacyl-CoA synthase 10, 3-ketoacyl-CoA synthase 19, and 3-ketoacyl-CoA

[1]https://primer3.ut.ee/

synthase 20 from *Arabidopsis*; three GDSL esterases/lipases, two of them similar to OSP1; and an O-acyltransferase WSD1. Although most of the DEGs were related to waxes, we also found two cutin-specific genes; a cytochrome P450 and a HXXXD-type acyl-transferase similar to cytochrome P450 86A2, and a BAHD acyltransferase DCR, respectively. Two genes encoding non-specific lipid-transfer proteins were also detected. Regarding the regulation of the cuticle formation, two transcription factors were also differentially expressed; ethylene-responsive WIN1 and MADS box, with a high homology to *Arabidopsis* WIN1 and tomato FRUITFULL-like MADS-box 1. On the other hand, the exocarp of 'Sinatra' fruit had 178 DEGs up-regulated with respect to 'Natura', of which only one could be associated with cuticle metabolism, constituting 0.56% of the total. This DEG corresponded to a Membrane Bound O-acyl transferase (MBOAT).

Cuticular Wax Morphology and Composition Before and After Storage at Low Temperature

SEM observations revealed that epicuticular wax in zucchini fruit mainly consisted of round-shaped or granule-like crystals scattered over the fruit surface (**Figure 2**). All samples analyzed had areas differing in the abundance of the wax coverage; however, in the 'Natura' fruit surface, the areas richer in agglomerations of granule-like crystals were more abundant in both conditions before and after the cold storage (**Figures 2A,C**). PCT fruit also had more regions whose surface was more enriched with epicuticular crystals (**Figure 2D**) when compared with non-treated 'Sinatra' fruit (**Figure 2E**). This finding suggests the formation of new waxes onto the cuticle surface what is also supported by their appearance when the images were analyzed under less magnification (**Supplementary Figure S2**).

The total cuticular wax load per surface area of the two zucchini varieties was different (**Figure 3A**). The cold-tolerant variety 'Natura' showed significantly more content of cuticular wax than the cold-sensitive variety 'Sinatra' at harvest and after 14 days of exposure to chilling. Total cuticular wax load only increased in 'Natura' during cold storage, as shown by values that doubled those exhibited in fruit at harvest after the 14 days of exposure. By contrast, 'Sinatra' fruit did not change significantly with storage. After 14 days at 4°C, 'Natura' fruit and the PCT exhibited significantly higher cuticular wax content than 'Sinatra' fruit, increasing about 4.4- and 1.8-fold, respectively.

Alkanes were one of the most important VLC aliphatic compounds in the cuticular wax of zucchini fruit. The total concentration of alkanes did not differ significantly between the two varieties in fruit at harvest (**Figure 3B**). The storage at low temperature induced the alkane-forming pathway in 'Natura' fruit, reaching very high levels, about 7-fold with respect to freshly-harvested fruit. On the contrary, 'Sinatra' fruit showed no significant changes in response to chilling stress, but with the preconditioning treatment, it increased 2.6-fold.

Nine VLC-alkanes ranging from C25 to C33 were detected in zucchini fruit (**Figure 3C**). Among the different alkanes identified, heptacosane (C27), nonacosane (C29), and hentriacontane (C31) were the most abundant in both varieties. Comparing the freshly-harvested fruit of the two varieties, no significant differences were observed in the amounts of heptacosane, nonacocosane and hentriacontane. However, these alkanes increased 5.5-, 8- and 7-fold respectively, in 'Natura' fruit kept at low temperature. The preconditioned fruit showed the same response as that observed in the cold-tolerant variety, but the increase was lower, 2.3-, 2.7 and 3-fold, respectively. By contrast, in the cold-sensitive variety, the content of these alkanes did not show significant differences between freshly-harvested and fruit stored at 4°C. In addition, the amounts of all alkanes per square cm, except for C28, did not significantly differ in 'Sinatra' fruit during cold storage with respect to harvest day.

The analysis of the cuticular wax composition in both zucchini varieties revealed that the fatty acids were the second dominant component (**Table 1**). Fourteen fatty acids ranging from C14 to C32 were detected in zucchini fruit, with hexadecanoic acid (C16:0), octadecanoic acid (C18:0), and hexacosanoic acid (C26:0) being predominant. The percentage of total fatty acids showed a contrary behavior to the obtained for the percentage of alkanes. The highest value was reached in 'Sinatra' fruit at harvest, although it did not change significantly during cold storage. The percentage of total fatty acids was lower in 'Natura' and PCT than in 'Sinatra'. In the cold-tolerant variety, a 13% reduction was also detected as a consequence of the storage at low temperature, whereas in PCT, a 17% reduction was observed with respect to freshly-harvested fruit. Studying the profile of saturated fatty acids in the cold-sensitive variety, all saturated fatty acids did not show statistical significant differences between freshly-harvested and fruit stored at 4°C. However, the preconditioning treatment reduced the percentage of hexadecanoic, heptadecanoic, octadecanoic, and octacosanoic acids.

Three primary alcohols were found in the cuticular wax of zucchini fruit (**Table 1**). The fatty alcohols profile was composed of hexacosanol, octacosanol, and triacontanol, but their percentage was relatively low with respect to the other compounds. The proportion of primary alcohols accounted for about 5% of the total wax found in zucchini fruit. The total percentage of alcohols did not change significantly in 'Natura' and 'Sinatra' fruit during storage at low temperature, and the preconditioning treatment did not affect the total percentage of alcohols either.

Two esters were detected in the cuticular wax of zucchini fruit (**Table 1**). It was noticeable that 1-monostearin content was predominant over 1-monopalmitin content in both varieties and storage times. The percentage of 1-monostearin decreased in response to low temperature, with a reduction of 13% observed in the cold-tolerant variety, 1.7% in cold-sensitive variety, and 4.4% when 'Sinatra' fruit was preconditioned. The percentage of 1-monopalmitin also diminished with cold storage in both varieties.

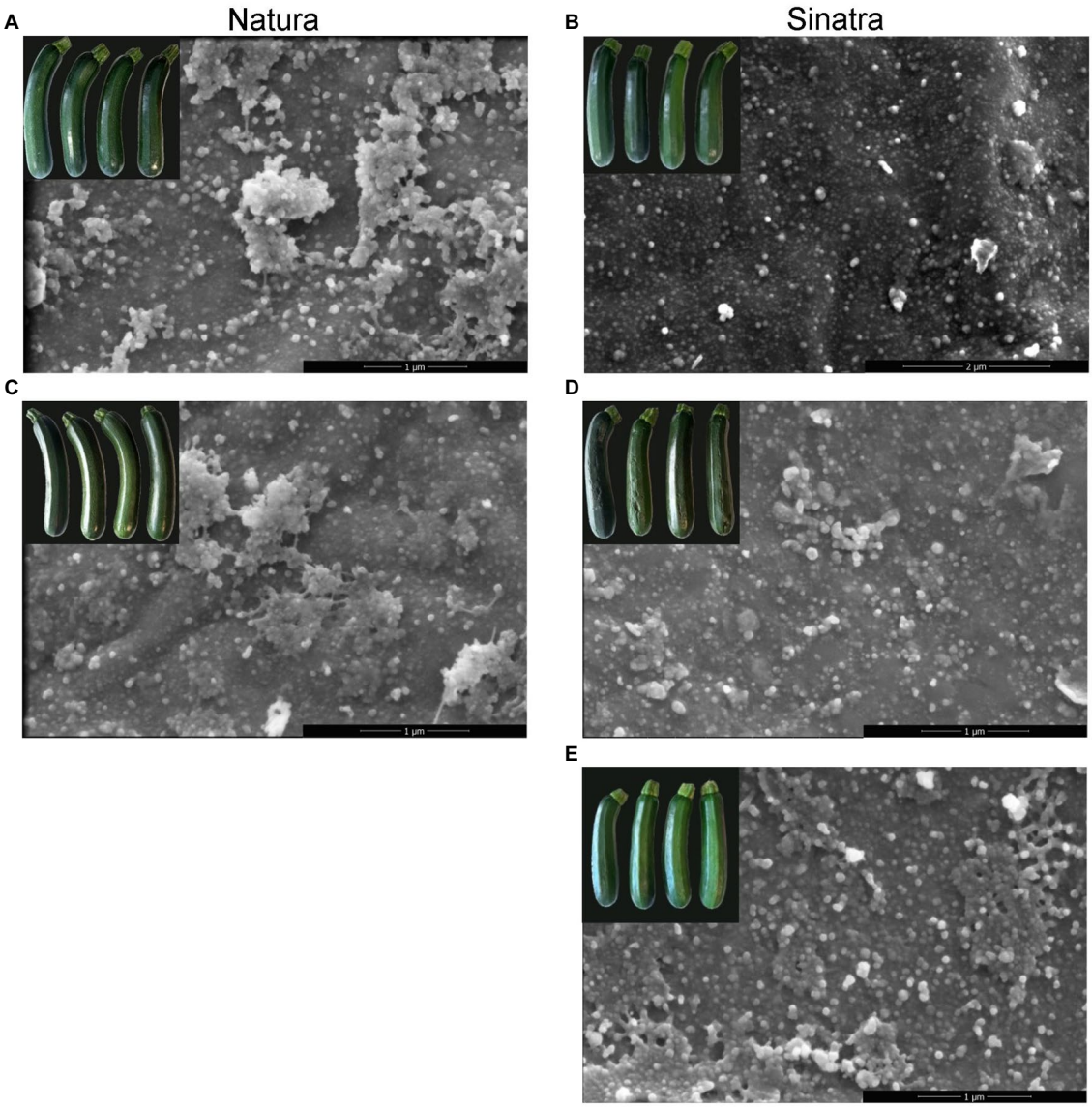

FIGURE 2 | Scanning electron micrographs of zucchini exocarp surface from 'Natura' and 'Sinatra' fruit, at harvest **(A,B)** and after 14 days of storage at 4°C **(C,D)** including preconditioned 'Sinatra' **(E)**. Scar bars: 1 or 2 µm.

Expression Profiles of Cuticle Related Genes During Postharvest

The relative expression of the VLC-alkane biosynthesis genes analyzed is shown in **Figure 4**. *CpCER2-like* transcripts only exhibited significant differences after 14 days of storage at low temperature in the variety 'Natura'. By contrast, the levels of *CpCER26-like* mRNA were 38% higher in the cold-tolerant variety with respect to the cold-sensitive one at harvest. Although in both varieties the expression values decreased, these significant differences were maintained and even increased by about 2-fold, after being kept at 4°C for 1 day. Nevertheless, no differences were found at the end of the storage period. With respect to *CpCER1-like* expression, it was about 13- and 8-fold higher in 'Natura' as compared with 'Sinatra' at harvest and after 24 h of exposure to cold, respectively. These results are in agreement with those found in the RNA-Seq analysis, where *CpCER1-like* was the DEG with the highest differences between freshly-harvested fruit from both varieties. After 14 days at 4°C, the expression values fell in all the fruits to barely detectable levels. Before the storage, the accumulation of the transcripts encoding for CpCER3-like was 64% higher in the cold-tolerant variety 'Natura' as compared to the cold-sensitive 'Sinatra'. These differences were accentuated after 1 day of cold stress, with 'Natura' reaching values that were about 3.4-fold higher than 'Sinatra'. PCT also affected *CpCER3-like* gene expression, with the treated 'Sinatra' fruit showing values about 2-fold higher

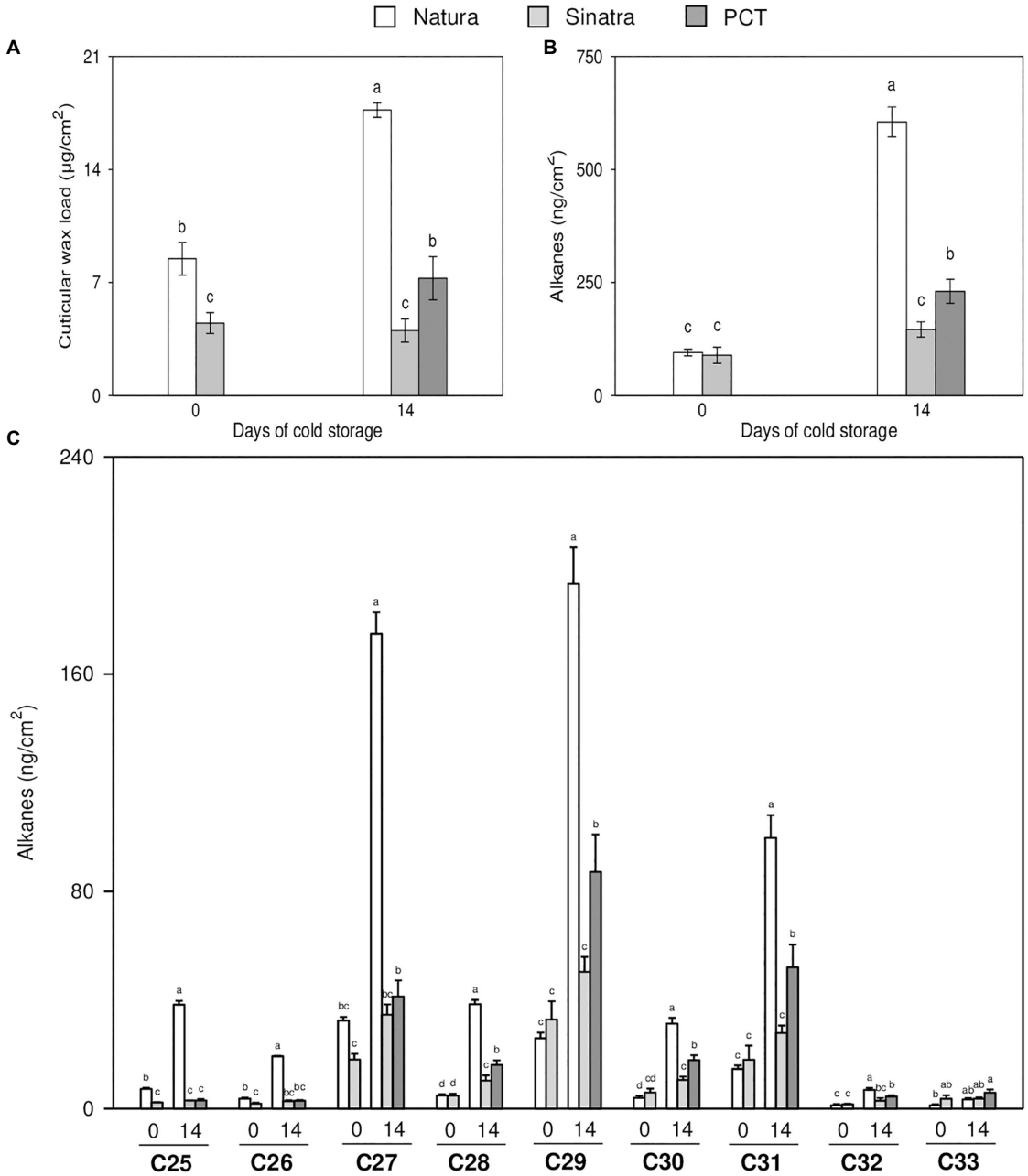

FIGURE 3 | Cuticular wax load **(A)**, total alkane content **(B)**, and individual alkanes per surface **(C)** measured in zucchini 'Natura' and 'Sinatra' fruit, at harvest and after 14 days of storage at 4°C, including preconditioned 'Sinatra'. Data presented are means ± SE of triplicate samples of six fruits each. Different letters indicate significant differences according to Duncan's test ($p < 0.05$).

than the control. As with *CpCER1-like*, *CpCER3-like* mRNA sharply decreased after a long-term storage at low temperature.

Expression results of the cuticle-related transcription factors analyzed are represented in **Figure 5**. *CpSHINE2* gene expression was induced in both varieties when fruits were exposed to 4°C for 1 day, with this increase being significantly higher in the cold-tolerant variety 'Natura'. After 14 days, the expression levels dropped in 'Natura' and 'Sinatra' but remained significantly higher in the latter. PCT fruit exhibited the highest accumulation of *CpSHINE2* transcripts at this time. The expression trend of *CpWIN1-like* was the same as *CpSHINE2* in the case of 'Natura' fruit; however, the results showed a differential trend between both genes in the cold-sensitive variety 'Sinatra'. Whereas *CpSHINE2* expression was induced by low temperature, *CpWIN1-like* did not show differences with the postharvest storage, and its values were very low. The high expression values found for this transcription factor in 'Natura' exocarp is remarkable, being about 21- and 30-fold higher when compared with

TABLE 1 | Relative content (%) of wax compounds in Natura (cold-tolerant variety), Sinatra (cold-sensitive variety) and PCT (preconditioned treatment in Sinatra) zucchini fruit at harvest and stored during 14 days at 4°C.

		At harvest		After 14 days at 4°C			LSD ($p < 0.05$)
		Natura	Sinatra	Natura	Sinatra	PCT	
Alkanes		**34.0^{c}**	**30.0^{c}**	**70.6^{a}**	**35.7^{c}**	**52.9^{b}**	**08.4**
Pentacosane	C25	02.6^{b}	00.8^{c}	04.5^{a}	00.8^{c}	00.7^{c}	00.6
Hexacosane	C26	01.3^{b}	00.6^{c}	02.3^{a}	00.7^{c}	00.7^{c}	00.2
Heptacosane	C27	11.7^{b}	06.2^{d}	20.4^{a}	08.4^{cd}	09.5^{bc}	02.4
Octacosane	C28	01.7^{d}	01.6^{d}	04.5^{a}	02.5^{c}	03.7^{b}	00.3
Nonacosane	C29	09.3^{b}	11.1^{b}	22.5^{a}	12.3^{b}	20.0^{a}	03.4
Triacontane	C30	01.4^{e}	02.0^{d}	03.6^{b}	02.6^{c}	04.1^{a}	00.4
Hentriacontane	C31	05.2^{b}	06.0^{b}	11.6^{a}	06.8^{b}	11.9^{a}	02.4
Dotriacontane	C32	00.4^{c}	00.5^{bc}	00.8^{ab}	00.7^{bc}	01.0^{a}	00.2
Tritriacontane	C33	00.4^{b}	01.2^{a}	00.4^{b}	00.9^{a}	01.3^{a}	00.5
Fatty Acids		**29.8^{b}**	**44.5^{a}**	**17.1^{c}**	**38.5^{a}**	**27.5^{b}**	**08.0**
Tetradecanoic acid	C14:0	00.4^{a}	00.5^{a}	00.3^{a}	00.2^{a}	00.2^{a}	00.6
Pentadecanoic acid	C15:0	00.2^{a}	00.3^{a}	00.2^{a}	00.1^{a}	00.2^{a}	00.4
Hexadecanoic acid	C16:0	09.4^{a}	10.7^{a}	04.5^{b}	07.9^{ab}	04.1^{b}	04.0
Heptadecanoic acid	C17:0	0nd	00.5^{a}	00.1^{b}	00.4^{a}	00.2^{b}	00.1
Octadecanoic acid	C18:0	04.0^{b}	07.3^{a}	02.6^{b}	06.0^{a}	03.0^{b}	01.3
Docosanoic acid	C22:0	00.6^{b}	01.9^{a}	00.4^{b}	01.7^{a}	01.3^{a}	01.0
Pentacosanoic acid	C25:0	00.6^{b}	01.1^{a}	00.5^{b}	01.2^{a}	01.0^{a}	00.4
Hexacosanoic acid	C26:0	04.2^{b}	06.9^{ab}	03.6^{b}	09.1^{a}	06.5^{ab}	03.5
Heptacosanoic acid	C27:0	00.5^{b}	01.1^{a}	00.4^{b}	01.1^{a}	01.1^{a}	00.4
Octacosanoic acid	C28:0	01.4^{c}	05.6^{a}	01.7^{c}	04.6^{ab}	03.6^{b}	01.2
Triacontanoic acid	C30:0	02.6^{a}	01.4^{bc}	00.7^{c}	01.6^{bc}	02.0^{ab}	00.9
Dotriacontanoic acid	C32:0	00.7^{b}	02.9^{a}	00.7^{b}	02.5^{a}	02.7^{a}	01.0
Palmitoleic acid	C16:1(9)	03.2^{a}	01.4^{ab}	00.9^{b}	00.6^{b}	00.6^{b}	02.1
Oleic acid	C18:1(9)	01.0^{bc}	02.9^{a}	00.5^{c}	01.5^{b}	01.0^{bc}	00.6
Fatty Alcohols		**02.7^{b}**	**05.2^{a}**	**03.0^{b}**	**06.1^{a}**	**05.1^{a}**	**01.2**
Hexacosanol	C26	00.9^{ab}	00.7^{b}	00.8^{b}	01.1^{a}	00.8^{b}	00.2
Octacosanol	C28	00.8^{b}	01.5^{a}	00.9^{b}	01.8^{a}	01.5^{a}	00.4
Triacontanol	C30	01.0^{b}	03.0^{a}	01.3^{b}	03.2^{a}	02.8^{a}	00.6
Esters		**19.9^{a}**	**09.3^{b}**	**06.1^{d}**	**07.3^{c}**	**04.6^{e}**	**01.1**
1-monopalmitin		00.6^{a}	00.6^{a}	00.2^{b}	00.3^{b}	00.2^{b}	00.2
1-monostearin		19.3^{a}	08.7^{b}	05.9^{c}	07.0^{c}	04.3^{d}	01.3

Relative content (%) was regarded as the percentage of each compound compared to the total content of compounds. Values represent means (nd, non-detectable). Different letters indicate significant differences according to Duncan's test ($p < 0.05$).

'Sinatra'. *CpFUL1-like* mRNA accumulation was also greater in the exocarp of 'Natura' fruit, about 3- and 2.7-fold, before the postharvest storage and after 24 h of exposure to cold as well, respectively. In this case, the differences found after 14 days at low temperature were not significant.

DISCUSSION

The implication of the cuticular waxes in the resistance to cold stress during postharvest storage of zucchini was investigated in the present study. A summary of the low temperature effects on the main quality parameters, weight loss, chilling-injury (CI) index, and firmness, throughout storage at 4°C is provided in **Supplementary Table S3**. These data show that Natura fruit, as well as fruit of Sinatra under a preconditioned treatment, were more tolerant to cold storage that Sinatra fruit, that were more sensitive and with more chilling injuries. Fruits from the more resistant variety 'Natura' showed a well-developed cuticle, whereas fruits from the very sensitive 'Sinatra' showed a slight stain that was not uniform, indicating a less developed cuticle in fruits that were more prone to developing CI. Cuticular waxes have been suggested to play an important role in fruit quality, postharvest storability, and pathogen susceptibility during postharvest of horticultural crops (Lara Ayala et al., 2014; Chu et al., 2018), being related to fruit postharvest water loss and resistance to environmental and biotic stresses. In zucchini fruit during cold storage after postharvest, the variety 'Natura' lost a smaller amount of water than the variety 'Sinatra' (**Supplementary Table S3**), which was also consistent with a better developed cuticle in 'Natura'. The chlorophyll leaching assay also showed that the cold-tolerant variety had a more reduced cuticular permeability that the cold-sensitive variety, as was also observed in leaves of *Arabidopsis* that overexpressed genes involved in the biosynthesis of VLCFAs (Yang et al., 2021). Transgenic cucumber overexpressing a gene involved in

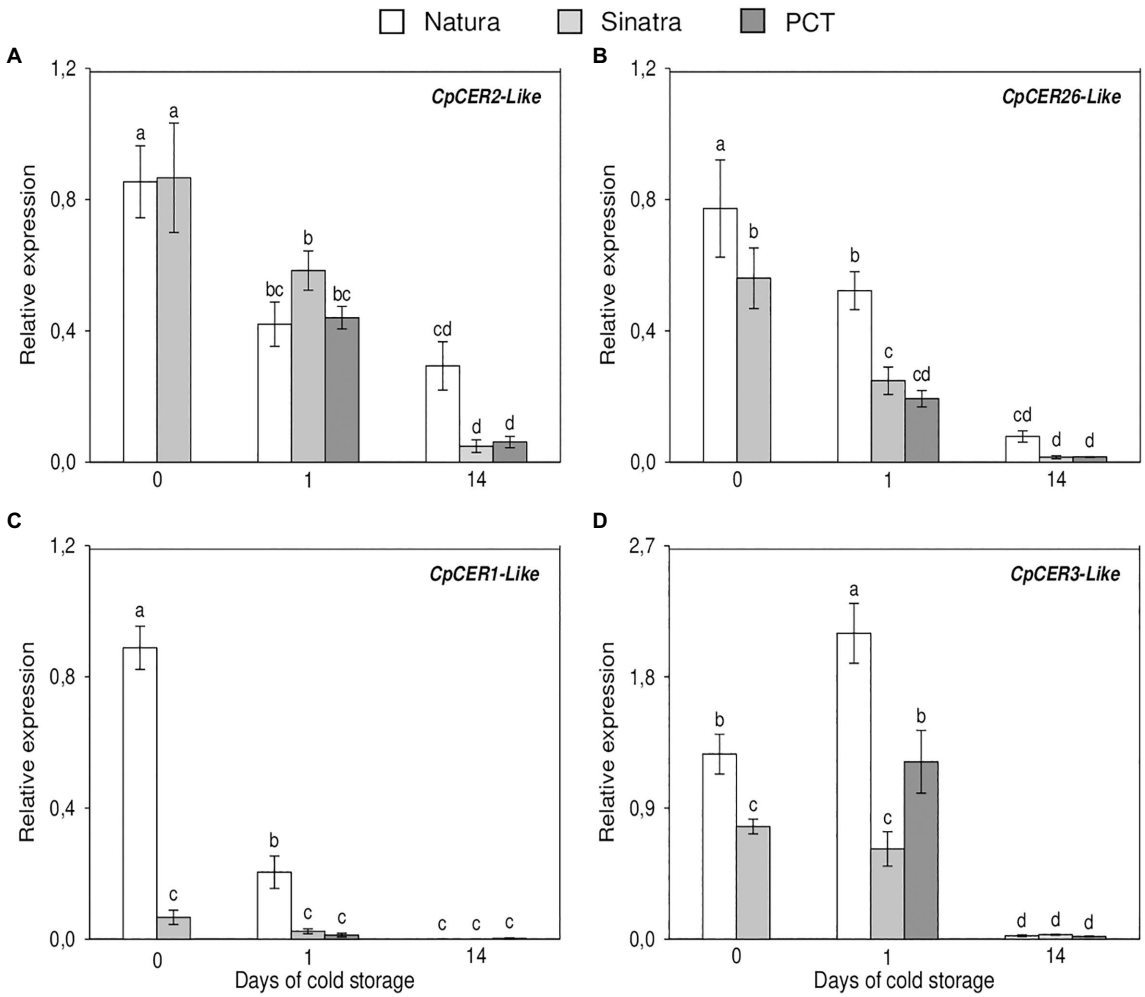

FIGURE 4 | Relative expression of the VLC-alkane biosynthesis genes *CpCER2-like* **(A)**, *CpCER26-like* **(B)**, *CpCER1-like* **(C)**, and *CpCER3-like* **(D)** in the exocarp of 'Natura' and 'Sinatra', including PCT 'Sinatra' fruit, at harvest and after 1 and 14 days of storage at 4°C. Data presented are means ± SE of triplicate samples of six fruits each. Different letters indicate significant differences according to Duncan's test ($p < 0.05$).

alkane synthesis also had a lower cuticular transpiration and chlorophyll leaching than the wild type (Wang et al., 2015b). Contradictory results have been reported as to the relevance of cuticle thickness in weight loss during storage, but most of the studies published reveal a positive relation between thickness and a decrease in weight loss, for example in pepper (Parsons et al., 2012). In blueberry, the removal of cuticular wax accelerated postharvest water loss and decay, and hence fruit quality (Chu et al., 2018). In zucchini, we conclude that cuticle thickness is related to chilling tolerance and helps to reduce water loss.

From a previous transcriptomic approach contrasting Natura and Sinatra fruits (Carvajal et al., 2018b), important differences among genes related to cuticle have been detected. Among the up-regulated DEGs in 'Natura', genes for wax and cutin synthesis were included. Homologous of these genes have been reported to be implicated cuticle development and also in water maintenance, such as GDSL lipase occluded stomatal pore 1 (At2g04570) from *Arabidopsis* (Tang et al., 2020), or the cytochrome P450, with a high identity with *Arabidopsis* CYP86A2, whose *att1* mutants showed a reduction of all cutin monomers and a consequent increase in cuticle permeability (Xiao et al., 2004). On the other hand, the only DEG up-regulated in 'Sinatra' with respect to 'Natura' at harvest corresponded with a MBOAT, a homolog to At5g55340, which catalyzes the final step in the synthesis of long-chain linear esters. The differences found at the gene expression level are related with the higher development of the cuticle in 'Natura', as observed at the microscopic level as well as its lower permeability; it also highlights the importance of the pre-harvest transcriptomic status on the subsequent postharvest behavior during cold storage.

In fruit of the varieties 'Natura' and 'Sinatra', differences in cuticular wax load were also detected, both at harvest, with a higher amount of waxes per surface area in 'Natura' than in 'Sinatra', and a sharp increase after 14 days of cold storage in 'Natura'. In fruits of the preconditioned 'Sinatra', a higher amount was also observed after 14 days at 4°C. These results are supported

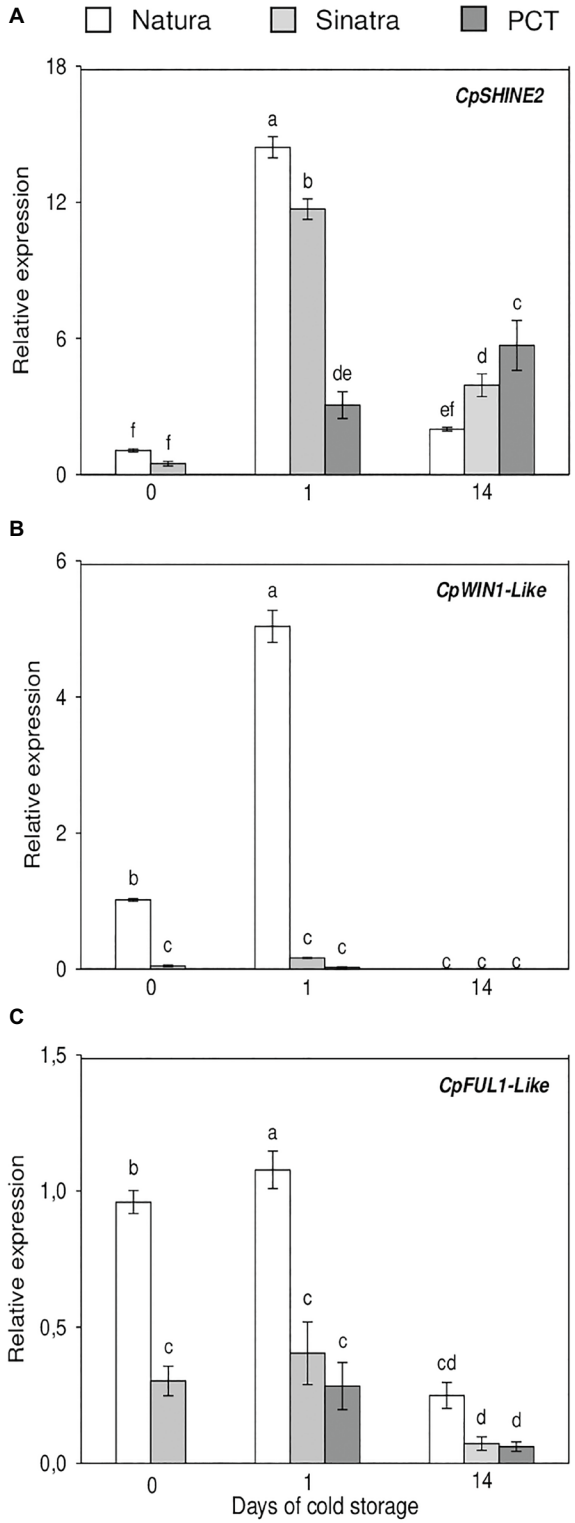

FIGURE 5 | Relative expression of the transcription factors *CpSHINE2* **(A)**, *CpWIN1-like* **(B)**, and *CpFUL1-like* **(C)** in the exocarp of 'Natura' and 'Sinatra', including PCT 'Sinatra' fruit, at harvest and after 1 and 14 days of storage at 4°C. Data presented are means ± SE of triplicate samples of six fruits each. Different letters indicate significant differences according to Duncan's test ($p < 0.05$).

by the SEM microscopy images, where higher wax crystal deposition was detected in 'Natura' and in PCT 'Sinatra' fruit surfaces. The preconditioned fruit showed images similar to those found in ethylene-treated orange fruit, where the formation of a new wax cover has been described (Cajuste et al., 2010). In that case, ethylene improved the postharvest behavior related to non-chilling peel pitting and increased cuticular wax yields. These results, together with the higher resistance to cold in 'Natura' and the great improvement in the postharvest performance of preconditioned 'Sinatra' fruit, point to an involvement of cuticular wax on the defense to cold stress conditions and the maintenance of the fruit water status (**Supplementary Table S3**).

With respect to the components of the cuticular wax, changes in composition and content during postharvest storage have been characterized in fruits such as apple (Chai et al., 2020), blueberry (Chu et al., 2018), and pear (Wang et al., 2021). These studies revealed that triterpenes and alkanes were, in general, the most prominent wax components of fruit cuticles in many species. The predominance of a wax compound has been associated to the taxonomic family of the species (Lara Ayala et al., 2014). We did not detect triterpenes in zucchini cuticular waxes. In fruits of *Cucumis sativus*, the main components were alkanes, aldehydes, and fatty acids (Wang et al., 2015a), similar to the components found in *Cucurbita pepo*. The most abundant alkanes, in our case, were heptacosane (C27), nonacosane (C29), and hentriacontane (C31); with the last two being the most abundant alkanes in fruit cuticles of many species (Wang et al., 2015a; Wu et al., 2018; Romero and Lafuente, 2020). The amount of alkanes increased in the cold-resistant fruit of 'Natura' during the storage at 4°C after 14 days, but remained unchanged in sensitive 'Sinatra' fruits, also increasing in PCT 'Sinatra' fruit, which indicates a mechanism to overcome chilling damages in which cuticular wax synthesis would be involved. The involvement of the alkanes in the defense to stresses has been reported for other species. In a study conducted with 50 pepper accessions, Parsons et al. (2012) found a positive correlation between water loss and alkane content/composition. When analyzing 10 apple cultivars during cold storage, the lowest alkane content was found in the 'Red Star' cultivar., which showed the highest weight loss rate during the storage period (Chai et al., 2020). In apple fruit peel, low temperatures induced the alkane-forming pathway and resulted in the accumulation of VLC-alkanes (C22, C27, C29, and C31; Hao et al., 2017), the same accumulation of C27, C29, and C31 alkanes detected in 'Natura' fruit and also in preconditioned fruit of 'Sinatra', which points to the implication of these compounds in chilling tolerance of zucchini fruit.

We have detected that the content of esters was higher in 'Natura' than in 'Sinatra' at harvest, whereas the fatty acids content showed the contrary behavior. This could be due to a higher rate of ester hydrolysis in the cold-sensitive variety. In apple fruit, an increase in the content of fatty acids has been described due to the hydrolysis of esters (Veraverbeke et al., 2001). Samuels et al. (2008) have described that most cuticular waxes are generated from the elongation of C16 and C18 free fatty acids, including two well characterized metabolic pathways for the formation of alkanes and for the production of primary alcohols and wax esters. In our analysis,

we detected only two esters in zucchini fruit: 1-monopalmitin and 1-monostearin. These two esters were also the only glyceride compounds identified in all 35 pear cultivars studied when the chemical composition of the cuticular wax in mature fruits was analyzed (Wu et al., 2018). The content of 1-monopalmitin and 1-monostearin diminished during the cold storage in both zucchini varieties, observing a greater decrease in 'Natura' than 'Sinatra' fruit. This behavior is indicative of an induction of the alkane biosynthesis pathway and the inhibition of the ester's biosynthesis pathway in the cold-tolerant fruit kept at 4°C. This finding is supported by different studies such as that of Wang et al. (2015a), where the knocked-down expression of CsCER1 in transgenic cucumber plants caused a decrease in alkanes content as well as an increase in esters, whereas overexpression of CsCER1 showed the opposite response. In a similar way, transgenic cucumber lines with an abnormal expression of *CsWAX2*, an *Arabidopsis CER3* homolog involved in alkane synthesis, showed an increased amount of esters in cuticular waxes, which decreased with the overexpression of this gene (Wang et al., 2015b). The alternation between the formation of alkanes and wax esters also seems to be regulated by abscisic acid (ABA). In cucumber, the expression of *CsCER1* was shown to be induced by this phytohormone (Wang et al., 2015a), whereas the ABA deficiency orange mutant Pinalate showed an induction in the gene *CsWSD1-like*, responsible for wax ester formation (Romero and Lafuente, 2020). These results suggest that ABA could act as a negative regulator of wax ester formation, and a positive regulator of alkane formation. In a previous work, we described that 'Natura' fruit drastically increased the ABA content during the first days of exposure to low temperature, whereas 'Sinatra' fruit did not show significant differences in ABA content during storage (Carvajal et al., 2017). This ABA response could be associated with the changes observed in the content of alkanes and esters in the two zucchini varieties, and should be investigated in the future.

It is obvious from this research that cuticular waxes, specifically alkanes, play an important role in defense against low temperature stress in fruits of *Cucurbita pepo*. Fruits of 'Natura', a cold resistant variety, and preconditioned 'Sinatra' had a higher content of alkanes after cold storage, and this correlated with a lower weight loss and CI damage during postharvest, as well as greater firmness. The biosynthetic pathway of cuticular waxes and regulatory genes have been researched and described in model species and in some fruits, but little is known in zucchini fruit. In this study, we analyzed the expression of 4 genes involved in proper cuticle development, and specifically involved in VLC-alkane biosynthesis. *CpCER2-like* only showed differences in the cold-tolerant variety 'Natura' at the end of the storage period. On the contrary, *CpCER26-like* gene expression was significantly higher in 'Natura' at harvest and after 1 day of cold exposure. Both genes, CER2 and CER26, are important components of the VLCFA elongation process (Haslam et al., 2017), with the *Arabidopsis cer2* mutant showing an impaired production of wax components longer than 28 carbons, and *cer2*6 mutant affected in the production of wax components longer than 30 carbons (Pascal et al., 2013). The higher expression of both genes in Natura fruit during storage, explains the accumulation of nonacosane (C29) and hentriacontane (C31).

The expression of the zucchini homolog genes, *CpCER1-like* and *CpCER3-like,* has been studied in this work. *CpCER1-like* mRNA was highly accumulated when 'Natura' fruit were harvested, whereas in 'Sinatra', very low levels were measured. Our results are supported by those found in *Arabidopsis cer1* insertional mutants, which showed a reduction in heptacosane (C27), nonacosane (C29), hentriacontane (C31), and tritriacontane (C33), with its overexpression resulting in an accumulation of these components (Bourdenx et al., 2011). The expression of *CpCER1-like* in zucchini decreased with storage at 4°C, similar to the results found by (Bourdenx et al., 2011), which reported a decreased expression of the CER1 gene in *Arabidopsis* plants subjected to dark and cold treatments. This behavior is in agreement with the trend described in previous works (Wang et al., 2015b) for its homolog *CsWAX2*, which was induced after 24 h of cold stress in cucumber plants. These authors also described a significant reduction in the concentration of the alkanes, pentacosane (C25), heptacosane (C27), nonacosane (C29), and hentriacontane (C31), in fruit from *CsWAX2* RNAi lines, as well as an increase of them in the *CsWAX2* overexpression lines. In zucchini fruit, the large difference found in *CpCER1-like* and *CpCER3-like* gene expression between varieties at harvest time and after 1 day of storage could explain, in part, the accumulation VLC-alkanes during cold stress.

Regarding the possible role of transcriptional regulators in wax biosynthesis, it has been reported that several members of the APETALA2/ETHYLENE-RESPONSIVE ELEMENTBINDING PROTEINS (AP2/EREBP) family regulate cuticle-related genes. In this work, we analyzed the expression of two cuticle-related AP2/EREBP transcription factors, *CpSHINE2* and *CpWIN1-like.* Cold storage induced *CpSHINE2* mRNA accumulation in both varieties in the short-term, with the increase being greater in the transcription detected in 'Natura'. On the contrary, this induction occurred in the long-term in PCT 'Sinatra' fruit. However, *CpWIN1-like* only showed a sharp increase in the cold-tolerant 'Natura' fruit after being exposed to low temperature, whereas no changes were detected in 'Sinatra'. Recently, Zhang et al. (2019) reported that the ectopic expression of the apple gene *MdSHINE2* in *Arabidopsis* resulted in a higher accumulation of wax crystals, and an increase in the alkanes, alcohols, aldehydes, and fatty acids wax components. These results correlated with an induction of CER1, CER3, and WIN1 gene expression, as well as an increase in drought tolerance. *WAX INDUCER1/SHINE1* has been associated with the induction of different wax biosynthesis genes such as *CER1* and *CER2* (Broun et al., 2004). *Arabidopsis* plants overexpressing *WIN1/SHN1* also showed enhanced drought tolerance (Aharoni et al., 2004). These results provide evidence that these genes play an important role on the regulation of the cuticular wax biosynthesis in zucchini fruit subjected to stress due to low temperatures.

Several MADS-box genes have been associated with the ripening process in tomato fruit, such as the FRUITFULL homologues, which may play a role in cuticle formation (Bemer et al., 2012; Shima et al., 2013; Fujisawa et al., 2014). In zucchini fruit, the

homolog to tomato TDR4/FUL1, *CpFUL1-like*, was significantly expressed in the cold-tolerant 'Natura' at harvest and after a short-term storage at 4°C. This response could be related with the lower percentage of weight loss observed in these fruits according to Bemer et al. (2012), who described an increase in the water loss rate in harvested tomato FUL1/2 RNAi fruits.

This study is the first comprehensive analysis of the cuticular wax structure, load, and composition in *Cucurbita pepo* fruit during postharvest, and its involvement in the defense against chilling injury, proving the importance of the biosynthesis of VLC-alkanes and its transcriptional regulation during the adaptation of the zucchini fruit to low temperatures. Overall, the results obtained can be the basis of future functional studies, and could serve in the identification of markers for the selection of cold-resistant varieties in zucchini breeding programs.

DATA AVAILABILITY STATEMENT

The original contributions presented in the study are included in the article/**Supplementary Material**, further inquiries can be directed to the corresponding authors.

AUTHOR CONTRIBUTIONS

DG and MJ designed the project and were responsible for funding acquisition. FC and FP conducted the research and analyzed the results. RJ-M and AC-C collaborated in part of the investigation. FC, FP, and DG wrote the original draft with contributions by MJ. All authors have read and accepted the final manuscript.

FUNDING

This work was supported by the Ministerio de Ciencia, Innovacion y Universidades (Project AGL2017-82885-C2-2-R and Project PID2020-118080RB-C22). AC-C is being funded by FPI Grants (MEC).

SUPPLEMENTARY MATERIAL

The Supplementary Material for this article can be found online at: https://www.frontiersin.org/articles/10.3389/fpls.2021.778745/full#supplementary-material

REFERENCES

Aharoni, A., Dixit, S., Jetter, R., Thoenes, E., van Arkel, G., and Pereira, A. (2004). The SHINE clade of AP2 domain transcription factors activates wax biosynthesis, alters cuticle properties, and confers drought tolerance when overexpressed in Arabidopsis. *Plant Cell* 16, 2463–2480. doi: 10.1105/tpc.104.022897

Alkio, M., Jonas, U., Sprink, T., van Nocker, S., and Knoche, M. (2012). Identification of putative candidate genes involved in cuticle formation in Prunusavium (sweet cherry) fruit. *Ann. Bot.* 110, 101–112. doi: 10.1093/aob/mcs087

Bauer, S., Schulte, E., and Thier, H.-P. (2004). Composition of the surface wax from tomatoes II. Quantification of the components at the ripe red stage and during ripening. *Eur. Food Res. Technol.* 219, 487–491. doi: 10.1007/s00217-004-0944-z

Bemer, M., Karlova, R., Ballester, A. R., Tikunov, Y. M., Bovy, A. G., Wolters-Arts, M., et al. (2012). The tomato FRUITFULL homologs TDR4/FUL1 and MBP7/FUL2 regulate ethylene-independent aspects of fruit ripening. *Plant Cell* 24, 4437–4451. doi: 10.1105/tpc.112.103283

Bernard, A., Domergue, F., Pascal, S., Jetter, R., Renne, C., Faure, J. D., et al. (2012). Reconstitution of plant alkane biosynthesis in yeast demonstrates That Arabidopsis ECERIFERUM1 and ECERIFERUM3 are Core components of a very-long-chain alkane synthesis complex. *Plant Cell* 24, 3106–3118. doi: 10.1105/tpc.112.099796

Bourdenx, B., Bernard, A., Domergue, F., Pascal, S., Léger, A., Roby, D., et al. (2011). Overexpression of Arabidopsis ECERIFERUM1 promotes wax very-long-chain alkane biosynthesis and influences plant response to biotic and abiotic stresses. *Plant Physiol.* 156, 29–45. doi: 10.1104/pp.111.172320

Broun, P., Poindexter, P., Osborne, E., Jiang, C. Z., and Riechmann, J. L. (2004). WIN1, a transcriptional activator of epidermal wax accumulation in Arabidopsis. *Proc. Natl. Acad. Sci. U. S. A.* 101, 4706–4711. doi: 10.1073/pnas.0305574101

Buda, G. J., Isaacson, T., Matas, A. J., Paolillo, D. J., and Rose, J. K. C. (2009). Three-dimensional imaging of plant cuticle architecture using confocal scanning laser microscopy. *Plant J.* 60, 378–385. doi: 10.1111/j.1365-313X.2009.03960.x

Buschhaus, C., and Jetter, R. (2011). Composition differences between epicuticular and intracuticular wax substructures: how do plants seal their epidermal surfaces? *J. Exp. Bot.* 62, 841–853. doi: 10.1093/jxb/erq366

Cajuste, J. F., González-Candelas, L., Veyrat, A., García-Breijo, F. J., Reig-Armiñana, J., and Lafuente, M. T. (2010). Epicuticular wax content and morphology as related to ethylene and storage performance of 'Navelate' orange fruit. *Postharvest Biol. Technol.* 55, 29–35. doi: 10.1016/j.postharvbio.2009.07.005

Carvajal, F., Martinez, C., Jamilena, M., and Garrido, D. (2011). Differential response of zucchini varieties to low storage temperature. *Sci. Hortic.* 130, 90–96. doi: 10.1016/j.scienta.2011.06.016

Carvajal, F., Palma, F., Jamilena, M., and Garrido, D. (2015). Preconditioning treatment induces chilling tolerance in zucchini fruit improving different physiological mechanisms against cold injury. *Ann. Appl. Biol.* 166, 340–354. doi: 10.1111/aab.12189

Carvajal, F., Palma, F., Jiménez-Muñoz, R., Jamilena, M., Pulido, A., and Garrido, D. (2017). Unravelling the role of abscisic acid in chilling tolerance of zucchini during postharvest cold storage. *Postharvest Biol. Technol.* 133, 26–35. doi: 10.1016/j.postharvbio.2017.07.004

Carvajal, F., Palma, F., Jiménez-Muñoz, R., Pulido, A., and Garrido, D. (2018a). Changes in the biosynthesis of cuticular waxes during postharvest cold storage of zucchini fruit (Cucurbita pepo L.). *Acta Hortic.* 1194, 1475–1480. doi: 10.17660/ActaHortic.2018.1194.206

Carvajal, F., Rosales, R., Palma, F., Manzano, S., Cañizares, J., Jamilena, M., et al. (2018b). Transcriptomic changes in Cucurbita pepo fruit after cold storage: differential response between two cultivars contrasting in chilling sensitivity. *BMC Genomics* 19, 125. doi: 10.1186/s12864-018-4500-9

Chai, Y., Li, A., Chit Wai, S., Song, C., Zhao, Y., Duan, Y., et al. (2020). Cuticular wax composition changes of 10 apple cultivars during postharvest storage. *Food Chem.* 324:126903. doi: 10.1016/j.foodchem.2020.126903

Chen, X., Goodwin, S. M., Boroff, V. L., Liu, X., and Jenks, M. A. (2003). Cloning and characterization of the WAX2 gene of Arabidopsis involved in cuticle membrane and WAX production. *Plant Cell* 15, 1170–1185. doi: 10.1105/tpc.010926

Chu, W., Gao, H., Chen, H., Fang, X., and Zheng, Y. (2018). Effects of cuticular wax on the postharvest quality of blueberry fruit. *Food Chem.* 239, 68–74. doi: 10.1016/j.foodchem.2017.06.024

Domínguez, E., Heredia-Guerrero, J. A., and Heredia, A. (2011). The biophysical design of plant cuticles: an overview. *New Phytol.* 189, 938–949. doi: 10.1111/j.1469-8137.2010.03553.x

Ensikat, H. J., Boese, M., Mader, W., Barthlott, W., and Koch, K. (2006). Crystallinity of plant epicuticular waxes: electron and X-ray diffraction studies. *Chem. Phys. Lipids* 144, 45–59. doi: 10.1016/j.chemphyslip.2006.06.016

Fujisawa, M., Shima, Y., Nakagawa, H., Kitagawa, M., Kimbara, J., Nakano, T., et al. (2014). Transcriptional regulation of fruit ripening by tomato FRUITFULL homologs and associated MADS box proteins. *Plant Cell* 26, 89–101. doi: 10.1105/tpc.113.119453

Fukumoto, S., and Fujimoto, T. (2002). Deformation of lipid droplets in fixed samples. *Histochem. Cell Biol.* 118, 423–428. doi: 10.1007/s00418-002-0462-7

Hao, S., Ma, Y., Zhao, S., Ji, Q., Zhang, K., Yang, M., et al. (2017). McWRI1, a transcription factor of the AP2/SHEN family, regulates the biosynthesis of the cuticular waxes on the apple fruit surface under low temperature. *PLoS One* 12:e0186996. doi: 10.1371/journal.pone.0186996

Haslam, T. M., Gerelle, W. K., Graham, S. W., and Kunst, L. (2017). The unique role of the ECERIFERUM2-LIKE clade of the BAHD acyltransferase superfamily in Cuticular wax metabolism. *Plan. Theory* 6:23. doi: 10.3390/plants6020023

Hen-Avivi, S., Lashbrooke, J., Costa, F., and Aharoni, A. (2014). Scratching the surface: genetic regulation of cuticle assembly in fleshy fruit. *J. Exp. Bot.* 65, 4653–4664. doi: 10.1093/jxb/eru225

Koch, K., and Ensikat, H. J. (2008). The hydrophobic coatings of plant surfaces: Epicuticular wax crystals and their morphologies, crystallinity and molecular self-assembly. *Micron* 39, 759–772. doi: 10.1016/j.micron.2007.11.010

Kosma, D. K., Bourdenx, B., Bernard, A., Parsons, E. P., Lü, S., Joubès, J., et al. (2009). The impact of water deficiency on leaf cuticle lipids of Arabidopsis. *Plant Physiol.* 151, 1918–1929. doi: 10.1104/pp.109.141911

Lara Ayala, I., Belge, B., and Goulao, L. F. (2014). The fruit cuticle as a modulator of postharvest quality. *Postharvest Biol. Technol.* 87, 103–112. doi: 10.1016/j.postharvbio.2013.08.012

Lara Ayala, I., Heredia, A., and Domínguez, E. (2019). Shelf life potential and the fruit cuticle: The unexpected player. *Front. Plant Sci.* 10, 1–18. doi: 10.3389/fpls.2019.00770

Lashbrooke, J., Aharoni, A., and Costa, F. (2015). Genome investigation suggests MdSHN3, an APETALA2-domain transcription factor gene, to be a positive regulator of apple fruit cuticle formation and an inhibitor of russet development. *J. Exp. Bot.* 66, 6579–6589. doi: 10.1093/jxb/erv366

Livak, K. J., and Schmittgen, T. D. (2001). Analysis of relative gene expression data using real-time quantitative PCR and the $2^{-\Delta\Delta CT}$ method. *Methods* 25, 402–408. doi: 10.1006/meth.2001.1262

Lolle, S. J., Berlyn, G. P., Engstrom, E. M., Krolikowski, K. A., Reiter, W.-D., and Pruitt, R. E. (1997). Developmental regulation of cell interactions in the Arabidopsis fiddlehead-1Mutant: A role for the epidermal Cell Wall and cuticle. *Dev. Biol.* 189, 311–321. doi: 10.1006/dbio.1997.8671

Martin, L. B. B., and Rose, J. K. C. (2013). There's more than one way to skin a fruit: formation and functions of fruit cuticles. *J. Exp. Bot.* 65, 4639–4651. doi: 10.1093/jxb/eru301

McNevin, J. P., Woodward, W., Hannoufa, A., Feldmann, K. A., and Lemieux, B. (1993). Isolation and characterization of eceriferum (cer) mutants induced by T-DNA insertions in Arabidopsis thaliana. *Genome* 36, 610–618. doi: 10.1139/g93-082

Palma, F., Carvajal, F., Jamilena, M., and Garrido, D. (2014a). Contribution of polyamines and other related metabolites to the maintenance of zucchini fruit quality during cold storage. *Plant Physiol. Biochem.* 82, 161–171. doi: 10.1016/j.plaphy.2014.06.001

Palma, F., Carvajal, F., Lluch, C., Jamilena, M., and Garrido, D. (2014b). Changes in carbohydrate content in zucchini fruit (*Cucurbita pepo* L.) under low temperature stress. *Plant Sci.* 217, 78–86. doi: 10.1016/j.plantsci.2013.12.004

Parsons, E. P., Popopvsky, S., Lohrey, G. T., Lü, S., Alkalai-Tuvia, S., Perzelan, Y., et al. (2012). Fruit cuticle lipid composition and fruit post-harvest water loss in an advanced backcross generation of pepper (capsicum sp.). *Physiol. Plant.* 146, 15–25. doi: 10.1111/j.1399-3054.2012.01592.x

Pascal, S., Bernard, A., Sorel, M., Pervent, M., Vile, D., Haslam, R. P., et al. (2013). The Arabidopsis cer26 mutant, like the cer2 mutant, is specifically affected in the very long chain fatty acid elongation process. *Plant J.* 73, 733–746. doi: 10.1111/tpj.12060

Romero, P., and Lafuente, M. T. (2020). Abscisic acid deficiency alters Epicuticular wax metabolism and morphology That leads to increased cuticle permeability During sweet Orange (Citrus sinensis) fruit ripening. *Front. Plant Sci.* 11:594184. doi: 10.3389/fpls.2020.594184

Samuels, L., Kunst, L., and Jetter, R. (2008). Sealing plant surfaces: Cuticular wax formation by epidermal cells. *Annu. Rev. Plant Biol.* 59, 683–707. doi: 10.1146/annurev.arplant.59.103006.093219

Schneider, C. A., Rasband, W. S., and Eliceiri, K. W. (2012). NIH image to ImageJ: 25 years of image analysis. *Nat. Methods* 9, 671–675. doi: 10.1038/nmeth.2089

Shi, J. X., Adato, A., Alkan, N., He, Y., Lashbrooke, J., Matas, A. J., et al. (2013). The tomato SlSHINE3 transcription factor regulates fruit cuticle formation and epidermal patterning. *New Phytol.* 197, 468–480. doi: 10.1111/nph.12032

Shima, Y., Kitagawa, M., Fujisawa, M., Nakano, T., Kato, H., Kimbara, J., et al. (2013). Tomato FRUITFULL homologues act in fruit ripening via forming MADS-box transcription factor complexes with RIN. *Plant Mol. Biol.* 82, 427–438. doi: 10.1007/s11103-013-0071-y

Tafolla-Arellano, J. C., Zheng, Y., Sun, H., Jiao, C., Ruiz-May, E., Hernández-Oñate, M. A., et al. (2017). Transcriptome analysis of mango (Mangiferaindica L.) fruit epidermal Peel to identify putative cuticle-associated genes. *Sci. Rep.* 7:46163. doi: 10.1038/srep46163

Tang, J., Yang, X., Xiao, C., Li, J., Chen, Y., Li, R., et al. (2020). GDSL lipase occluded stomatal pore 1 is required for wax biosynthesis and stomatal cuticular ledge formation. *New Phytol.* 228, 1880–1896. doi: 10.1111/nph.16741

Trivedi, P., Nguyen, N., Hykkerud, A. L., Häggman, H., Martinussen, I., Jaakola, L., et al. (2019). Developmental and environmental regulation of Cuticular wax biosynthesis in fleshy fruits. *Front. Plant Sci.* 10:431. doi: 10.3389/fpls.2019.00431

Veraverbeke, E. A., Lammertyn, J., Saevels, S., and Nicolaï, B. M., (2001). Changes in chemical wax composition of three different apple (Malus domesticaBorkh.) cultivars during storage. *Postharvest Biol. Technol.* 23, 197–208. doi: 10.1016/S0925-5214(01)00128-4

Wang, W., Liu, X., Gai, X., Ren, J., Liu, X., Cai, Y., et al. (2015a). Cucumissativus L. WAX2 plays a pivotal role in WAX biosynthesis, influencing pollen fertility and plant biotic and abiotic stress responses. *Plant Cell Physiol.* 56, 1339–1354. doi: 10.1093/pcp/pcv052

Wang, Y., Mao, H., Lv, Y., Chen, G., and Jiang, Y. (2021). Comparative analysis of total wax content, chemical composition and crystal morphology of cuticular wax in Korla pear under different relative humidity of storage. *Food Chem.* 339:128097. doi: 10.1016/j.foodchem.2020.128097

Wang, W., Zhang, Y., Xu, C., Ren, J., Liu, X., Black, K., et al. (2015b). Cucumber ECERIFERUM1 (CsCER1), which influences the cuticle properties and drought tolerance of cucumber, plays a key role in VLC alkanes biosynthesis. *Plant Mol. Biol.* 87, 219–233. doi: 10.1007/s11103-014-0271-0

Wu, X., Yin, H., Shi, Z., Chen, Y., Qi, K., Qiao, X., et al. (2018). Chemical composition and crystal morphology of Epicuticular wax in mature fruits of 35 pear (Pyrus spp.). *Cultivars. Front. Plant Sci.* 9:679. doi: 10.3389/fpls.2018.00679

Xiao, F., Goodwin, S. M., Xiao, Y., Sun, Z., Baker, D., Tang, X., et al. (2004). Arabidopsis CYP86A2 represses pseudomonas syringae type III genes and is required for cuticle development. *EMBO J.* 23, 2903–2913. doi: 10.1038/sj.emboj.7600290

Yang, H., Mei, W., Wan, H., Xu, R., and Cheng, Y. (2021). Comprehensive analysis of KCS gene family in Citrinae reveals the involvement of CsKCS2 and CsKCS11 in fruit cuticular wax synthesis at ripening. *Plant Sci.* 310:110972. doi: 10.1016/j.plantsci.2021.110972

Yeats, T. H., Howe, K. J., Matas, A. J., Buda, G. J., Thannhauser, T. W., and Rose, J. K. C. (2010). Mining the surface proteome of tomato (*Solanum lycopersicum*) fruit for proteins associated with cuticle biogenesis. *J. Exp. Bot.* 61, 3759–3771. doi: 10.1093/jxb/erq194

Yeats, T. H., and Rose, J. K. C. (2013). The formation and function of plant cuticles. *Plant Physiol.* 163, 5–20. doi: 10.1104/pp.113.222737

Zhang, Y.-L., Zhang, C.-L., Wang, G.-L., Wang, Y.-X., Qi, C.-H., You, C.-X., et al. (2019). Apple AP2/EREBP transcription factor MdSHINE2 confers drought resistance by regulating wax biosynthesis. *Planta* 249, 1627–1643. doi: 10.1007/s00425-019-03115-4

Conflict of Interest: The authors declare that the investigation was conducted in the absence of any financial interests that could be interpreted as a potential conflict of interest.

be evaluated in this article, or claim that may be made by its manufacturer, is not guaranteed or endorsed by the publisher.

frontiers in Plant Science

MINI REVIEW
published: 10 December 2021
doi: 10.3389/fpls.2021.782773

The Complex Architecture of Plant Cuticles and Its Relation to Multiple Biological Functions

*Nicolas Reynoud[1], Johann Petit[2], Cécile Bres[2], Marc Lahaye[1], Christophe Rothan[2], Didier Marion[1] and Bénédicte Bakan[1]**

[1] INRAE, Unité Biopolymères, Interactions, Assemblages, Nantes, France, [2] INRAE, University of Bordeaux, UMR BFP, Villenave d'Ornon, France

Terrestrialization of vascular plants, i.e., Angiosperm, is associated with the development of cuticular barriers that prevent biotic and abiotic stresses and support plant growth and development. To fulfill these multiple functions, cuticles have developed a unique supramolecular and dynamic assembly of molecules and macromolecules. Plant cuticles are not only an assembly of lipid compounds, i.e., waxes and cutin polyester, as generally presented in the literature, but also of polysaccharides and phenolic compounds, each fulfilling a role dependent on the presence of the others. This mini-review is focused on recent developments and hypotheses on cuticle architecture–function relationships through the prism of non-lipid components, i.e., cuticle-embedded polysaccharides and polyester-bound phenolics.

Keywords: plant cuticle, architecture–function relationship, cutin, cell wall polysaccharides, phenolics

OPEN ACCESS

Edited by:
Isabel Molina, Algoma University, Canada

Reviewed by:
Victoria Fernandez, Polytechnic University of Madrid, Spain
Dylan Kosma, University of Nevada, Reno, United States

****Correspondence:***
Bénédicte Bakan
benedicte.bakan@inrae.fr

Specialty section:
This article was submitted to Plant Physiology, a section of the journal Frontiers in Plant Science

Received: *24 September 2021*
Accepted: *18 November 2021*
Published: *10 December 2021*

Citation:
Reynoud N, Petit J, Bres C, Lahaye M, Rothan C, Marion D and Bakan B (2021) The Complex Architecture of Plant Cuticles and Its Relation to Multiple Biological Functions. Front. Plant Sci. 12:782773. doi: 10.3389/fpls.2021.782773

INTRODUCTION

Terrestrial colonization of plants came along with the development of four sophisticated hydrophobic macromolecular assemblies, i.e., cuticle, suberin, lignin and sporopollenin (Yeats and Rose, 2013; Graça, 2015; Li et al., 2019; Ralph et al., 2019), which enabled plants to resist to the harsh conditions of the environment, to stiffen their architecture, to ensure nutrient and water adsorption, their reproduction and land dispersion. Cuticle has a high plasticity, especially adapted to organ growth. This plasticity was recently illustrated in the case of the cuticle of lateral root primordia which controls further lateral root emergence (Berhin et al., 2019). Indeed, any defects in the cuticle biosynthetic pathways induce defects in cuticle assembly and impact organ growth and morphology (Fich et al., 2016; Berhin et al., 2019). Cuticle fulfills multiple functions, e.g., in the control of water and gas exchanges, in the defense signaling against biotic and abiotic stresses, in plant development with many interactions with hormone signaling and cell wall biosynthesis, in the protection against UV radiation, in the retention of environmental pollutants, in the induction of responses to mechanical stimuli, and constitute an habitat for the plant microbiome (Schönherr and Riederer, 1989; Martin and Rose, 2014; Meder et al., 2018; Cordovez et al., 2019). These multiple functions impact crop yields and quality, including post-harvest quality and processing which has boosted research on the structure, assembly, and biosynthesis of their macromolecular and molecular constituents. Finally, recent data showed that cuticle functions could not be regarded only through the lens of their chemical composition, but resulted from a spatial organization of molecules and macromolecules, i.e., a 3D architecture, finely regulated at the genetic and physiological levels. This mini-review reports recent data on cuticle structural features and the

ensuing hypotheses on its architecture, its evolution during organ development and its relationship with their functional properties.

FROM MOLECULAR DIVERSITY TO CUTICLE ARCHITECTURE

Plant cuticles are composed of three main types of chemical components, i.e., lipids, carbohydrates, and phenolics. Lipids give the cuticles their hydrophobic properties. They consist of molecules easily extractable with organic solvents, i.e., epi- and intra-cuticular waxes, dispersed at the surface and within the cuticles, respectively, and of insoluble lipid polymers, i.e., cutan and cutin. While cutan polymer contains non-hydrolysable bounds that limit structural investigation (Bhanot et al., 2021), cutin is a polyester of oxygenated fatty acids (mainly with hydroxyl and/or epoxide groups, but in less proportion with oxo groups) of 16 and 18 carbon atoms (Yeats and Rose, 2013). In some plants and, especially those of the Brassicaceae family, high amounts of dicarboxylic acids (DCA) are found while they are minor compounds in other plants (Franke et al., 2005; Razeq et al., 2021).

The diversity of cutin monomer compositions has to be analyzed in relation to the architecture of the cutin polyester. Two physical parameters characterize the architecture of polymers, their size and their reticulation (Caccavo et al., 2018). In contrast with synthetic polyesters, measuring precisely the size of the cutin polymer is not possible since it cannot be solubilized. However, *in planta*, the cutin synthase (CUS1)-catalyzed cutin polymerization from 2-monoacylglycerol (2-MAG), gives rise to polyester with glycerol at the carboxylate terminus (Yeats and Rose, 2013). Therefore, the molar ratio of glycerol to hydroxy-fatty acid (HOFA) ratio allows the comparison of the polymer sizes of cutins between plant species or mutants. Indeed, this ratio is highly variable between plants suggesting a diversity of cutin molecular sizes (Graça et al., 2002) and in *cus1* tomato mutants, the increase of this ratio regarding the wild-type suggested a lower cutin polymer size (Philippe et al., 2016). This chemical rule has however some limit for DCA-rich cutins of Brassicaceae, where this particular composition came along with a high amount of glycerol and a DCA:glycerol molar ratio of 1:2 consistent with the formation of glycerol-DCA-glycerol polyesters (Yang et al., 2016).

Concerning cutin reticulation, it is necessary to consider the basic chemical reaction of polyesterification of components bearing both hydroxyl and carboxylate groups and two carboxylate groups and leading to branched polyesters (McKee et al., 2005) or cross-linked polymer networks (Gu et al., 2019). Branched vs. linear cutin polyesters, will depend (i) on the presence of mid-chain hydroxyls as for the 9(10),16-dihydroxy hexadecanoic acid (diOHC16) and (ii) on the OH/COOH molar ratio in the global monomer composition and especially on the level of DCA. It is also important to consider the hydroxyls of glycerol in this ratio, although this triol displays relatively low contents in cuticles. Indeed, as a branching point, it seems involved in the reticulation of tomato cutin (Philippe et al., 2016).

However, while tomato cutin contains more than 75% diOHC16, it is surprising to observe that more than 80% of the midOH groups of tomato cutin are esterified and can reach up to 90% in the cutin of red ripe fruit (Philippe et al., 2016). Furthermore, in the *cus1* mutant, the lower expression of CUS1 induces a high decrease of midOH esterification (Philippe et al., 2016). In these mutants, the cutin deposition and cutin density are also lowered suggesting that CUS1 could also facilitate esterification of the mid-chain secondary alcohol group when the cutin density is sufficient to create a favorable hydrophobic environment (Girard et al., 2012; Philippe et al., 2016). Esterification of midchain hydroxyl could also involve another enzyme and especially a cutin: cutin transacylase activity recently described (Xin et al., 2021). Whatever the mechanism of polymerization, in diOHC16-rich cutins, the polyesterification would typically lead to hyperbranched macromolecules that are easily soluble in organic solvents (Testud et al., 2017) while cutin is insoluble. Furthermore, branching through the midOH group should lead to an increase of non-esterified ω-OH groups while this was not observed (Philippe et al., 2016). It is therefore necessary to consider the links between cutin and the other cuticle compounds, i.e., phenolics and polysaccharides (**Figure 1**).

Phenolics, generally regarded as minor components, are also embedded in the cuticles. These phenolics comprise two main types of molecules, phenolic acids (e.g., para-coumarate) and flavonoids (e.g., naringenin). Hunt and Baker (1980) suggested that they are associated with the cutin by ester bonds since all the phenolic acids are released after alkaline hydrolysis (Hunt and Baker, 1980). However, ester links with polysaccharides is also possible and are described in the xylan and pectin fractions of the cell walls of both monocots and dicots (Mnich et al., 2020). An ester link with the cutin polymer must be also considered regarding the characterization of an enzyme of the BAHD family capable to esterify the ω-position of HOFA by a phenolic acid (Rautengarten et al., 2012; Molina and Kosma, 2015). Unexpectedly, these minor ester bonds of the cutin polymer seem essential for the cuticle architecture of tomato fruit (Lashbrooke et al., 2016). The importance of such chemical bonds is also strengthened by the evolution of plant hydrophobic polymers, and especially in mosses where cutin is a co-polyester of HOFA and phenolic acids (Renault et al., 2017). On the contrary, a part of flavonoids is extractible with methanol while the other was extracted only after alkaline hydrolysis of the cuticle (Hunt and Baker, 1980). Ester bonds between cutin and flavonoids are unlikely due to the absence of carboxylate on these molecules. From sorption studies of naringenin into tomato cuticles, it was suggested that flavonoids can form solid clusters within the cuticles which can be dissociated only after cutin depolymerization (Dominguez et al., 2009). In agreement with this equilibrium partition within the cuticle, the ketone group of flavonoids could form hemiacetal and/or acetal derivatives with the alcohol group of cutin, and especially with the glycerol moieties of cutins (Moity et al., 2015) (**Figure 1**). In this regard, such bonds can be also considered with minor cutin fatty acids containing oxo groups.

The ester bonds between phenolic acids and cutin could be questioned regarding cutin reticulation. These HOFA-phenolic

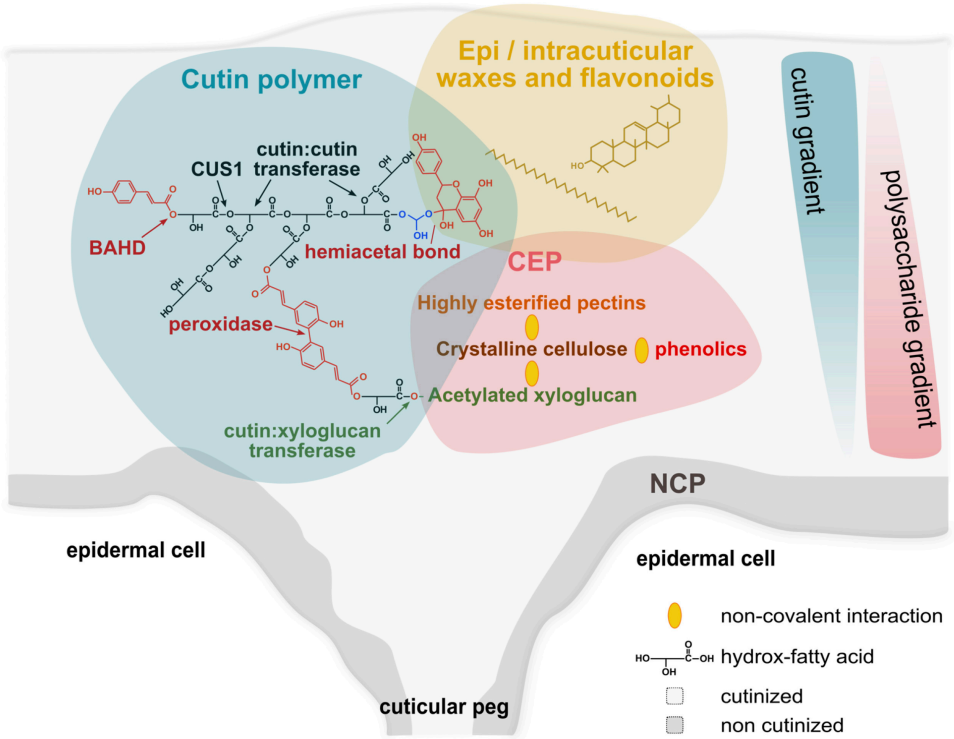

FIGURE 1 | Schematic model for the complex architecture of plant cuticles. Plant cuticle (gray background) is a natural hydrophobic composite. The lipid scaffold of the cuticle is the cutin polymer (blue background) embedded with waxes (yellow background), and associated to the cuticle-embedded polysaccharides (CEP, red background). Cutin is a polyester network of HOFA mainly formed by the activities of CUS1 (a protein from the multigenic GDSL family of esterase/lipase) (Girard et al., 2012) and cutin:cutin acyl transferase (CCAT, the protein associated with this activity has not yet been identified) during the expansion of the plant cuticle (Xin et al., 2021). Para-coumaric acid esterification of the primary alcohol group of HOFA (co-position) is catalyzed by an enzyme of the multigenic BAHD family (Molina and Kosma, 2015) and could form covalent bridges between the polyester chains through peroxidase oxidation (Kerr and Fry, 2004; Arrieta-Baez and Stark, 2006). The strong association of flavonoids (e.g., naringenin and naringenin chalcone in tomato), especially at the end of fruit growth (Hunt and Baker, 1980) could involve hemiacetal bond with primary hydroxyl groups (e.g., with the glycerol end residue of 2-monoacylglycerol, the precursor of CUS1). The cutin:xyloglucan transferase is a good candidate to link covalently the cutin network to the CEP (Xin and Fry, 2021). In contrast to the non-cutinized polysaccharides (NCP), the CEP concentrates crystalline cellulose, highly esterified pectins and acetylated xyloglucans (Philippe et al., 2020) associated by non-covalent bonds (yellow ellipses). In addition, the hydrophobicity of these polysaccharides is compatible with non-covalent interactions (Ngouémazong et al., 2015; Dai et al., 2020; Lindman et al., 2021) with the cutin network and intracuticular waxes. Finally, cellulose can also interact with phenolics (Phan et al., 2015). The cutin network and CEP form gradients in the cuticle thickness create a spatial heterogeneity in the plant cuticles.

esters could dimerize through carbon–carbon bonds under oxidative reactions as suggested for suberin (Arrieta-Baez and Stark, 2006). As for arabinoxylan cross-linking (Kerr and Fry, 2004), a similar chemical mechanism could be considered for the anchoring of polysaccharides and cutin (though phenolic acids in plant cell walls are commonly found on arabinose moieties that are not a dominant sugar in tomato cuticle) and/or for the cross-linking of cutin linear chains. The role of phenolics is strengthened by the polyesterification of diOHC16 and phenolic-rich fractions of tomato pomaces. This non-catalyzed and temperature-controlled process induces oxidation of the phenolic compounds and the formation of an insoluble cross-linked polymer network and not of soluble branched polyesters (Marc et al., 2021). *In planta*, this oxidation could be driven by peroxidases that accumulate at the end of fruit growth (Andrews et al., 2000).

The presence of polysaccharides in the cuticular layer leads to the concept of the cell wall continuum of the epidermis (Fich et al., 2016). The fine structure of the cutin-embedded polysaccharides (CEP) was first investigated by immunolabeling studies on leaves or fruit epidermis from pear and tomato and resulted in either very faint or no labeling of cellulose and pectin within the cutin matrix (Guzman et al., 2014a,b; Segado et al., 2016) probably due to the masking of the glycoside epitopes. By combining different investigation methods, it was recently shown that these CEP display specific features regarding those of the sub-cuticular, non-cutinized cell walls. Especially, in the tomato cuticle, the pectin and hemicelluloses (enriched in xyloglucan) are highly esterified, while a higher content in crystalline cellulose is observed (Philippe et al., 2020). Pectins embedded in the cuticle display a low ramification of rhamnogalacturonan (RGI). These CEP structural features are in favor of a lipid-polysaccharide association. Indeed, high methyl- and acetyl-esterification of pectin and hemicellulose increase their apolarity making interactions with lipids possible. Indeed, pectin methyl- and acetyl-esters have often been

related to oil/water emulsification and emulsion stabilization (Ngouémazong et al., 2015). Low ramified RGI in the CEP with the apolar rhamnose residue and the acetyl esters are also expected to participate in pectin–lipid interactions. Cellulose is an amphiphilic polysaccharide that stabilizes lipid emulsion through hydrophobic interactions (Lindman et al., 2021). Its crystalline assemblies also interact with lipids to stabilize emulsions via the hydrophobic face of the crystals (Dai et al., 2020). Furthermore, phenolic derivatives of lipids can also contribute to lipid–polysaccharides interactions since phenolics can interact with cellulose (Phan et al., 2015). Thus, lipids and derivatives can physically form hydrophobic association with polysaccharides in the cutinized cell-wall domain of the cuticle. As observed for the xyloglucan-cellulose-pectin assemblies of cell walls, the non-covalent links between the polysaccharides and cutin should be sufficient to give the cuticle both strength and flexibility needed for organ growth.

If a covalent link was highlighted after partial depolymerization of lime fruit (Tian et al., 2008), no other studies reported similar heteromers in plant cuticles. Interestingly, an enzyme activity capable of linking HOFA and polysaccharides, and specific for xyloglucans, i.e., a cutin:xyloglucan transacylase (CXT), was recently characterized (Xin and Fry, 2021). Furthermore, in tomato fruit, both the CXT activity and xyloglucan contents increase in the epidermis during fruit expansion (Takizawa et al., 2014). CXT could play a significant role in the construction of the cuticle architecture since xyloglucans are embedded in cuticles (Philippe et al., 2020).

In summary, the cutin polyester can be considered as a branched or hyperbranched polyester architecture which is insolubilized by the multiple covalent and non-covalent links created during organ growth with polysaccharides and phenolics (**Figure 1**). The cuticle image portrayed from numerous microscopy investigations described cuticle architecture as two hierarchically organized layers including an upper cuticular proper mixing cutin and waxes, and a lower cuticular layer containing cutin, polysaccharides, and intra-cuticular waxes (Jeffree, 2006). Much progress has been done in imaging, especially thanks to the development of Raman, infrared and MALDI mass imaging that provide information on the distribution of lipid, carbohydrate and phenolic compounds within cuticles (Vrkoslav et al., 2010; Velickovic et al., 2014; Philippe et al., 2016; Sasani et al., 2021). Actually, compositional gradients were observed both on the surface (Philippe et al., 2016) and within the thickness of the cuticular layer (Philippe et al., 2020; Sasani et al., 2021). The cutin/polysaccharide ratio decreases from the outer cuticle to the inner cell wall-cuticle interface (Philippe et al., 2020) while phenolic compounds are mainly associated with the waxes and cutin-rich regions (Sasani et al., 2021). The question of the lipid-polysaccharides molecular orientational order was also raised recently on leaves models (Hama et al., 2019). Furthermore, deep cutinization of cell walls can occur between epidermal cells creating anticlinal pegs adjacent to epidermis cells (Buda et al., 2009). Discontinuities can also occur with the presence of trichomes creating small polysaccharide transcuticular channels (Fich et al., 2020) or the presence of suberized lenticels in apple fruit (Velickovic et al., 2014). Therefore, cuticle architecture displays chemical heterogeneities in all the dimensions of the 3D space. This architecture seems also finely regulated and mutations affecting a specific component of the cuticles induce modification of the expression of genes involves in the synthesis and assembly of the others. For example, in tomatoes, downregulation of GPAT6, an enzyme involved in the biosynthesis of the cutin substrate of *cus1*, modifies the expression of genes involved in the synthesis of polysaccharides and phenolics (Petit et al., 2016). It is also interesting to note that major cuticle-associated transcription factors, e.g., SHINE or MIXTA regulate coordinately the synthesis of polysaccharides, cutin monomer, wax and phenolics, and epidermal patterning (Shi et al., 2011; Lashbrooke et al., 2016). This fine regulation comes along with a dynamic of the cuticle architecture needed for and occurring during organ growth. This is well illustrated with the recent observation of a cutin: cutin transacylase activity capable of rearranging the architecture of the cutin polyester by a cut and paste mechanism during the growth of plant epidermis (Xin and Fry, 2021), similar to the xyloglucan endotransglucosylase/hydrolase (XTH) for polysaccharides remodeling during organ growth (Rose et al., 2002) or to the suberin polymerization-degradation process catalyzed by clusters of enzymes from the GDSL-family of esterase/lipase during lateral root formation (Ursache et al., 2021).

FROM CUTICLE ARCHITECTURE TO FUNCTIONAL PROPERTIES

The complexity of the architecture of plant cuticles can explain controversies in the role of the different components in their properties. This is well illustrated by the role of waxes and cutin on the water permeability of cuticles. If a consensus exists on the major role of waxes on water permeability, this is still debated for cutin. Previous studies showed differences in *Clivia miniata* leaf cuticle permeability between young and old leaves and were related to structural differences of the cutin matrix reticulation (Schmidt et al., 1981). It was suggested that wax filling of the cutin matrix depends on the cutin scaffold to explain the impact of cutin defects on cuticle water permeability (Goodwin and Jenks, 2005). However, water permeance of tomato cutin from *gpat6* tomato mutant (not affected in cutin polymerization) and from *cus1* mutants (affected in cutin polymerization) was not significantly different (Philippe et al., 2016), suggesting that the rule developed by Goodwin and Jenks cannot be applied to the cuticle of tomato fruit. Cuticle water permeability seems also related to the presence of small polysaccharide transcuticular channels, as illustrated in remnants of trichomes in some tomato accessions (Fich et al., 2020; Slot et al., 2021). The data on cuticle water permeability clearly illustrate that the functional properties of cuticles are due to the combination of the properties of each cuticular component and their hierarchical organization in a complex architecture.

Likewise, the cuticle mechanical properties are driven by the association of the cuticular components, while the direct contribution of each cuticle component is difficult to determine

in planta. Many studies have examined the mechanical properties of isolated cuticles from different botanical origins, primarily through tensile tests (Khanal and Knoche, 2017). The resulting data demonstrated that the mechanical properties of cuticles are mainly determined by their: (i) anatomy (Allende et al., 2004; Matas et al., 2004), (ii) relative humidity (Matas et al., 2005), and (iii) relative proportions of constituents in particular during the fruit development. The accumulation of waxes and non-esterified flavonoids has been associated with an increase in cuticle stiffness (Bargel and Neinhuis, 2004; Espana et al., 2014). Notably, the contribution of esterified phenolic acids to cuticle mechanical properties is not documented although the absence of this link impairs the mechanical properties of the cuticle (Lashbrooke et al., 2016).

The cutin polyester fraction is described as a typical viscoelastic material (Knoche and Lang, 2017) whose mechanical properties would be impacted by its reticulation index. Indeed, AFM surface analyses of cutin from *cus1* tomato mutant showed a lower Young's elastic modulus than the corresponding wild-type (Isaacson et al., 2009). This result was recently strengthened by studies on synthetic biomimetic copolyesters of cutin HOFA and glycerol where a decrease in the cutin-like polyester reticulation has been associated with a decrease in Young's elastic modulus and a twofold increase in the strain at break (Marc et al., 2021).

The impact of different CEP on mechanical properties is less documented (Khanal and Knoche, 2017). However, paralleling the data available from the cell wall polysaccharides models, the recent identification of the specific feature of the CEP should bring new hypotheses on their impact on the cuticle mechanical properties. Indeed, reversible interactions of methyl esterified pectin with cellulose have been observed *in vitro* (Lin et al., 2016, 2018). Moreover, in pectin-cellulose model composites, an increase in the methyl esterification rate was associated with an increase in their elastic storage modulus (Lin et al., 2016, 2018). In similar model composites, hemicellulose (xyloglucan and glucomannan) affects the cellulose structuring and the mechanical properties of the composites. In particular, xyloglucan increases the composite extensibility and the decrease of its tensile elastic modulus while glucomannan leads to the opposite effect (Chanliaud et al., 2002; Berglund et al., 2020). These data open the way to the conception of new biomimetic models combining pectin, hemicellulose, and cellulose with lipids and to target specific genes in plant mutants to affect the construction and assembly of these polysaccharides and lipids to assess their specific function on the viscoelastic mechanical and/or barrier properties of cuticle.

CONCLUSION

The cuticle can be considered as a polymeric composite displaying spatial heterogeneity. Our knowledge of the architecture of cuticles is rapidly progressing thanks to the development of physical instrumentation and in the future, probably with the development of correlative investigations coupling different physical techniques and modeling. Most of the studies are performed with tomato fruit which is amenable to delineate cuticle architecture. Indeed, tomato cuticle can be isolated easily, has a thickness compatible with the resolution of most physical techniques, its cutin is dominated by diOHC16 and different genetic tools are available to modify their composition. The architecture–function relationships of cuticles are still in their infancy, but should also progress rapidly and should benefit in particular (i) from the delineation of the architecture-associated enzyme network (CUS1, CXT, CCT, etc.) and (ii) from biomimicry approaches. Biomimicry will especially extend the concept of a spatially tunable architecture of the cuticle to fulfill their multiple functionalities while tailoring original bioinspired materials (Heredia-Guerrero et al., 2017).

AUTHOR CONTRIBUTIONS

BB, DM, and NR wrote the first draft. All authors contributed to the article and approved the submitted version.

FUNDING

NR was supported by a Ph.D. grant (SeaSCAPE) from INRAE and the Region Pays de la Loire.

REFERENCES

Allende, A., Desmet, M., Vanstreels, E., Verlinden, B. E., and Nicolai, B. M. (2004). Micromechanical and geometrical properties of tomato skin related to differences in puncture injury susceptibility. *Postharvest. Biol. Tec.* 34, 131–141. doi: 10.1016/j.postharvbio.2004.05.007

Andrews, J., Malone, M., Thompson, D. S., Ho, L., and Burton, K. (2000). Peroxidase isozyme patterns in the skin of maturing tomato fruit. *Plant Cell Environ.* 23, 415–422. doi: 10.1046/j.1365-3040.2000.00555.x

Arrieta-Baez, D., and Stark, R. E. (2006). Modeling suberization with peroxidase-catalyzed polymerization of hydroxycinnamic acids: cross-coupling and dimerization reactions. *Phytochemistry* 67, 743–753. doi: 10.1016/j.phytochem.2006.01.026

Bargel, H., and Neinhuis, C. (2004). Altered tomato fruit cuticle biomechanics of a pleiotropic non ripening mutant. *J. Plant Growth Regul.* 23, 61–75. doi: 10.1007/s00344-004-0036-0

Berglund, J., Mikkelsen, D., Flanagan, B. M., Dhital, S., Gaunitz, S., Henriksson, G., et al. (2020). Wood hemicelluloses exert distinct biomechanical contributions to cellulose fibrillar networks. *Nat. Comm.* 11, 1–16. doi: 10.1038/s41467-020-18390-z

Berhin, A., de Bellis, D., Franke, R. B., Buono, R. A., Nowack, M. K., and Nawrath, C. (2019). The root cap cuticle: A cell wall structure for seedling establishment and lateral root formation. *Cell* 176, 1367–1378. doi: 10.1016/j.cell.2019.01.005

Bhanot, V., Fadanavis, S. V., and Panwar, J. (2021). Revisiting the architecture, biosynthesis and functional aspects of the plant cuticle: There is more scope. *Environ. Exp. Bot.* 183:104364. doi: 10.1016/j.envexpbot.2020.104364

Buda, G. J., Isaacson, T., Matas, A. J., Paolillo, D. J., and Rose, J. K. (2009). Three-dimensional imaging of plant cuticle architecture using confocal scanning laser microscopy. *Plant J.* 60, 378–385. doi: 10.1111/j.1365-313X.2009.03960.x

Caccavo, D., Cascone, S., Lamberti, G., and Barba, A. (2018). Hydrogels: experimental characterization and mathematical modelling of their mechanical and diffusive behaviour. *Chem. Soc. Rev.* 47, 2357–2373. doi: 10.1039/C7CS00638A

Chanliaud, E., Burrows, K. M., Jeronimidis, G., and Gidley, M. J. (2002). Mechanical properties of primary plant cell wall analogues. *Planta* 215, 989–996. doi: 10.1007/s00425-002-0783-8

Cordovez, V., Dini-Andreote, F., Carrión, V. J., and Raaijmakers, J. M. (2019). Ecology and evolution of plant microbiomes. *Annu. Rev. Microbiol.* 73, 69–88. doi: 10.1146/annurev-micro-090817-062524

Dai, H., Wu, J., Zhang, H., Chen, Y., Ma, L., Huang, H., et al. (2020). Recent advances on cellulose nanocrystals for Pickering emulsions: development and challenge. *Trends Food Sci. Tech.* 102, 16–29. doi: 10.1016/j.tifs.2020.05.016

Dominguez, E., Luque, P., and Heredia, A. (2009). Sorption and interaction of the flavonoid naringenin on tomato fruit cuticles. *J. Agric. Food Chem.* 57, 7560–7564. doi: 10.1021/jf9011455

Espana, L., Heredia-Guerrero, J. A., Segado, P., Benitez, J. J., Heredia, A., and Dominguez, E. (2014). Biomechanical properties of the tomato (*Solanum lycopersicum*) fruit cuticle during development are modulated by changes in the relative amounts of its components. *New Phytol.* 202, 790–802. doi: 10.1111/nph.12727

Fich, E. A., Fisher, J., Zamir, D., and Rose, J. K. C. (2020). Transpiration from tomato fruit occurs primarily via trichome-associated transcuticular polar pores. *Plant Physiol.* 184, 1840–1852. doi: 10.1104/pp.20.01105

Fich, E. A., Segerson, N. A., and Rose, J. K. (2016). The plant polyester cutin: biosynthesis, structure, and biological roles. *Annu. Rev. Plant Biol.* 67, 207–233. doi: 10.1146/annurev-arplant-043015-111929

Franke, R., Briesen, I., Wojciechowski, T., Faust, A., Yephremov, A., Nawrath, C., et al. (2005). Apoplastic polyesters in Arabidopsis surface tissues-a typical suberin and a particular cutin. *Phytochemistry* 66, 2643–2658. doi: 10.1016/j.phytochem.2005.09.027

Girard, A. L., Mounet, F., Lemaire-Chamley, M., Gaillard, C., Elmorjani, K., Vivancos, J., et al. (2012). Tomato GDSL1 is required for cutin deposition in the fruit cuticle. *Plant Cell* 24, 3119–3134. doi: 10.1105/tpc.112.101055

Goodwin, S. M., and Jenks, M. A. (2005). "Plant cuticle function as a barrier to water loss," in *Plant Abiotic Stress*, eds M. A. Jenks and P. M. Hasegawa (Hoboken, NJ: Blackwell Publishing Ltd), 14–36. doi: 10.1002/9780470988503.ch2

Graça, J. (2015). Suberin: the biopolyester at the frontier of plants. *Front. Chem.* 3:62. doi: 10.3389/fchem.2015.00062

Graça, J., Schreiber, L., Rodrigues, J., and Pereira, H. (2002). Glycerol and glyceryl esters of ω-hydroxyacids in cutins. *Phytochemistry* 61, 205–215. doi: 10.1016/S0031-9422(02)00212-1

Gu, Y., Zhao, J., and Johnson, J. A. (2019). A (macro) molecular-level understanding of polymer network topology. *Trends Chem.* 1, 318–334. doi: 10.1016/j.trechm.2019.02.017

Guzman, P., Fernandez, V., Garca, M. A. L., Khayet, M., Fernendez, A. N., and Gil, L. (2014a). Localization of polysaccharides in isolated and intact cuticles of eucalypt, poplar and pear leaves by enzyme-gold labelling. *Plant Physiol. Biochem.* 76, 1–6. doi: 10.1016/j.plaphy.2013.12.023

Guzman, P., Fernández, V., Graça, J., Cabral, V., Kayali, N., Khayet, M., et al. (2014b). Chemical and structural analysis of Eucalyptus globulus and E. camaldulensis leaf cuticles: a lipidized cell wall region. *Front. Plant Sci.* 5:481. doi: 10.3389/fpls.2014.00481

Hama, T., Seki, K., Ishibashi, A., Miyazaki, A., Kouchi, A., Watanabe, N., et al. (2019). Probing the Molecular Structure and Orientation of the Leaf Surface of Brassica oleracea L. by Polarization Modulation-Infrared Reflection-Absorption Spectroscopy. *Plant Cell Physiol.* 60, 1567–1580. doi: 10.1093/pcp/pcz063

Heredia-Guerrero, J. A., Benitez, J. J., Cataldi, P., Paul, U. C., Contardi, M., Cingolani, R., et al. (2017). All-natural sustainable packaging materials inspired by plant cuticles. *Adv. Sustain. Syst.* 1:1600024. doi: 10.1002/adsu.201600024

Hunt, G. M., and Baker, E. A. (1980). Phenolic constituents of tomato fruit cuticles. *Phytochemistry* 19, 1415–1419. doi: 10.1016/0031-9422(80)80185-3

Isaacson, T., Kosma, D. K., Matas, A. J., Buda, G. J., He, Y., Yu, B., et al. (2009). Cutin deficiency in the tomato fruit cuticle consistently affects resistance to microbial infection and biomechanical properties, but not transpirational water loss. *Plant J.* 60, 363–377. doi: 10.1111/j.1365-313X.2009.03969.x

Jeffree, C. E. (2006). "The fine structure of the plant cuticle," in *Biology of the Plant Cuticle* (Oxford: Blackwell Publishing Ltd), 11–125. doi: 10.1002/9780470988718.ch2

Kerr, E. M., and Fry, S. C. (2004). Extracellular cross-linking of xylan and xyloglucan in maize cell-suspension cultures: the role of oxidative phenolic coupling. *Planta* 219, 73–83. doi: 10.1007/s00425-004-1210-0

Khanal, B. P., and Knoche, M. (2017). Mechanical properties of cuticles and their primary determinants. *J. Exp. Bot.* 68, 5351–5367. doi: 10.1093/jxb/erx265

Knoche, M., and Lang, A. (2017). Ongoing growth challenges in fruit skin integrity. *CRC CR. Rev. Plant Sci.* 36, 190–215. doi: 10.1080/07352689.2017.1369333

Lashbrooke, J., Cohen, H., Levy-Samocha, D., Tzfadia, O., Panizel, I., Zeisler, V., et al. (2016). MYB107 and MYB9 homologs regulate suberin deposition in Angiosperms. *Plant Cell* 28, 2097–2116. doi: 10.1105/tpc.16.00490

Li, F.-S., Phyo, P., Jacobowitz, J., Hong, M., and Weng, J.-K. (2019). The molecular structure of plant sporopollenin. *Nat. Plants* 5, 41–46. doi: 10.1038/s41477-018-0330-7

Lin, D., Lopez-Sanchez, P., and Gidley, M. J. (2016). Interactions of pectins with cellulose during its synthesis in the absence of calcium. *Food Hydrocolloid.* 52, 57–68. doi: 10.1016/j.foodhyd.2015.06.004

Lin, D., Lopez-Sanchez, P., Selway, N., and Gidley, M. J. (2018). Viscoelastic properties of pectin/cellulose composites studied by QCM-D and oscillatory shear rheology. *Food Hydrocolloid.* 79, 13–19. doi: 10.1016/j.foodhyd.2017.12.019

Lindman, B., Medronho, B., Alves, L., Norgren, M., and Nordenskiöld, L. (2021). Hydrophobic interactions control the self-assembly of DNA and cellulose. *Q. Rev. Biophys.* 54:19. doi: 10.1017/S0033583521000019

Marc, M., Risani, R., Desnoes, E., Falourd, X., Pontoire, B., Rodrigues, R., et al. (2021). Bioinspired co-polyesters of hydroxy-fatty acids extracted from tomato peel agro-wastes and glycerol with tunable mechanical, thermal and barrier properties. *Ind. Crop. Prod.* 170:113718. doi: 10.1016/j.indcrop.2021.113718

Martin, L. B., and Rose, J. K. (2014). There's more than one way to skin a fruit: formation and functions of fruit cuticles. *J. Exp. Bot.* 65, 4639–4651. doi: 10.1093/jxb/eru301

Matas, A. J., Cobb, E. D., Bartsch, J. A., Paolillo, D. J. Jr., and Niklas, K. J. (2004). Biomechanics and anatomy of Lycopersicon esculentum fruit peels and enzyme-treated samples. *Am. J. Bot.* 91, 352–360. doi: 10.3732/ajb.91.3.352

Matas, A. J., Lopez-Casado, G., Cuartero, J., and Heredia, A. (2005). Relative humidity and temperature modify the mechanical properties of isolated tomato fruit cuticles. *Am. J. Bot.* 92, 462–468. doi: 10.3732/ajb.92.3.462

McKee, M. G., Unal, S., Wilkes, G. L., and Long, T. E. (2005). Branched polyesters: recent advances in synthesis and performance. *Prog. Polym. Sci.* 30, 507–539. doi: 10.1016/j.progpolymsci.2005.01.009

Meder, F., Must, I., Sadeghi, A., Mondini, A., Filippeschi, C., Beccai, L., et al. (2018). Energy conversion at the cuticle of living plants. *Adv. Func. Mat.* 28:1806689. doi: 10.1002/adfm.201806689

Mnich, E., Bjarnholt, N., Eudes, A., Harholt, J., Holland, C., Jørgensen, B., et al. (2020). Phenolic cross-links: building and de-constructing the plant cell wall. *Nat. Prod. Rep.* 37, 919–961. doi: 10.1039/C9NP00028C

Moity, L., Benazzouz, A., Molinier, V., Nardello-Rataj, V., Elmkaddem, M. K., De Caro, P., et al. (2015). Glycerol acetals and ketals as bio-based solvents: positioning in Hansen and COSMO-RS spaces, volatility and stability towards hydrolysis and autoxidation. *Green Chem.* 17, 1779–1792. doi: 10.1039/C4GC02377C

Molina, I., and Kosma, D. (2015). Role of HXXXD-motif/BAHD acyltransferases in the biosynthesis of extracellular lipids. *Plant Cell Rep.* 34, 587–601. doi: 10.1007/s00299-014-1721-1725

Ngouémazong, E. D., Christiaens, S., Shpigelman, A., Van Loey, A., and Hendrickx, M. (2015). The emulsifying and emulsion-stabilizing properties of pectin: a review. *Compr. Rev. Food Sci. Food Saf.* 14, 705–718. doi: 10.1111/1541-4337.12160

Petit, J., Bres, C., Mauxion, J. P., Tai, F. W., Martin, L. B., Fich, E. A., et al. (2016). The glycerol-3-phosphate acyltransferase GPAT6 from tomato plays a central role in fruit cutin biosynthesis. *Plant Physiol.* 171, 894–913. doi: 10.1104/pp.16.00409

Phan, A. D. T., Netzel, G., Wang, D., Flanagan, B. M., D'Arcy, B. R., and Gidley, M. J. (2015). Binding of dietary polyphenols to cellulose: structural and nutritional aspects. *Food Chem.* 171, 388–396. doi: 10.1016/j.foodchem.2014.08.118

Philippe, G., Gaillard, C., Petit, J., Geneix, N., Dalgalarrondo, M., Bres, C., et al. (2016). Ester cross-link profiling of the cutin polymer of wild-type and cutin synthase tomato mutants highlights different mechanisms of polymerization. *Plant Physiol.* 170, 807–820. doi: 10.1104/pp.15.01620

Philippe, G., Geneix, N., Petit, J., Guillon, F., Sandt, C., Rothan, C., et al. (2020). Assembly of tomato fruit cuticles: a cross-talk between the cutin polyester and cell wall polysaccharides. *New Phytol.* 226, 809–822. doi: 10.1111/nph.16402

Ralph, J., Lapierre, C., and Boerjan, W. (2019). Lignin structure and its engineering. *Curr. Opin. Biotechnol.* 56, 240–249. doi: 10.1016/j.copbio.2019.02.019

Rautengarten, C., Ebert, B., Ouellet, M., Nafisi, M., Baidoo, E. E., Benke, P., et al. (2012). Arabidopsis Deficient in Cutin Ferulate encodes a transferase required for feruloylation of omega-hydroxy fatty acids in cutin polyester. *Plant Physiol.* 158, 654–665. doi: 10.1104/pp.111.187187pp.111.187187

Razeq, F. M., Kosma, D. K., França, D., Rowland, O., and Molina, I. (2021). Extracellular lipids of *Camelina sativa*: Characterization of cutin and suberin reveals typical polyester monomers and unusual dicarboxylic fatty acids. *Phytochemistry* 184:112665. doi: 10.1016/j.phytochem.2021.112665

Renault, H., Alber, A., Horst, N. A., Basilio Lopes, A., Fich, E. A., Kriegshauser, L., et al. (2017). A phenol-enriched cuticle is ancestral to lignin evolution in land plants. *Nat. Commun.* 8:14713. doi: 10.1038/ncomms14713

Rose, J. K., Braam, J., Fry, S. C., and Nishitani, K. (2002). The XTH family of enzymes involved in xyloglucan endotransglucosylation and endohydrolysis: current perspectives and a new unifying nomenclature. *Plant Cell Physiol.* 43, 1421–1435. doi: 10.1093/pcp/pcf171

Sasani, N., Bock, P., Felhofer, M., and Gierlinger, N. (2021). Raman imaging reveals in-situ microchemistry of cuticle and epidermis of spruce needles. *Plant Methods* 17:17. doi: 10.1186/s13007-021-00717-6

Schmidt, H., Mérida, T., and Schönherr, J. (1981). Water permeability and fine structure of cuticular membranes isolated enzymatically from leaves of *Clivia miniata Reg. Z.Pflanzenphysiol.* 105, 41–51. doi: 10.1016/S0044-328X(81)80006-2

Schönherr, J., and Riederer, M. (1989). "Foliar penetration and accumulation of organic chemicals in plant cuticles," in *Reviews of Environmental Contamination and Toxicology*, Vol. 108, ed. G. W. Ware (New York, NY: Springer), 1–70. doi: 10.1007/978-1-4613-8850-0_1

Segado, P., Dominguez, E., and Heredia, A. (2016). Ultrastructure of the Epidermal Cell Wall and Cuticle of Tomato Fruit (Solanum lycopersicum L.) during Development. *Plant Physiol.* 170, 935–946. doi: 10.1104/pp.15.01725

Shi, J. X., Malitsky, S., De Oliveira, S., Branigan, C., Franke, R. B., Schreiber, L., et al. (2011). SHINE transcription factors act redundantly to pattern the archetypal surface of Arabidopsis flower organs. *PLoS Genet.* 7:e1001388. doi: 10.1371/journal.pgen.1001388

Slot, M., Nardwattanawong, T., Hernández, G. G., Bueno, A., Riederer, M., and Winter, K. (2021). Large differences in leaf cuticle conductance and its temperature response among 24 tropical tree species from across a rainfall gradient. *New Phytol.* 2021:17626. doi: 10.1111/nph.17626

Takizawa, A., Hyodo, H., Wada, K., Ishii, T., Satoh, S., and Iwai, H. (2014). Regulatory specialization of xyloglucan (XG) and glucuronoarabinoxylan (gax) in pericarp cell walls during fruit ripening in tomato (*Solanum lycopersicum*). *PLoS One* 9, 3–10. doi: 10.1371/journal.pone.0089871

Testud, B., Pintori, D., Grau, E., Taton, D., and Cramail, H. (2017). Hyperbranched polyesters by polycondensation of fatty acid-based AB n-type monomers. *Green Chem.* 19, 259–269. doi: 10.1039/C6GC02294D

Tian, S., Fang, X., Wang, W., Yu, B., Cheng, X., Qiu, F., et al. (2008). Isolation and identification of oligomers from partial degradation of lime fruit cutin. *J. Agric. Food Chem.* 56, 10318–10325. doi: 10.1021/jf801028g

Ursache, R., DeJesusVieiraTeixeira, C., DenervaudTendon, V., Gully, K., DeBellis, D., and Schmid-Siegert, E. (2021). GDSL-domain proteins have key roles in suberin polymerization and degradation. *Nat. Plants* 7, 353–364. doi: 10.1038/s41477-021-00862-9

Velickovic, D., Herdier, H., Philippe, G., Marion, D., Rogniaux, H., and Bakan, B. (2014). Matrix-assisted laser desorption/ionization mass spectrometry imaging: a powerful tool for probing the molecular topology of plant cutin polymer. *Plant J.* 80, 926–935. doi: 10.1111/tpj.12689

Vrkoslav, V., Muck, A., Cvačka, J., and Svatoš, A. (2010). MALDI imaging of neutral cuticular lipids in insects and plants. *J. Am. Soc. Mass Spectrom.* 21, 220–231. doi: 10.1016/j.jasms.2009.10.003

Xin, A., Fei, Y., Molnar, A., and Fry, S. C. (2021). Cutin: cutin-acid endo-transacylase (CCT), a cuticle-remodelling enzyme activity in the plant epidermis. *Biochem. J.* 478, 777–798. doi: 10.1042/BCJ20200835

Xin, A., and Fry, S. C. (2021). Cutin: xyloglucan transacylase (CXT) activity covalently links cutin to a plant cell-wall polysaccharide. *J. Plant Physiol.* 2021:153446. doi: 10.1016/j.jplph.2021.153446

Yang, W., Pollard, M., Li-Beisson, Y., and Ohlrogge, J. (2016). Quantitative analysis of glycerol in dicarboxylic acid-rich cutins provides insights into Arabidopsis cutin structure. *Phytochemistry* 130, 159–169. doi: 10.1016/j.phytochem.2016.03.017

Yeats, T. H., and Rose, J. K. (2013). The formation and function of plant cuticles. *Plant Physiol.* 163, 5–20. doi: 10.1104/pp.113.222737

Conflict of Interest: The authors declare that the research was conducted in the absence of any commercial or financial relationships that could be construed as a potential conflict of interest.

Publisher's Note: All claims expressed in this article are solely those of the authors and do not necessarily represent those of their affiliated organizations, or those of the publisher, the editors and the reviewers. Any product that may be evaluated in this article, or claim that may be made by its manufacturer, is not guaranteed or endorsed by the publisher.

frontiers in Plant Science

ORIGINAL RESEARCH
published: 17 December 2021
doi: 10.3389/fpls.2021.787839

Mechanical Performances of Isolated Cuticles Along Tomato Fruit Growth and Ripening

José J. Benítez[1], Susana Guzmán-Puyol[2], Francisco Vilaplana[3], José A. Heredia-Guerrero[2], Eva Domínguez[2] and Antonio Heredia[4]*

[1]Instituto de Ciencia de Materiales de Sevilla, Centro Mixto Consejo Superior de Investigaciones Científicas-Universidad de Sevilla, Seville, Spain, [2]Departamento de Mejora Genética y Biotecnología, Instituto de Hortofruticultura Subtropical y Mediterránea "La Mayora", Universidad de Málaga-Consejo Superior de Investigaciones Científicas, Estación Experimental La Mayora, Málaga, Spain, [3]Division of Glycoscience, Department of Chemistry, School of Engineering Sciences in Chemistry, Biotechnology and Health, KTH Royal Institute of Technology, Stockholm, Sweden, [4]Departamento de Biología Molecular y Bioquímica, Instituto de Hortofruticultura Subtropical y Mediterránea "La Mayora", Universidad de Málaga-Consejo Superior de Investigaciones Científicas, Universidad de Málaga, Málaga, Spain

The cuticle is the most external layer that protects fruits from the environment and constitutes the first shield against physical impacts. The preservation of its mechanical integrity is essential to avoid the access to epidermal cell walls and to prevent mass loss and damage that affect the commercial quality of fruits. The rheology of the cuticle is also very important to respond to the size modification along fruit growth and to regulate the diffusion of molecules from and toward the atmosphere. The mechanical performance of cuticles is regulated by the amount and assembly of its components (mainly cutin, polysaccharides, and waxes). In tomato fruit cuticles, phenolics, a minor cuticle component, have been found to have a strong influence on their mechanical behavior. To fully characterize the biomechanics of tomato fruit cuticle, transient creep, uniaxial tests, and multi strain dynamic mechanical analysis (DMA) measurements have been carried out. Two well-differentiated stages have been identified. At early stages of growth, characterized by a low phenolic content, the cuticle displays a soft elastic behavior. Upon increased phenolic accumulation during ripening, a progressive stiffening is observed. The increment of viscoelasticity in ripe fruit cuticles has also been associated with the presence of these compounds. The transition from the soft elastic to the more rigid viscoelastic regime can be explained by the cooperative association of phenolics with both the cutin and the polysaccharide fractions.

Keywords: tomato fruit cuticles, mechanical characterization, dynamic mechanical analysis, fruit growth and ripening, phenolic compounds

OPEN ACCESS

Edited by:
Kazimierz Trebacz, Maria Curie-Skłodowska University, Poland

Reviewed by:
Georgios Liakopoulos, Agricultural University of Athens, Greece
Luis Morales-Quintana, Autonomous University of Chile, Chile

****Correspondence:***
José J. Benítez
benitez@icmse.csic.es

Specialty section:
This article was submitted to Plant Physiology, a section of the journal Frontiers in Plant Science

Received: *01 October 2021*
Accepted: *25 November 2021*
Published: *17 December 2021*

Citation:
Benítez JJ, Guzmán-Puyol S, Vilaplana F, Heredia-Guerrero JA, Domínguez E and Heredia A (2021) Mechanical Performances of Isolated Cuticles Along Tomato Fruit Growth and Ripening. Front. Plant Sci. 12:787839. doi: 10.3389/fpls.2021.787839

INTRODUCTION

The aerial parts of higher plants are covered by the cuticle, a hydrophobic extracellular layer that protects fruits, leaves, seeds, petals, and green stems from the environment. The main functions of the cuticle are to prevent water loss, to regulate the gas exchange, and to act as an effective shield against other external physical agents, such as heat, light, and pressure

exerted by insects and pathogens (Domínguez et al., 2011; Heredia-Guerrero et al., 2018).

Fruit firmness and the absence of cracks are features that condition the marketability of many commercial fruits. For this reason, understanding the factors that affect the mechanical endurance of the fruit skin is essential to adopt profitable production and postharvest strategies (Lara et al., 2014). The mechanical integrity of fruits is attributed to the skin (cuticle, epidermis, and hypodermal cell layers; Bargel and Neinhuis, 2005; Khanal and Knoche, 2014). However, most of the biomechanical characterization has been carried out on isolated cuticles, as they mirror the skin performances and constitute a relevant structural component for the integrity of the fruit (Thompson, 2001; Matas et al., 2004a,b; Bargel and Neinhuis, 2005). Currently, there are a number of studies addressing the mechanical characterization of isolated cuticles of fruits and leaves and several comprehensive reviews have been published (Domínguez et al., 2011; Khanal and Knoche, 2017). Thus, parameters, such as stiffness, elastic modulus, rupture stress, and strain as well as the elastic, plastic, and viscoelastic behavior, have been related to the cuticle structure, composition, environmental conditions, and growth stage. For that purpose, procedures, such as uniaxial and biaxial tensile, transient creep and creep-relaxation, and progressive loading and unloading cycle tests, have been performed and reported (Petracek and Bukovac, 1995; Wiedemann and Neinhuis, 1998; Bargel and Neinhuis, 2004, 2005; Matas et al., 2004a,b; Edelmann et al., 2005; López-Casado et al., 2007, 2010; Domínguez et al., 2009; Takahashi et al., 2012; Tsubaki et al., 2012, 2013; Khanal et al., 2013; España et al., 2014; Khanal and Knoche, 2014).

The accuracy and representativeness of these methodologies are conditioned by several factors. Among them: (1) most testing is carried out using isolated specimens, far from the actual *in vivo* stress, hydration, and structural integration conditions; (2) the cuticle is not an isotropic material; in fact, it can be described as a C_{16}-C_{18} polyester (cutin) matrix with embedded phenolic compounds and waxes, an important remnant polysaccharide fraction from the cell wall mostly concentrated at the inner side and epicuticular waxes covering the outer region (Domínguez et al., 2011; Yeats and Rose, 2013); and (3) the cuticle thickness is not always uniform since in many species, this continuous layer can infiltrate the anticlinal epidermal cell walls to a variable degree forming wedge-shaped protrusions (pegs). This is common in tomato fruit, where the cuticle can completely encase the epidermis and even extend underneath hypodermal cell layers (Matas et al., 2004a; Bargel and Neinhuis, 2005; Domínguez et al., 2008; Barraj Barraj et al., 2021). As far as key mechanical parameters, such as the Young's modulus, the rupture stress, and toughness, are calculated considering the cuticle cross-section, the uncertainty in the thickness value compromises an accurate quantification. Despite these difficulties, some general conclusions have been attained. Thus, it has been possible to state the role of water as a plasticizer upon hydration, to elucidate the stiffening effect of waxes and flavonoids acting as fillers, and to relate the elastic and viscoelastic behavior of the cuticle with the polysaccharide and cutin fractions, respectively (Khanal and Knoche, 2017).

The non-elastic (i.e., the viscoelastic and plastic) response of isolated cuticles has been usually obtained from holding or relaxation stages after an applied stress in single or successive creep experiments (Khanal and Knoche, 2017). Often, in these type of experiments, it is difficult to set the limit between the elastic (instantaneous) and non-elastic (time-dependent) regions from the strain-time curves. Additionally, when successive load-unload cycles are used, the final results may be conditioned by an insufficient length of the holding or relaxation period. To avoid these problems, a more refined analytical method, such as dynamic mechanical analysis (DMA), can be employed. In DMA, no time-dependent relaxation or holding is requested and the on-phase strain response to the low amplitude oscillatory stress characterizes the elastic component while the off-phase output corresponds to the viscous element (Menard, 2008). In the literature, there is a limited number of DMA studies on this topic. Some of them were performed with apple cortex tissues (Videcoq et al., 2017) and tomato fruit peels (Wang et al., 2014; Vidyarthi et al., 2020), others with isolated cuticles of persimmon fruits and olive and ivy leaves (Tsubaki et al., 2013; Kamtsikakis et al., 2021). However, to our knowledge, no results using isolated tomato cuticles have been published yet. In this work, the contribution of DMA to the mechanical characterization of a series of isolated cuticles of tomato fruit, collected a different growing stages, is addressed and results are rationalized with those obtained from other techniques. In particular, viscoelasticity has been determined as a function of strain and related to the presence of phenolic compounds along growth and ripening.

MATERIALS AND METHODS

Cuticle Isolation, Composition, and Morphological Analysis

The protocols for sample isolation have been described by España et al. (2014). Briefly, cuticles were enzymatically isolated from *Solanum lycopersicum* "Cascada" using a mixture of fungal cellulase and pectinase in sodium citrate buffer and NaN_3 to inhibit microbial growth (Petracek and Bukovac, 1995). The cuticles were then separated from the epidermis, rinsed in distilled water, and stored under dry conditions until analysis. The fruit developmental stage is defined as days after anthesis (daa).

Polysaccharide Analysis

The polysaccharide fraction was isolated after cuticle dewaxing and further cutin degradation. Wax removal was carried out after treating isolated cuticles with a hot chloroform: methanol (2: 1, v:v) mixture for several hours. Cutin degradation was performed in KOH 1% in methanol for 7 days at 40°C. The monosaccharide composition was determined after digestion in trifluoroacetic acid. Briefly, 1 mg sample was weighted accurately and treated with 1 ml TFA 2 M at 121°C for 3 h. Then, 100 µl of solution was diluted until a final volume of 1 ml and filtered through a 0.2 µm PVDF membrane. The monosaccharide analysis was performed using high performance anion exchange chromatography with pulsed amperometry

detection (HPAEC-PAD) system (Dionex ICS 3000) equipped with a CarboPac PA1 column. The quantification of monosaccharides was done after calibration with neutral sugars and uronic acid standards at concentrations between 0.005 and 0.1 g/l. The measurements were repeated for 3 replicates. Monosaccharides detected were as: glucose (Glu), xylose (Xyl), manose (Man), glucuronic acid (GlcA), arabinose (Ara), galactose (Gal), and galacturonic acid (GalA). Cellulose content was calculated from the amount of (Glu), while hemicellulose and pectin were the sum of (Xyl + Man+GlcA) and (Ara + Gal+GalA), respectively.

Infrared Spectroscopy

Attenuated Total Reflected (ATR-FTIR) IR spectra were obtained from both sides of the cuticles using a single reflection ATR accessory (MIRacle ATR, PIKE Technologies, Madison, WI, USA) with a diamond crystal at 45° incidence and coupled to a FTIR spectrometer (FT/IR-6200, Jasco, Tokyo, Japan). All spectra were acquired with a liquid nitrogen cooled MCT detector in the 4,000–600 cm^{-1} range at 4 cm^{-1} resolution and by accumulating 50 scans. Spectrum absorbance was corrected to account for the dependence between the penetration depth and the radiation wavelength in ATR-FTIR measurements. Band areas were calculated using the Jasco SpectraManager software V.2 (Jasco Corporation, Tokyo, Japan).

Mechanical Characterization

Uniaxial tensile tests of cuticles were conducted using a Criterion 42 (MTS Systems, Eden Prairie, MN, United States) machine equipped with a 10 N load cell and applying a 0.02 N preload. Rectangular uniform pieces (5 mm x 15 mm) were cut and brought to rupture at a constant deformation rate of about 3% min^{-1} at room conditions (~23°C and 45% RH). Samples were inspected with a stereo microscope to check for the absence of cracks. Tomato fruit cuticle changes their color during ripening, reaching an orange-yellow color at red ripe. Given the color variability, within fruits and among them, exhibited in the ripening stages prior to red ripe, samples showing a color representative of the ripening stage were selected. Stress–strain curves were acquired using the specimen cross-section value under no applied load. The cross-section was calculated from the thickness of the continuous cuticle layer on top of the periclinal wall of epidermal cells (t_L) as observed from optical microscopy. The Young's modulus was calculated from the maximum slope of the stress–strain curve (typically around 1–2% strain). Experiments were repeated for at least 10 specimens at each ripening stage. Errors in mechanical parameters are expressed as the standard deviation.

Transient creep measurement of the 55 daa Cascada cuticle was performed with a Q800 DMA (TA Instruments, New Castle, DE, United States) and using the tension clamp at room conditions. Sample inspection and dimensions were the same as in uniaxial tensile test. Conditions used, i.e., force increments (ΔF) of 0.04 N and holding times (t_H) of 1200 s were similar to those used in previous studies (López-Casado et al., 2007; España et al., 2014). Here, only the 55 daa sample was measured in transient creep mode to compare with the already published data using a different equipment (España et al., 2014).

Multi strain DMA tests have been done at room conditions with the same analyzer and samples 3 mm wide and with an effective length (distance between grips) of 8 mm. The amplitude of the oscillation was increased from 10 µm in 5 µm increments up to sample rupture. The initial preload force was 0.005 N and the instrument sets an additional static force (Fs) to prevent sample warping. Storage (E') and loss (E'') moduli, as well as their ratio (Tan δ), were recorded as a function of sample strain. Measurements were carried out for 5 specimens at each ripening time. In stages showing evident color variation (35 to 45 daa), samples were sorted in clearer, darker and average and five of each category were analyzed. In addition to the strain evolution of E', E'', and Tan δ, rupture stress and strain were also determined from multi strain DMA tests.

Statistical Analysis

Regression analysis and the calculation of mean and standard deviation values were performed using OriginPro, Version 2019 software (OriginLab Corporation, Northampton, MA, United States).

Mechanical Characterization Methods Overview

This section provides a brief description of the methods used for the mechanical characterization of isolated cuticles.

Transient creep tests consist in the accumulative application of a force gradient (ΔF) for a relatively long holding time (t_H; **Figure 1A**). The strain response is then decomposed into an instantaneous (elastic) and a time-dependent (inelastic: viscoelastic + plastic) contributions. At low total forces, the elastic behavior predominates while viscoelastic and plastic deformations progressively show up at higher loads. In addition to the characterization of the elastic and viscoelastic regions of samples, the number of stretch and hold steps can be increased up to sample failure to collect the rupture stress and strain values. However, the main disadvantage of this method is the low productivity. With holding times in the order of several minutes, the number of cycles per time unit is very low. Furthermore, if the value of ΔF is reduced to gain resolution in the corresponding stress–strain curve, the duration of a single experiment may take several hours. When dealing with samples with high variability, such as plant cuticles and to ensure data representativeness, the collection of several replicates significantly slows down obtaining accurate results.

Uniaxial tensile testing is likely the most used procedure to study the mechanical response of films to an applied load. Most of the commercial available instrumentation uses a servomotor to strain the sample at a constant speed and a force transductor to measure the stress exerted to keep such constant deformation rate (**Figure 1B**). The stress–strain curve of a viscoelastic material commonly displays an initial linear elastic behavior followed by a non-linear segment before failure. The Young's modulus is calculated as the slope of the linear

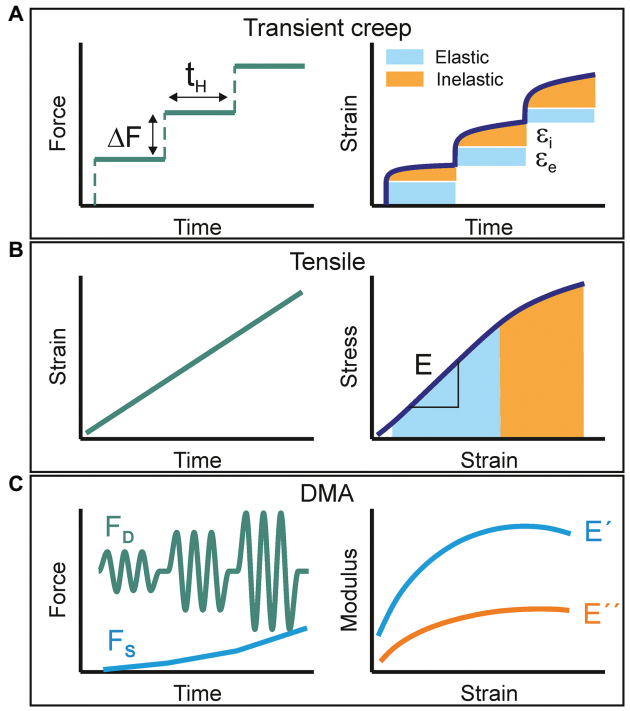

FIGURE 1 | Schematic representation of the mechanical characterization methods used in this study: **(A)** transient creep, **(B)** uniaxial tensile, and **(C)** multi strain dynamic mechanical analysis. The applied perturbation signal is shown on the left side while the collected response is plotted on the right.

part, typically around 1% deformation. The area under the curve is the energy per volume needed to break the sample and is an indicator for toughness. Usual strain rates are in the order of several % min^{-1}, which leads to experiment duration of few minutes and hundreds of acquired points per stress–strain curve. Test replication is then feasible in a reasonable working time and the productivity and reproducibility of the mechanical characterization improve. However, since there is not a proper static force-time segment, as in creep experiments, it is not possible to accurately define the elastic and inelastic responses.

Dynamic Mechanical Analysis (DMA) is a methodology that combines both the productivity and the capability to characterize the viscoelastic behavior. In a typical DMA experiment, the sample is subjected to a low amplitude sinusoidal stress and the strain response vs. time is monitored. In a pure elastic material, the energy provided by the applied force is stored and released instantly as the stimulus ceases. Consequently, the strain response is synchronized with the stress and their amplitude ratio (stress–strain) is the so-called storage (E') modulus. In a pure viscous material, the energy is fully absorbed (loss) to induce mass flow and there is no instant recovery. A real viscoelastic material can be described by a combination of both models. The total resulting strain response is then delayed (δ) with respect to the oscillating stress and it can be decomposed into an in-phase and an out-of-phase components.

TABLE 1 | Invagination degree (V_{peg}/V_L) values for tomato Cascada cuticles as a function of fruit development time (daa).

daa (day)	V_{peg}/V_L
15	0.784
20	0.979
25	1.252
30	1.076
35	0.814
40	0.687
45	0.700
50	0.856
55	0.759

The first one provides the pure elastic (storage) modulus (E') and the second one the so-called loss modulus (E"). Their ratio E"/E' is defined as Tan δ (or damping factor) and constitutes a direct measurement of viscoelasticity. In a DMA experiment, the amplitude of the stress perturbation can be progressively increased (the so-called multi strain mode; **Figure 1C**). This is achieved by applying a growing dynamic force (F_D) while a static (F_S) backup component is added to prevent sample warping and to ensure a periodic response to the oscillation stress. The net applied force can be raised until sample failure and fracture parameters can also be obtained as in transient creep and tensile tests. In this mode, DMA is also capable of evaluating the viscoelasticity (Tan δ) as a function of strain.

RESULTS

Physical Parameters and Fraction Composition of Isolated Cascada Tomato Fruit Cuticles

The weight per area (w), density (d), and thickness (t_L) of the isolated Cascada cuticles as a function of fruit development time (days after anthesis or daa) are compiled in **Supplementary Table S1**. As observed, the weight per area slightly increases up to 25 daa, stabilizes between 25 and 45 daa, and decreases above 45 daa. The density drops almost to half from 15 to 30 daa and later increases around 30–40% up to 55 daa. The thickness displays a more defined evolution starting with a sharp increment from 15 to 30 daa followed by a progressive reduction above such development time. In general, 30 daa sets a limit for an initial trend involving an increment of weight per area and thickness and a reduction of density. Above 30 daa, these trends reverse but with a less pronounced tendency. These morphological parameters allow the calculation of the ratio between the volume associated to pegs (V_{peg}) and that of the uniform and non-invaginated layer (V_L) of the isolated cuticles according to equation (1). Data in **Table 1** show that invagination (V_{peg}/V_L) increases up to a maximum at 25 daa followed by a reduction until 35 daa and a stabilization in the 35–55 daa period.

$$V_{peg} / V_L = \left[w / \left(d \times t_L \right) \right] - 1 \quad (1).$$

TABLE 2 | Polysaccharide fraction analysis of cuticles isolated from Cascada tomato fruits harvested at 15, 30, 45, and 55 daa.

daa (day)	Cellulose (%)	Hemicellulose (H) (%)	Pectin (P) (%)	H/cellulose	P/cellulose	(H + P)/cellulose
15	35.5 ± 3.9	40.7 ± 5.7	23.7 ± 3.7	1.15	0.67	1.81
30	36.4 ± 4.4	37.7 ± 4.6	25.8 ± 3.6	1.04	0.71	1.74
45	35.3 ± 4.0	35.9 ± 4.1	28.7 ± 3.0	1.02	0.81	1.83
55	36.1 ± 4.3	36.8 ± 2.9	27.1 ± 2.9	1.02	0.75	1.77

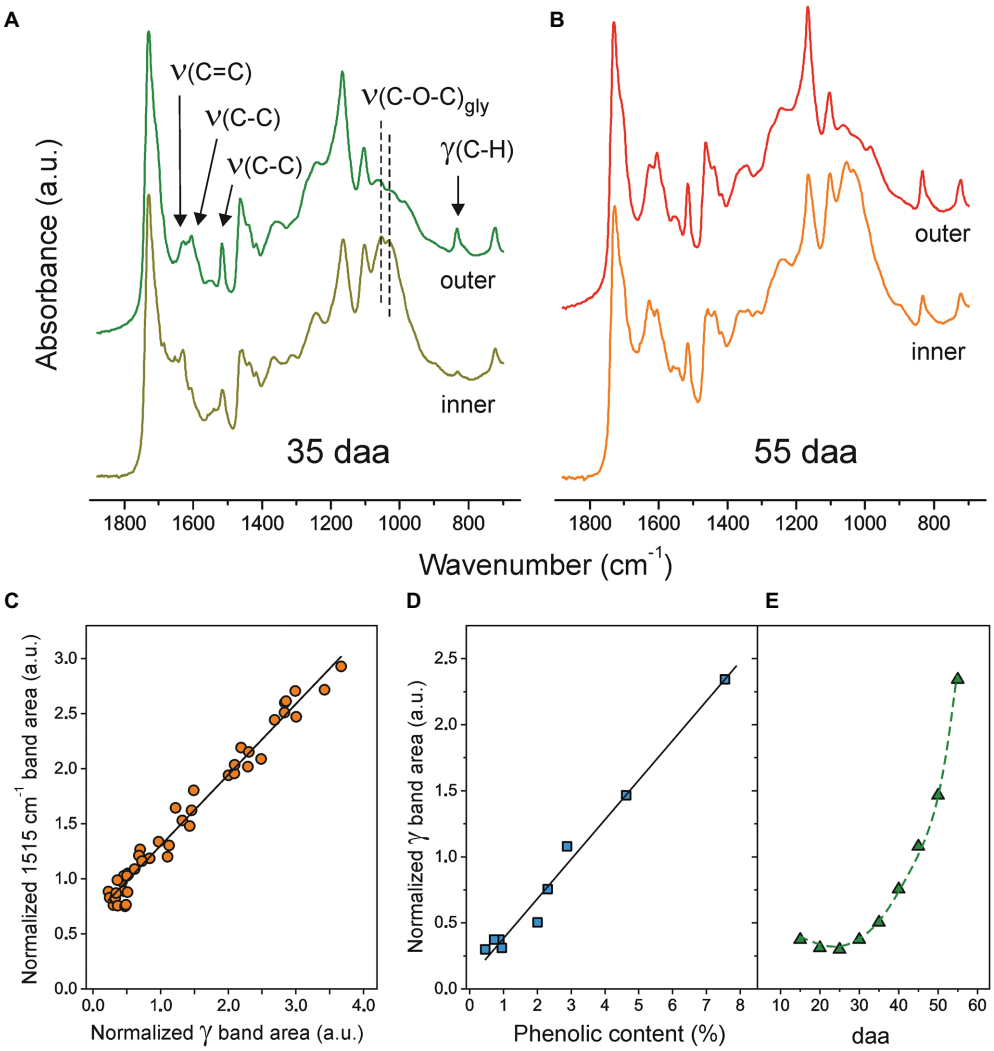

FIGURE 2 | **(A)** and **(B)** Normalized ATR-FTIR spectra (700–1875 cm^{-1}) of both sides of Cascada cuticles at 35 and 55 daa, respectively. **(C)** Relationship between normalized areas of bands at 1515 cm^{-1} and (γ) at 835 cm^{-1}. **(D)** Correlation between the normalized area of the (γ) band and the phenolic content obtained from UV–Vis spectroscopy. **(D)** Phenolics evolution in Cascada cuticles along fruit development as monitored by the normalized (γ) ATR-FTIR band.

The chemical composition of Cascada cuticles along fruit development is shown in **Supplementary Table S2**. In general, there is not a well-defined evolution of the main fractions (cutin and polysaccharides) and percentages are quite constant. At most, a subtle reduction of the polysaccharide/cutin ratio can be observed at 50 daa and above, which suggests a mild degradation of cell walls at the red-ripe stage. By far, the most noticeable modification during ripening is the accumulation of phenolic compounds. The concentration rapidly increases above 30 daa and it peaks at 55 daa with an order of magnitude increment.

The polysaccharide fraction analysis at selected fruit development times is indicated in **Table 2**. Samples are quite homogenous in cellulose content though an overall small reduction in hemicellulose and a slight enrichment of pectin can be observed.

ATR-FTIR Characterization of Tomato Cascada Cuticles and the Relative Quantification of Phenolic Compounds

The ATR-FTIR spectra of both, the inner and outer, sides of isolated Cascada cuticles at 35 and 55 daa in the 700–1875 cm^{-1} range are shown in **Figures 2A,B**. Characteristic ester bands ν(C=O) at 1731 cm^{-1} and ν(C-O-C) at 1168 and 1105 cm^{-1} as well as those of aliphatic chains at 2926 and 2854 cm^{-1} [$\nu_a(CH_2)$ and $\nu_s(CH_2)$, respectively, (not shown)] and 1463 and 725 cm^{-1} [scissoring and rocking $\delta(CH_2)$, respectively] are common to both sides and developmental stages. In addition to these peaks (mostly due to cutin), on the inner side, the presence of polysaccharides is revealed by glycosidic $\nu(C\text{-}O\text{-}C)_{gly}$ peaks at 1053 and 1034 cm^{-1} (Heredia-Guerrero et al., 2014). Apart from the accumulation of cutin on the outer side and polysaccharides on the inner surface, the main differences between spectra involve the ν(C=C), ν(C-C), and δ(C-H) modes assigned to aromatic rings in phenolic compounds (Ramírez et al., 1992; España et al., 2014). The evolution of their intensities reveals a noticeable increment of such compounds upon fruit development and their preferential accumulation on the outer regions of the cuticles. The phenolic content in Cascada tomato cuticles throughout development has been reported after cutin depolymerization (España et al., 2014). Here, we propose a new method based on the direct quantification of phenolics ATR-FTIR bands. For this purpose, the ν(C-C) at 1515 cm^{-1} and the so-called gamma (γ) band at 835 cm^{-1} have been selected because they are relatively intense, well separated from other absorptions and the base line can be easily defined. However, band intensity in ATR-FTIR is not an absolute measurement and areas should be normalized to allow for the spectra comparison. For normalization, the intense $\nu(CH_2)$ stretching peaks at 2926 and 2854 cm^{-1} have been used as the reference. **Figure 2C** shows the correlation between the normalized areas of the ν(C-C; 1515 cm^{-1}) and γ (835 cm^{-1}) bands from both sides of the whole series of Cascada cuticles. Despite the good linearity, there is an offset for the 1515 cm^{-1} absorption at zero (γ) area. This may indicate that, besides the phenolic compounds, other components may be contributing to the 1515 cm^{-1} peak which invalidate its use for the intended quantitative analysis. Also, when using ATR-FTIR, it has to be considered that its analysis depth is limited. In the experimental conditions used, the effective value is around 4–5 µm, which is below the (t_L) values for the series (4.4–7.4 µm, **Supplementary Table S1**). This means that there are regions out of the IR beam penetration range and do not contribute to the spectrum. To overcome this problem and to provide a more precise quantification using ATR-FTIR, the cuticles were analyzed from both sides and the normalized area values averaged. To validate this procedure, results obtained from ATR-FTIR have been compared with those provided by UV–Vis spectroscopy, **Figure 2D**. As observed, there is a good linearity and no offset at zero coordinate value using the gamma band. Consequently, the normalized (γ) ATR-FTIR band area has proven to be an *in-situ*, accurate and fast method to detect the evolution of phenolic content in isolated Cascada cuticles upon fruit development. Such evolution can be observed in **Figure 2E**: Initially (15–30 daa), the concentration is very low, but it grows very quickly up to a maximum at full maturation (55 daa).

Comparative Mechanical Characterization of Isolated Tomato Cascada Cuticles

Figure 3 shows the mechanical characterization of the 55 daa cuticle using the three methods above described. The uniaxial tensile test (**Figure 3B**) has been performed using a universal testing machine while the transient creep (**Figure 3A**) and the multi strain (**Figure 3C**) experiments have been collected

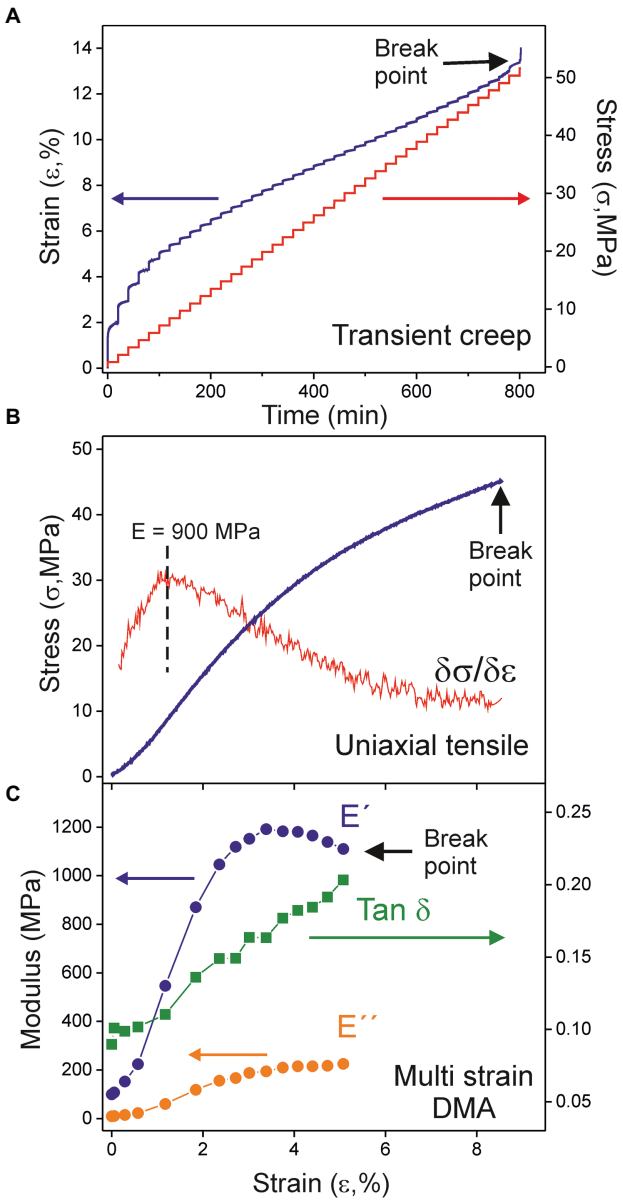

FIGURE 3 | Mechanical analysis of the 55 daa tomato Cascada cuticle by **(A)** transient creep, **(B)** uniaxial tensile, and **(C)** multi strain dynamic mechanical analysis (DMA).

with the DMA in specific configurations. The transient creep study of the whole Cascada cuticle series has already been reported (España et al., 2014). However, for reproducibility and comparative purposes, the 55 daa has been reanalyzed using the DMA. Results obtained here were a Young's modulus of 1000 MPa, a breaking stress of 52 MPa and a rupture strain around 13%, which are in good agreement with those reported (884 MPa, 59 MPa, and 14%, respectively) by España et al. (2014).

Figures 3B,C illustrate the general behavior within the Cascada series. The stress–strain curves (**Figure 3B**) are characteristic for viscoelastic materials, i.e., an initial relatively linear response to the applied force followed by a progressive decay of the slope until sudden rupture. In most cases, stress–strain curves display a subtle "S" shape caused by the lower stress needed to keep the strain rate at the very beginning of the uniaxial test. This effect is likely caused by the fact that cuticle pieces are not macroscopically flat because of the underlying uneven texture of epidermal cells and the inherent curvature of the fruit. Stress is not then uniformly transmitted along the full cross-section of the cuticle and it concentrates in some regions. Consequently, the effective area is smaller than the geometric one and requires less stress to be deformed. As the strain is raised, the area of the effective cross-section increases and stabilizes and the linearity in the mechanical response is regained. Accordingly, the reported Young's moduli (E) correspond to the maximum slope of the stress–strain curve.

In multi strain DMA tests, both the storage (E') and loss (E'') moduli of cuticles increase with strain until a maximum value is reached, **Figure 3C**. At higher strain, there is a smooth diminishment before sample break up. This behavior reveals an initial strain-hardening stage followed by a strain-softening one, as previously observed for cuticles of a crack-prone cultivar, such as Sweet 100 (Matas et al., 2004a). In every case, the increment rate of (E'') is higher than (E') as shown by the evolution of their ratio (Tan δ). This result indicates that viscoelasticity increases almost linearly with the strain applied to the cuticles and no well-differentiated limits for the elastic and viscoelastic regions can be stablished.

Modulus and Rupture Parameters of Tomato Cascada Cuticles

The modulus, as well as the breaking stress and strain, values are plotted vs. the fruit development time (daa) in **Figure 4** (numeric data and errors are provided in **Supplementary Table S3**). Several peculiarities can be observed from the comparison of the mechanical parameters determined from the three methods used. First, the good concordance between the breaking parameters calculated by tensile and multi strain DMA and the higher values observed in transient creep tests, **Figures 4B,C**. The most plausible explanation for such difference is based on the long holding times between successive loads in transient creep tests. This procedure adds a viscous extension component to strain and allows the relaxation of local stresses by mass rearrangement and energy dissipation that prevents the formation of a point of fracture and extends the stress limit. Second, the difference between the storage modulus (E') from multi strain DMA and the Young's modulus from transient creep and uniaxial tensile tests, **Figure 4A**. Strictly, they are not the same magnitude. The storage modulus (E') is a pure elastic component extracted from a sample subjected to a minimal cyclic stress/relaxation signal with energy being continuously provided and released. Meanwhile, the Young's modulus is obtained from a unidirectional experiment

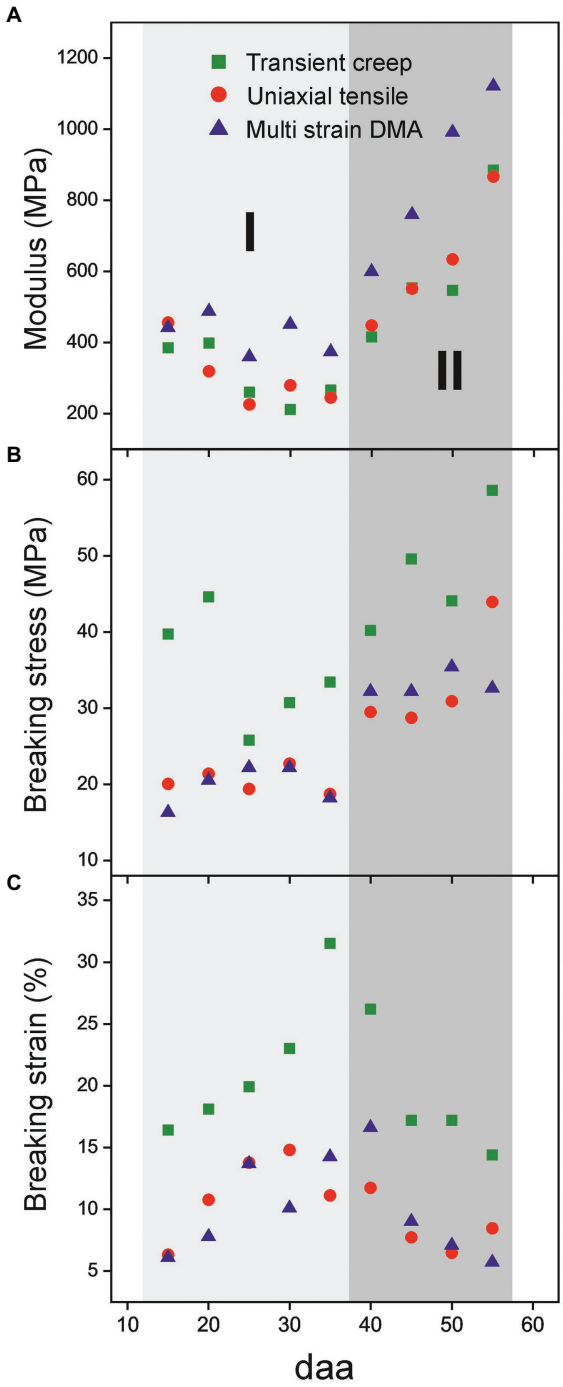

FIGURE 4 | Evolution of mechanical parameters of isolated cuticles along tomato fruit development. **(A)** Modulus, **(B)** breaking stress and **(C)** breaking strain. Two stages (I, 15-35 daa and II, 40-55 daa) can be distinguished.

in which energy is only accumulated by the sample. Besides, it is obtained at larger deformations and it contains a viscous contribution. In this sense, E' can be envisaged as the Young's value extrapolated to virtually zero strain and, therefore, it is expected to be higher. The same difference between these parameters has been observed for isolated persimmon fruit cuticles (Tsubaki et al., 2013).

Despite the characterization method employed, mechanical parameters of the Cascada series display a reproducible trend along fruit development. In **Figure 4**, two different stages can be distinguished. Stage I (from 15 to 35 daa) is characterized by a small diminishment of the modulus, an increment of breaking strain and a low, but constant, rupture stress. In stage II (35 to 55 daa), the modification of parameters is more drastic and there is a strong increment of modulus and a noticeable reduction of breaking strain while the breaking stress reaches a maximum plateau within the series.

Uniaxial tensile testing allows the obtaining of additional interesting mechanical parameters, such as toughness (U_T) and breaking force (F_{rup}). They, respectively, represent the amount of absorbed energy per volume and the force needed for sample breakup. U_T is calculated as the area below the stress–strain curve, while F_{rup} is an absolute magnitude directly measured at the point of failure and normalized to 1 m sample width. **Figure 5** shows the values for the Cascada series. As observed, there is a sustained growth of toughness from 15 to 30 daa (**Figure 5A**), mostly caused by the increment in the rupture strain. Above 30 daa, there is not a well-defined behavior due to the opposed evolution of breaking stress and strain values, **Figures 4B,C**. On the other side, the breaking force increases up to a maximum at 55 daa, **Figure 5B**. The growth of breaking force in the early stages of development (15–35 daa) seems to be linked to the increment of thickness of the cuticle; however, above 35 daa, the mechanical resistance to rupture improved despite the observed thickness reduction, which suggests the participation of a reinforcing agent surpassing the thickness effect.

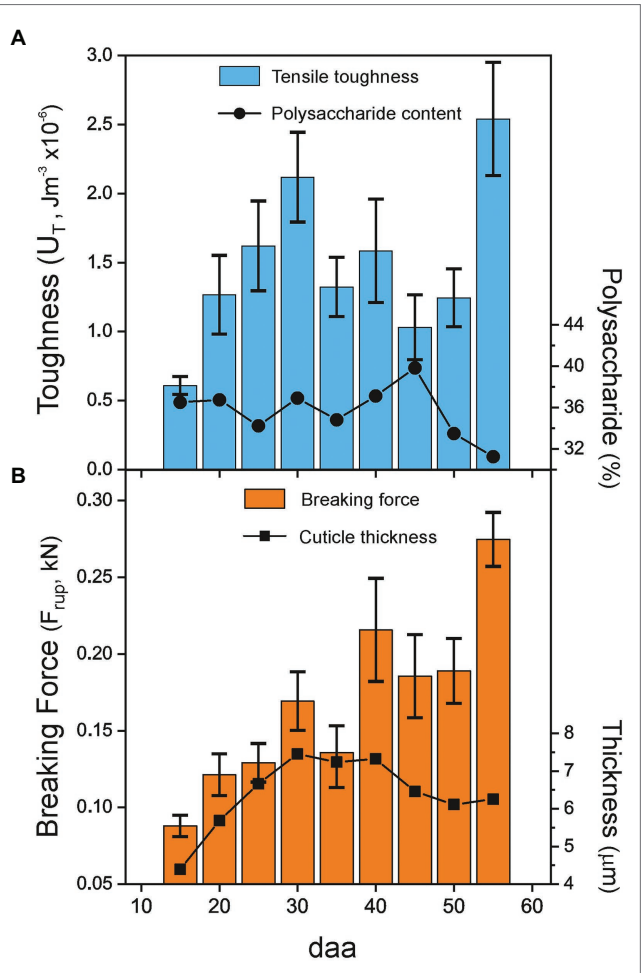

FIGURE 5 | (A) Toughness (U_T) and **(B)** net breaking force (F_{rup}) of tomato Cascada cuticles vs. fruit development. For reference, the polysaccharide content (circles) and the cuticle thickness (t_L; squares) values are included in the plots. Percentage of cuticle polysaccharides and cuticle thickness taken from Domínguez et al. (2008).

Viscoelastic Behavior of Isolated Tomato Cascada Cuticles

Viscoelastic properties of Cascada cuticles have been studied by DMA. Multi strain experiments allow the calculation of the storage (E') and loss (E") moduli as well as their ratio (Tan δ or damping factor) as a function of strain. Curves for the whole Cascada series are shown in **Figures 6A–C**. As observed, the shape of the curves depends on the fruit developmental state. The behavior of young, low coloration cuticles is well differentiated from that of ripe ones. Moduli curves within the 15–40 daa period are similar and display a mild increment with strain (strain hardening). At 45 daa and above the evolution of E' and E" are more pronounced and the growth is clearly associated with ripening time. Tan δ follows a linear trend with strain and the inclination is noticeably incremented at 45 daa and above. Tan δ reveals a linear and progressive increment of viscoelasticity with strain as E" grows faster than E', but no well-defined transition point between the elastic and viscoelastic behavior of tomato Cascada cuticles is observed.

The evolution of DMA parameters with fruit development time is better appreciated in **Figures 6D–F**, where E', E", and Tan δ values at low strain (1.6%) are plotted. Such strain value has been selected because it is below the reported values (2–3%) for the transition between the elastic and viscoelastic regimes in tomato cuticles (Khanal and Knoche, 2017 and references there in) and once the initial non-linear stress–strain stage in cuticles is surpassed (see **Figure 3B**). **Figures 6D–E** show the relationship between the moduli and ripening. The initial lower plateau extends from 15 to 35 daa and it is followed by a fast increment up to 55 daa. Tan δ seems to slightly grow from 15 to 40 daa (**Figure 6F**) and jumps to the highest value in the 45–55 daa period, which indicates a reduction of elasticity and an increment of the viscous component with ripening.

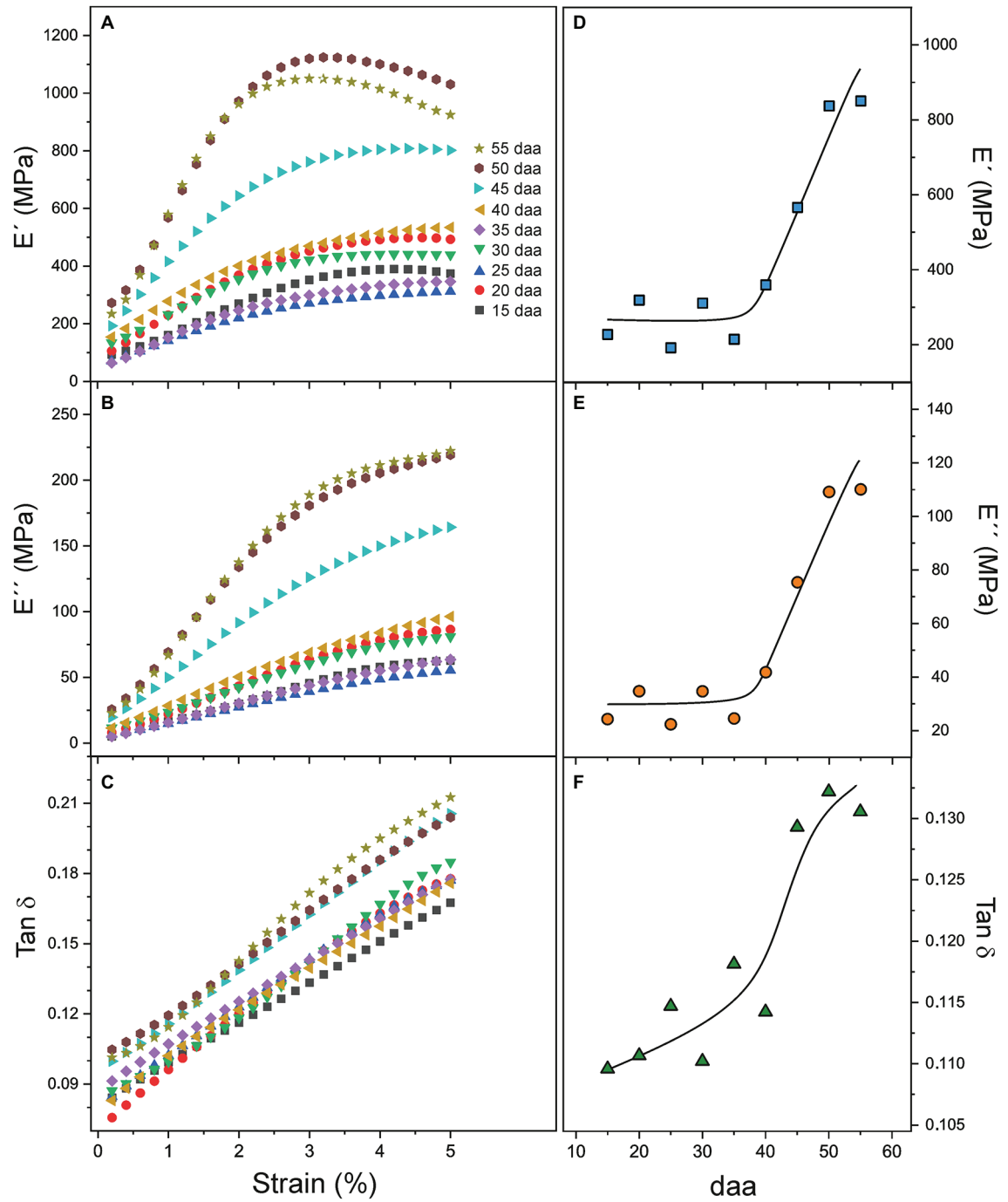

FIGURE 6 | (A–C) E', E'', and Tan δ dependence with strain for tomato Cascada cuticles. **(D–F)** E', E'', and Tan δ evolution with ripening time.

To further investigate the relationship between DMA parameters and the color variability, additional measurements have been performed with cuticles showing a noticeable color variation within a same fruit developmental stage. Visually, samples above (darker) and below (clearer) the average color have been selected for each stage within the 35–45 daa period. E', E'', and Tan δ curves vs. strain are displayed in **Figure 7**. As noticed, values of clear samples (open symbols) are systematically lower than those of the corresponding darker ones (filled symbols), particularly for younger cuticles (35 and 40 daa). Differences are reduced as ripening progresses to the point that the behavior of clear 45 daa specimens is comparable to the dark set of 35 and 40 daa, while the dark 45 daa resembles the red-ripe stage.

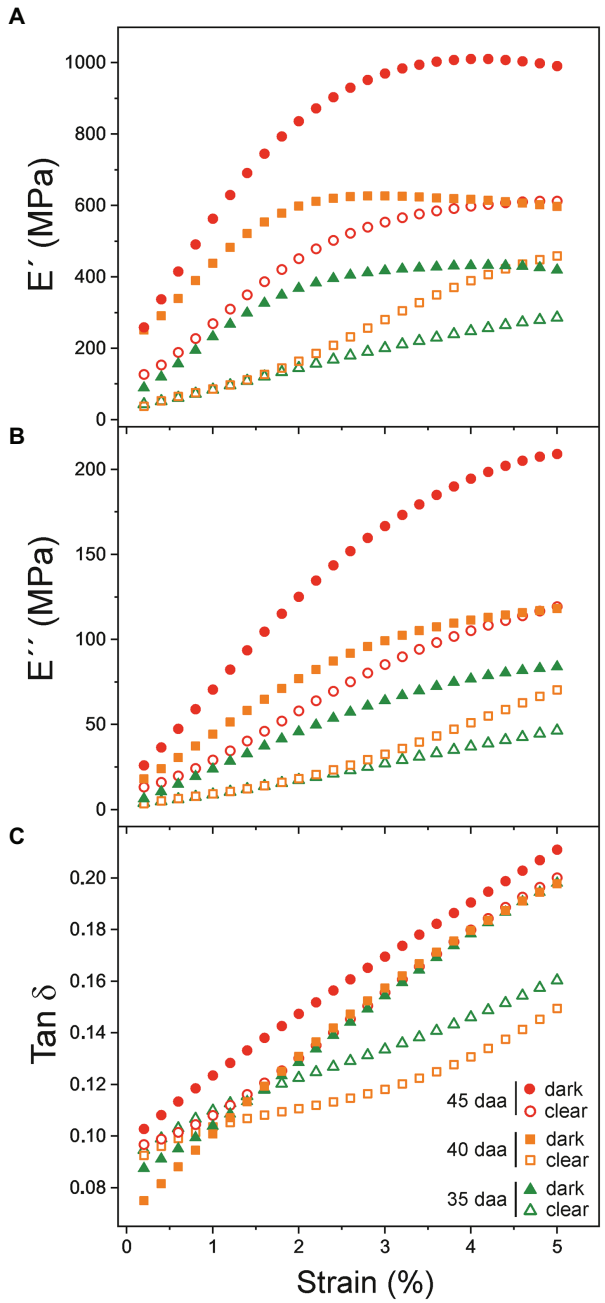

FIGURE 7 | (A) Storage (E'), **(B)** loss E'' moduli, and **(C)** Tan δ dependence with strain for cuticles showing differentiated coloration within the same ripening time. The color variability in tomato Cascada cuticles is observed in the 35–45 daa range.

DISCUSSION

The characterization of isolated tomato Cascada cuticles with a combination of continuous, stepped, and oscillatory mechanical methods has contributed to the elaboration of a more defined model with several stages involving chemical and structural changes along fruit growth and ripening.

Peg Development Induces Tomato Cuticle Softening at Early Stages of Fruit Growth (Stage I)

The first stage (Stage I) extends from 15 and up to 30–35 daa and it is characterized by a progressive softening, i.e., the reduction of the Young's modulus and the increment of extensibility before rupture, **Figure 4**. In this stage, the cuticles are elastic but with slightly growing viscoelasticity, **Figure 6F**.

Many factors have been reported to affect the mechanical performances of tomato cuticles (Khanal and Knoche, 2017). Among them, the relative amounts of their components. The main fraction of isolated tomato cuticles is cutin and it is generally accepted that cutin increases extensibility and reduces stiffness of cuticles while adding viscoelasticity. The observed evolution of mechanical parameters in tomato cuticles within stage I would be then justified by an increment of the cutin content. However, neither the amount of cuticle per surface area nor the percentage of cutin was reported to change significantly during this period (Domínguez et al., 2008; **Supplementary Table S2**). Moreover, ATR-FTIR data reveals that there is no reduction of the esterification index in the 15–30 daa range, which rules out the possibility of softening *via* the diminishment of the molecular weight or cross-linking within the cutin polyester matrix due to partial depolymerization.

Quantitatively, polysaccharides are the second component of Cascada cuticles. The presence of the embedded polysaccharides in tomato cuticles has been reported to drastically increase the stiffness of the cutin matrix (López-Casado et al., 2007). Furthermore, the polysaccharide fraction is considered to control the initial elastic stage of the cuticle deformation where the Young's modulus is calculated. Consequently, it would be reasonable to consider that modifications in the polysaccharide content may induce a change in the elastic response and, thus, the observed cuticle softening in stage I could be tentatively assigned to a reduction of polysaccharides. However, as it was above mentioned for cutin, the percentage of polysaccharides was not reported to change during the 15–30 daa period (Domínguez et al., 2008). Despite the amount of polysaccharides remaining constant, the relative amounts of cellulose, hemicellulose, and pectin displayed small changes, **Table 2**. The incorporation of pectin and/or hemicellulose to a cellulose matrix has been reported to increase elasticity and extensibility (Chanliaud et al., 2002). However, the observed differences in the relative pectin/cellulose, hemicellulose/cellulose, or pectin+hemicellulose/cellulose ratios (**Table 2**) are not consistent with the observed 40–45% reduction of the Young's modulus and the 2-fold increment of the breaking strain in the 15–30 daa stage.

Finally, intracuticular waxes and phenolics have been described as reinforcing fillers in tomato cuticles causing the increment of modulus and rupture strength and the reduction of extensibility (Domínguez et al., 2009; Khanal et al., 2013; España et al., 2014). Yet, as it was the case for the main cuticle components, their reported variation during the 15–30 daa period (Domínguez et al., 2008; España et al., 2014) does not seem to explain the detected tomato cuticle softening.

Data in **Supplementary Tables S1, S2** reveal that parameters showing a noticeable modification in stage I (between 15 and 30 daa) are morphological rather than compositional. For instance, cuticle density progressively decreases from 1.665 to 0.908 g cm^{-3} in this period. To explain such reduction, the formation of microscopic and/or nanoscopic cavities along the growth has been suggested (Domínguez et al., 2008). The presence of such cavities would lead to an overestimation of the thickness values (t_L) used to calculate the Young's modulus and the breaking stress. Indeed, the modulus reduction in stage I (**Figure 3A**) would be consistent with such overestimation. Furthermore, the higher elongation at break could also be explained by the formation of a "hollow" structure, as cavities may facilitate the deformation under stress and allow a larger extensibility. However, the breaking stress should also diminish as it is also calculated considering the thickness of the specimen, but the values are quite constant. In other words, there is a direct correlation between the net force needed to break the sample and thickness up to 30 daa (**Figure 5B**), which is not coherent with the argument of an overestimated thickness caused by void cavities in this growth range. Consequently, other arguments should be provided to explain the tomato Cascada cuticle softening in stage I.

Figure 8A is a schematic representation of the cross-section of tomato Cascada cuticles based on histological studies (Domínguez et al., 2008). Equation (1) allows the calculation of the ratio between the volumes of the peg and parallel regions (V_{peg}/V_L), which can be regarded as an invagination parameter. Its evolution with fruit growth is represented in **Figure 8C**. As observed, the invagination generally increases from 15 to 25 daa; then, it slightly decreases up to 35 daa and remains virtually constant up to full ripening. Interestingly, in stage I, and irrespective of the mechanical characterization method used, the modulus correlates negatively with the invagination degree ($p < 0.01$; **Figure 8D**), while the breaking strain follows the opposite trend ($p < 0.01$; **Figure 8E**). Matas et al. (2004a) proposed a model in which the rheology of cuticles of tomato cuticles is conditioned by the presence of embedded polysaccharide microfibrils within the cutin matrix. They indicated that the application of a mechanical stress induced the fibril alignment in the direction of the acting force (**Figure 8B**) which resulted in an increment of the Young's modulus (strain-hardening). In tomato Cascada cuticles, and according to this model, peg regions would need a higher deformation to rearrange the microfibrils toward a given applied stress resulting in a lower modulus and a higher extensibility. This hypothesis would justify the observed softening in the 15–30 daa period (Stage I) indicating the contribution of peg regions to the overall rheology of the cuticle.

The Accumulation of Phenolic Compounds Stiffens the Tomato Cuticle (Stage II)

Around the onset of ripening, from 35 daa until red ripe (55 daa; Stage II), the mechanical performance of tomato Cascada cuticles changes drastically. They undergo a stiffening process

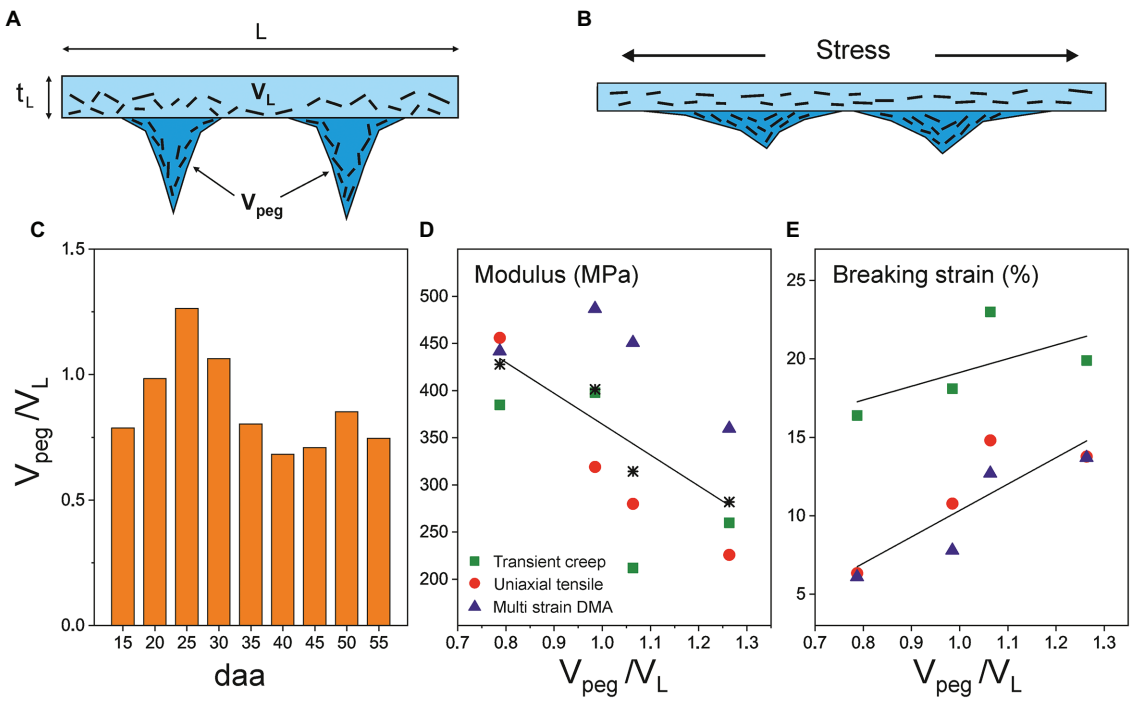

FIGURE 8 | (A) Schematic representation of a cross-section of isolated tomato Cascada cuticles and **(B)** under an applied stress. **(C)** Evolution of V_{peg}/V_L (invagination) along ripening. Correlation between the invagination degree and **(D)** the Young's modulus and **(E)** the breaking strain in the softening stage (15–30 daa) of tomato Cascada cuticles. Asterisks in **(D)** are the modulus average values.

with a noticeable increment of modulus and breaking stress and a reduction of rupture strain, **Figure 4**. These changes cannot be explained by the modification of morphological traits as invagination and density are relatively constant and the net breaking force increases despite the slight diminishment of thickness, **Figure 5B**. The cuticle stiffening in the ripening stage (35–55 daa) cannot be associated with the amount and/or type of polysaccharides. Though there is an initial increment of polysaccharide content from 35 to 45 daa (**Figure 5A**), the amount is significantly reduced at 50 and 55 daa coinciding with the highest cuticle rigidity, **Figure 4A**. Besides, no meaningful increment of the cellulose and hemicellulose percentages supporting the noticeable increment of modulus is observed from 45 to 55 daa (**Table 2**). Additionally (see **Supplementary Figure S1**), no modification of the ATR-FTIR spectra suggesting a modification of the polymerization degree of the polysaccharide fraction has been detected (Castro and Morales-Quintana, 2019). Furthermore, the clear reduction of the esterification index in the 30–55 daa range also discards the possibility of a denser and/or more cross-liked cutin polyester network contributing to the cuticle stiffening. In this scenario, the mechanical behavior of cuticles is univocally conditioned by the accumulation of phenolic species, as previously reported by España et al. (2014). Indeed, a direct correlation ($p < 0.01$) between the modulus and the normalized area of the (γ) band can be found for the Cascada series in stage II, **Figure 9**. Such a direct relationship between the amount of phenolics and the cuticle stiffening can also be found within the same fruit developmental stage when analyzing specimen with variable coloration in the 35–45 daa range (see **Supplementary Figure S2**). The stage I region falls outside the fit because of the low amount of phenolics and the occurrence of the aforementioned peg-induced softening in such early stage of fruit development.

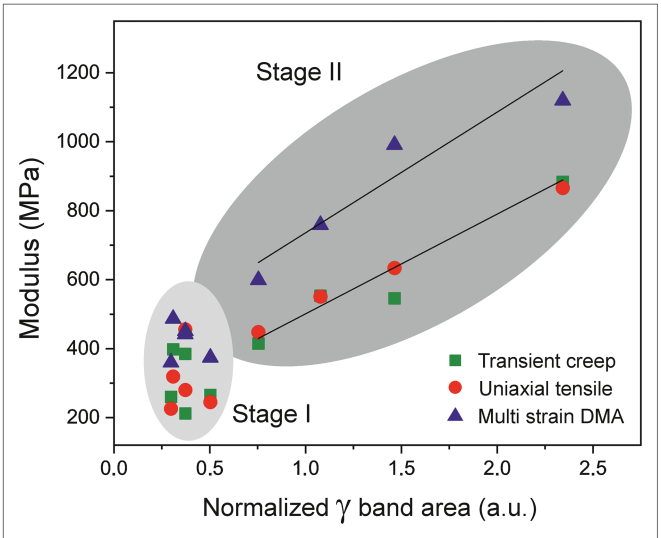

FIGURE 9 | Evolution of Young's (squares and circles) and storage (triangles) moduli vs. the normalized area of gamma band (phenolics) of cuticles along fruit development. The modulus is correlated with the phenolic content in the 35–55 daa period (Stage II).

The stiffening effect of phenolics in tomato cuticles has been associated with their role as molecular fillers in the cutin fraction. Earlier results indicated that phenolics may form clusters trapped in the cutin network (Luque and Heredia, 1994; Laguna et al., 1999) and the affinity of phenolics for the polyester environment is confirmed by ATR-FTIR that shows their accumulation in the outer cutin-enriched regions rather than on the inner polysaccharide-rich fraction of cuticles (**Figures 2A,B**). The integration of phenolics in the cutin framework is supported by the availability of nanometer size cavities as revealed by computational modeling (Matas and Heredia, 1999) and the induced structural compacting of the cutin network found by XRD (Segado et al., 2020). The rigidity of the cutin matrix has been correlated with the amount of phenolics (López-Casado et al., 2007) and the derived segmental mobility restriction of polyester chains and the reduction of free volume have been evidenced by the increment of the glass transition temperature (T_g; Luque and Heredia, 1997; Matas et al., 2004c). Such interaction of phenolics with cutin and their impact on the mechanical properties of the tomato cuticles is comparable to the effect of the intracuticular triterpenoids on cuticles of persimmon fruits (Tsubaki et al., 2013).

Phenolics Stiffen Isolated Tomato Cuticles by Interacting With Both the Cutin and the Polysaccharide Fractions

In isolated tomato cuticles, the modulus is the mechanical parameter that experiments the most direct and consistent effect of phenolics. Such parameter is obtained at the elastic regime, which is reported to be conditioned by the polysaccharide fraction and the re-orientation of their microfibrils along the stress direction (Matas et al., 2004a). This consideration would bring the focus on the relevance of polysaccharides on the control of the structural assembly and the mechanical properties of the cuticle (Guzmán et al., 2014; Fernández et al., 2016), a role usually assigned to the polyester cutin. In this sense, it has to be kept in mind that the moduli of tomato cuticles are closer to those of polysaccharides, such as cellulose, hemicellulose, and pectin (in the GPa range) than to cutin and amorphous synthetic cutin-alike polyesters (~10–50 MPa; López-Casado et al., 2007; Benítez et al., 2018). Thus, the massive phenolic incorporation to the cuticle that occurs during ripening could be affecting polysaccharide re-orientation by acting as a compatibilizer on the interface between polysaccharide fibrils and polyester cutin matrix. The potential improvement of polysaccharide-cutin adhesion caused by phenolics would be a shear hindrance to microfibril orientation and a higher stress per deformation unit would be required. Consequently, phenolic compounds may have a new function in cuticles by acting as coupling agents and establishing bridging linkages between polysaccharides and cutin, as proposed for cementing polysaccharides (Fich et al., 2016; Philippe et al., 2020).

A closer look to ATR-FTIR data supports the proposed association of phenolics with the polysaccharide fraction. In **Figure 10A**, the ratio between the normalized (γ) band areas corresponding to the inner (polysaccharide-rich) and outer (cutin-rich) sides of Cascada cuticles is plotted versus fruit development

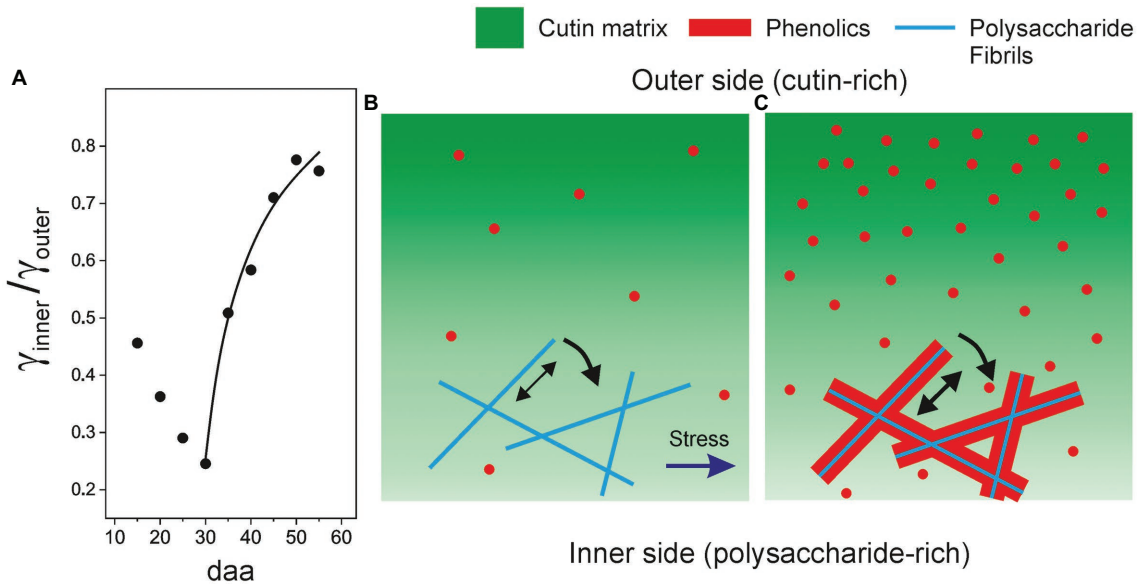

FIGURE 10 | (A) Evolution of the ratio of normalized (γ) bands as obtained from the ATR-FTIR spectra from the inner (γ_{inner}) and outer (γ_{outer}) sides of tomato Cascada cuticles. Structural model showing the fractions (cutin, polysaccharides, and phenolics) distributions in: **(B)** young and **(C)** ripe cuticles.

time time. As observed, there is a noticeable increment of the $\gamma_{inner}/\gamma_{outer}$ ratio matching the phenolic accumulation stage (30 to 55 daa). The thickness and invagination variations in this range are small (**Table 1; Supplementary Table S1**) and, consequently, data should be considered to be free of the inherent thickness distortion of ATR-FTIR measurements (see Additional Text in **Supplementary Material**). The interpretation of the $\gamma_{inner}/\gamma_{outer}$ increment is that, during ripening in stage II, the rate of accumulation of phenolics in the polysaccharide-rich region is faster than in the cutin-rich one, as expected from the proposed phenolics-polysaccharide association. The initial $\gamma_{inner}/\gamma_{outer}$ diminishment observed between 15 and 30 daa is very likely a thickness artifact (see Additional Text in **Supplementary Material**).

The structural model proposed here is schematized in **Figures 10B,C** and combines two effects caused by phenolics: (1) their association with polysaccharide fibrils and the increment of adhesion between fibrils and cutin and (2) the stiffening of the cutin matrix resulting from their accommodation as nanofillers. Since tomato fruit cuticle phenolics are mainly phenolic acids, which are present throughout development but significantly increase their accumulation during ripening, and the flavonoid chalconaringenin, that is only incorporated to the cuticle during ripening (España et al., 2014), it would be important to ascertain whether both phenolic compounds can act as nanofillers and compatibilizers.

Viscoelasticity of Isolated Tomato Cuticles Is Modulated by the Presence of Phenolic Compounds

The evolution of the storage modulus (E') with strain displays an initial increment (strain-hardening; **Figure 6A**) caused by the re-orientation of fibrils along the stress direction. At low phenolic content, the interfacial adhesion between polysaccharides and cutin is comparatively low and, consequently, the re-orientation requires a low stress. As phenolics accumulate, they associate with polysaccharides and the cutin-polysaccharide interaction gets reinforced. The higher interfacial adhesion between fibrils and cutin, as well as the stiffening of the cutin itself, caused by phenolics entail a higher stress for the re-orientation and the storage modulus (E') increases significantly (**Figures 6A,D**). At higher strains, the strain-hardening is followed by a strain-softening assigned to the slippage of polysaccharide fibrils within a plastic deformed cutin matrix (Spatz et al., 1999; Köhler and Spatz, 2002). The transition between both regimes sets a (E') maximum which is also affected by the fruit developmental stage. The maximum is higher, more pronounced and displaced toward lower strains upon phenolics irruption because the stress required for the orientation of fibrils raises so quickly that reaches the slippage limit at lower strain values. The cuticle stiffening induced by these compounds is so intense that compensates and surpasses the effect of the polysaccharide reduction in the 45–55 daa range (**Figure 5A**). Indeed, evaluation of the effect of phenolics on the elastic modulus was shown to be an order of magnitude higher than the one of polysaccharides (Domínguez et al., 2009).

It has been suggested that the predominance of the viscoelastic performance of cuticles is related to the absence of phenolics (Domínguez et al., 2009). This conclusion is based on the analysis of the shape of the stress–strain curve in transient creep experiments. However, DMA analysis is capable to isolate the pure elastic and viscous components from the very beginning of deformation. Thus, **Figure 6C** shows that the viscoelasticity (Tan δ) increases with the phenolic content even within the elastic region ($\varepsilon < 2$–3%). This behavior can be due to a higher contribution of the viscous

component arising from a better compatibilization between polysaccharides and cutin phases favored by phenolics. Nevertheless, an effect of the polysaccharide decrease observed in the 45–55 daa period cannot be dismissed (López-Casado et al., 2007).

The increased accumulation of phenolic compounds in tomato cuticle during ripening allows the transition from a soft elastic regime to a more rigid and viscous state. Such rheological modification is relevant to the understanding of key phenomena, such as mass flow, diffusion, and transpiration processes across this barrier layer. The association of phenolics with polysaccharides and its contribution to the modification of the biomechanical performance of tomato cuticles are issues that deserve further research.

DATA AVAILABILITY STATEMENT

The raw data supporting the conclusions of this article will be made available by the authors, without undue reservation.

AUTHOR CONTRIBUTIONS

JB, ED, and AH conceived and planned the research. JB performed the experiments. SG-P and FV were responsible for the polysaccharide analysis. JH-G supervised the experiments. JB, JH-G, and ED wrote the article with contributions and supervision of all authors. All authors approved the submitted text.

FUNDING

This work was supported by grant RTI2018-094277-B/AEI/10.13039/501100011033 from Agencia Estatal de Investigación, Ministerio de Ciencia e Innovación, Spain (co-financed by the European Regional Development Fund, ERDF). JH-G acknowledges the support by the Spanish "Ministerio de Ciencia, Innovación y Universidades" project RYC2018-025079-I/AEI/10.13039/501100011033 (co-financed by the European Social Fund, ESF). SG-P thanks the support of the PIE project 202040E003 funded by the Spanish Research Council (CSIC).

SUPPLEMENTARY MATERIAL

The Supplementary Material for this article can be found online at: https://www.frontiersin.org/articles/10.3389/fpls.2021.787839/full#supplementary-material

REFERENCES

Bargel, H., and Neinhuis, C. (2004). Altered tomato (*Lycopersicon esculentum* mill.) fruit cuticle biomechanics of a pleiotropic non ripening mutant. *J. Plant Growth Regul.* 23, 61–75. doi: 10.1007/s00344-004-0036-0

Bargel, H., and Neinhuis, C. (2005). Tomato (*Lycopersicon esculentum* mill.) fruit growth and ripening as related to the biomechanical properties of fruit skin and isolated cuticle. *J. Exp. Bot.* 56, 1049–1060. doi: 10.1093/jxb/eri098

Barraj Barraj, R., Segado, P., Moreno-González, R., Heredia, A., Fernández-Muñoz, R., and Domínguez, E. (2021). Genome-wide QTL analysis of tomato fruit cuticle deposition and composition. *Hortic. Res.* 8:113. doi: 10.1038/s41438-021-00548-5

Benítez, J. J., Castillo, P. M., del Río, J. C., León-Camacho, M., Domínguez, E., Heredia, A., et al. (2018). Valorization of tomato processing by-products: fatty acid extraction and production of bio-based materials. *Materials* 11:2211. doi: 10.3390/ma11112211

Castro, R. I., and Morales-Quintana, L. (2019). Study of the cell wall components produced during different ripening stages through thermogravimetric analysis. *Cellulose* 26, 3009–3020. doi: 10.1007/s10570-019-02305-3

Chanliaud, E., Burrows, K. M., Jeronimidis, G., and Gidley, M. J. (2002). Mechanical properties of primary plant cell wall analogues. *Planta* 215, 989–996. doi: 10.1007/s00425-002-0783-8

Domínguez, E., Cuartero, J., and Heredia, A. (2011). An overview on plant cuticle biomechanics. *Plant Sci.* 181, 77–84. doi: 10.1016/j.plantsci.2011.04.016

Domínguez, E., España, L., López-Casado, G., Cuartero, J., and Heredia, A. (2009). Biomechanics of isolated tomato (*Solanum lycopersicum*) fruit cuticles during ripening: the role of flavonoids. *Funct. Plant Biol.* 36, 613–620. doi: 10.1071/FP09039

Domínguez, E., López-Casado, G., Cuartero, J., and Heredia, A. (2008). Development of fruit cuticle in cherry tomato (*Solanum lycopersicum*). *Funct. Plant Biol.* 35, 403–411. doi: 10.1071/FP08018

Edelmann, H. G., Neinhuis, C., and Bargel, H. (2005). Influence of hydration and temperature on the rheological properties of plant cuticles and their impact on plant organ integrity. *J. Plant Growth Regul.* 24, 116–126. doi: 10.1007/s00344-004-0015-5

España, L., Heredia-Guerrero, J. A., Segado, P., Benítez, J. J., Heredia, A., and Domínguez, E. (2014). Biomechanical properties of the tomato (*Solanum lycopersicum*) fruit cuticle during development are modulated by changes in the relative amounts of its components. *New Phytol.* 202, 790–802. doi: 10.1111/nph.12727

Fernández, V., Guzmán-Delgado, P., Graça, J., Santos, S., and Gil, L. (2016). Cuticle structure in relation to chemical composition: re-assessing the prevailing model. *Front. Plant Sci.* 7:427. doi: 10.3389/fpls.2016.00427

Fich, E. A., Segerson, N. A., and Rose, J. K. C. (2016). The plant polyester cutin: biosynthesis, structure and biological roles. *Annu. Rev. Plant Biol.* 67, 207–233. doi: 10.1146/annurev-arplant-043015-111929

Guzmán, P., Fernández, V., Graça, J., Cabral, V., Kayali, N., Khayet, M., et al. (2014). Chemical and structural analysis of Eucalyptus globulus and E. camaldulensis leaf cuticles: a lipidized cell wall region. *Front. Plant Sci.* 5:481. doi: 10.3389/fpls.2014.00481

Heredia-Guerrero, J. A., Benítez, J. J., Domínguez, E., Bayer, I. S., Cingolani, R., Athanassiou, A., et al. (2014). Infrared and Raman spectroscopic features of plant cuticles: a review. *Front. Plant Sci.* 5:305. doi: 10.3389/fpls.2014.00305

Heredia-Guerrero, J. A., Guzman-Puyol, S., Benítez, J. J., Athanassiou, A., Heredia, A., and Domínguez, E. (2018). Plant cuticle under global change: biophysical implications. *Glob. Chang. Biol.* 24, 2749–2751. doi: 10.1111/gcb.14276

Kamtsikakis, A., Baales, J., Zeisler-Diehl, V. V., Vanhecke, D., Zoppe, J. O., Schreiber, L., et al. (2021). Asymmetric water transport in dense leaf cuticles and cuticle-inspired compositionally graded membranes. *Nat. Commun.* 12:1267. doi: 10.1038/s41467-021-21500-0

Khanal, B. P., Grimm, E., Finger, S., Blume, A., and Knoche, M. (2013). Intracuticular was fixes and restricts strain in leaf and fruit cuticles. *New Phytol.* 200, 134–143. doi: 10.1111/nph.12355

Khanal, B. P., and Knoche, M. (2014). Mechanical properties of apple skin are determined by epidermis and hypodermis. *J. Amer. Soc. Hort. Sci.* 139, 139–147. doi: 10.21273/JASHS.139.2.139

Khanal, B. P., and Knoche, M. (2017). Mechanical properties of cuticles and their primary determinants. *J. Exp. Bot.* 68, 5351–5367. doi: 10.1093/jxb/erx265

Köhler, L., and Spatz, H. C. (2002). Micromechanics of plant tissues beyond the linear-elastic range. *Planta* 215, 33–40. doi: 10.1007/s00425-001-0718-9

Laguna, L., Casado, C. G., and Heredia, A. (1999). Flavonoid biosynthesis in tomato fruit cuticles after in vivo incorporation of H^3-phenylamine precursor. *Physiol. Plant.* 105, 491–498. doi: 10.1034/j.1399-3054.1999.105314.x

Lara, I., Belge, B., and Goulao, L. F. (2014). The fruit cuticle as modulator of postharvest quality. *Postharvest Biol. Technol.* 87, 103–112. doi: 10.1016/j.postharvbio.2013.08.012

López-Casado, G., Matas, A. J., Domínguez, E., Cuartero, J., and Heredia, A. (2007). Biomechanics of isolated tomato (Solanum lycopersicum L.) fruit cuticles: the role of the cutin matrix and polysaccharides. *J. Exp. Bot.* 58, 3875–3883. doi: 10.1093/jxb/erm233

López-Casado, G., Salamanca, A., and Heredia, A. (2010). Viscoelastic nature of isolatated tomato (*Solanum lycopersicum*) fruit cuticles: a mathematical model. *Physiol. Plant.* 140, 79–88. doi: 10.1111/j.1399-3054.2010.01379.x

Luque, P., and Heredia, A. (1994). Glassy state in plant cuticles during growth. *Z. Naturforsch. C* 49, 273–275. doi: 10.1515/znc-1994-3-419

Luque, P., and Heredia, A. (1997). The glassy state in isolated cuticles: differential scanning calorimetry of tomato fruit cuticular membranes. *Plant Physiol. Biochem.* 35, 251–256.

Matas, A. J., Cobb, E. D., Bartsch, J. A., Paolillo, D. J., and Niklas, K. J. (2004a). Biomechanics and anatomy of *Lycopersicon esculentum* fruit peels and enzyme-treated samples. *Am. J. Bot.* 91, 352–360. doi: 10.3732/ajb.91.3.352

Matas, A. J., Cobb, J. A., Paolillo, D. J., and Niklas, K. J. (2004b). Crack resistance in cherry tomato fruit correlates with cuticular membrane thickness. *HortScience* 39, 1354–1358. doi: 10.21273/HORTSCI.39.6.1354

Matas, A., Cuartero, J., and Heredia, A. (2004c). Phase transitions in the biopolyester cutin isolated from tomato fruit cuticles. *Thermochim. Acta* 409, 165–168. doi: 10.1016/S0040-6031(03)00357-5

Matas, A., and Heredia, A. (1999). Molecular dynamics modellization and simulation of water diffusion through plant cutin. *Z. Naturforsch. C* 54, 896–902. doi: 10.1515/znc-1999-1107

Menard, K. P. (2008). *Dynamic Mechanical Analysis: A Practical Introduction* (Boca Raton: CRC Press).

Petracek, P. D., and Bukovac, M. J. (1995). Rheological properties of enzymatically isolated tomato fruit cuticle. *Plant Physiol.* 109, 675–679. doi: 10.1104/pp.109.2.675

Philippe, G., Geneix, N., Petit, J., Guillon, F., Sandt, C., Rothan, C., et al. (2020). Assembly of tomato fruit cuticles: a cross-talk between the cutin polyester and cell wall polysaccharides. *New Phytol.* 226, 809–822. doi: 10.1111/nph.16402

Ramírez, F. J., Luque, P., Heredia, A., and Bukovac, M. J. (1992). Fourier transform IR of enzymatically isolated tomato cuticular membrane. *Biopolymers* 32, 1425–1429. doi: 10.1002/bip.360321102

Segado, P., Heredia-Guerrero, A., Heredia, A., and Domínguez, E. (2020). Cutinsomes and CUTIN SYNTHASE1 function sequentially in tomato fruit cutin deposition. *Plant Physiol.* 183, 1622–1637. doi: 10.1104/pp.20.00516

Spatz, H. C. H., Köhler, L., and Niklas, K. J. (1999). Mechanical behavior of plant tissues: composite materials or structures? *J. Exp. Biol.* 202, 3269–3272. doi: 10.1242/jeb.202.23.3269

Takahashi, Y., Tsubaki, S., Sakamoto, M., Watanabe, S., and Azuma, J. (2012). Growth-dependent chemical and mechanical properties of cuticular membranes from leaves of Sonneratia alba. *Plant Cell and Environ.* 35, 1201–1210. doi: 10.1111/j.1365-3040.2012.02482.x

Thompson, D. S. (2001). Extensiometric determination of the rheological properties of the epidermis of growing tomato fruit. *J. Exp. Bot.* 52, 1291–1301. doi: 10.1093/jexbot/52.359.1291

Tsubaki, S., Ozaki, Y., Yonemori, K., and Azuma, J. (2012). Mechanical properties of fruit-cuticular membranes isolated from 27 cultivars of Diospyros kaki Thunb. *Food Chem.* 132, 2135–2139. doi: 10.1016/j.foodchem.2011.12.039

Tsubaki, S., Sugimura, K., Teramoto, Y., Yonemori, K., and Azuma, J. (2013). Cuticular membrane of Fuyu Persimon fruit is strengthened by triterpenoid nano-fillers. *PLoS One* 8:e75275. doi: 10.1371/journal.pone.0075275

Videcoq, P., Barbacci, A., Assor, C., Magnenet, V., Arnould, O., Le Gall, S., et al. (2017). Examining the contribution of cell wall polysaccharides to the mechanical properties of apple parenchyma tissue using exogenous enzymes. *J. Exp. Bot.* 68, 5137–5146. doi: 10.1093/jxb/erx329

Vidyarthi, S. K., El Mashad, H. M., Khir, R., Zhang, R., Sun, G., Tiwari, R., et al. (2020). Viscoelastic properties of tomato peels produced from catalytic infrared and lye peeling methods. *Food Bioprod. Process.* 119, 337–344. doi: 10.1016/j.fbp.2019.11.019

Wang, Y., Li, X., Sun, G., Li, D., and Pan, A. (2014). A comparison of dynamic mechanical properties of processing-tomato peel as affected by hot lye and infrared radiation heating for peeling. *J. Food Eng.* 126, 27–34. doi: 10.1016/j.jfoodeng.2013.10.032

Wiedemann, P., and Neinhuis, C. (1998). Biomechanics of isolated plant cuticles. *Bot. Acta* 111, 28–34. doi: 10.1111/j.1438-8677.1998.tb00673.x

Yeats, T. H., and Rose, J. K. C. (2013). The formation and function of plant cuticles. *Plant Physiol.* 163, 5–20. doi: 10.1104/pp.113.222737

Conflict of Interest: The authors declare that the research was conducted in the absence of any commercial or financial relationships that could be construed as a potential conflict of interest.

Publisher's Note: All claims expressed in this article are solely those of the authors and do not necessarily represent those of their affiliated organizations, or those of the publisher, the editors and the reviewers. Any product that may be evaluated in this article, or claim that may be made by its manufacturer, is not guaranteed or endorsed by the publisher.

frontiers in Plant Science

METHODS
published: 17 December 2021
doi: 10.3389/fpls.2021.793330

A Guide to Elucidate the Hidden Multicomponent Layered Structure of Plant Cuticles by Raman Imaging

*Peter Bock†, Martin Felhofer†, Konrad Mayer and Notburga Gierlinger**

Department of Nanobiotechnology, Institute of Biophysics, University of Natural Resources and Life Sciences, Vienna, Austria

The cuticle covers almost all plant organs as the outermost layer and serves as a transpiration barrier, sunscreen, and first line of defense against pathogens. Waxes, fatty acids, and aromatic components build chemically and structurally diverse layers with different functionality. So far, electron microscopy has elucidated structure, while isolation, extraction, and analysis procedures have revealed chemistry. With this method paper, we close the missing link by demonstrating how Raman microscopy gives detailed information about chemistry and structure of the native cuticle on the microscale. We introduce an optimized experimental workflow, covering the whole process of sample preparation, Raman imaging experiment, data analysis, and interpretation and show the versatility of the approach on cuticles of a spruce needle, a tomato peel, and an Arabidopsis stem. We include laser polarization experiments to deduce the orientation of molecules and multivariate data analysis to separate cuticle layers and verify their molecular composition. Based on the three investigated cuticles, we discuss the chemical and structural diversity and validate our findings by comparing models based on our spectroscopic data with the current view of the cuticle. We amend the model by adding the distribution of cinnamic acids and flavonoids within the cuticle layers and their transition to the epidermal layer. Raman imaging proves as a non-destructive and fast approach to assess the chemical and structural variability in space and time. It might become a valuable tool to tackle knowledge gaps in plant cuticle research.

Keywords: plant surfaces, waxes, cutin, chalcones, flavonoids, multivariate data analysis, epidermal cell wall, pectin

OPEN ACCESS

Edited by:
Antonio Heredia,
University of Malaga, Spain

Reviewed by:
Jozef Mravec,
University of Copenhagen, Denmark
Wieslaw Gruszecki,
Maria Curie-Skłodowska University, Poland

***Correspondence:**
Notburga Gierlinger
burgi.gierlinger@boku.ac.at

† These authors have contributed equally to this work and share first authorship

Specialty section:
This article was submitted to Plant Physiology, a section of the journal Frontiers in Plant Science

Received: *12 October 2021*
Accepted: *09 November 2021*
Published: *17 December 2021*

Citation:
Bock P, Felhofer M, Mayer K and Gierlinger N (2021) A Guide to Elucidate the Hidden Multicomponent Layered Structure of Plant Cuticles by Raman Imaging. Front. Plant Sci. 12:793330. doi: 10.3389/fpls.2021.793330

INTRODUCTION

The cuticle is the outermost layer of the plant in direct contact with the environment. It consists of an epicuticular wax layer on top of a lipidized region of the epidermal cell wall. The various functions include controlling water and gas exchange, defense against pathogens, separating plant organs, and light protection and manipulation for the underlying tissues (Yeats and Rose, 2013; Martin and Rose, 2014; Pfündel et al., 2018). To fulfill these different tasks, lipidic and aromatic components build layers upon a carbohydrate-rich epidermal layer.

On top, the epidermal waxes are in direct contact with the atmosphere and maintain a clean surface to avoid reduced transmission of active photosynthetic radiation. Additionally, they scatter excess light (Pfündel et al., 2018) and impede the attachment of fungal spores and insect tarsae (Berto et al., 1999; Eigenbrode and Jetter, 2002). The beneath cuticular layer's primary role seems to be controlling water diffusion (Martin and Rose, 2014). Depending on species and developmental stages, aromatic components impregnate the cuticle and transition to the epidermal layer (Sasani et al., 2021). In the last decade, the view of the cuticle shifted from a stand-alone layer on top of the epidermis to more integrated concepts (Yeats and Rose, 2013; Guzman et al., 2014b; Fernandez et al., 2016; Sasani et al., 2021). However, the chemical composition in context with the biological architecture of the plant cuticle is still under debate. To close this knowledge gap, we present Raman microspectroscopy as a valuable tool for cuticle research.

Chemical Imaging: The Missing Link?

In the past, cuticles have been studied mainly through electron microscopy for elucidating their structure (Jeffree and Sandford, 1982; Wattendorff and Holloway, 1982; Tenberge, 1992; Lopez-Casado et al., 2007; Guzman et al., 2014a,c; Kwiatkowska et al., 2014; Segado et al., 2016), while the chemistry was revealed by lipid extraction and separation procedures (Franich et al., 1978; Hunt and Baker, 1980; Tulloch and Bergter, 1981; Jetter and Riederer, 1994, 2016; Kögel-Knabner et al., 1994; Prügel and Lognay, 1996; Oros et al., 1999; Villena et al., 1999; Jetter et al., 2000; Goodwin et al., 2003; Solovchenko and Merzlyak, 2003; Wen et al., 2006; Buschhaus et al., 2007, 2015; Szafranek et al., 2008; Guzman et al., 2014b; Guzman-Delgado et al., 2016; Bourgault et al., 2020; Moreira et al., 2020). However, both approaches faced the same problem: destroying the native structure by peeling/scratching off cuticles. Electron microscopy better retains the structure but linking it to chemistry is problematic as stainings can be affected by different infiltration into the sample (Fernandez et al., 2016). Extraction and separation yield detailed chemical information, but it can hardly be linked to the cuticle structure destroyed in the process. The heterogeneous nature of the cuticle, comprising compounds with different solubilities and high spatial variability, calls for approaches, which link chemistry with structure (Guzman et al., 2014b; Fernandez et al., 2016; Guzman-Delgado et al., 2016). Here, we show how Raman microscopy offers an *in situ* method that links the chemical to structural information on the micro-scale. It is already successfully used in plant sciences for studying flower (Gamsjaeger et al., 2011), stem (Gierlinger et al., 2008; Zeise et al., 2018), leaves (Baranska et al., 2006; Richter et al., 2011), fruits (Cai et al., 2010; Szymanska-Chargot et al., 2016), and roots (Schreiber et al., 2010; Heiner et al., 2018), but so far only a few Raman studies on cuticles are available (Littlejohn et al., 2015; Prats Mateu et al., 2016; Philippe et al., 2020; Sasani et al., 2021).

In this method article, we explore the potential of Raman imaging on cuticles of three plant species and provide an informative guide for successful applications. We share our experiences from sample preparation to spectra acquisition, from spectra analysis to image generation, and give new insights into the spectral interpretation of cuticle components.

MATERIALS AND METHODS

Samples and Microtomes

Fresh samples (**Figure 1A**) and proper storage are essential to exclude unwanted chemical or biological reactions (oxidation, microbial growth, etc.). Before micro sectioning, cutting small blocks with a sharp razor blade is simple and straightforward (**Figure 1A**). To stabilize soft tissues, samples often need to be embedded in polymers or resins before cutting. However, the Raman signal of embedding media can superimpose with those from the tissue (Coste et al., 2021). Therefore, water-soluble polyethylene glycol (PEG) is recommended (Gierlinger et al., 2012; Prats Mateu et al., 2016). However, cryo-microtomes cut native samples in the frozen state without any treatment. Therefore we consider cryomicrotomy as the best sample preparation for Raman imaging and use a cryo-microtome (CM 3050 S) from Leica (Biosystems Nussloch GmbH, Germany).

Cryosectioning and Sample Preparation

For successful imaging and reproducibility, selection of target regions (developmental and tissue-specific) and the orientation is crucial (Gierlinger et al., 2012; Butler et al., 2016). Thus, before mounting, it should be considered whether the abaxial or adaxial cuticle or the tip or middle portion of a needle or leaf is the area of interest. Furthermore, different sample orientations allow probing orientation of molecules with respect to stem axis or leaf surface. Here, the cryo approach provides easy adjustment of the sample's angle during mounting or by moving the sample holder in the cryostat (**Figures 1B,C**).

Disposable blades are valuable and easy to handle; for example, the N35 blade (35°) from Feather (Japan) is particularly suitable for frozen tissues and allows the sectioning of flat, thin (1–20 μm) and relatively large sections. Using a trimmed, clean, and fine brush allows collecting the micro section after cutting and transferring onto a cooled glass slide. Next, the micro section is directly covered with a cooled coverslip in the cryostat (**Figure 1C**). Finally, the sample can be taken out of the cryostat and slowly accommodated to room temperature. A water drop might also be added. After rinsing several times with water, the coverslip is sealed with nail polish to avoid dehydration (**Figure 1D**). More information about sample preparation can be found in Gierlinger et al. (2012), Butler et al. (2016), Prats-Mateu et al. (2020).

Other Cuticle Preparation Techniques and Their Potential for Raman Experiments

Most studies used sample preparation techniques other than cryo-sectioning, relying on different chemical and mechanical treatments. Recently (Vráblová et al., 2020) reported a modified enzymatic method, which isolates abaxial and adaxial cuticles and avoids the formation of wrinkles (**Figure 1E**). This method

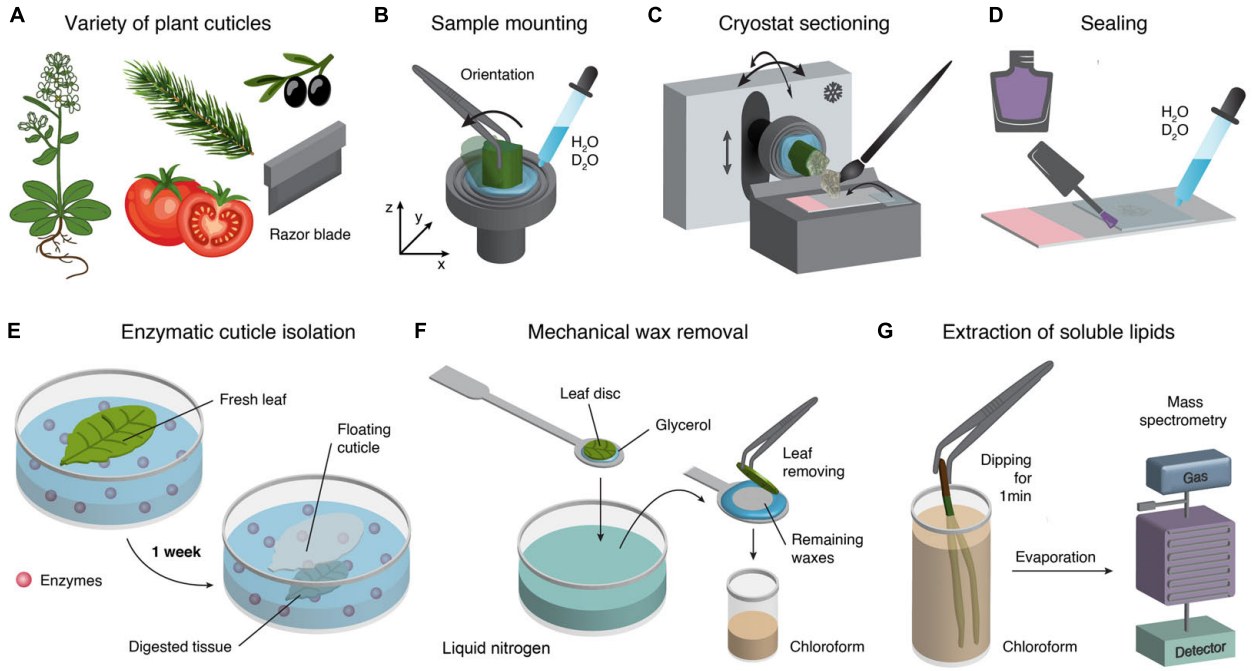

FIGURE 1 | Cuticle sample preparation techniques. **(A)** For a wide variety of plant cuticles different sample preparation techniques are available. In a first step a sharp razor blade separates fast and easy areas of interest in form of small pieces for microtome sectioning. **(B)** For cryo-cutting, the mounting of a sample can be easily achieved by freezing a tissue on the sample holder. The advantage is that the sample orientation can be adjusted, and no embedding medium is needed. **(C)** Cutting in the cryostat allows the adjusting of the temperature of the chamber and the sample holder separately. Furthermore, the orientation of the sample holder can also be adjusted accordingly. **(D)** Cross-sections embedded on glass slides with a drop of water and coverslip and finally sealed with nail polish. **(E)** Enzymatic separation of cuticles (Vráblová et al., 2020). **(F)** Mechanical wax removal (Jetter et al., 2000). **(G)** Easy and fast extraction of soluble lipids by dipping samples into chloroform (Guzmán-Delgado et al., 2017).

can potentially be applied to Raman studies because following the separation of the cuticle *in situ* would shed new light on the interface between the cuticle and the epidermal cell wall. In addition (Jetter et al., 2000) showed that a cryo-adhesive-based approach allows for mechanical isolation of the epicuticular wax film (**Figure 1F**). This technique can be employed directly under the Raman microscope equipped with a heating and freezing stage (e.g., Linkam, United Kingdom) to follow the separation *in situ*. Another study showed an easy and fast extraction method of soluble lipids from the cuticle surface by dipping the leaves directly in chloroform and subsequent analysis with mass spectrometry (Guzman-Delgado et al., 2016; **Figure 1G**). A very recent study by Chang and Keller (2021) used chloroform and hydrogen peroxide treatments to test the mechanical influence of the cuticle and skin cell walls during berry splitting. Lim et al. (2020) used cuticle-defective mutants with increased transpiration and reduced water potential to show the movement of salicylic acid toward the cuticle. They also used chloroform to extract the cuticular waxes. Here, Raman experiments before and after extraction would add tissue-specific and spatial information about the extraction progress and mutants.

Raman Microspectroscopy

Raman spectroscopy probes molecular vibrations and changes in the polarizability of molecules (inducing a dipole) by using a monochromatic laser (Colthup et al., 1990). The excitation wavelength and the numerical aperture (NA) of the objective determine the spatial resolution. For example, using an oil objective (NA = 1.4) and a standard 532 nm or 785 nm laser, the theoretical resolution is about 232 and 342 nm, respectively. In addition, a short wavelength (e.g., 532 nm) is preferred because of the higher Raman intensity gained. However, if samples absorb at these wavelengths, fluorescence can swamp the Raman signal to levels where a high background masks all peaks. For example, in previous studies (Sasani et al., 2021), flavonoids often caused high fluorescence at 532 nm and scanning with 785 nm laser gave better results. Choosing the right laser wavelength is based on individual samples and trial and error.

Integration Time and Laser Power

If a sample cannot sustain laser power for the length of a measurement, then laser power, point density and integration time can be adjusted. A choice has to be made between the quality of the spectra and the spatial resolution of the image. For higher spectral quality, increasing the distance between measurement points reduces the time the sample is exposed to the laser. If the spatial resolution should not be compromised, then the laser power or the time the laser remains on a single measurement spot (called integration time) can be reduced. However, lower integration time means noisier spectra. In our experiments, laser

powers of 10–30 mW and integration times of 0.01 seconds have proven optimal parameters for a wide range of samples. Time series measurements (0.01 s resolution) are suitable to check whether a sample is prone to laser degradation.

Avoiding Fluorescence

The most problematic drawback of Raman spectroscopy is fluorescence. This means that a molecule absorbs radiation at a particular wavelength, lifting electrons into a higher energy state. After falling back to the ground state, the electrons release energy as radiation and create more photons than Raman scattering. The consequence is that if the absorption of a sample coincides with the laser wavelength, fluorescence can mask the Raman spectrum (Colthup et al., 1990; Smith and Dent, 2005; Nebu and Sony, 2017). In this case, changing the laser wavelength, adding freshwater, or extracting some compounds from the sample can be helpful. If cells with chlorophyll are within the region of interest, a preliminary fast scan with short integration time is recommended to bleach the chlorophyll; the subsequent scan will be without fluorescence.

Polarizability and Molecule Orientation

One characteristic of Raman spectroscopy is that molecules with extended delocalized π-electrons (carotenes, cinnamic acids, flavonoids, stilbenes) induce bands with a very high Raman intensity (Schmid and Brosa, 1971; Schmid and Topsom, 1981; Felhofer et al., 2018; Maia et al., 2021). Therefore, even low quantities of molecules can be tracked within a sample and particularly in the cuticle. However, their signal can be so strong that the discrimination of other compounds is difficult, but changing the wavelength might be helpful (Bock and Gierlinger, 2019). Furthermore, a change of bond polarizability concerning laser polarization can be seen in crystalline structures like the wax layers. The highest polarizability is often along bond axes and allows statements about molecular order and orientation by Raman spectroscopy (Gierlinger et al., 2010; Sasani et al., 2021).

Water as a Native Embedding Medium

The substantial benefit of Raman microspectroscopy is the possibility of studying plants in their native (wet) state. The reason is that the water Raman intensity is relatively low and shows only one band. If an embedding medium other than water is used, its Raman spectrum can be subtracted in a post-processing step. In practice, however, the impregnation of embedding media varies with different tissues (Coste et al., 2021), and their spectral contribution cannot entirely be removed, causing spectral artifacts to remain. Therefore, it is advisable to use water or deuterium oxide as an embedding medium because of its relatively weak Raman signal and only one notable band at around 3400 cm^{-1}. In addition, tracking the water distribution within different tissues and layers is possible (Horvath et al., 2012; Prats Mateu et al., 2016).

Raman Imaging

A piezo motorized scan stage allows fast stitching of the entire sample, which supports selecting the region of interest for area scans (x,y). In addition, depth scans (z) are possible to elucidate the three-dimensional chemical distribution. However, in practice, quantitative depth scanning is only possible in more or less transparent samples, like silica protrusion in horsetail (Gierlinger et al., 2008). Before measuring, it is crucial to adjust and fix the sample on the scan stage according to the laser polarization. Rastering a sample with a laser point by point creates a hyperspectral data cube, including the spatial position (x,y,z) and the molecular fingerprint (spectrum). Finally, the hyperspectral data cube allows the calculation of Raman images based on univariate and multivariate approaches (Gierlinger, 2018).

Image Processing

Applying different image processing approaches can reveal the multicomponent chemical structure. Before image processing, it is necessary to remove cosmic rays by a software algorithm and check whether intensity differences are due to chemical differences or the focal plane (sample flatness). If the measured surface has not been even, regions out of focus can appear with less signal and cannot be separated from areas with a lower number of molecules. As the multicomponent spectra with overlapping bands are often difficult to explore by band integration and marker bands (see section "Results and Discussion" Step1), it is helpful to include multivariate methods taking care of the whole wavenumber range instead of selected wavenumbers/bands. However, before applying these methods, a suitable background correction algorithm (see e.g., Prats-Mateu et al., 2020), which works on every hyperspectral data cube pixel, is recommended.

True Component Analysis and Mixture Analysis

The "True Component" post-processing function included in the WITec5 software establishes the number of components in a dataset, locates them in the image, and differentiates their spectra. The function calculates the hyperspectral dataset as a linear combination of the most different spectra with a basis analysis algorithm (Dieing and Ibach, 2011). The number of components was increased step by step as long as different and meaningful spectra could be retrieved. To further analyze the multicomponent nature of the derived spectrum (layer), we modeled in the next step the "layer spectra" as a linear combination of measured reference spectra using the Orthogonal Matching Pursuit (Pati et al., 1993). This algorithm compares the spectral signature of the distinguished cuticle layers with spectra of known compounds of a reference library, including 326 entities, from aromatics to lipids to carbohydrates. The orthogonal matching pursuit (OMP) is an iterative approach, running fast enough to handle hyperspectral datacubes. A member from the spectral reference library that best correlates with the residual of the linear combination of references selected in the previous iterations is sought at each iteration. This reference is then added to the predictor set. A termination criterion such as a threshold for the residual error or a maximum number of iterations stops the search for additional members. The predictor set of the final model contains the selected members of the mixture, and the coefficients indicate the frequency of the respective compounds. Completeness and

scaling of the spectral library, the analyzed spectral range, preprocessing (most important baseline correction), among others, have a substantial effect on the result and must be carefully evaluated. Yet, coupled with an exhaustive assessment of the plausibility of the result and testing the robustness of the fit, mixture analysis is an invaluable tool in analyzing complex biological spectra, like the cuticle.

RESULTS AND DISCUSSION

We use Raman images of cuticles of spruce, tomato, and Arabidopsis to show the procedure of image acquisition and analysis as well as cuticle spectral variability across plant species, organs, and layers. We offer an extensive analysis of the cuticle of spruce needles with our optimized experimental workflow, including:

1. Initial univariate exploration by band integration.
2. Determination of molecular orientation.
3. Multivariate image decomposition.
4. Mixture analysis of the resulting spectra.

We then discuss special issues of fluorescence and aromatic signal dominance on cuticles of tomato and show the cuticle of Arabidopsis as a counterexample with much fewer phenolic compounds.

Step 1–Exploring the Sample via Band Integration

A thin section of a needle of spruce was imaged with a Raman microscope (**Figure 2A**). The resulting Raman image displays the CCD counts of the Raman band integrated over a defined wavenumber range at every pixel (**Figures 2B,C**). Pixels with higher band intensity are usually highlighted in brighter colors than areas with low signal. Since the bands of biological samples are often unknown beforehand, the Raman image is explored by changing the center wavenumber, that is, moving the slider through the spectrum. Then, the Raman image constantly changes from noise to clear pictures, similar to tuning a TV to a specific program (**Supplementary Video 1**). Peaks of biological samples often have bandwidths of 20–30 cm^{-1} (FWHM), which is a reasonable first choice for the slider width. This way, the sample is explored, and areas of similar chemistry can be found. They may correspond to structures seen in the visual image but can also reveal hidden structures not visible in light microscopy.

We used the strong CH-stretching band centered at 2900 cm^{-1} to visualize all organic components throughout the whole tissue (**Figures 2B,C**). As this band's intensity also depends on the focus of the image, it can be used to check the quality of the scan before further analysis. We also detected a solid aromatic signal centered at 1600 cm^{-1}, clearly visible in the inner part, as it is also the predominant spectral feature of lignin. In addition, we used a band representing the wax layer in the outer part of the tissue centered at 1065 cm^{-1} (**Figures 2B,C**). The strongest bands give clear pictures but often comprise contributions from more than one component and are suitable for visualization, but often not so informative. Weaker bands (e.g., 1065 cm^{-1}) usually result in noisy images but can have high selectivity if they represent a marker band for a specific component.

Step 2–Determining Molecular Orientation Within the Sample by Laser Polarization Experiments

By using a polarized monochromatic light source, the crystallinity and orientation of molecules can be probed. Controlling the orientation of the laser polarization relative to the sample orientation can provide spectra with information on the preferred orientation of molecules within the sample. This builds on the fact that the polarizability is normally greatest along a chemical bond. Raman polarization measurements have already been shown on biological materials (Cao et al., 2006; Gierlinger et al., 2010; Dong et al., 2021) and recently on cuticles of spruce needles (Sasani et al., 2021).

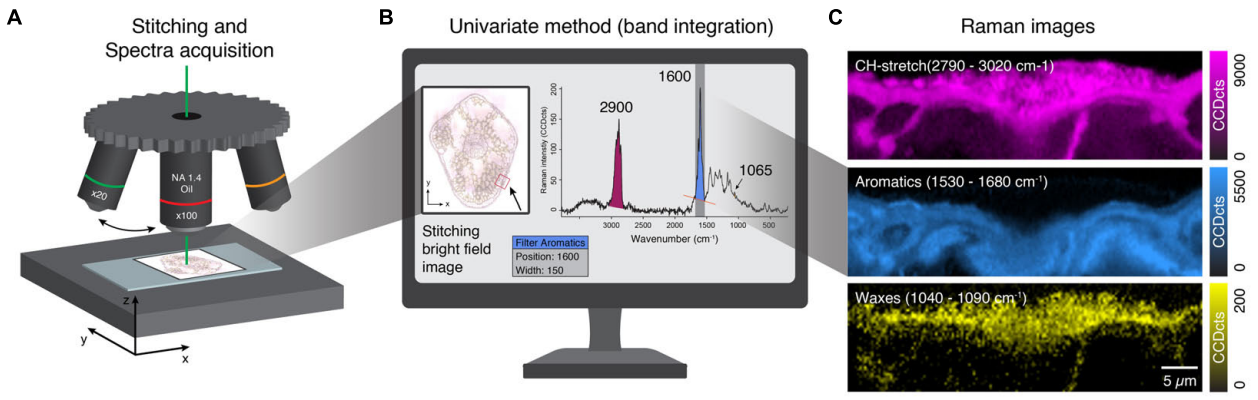

FIGURE 2 | Stitching, Raman spectra acquisition, and image generation. **(A)** Different objective lenses for stitching and high-resolution Raman imaging. **(B)** Stitched bright-field image based on the x20 objective lens provides a good sample overview to select and show regions of interest. Univariate spectra analysis uses filters to plot Raman intensity of selected bands (wavenumber ranges). **(C)** Calculated Raman images based on Raman intensity of different wavenumber ranges corresponding to all components (CH stretching) and selected chemical groups (aromatics, waxes). See also Raman TV (**Supplementary Video 1**).

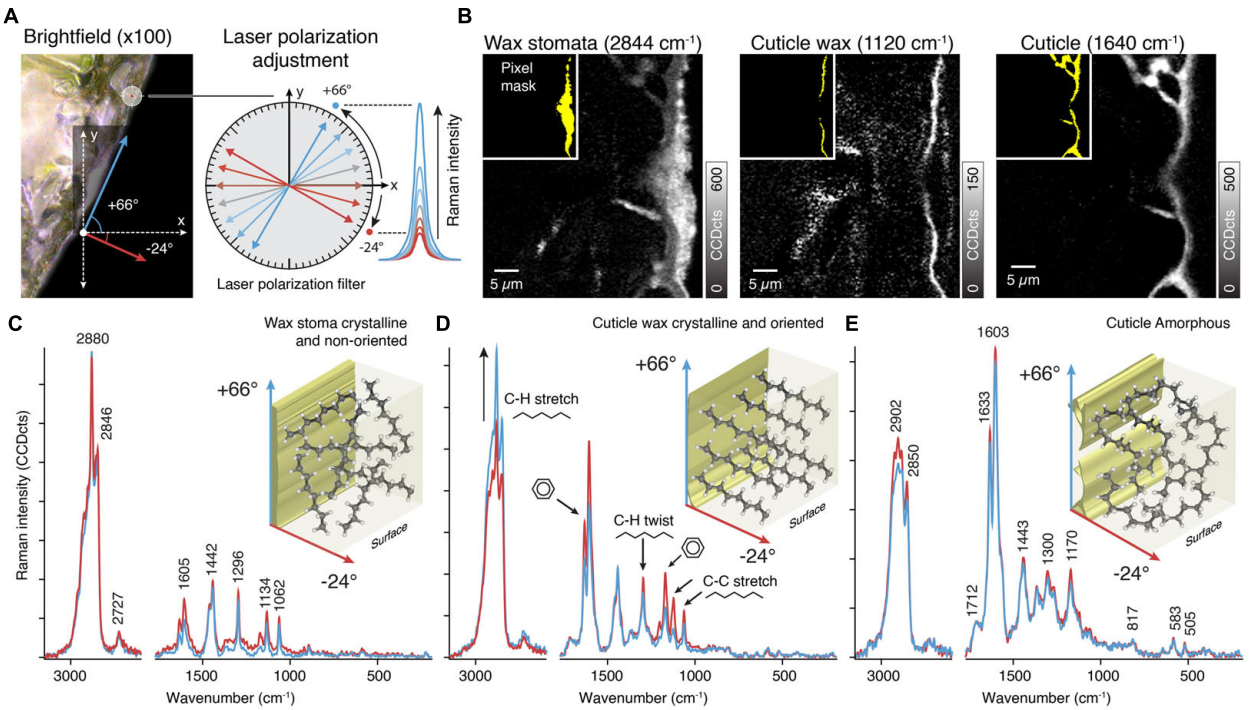

FIGURE 3 | Orientation of molecules in plant tissues. **(A)** Changing the laser polarization allows probing molecular orientations by following the change in Raman intensity with respect to different laser polarizations angles. In the tilted investigated area the maximum and minimum intensity was found at +66° and −24°, respectively. As these angles represents the tilt of the sample, the molecules are orientated parallel and/or perpendicular to the surface. **(B)** The Raman images are based on integrating specific bands sensitive to laser orientation. The inlays (yellow) show pixel masks for extracting average spectra for the different layers. **(C)** Average Raman spectra of the wax in the stomata show sharp bands of a crystalline structure but no change in Raman intensity and thus no orientation. **(D)** The thin cuticle wax layer spectra show high crystallinity and oriented structures by changes in the Raman intensity of specific bands (C-H stretch, black arrow, C-H twist, and C-C stretch). **(E)** The underlying cuticle spectra are identical at different laser polarization and thus indicate amorphous components.

The first step is checking for molecular orientation in the sample. This is done by recording several Raman spectra of the same position but with varying polarization angles (e.g., 30° steps) and looking for differences between the spectra (**Figure 3A**). The subsequent acquisition of spectra exposes the sample over seconds to a focused laser beam. This can alter its chemistry, thus rendering the polarization experiment useless, because band intensity shifts cannot be solely related to orientation anymore. Hence it can be impossible to perform polarization experiments on samples prone to laser degradation and sample behavior have to be checked prior to such experiments (see Prats-Mateu et al., 2018 for details). In the shown example, peak maxima and minima were determined at the angles of +66° and −24°, which are related to the sample's parallel and perpendicular orientation in relation to the surface. The spectral changes are consistent with previous measurements on cuticles and on pure references (Sasani et al., 2021).

The next step is to perform Raman imaging with the predetermined angles. We show average spectra extracted from the wax filling the stomatal antechamber, the epicuticular wax as well as the cuticle (**Figure 3B**). Two measurements were sufficient in our case, because we only observed spectral changes in the epicuticular wax layer. In case there are regions differing from each other in terms of peak maxima angles (that is their molecular orientation differs), each region has to be measured separately with its own angles.

Spectra of the stomatal wax (**Figure 3C**) showed no differences with regard to laser polarization but exhibited clear signs of wax crystallinity (sharp bands at 1134 and 1062 cm^{-1}). This matches with prior observations that the plug consists of intermeshed and randomly oriented wax tubes (Jeffree et al., 1971; Jeffree, 2006).

On the contrary, spectra of the epicuticular wax showed differences (**Figure 3D**). Signal of CH stretches and C-C stretches showed opposite behavior, indicating that there is a net orientation of aliphatic chains. As the aromatic signal shows a concomitant change we conclude that coumaric acids are oriented along the wax chains. Both are oriented perpendicularly to the surface, corroborating previous ideas of wax orientation (Ensikat et al., 2006).

In the cuticle spectral differences between polarizations and the crystal bands are missing (**Figure 3E**). We therefore conclude on non-oriented and amorphous aliphatic chains in the cuticle.

This example shows that polarization experiments require more effort, may not work on some samples, but generate great insights into the molecular organization of the cuticle.

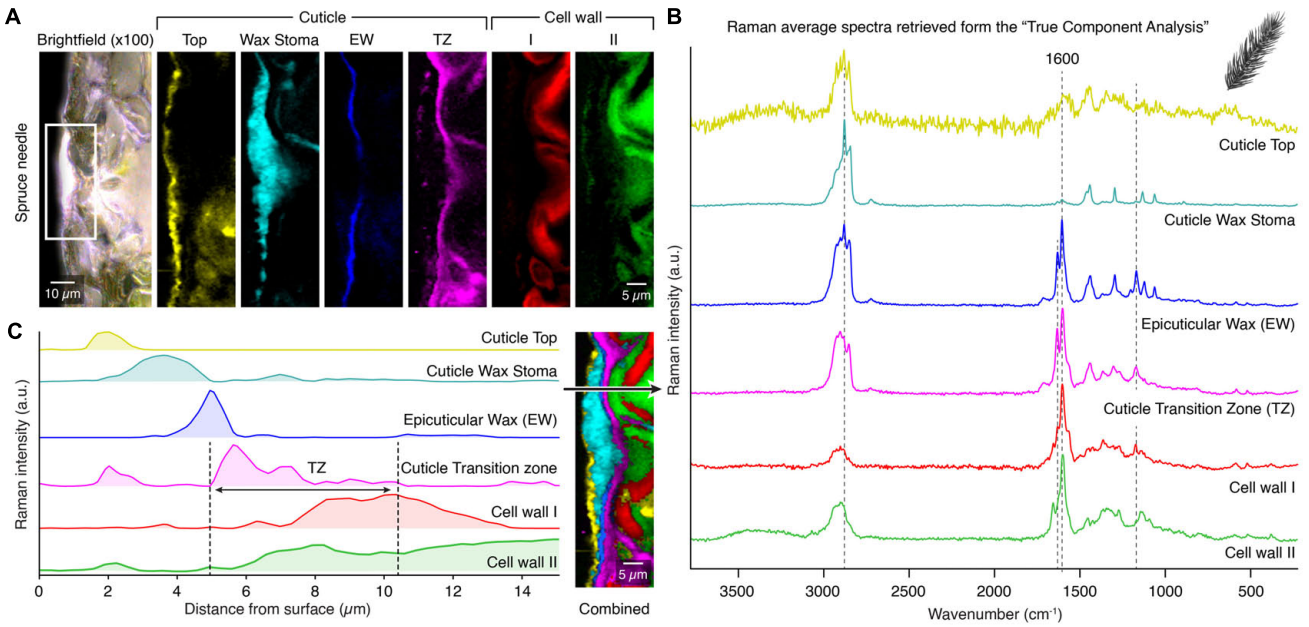

FIGURE 4 | True component analysis of spruce needle cuticle **(A)** Bright-field image with the measured area marked with the white rectangle and the six gained Raman images by the "True Component Analysis." First, four different components within the cuticle with varying chemical compositions. Second, two different cell wall layers. **(B)** Corresponding Raman spectra. **(C)** Raman intensity profile from the surface inwards to the epidermal cells. Note the special cuticle transition zone (TZ), which overlays with the epidermal cell wall. Legend: (EW) Epicuticular wax, (TZ) Transition zone.

Step 3–Revealing Hidden Layers and Components by Multivariate Analysis

Although simple band integration combined with polarization measurements already provides insights into the chemical structure of the cuticle, the spectral components often cannot be unambiguously determined. In addition, the overlap of Raman bands of different components is difficult to estimate when marker bands coincide. Then multivariate statistical methods come into play as they do not only consider single peaks, but include the whole spectrum for analysis. As an example, out of the many different multivariate methods (Felten et al., 2015; Gierlinger, 2018; Prats-Mateu et al., 2018; Sasani et al., 2021), we chose to show the very simple and fast to apply "True Component Analysis" (TCA) implemented in the Project FIVE software.

On the spruce needle cuticle, this analysis revealed seven spectral components with different spatial distribution patterns based on various chemical entities of the cuticle (**Figure 4A**). The corresponding average spectra exhibit the chemical nature of these layers (**Figure 4B**). On top, a thin outer layer was identified with marked fluorescence and thus noisy spectra (**Figures 4A,B**, yellow). As a second layer, the wax sealing with distinct bands at 2900 and 1440 cm^{-1} was retrieved (**Figures 4A,B**, cyan). Also, the underlying epicuticular wax layer was separated with a thickness of only one micrometer (**Figures 4A,B**, blue). Below this, a lipid-rich layer, even extending to the inner walls of epidermal cells, was identified (**Figures 4A,B**, pink). The underlying epidermal cell walls show no lipid signal, but the analysis separated two individual components with different aromatic compositions (**Figures 4A,B**, red and green).

In **Figure 4C**, we show an additional feature of Raman imaging. The intensity of the different components can be displayed along a line from the outer surface inwards, representing the depth distribution in the cuticle. The different components display individual layers with minimal overlap and the transition zone (**Figure 4C**, black arrow). This novel method highlights the capability of Raman spectroscopy to determine the micro spatial distribution of chemical components inaccessible by many other methods.

Step 4–Decoding the Spectra by Mixture Analysis

Different chemical components are often co-localized in biological materials and can therefore not be separated with a simplistic analysis. Thus, the last step of our comprehensive approach was to identify the chemical identity of the received spectra by comparing them with reference compounds spectra from a library. For this purpose, we used a mixture analysis strategy based on the orthogonal matching pursuit, which models the experimental spectrum as a linear combination of selected compound spectra from a spectral reference library (see section "Methods" for details). In addition, we discuss the advantages of this method and point out some pitfalls and how to avoid them. The mixture analysis results shown in **Figure 5** and **Supplementary Figure 1** are based on the obtained spectra from the "True Component Analysis" of the spruce needle measurement (**Figure 4**).

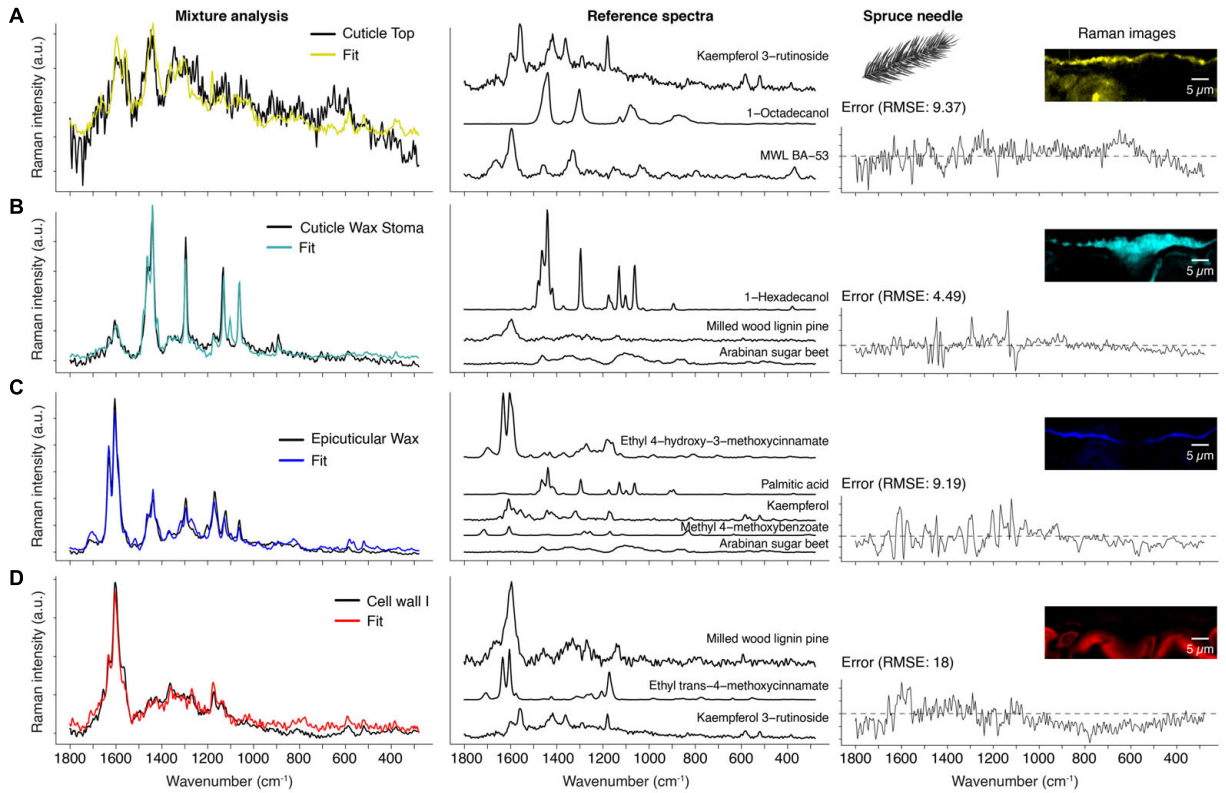

FIGURE 5 | Mixture analysis of spruce needle spectra. Based on a reference library the spectra from the True Component Analysis are fit by a mixture alogorithm (see method part). **(A)** Cuticle top layer (black spectrum) compared with the fit result (yellow), which is a linear combination of a flavonol (Kaempferol 3-rutionside), saturated fatty alcohol (1-Octadecanol), and milled wood lignin (MWL BA-53). The residual error is shown on the right and the Raman images from **Figure 4** for better orientation. **(B)** Spectrum of the cuticle wax sealing of the stoma (black) and the resulting fit (cyan) and reference spectra. **(C)** The thin epicuticular wax layer spectrum (black) and its fit (blue) and reference spectra. Note that this layer also has incorporated cinnamic acid and flavonol. **(D)** The first cell wall layer (red) is mainly fit by lignin, but also cinnamic acid and flavonol (see also **Supplementary Figure 1**).

The Fluorescing Top Layer

The first component is already an excellent example of the limits of this method because the experimental spectrum shows a high fluorescence background (**Figure 5A**). Baseline correction removes the elevated background, but this does not affect the high noise level. Consequently, the algorithm has little guidance for optimizing the fit. Despite this, the chosen references fit surprisingly well because the selected compounds make sense in the context of a spruce needle. For example, kaempferol-3-glycosides were found in the cell walls of spruce needles (Heilemann and Strack, 1990; Slimestad et al., 1992; Ganthaler et al., 2017). Although the spectrum alone cannot prove the occurrence of kaempferol at this position, the strong fluorescence of pure reference compounds (kaempferol, kaempferol-3-O-glycoside, and kaempferol-3-O-rutinoside) is an indication for the presence. Thus, researchers should not focus only on the fit and its error alone but also critically examine the reference spectra chosen by the algorithm.

Moreover, the exact compound identification in a complex mixture below the group level is challenging (e.g., group: flavonoids) because the algorithm takes the compound spectrum, which gives the best fit over the whole range, but the basic structure or origin is unclear. For example, flavones (e.g., kaempferol) can be distinguished from flavone glycosides (e.g., kaempferol-3-O-glycosides), but the glycoside nature cannot (e.g., it is impossible to differentiate between kaempferol-3-O-glucopyranoside and kaempferol-3-O-rutinoside). The second compound, octadecanol, represents the wax occurring at the top layer (**Figure 5A**). Finally, the fitted milled wood lignin spectrum is the third component, which underlines the aromatic nature of the unknown component(s).

Wax Sealing the Stomatal Entrance

Figure 5B shows the model result of the wax component, correctly identified as crystalline wax. The fitted compound 1-hexadecanol serves as a representative for waxes in general. Our library currently only contains C16 and C18 waxes; nevertheless, this is not problematic because the Raman spectra show very subtle changes concerning the number of carbons in the chain. The weak aromatic ring stretch at 1604 cm^{-1} is likely the cause for the inclusion of the milled wood lignin spectrum. However, cinnamic acid as the origin is more plausible due to the band at 1630 cm^{-1}. Finally, arabinan is perceived as a component to account for the background in the experimental spectrum.

The Cuticular Layer

The fit in **Figure 5C** shows the method's power because the cuticle's experimental spectrum is fitted by five different compounds (**Figure 5C**). For example, the ferulic acid ester is the main component consistent with the literature, where p-cinnamic and ferulic acid are found in the cutin of fruits (Wang et al., 2016; Ding et al., 2020). Depending on the parameters, the algorithm often also chooses p-cinnamic acid esters (data not shown) because both acids have similar Raman spectra. The lipidic fraction of the cuticle is represented by palmitic acid (C16), in perfect agreement with the literature, which reports cutin being mainly composed of C16 and C18 fatty acids (Holloway, 1994; Lara et al., 2015). Kaempferol is singled out as representing a flavonoid component and is the dominant flavone in spruce needles (Ganthaler et al., 2017; Szwajkowska-Michałek et al., 2020). Also, several hydroxybenzoic acids were found in needles (Szwajkowska-Michałek et al., 2020), represented in our analysis by methyl-4-methoxybenzoate. Lastly, the algorithm also attributed a minor role to a polysaccharide. At least in cuticles of tomatoes, polysaccharides have been found (Lopez-Casado et al., 2007; Philippe et al., 2020).

The Spectrum of the Cell Wall

The cell wall spectrum is another prime example of capturing all main spectral contributors (**Figure 5D**). The method chose the milled wood lignin of pine as the best fitting lignin spectrum, which is very close to spruce, considering that hardwood lignin spectra are also in the library. The second component is a p-coumaric acid ester, representing coumarates and ferulates in the cell wall (clearly identified by intense bands at 1630 and 1180 cm^{-1}). Again, a kaempferol glycoside was chosen, accounting for the bands at 1570, 595, and 521 cm^{-1}.

Tomato Cuticle as an Example for High Fluorescence

The previous section showed the spruce's cuticle analysis, where reasonable Raman spectra could be obtained with 532 nm laser despite fluorescence. Nevertheless, tomatoes show a high tendency for fluorescence background, masking most of the Raman signal (see **Supplementary Figure 2**) and making the experiment prone to sample degradation and sample burning. Fluorescence occurs when the excitation wavelength is close to

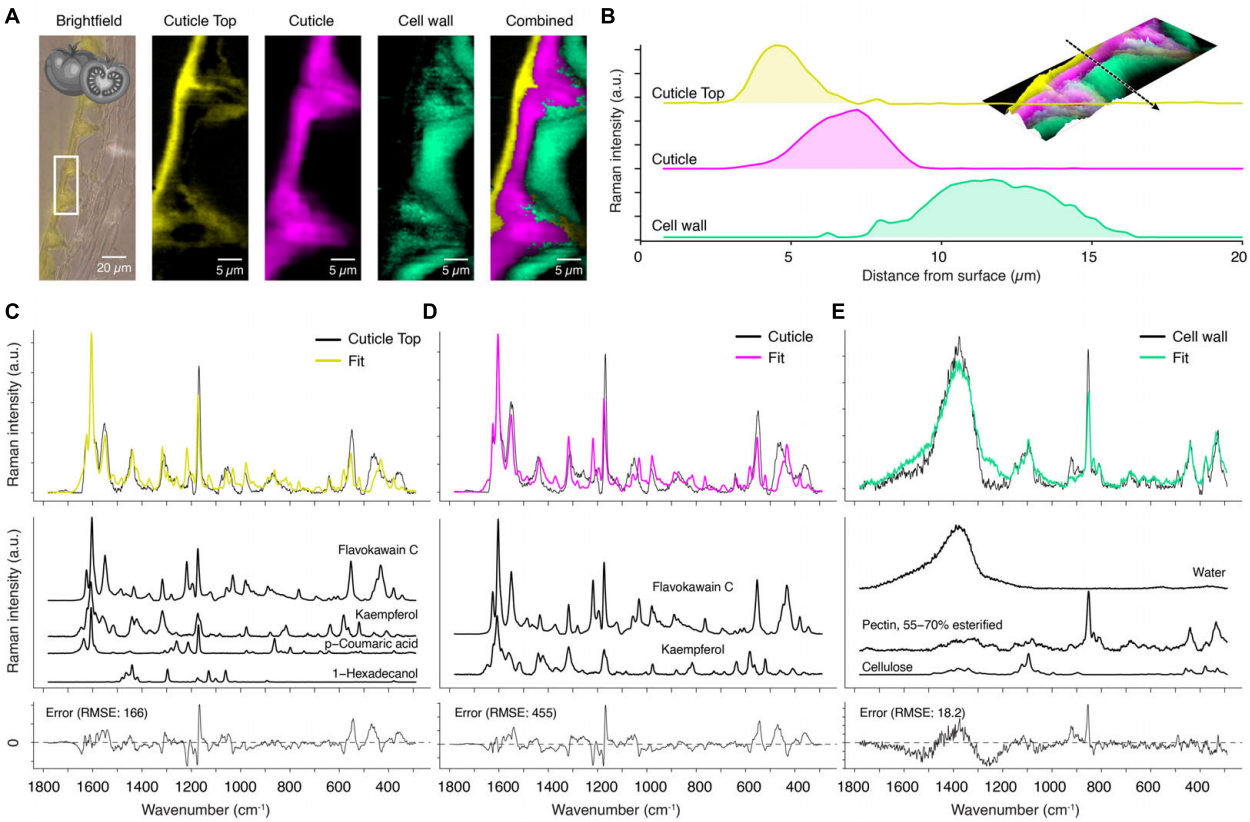

FIGURE 6 | True component and mixture analysis of tomato cuticle. **(A)** Bright-field image with the measurement area (white rectangle), calculated component images and a combination of all. **(B)** Raman intensity profile along the dotted arrow of the various layers from the surface inwards (see inlay: 3D Raman intensity (in the z-direction) combined image). **(C)** For the fit of the cuticle top layer spectrum (yellow) a precursor of flavones, the chalcone flavokawain-C, an aromatic ketone, was chosen. The flavone kaempferol and p-coumaric acid are further aromatic compounds in the top layer. Finally, C-16 fatty alcohol (hexadecanol) was modeled into as the wax component of the top layer. **(D)** The main cuticle (pink) was composed of mainly chalcone and flavone. **(E)** The cell wall component (green) was explained as a combination of water, pectin and cellulose.

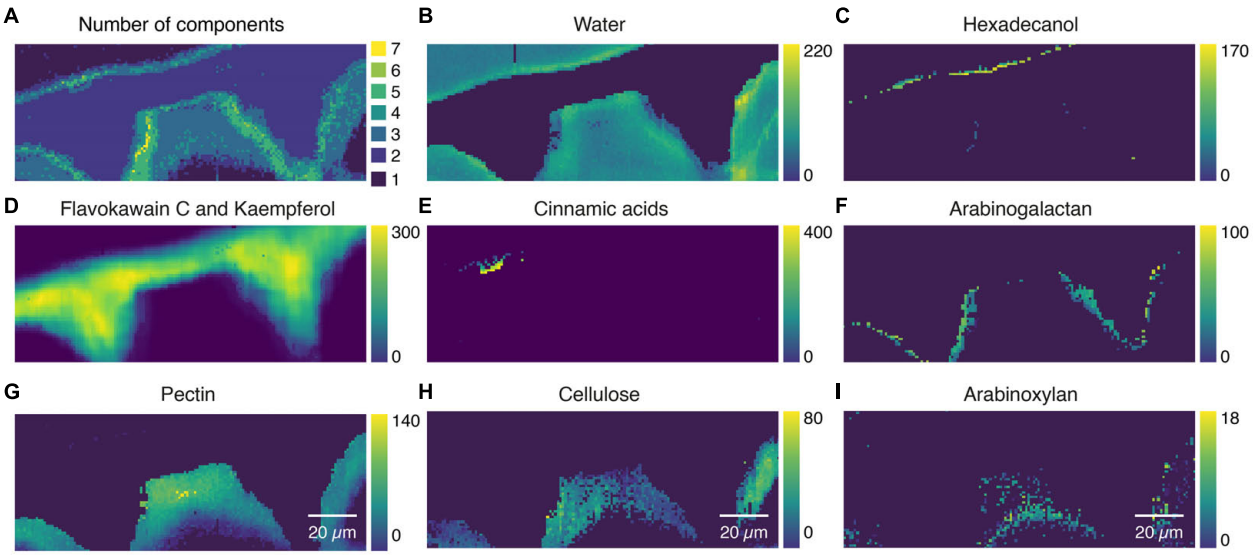

FIGURE 7 | Mixture image analysis of tomato cuticle. **(A)** The number of components used from the library to fit the sample spectrum at every pixel. **(B)** Water distribution confirms the hydrophobic nature of the cuticle and reveals a hydrophilic interface toward the cell wall. **(C)** Epicuticular wax layer is imaged based on Hexadecanol distribution. **(D)** Flawokawain C and kaempferol are fitted as the two dominant spectral contributors within the main part of the cuticle. **(E)** Cinnamic acids accumulated toward the epicuticular wax layer. **(F)** Interface toward the epidermal cell wall included Arabinogalactan. **(G)** The epidermal cell wall was composed of pectin and **(H)** cellulose and **(I)** toward the lumen xyloglucan.

molecular absorption and can be avoided by changing the laser wavelength (e.g., 532 to 785 nm). Thus, we used a 785 nm laser and obtained spectra with much lower background and better signal-to-noise ratio.

The "True Component Analysis" on the tomato measurement identified three main components (**Figure 6A**), from which the top layer and the underlying cuticle strongly overlap (**Figure 6B**). The spectra of these two look very similar, and most notably, the signal of waxes and fatty acids seems to be completely absent in the fingerprint region (**Figures 6C,D**). The reason is that some aromatic compounds have increased Raman cross-sections if they contain conjugated aromatic rings (Schmid and Brosa, 1971, 1972, 1973; Schmid et al., 1977; Schmid and Topsom, 1981; Schmid and Brodbek, 1983). The signal further rises if a charge transfer path coincides with one or more displacement coordinates (Zerbi et al., 1991; Del Zoppo et al., 1998; Tommasini et al., 1999). Therefore, almost all peaks in the cuticle spectra can belong to naringenin chalcone (**Figures 6C,D**, yellow and pink), the predominant flavonoid in tomato cuticles (Hunt and Baker, 1980; Luque et al., 1995).

Applying mixture analysis on the derived component spectra confirms that chalcones play the main role by fitting flavokawain C as the main component in the first place (**Figures 6C,D**, yellow and pink component). Naringenin chalcone was included in the library, but the algorithm chose the methylated variant (flavokawain C) and additional kaempferol. Inspection of the spectra shows that naringenin chalcone has a strong band at 1509 cm^{-1} which is absent in the experimental spectrum. The better fit of its methylated form is an indication that naringenin chalcone occurs in a bound state in the cuticle of the tomato, meaning that the molecule is covalently bonded to other chemical components over its OH-groups. However, the nature of these different components cannot be inferred from the Raman spectra and requires other methods. Yet, this shows that detailed insights into a molecular structure can be acquired by Raman spectroscopy.

In the top layer, the fit included beside the flavonoids also p-coumaric acid and 1-hexadecanol, a representative for the wax (**Figure 6C**, yellow spectrum). The third chemical component, the epidermal layer, is fitted with pectin as a major component. The fit suggests a high water content of the cell wall because the reference library also includes pure water spectra (**Figure 6E**). In this layer, polysaccharides become visible in the spectrum as the masking effect of the stong scatterers is absent [compare the cell wall spectrum of spruce, which had only aromatic components (**Figure 5D**)].

As the mixture analysis gave reasonable results with good fits on the extracted component spectra, we went a step further and applied the mixture analysis on the whole hyperspectral data set. The first interesting result is the number of references used to fit the spectrum at every pixel (**Figure 7A**). While the main cuticle was fitted using two components (flavokawain C, kaempferol), a transition layer (green, yellow) toward the epidermal and the top layer showed higher chemical heterogeneity. The water distribution image (**Figure 7B**) confirms the hydrophobic nature of the main part of the cuticle and reveals a hydrophilic interface toward the epidermal layer. The epicuticular wax layer was imaged by hexadecanol distribution (**Figure 7C**), the main part of the cuticle by flavokavain C and kaempferol (**Figure 7D**), while cinnamic acids seem to accumulate near the

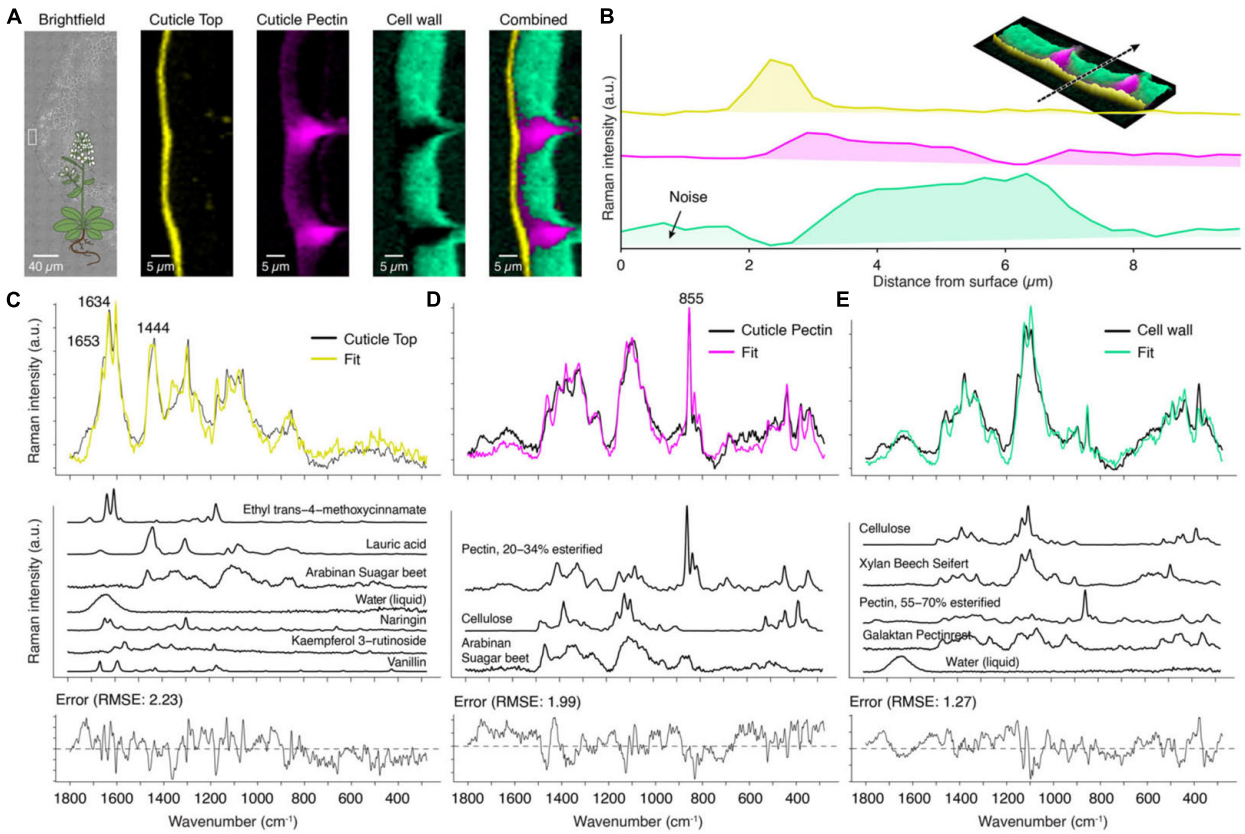

FIGURE 8 | True component and mixture analysis of *Arabidopsis* cuticle. **(A)** Bright-field image with the measurement area (white rectangle), component images and a combination of all. **(B)** Raman intensity profile of the various layers from the surface inward (see inlay: 3D combined image along the dotted arrow). **(C)** The cuticle top layer showed a fitted spectrum (yellow) based on seven components, but still some misfits were observed. **(D)** The layer beneath was fitted based on pectin and polysaccharides. **(E)** The cell wall spectrum was modeled as a combination of cellulose, pectin, and hemicelluloses.

top layer (**Figure 7E**). In the interface toward the epidermal layer, arabinogalactan was chosen by the algorithm (**Figure 7F**), while the epidermal layer is represented by pectin (**Figure 7G**), cellulose (**Figure 7H**), and toward the lumen arabinoxylan (**Figure 7I**). A carbohydrate-rich cuticle layer toward the epidermis agrees with a current cuticle model (Heredia-Guerrero et al., 2014).

The Components in the Shadow–Arabidopsis Without Strong Aromatic Scatterers

The previous examples, spruce (**Figures 4**, **5**) and tomato (**Figures 6**, **7**), included areas where spectra mainly showed a solid aromatic signal. Weaker Raman scatterers like linear aliphatics or polysaccharides contributed little to the spectra, although they are the primary mass component of the respective areas. Arabidopsis cuticles show less aromatic contributions, and so lipids and carbohydrates become more visible.

The "True Component Analysis" identifies three distinct areas: cuticle, pectin-rich layer, and the cell wall beneath (**Figure 8A**). The pectin-rich layer overlays with the top cuticle layer and the cell wall (**Figure 8B**). An aromatic signal centered around 1600 cm^{-1} is only visible in the spectrum averaged from the top layer (**Figure 8C**). Other studies also found that the cuticular waxes of Arabidopsis are chemically different from many other species because the main components are unsaturated diacids (Bonaventure et al., 2004; Yeats and Rose, 2013). This is in line with our recorded spectrum (**Figure 8C**), which has a distinct band at 1654 cm^{-1}, originating from the C = C stretch of the unsaturated moieties. This band is absent in the wax spectra of spruce (**Figure 5B**, yellow) and tomato (**Figure 6B**, yellow).

The layer beneath shows only a weak signal of lipidic components (CH-stretching, not shown), and the mixture analysis does not fit in aliphatic components (**Figure 8D**). Instead, the assigned Raman band centered at 855 cm^{-1} reveals pectin as the main component (**Figure 8D**, pink) (Synytsya et al., 2003). This band is also visible in the spectrum of the cell wall, which shows a mixture of cellulose/hemicellulose and pectin (**Figure 8E**, cyan).

Step 5–Band Shapes and Assignment of Major Cuticle Compounds

The bottleneck of many applications of Raman spectroscopy on biological materials is the interpretation of the spectra

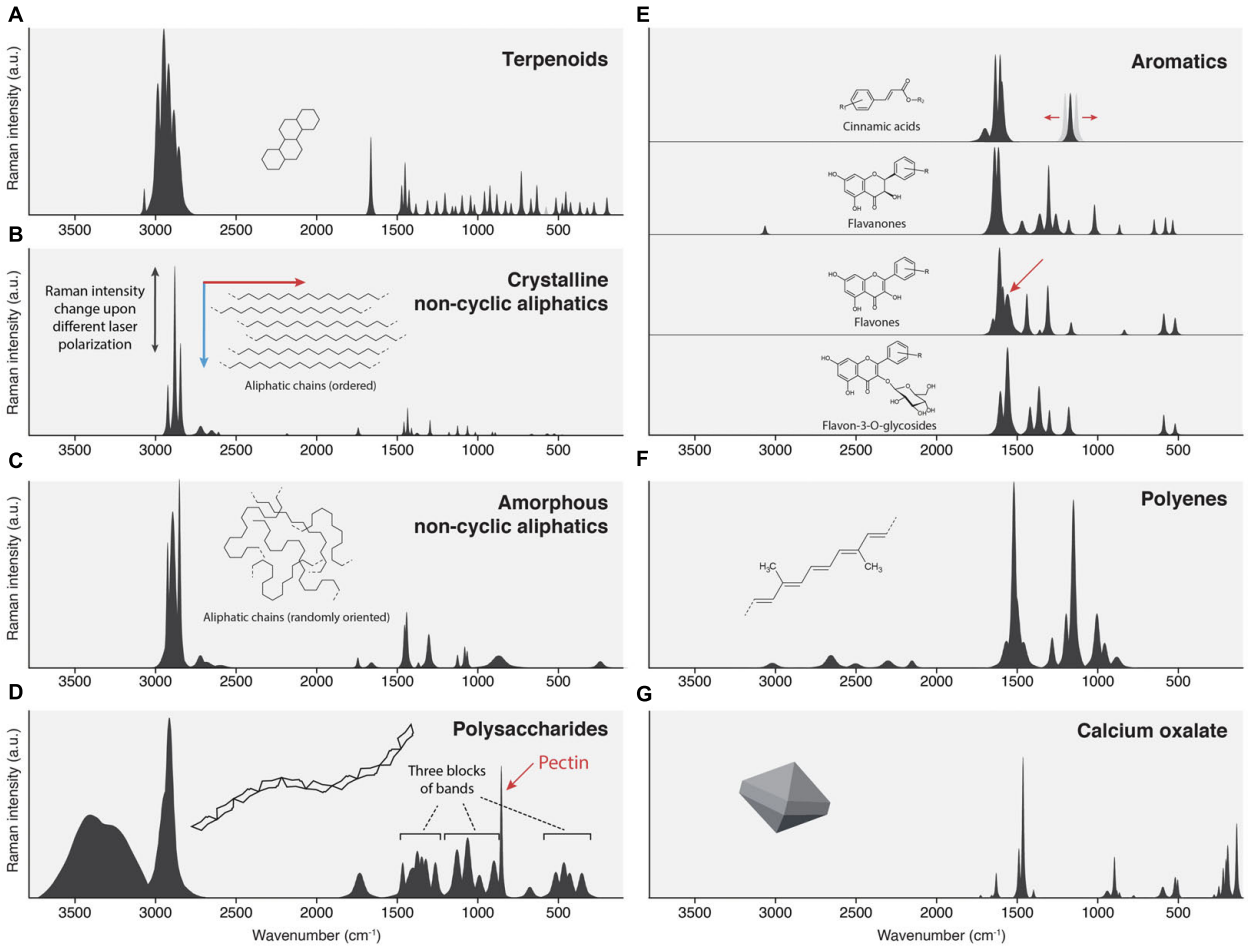

FIGURE 9 | Idealized spectral patterns of several cuticular compounds. **(A)** Terpenoids: Strong CH stretch, many sharp bands in the fingerprint zone. **(B)** Crystalline waxes: Sharp bands, intense CH stretch, weak to medium CH bends, and C-C stretches. **(C)** Amorphous alkane chains in cutin: Similar wavenumbers like waxes, but broader bands; CH stretch is the strongest. **(D)** Polysaccharides: Notable OH stretch, undifferentiated CH stretch, fingerprint zone often containing three blocks of bands. **(E)** Aromatic compounds: Very weak CH stretches, dominant 1600 ring stretch. Most strong bands occur from 1660 – 1000 cm^{-1}. **(F)** Polyenes: No CH stretches, three characteristic bands in the fingerprint zone (1520, 1150, and 1000 cm^{-1}). **(G)** Calcium oxalate.

and assigning molecular structures to individual bands. This assignment strongly depends on the chemistry of the sample and can hardly be generalized. The desired result for most users is the assignment of *chemical components*. A vibrational band, however, first and foremost relates only to *a vibrational mode* (e.g., C = O stretch at 1720 cm^{-1}), and such a mode can occur in many different molecules. Information about the sample's chemistry is therefore required.

Many cuticle components are well characterized, and we discuss their spectral characteristics in the following paragraphs. Finally, we show idealized band shapes (**Figure 9**) and wavenumbers (**Table 1**) based on numerous measurements of pure compounds and compare them to experimentally observed values of cuticles.

Waxes

Epicuticular waxes consist of long-chain aliphatics (C20-C34), modified by acid-, aldehyde-, keto-, alcohol, and ester functional groups (Yeats and Rose, 2013; Lara et al., 2015; Chu et al., 2017; Zhu et al., 2018) and triterpenoids, the most common being α-amyrin, β-amyrin, ursolic and oleanolic acid (Haliński et al., 2015; Lara et al., 2015; Chu et al., 2017). The most apparent feature of crystalline waxes is many sharp bands. This is due to the limited rotational freedom of the aligned chains or the rigid molecular body in the case of terpenoids. This alignment can often be seen in Raman spectra of different laser polarization (see also **Figure 3D**).

Terpenoids

The typical feature of terpenoid Raman spectra is very strong CH stretching bands (3000-2800 cm^{-1}), the occurrence of bands around 1660 cm^{-1}, and many sharp bands of more or less equal intensity in the fingerprint zone. The CH-stretching region is the strongest in the spectrum and consists of many sharp bands originating from various CH_2 groups and lone hydrogens. Cuticle terpenoids can easily be distinguished from saturated

TABLE 1 | Idealized wavenumbers of standard cuticular components compared to experimental wavenumbers of cuticle spectra of spruce, tomato, and *Arabidopsis*. Assignments based on text.

Terpenoids	Waxes	Cutin	Carbohydrates	Cinnamic acids	Flavanones	Flavones	Flavon-3-O-glycosides	Polyenes	Cuticle 2 spruce	Assignment	Wax tomato	Assignment	Cuticle Arabidopsis	Assignment
			3400										3398	ν O-H (polysaccharides, water)
			3280										3247	ν O-H (polysaccharides, water)
								3200						
3070					3065				3063	ν C-H ring Φ2 (flavanones)			3066	ν C-H ring Φ2 (flavanones?)
2985														
2950														
			2940											
2920	2925	2925							2923	ν C-H (lipids)			2930	ν C-H (lipids, polysaccharides)
			2915										2914	ν C-H (lipids, polysaccharides)
		2895							2904	ν C-H (lipids)			2900	ν C-H (lipids, polysaccharides)
	2880												2882	ν C-H (lipids, polysaccharides)
2870														
2855		2850							2853	ν C-H (lipids)			2862	ν C-H (lipids, polysaccharides)
	2845													
	2720	2725							2725	δ C-H (lipids: overtone/combination)			2727	δ C-H (lipids: overtone/combination)
	2650							2650						
	2610													
								2500						
								2300						
								2150						
	1740	1745	1730											
				1700					1716	ν C = O (cinnamates)			1722	ν C = O (cinnamates, toward 1740 also ester groups of polysaccharides)
1660		1660											1654	ν C = C of unsaturated fatty acids
						1650								
				1635	1640				1633	ν C = C (cinnamic acids/esters)	1624	ν C = O (naringenin chalcone)	1633	ν C = C (cinnamic acids, esters)
					1615									
				1605		1610	1605		1603	ν C = C ring Φ8	1605	ν C = C ring Φ8a; ν C = C (naringenin chalcone)	1606	ν C = C ring Φ8
				1595		1590					1587	ν C = C ring Φ8b (cinnamic acids)		

(Continued)

TABLE 1 | (Continued)

Terpenoids	Waxes	Cutin	Carbohydrates	Cinnamic acids	Flavanones	Flavones	Flavon-3-O-glycosides	Polyenes	Cuticle 2 spruce Assignment		Wax tomato Assignment		Cuticle Arabidopsis Assignment	
								1570	1570	ν C = C ring Φ8 (cinnamic acids/flavones)				
						1560	1560				1552	ν C = C ring Φ8b (naringenin chalcone)	1560	ν C = C ring Φ8b + ν C = O (flavones)
								1520					1527	
1470					1470									
	1460							1460						
1450		1455	1455											
	1440	1440				1440	1420		1445	δ C-H (lipids), flavone mode	1440	δ C-H (lipids), flavone/chalcone mode	1441	δ CH (lipids)
1430														
	1410													
			1400											
	1380	1370	1375										1383	δ CH (polysaccharides)
					1360	1360	1365		1365	ν C-X ring Φ20a (flavones)				
multiple bands			1350											
			1320											
	1300	1305			1305	1310	1300		1303	γ_t CH (lipids); flavone mode	1310	γ_t CH (lipids); flavone/chalcone mode	1296	γ_t CH (lipids)
								1280						
strong band 800-500			1260		1260				1268	ν C-X ring Φ7a ferulic acids/ferulates	1261		1273	ν C-X ring Φ7a ferulic acids/ferulates
								1195			1205	ν_{as} C-C-O (coumaric acid/ester)	1204	ν_{as} C-C-O (coumaric acid/ester)
	1180				1180		1180							
				1170		1165			1171	δ CH ring Φ9a (coumaric acid/ester); Φ18a (flavone A-Ring); ν C-C (ferulate)	1168	δ CH ring Φ9a (coumaric acid/ester, naringenin chalkone B-ring)	1170	δ CH ring Φ9a (coumaric acid/ester); Φ18a (flavone A-Ring); ν C-C (ferulate)
								1150					1131	ν C-C (lipids)
	1135	1125	1130						1122	ν C-C (lipids)			1114	ν C-C/C-O (polysaccharides)
		1080							1086	ν C-C (lipids)	1074	ν C-C (lipids)	1081	ν C-C/C-O (polysaccharides)
	1065	1065	1060						1063	ν C-C (lipids)	1053	ν C-C (lipids)	1063	ν C-C (lipids)
	1020				1020				1033	ν C-C (lipids)				
								1000					1007	
			990								981	flavone/chalkone mode		
								960						
	910		900										933	

(Continued)

TABLE 1 | (Continued)

Terpenoids	Waxes	Cutin	Carbohydrates	Cinnamic acids	Flavanones	Flavones	Flavon-3-O-glycosides	Polyenes	Cuticle 2 spruce Assignment		Wax tomato Assignment		Cuticle Arabidopsis Assignment	
	890												892	
								880			870	ν C-C + γ_r CH (lipids)		
		865			865									
			855										856	ν C-C/C-O (pectin)
						835			820	ν C-C (lipids)				
	670		670											
					650				648	δ C = C ring Φ6a (flavone A-Ring)	642	γ C = C ring Φ16b (naringenin chalcone A-ring)		
						590	590							
					580				583	ν C = C ring Φ1 (flavone A-Ring)				
											550	ν C = C ring Φ1 (naringenin chalcone A-Ring)		
					535									
			515			520	520		521	δ C = C ring Φ6b (flavone A-Ring)				
			470								459		443	
			430						413					
			355								357			
		240												
	205													

Assignments based on text. ν: stretching; δ: in-plane bending; γ: out-of-plane bending; γ_t: twisting; γ_r: rocking; γ_w: wagging; Φ: ring mode (Varsanyi designation, Varsanyi, 1969); C-X: ring mode involving substituents.

alkyl chains by the signal from their C = C bonds, and the internal C = C stretch comes at ∼1660 cm^{-1}, the vinyl C = C stretch at 1640 cm^{-1}. Their hydrogens often produce a band near 3070 cm^{-1}. The C = O stretch of acids is very weak in Raman and, therefore, not a useful band. The fingerprint region shows medium intense CH bending bands (∼1440 cm^{-1}) and many needle-like bands of equal intensity, stemming from numerous CH and C-C modes of the stiff molecular skeleton (**Figure 9A**). Some modes can acquire substantial Raman intensity, and several strong bands are often observed in the region 800–500 cm^{-1}.

Linear Alkyl Chains in the Crystalline State

Linear alkyl chains (cuticular waxes) can be identified by two sharp CH stretching bands and medium intense CH/C-C modes (2880, 2850, 1440, 1300, 1135, 1065 cm^{-1}) (**Figure 9B**). There are fewer bands observed compared to terpenoids because the CH and C-C modes are chemically very similar. In crystalline alkyl chains, the CH-stretching region shows typical bands for CH_2-stretching (antisymmetric: 2940, 2920 cm^{-1}; symmetric: 2880, 2845 cm^{-1}) (Colthup et al., 1990). Overtones of wagging and twisting modes cause a distinctive set of bands on the low-frequency side of the CH stretches (2720, 2650, 2610 cm^{-1}). Carbonyl groups cause only weak Raman scattering (esters 1740 cm^{-1}; aldehydes 1730 cm^{-1}; ketones 1720 cm^{-1}) and are often hidden under stronger aromatic carbonyls. A set of bands around 1440 cm^{-1} (CH bendings), one at 1300 cm^{-1} (CH twisting) (Colthup et al., 1990), and several C-C stretching modes in the range of 1150–800 cm^{-1} (Machado et al., 2012) are other characteristic bands of waxes in a cuticle. Below 800 cm^{-1}, the spectrum is devoid of any notable bands. Varying the chain length does not affect the spectra much because the principal modes of the molecules are the same. Therefore, measurements of waxes with shorter chain lengths than usually found in most cuticles (C16 vs. C34) are valid. Because the chains are ordered in a parallel fashion in most crystalline forms, the intensity of CH and C-C bands differs relative to each other when probed by a linearly polarized laser. If the laser is parallel to the chain, the C-C stretching and CH-twisting will be stronger, while being orthogonal, the CH stretching band is by far the most intense.

Cutin Fatty Acids (Linear Alkyl Chains in the Amorphous State)

Cutin monomers are mainly C16 and C18 alkanoic acids (Holloway, 1994; Lara et al., 2015; Wang et al., 2016). Their spectra show the typical bands of alkylic chains, namely CH_2 stretches (2926, 2851 cm^{-1}), CH2 bendings and twistings (1455, 1440, 1303 cm^{-1}). In contrast to cuticular waxes, they show broader bands because the amorphous structure allows many more conformations; therefore, the frequencies of individual modes vary stronger and blur into each other (**Figure 9C**). However, the CH_2 and C-C modes are still at similar wavenumbers as in the crystalline state, so the principal distinction is made by spectral shape (see **Figures 3D,E**). Ester carbonyls are seen as weak bands at 1740 cm^{-1}, the free acids at 1660 cm^{-1}. The cuticle of Arabidopsis seems to be atypical (Yeats and Rose, 2013) and consists mainly of unsaturated diacids (Bonaventure et al., 2004). They show a strong Raman band at ∼1660 cm^{-1}, stemming from the C = C stretch (see also **Figure 8C**).

Polysaccharides

Polysaccharides may function as the scaffold for lipids (Guzman et al., 2014b). Pectin, hemicelluloses (e.g., xyloglucan), and cellulose are reported in cuticles (Lopez-Casado et al., 2007; Guzman et al., 2014a; Philippe et al., 2020). Although plant polysaccharides are diverse compounds, their Raman spectra do not differ that much because the involved chemical bonds are essentially the same (OH, CH, C-C, C-O). **Figure 9D** shows a typical Raman spectrum. The high number of OH-groups causes a Raman band of notable intensity (∼3400, 3280 cm^{-1}). It is neighbored by a high CH-stretching peak, which is often not resolved into individual bands. The band position is around 2915 cm^{-1}, well set apart from the lower-lying stretches of alkyl chains centered at 2880 cm^{-1}. Esterification can result in a weak to medium Raman band at ∼1730 cm^{-1}. The fingerprint area shows three separated blocks of bands: CH bending modes (1500–1250 cm^{-1}), C-O/C-C stretching modes (1180–900 cm^{-1}), and various bending and twisting modes (500–350 cm^{-1}). Pectin has a distinct Raman band at 855 cm^{-1} (Synytsya et al., 2003).

Aromatic Compounds

A variety of aromatic compounds is found in cuticles: cinnamic acids, hydroxybenzoic acids, benzyl esters, phenethyl esters, phthalate esters, and several flavonoids are reported (Kisser-Priesack et al., 1990; Luque et al., 1995; Laguna et al., 1999; Steinbauer et al., 2009; Bernal et al., 2013; Zhu et al., 2018). Aromatic rings are typically identified in Raman by a strong band at 1600 cm^{-1}. If the ring is part of a delocalized π-electron system, the Raman cross-section of the whole conjugated system is significantly increased (Schmid and Brosa, 1971, 1972, 1973; Schmid et al., 1977; Schmid and Topsom, 1981). Cinnamic acids and flavonoids contain extended π-systems and correspondingly cause intense Raman peaks. It is important to note that all modes having bond movement of the charge-transfer-path in charge-transfer systems are enhanced (Tommasini et al., 1999). The result is that even small quantities of cinnamic acids and flavonoids cause strong Raman bands and, at some point, start to mask bands from non-enhanced molecular structures in a similar way as it is observed in lignin (Bock and Gierlinger, 2019). Furthermore, judging from absorption spectra, aromatic compounds are often responsible for fluorescence in Raman spectra if absorption bands hit the excitation wavelength or overtones (Bock, 2020). In the cuticle, aromatic compounds are primarily identified by bands in the region 1650–1550 cm^{-1}. Many of them have no notable bands in the CH stretching region (**Figure 9E**).

Cinnamic acids show two strong bands at 1630 (C = C stretch) and 1605 cm^{-1} (ring stretch), esters an additional weak band at 1700 cm^{-1} (C = O stretch). Cinnamic acids show only a few other bands in the range 1500–1000 cm^{-1} and only weak to very weak bands below 1000 cm^{-1} (**Figure 9E**). Thus, the nature of the ring system can often be deduced from characteristic bands. However, in the case of cinnamic acids, ferulic acids/esters show an unusual strong band at 1180 cm^{-1}, which is usually a marker band of coumaric acids/esters and is typical for para-substituted aromatic rings (Varsanyi, 1969). Since all other bands are so weak or hidden, these two cannot be separated with confidence (see also **Figures 5C,D**, where each of them is selected by mixture analysis).

Flavones and chalcones often have a very strong marker band at 1560 cm^{-1} (**Figure 9E**, arrow). They share a very strong band at 1600 cm^{-1} with all other conjugated aromatic compounds. In contrast to cinnamic acids, flavonoids show more strong bands over the whole fingerprint range; notable is a characteristic set around 600 cm^{-1}, which is often stronger than modes of other molecules in this range, thus enabling confirmation of a flavone structure. Based on our observation, flavanones show less Raman intensity, and we attribute this to the reduced size of the conjugated system (the B-ring is not in conjugation). The consequence is that it might be more challenging to identify them in mixtures.

In contrast to flavones, weak CH stretches are often observed. We also note a difference in the spectra of flavones and their respective 3-O-glycosides. DFT-Studies show that the B-Ring is rotated out of the plane, reducing its conjugation with the chromone system (Cai et al., 2013; Paczkowska et al., 2015). Our interpretation is that this increases the relative intensity of A-ring modes in the spectrum and results in flavone-3-O-glycoside spectra being notably different from their respective aglycones (see **Figure 9E**).

Polyenes

Polyenes are identified by two characteristic bands, the C = C stretching (1520 cm^{-1}) and C-C stretching (1150 cm^{-1}) vibrations (**Figure 9F**). The 1000 cm^{-1} band is a more complex displacement, best described as CH_3 wag (Novikov et al., 2021). Overtones and combinations can be seen at >2000 cm^{-1}.

Calcium Oxalate Cystoliths

Calcium oxalate cystoliths were found in the lowest cuticle layers or directly underneath (Fink, 1991; Pennisi et al., 2001; Sasani et al., 2021), where one function is light scattering (Gal et al., 2012). The bands of calcium oxalate monohydrate

are shown in **Figure 9G**. Mineral crystals, in general, have sharp bands stemming from rigid molecular structures and have strong bands at low wavenumbers (these are motions involving the heavy atoms like Ca).

Spectral Assignments of Three Experimental Spectra

In the last step, we compare the band assignments of pure, idealized components with spectra of the "True component analysis" as discussed in step 3 of this manuscript. Note that mixture analysis (step 4) and band assignment via pure reference compounds (step 5) are complementary. Mixture analysis results indicate certain compounds which should be checked for plausibility with known assignments. Conversely, individual band assignments should be cross-checked by modeling spectra of assumed substances into the experimental spectrum.

Table 1 shows a comparison of wavenumbers of chemical components with one spectrum of a cuticle from each of the three samples discussed so far. We chose a cuticle component of the spruce needle, the wax of the tomato, and the cuticle of Arabidopsis. We observe that our idealized wavenumbers, derived solely from pure reference compounds, match well with experimental cuticle spectra. We see this as a confirmation of our new approach using averaged and adjusted wavenumber sets to account for variability within a chemical group.

The assignments are now adjusted for the compounds known to occur in a cuticle. This means that chemical groups can be narrowed down. For example, in the tomato wax, the band at 1560 cm^{-1}, indicating flavones and chalcones, can be narrowed down to naringenin chalcone or a very similar substance, with the help of mixture analysis. Hence the assignment specifically states "naringenin chalcone."

The multicomponent nature of the needle cuticle of spruce (see **Figure 5**) is reflected in its band assignment. The lipidic fraction is best seen in the high wavenumber region (∼3000 cm^{-1}), whereas most of the observed bands in the fingerprint region (∼1500–0 cm^{-1}) are from aromatic compounds. Thus, the bands around 3000 cm^{-1} can be assigned to aliphatic components, in this case mainly cutin esters. However, a small band at 3063 cm^{-1} is of aromatic origin. Based on our observation that flavones, cinnamic and benzoic acids do not show bands in this region at 532 nm, we assign this band to flavanones, which display bands in this region and are still sufficiently strong scatterers to be seen. However, this does not exclude other aromatic compounds which might be undetermined yet. The strong band at 1603 cm^{-1} is unspecific for (conjugated) aromatic compounds. The bands 1633 and 1171 cm^{-1} are assigned to ferulic and or p-coumaric acid, while the band at 1268 cm^{-1} seems to be exclusively from ferulic acid. The presence of flavonoids is deduced from the shoulder at 1570 cm^{-1} together with bands at 648, 583, and 521 cm^{-1}, which are assigned to various modes of the flavone A-ring. Lipids show only two clear bands, 1439 and 1303 cm^{-1}, although both fall together with flavone modes, the bands being regarded as mixtures of both.

Compared to spruce, the wax of tomato shows a simple spectrum–simple because almost all bands are caused by a single chemical component, naringenin chalcone or a very similar structure (see also mixture analysis, **Figure 6**), in agreement with previous studies (Piringer and Heinze, 1954; Hunt and Baker, 1980; Luque et al., 1995). At 785 nm, the presence of lipids can only be derived from the bands at 1440, 1310, and 870 cm^{-1}, although flavones/chalcones also have bands at these wavenumbers.

The assignment of the Arabidopsis cuticle is a little different because it also includes polysaccharides. These can be seen due to the weaker scattering of aromatic compounds in comparison to spruce or tomato. Polysaccharides and water cause the strong OH bands (3398, 3247 cm^{-1}), the weak band at 3066 cm^{-1} is of aromatic origin, and the neighboring CH stretches come from polysaccharides and lipids. The bands at 1722, 1633, and 1606 cm^{-1} indicate cinnamic esters. There is an additional band at 1654 cm^{-1}, which either comes from a C = C in conjugation with a ring (e.g., a cinnamyl alcohol moiety) or from an unsaturated fatty acid. We have not found studies reporting cinnamyl alcohols in the cuticle of Arabidopsis, but unsaturated cutin monomers were found by GC-MS (Bonaventure et al., 2004). We, therefore, assign this band to the C = C stretch of unsaturated fatty acids and do not count on the result of the mixture analysis in this case (**Figure 8C**). Polysaccharides are seen at 1380 cm^{-1}, and pectin displays its marker band at 856 cm^{-1}. We interpret the bands at 1131 and 1063 cm^{-1} as signs for crystalline aliphatic components (waxes). Furthermore, the measurement was performed with a laser polarization perpendicular to the surface, enhancing the C-C stretches if the chains are in line with the laser (see **Figure 3** for wax orientation). This indicates that these waxes are also oriented in the cuticle or on top of it, although a more rigorous determination is required.

SUMMARY AND OUTLOOK

This method article highlights Raman microscopy as an *in situ* method to study the relationship of chemistry and structure on the microscale. We present a comprehensive workflow starting with the sample in hand and ending with detailed insights into chemical compounds and their spatial distributions within different cuticle layers. Native sample preparation, label-free imaging, detailed chemical information about all involved molecules and in context with the anatomical structures are essential assets of the Raman imaging approach. The examples confirm that even the molecule orientation can be deduced in an about 500 nm thick epicuticular wax layer (**Figure 3**), and transition and top layers can be distinguished with a spatial resolution of 300 nm and minor changes in composition (**Figures 4–8**). Furthermore, we show and discuss that especially aromatic components are strong Raman scatterers and can therefore be tracked even in small amounts. But in fact, researchers even pushed the limits of tracing compounds in attomolar concentrations (Yang et al., 2016) and sub-nanometer resolutions (Chen et al., 2019; Lee et al., 2019), showing the potential of the Raman toolbox.

We worked through cuticles of a spruce needle (**Figures 3–5**), a tomato peel (**Figures 6** and **7**), and an Arabidopsis stem (**Figure 8**), revealing common features as well as differences.

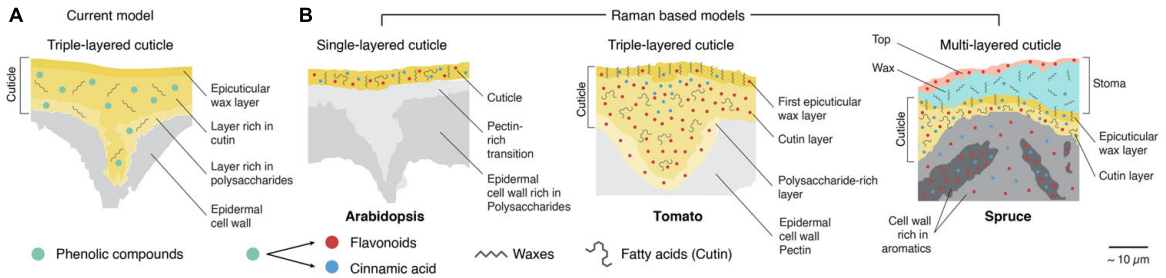

FIGURE 10 | Extended models for different plant cuticles based on the Raman results. **(A)** The current model shows three different layers. An epicuticular wax layer is followed by a layer rich in cutin and a third rich in polysaccharides. Note that this model puts phenolic compounds mainly in the second layer. Model adapted from Heredia-Guerrero et al. 2014. **(B)** Models based on our Raman results (**Figures 3–8**). Left, *Arabidopsis*, showing only a single cuticle layer with additional flavonoids and cinnamic acids. Waxes are presumably crystalline and oriented. In the center, the triple-layered cuticle of tomato is shown. The top layer is composed of oriented waxes and cinnamic acids, while the subjacent layer is rich in amorphous cutin. Interestingly, cinnamic acids were mainly detected in the cuticle bulge and close to the top layer in this layer. The third layer is rich in polysaccharides. Flavonoids are found throughout the whole cuticle. On the right, the complex, multilayered model of a cuticle at a stomatal opening of the spruce needle is shown. A thin layer rich in flavonoids is observed on the top of the stoma wax (cyan). However, the stoma wax sealing seems to contain only a tiny amount of cinnamic acids and consists mainly of crystalline but random oriented wax crystals (see **Figure 3C**). In contrast, the underlying epicuticular wax layer (generally on the surface) shows clear signs of oriented crystalline waxes and co-oriented cinnamic acids (see also **Figure 3D**). The last cuticle layer is rich in amorphous fatty acids and aromatic compounds (flavones and cinnamic acids). Those aromatics transition into the subjacent cell walls where they co-localize with lignin but are not found in deeper-lying cells.

The differences start already in the measurement setup, as cuticles with a higher amount of aromatic components (e.g., tomato) are more prone to sample degradation and more challenging to get spectra with a good signal-to-noise ratio using the 532 nm laser. So the 785 nm laser was the best choice for the tomato cuticle, although we lost spatial resolution. At high concentrations, aromatic components start to mask bands from non-enhanced molecular structures like carbohydrates and lipids. Therefore, probing different developmental stages of the cuticle might be interesting. Anticipating that lipids and carbohydrates are first deposited, the aromatic impregnation can be followed step by step. Or moving backward, using different solvents to see effects of the extraction procedure on the sample as well as characterizing the extracted components. Chemical environments, as well as bonding, can also be reflected in the Raman spectra. The here presented mixture analysis (orthogonal matching pursuit) of the native tomato cuticle spectrum suggested that naringenin chalcone is covalently bonded to other chemical components over its OH-groups as the methylated form better explained the spectrum (**Figure 6**). The power of this hyperspectral analysis was also proven on the hyperspectral dataset by spatially resolving even tiny layers with a high chemical precision (**Figure 7**). We showed the power of such methods with a library including the most relevant reference spectra in high quality but also displayed on the Arabidopsis cuticle that a thorough check of the results due to many possibilities and influence factors is necessary. As additional help for successful Raman spectra interpretation, we derived band shapes of the main cuticular component groups and their assignment (**Figure 9** and **Table 1**).

Based on the calculated Raman images, schematic models can be derived with unprecedented details and compared with current cuticle models (**Figures 10A,B**). Imaging micro sections allows to include the underlying epidermis and probe the transition or look at special cases like the cuticle above a stoma. What is seen at first sight is the diversity of the three investigated cuticles in dimension, layering, and chemistry. In Arabidopsis, we could only derive one layer with a relatively low amount of aromatic components (**Figure 10B**, Arabidopsis). Between the cuticle and cell wall, a pectin-rich layer was imaged. In the native tomato also a pectin-rich epidermal wall was found, but additionally a polysaccharide layer with flavonoids as a transition zone (**Figure 10B**, Arabidopsis). The high impregnation with chalcones was found throughout the whole tomato cuticle. These increased amounts probably mask other components present in lower entities, and cinnamic acids and lipids were only detected in the top region. Cinnamic acids accumulate near the epicuticular wax layer, and then transit into flavonoids; this is also a feature of the multilayered spruce cuticle (**Figure 10B**, spruce needle).

In contrast to the other examples, the cuticle in spruce needles is built upon a lignified epidermal cell wall, which is additionally impregnated with flavonoids found in the cuticle (Sasani et al., 2021). In spruce needles, the periclinal cell walls often present themselves as chemical hybrids of cell walls and cuticles, which we interpret as an additional reinforcement of the outermost cells. The complex cuticular setup of the spruce needle is even topped at the stomatal opening by two additional layers (**Figure 10B**, spruce).

Among the three derived Raman models, the tomato fits very well with the current model of the cuticle by distinguishing the epicuticular wax layer and a carbohydrate-rich transition layer towards the epidermis from the main part of the cuticle. But we now add detailed information about the aromatic components, which have so far only been indicated in the primary layer. Although our three investigated cuticles differed in their setup and layering, we can derive underlying chemical concepts: (1) cinnamic acids are co-localized with waxes and directly contact the outside world. (2) underlying layers are composed of amorphous cutin esters and contain flavonoids in addition

to cinnamic acids. (3) these compounds stop at the border in unlignified cell walls (Arabidopsis, tomato) but gradually fade into the lignified cell walls.

With these measurement examples and informative guide we hope to spur the community to include Raman imaging in their cuticle research. Diving deeper into cuticle structure and revealing more hidden features will advance a comprehensive and holistic biological understanding of the plant cuticle.

DATA AVAILABILITY STATEMENT

The raw data supporting the conclusions of this article will be made available by the authors, without undue reservation.

AUTHOR CONTRIBUTIONS

NG, MF, and PB conceptualized the article and wrote the manuscript. NG and PB analyzed the data and interpreted the results. MF illustrated the figures. KM programmed the R-interface for the mixture analysis approach. All authors discussed the results, read and approved the article.

FUNDING

Austrian Science Fund (FWF): START Project (Y-728-B16).

ACKNOWLEDGMENTS

We thank Nadia Sasani for cutting the spruce needle, Martin Niedermeier, Ana Gonzalez and Batirtze Prats-Mateu for cutting and measuring the tomato peel and *Arabidopsis* stem.

SUPPLEMENTARY MATERIAL

The Supplementary Material for this article can be found online at: https://www.frontiersin.org/articles/10.3389/fpls.2021.793330/full#supplementary-material

REFERENCES

Baranska, M., Schulz, H., Joubert, E., and Manley, M. (2006). In situ flavonoid analysis by FT-Raman spectroscopy: identification, distribution, and quantification of aspalathin in green rooibos (Aspalathus linearis). *Anal. Chem.* 78, 7716–7721. doi: 10.1021/ac061123q

Bernal, M., Llorens, L., Julkunen-Tiitto, R., Badosa, J., and Verdaguer, D. (2013). Altitudinal and seasonal changes of phenolic compounds in Buxus sempervirens leaves and cuticles. *Plant Physiol. Biochem.* 70, 471–482. doi: 10.1016/j.plaphy.2013.06.012

Berto, P., Comménil, P., Belingheri, L., and Dehorter, B. (1999). Occurrence of a lipase in spores of Alternaria brassicicola with a crucial role in the infection of cauliflower leaves. *FEMS Microbiol. Lett.* 180, 183–189. doi: 10.1111/j.1574-6968.1999.tb08794.x

Bock, P. (2020). *The Vibrations Of Lignin*. Ph.D. thesis. Austria: University of Natural Resources and Life Sciences.

Bock, P., and Gierlinger, N. (2019). Infrared and Raman spectra of lignin substructures: coniferyl alcohol, abietin, and coniferyl aldehyde. *J. Raman Spectrosc.* 50, 778–792. doi: 10.1002/jrs.5588

Bonaventure, G., Beisson, F., Ohlrogge, J., and Pollard, M. (2004). Analysis of the aliphatic monomer composition of polyesters associated with Arabidopsis epidermis: occurrence of octadeca-cis-6, cis-9-diene-1, 18-dioate as the major component. *Plant J.* 40, 920–930. doi: 10.1111/j.1365-313X.2004.02258.x

Bourgault, R., Matschi, S., Vasquez, M., Qiao, P., Sonntag, A., Charlebois, C., et al. (2020). Constructing functional cuticles: analysis of relationships between cuticle lipid composition, ultrastructure and water barrier function in developing adult maize leaves. *Ann. Bot.* 125, 79–91. doi: 10.1093/aob/mcz143

Buschhaus, C., Hager, D., and Jetter, R. (2015). Wax layers on Cosmos bipinnatus petals contribute unequally to total petal water resistance. *Plant Physiol.* 167, 80–88. doi: 10.1104/pp.114.249235

Buschhaus, C., Herz, H., and Jetter, R. (2007). Chemical composition of the epicuticular and intracuticular wax layers on the adaxial side of Ligustrum vulgare leaves. *New Phytol.* 176, 311–316. doi: 10.1111/j.1469-8137.2007.02190.x

Butler, H. J., Ashton, L., Bird, B., Cinque, G., Curtis, K., Dorney, J., et al. (2016). Using Raman spectroscopy to characterize biological materials. *Nat. Protoc.* 11, 664–687. doi: 10.1038/nprot.2016.036

Cai, W., Chen, Y., Xie, L., Zhang, H., and Hou, C. (2013). Characterization and density functional theory study of the antioxidant activity of quercetin and its sugar-containing analogues. *Eur. Food Res. Technol.* 238, 121–128. doi: 10.1007/s00217-013-2091-x

Cai, Y., Li, G., Nie, J., Lin, Y., Nie, F., Zhang, J., et al. (2010). Study of the structure and biosynthetic pathway of lignin in stone cells of pear. *Sci. Hortic.* 125, 374–379. doi: 10.1016/j.scienta.2010.04.029

Cao, Y., Shen, D., Lu, Y., and Huang, Y. (2006). A Raman-scattering study on the net orientation of biomacromolecules in the outer epidermal walls of mature wheat stems (Triticum aestivum). *Ann. Bot.* 97, 1091–1094. doi: 10.1093/aob/mcl059

Chang, B. M., and Keller, M. (2021). Cuticle and skin cell walls have common and unique roles in grape berry splitting. *Hortic. Res.* 8:168. doi: 10.1038/s41438-021-00602-2

Chen, X., Liu, P., Hu, Z., and Jensen, L. (2019). High-resolution tip-enhanced Raman scattering probes sub-molecular density changes. *Nat. Commun.* 10:2567. doi: 10.1038/s41467-019-10618-x

Chu, W., Gao, H., Cao, S., Fang, X., Chen, H., and Xiao, S. (2017). Composition and morphology of cuticular wax in blueberry (Vaccinium spp.) fruits. *Food Chem.* 219, 436–442. doi: 10.1016/j.foodchem.2016.09.186

Colthup, N. B., Daly, L. H., and Wiberley, S. E. (1990). *Introduction To Infrared And Raman Spectroscopy*. New York: Academic Press Inc.

Coste, R., Soliman, M., Bercu, N. B., Potiron, S., Lasri, K., Aguié-Béghin, V., et al. (2021). Unveiling the impact of embedding resins on the physicochemical traits of wood cell walls with subcellular functional probing. *Compos. Sci. Technol.* 201:108485. doi: 10.1016/j.compscitech.2020.108485

Del Zoppo, M., Tommasini, M., Castiglioni, C., and Zerbi, G. (1998). A relationship between Raman and infrared spectra: the case of push-pull molecules. *Chem. Phys. Lett.* 287, 100–108.

Dieing, T., and Ibach, W. (2011). "Software Requirements and Data Analysis in Confocal Raman Microscopy," in *Confocal Raman Microscopy*, eds T. Dieing, O. Hollricher, and J. Toporski (Berlin: Springer), 61–89.

Ding, S., Zhang, J., Yang, L., Wang, X., Fu, F., Wang, R., et al. (2020). Changes in cuticle components and morphology of 'Satsuma'Mandarin (Citrus unshiu) during ambient storage and their potential role on Penicillium digitatum infection. *Molecules* 25:412. doi: 10.3390/molecules25020412

Dong, P.-T., Zong, C., Dagher, Z., Hui, J., Li, J., Zhan, Y., et al. (2021). Polarization-sensitive stimulated Raman scattering imaging resolves amphotericin B orientation in Candida membrane. *Sci. Adv.* 7:eabd5230. doi: 10.1126/sciadv.abd5230

Eigenbrode, S. D., and Jetter, R. (2002). Attachment to plant surface waxes by an insect predator. *Integr. Compar. Biol.* 42, 1091–1099. doi: 10.1093/icb/42.6.1091

Ensikat, H. J., Boese, M., Mader, W., Barthlott, W., and Koch, K. (2006). Crystallinity of plant epicuticular waxes: electron and X-ray diffraction studies. *Chem. Phys. Lipids* 144, 45–59. doi: 10.1016/j.chemphyslip.2006.06.016

Felhofer, M., Prats-Mateu, B., Bock, P., and Gierlinger, N. (2018). Antifungal stilbene impregnation: transport and distribution on the micron-level. *Tree Physiol.* 38, 1526–1537. doi: 10.1093/treephys/tpy073

Felten, J., Hall, H., Jaumot, J., Tauler, R., de Juan, A., and Gorzsas, A. (2015). Vibrational spectroscopic image analysis of biological material using multivariate curve resolution-alternating least squares (MCR-ALS). *Nat. Protoc.* 10, 217–240. doi: 10.1038/nprot.2015.008

Fernandez, V., Guzman-Delgado, P., Graca, J., Santos, S., and Gil, L. (2016). Cuticle Structure in Relation to Chemical Composition: re-assessing the Prevailing Model. *Front. Plant Sci.* 7:427. doi: 10.3389/fpls.2016.00427

Fink, S. (1991). Comparative microscopical studies on the patterns of calcium oxalate distribution in the needles of various conifer species. *Bot. Acta* 104, 306–315.

Franich, R. A., Wells, L. G., and Holland, P. T. (1978). Epicuticular wax of Pinus radiata needles. *Phytochemistry* 17, 1617–1623.

Gal, A., Brumfeld, V., Weiner, S., Addadi, L., and Oron, D. (2012). Certain biominerals in leaves function as light scatterers. *Adv. Mater.* 24, O77–O83. doi: 10.1002/adma.201104548

Gamsjaeger, S., Baranska, M., Schulz, H., Heiselmayer, P., and Musso, M. (2011). Discrimination of carotenoid and flavonoid content in petals of pansy cultivars (Viola x wittrockiana) by FT-Raman spectroscopy. *J. Raman Spectrosc.* 42, 1240–1247. doi: 10.1002/jrs.2860

Ganthaler, A., Stoggl, W., Kranner, I., and Mayr, S. (2017). Foliar Phenolic Compounds in Norway Spruce with Varying Susceptibility to Chrysomyxa rhododendri: analyses of Seasonal and Infection-Induced Accumulation Patterns. *Front. Plant Sci.* 8:1173. doi: 10.3389/fpls.2017.01173

Gierlinger, N. (2018). New insights into plant cell walls by vibrational microspectroscopy. *Appl. Spectrosc. Rev.* 53, 517–551. doi: 10.1080/05704928.2017.1363052

Gierlinger, N., Keplinger, T., and Harrington, M. (2012). Imaging of plant cell walls by confocal Raman microscopy. *Nat. Protoc.* 7, 1694–1708. doi: 10.1038/nprot.2012.092

Gierlinger, N., Luss, S., Konig, C., Konnerth, J., Eder, M., and Fratzl, P. (2010). Cellulose microfibril orientation of Picea abies and its variability at the micron-level determined by Raman imaging. *J. Exp. Bot.* 61, 587–595. doi: 10.1093/jxb/erp325

Gierlinger, N., Sapei, L., and Paris, O. (2008). Insights into the chemical composition of *Equisetum hyemale* by high resolution Raman imaging. *Planta* 227, 969–980. doi: 10.1007/s00425-007-0671-3

Goodwin, S. M., Kolosova, N., Kish, C. M., Wood, K. V., Dudareva, N., and Jenks, M. A. (2003). Cuticle characteristics and volatile emissions of petals in Antirrhinum majus. *Physiol. Plant.* 117, 435–443. doi: 10.1034/j.1399-3054.2003.00047.x

Guzman, P., Fernandez, V., Garcia, M. L., Khayet, M., Fernandez, A., and Gil, L. (2014a). Localization of polysaccharides in isolated and intact cuticles of eucalypt, poplar and pear leaves by enzyme-gold labelling. *Plant Physiol. Biochem.* 76, 1–6. doi: 10.1016/j.plaphy.2013.12.023

Guzman, P., Fernandez, V., Graca, J., Cabral, V., Kayali, N., Khayet, M., et al. (2014b). Chemical and structural analysis of Eucalyptus globulus and E. camaldulensis leaf cuticles: a lipidized cell wall region. *Front. Plant Sci.* 5:481. doi: 10.3389/fpls.2014.00481

Guzman, P., Fernandez, V., Khayet, M., Garcia, M. L., Fernandez, A., and Gil, L. (2014c). Ultrastructure of plant leaf cuticles in relation to sample preparation as observed by transmission electron microscopy. *Sci. World J.* 2014:963921. doi: 10.1155/2014/963921

Guzman-Delgado, P., Graca, J., Cabral, V., Gil, L., and Fernandez, V. (2016). The presence of cutan limits the interpretation of cuticular chemistry and structure: ficus elastica leaf as an example. *Physiol. Plant* 157, 205–220. doi: 10.1111/ppl.12414

Guzmán-Delgado, P., Fernández, V., Venturas, M., Rodríguez-Calcerrada, J., and Gil, L. (2017). Surface properties and physiology of Ulmus laevis and U. minor samaras: implications for seed development and dispersal. *Tree physiology* 37(6), 815–826.

Haliński, Ł. P., Kalkowska, M., Kalkowski, M., Piorunowska, J., Topolewska, A., and Stepnowski, P. (2015). Cuticular wax variation in the tomato (Solanum lycopersicum L.), related wild species and their interspecific hybrids. *Biochem. Syst. Ecol.* 60, 215–224. doi: 10.1016/j.bse.2015.04.030

Heilemann, J., and Strack, D. (1990). Incorporation of kaempferol 3-O-glucoside into the cell walls of Norway spruce needles. *Planta* 181, 599–603. doi: 10.1007/BF00193016

Heiner, Z., Zeise, I., Elbaum, R., and Kneipp, J. (2018). Insight into plant cell wall chemistry and structure by combination of multiphoton microscopy with Raman imaging. *J. Biophotonics* 11:e201700164. doi: 10.1002/jbio.201700164

Heredia-Guerrero, J. A., Benitez, J. J., Dominguez, E., Bayer, I. S., Cingolani, R., Athanassiou, A., et al. (2014). Infrared and Raman spectroscopic features of plant cuticles: a review. *Front. Plant Sci.* 5:305. doi: 10.3389/fpls.2014.00305

Holloway, P. J. (1994). "Plant cuticles: physicochemical characteristics and biosynthesis," in *Air Pollutants And The Leaf Cuticle*, eds K. E. Percy, J. N. Cape, R. Jagels, and C. J. Simpson (Berlin: Springer), 1–13.

Horvath, L., Peszlen, I., Gierlinger, N., Peralta, P., Kelley, S., and Csoka, L. (2012). Distribution of wood polymers within the cell wall of transgenic aspen imaged by Raman microscopy. *Holzforschung* 66, 717–725. doi: 10.1515/hf-2011-0126

Hunt, G. M., and Baker, E. A. (1980). Phenolic constituents of tomato fruit cuticles. *Phytochemistry* 19, 1415–1419.

Jeffree, C., and Sandford, A. (1982). Crystalline structure of plant epicuticular waxes demonstrated by cryostage scanning electron microscopy. *New Phytol.* 91, 549–559.

Jeffree, C. E. (2006). The Fine Structure of the Plant Cuticle. *Annu. Plant Rev.* 23, 11–125. doi: 10.1002/9780470988718.ch2

Jeffree, C. E., Johnson, R. P. C., and Jarvis, P. G. (1971). Epicuticular wax in the stomatal antechamber of sitka spruce and its effects on the diffusion of water vapour and carbon dioxide. *Planta* 98, 1–10. doi: 10.1007/BF00387018

Jetter, R., and Riederer, M. (1994). Epicuticular crystals of nonacosan-10-ol: in-vitro reconstitution and factors influencing crystal habits. *Planta* 195, 257–270.

Jetter, R., and Riederer, M. (2016). Localization of the Transpiration Barrier in the Epi- and Intracuticular Waxes of Eight Plant Species: water Transport Resistances Are Associated with Fatty Acyl Rather Than Alicyclic Components. *Plant Physiol.* 170, 921–934. doi: 10.1104/pp.15.01699

Jetter, R., Schäffer, S., and Riederer, M. (2000). Leaf cuticular waxes are arranged in chemically and mechanically distinct layers: evidence from Prunus laurocerasus L. *Plant Cell Environ.* 23(6), 619–628. doi: 10.1046/j.1365-3040.2000.00581.x

Kisser-Priesack, G., Bieniek, D., and Ziegler, H. (1990). NO2 binding to defined phenolics in the plant cuticle. *Naturwissenschaft* 77, 492–493.

Kögel-Knabner, I., de Leeuw, J. W., Tegelaar, E. W., Hatcher, P. G., and Kerp, H. (1994). A lignin-like polymer in the cuticle of spruce needles: implications for the humification of spruce litter. *Org. Geochem.* 21, 1219–1228.

Kwiatkowska, M., Wojtczak, A., Poplonska, K., Polit, J. T., Stepinski, D., Dominguez, E., et al. (2014). Cutinsomes and lipotubuloids appear to participate in cuticle formation in Ornithogalum umbellatum ovary epidermis: EM-immunogold research. *Protoplasma* 251, 1151–1161. doi: 10.1007/s00709-014-0623-2

Laguna, L., Casado, C. G., and Heredia, A. (1999). Flavonoid biosynthesis in tomato fruit cuticles after in vivo incorporation of H-phenylalanine precursor. *Physiol. Plant.* 105, 491–498.

Lara, I., Belge, B., and Goulao, L. F. (2015). A focus on the biosynthesis and composition of cuticle in fruits. *J. Agric. Food Chem.* 63, 4005–4019. doi: 10.1021/acs.jafc.5b00013

Lee, J., Crampton, K. T., Tallarida, N., and Apkarian, V. A. (2019). Visualizing vibrational normal modes of a single molecule with atomically confined light. *Nature* 568, 78–82. doi: 10.1038/s41586-019-1059-9

Lim, G.-H., Liu, H., Yu, K., Liu, R., Shine, M., Fernandez, J., et al. (2020). The plant cuticle regulates apoplastic transport of salicylic acid during systemic acquired resistance. *Sci. Adv.* 6:eaaz0478. doi: 10.1126/sciadv.aaz0478

Littlejohn, G. R., Mansfield, J. C., Parker, D., Lind, R., Perfect, S., Seymour, M., et al. (2015). In vivo chemical and structural analysis of plant cuticular waxes using stimulated Raman scattering microscopy. *Plant Physiol.* 168, 18–28. doi: 10.1104/pp.15.00119

Lopez-Casado, G., Matas, A. J., Dominguez, E., Cuartero, J., and Heredia, A. (2007). Biomechanics of isolated tomato (Solanum lycopersicum L.) fruit cuticles: the role of the cutin matrix and polysaccharides. *J. Exp. Bot.* 58, 3875–3883. doi: 10.1093/jxb/erm233

Luque, P., Bruque, S., and Heredia, A. (1995). Water permeability of isolated cuticular membranes: a structural analysis. *Arch. Biochem. Biophys.* 317, 417–422. doi: 10.1006/abbi.1995.1183

Machado, N. F. L., de Carvalho, L. A. E. B., Otero, J. C., and Marques, M. P. M. (2012). The autooxidation process in linoleic acid screened by Raman spectroscopy. *J. Raman Spectrosc.* 43, 1991–2000. doi: 10.1002/jrs.4121

Maia, L. F., De Oliveira, V. E., Edwards, H. G. M., and De Oliveira, L. F. C. (2021). The Diversity of Linear Conjugated Polyenes and Colours in Nature: raman Spectroscopy as a Diagnostic Tool. *Chemphyschem* 22, 231–249. doi: 10.1002/cphc.202000818

Martin, L. B., and Rose, J. K. (2014). There's more than one way to skin a fruit: formation and functions of fruit cuticles. *J. Exp. Bot.* 65, 4639–4651. doi: 10.1093/jxb/eru301

Moreira, C. J. S., Bento, A., Pais, J., Petit, J., Escorcio, R., Correia, V. G., et al. (2020). An Ionic Liquid Extraction That Preserves the Molecular Structure of Cutin Shown by Nuclear Magnetic Resonance. *Plant Physiol.* 184, 592–606. doi: 10.1104/pp.20.01049

Nebu, J., and Sony, G. (2017). Raman Spectroscopy. *Spectrosc. Methods Nanomater. Charact.* 2017, 95–127. doi: 10.1016/b978-0-323-46140-5.00005-4

Novikov, V. S., Kuzmin, V. V., Kuznetsov, S. M., Darvin, M. E., Lademann, J., Sagitova, E. A., et al. (2021). DFT study of Raman spectra of polyenes and ss-carotene: dependence on length of polyene chain and isomer type. *Spectrochim. Acta A Mol. Biomol. Spectrosc.* 255:119668. doi: 10.1016/j.saa.2021.119668

Oros, D. R., Standley, L. J., Chen, X., and Simoneit, B. R. (1999). Epicuticular wax compositions of predominant conifers of western North America. *Zeitschrift für Naturforschung C* 54, 17–24.

Paczkowska, M., Lewandowska, K., Bednarski, W., Mizera, M., Podborska, A., Krause, A., et al. (2015). Application of spectroscopic methods for identification (FT-IR, Raman spectroscopy) and determination (UV, EPR) of quercetin-3-O-rutinoside. Experimental and DFT based approach. *Spectrochim. Acta A Mol. Biomol. Spectrosc.* 140, 132–139. doi: 10.1016/j.saa.2014.12.050

Pati, Y. C., Rezaiifar, R., and Krishnaprasad, P. S. (1993). "Orthogonal matching pursuit: Recursive function approximation with applications to wavelet decomposition," in *Proceedings of 27th Asilomar conference on signals, systems and computers*: IEEE, (Pacific Grove: IEEE), 40–44.

Pennisi, S. V., McConnell, D. B., Gower, L. B., Kane, M. E., and Lucansky, T. (2001). Intracellular calcium oxalate crystal structure in Dracaena sanderiana. *New phytol.* 150, 111–120.

Pfündel, E. E., Agati, G., and Cerovic, Z. G. (2018). Optical Properties of Plant Surfaces. *Annu. Plant Rev.* 23, 216–249. doi: 10.1002/9781119312994.apr0234

Philippe, G., Geneix, N., Petit, J., Guillon, F., Sandt, C., Rothan, C., et al. (2020). Assembly of tomato fruit cuticles: a cross-talk between the cutin polyester and cell wall polysaccharides. *New Phytol.* 226, 809–822. doi: 10.1111/nph.16402

Piringer, A., and Heinze, P. (1954). Effect of light on the formation of a pigment in the tomato fruit cuticle. *Plant Physiol.* 29:467. doi: 10.1104/pp.29.5.467

Prats Mateu, B., Hauser, M. T., Heredia, A., and Gierlinger, N. (2016). Waterproofing in Arabidopsis: following Phenolics and Lipids In situ by Confocal Raman Microscopy. *Front. Chem.* 4:10. doi: 10.3389/fchem.2016.00010

Prats-Mateu, B., Bock, P., Schroffenegger, M., Toca-Herrera, J. L., and Gierlinger, N. (2018). Following laser induced changes of plant phenylpropanoids by Raman microscopy. *Sci. Rep.* 8:11804. doi: 10.1038/s41598-018-30096-3

Prats-Mateu, B. P., Bock, P., and Gierlinger, N. (2020). "Raman Imaging of Plant Cell Walls," in *The Plant Cell Wall: Methods and Protocols*, ed. Z. A. Popper (New York: Springer), 251–295.

Prügel, B., and Lognay, G. (1996). Composition of the cuticular waxes of Picea abies and P. sitchensis. *Phytochem. Anal.* 7, 29–36.

Richter, S., Mussig, J., and Gierlinger, N. (2011). Functional plant cell wall design revealed by the Raman imaging approach. *Planta* 233, 763–772. doi: 10.1007/s00425-010-1338-z

Sasani, N., Bock, P., Felhofer, M., and Gierlinger, N. (2021). Raman imaging reveals in-situ microchemistry of cuticle and epidermis of spruce needles. *Plant Methods* 17:17. doi: 10.1186/s13007-021-00717-6

Schmid, E. D., and Brodbek, E. (1983). Raman Intensity Calculations of Formamide with the Cndo Method. *J. Chem. Phys.* 78, 1117–1120. doi: 10.1063/1.444895

Schmid, E. D., and Brosa, B. (1971). Raman Intensity and Conjugation .1. Substituent Dependence of Raman Intensities of 1600 1/Cm Ring Vibrations of Monosubstituted Benzene Derivatives. *Berichte Der Bunsen-Gesellschaft Fur Physikalische Chemie* 75, 1334–1343.

Schmid, E. D., and Brosa, B. (1972). Determination of Conjugation and Angle of Twist in Biphenyls by Raman Intensity. *J. Chem. Phys.* 56:2.

Schmid, E. D., and Brosa, B. (1973). Raman Intensity and Conjugation .3. Conjugation and Resonance Raman Effect on Raman Intensities of Diphenylpolyenes. *J. Chem. Phys.* 58, 3871–3877. doi: 10.1063/1.1679742

Schmid, E. D., Schlenker, P., and Brand, R. R. M. (1977). Raman Intensity and Conjugation .4. Determination of Conjugation between a Phenyl Ring and a Carbonyl Group by Raman Intensity. *J. Raman Spectrosc.* 6, 314–318. doi: 10.1002/jrs.1250060610

Schmid, E. D., and Topsom, R. D. (1981). Raman Intensity and Conjugation .5. A Quantitative Relationship between Raman Intensity and the Length of Conjugation and an Analysis of the Raman Intensities of Some Substituted Benzenes and Biphenyls. *J. Am. Chem. Soc.* 103, 1628–1632. doi: 10.1021/Ja00397a004

Schreiber, N., Gierlinger, N., Putz, N., Fratzl, P., Neinhuis, C., and Burgert, I. (2010). G-fibres in storage roots of Trifolium pratense (Fabaceae): tensile stress generators for contraction. *Plant J.* 61, 854–861. doi: 10.1111/j.1365-313X.2009.04115.x

Segado, P., Dominguez, E., and Heredia, A. (2016). Ultrastructure of the Epidermal Cell Wall and Cuticle of Tomato Fruit (Solanum lycopersicum L.) during Development. *Plant Physiol.* 170, 935–946. doi: 10.1104/pp.15.01725

Slimestad, R., Nerdal, W., Francis, G. W., and Andersen, ØM. (1992). Myricetin 3, 4'-diglucoside and kaempferol derivatives from needles of Norway spruce, Picea abies. *Phytochemistry* 32, 179–181.

Smith, E., and Dent, G. (2005). *Modern Raman Spectroscopy: A Practical Approach*. Hoboken: John Wiley & Sons.

Solovchenko, A., and Merzlyak, M. (2003). Optical properties and contribution of cuticle to UV protection in plants: experiments with apple fruit. *Photochem. Photobiol. Sci.* 2, 861–866. doi: 10.1039/b302478d

Steinbauer, M. J., Davies, N. W., Gaertner, C., and Derridj, S. (2009). Epicuticular waxes and plant primary metabolites on the surfaces of juvenile Eucalyptus globulus and E. nitens (Myrtaceae) leaves. *Aust. J. Bot.* 57, 474–485.

Synytsya, A., Copıkova, J., Matejka, P., and Machovic, V. (2003). Fourier transform Raman and infrared spectroscopy of pectins. *Carbohydr. Polym.* 54, 97–106. doi: 10.1016/S0144-8617(03)00158-9

Szafranek, B., Tomaszewski, D., Pokrzywinska, K., and Gołębiowski, M. (2008). Microstructure and chemical composition of Leaf cuticular waxes in two Salix species and their hybrid. *Acta Biol. Crac. Ser. Bot.* 50, 49–54.

Szwajkowska-Michałek, L., Przybylska-Balcerek, A., Rogoziński, T., and Stuper-Szablewska, K. (2020). Phenolic Compounds in Trees and Shrubs of Central Europe. *Appl. Sci.* 10:6907. doi: 10.3390/app10196907

Szymanska-Chargot, M., Chylinska, M., Pieczywek, P. M., Rosch, P., Schmitt, M., Popp, J., et al. (2016). Raman imaging of changes in the polysaccharides distribution in the cell wall during apple fruit development and senescence. *Planta* 243, 935–945. doi: 10.1007/s00425-015-2456-4

Tenberge, K. B. (1992). Ultrastructure and development of the outer epidermal wall of spruce (Picea abies) needles. *Can. J. Bot.* 70, 1467–1487.

Tommasini, M., Castiglioni, C., Del Zoppo, M., and Zerbi, G. (1999). Relationship between infrared and Raman intensities in molecules with polarized pi electrons. *J. Mol. Struct.* 481, 179–188. doi: 10.1016/S0022-2860(98)00915-6

Tulloch, A. P., and Bergter, L. (1981). Epicuticular wax of Juniperus scopulorum. *Phytochemistry* 20, 2711–2716.

Varsanyi, G. (1969). *Vibrational Spectra of Benzene Derivatives*. New York: Academic Press.

Villena, J. F., Domínguez, E., Stewart, D., and Heredia, A. (1999). Characterization and biosynthesis of non-degradable polymers in plant cuticles. *Planta* 208, 181–187. doi: 10.1007/s004250050548

Vráblová, M., Vrabl, D., Sokolová, B., Marková, D., and Hronková, M. (2020). A modified method for enzymatic isolation of and subsequent wax extraction from Arabidopsis thaliana leaf cuticle. *Plant Methods* 16(1), 1–11. doi: 10.1186/s13007-020-00673-7

Wang, J., Sun, L., Xie, L., He, Y., Luo, T., Sheng, L., et al. (2016). Regulation of cuticle formation during fruit development and ripening in 'Newhall' navel orange (Citrus sinensis Osbeck) revealed by transcriptomic and metabolomic profiling. *Plant Sci.* 243, 131–144. doi: 10.1016/j.plantsci.2015.12.010

Wattendorff, J., and Holloway, P. (1982). Studies on the ultrastructure and histochemistry of plant cuticles: isolated cuticular membrane preparations of

Agave americana L. and the effects of various extraction procedures. *Ann. Bot.* 49, 769–804.

Wen, M., Buschhaus, C., and Jetter, R. (2006). Nanotubules on plant surfaces: chemical composition of epicuticular wax crystals on needles of Taxus baccata L. *Phytochemistry* 67, 1808–1817. doi: 10.1016/j.phytochem.2006.01.018

Yang, S., Dai, X., Stogin, B. B., and Wong, T. S. (2016). Ultrasensitive surface-enhanced Raman scattering detection in common fluids. *Proc. Natl. Acad. Sci. U. S. A.* 113, 268–273. doi: 10.1073/pnas.1518980113

Yeats, T. H., and Rose, J. K. (2013). The formation and function of plant cuticles. *Plant Physiol.* 163, 5–20. doi: 10.1104/pp.113.222737

Zeise, I., Heiner, Z., Holz, S., Joester, M., Buttner, C., and Kneipp, J. (2018). Raman Imaging of Plant Cell Walls in Sections of Cucumis sativus. *Plants* 7:7. doi: 10.3390/plants7010007

Zerbi, G., Castiglioni, C., and Gussoni, M. (1991). Understanding of Vibrational-Spectra of Polyconjugated Molecules by Means of the Effective Conjugation Coordinate. *Synth. Met.* 43, 3407–3412. doi: 10.1016/0379-6779(91)91315-2

Zhu, X., Zhang, Y., Du, Z., Chen, X., Zhou, X., Kong, X., et al. (2018). Tender leaf and fully-expanded leaf exhibited distinct cuticle structure and wax lipid composition in Camellia sinensis cv Fuyun 6. *Sci. Rep.* 8:14944. doi: 10.1038/s41598-018-33344-8

Conflict of Interest: The authors declare that the research was conducted in the absence of any commercial or financial relationships that could be construed as a potential conflict of interest.

Publisher's Note: All claims expressed in this article are solely those of the authors and do not necessarily represent those of their affiliated organizations, or those of the publisher, the editors and the reviewers. Any product that may be evaluated in this article, or claim that may be made by its manufacturer, is not guaranteed or endorsed by the publisher.

frontiers in Plant Science

ORIGINAL RESEARCH
published: 05 January 2022
doi: 10.3389/fpls.2021.766602

Building a Barrier: The Influence of Different Wax Fractions on the Water Transpiration Barrier of Leaf Cuticles

Pascal Seufert[†‡], *Simona Staiger*[†‡], *Katja Arand*[‡], *Amauri Bueno*, *Markus Burghardt and Markus Riederer**

Chair of Botany II – Ecophysiology and Vegetation Ecology, Julius von Sachs Institute of Biological Sciences, University of Würzburg, Würzburg, Germany

Waxes are critical in limiting non-stomatal water loss in higher terrestrial plants by making up the limiting barrier for water diffusion across cuticles. Using a differential extraction protocol, we investigated the influence of various wax fractions on the cuticular transpiration barrier. Triterpenoids (TRPs) and very long-chain aliphatics (VLCAs) were selectively extracted from isolated adaxial leaf cuticles using methanol (MeOH) followed by chloroform (TCM). The water permeabilities of the native and the solvent-treated cuticles were measured gravimetrically. Seven plant species (*Camellia sinensis*, *Ficus elastica*, *Hedera helix*, *Ilex aquifolium*, *Nerium oleander*, *Vinca minor,* and *Zamioculcas zamiifolia*) with highly varying wax compositions ranging from nearly pure VLCA- to TRP-dominated waxes were selected. After TRP removal with MeOH, water permeability did not or only slightly increase. The subsequent VLCA extraction with TCM led to increases in cuticular water permeabilities by up to two orders of magnitude. These effects were consistent across all species investigated, providing direct evidence that the cuticular transpiration barrier is mainly composed of VLCA. In contrast, TRPs play no or only a minor role in controlling water loss.

Keywords: leaf cuticles, non-stomatal transpiration, selective wax extraction, triterpenoids, very long-chain aliphatics, weighted average chain length, leaf cuticular wax properties

OPEN ACCESS

Edited by:
Cécile Raynaud, UMR9213 Institut des Sciences des Plantes de Paris Saclay (IPS2), France

Reviewed by:
Paula Guzmán-Delgado, University of California, Davis, United States
Shuai Li, University of Illinois at Urbana-Champaign, United States

***Correspondence:**
Markus Riederer
riederer@uni-wuerzburg.de

[†]These authors have contributed equally to this work and share first authorship

[‡]Present address:
Pascal Seufert, Labor LS SE & Co. KG, Bad Bocklet, Germany
Simona Staiger, Syngenta Crop Protection, Global Application Technology Group, Münchwilen, Switzerland
Katja Arand, Bavarian State Institute for Viticulture and Horticulture, Institute for Urban Green Space and Landscaping, Veitshöchheim, Germany

Specialty section:
This article was submitted to Plant Physiology, a section of the journal Frontiers in Plant Science

Received: *29 August 2021*
Accepted: *08 December 2021*
Published: *05 January 2022*

Citation:
Seufert P, Staiger S, Arand K, Bueno A, Burghardt M and Riederer M (2022) Building a Barrier: The Influence of Different Wax Fractions on the Water Transpiration Barrier of Leaf Cuticles. Front. Plant Sci. 12:766602. doi: 10.3389/fpls.2021.766602

INTRODUCTION

Plant waxes are complex mixtures varying across species. They are heterogeneous mixtures with more than a hundred compounds, sometimes dominated by a single compound by up to 70%. These complex blends have evolved to fulfill various biological functions, like protection against UV radiation, fungi and insects, self-cleaning of the surface, and building an uptake barrier (Yeats and Rose, 2013). The most important function is to limit cuticular transpiration, especially during periods of drought. It is well known that cuticular waxes build the main barrier to non-stomatal water loss across the leaf surface since the extraction of the cuticular wax leads to a drastic increase of cuticular water permeability (Schönherr, 1976; Schönherr and Lendzian, 1981). However, what wax traits are responsible for its barrier properties remain unclear.

Contrary to intuitive expectation and the statements in many plant ecology text books, the water permeability of cuticles is neither correlated to their thickness (Kamp, 1930; Evans, 1932; Schönherr, 1976, 1982; Becker et al., 1986; Schreiber and Riederer, 1996; Riederer and Schreiber, 2001; Burghardt and Riederer, 2006) nor to total wax, intracuticular wax, or epicuticular wax

coverage (Riederer and Schneider, 1990; Riederer and Schreiber, 2001; Jetter and Riederer, 2016; Bueno et al., 2020). Hence, after more than one century of research into the ecophysiology of cuticular transpiration, the molecular mechanism underlying the barrier properties of plant cuticles is still largely unknown. This could be because the scientists in this field asked the wrong questions and, therefore, got just such answers. The present work aims to clarify what we have to understand by "wax" when we want to elucidate the chemical and physical foundations of the cuticular transpiration barrier.

The composition of leaf cuticular waxes differs widely between plant species, but alicyclic triterpenoids (TRPs) and very long-chain aliphatics (VLCAs) are usually the most abundant constituents (Jetter et al., 2006; Busta and Reinhard, 2018). In the adaxial leaf wax of *Prunus laurocerasus*, the former constitutes about 70% of the total wax coverage. Although VLCAs make up a significant wax fraction in many leaf cuticles analyzed so far, TRPs can nevertheless constitute the major wax fraction. Within the VLCAs, alkanes, primary alcohols, and fatty acids are usually the most abundant substance classes. In several species, a significant difference regarding their chemical composition between intra- and epicuticular waxes was found. While epicuticular wax only contains aliphatic compounds, intracuticular wax comprises both TRPs and VLCAs (Jetter et al., 2000; Jetter and Riederer, 2016; Zeisler and Schreiber, 2016). Several studies have shown that the transpiration barrier is located within the intracuticular wax in most plant species, embedded in the cutin matrix (Jetter and Riederer, 2016; Zeisler and Schreiber, 2016; Zeisler-Diehl et al., 2018). Jetter and Riederer (2016) proposed that the transpiration barrier is mainly formed by the intracuticular VLCAs, while alicyclic TRPs play no or only a minor role. Other studies comparing the wax composition of genetically modified plants (Vogg et al., 2004) or intra- and epicuticular wax of the same cuticle (Jetter and Riederer, 2016) also suggested that the VLCAs mainly constitute the cuticular transpiration barrier. VLCAs at physiological temperatures form semi-crystalline solids (Merk et al., 1998; Dorset, 2005; Fagerström et al., 2013) with crystalline domains consisting of the tightly aligned long hydrocarbon chains of the aliphatic compounds (Reynhardt and Riederer, 1991, 1994; Dorset, 1999) and having a low permeability for water. TRPs have been shown to provide mechanical (Tsubaki et al., 2013) and thermal stability to the plant cuticle (Schuster et al., 2016).

The present study aims to shed light on the roles of the VLCA and TRP fractions in plant cuticular waxes in building the barrier against the transcuticular diffusion of water. A suite of seven plant species was selected for the experiments, which fulfilled the following conditions: (1) astomatous leaf cuticles can be isolated, (2) presence of TRPs varying from absent to making up high proportions, and (3) absence of pronounced epicuticular wax crystals. To examine the respective impact of the two wax fractions on the permeability properties of the cuticle, TRPs and VLCAs were selectively removed by solvent extraction of isolated cuticles. Permeances for water were obtained for (1) native isolated cuticular membranes (CMs) containing both the VLCA fraction and if present, the TRP fraction of cuticular wax, (2) MeOH-extracted cuticular membranes (Ms) containing the VLCA fraction but TRPs having been selectively removed, and (3) chloroform-extracted and thus completely dewaxed matrix membranes (MXs). This approach was taken to clarify which wax fractions we must keep in mind when we want to understand cuticular barrier properties.

Abbreviations: CM, Cuticular membrane; FE, Full extracts; M, Methanol extracted cuticle; MX, Dewaxed cuticles; MeOH, Methanol; TCM, Chloroform; TRP, Triterpenoid; VLCA, Very long-chain aliphatic.

MATERIALS AND METHODS

Plant Material and Cuticle Isolation

Plants of *Vinca minor*, *Hedera helix*, and *Ilex aquifolium* were grown outdoors in the Botanical Garden of the University of Würzburg. *Ficus elastica*, *Camellia sinensis*, and *Zamioculcas zamiifolia* were cultivated in the greenhouse all year round. At the same time, potted *Nerium oleander* plants were held in the greenhouse during winter and outdoors during summer.

Astomatous CMs were isolated according to a method adapted from Schönherr and Riederer (1986). For all plants except *V. minor*, disks with a diameter of 1.89 cm were punched out of fresh, fully mature leaves, avoiding major veins as far as possible. From the tiny leaves of *V. minor,* disks with a diameter of only 1.66 cm were punched out, and it was impossible to avoid the major vein. After marking the adaxial, astomatous side at the edge of the leaf disks with a permanent marker pen, the disks were incubated in an enzyme solution containing 1% pectinase (Trenolin, Erbslöh, Geisenheim, Germany), 1% cellulase (Celluclast, NCBE, University of Reading, U.K.), 1 mm citric acid monohydrate (Applichem, Darmstadt, Germany) as a buffer, and 1 mm sodium azide (Sigma-Aldrich, Steinheim, Germany) to prevent bacterial growth. The solution was kept at room temperature and was replaced twice a week. After the disintegration of the leaf tissue, astomatous cuticles (CM) were identified by the pen marks, washed thoroughly with distilled water and stored in distilled water until further use (maximum period of 7 weeks).

Wax Extraction and Analysis

For full extracts (FE), samples comprised of five CMs per plant species (two for *H. helix*) were extracted twice, first overnight and then for 30 min, in 10 ml TCM (≥99.8%; Roth, Karlsruhe, Germany) at room temperature, yielding completely dewaxed matrix membranes (MX). N-tetracosane (Sigma-Aldrich, Steinheim, Germany) was added as an internal standard before the first extraction. TCM extracts were combined, and the solvent was evaporated under a gentle stream of N_2. Derivatization for gas chromatography of an aliquot of the wax samples was performed using N,O-bis (trimethylsilyl) trifluoroacetamide (Macherey-Nagel Düren, Germany) in dry pyridine (Roth, Karlsruhe, Germany) for 45 min at 70°C. Quantitative analyses were performed using a gas chromatograph coupled with a flame ionization detector (FID). Samples were injected by an on-column injector (7890A, Agilent Technologies, Waldbronn, Germany) into a fused silica capillary column (DB1-ms, 30 m length×0.32 mm ID, 0.1 µm film, Agilent Technologies) using H_2 as the carrier gas. The temperature

program was as: injection at 50°C and held for 2 min, raised by 40°C min^{-1} to 200°C and held for 2 min, and increased by 3°C min^{-1} to 320°C and held for 30 min. Quantification was achieved by comparing the internal standard's peak area with the analytes' peak area. Gas chromatography coupled with mass spectrometry (5975iMSD, Agilent Technologies) was used for qualitative analysis. The separation was performed under the same conditions except that helium was used as the carrier gas.

For selective wax extraction, five CMs per sample were extracted overnight with 20 ml MeOH (UPLC-grade; Roth, Karlsruhe, Germany) at room temperature. Depending on the plant species, four to eight samples were prepared. The cuticles were removed and washed with MeOH. The extracts and washings were combined. Part of the MeOH-extracted cuticles (Ms) were saved for permeability measurements. The remaining Ms were gently flattened, dried under a stream of air on Teflon platelets, and immersed twice, first overnight, then for 30 min in 20 ml TCM (≥99.8%; Roth, Karlsruhe, Germany) at room temperature to ensure complete wax removal. This extraction process yielded dewaxed matrix membranes (MXs) equivalent to the MXs obtained by TCM extraction of CMs. The MXs were washed with TCM, flattened on Teflon platelets, and dried under a gentle stream of air. TCM extracts and washings were combined, and n-tetracosane was added as an internal standard. Wax analysis was performed as described above.

Measurement of Cuticular Permeance

Permeances of CMs, Ms, and MXs were measured by a method adapted from Schönherr and Lendzian (1981). The cuticles were mounted on stainless steel transpiration chambers using Teflon paste (Roth, Karlsruhe, Germany) and fixed with a ring-like lid. The physiological outer side of the isolated cuticles faced the atmosphere with a surface area of 1.12 cm^2 available for transpiration. After adding deionized water through a small opening in the bottom of the transpiration chamber, the latter was sealed with adhesive tape. The transpiration chambers were placed into a sealed plastic container upside down on a grid over dried silica gel (Applichem, Darmstadt, Germany). The chambers were kept at 25°C. The transpirational water loss was determined gravimetrically. Samples were weighted once or twice a day, depending on the plant species and treatment with a total of 6 measurements. Water permeance P ($m\,s^{-1}$) was obtained from

$$P = \frac{J}{A \times \Delta c} \quad (1)$$

with J being the loss of water ($g\,s^{-1}$), A the cuticle surface area exposed to the air (m^2), and Δc the difference of water vapor concentration at the inner ($C_i = 23.074\,g\,m^{-3}$) and outer ($C_o = 0\,g\,m^{-3}$) sides of the cuticle.

Scanning Electron Microscopy

The surface structure of the outer sides of the isolated cuticles was investigated using scanning electron microscopy (SEM, JEOL JSM-7500F, JEOL GmbH, Freising, Germany) with an accelerating voltage of 5.0 kV and a working distance of 7.9 mm equipped with a field emission gun and a lower secondary electron (LEI) detector. CMs, Ms, and MXs were carefully mounted on aluminum holders and sputter-coated with an 80/20 gold/palladium mixture.

Statistics

OriginPro 2018b (Systat Software GmbH) was used for statistical analysis. Water permeance values and their log transformations were rejected for normal distribution with the Shapiro–Wilk normality test. Therefore, medians (median; 25th–75th percentile) and nonparametric statistics were used. Permeances were tested for significant differences by Kruskal-Wallis test ANOVA with post-hoc Dunn's test ($p < 0.05$). For wax analyses, normal distribution was found for all species except for the VLCAs of the MeOH and TCM extracts of *V. minor* and the VLCAs of the MeOH extract of *Z. zamiifolia*. For normally distributed data, significant differences were investigated using one-way ANOVA ($p < 0.05$). Otherwise, the Kruskal-Wallis test ANOVA with post-hoc Dunn's test was used.

RESULTS

Cuticular Wax

A complex mixture of cuticular waxes was found in MeOH and following TCM extracts, and full TCM extracts of cuticles from the seven plant species investigated (**Supplementary Table 1**). *Z. zamiifolia* and *H. helix* had low total wax coverages (around 10 $\mu g\,cm^{-2}$), consisting almost exclusively of VLCAs. *C. sinensis* showed a wax composition of about one-third of VLCAs and two-thirds of TRPs. *V. minor* and *F. elastica* had intermediate wax coverages (40–60 $\mu g\,cm^{-2}$) with minor VLCA content. *N. oleander* and *I. aquifolium* exhibited high wax coverages (around 180 $\mu g\,cm^{-2}$) dominated by TRPs and only minor contributions of VLCAs (**Supplementary Table 2**). No significant differences of the total removed TRP and VLCA wax coverages between the combined MeOH and following TCM extracts and FEs were observed (**Figure 1**).

MeOH treatment removed TRPs exhaustively or almost exhaustively in all TRP-containing species. In most species, VLCA in the MeOH extract ranged from 11 to 44% of the total extracted VLCAs. Only from *I. aquifolium*, about 60% of the VLCAs were removed with MeOH (**Supplementary Table 2**). Subsequent TCM treatment of these cuticles released almost exclusively VLCAs and minor residues of TRPs (**Figure 2**; **Supplementary Table 2**). All plant species showed a significant decrease of extracted TRPs between the MeOH and the following TCM extract ($p < 0.05$). Except for *I. aquifolium* and *N. oleander*, all plant species showed a significant increase of extracted VLCAs between the MeOH and the following TCM extract ($p < 0.05$). Despite considerable differences in wax coverages and compositions, these trends were observed for all plant species (**Supplementary Table 2**).

The chain length distribution of the VLCAs varied strongly between the plant species. In all plant species, except *N. oleander,*

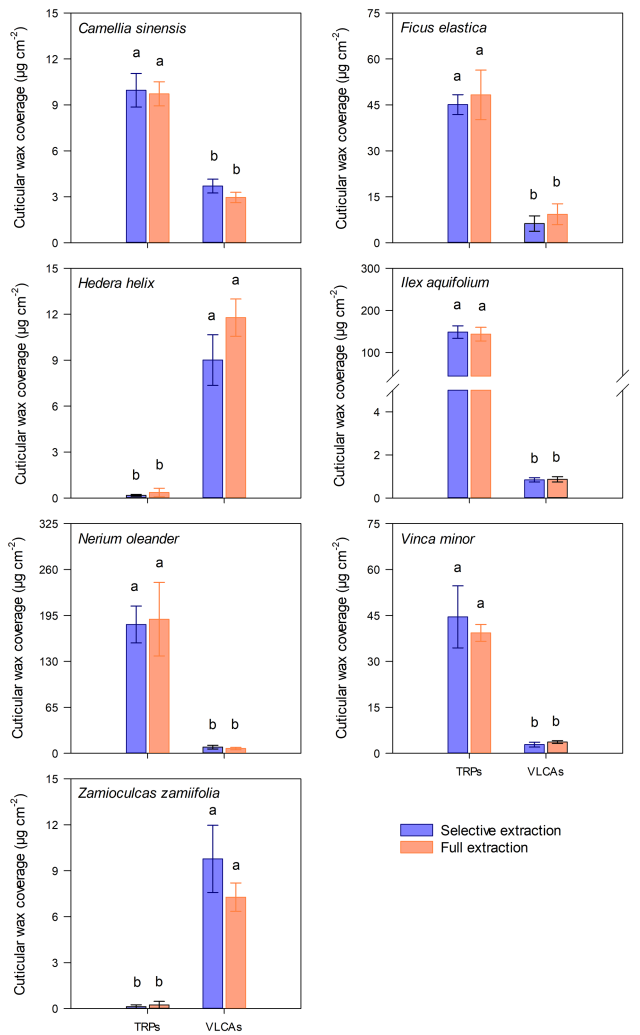

FIGURE 1 | Comparison of total cuticular loads of very long-chain aliphatics (VLCA) and triterpenoids (TRP) in selective wax extracts (purple) and full extracts (orange) of seven plant species. Data were normally distributed. Differences were tested using one-way ANOVA. Different letters stand for significant differences ($p < 0.05$) between the two extraction methods within a wax fraction. Columns show mean values and whiskers standard deviations ($n = 4–8$).

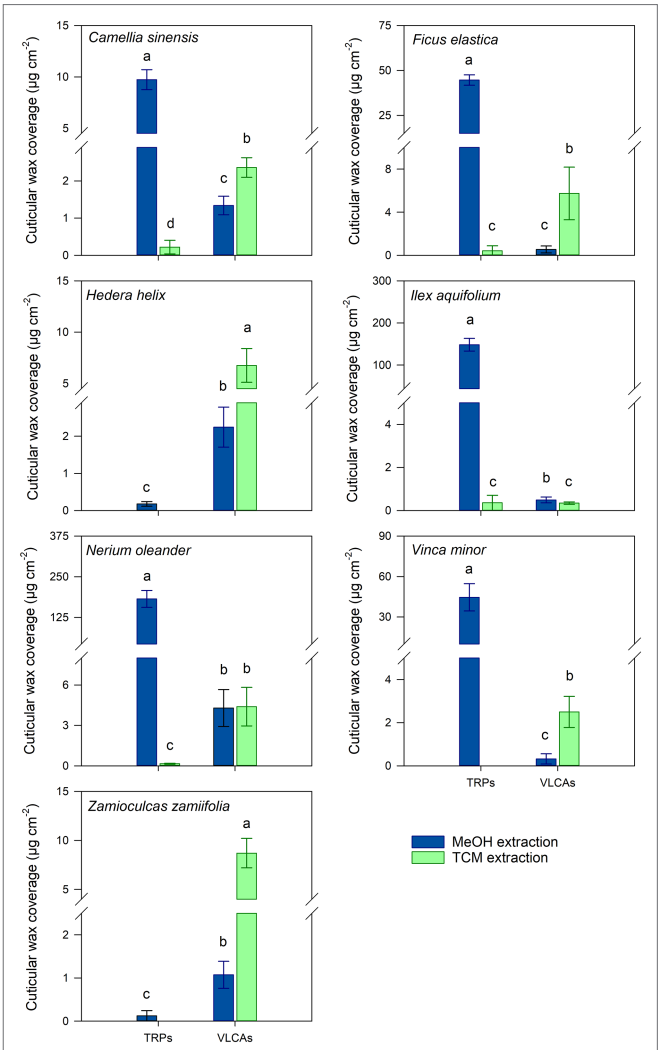

FIGURE 2 | Comparison of cuticular wax compositions extracted from isolated cuticles with consecutive methanol (MeOH; blue) and chloroform (TCM; green) extraction steps. Normal distribution was found for data of all species except for the VLCA of both steps of *V. minor* and the VLCAs of the MeOH extraction of *Z. zamiifolia*. For normally distributed data, differences were tested for significance with one-way ANOVA. In all other cases, the Kruskal-Wallis test ANOVA with post-hoc Dunn's test was used. Different letters stand for significant differences ($p < 0.05$) between the two extraction methods within a wax fraction. Columns show mean values and whiskers standard deviation ($n = 4–8$).

the MeOH extraction tended to remove VLCAs with shorter chain lengths (< 32 carbon atoms). In comparison, the following TCM extraction also removed VLCAs with longer chain lengths (**Figure 3**).

Water Permeance

The cuticular water permeance was measured for CMs, Ms, and MXs (**Supplementary Table 3**). Median permeances of CMs ranged from $0.40 \times 10{-}5\,m\,s{-}1$ (*H. helix*) to $4.27 \times 10^{-5}\,m\,s^{-1}$ (*C. sinensis*). Permeances of Ms ranged from $0.57 \times 10^{-5}\,m\,s^{-1}$ (*Z. zamiifolia*) to $9.19 \times 10^{-5}\,m\,s^{-1}$ (*N. oleander*). The permeances of Ms of *C. sinensis*, *F. elastica*, *H. helix*, *I. aquifolium*, and *Z. zamiifolia* were not significantly different ($p > 0.05$) from the values of the untreated cuticles (**Figure 4**). Permeances of Ms of *N. oleander* and *V. minor* showed a small but significant increase ($p < 0.05$) in comparison with the values of CMs (**Figure 4**). Permeances of MXs ranged from $1.07 \times 10^{-5}\,m\,s^{-1}$ (*Z. zamiifolia*) to $50.9 \times 10{-}5\,m\,s{-}1$ (*V. minor*). The permeances of the completely dewaxed MXs of the species investigated were significantly higher ($p < 0.05$) than those of CMs and Ms (Figure 4).

Scanning Electron Microscopy

The surfaces of CMs of all species investigated were smooth, lacking pronounced and well-defined epicuticular wax crystals (**Supplementary Figures 1–4**). The surface of *C. sinensis* displayed

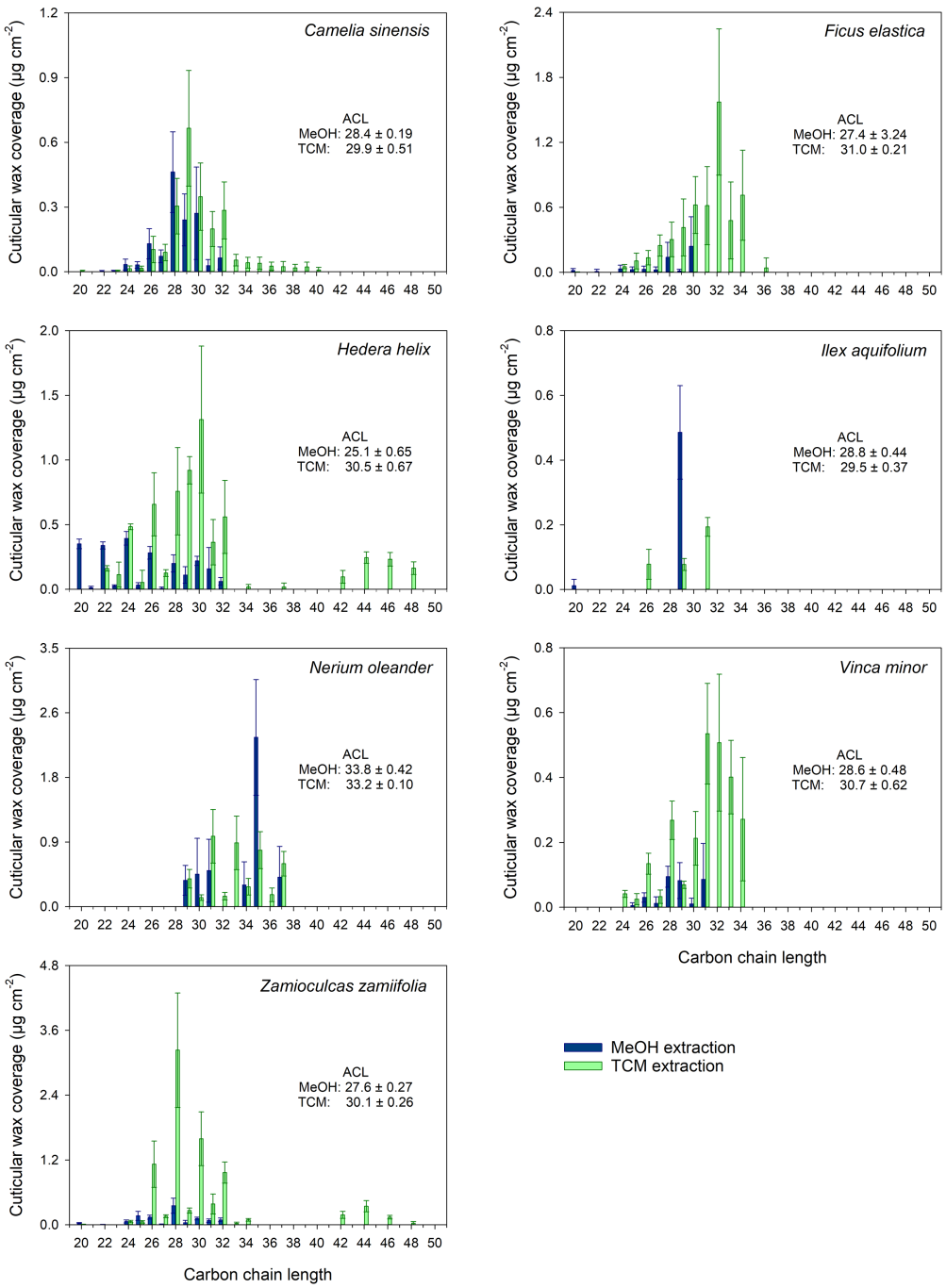

FIGURE 3 | Chain length distribution of VLCA in the methanol (MeOH; blue) and the subsequent chloroform (TCM; green) extracts of seven plant species. Columns show mean values and whiskers standard deviation ($n = 4–8$).

tiny, scattered wax accumulations. The *F. elastica* surface appeared encrusted. Ms of both plant species showed a slight decrease in surface roughness. (**Supplementary Figure 1**). Aside from small wax accumulations, the surfaces of *H. helix* and *I. aquifolium* had an overall smooth appearance. The M of *I. aquifolium* showed relatively small differences to the corresponding CM. The M of *H. helix* appeared slightly more granulated than the corresponding CM. (**Supplementary Figure 2**). The wax on the surface of CM and M of *N. oleander* had a smooth appearance. The CM and M of *V. minor* were encrusted with wax (**Supplementary Figure 3**). The surface CM and M of *Z. zamiifolia* had a partially granulated appearance. (**Supplementary Figure 4**). Aside from minor remnants, the surfaces of MXs of all plants appeared devoid of cuticular wax (**Supplementary Figures 1–4**).

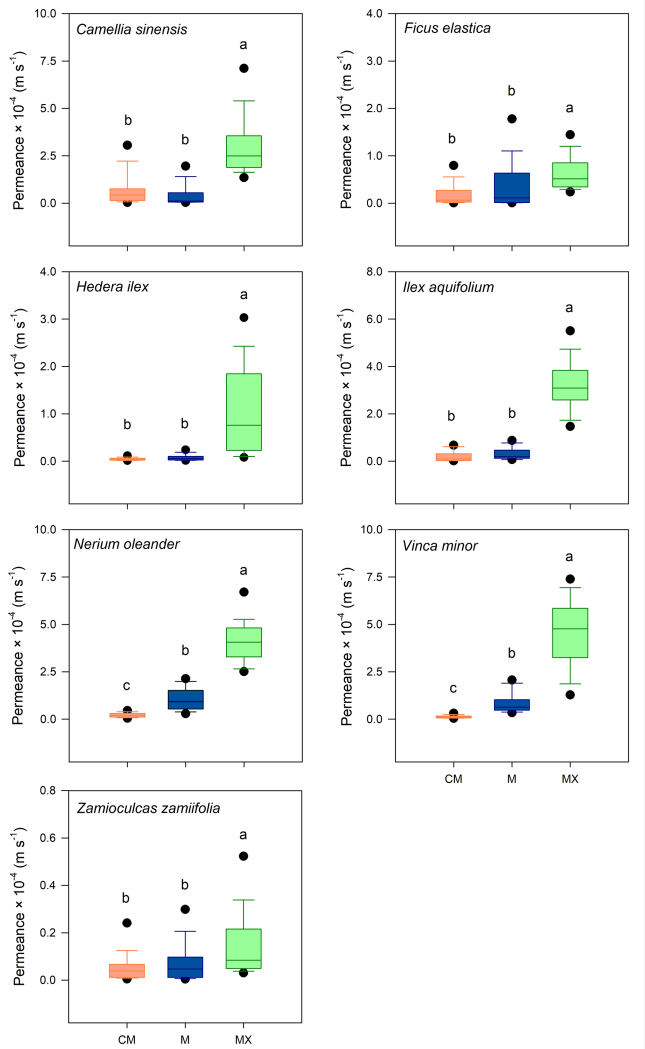

FIGURE 4 | Water permeability of isolated cuticles of seven plant species in untreated (CM; orange), methanol (M; blue), and subsequent chloroform (MX; green) extracted conditions. Investigation of significant differences was conducted by Kruskal-Wallis test ANOVA with post-hoc Dunn's test. Boxes are interquartile ranges from 25 to 75%, whiskers 10–90% and dots designate outliers. Different letters stand for significant differences ($p < 0.05$) among treatments ($p \geq 28$).

DISCUSSION

The objective of our study was to experimentally identify the respective contributions of the two main cuticular wax fractions VLCAs and TRPs to the barrier against non-stomatal water loss. The effects of the complete and the selective removal of TRPs and VLCAs, respectively, on the water permeability barrier were measured using isolated cuticles from seven plant species with a varying contribution of TRPs to the total of their cuticular waxes.

The primary challenge was to find a solvent suitable for TRP extraction, which leaves the VLCA fraction of the cuticular wax as intact as possible. Reports dealing with the solubility of VLCA compounds in organic solvents indicate a common trend of a sharply decreasing solubility of these substances with increasing chain lengths (Hoerr et al., 1944; Kiser et al., 1961). Hoerr et al. (1944) showed this trend in several solvents varying in polarity for primary *n*-alcohols with even carbon chain lengths between 10 and 18. A similar result was found for the solubility of hydrocarbons with chain lengths between five and 10 in MeOH (Kiser et al., 1961). Riederer and Schneider (1989) recalculated data from several publications and reported the relative solubility compared to their solubility in TCM of three substances found in cuticular wax. TCM was by far the best solvent for both 1-octacosanol and octadecanoic acid. However, both compounds were only slightly soluble in MeOH, and the solubility of dotriacontane was higher in more nonpolar solvents (Riederer and Schneider, 1989). Jin et al. (1997) investigated the solubility of oleanolic and ursolic acid in different solvents, and their solubility in MeOH was similar to that in TCM. From the present data, assuming equal accessibility of the wax components for the solvent, we expected a good solubility of TRPs in MeOH but not of VLCAs, allowing us to extract the two fractions separately from the cuticle.

Treating isolated cuticles containing a TRP wax fraction with MeOH led to almost complete removal of this distinctly polar alicyclic fraction. In addition to TRPs, minor amounts of the more polar VLCAs were released, mainly those with shorter chain lengths and polar functional groups, like alcohols and fatty acids. Most importantly, the majority of the VLCAs with higher carbon numbers remained in the cuticle. They could be extracted with a subsequent TCM treatment (**Figure 2**). Despite a relatively poor solubility of VLCAs in MeOH, a significant fraction of the total VLCA amount was extracted in *I. aquifolium* and *N. oleander*. These results show that our method could remove TRPs quite selectively, however, not without avoiding VLCA removal. This may indicate that in some species, TRPs and VLCAs are not as distinctly separated in different layers as postulated by Jetter and Riederer (2016) but may intermix to some degree. It is conceivable that a portion of VLCAs is extracted by MeOH when the surrounding TRPs are removed, and the connection to the cutin matrix gets lost. The chain length distributions of VLCAs extracted with MeOH and TCM differed strongly. MeOH dissolved VLCAs preferentially with shorter chain lengths (**Figure 3**), while TCM did not discriminate chain lengths. VLCAs with a polar functional group dominated the long-chain fraction of the MeOH extracts, which also contained alkanes to a minor extent. VLCAs with longer chain lengths, including alkyl esters with carbon numbers above 40, could be found in the following TCM extract. VLCAs were extracted exhaustively using TCM, regardless their functional groups or chain lengths.

To characterize the VLCAs extracted from CMs with MeOH and from Ms with TCM, we calculated the weighted average chain length (ACL) as an indicator for the ability of the solvent to dissolve VLCAs with varying carbon numbers. ACLs were calculated according to:

$$\mathrm{ACL} = \frac{\sum(\mathrm{C_n} \times \mathrm{n})}{\sum(\mathrm{C_n})} \quad (2)$$

where c_n is the amount per unit area of all aliphatic compounds with carbon chain length n. The chain length distribution of the MeOH extracts was characterized by an ACL < 30. *N. oleander* was the only species with an ACL > 30 in the MeOH extract. The TCM extracts from Ms showed ACLs >30 except those of *C. sinensis* and *I. aquifolium*, which were dominated by shorter chain aliphatics. Combining the results for the two extracts yielded ACLs >30 for *F. elastica, N. oleander*, and *V. minor,* while all other species exhibited ACLs below 30. The same was found for FEs (obtained by TCM extraction of CMs); *F. elastica*, *N. oleander,* and *V. minor* showed ACL values above 30, all other plant species below 30 (**Supplementary Table 4**). The ACLs of TCM extracts of all plants, except *N. oleander,* displayed a significant increase ($p < 0.05$) compared to the ACLs of MeOH extracts, indicating a reduced VLCA extraction capability of MeOH compared to TCM with the increasing chain length of the wax constituent. The ACLs of the combined MeOH and TCM extracts and FEs did not differ significantly ($p > 0.05$).

Removing the TRPs from CMs with MeOH did not significantly affect the cuticular water permeance of isolated cuticles except for *N. oleander* and *V. minor*. However, the subsequent extraction of the remaining VLCAs with TCM substantially increased the permeances of the cuticles of all plant species compared to untreated and MeOH-extracted ones (**Figure 4**). These findings are rigorous experimental evidence that the VLCA and not the TRP fraction of cuticular wax constitutes the actual barrier to water permeability. The results for *I. aquifolium*, *N. oleander*, and *V. minor* indicate a more complex relationship between water permeance and the VLCAs, which needs further study. One can be imagined that not only the composition of cuticular waxes influences the barrier properties but also their location and distribution within the cuticle.

Since the MeOH treatment did not alter the integrity of the transpirational barrier made up by the VLCAs in the majority of the species investigated, we propose that the VLCA and TRP wax fractions are located in different regions of the cuticle depending on their polarity with some degree of intermixing. As already shown for several plant species, the VLCAs tend to accumulate at and on the outer surface of the cuticle facing the environment, while TRPs are deposited in the interior of the cuticle, facing the hydrophilic cell wall (Jetter et al., 2000; Buschhaus and Jetter, 2011; Jetter and Riederer, 2016). Jetter and Riederer (2016) postulated that cuticular waxes are arranged in a VLCA layer associated with the outer surface of the cuticle and a TRP layer in its interior. This view was supported by a previous study (Staiger et al., 2019) describing that no TRPs could be extracted when dipping whole leaves into MeOH. This indicates that the external VLCA layer prevents MeOH from penetrating into deeper layers of the cuticle from the outside and extracting TRPs from these locations. Extraction of TRPs with MeOH was only possible with isolated cuticles, whose inner side is fully accessible to the solvent.

Our findings provide, to our knowledge, for the first time direct experimental evidence for the fact that the cuticular transpiration barrier is mainly composed of the VLCA fraction of the wax. This experimental approach makes it possible to more clearly formulate questions concerning the significance of waxes or specific fractions thereof for the cuticular transpiration barrier and to generate hypotheses that can be tested experimentally. This may translate into a significant advance in the scientific understanding of the role of the cuticle in the ecophysiology of non-stomatal transpiration beyond the intuitive but mostly wrong views prevalent in this field.

DATA AVAILABILITY STATEMENT

The raw data supporting the conclusions of this article will be made available by the authors, without undue reservation.

AUTHOR CONTRIBUTIONS

PS and SS conducted the experiments and evaluated the results together with KA. SS, KA, AB, MB, and MR revised the manuscript. PS wrote the manuscript. AB implemented the changes. KA, MB, and MR supervised the work. Results and content were discussed with all authors. All authors contributed to the article and approved the submitted version.

ACKNOWLEDGMENTS

The authors gratefully acknowledge the skillful technical assistance by Jutta Winkler-Steinbeck, Yvonne Heppenstiel, Tanja Röder, and Christine Gernert.

SUPPLEMENTARY MATERIAL

The Supplementary Material for this article can be found online at: https://www.frontiersin.org/articles/10.3389/fpls.2021.766602/full#supplementary-material

REFERENCES

Becker, M., Kerstiens, G., and Schönherr, J. (1986). Water permeability of plant cuticles: permeance, diffusion and partition coefficients. *Trees - Struct. Funct.* 1, 54–60. doi: 10.1007/BF00197025

Bueno, A., Sancho-Knapik, D., Gil-Pelegrín, E., Leide, J., Peguero-Pina, J. J., Burghardt, M., et al. (2020). Cuticular wax coverage and its transpiration barrier properties in *Quercus coccifera* L. leaves: does the environment matter? *Tree Physiol.* 40, 827–840. doi: 10.1093/treephys/tpz110

Burghardt, M., and Riederer, M. (2006). "Cuticular transpiration," in *Biology of the Plant Cuticle*. eds. M. Riederer and C. Müller (Oxford: Blackwell Publishing), 291–310.

Buschhaus, C., and Jetter, R. (2011). Composition differences between epicuticular and intracuticular wax substructures: how do plants seal their epidermal surfaces? *J. Exp. Bot.* 62, 841–853. doi: 10.1093/jxb/erq366

Busta, L., and Reinhard, J. (2018). Moving beyond the ubiquitous: the diversity and biosynthesis of specialty compounds in plant cuticular waxes. *Phytochem. Rev.* 17, 1275–1304. doi: 10.1007/s11101-017-9542-0

Dorset, D. L. (1999). Development of lamellar structures in natural waxes-an electron diffraction investigation. *J. Phys. D. Appl. Phys.* 32, 1276–1280. doi: 10.1088/0022-3727/32/11/315

Dorset, D. L. (2005). *Crystallography of the Polymethylene Chain: An Inquiry Into the Structure of Waxes. Vol. 17*. Oxford: Oxford University Press on Demand.

Evans, H. (1932). The physiology of succulent plants. *Biol. Rev.* 7, 181–211. doi: 10.1111/j.1469-185X.1962.tb01040.x

Fagerström, A., Kocherbitov, V., Westbye, P., Bergström, K., Mamontova, V., and Engblom, J. (2013). Characterization of a plant leaf cuticle model wax, phase behaviour of model wax-water systems. *Thermochim. Acta* 571, 42–52. doi: 10.1016/j.tca.2013.08.025

Hoerr, C. W., Harwood, H. J., and Ralston, A. W. (1944). Solubilities of high molecular weight normal aliphatic primary alcohols. *J. Organomet. Chem.* 9, 267–280. doi: 10.1021/jo01185a010

Jetter, R., Kunst, L., and Samuels, A. L. (2006). "Composition of plant cuticular waxes," in *Biology of the Plant Cuticle*. eds. M. Riederer and C. Müller (Oxford: Blackwell Publishing), 145–181.

Jetter, R., and Riederer, M. (2016). Localization of the transpiration barrier in the epi- and intracuticular waxes of eight plant species: water transport resistances are associated with fatty acyl rather than alicyclic components. *Plant Physiol.* 170, 921–934. doi: 10.1104/pp.15.01699

Jetter, R., Schäffer, S., and Riederer, M. (2000). Leaf cuticular waxes are arranged in chemically and mechanically distinct layers: evidence from *Prunus laurocerasus* L. *Plant Cell Environ.* 23, 619–628. doi: 10.1046/j.1365-3040.2000.00581.x

Jin, I., Ko, Y., Kim, Y., and Han, S. (1997). Solubilization of oleanolic acid and ursolic acid by cosolvency. *Arch. Pharm. Res.* 20, 269–274. doi: 10.1007/BF02976156

Kamp, H. (1930). Untersuchungen über Kutikularbau und kutikuläre Transpiration von Blättern. *Jahrb. Wiss. Bot.* 72, 403–464.

Kiser, R., Johnson, G., and Shetlar, M. (1961). Solubilities of various hydrocarbons in methanol. *J. Chem. Eng. Data* 6, 338–341. doi: 10.1021/je00103a009

Merk, S., Blume, A., and Riederer, M. (1998). Phase behaviour and crystallinity of plant cuticular waxes studied by Fourier transform infrared spectroscopy. *Planta* 204, 44–53. doi: 10.1007/s004250050228

Reynhardt, E. C., and Riederer, M. (1991). Structure and molecular dynamics of the cuticular wax from leaves of *Citrus aurantium* L. *J. Phys. D. Appl. Phys.* 24, 478–486. doi: 10.1088/0022-3727/24/3/036

Reynhardt, E. C., and Riederer, M. (1994). Structures and molecular dynamics of plant waxes II. Cuticular waxes from leaves of *Fagus sylvatica* L. and *Hordeum vulgare* L. *Eur. Biophys. J.* 23, 59–70.

Riederer, M., and Schneider, G. (1989). Comparative study of the composition of waxes extracted from isolated leaf cuticles and from whole leaves of *citrus*: evidence for selective extraction. *Physiol. Plant.* 77, 373–384. doi: 10.1111/j.1399-3054.1989.tb05656.x

Riederer, M., and Schneider, G. (1990). The effect of the environment on the permeability and composition of citrus leaf cuticles: II. Composition of soluble cuticular lipids and correlation with transport properties. *Planta* 180, 154–165. doi: 10.1007/BF00193990

Riederer, M., and Schreiber, L. (2001). Protecting against water loss: analysis of the barrier properties of plant cuticles. *J. Exp. Bot.* 52, 2023–2032. doi: 10.1093/jexbot/52.363.2023

Schönherr, J. (1976). Water permeability of isolated cuticular membranes: The effect of cuticular waxes on diffusion of water. *Planta* 131, 159–164. doi: 10.1007/BF00389989

Schönherr, J. (1982). "Resistance of plant surfaces to water loss: transport properties of cutin, suberin and associated lipids," in *Physiological Plant Ecology*. eds. O. L. Lange, P. S. Nobel, C. B. Osmond and H. Ziegler (Berlin: Springer-Verlag), 153–179.

Schönherr, J., and Lendzian, K. (1981). A simple and inexpensive method of measuring water permeability of isolated plant cuticular membranes. *Z. Pflanzenphysiol.* 102, 321–327. doi: 10.1016/S0044-328X(81)80203-6

Schönherr, J., and Riederer, M. (1986). Plant cuticles sorb lipophilic compounds during enzymatic isolation. *Plant Cell Environ.* 9, 459–466. doi: 10.1111/j.1365-3040.1986.tb01761.x

Schreiber, L., and Riederer, M. (1996). Ecophysiology of cuticular transpiration: comparative investigation of cuticular water permeability of plant species from different habitats. *Oecologia* 107, 426–432. doi: 10.1007/BF00333931

Schuster, A.-C., Burghardt, M., Alfarhan, A., Bueno, A., Hedrich, R., Leide, J., et al. (2016). Effectiveness of cuticular transpiration barriers in a desert plant at controlling water loss at high temperatures. *AoB Plants* 8:plw027. doi: 10.1093/aobpla/plw027

Staiger, S., Seufert, P., Arand, K., Burghardt, M., Popp, C., and Riederer, M. (2019). The permeation barrier of plant cuticles: uptake of active ingredients is limited by very long-chain aliphatic rather than cyclic wax compounds. *Pest Manag. Sci.* 75, 3405–3412. doi: 10.1002/ps.5589

Tsubaki, S., Sugimura, K., Teramoto, Y., Yonemori, K., and Azuma, J. I. (2013). Cuticular membrane of Fuyu persimmon fruit is strengthened by triterpenoid nano-fillers. *PLoS One* 8:e75275. doi: 10.1371/journal.pone.0075275

Vogg, G., Fischer, S., Leide, J., Emmanuel, E., Jetter, R., Levy, A. A., et al. (2004). Tomato fruit cuticular waxes and their effects on transpiration barrier properties: functional characterization of a mutant deficient in a very-long-chain fatty acid β-ketoacyl-CoA synthase. *J. Exp. Bot.* 55, 1401–1410. doi: 10.1093/jxb/erh149

Yeats, T., and Rose, J. (2013). The Formation and Function of Plant Cuticles. *Plant Physiol.* 163, 5–20. doi: 10.1104/pp.113.222737

Zeisler, V., and Schreiber, L. (2016). Epicuticular wax on cherry laurel (*Prunus laurocerasus*) leaves does not constitute the cuticular transpiration barrier. *Planta* 243, 65–81. doi: 10.1007/s00425-015-2397-y

Zeisler-Diehl, V., Müller, Y., and Schreiber, L. (2018). Epicuticular wax on leaf cuticles does not establish the transpiration barrier, which is essentially formed by intracuticular wax. *J. Plant Physiol.* 227, 66–74. doi: 10.1016/j.jplph.2018.03.018

Conflict of Interest: The authors declare that the research was conducted in the absence of any commercial or financial relationships that could be construed as a potential conflict of interest.

Publisher's Note: All claims expressed in this article are solely those of the authors and do not necessarily represent those of their affiliated organizations, or those of the publisher, the editors and the reviewers. Any product that may be evaluated in this article, or claim that may be made by its manufacturer, is not guaranteed or endorsed by the publisher.

frontiers in Plant Science

PERSPECTIVE
published: 05 January 2022
doi: 10.3389/fpls.2021.786874

Trafficking Processes and Secretion Pathways Underlying the Formation of Plant Cuticles

*Glenn Philippe[1], Damien De Bellis[2,3], Jocelyn K. C. Rose[1] and Christiane Nawrath[2]**

[1]Plant Biology Section, School of Integrative Plant Science, Cornell University, Ithaca, NY, United States, [2]Department of Plant Molecular Biology, University of Lausanne, Lausanne, Switzerland, [3]Electron Microscopy Facility, University of Lausanne, Lausanne, Switzerland

Cuticles are specialized cell wall structures that form at the surface of terrestrial plant organs. They are largely comprised lipidic compounds and are deposited in the apoplast, external to the polysaccharide-rich primary wall, creating a barrier to diffusion of water and solutes, as well as to environmental factors. The predominant cuticle component is cutin, a polyester that is assembled as a complex matrix, within and on the surface of which aliphatic and aromatic wax molecules accumulate, further modifying its properties. To reach the point of cuticle assembly the different acyl lipid-containing components are first exported from the cell across the plasma membrane and then traffic across the polysaccharide wall. The export of cutin precursors and waxes from the cell is known to involve plasma membrane-localized ATP-binding cassette (ABC) transporters; however, other secretion mechanisms may also contribute. Indeed, extracellular vesiculo-tubular structures have recently been reported in *Arabidopsis thaliana* (Arabidopsis) to be associated with the deposition of suberin, a polyester that is structurally closely related to cutin. Intriguingly, similar membranous structures have been observed in leaves and petals of Arabidopsis, although in lower numbers, but no close association with cutin formation has been identified. The possibility of multiple export mechanisms for cuticular components acting in parallel will be discussed, together with proposals for how cuticle precursors may traverse the polysaccharide cell wall before their assimilation into the cuticle macromolecular architecture.

Keywords: cutin, suberin, cuticle, cell wall, ABC-transporter, secretion, transport, extracellular vesiculo-tubular body

OPEN ACCESS

Edited by:
Eva Domínguez, Institute of Subtropical and Mediterranean Horticulture La Mayora, Spain

Reviewed by:
Agnieszka Zienkiewicz, Nicolaus Copernicus University in Toruń, Poland
Luciana Renna, Michigan State University, United States
Johann Petit, Institut National de la Recherche Agronomique (INRA), France

****Correspondence:***
Christiane Nawrath
christiane.nawrath@unil.ch

Specialty section:
This article was submitted to Plant Physiology, a section of the journal Frontiers in Plant Science

Received: *30 September 2021*
Accepted: *10 November 2021*
Published: *05 January 2022*

Citation:
Philippe G, De Bellis D, Rose JKC and Nawrath C (2022) Trafficking Processes and Secretion Pathways Underlying the Formation of Plant Cuticles. Front. Plant Sci. 12:786874. doi: 10.3389/fpls.2021.786874

INTRODUCTION

During plant organ development, a lipidic, hydrophobic cuticle is deposited on the nascent epidermal surface of the entire embryo (Ingram and Nawrath, 2017; Berhin et al, 2019), where it forms an intimate association with the underlying hydrated polysaccharide cell wall. Cuticle biosynthesis continues during organ expansion and is fine-tuned by developmental signals and environmental conditions to fulfill multiple roles. These include biomechanical support to maintain organ integrity, a barrier that limits the diffusion of a wide range of molecules between epidermal cells and the plant surface, and a layer that prevents organ fusion (Yeats and Rose, 2013; Ingram and Nawrath, 2017). The cuticle of the shoot of a

seedling is maintained on the surface of organs in their primary growth stage during the entire life of the plant (**Figure 1A**), and cuticles can also line internal structures, such as the sub-stomatal chamber and locular cavity of some fruits. In contrast, the cuticle encasing the root of a seedling is shed with the embryonal root cap cell layer after seedling establishment (**Figure 1A**), at which time other extracellular protective structures, including mucilage sheaths, Casparian strips and suberin lamellae, have been formed in different cell types (Berhin et al., 2019).

The most abundant component of the cuticle is the polyester cutin, which is mainly composed of fatty acids C16–C18 in length carrying an oxygen-containing group (hydroxy, epoxy, or carboxy) in the ω or mid-chain positions of the acyl chain. In addition, relatively low amounts of glycerol and hydroxycinnamic acids are often detected as components of the polyester (Fich et al., 2016). Cuticular waxes, composed of very-long chain fatty acids (VLCFA) of C26–C34 and their derivatives (aldehydes, ketones, alcohols, alkanes, and wax esters), and alicyclic compounds

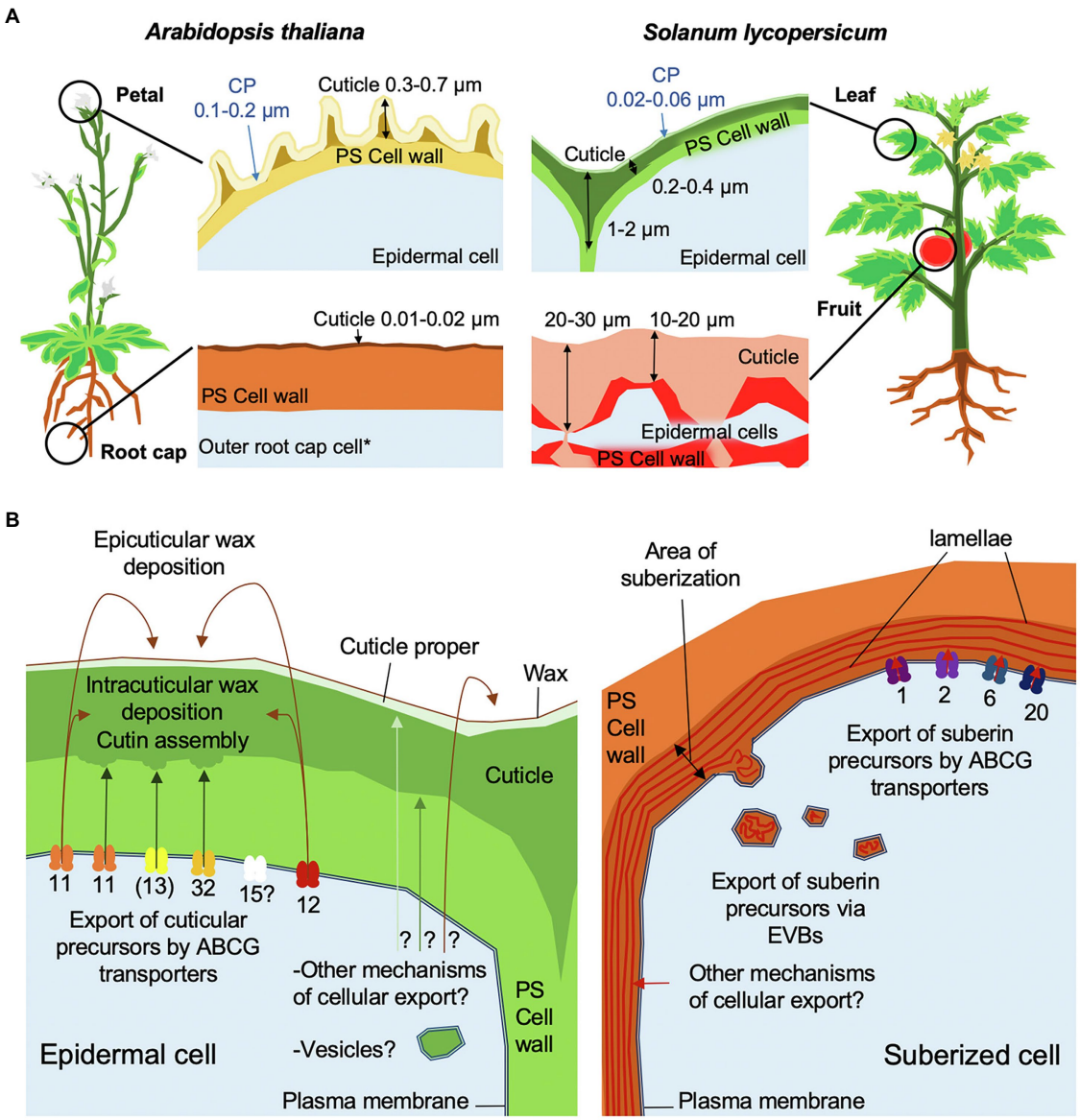

FIGURE 1 | Schematic overview of cuticle assembly. **(A)** Morphologies of cuticles from different organs of tomato and Arabidopsis. Cuticle thickness measurements were based on TEM images from Martin et al. (2017), Mazurek et al. (2017), and Berhin et al. (2019). The cuticle proper (CP) is indicated by blue arrows. *The root cap cuticle is only present on the first outer root cap layer formed during the development of a main root or lateral root. **(B)** Models of cuticle and suberin cellular export and trafficking mechanisms. ABCG transporters are annotated by their respective numbers in Arabidopsis. Brackets indicate that ABCG13 is only involved flowers. Arrows show the trafficking direction of lipidic components to their final destination. Question marks indicate hypothetical mechanisms. Note that LTPs have not been included in this model.

(triterpenoids and flavonoids) impregnate the cutin matrix (intracuticular) or accumulate on the surface (epicuticular), where they may form films or crystal structures, depending on their amount and composition (Jetter et al., 2006; Jetter and Riederer, 2016).

Cutin is assembled in the apoplast from precursors that are generated within the cell (Fich et al., 2016; Philippe et al., 2020b). Hydroxylated fatty acids, synthesized by members of the cytochrome P450 families 77 and 86 are covalently linked to glycerol by glycerol 3-phosphate acyl transferase (GPAT) proteins at the endoplasmic reticulum (ER) membrane, resulting in monoacylglycerols (Gidda et al., 2009; Yang et al., 2012). Several acyl transferases of the BAHD family that are localized in the cytoplasm are also essential for the formation of the cutin polyester: for example, DEFECTIVE IN CUTICULAR RIDGES (DCR) is required for the incorporation of mid-chain oxygenated fatty acids into cutin (Panikashvili et al., 2009; Lashbrooke et al., 2016). In addition, DEFICIENT IN CUTIN FERULATE (DCF), a member of the BAHD family that has acyl-coenzyme A (CoA)-dependent acyl-transferase activity involving ferulic and sinapic acids, incorporates ferulate into cutin (Rautengarten et al., 2012). The formation of adducts with glycerol or other molecules may provide a mechanism to circumvent potential disturbance of membranes caused by free hydroxyacids (Douliez, 2004). Notably, all known cutin precursors are amphiphilic, reflecting the oxygenation of the component fatty acids and the conjugation to hydrophilic compounds (glycerol) or other amphiphilic compounds, such as hydroxycinnamic acids. Cuticular wax components are synthesized at the ER *via* the alkane-forming or alcohol-forming pathways after fatty acid elongation (Lewandowska et al., 2020). Wax molecules, particularly alkanes, are considerably more hydrophobic than cutin precursors.

While the core frameworks of the biosynthetic pathways of cutin and waxes have been generally defined, many questions remain regarding the export mechanisms of the cutin precursors and waxes; the trafficking processes across the hydrated primary cell wall to their point of assembly on the outer face of the wall, and factors that influence the subsequent assembly of the cutin scaffold and associated waxes.

In this article, we discuss the routes of export of cutin precursors and wax components across the plasma membrane (PM) and through the cell wall to their final destination in the cuticle. We compare these processes with the export of precursors of suberin, a polyester that is closely related to cutin, but that is often described as having longer monomer acyl chain lengths (C18–C28) than cutin and a higher content of phenolic compounds. Suberin is deposited in specialized cell types, or in response to tissue damage, often in the form of lamellae that are present between the PM and the bulk of the primary polysaccharide wall. This is a notable difference from cutin, which accumulates on the outer face of the primary wall. The mechanistic or structural basis for the differences in localization of the two polyester types has not yet been elucidated (Philippe et al., 2020b).

EXPORT OF CUTICULAR COMPONENTS BY ABC TRANSPORTERS

In organisms of all kingdoms ABC-transporters, consisting of nucleotide binding domains (NBD) and transmembrane domains (TMD), transport a broad range of molecules with different structure and properties across the PM. Some act as flippases, translocating acyl lipids from one leaflet of the membrane to the other (Lopez-Marques et al., 2015). Reaction mechanisms for binding different types of substrates and for the transport process (import/export/flippase) have been elucidated (Lopez-Marques et al., 2015; Lewinson et al., 2020). The different domains of ABC-transporters may be comprised of separate polypeptide chains, as is typical in bacteria. In eukaryotes, so-called ABC half-transporters, each of which is encoded by a single gene, are composed of one TMD and one NBD. These are thought to require dimerization to form a functional unit. Full ABC transporters, composed of two TMDs and NBDs, are formed by a single polypeptide chain. ABC-transporters in plants can be grouped into eight different families (ABCA–ABCI; ABCH is not found in plants). ABC-transporters of the G-family have the NBD at the N-terminus and the TMD at the C-terminus of the protein. In fungi and plants, in addition to ABCG half-transporters (previously called as WBC transporters), full ABCG transporters (termed Pleiotropic Drug Resistance (PDR)-type ABCG transporters) are also present (Verrier et al., 2008).

ABCG Half-Transporters Are Required for Cuticle Formation

A clade of closely related ABCG half-transporters has been associated with the export of cuticular components (Do et al., 2018), which in Arabidopsis comprises four members: AtABCG11, AtABCG12, AtABCG13, and the currently uncharacterized AtABCG15 (Pighin et al., 2004; Bird et al., 2007; Luo et al., 2007; Ukitsu et al., 2007; Panikashvili et al., 2010, 2011; **Figure 1B**). Notably, a different clade of ABCG half-transporters (AtABCG1, AtABCG2, AtABCG6, and AtABCG20) is involved in the extracellular deposition of suberin (Yadav et al., 2014; Shanmugarajah et al., 2019; **Figure 1B**). AtABCG11 contributes to both wax and cutin export, while AtABCG12 is only required for wax export and AtABCG13 only for cutin precursor export (Pighin et al., 2004; Bird et al., 2007; Panikashvili et al., 2011).

Substrate specificities of ABCG-half transporters seem to be largely dependent on homodimer or heterodimer formation: for example, AtABCG11 forms homodimers and heterodimers with AtABCG12 *in vivo* (Bird, 2008; McFarlane et al., 2010). ABCG11 likely transports cutin precursors as a homodimer that forms with high affinity (Bird et al., 2007). The heterologous expression of AtABCG11 in protoplasts of *Nicotiana benthamiana* was observed to lead to the export of free and glycerol-bound hydroxylated fatty acids, consistent with a role in cutin precursor export (Elejalde-Palmett et al., 2021). Nevertheless, the possibility of heterodimerization with other ABCG half-transporters cannot be excluded. While *AtABCG11*

is expressed in all Arabidopsis organs, *ABCG13* expression is restricted to inflorescences and specific positions in other organs. Whether this specific expression pattern relates to particular cutin precursor export capacities needs further investigation.

PpABCG7, a member of this clade of ABCG half-transporters, is required for wax export in the moss *Physcomitrium* (*Physcomitrella*) *patens* indicating that the role of this ABCG transporter clade has been conserved over at least 450 million years of plant evolution (Buda et al., 2013). ABCG function in the formation of impregnations of the cell wall with lipidic components may have arisen even earlier in various charophyte algal lineages (Kondo et al., 2016; Philippe et al., 2020b). Indeed, *ABCG11* homologues have been identified in extant charophyte algae, the sister lineage of embryophytes, and the size of the family has increased substantially during the emergence and evolution of land plants (Philippe et al., 2020b). This is consistent with the capacity to secrete and assemble hydrophobic cuticles being a prerequisite for plant colonization of truly terrestrial habitats.

ABCG Full-Transporters Export Cutin Precursors

In addition to ABCG half-transporters, ABCG full-transporters play essential roles in cutin precursor export (Bessire et al., 2011; Chen et al., 2011b; Garroum et al., 2016; **Figure 1B**). The downregulation or knockout of *AtABCG32* homologs (named as *ABCG31* in monocots) in rice (*Oryza sativa*) and barley (*Hordeum vulgare*) results in severely impaired cuticle diffusion barrier properties (Chen et al., 2011a,b; Garroum et al., 2016). Additionally, the polysaccharide cell wall-cuticle interface is severely disrupted in the rice mutant (Garroum et al., 2016). In Arabidopsis, which has a cutin composition that is unusually rich in unsaturated dicarboxylic acids, ABCG32 plays a more pronounced role in cuticle formation of organs with a higher proportion of hydroxy acids (Bessire et al., 2011; Fabre et al., 2016). Although *AtABCG32* homologs have been tentatively identified in a few non-vascular plant lineages, it appears that at least one homolog is present in all seed plants (Philippe et al., 2020b). A duplication of *AtABCG32* has been identified in members of the Solanaceae (Elejalde-Palmett et al., 2021); however, whether the two paralogs have evolved different substrate specificities is still an open question. In the tobacco protoplast system, ABCG32 homologs transport oxygenated cutin precursors without selectivity for the structure at the terminal carbons or the mid-chain position, raising the possibility that these proteins may also transport yet uncharacterized cutin precursors (Elejalde-Palmett et al., 2021).

Full ABCG transporters are often expressed in the same organ and developmental stage as the ABCG half-transporters: for example, *AtABCG11*, *AtABCG13*, and *AtABCG32* are all expressed in floral organs. However, single *atabcg* mutants exhibit significant reductions in cutin levels, as well as other specific phenotypes, highlighting their non-redundant functions (Bird, 2008; Bessire et al., 2011; Panikashvili et al., 2011).

An important unanswered question is the mode by which the lipid-derived substrates interact with the ABCG transporters, i.e., as free molecules, as ligand-bound forms, or *via* the PM. This question is particular pertinent for the hydrophobic wax molecules. The export of the amphiphilic cutin precursors can be directly addressed with transport assays using radiolabeled precursors. However, the export of the more hydrophobic wax molecules has not yet been characterized since they partition into membranes *in vitro*. Consequently, there is not yet direct experimental evidence that the ABCG transporter formed by the AtABCG11/AtABCG12 heterodimer exports waxes.

UNDERSTANDING CELLULAR TRAFFICKING OF CUTICLE BUILDING BLOCKS AND AN ASSESSMENT OF ALTERNATIVE EXPORT PATHWAYS

A broad range of cell wall components, including structural proteins and cell wall matrix polysaccharides, such as hemicelluloses and pectins, are secreted *via* the canonical secretory pathway, in which vesicles derived from the trans-Golgi network fuse with the PM and deposit their cargo into the apoplast (Driouich et al., 2012). Lipophilic apoplastic components may follow similar transport pathways, and indeed early histological studies of the root endodermis revealed the presence of vesicles coincident with the deposition of suberin (Scott and Peterson, 1979). Consistent with this idea, the *atmin7* mutant, which is deficient in an ADP-ribosylation factor guanine exchange factor (ARF-GEF) protein, homologs of which function as regulators of the secretion pathway, exhibits reduced cutin deposition (Zhao et al., 2020). Similarly, the Arabidopsis *echidna* mutant, which has perturbed post trans-Golgi network (TGN) formation, shows decreased wax accumulation, although the presence of pleiotropic phenotypes complicates interpretation of these relationships (Gendre et al., 2013).

Besides export through the canonical secretion pathway, cell wall material may also be exported at direct contact sites between the cortical ER and the PM, independent of vesicular traffic (Samuels and McFarlane, 2012). In animal cells too, lipids traffic between the ER and other cell compartments *via* ER contact sites, and such a mechanism might also be used for the transport of cuticular lipids from the ER to the PM (Stefan et al., 2013; Wu et al., 2018).

Recently, a study of suberin formation in the root endodermis of Arabidopsis revealed that membrane-enclosed vesiculo-tubular structures (300–900 nm diameter), so called extracellular vesiculo-tubular bodies (EVBs), are tightly associated with the suberization process (**Figure 1B**; De Bellis et al., 2021). Notably, these EVBs are considerably larger in diameter than the vesicles of the canonical secretion pathway (30–100 nm). Remarkably, despite the resemblance of EVBs to multi-vesicular bodies (MVB), a specialized subset of endosomes that contain membrane-bound intraluminal vesicles, no evidence was found that EVBs are involved in recycling

endosomes or are derived from Golgi vesicles, the trans-Golgi-network (TGN), or vacuoles (De Bellis et al., 2021). Moreover, cryo-fixation procedures reveal that the MVB-like appearance of these structures might be largely due to their swelling upon chemical fixation, and that their *in vivo* appearance is more lens-shaped, containing larger, less fragmented extracellular membrane tubules (De Bellis et al., personal communication). While blocking endosomal trafficking did not interfere with EVB- or suberin formation, blocking ER-to-*cis*-Golgi trafficking, as well as post-TGN secretory trafficking, affected both EVB accumulation and suberin formation, indicating that both early and later secretory pathway are required for EVB formation. The cargo of EVBs is hypothesized to be suberin precursors, since punctate structures of approximately 1 µm diameter, possibly corresponding to EVBs, were stained with the lipid dye fluorol yellow in early suberizing cells (De Bellis et al., 2021). In this context, it has been reported that free polyhydroxy acids form vesicles *in vitro* (Heredia-Guerrero et al., 2008), although it is not known whether suberin precursors, i.e., largely ω-hydroxy and dicarboxylic acids bound to glycerol, spontaneously form vesicles, nor whether such a process occurs *in vivo*. Recently, EVBs have also been reported in suberized bundle sheath cells in maize, further supporting the link between EVBs and suberin formation (Gao et al., 2021). In addition to suberin precursors, the EVB cargo may include enzymes catalyzing suberin formation, polymerization, or a broader collection of cell wall components.

An intriguing question is whether EVBs may also be associated with cutin formation. We addressed this using histological approaches to study tomato (*Solanum lycopersicum*) fruit and Arabidopsis petals, both of which have cutin that is rich in 10, 16 diOH C16:0 acids (Martin and Rose, 2014; Mazurek et al., 2017). In addition to wild-type (WT) Arabidopsis, we examined several mutants that have a reduction in cutin abundance (including in 10,16-diOH C16:0 levels) due to distinct changes in cutin precursor formation (*cyp77a6*, *gpat6*, *dcr* single and double mutants) or a deficiency in ABCG32 (*pec1*) expression (Bessire et al., 2011; Mazurek et al., 2017).

Notably, no EVB-like structures were observed during the expansion phase of WT tomato fruit development, at which point very large amounts of cutin are synthesized and deposited. In Arabidopsis, WT petals only very small EVB-like structures were present (**Figure 2**). However, large EVB-like structures (up to 2,500 nm in diameter), similar to these associated with suberization of Arabidopsis root tissues, were observed in all the investigated cutin-related mutants (Bessire et al., 2011; Mazurek et al., 2017). Interestingly, large EVBs were also seen in WT leaves, which have a cutin composition that it more similar to suberin than is cutin from petals (Nawrath et al., 2013). Nevertheless, in shoots, EVBs were not only specific to epidermal cells, but were also present at the periphery of internal cells, suggesting a role in the formation of multiple specialized cell wall types (**Figure 2**). Furthermore, EVBs in organs of the shoot were present in lower numbers (a maximum of 0.5 EVBs/cell section) than in suberizing root tissues (eight EVBs/cell section; De Bellis et al., 2021). In addition, the size and internal structure of EVBs varied considerably, not only between different genotypes but also between different preparations of sections from the same sample. This raises the question of whether these phenotypic characteristics are not only influenced by cellular metabolism and developmental trajectories, but also by the barrier properties of the cuticle affecting the chemical fixation and embedding procedure. Accordingly, the use of fixation methods that minimize the introduction of artefacts, such as cryo-fixation, will be important for further studies of EVBs in the formation of different cell wall types.

Our observations and published data suggest that EVBs are related to the deposition of suberized cell walls, rather than to the formation of cutin. However, the possibility that they also carry other cargo cannot be excluded (**Figure 1B**).

THE MYSTERIOUS PATH THROUGH THE CELL WALL TO THE SITE OF CUTICLE ASSEMBLY

The mechanism by which cutin precursors traffic from the point of their deposition into the apoplast and then across the highly hydrated primary cell wall to the site of cutin assembly remains a poorly understood aspect of cuticle formation. An earlier suggestion was that lipid-transfer proteins (LTPs), which are small (7–9 kDa) and often abundant extracellular proteins, function as carriers that mediate the transport of cuticular components across the wall (Sterk et al., 1991; Pyee et al., 1994; Hollenbach et al., 1997; Yeats and Rose, 2008; Salminen et al., 2016). Consistent with this model, LTPs have been found to accumulate at the plant surface (Pyee et al., 1994; Yeats et al., 2010). There is also evidence that LTPs play a role in the deposition of cuticular waxes, as evidenced by a reduction in the very long chain fatty acid (VLCFA) content in Arabidopsis LTP mutants (DeBono et al., 2009; Lee et al., 2009; Kim et al., 2012). However, the reported decrease in wax load in the mutants did not exceed 25% and there did not appear to be an effect on the composition or amount of cutin monomers. It is also notable that none of the many cuticle-related mutants that have been identified in a range of plant species to date has been attributed to a defect in a non-anchored LTP protein. Indeed, the energy cost of synthesizing proteins that would act as chaperones and transport cutin and waxes, in the absence of a recycling mechanism, suggests that such a process is unlikely. This would, presumably, particularly be the case with organs that deposit massive cuticles such as fleshy fruits. Thus, LTPs may instead have other roles such as antimicrobial defense and signaling (Bakan et al., 2006; Yeats and Rose, 2008; Salminen et al., 2016; Balmant et al., 2021).

Given the large amounts of material needed to assemble the thick cuticles of some organs, such as tomato and pepper fruit cuticles (>1 mg/cm^{-2} cutin monomers; **Figure 1A**; Graça et al., 2002), we suggest that the movement of cuticular lipids across the apoplast is more likely to be a passive process that avoids

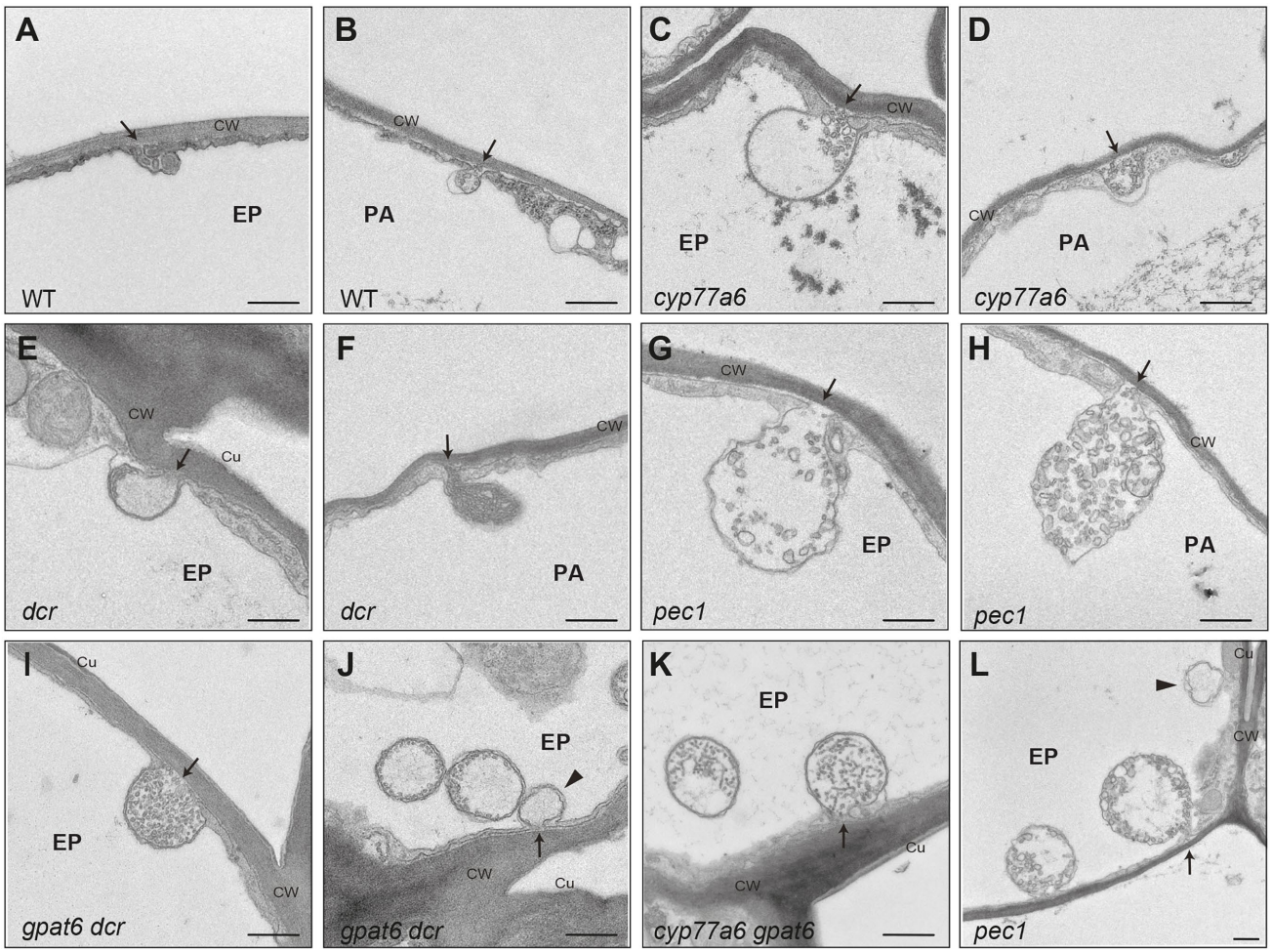

FIGURE 2 | Extracellular vesiculo/tubular bodies in Arabidopsis. Transmission electron micrographs of extracellular vesiculo/tubular bodies (EVBs) visualized in Arabidopsis petals have connections to the cell wall. In addition, similar bodies were seen that were hypothesized to have the cell wall connection in a different plane of section. **(A,B)** Small EVBs in WT; **(C–L)** large EVBs in Arabidopsis cutin mutants. Arrows point to the connection to the cell wall; arrow head points to plasma filled bodies potentially having vesicles in another plane of section; Ep, epidermal cell; pa, parenchyme cell; CW, cell wall; Cu, cuticle. Scale bar represents 500 nm.

investment in metabolically expensive transport proteins (Fich et al., 2016; Philippe et al., 2020b). Such a mechanism would involve the diffusion of amphiphilic cutin precursors and hydrophobic waxes in the hydrophilic environment of the cell wall as a physicochemical phase-separation process. Bakan and Marion (2017) suggested that cutin precursors might aggregate in aqueous environments due to their chemical properties and may be stabilized as lyotropic structures through association with polysaccharides and non-polar waxes (Bakan and Marion, 2017). Indeed, the studies of the behavior of mixtures of cutin fatty acids with pectin *in vitro* have led to the observation of stable aggregation (Guzman-Puyol et al., 2015; Manrich et al., 2017). An early association of cutin precursors with waxes and polysaccharides is consistent with features of maturing cuticles, such as deposition of intracuticular waxes and the embedding of specific polysaccharides within the cuticle characterized by their hydrophobicity (Philippe et al., 2020a). While there is not currently direct evidence of phase separation of cuticle components *in muro*, transmission electron microscopy images of the outer epidermal wall and thick cuticles of tomato fruit often show patches of electron-dense material of increasing size nearer to the wall-cuticle interphase (Girard et al., 2012; Yeats et al., 2012) that are reminiscent of the coalescence of materials of differing hydrophobicity. It may be that a gradient of increasing hydrophobicity provides specific micro-/nano-scale environments for the aggregation of certain wall components, favoring the activities of specific enzymes that catalyze wall assembly. For example, tomato cutin synthase 1 (SlCUS1) was shown to localize in the cuticle and not the primary wall, indicative of the site of cutin polymerization (Girard et al., 2012; Yeats et al., 2012). Interestingly, over-expression of SlCUS1 using a constitutive promoter resulted in the appearance of polymeric cutin in non-epidermal wall layers, suggesting that the polymerizing activity is a limiting factor and that the cutin precursor substrate is mobile and not solely targeted to the organ surface (Yeats et al., 2012). The deposition of cutin in the anticlinal and sub-epidermal

walls observed in some fruits suggests additional complexity in the modes and directionality of the secretion of cuticle components.

Phase separation of cuticle components may also result in compositional heterogeneity within a single cuticle. The cuticle is sometimes broadly described as a bi-layer, comprising an upper stratum, referred to as the 'cuticle proper', overlying the 'cuticle layer', which is thought to be less abundant in waxes but enriched with polysaccharides (**Figure 1A**; Yeats and Rose, 2013; Fernandez et al., 2016). While distinctly demarcated layers are not apparent in microscopic images of some cuticles, and a simple two-layer model may be overly simplistic, trafficking models should accommodate the formation of distinct zones (**Figure 1B**). For example, populations of epicuticular waxes are distinct from those of intracuticular waxes. However, it is not known whether cutin structure on the outer and inner face differ from each other, and new technologies are needed to resolve cuticle architecture at a higher degree of resolution. Regardless, phase separation of cuticular lipids with differing physicochemical properties seems a viable mechanism to both drive deposition of the cuticle and to establish higher order structures within the macromolecular cuticular matrix.

Another mystery is the basis of the different sites of deposition of the structurally related suberin and cutin polyesters, on the inner and outer faces of the polysaccharide wall, respectively (Philippe et al., 2020b). Suberin accumulates immediately after cell export and there is no evidence of diffusion of its precursors. An important factor in this regard may be that suberin has a relatively high phenolic content, which could affect the mobility of its precursors and promote physical associations with lignin, a phenolic polymer that is deposited in cell secondary walls close to the PM (Philippe et al., 2020b). Another feature that may influence the sites of cutinization or suberization is the potential involvement of multiple classes of proteins associated with their coordinated secretion at the PM. For example, it has been reported that membrane-anchored LTPs may be involved in suberin export or deposition, consistent with polymerization immediately after secretion (Deeken et al., 2016; Lee and Suh, 2018). Clearly, much remains to be learnt about this process, and the underlying mechanistic basis and potential differences between the deposition of canonical cutin and suberin, or other structural intermediates, represents an exciting area of future study.

CONCLUSION

Key aspects of transport processes underlying the formation of plant extracellular lipid matrices are slowly coming into focus. This has been enabled by advances in high-resolution imaging, molecular probes and reverse genetic targeting of candidate genes, as well as mutant characterization. However, fundamental questions remain regarding the relationship between composition, architecture and assembly, and the molecular and physicochemical basis for the organization of the cuticle and the cell wall-cuticle continuum is still essentially a blank canvas.

MATERIALS AND METHODS

Transmission Electron Microscopy

Transmission electron micrographs of *A. thaliana* (accession Col) petals were obtained as described previously (Fabre et al., 2016; Mazurek et al., 2017). Micrographs of the areas of interest were taken as tiled scans with a transmission electron microscope JEOL JEM-2100Plus (JEOL Ltd., Akishima, Tokyo, Japan) at an acceleration voltage of 80 kV with a TVIPS TemCamXF416 digital camera (TVIPS GmbH, Gauting, Germany) using the SerialEM software package (Mastronarde, 2005). Tiled scans were aligned with the software IMOD (Kremer et al., 1996).

DATA AVAILABILITY STATEMENT

The raw data supporting the conclusions of this article will be made available by the authors, without undue reservation.

AUTHOR CONTRIBUTIONS

DB did experiments. CN evaluated data. GP, JR, and CN wrote the article. All authors contributed to the article and approved the submitted version.

FUNDING

This work was supported by the Swiss National Science Foundation, Switzerland (grant 31003A-170127 to CN). JR was supported by an award (59-8062-9-003P) from the Agricultural Research Service, and a grant (2020-03667) from the Agriculture and Food Research Initiative, United States Department of Agriculture.

ACKNOWLEDGMENTS

We thank Markus Geisler, Marie Barberon, and Niko Geldner for critically reading the manuscript. We also thank David Domozych (Skidmore College) for his expert guidance with TEM analyses of tomato tissues.

REFERENCES

Bakan, B., Hamberg, M., Perrocheau, L., Maume, D., Rogniaux, H., Tranquet, O., et al. (2006). Specific adduction of plant lipid transfer protein by an allene oxide generated by 9-lipoxygenase and allene oxide synthase. *J. Biol. Chem.* 281, 38981–38988. doi: 10.1074/jbc.M608580200

Bakan, B., and Marion, D. (2017). Assembly of the cutin polyester: from cells to extracellular cell walls. *Plan. Theory* 6:57. doi: 10.3390/plants6040057

Balmant, K. M., Lawrence, S. R. II, Duong, B. V., Zhu, F., Zhu, N., Nicklay, J., et al. (2021). Guard cell redox proteomics reveals a role of lipid transfer protein in plant defense. *J. Proteome* 242:104247. doi: 10.1016/j.jprot.2021.104247

Berhin, A., de Bellis, D., Franke, R. B., Buono, R. A., Nowack, M. K., and Nawrath, C. (2019). The root cap cuticle: a cell wall structure for seedling

establishment and lateral root formation. *Cell* 176, 1367–1378.e8. doi: 10.1016/j.cell.2019.01.005

Bessire, M., Borel, S., Fabre, G., Carraca, L., Efremova, N., Yephremov, A., et al. (2011). A member of the PLEIOTROPIC DRUG RESISTANCE family of ATP binding cassette transporters is required for the formation of a functional cuticle in Arabidopsis. *Plant Cell* 23, 1958–1970. doi: 10.1105/tpc.111.083121

Bird, D. A. (2008). The role of ABC transporters in cuticular lipid secretion. *Plant Sci.* 174, 563–569. doi: 10.1016/j.plantsci.2008.03.016

Bird, D., Beisson, F., Brigham, A., Shin, J., Greer, S., Jetter, R., et al. (2007). Characterization of Arabidopsis ABCG11/WBC11, an ATP binding cassette (ABC) transporter that is required for cuticular lipid secretion. *Plant J.* 52, 485–498. doi: 10.1111/j.1365-313X.2007.03252.x

Buda, G. J., Barnes, W. J., Fich, E. A., Park, S., Yeats, T. H., Zhao, L., et al. (2013). An ATP-binding cassette transporter is required for cuticular wax deposition and desiccation tolerance in the moss *Physcomitrella patens*. *Plant Cell* 25, 4000–4013. doi: 10.1105/tpc.113.117648

Chen, G., Komatsuda, T., Ma, J. F., Li, C., Yamaji, N., and Nevo, E. (2011a). A functional cutin matrix is required for plant protection against water loss. *Plant Signal. Behav.* 6, 1297–1299. doi: 10.4161/psb.6.9.17507

Chen, G., Komatsuda, T., Ma, J. F., Nawrath, C., Pourkheirandish, M., Tagiri, A., et al. (2011b). An ATP-binding cassette subfamily G full transporter is essential for the retention of leaf water in both wild barley and rice. *Proc. Natl. Acad. Sci. U. S. A.* 108, 12354–12359. doi: 10.1073/pnas.1108444108

De Bellis, D., Kalmbach, L., Marhavy, P., Daraspe, J., Geldner, N., and Barberon, M. (2021). Extracellular membrane tubules involved in suberin deposition in plant cell walls. bioRxiv [Preprint]. doi: 10.1101/2021.02.02.429332

DeBono, A., Yeats, T. H., Rose, J. K. C., Bird, D., Jetter, R., Kunst, L., et al. (2009). Arabidopsis LTPG is a glycosylphosphatidylinositol-anchored lipid transfer protein required for export of lipids to the plant surface. *Plant Cell* 21, 1230–1238. doi: 10.1105/tpc.108.064451

Deeken, R., Saupe, S., Klinkenberg, J., Riedel, M., Leide, J., Hedrich, R., et al. (2016). The nonspecific lipid transfer protein AtLTPI-4 is involved in suberin formation of *Arabidopsis thaliana* crown galls. *Plant Physiol.* 172, 1911–1927. doi: 10.1104/pp.16.01486

Do, T. H. T., Martinoia, E., and Lee, Y. (2018). Functions of ABC transporters in plant growth and development. *Curr. Opin. Plant Biol.* 41, 32–38. doi: 10.1016/j.pbi.2017.08.003

Douliez, J. P. (2004). Cutin and suberin monomers are membrane perturbants. *J. Colloid Interf. Sci.* 271, 507–510. doi: 10.1016/j.jcis.2003.12.020

Driouich, A., Follet-Gueye, M. L., Bernard, S., Kousar, S., Chevalier, L., Vicre-Gibouin, M., et al. (2012). Golgi-mediated synthesis and secretion of matrix polysaccharides of the primary cell wall of higher plants. *Front. Plant Sci.* 3:79. doi: 10.3389/fpls.2012.00079

Elejalde-Palmett, C., San Segundo, I. M., Garroum, I., Charrier, L., De Bellis, D., Mucciolo, A., et al. (2021). ABCG transporters export cutin precursors for the formation of the plant cuticle. *Curr. Biol.* 31, 2111–2123.e9. doi: 10.1016/j.cub.2021.02.056

Fabre, G., Garroum, I., Mazurek, S., Daraspe, J., Mucciolo, A., Sankar, M., et al. (2016). The ABCG transporter PEC1/ABCG32 is required for the formation of the developing leaf cuticle in Arabidopsis. *New Phytol.* 209, 192–201. doi: 10.1111/nph.13608

Fernandez, V., Guzman-Delgado, P., Graca, J., Santos, S., and Gil, L. (2016). Cuticle structure in relation to chemical composition: re-assessing the prevailing model. *Front. Plant Sci.* 7:427. doi: 10.3389/fpls.2016.00427

Fich, E. A., Segerson, N. A., and Rose, J. K. C. (2016). The plant polyester cutin: biosynthesis, structure, and biological roles. *Ann. Rev. Plant Biol.* 67, 207–233. doi: 10.1146/annurev-arplant-043015-111929

Gao, P., Wang, P., Du, B., Li, P., and Kang, B.-H. (2021). Accelerated remodeling of the mesophyll-bundle sheath interface in the maize C4 cycle mutant leaves. Research Square [Preprint]. doi: 10.21203/rs.3.rs-442351/v1

Garroum, I., Bidzinski, P., Daraspe, J., Mucciolo, A., Humbel, B. M., Morel, J. B., et al. (2016). Cuticular defects in *Oryza sativa* ATP-binding cassette transporter G31 mutant plants cause dwarfism, elevated defense responses and pathogen resistance. *Plant Cell Physiol.* 57, 1179–1188. doi: 10.1093/pcp/pcw066

Gendre, D., McFarlane, H. E., Johnson, E., Mouille, G., Sjodin, A., Oh, J., et al. (2013). Trans-Golgi network localized ECHIDNA/Ypt interacting protein complex is required for the secretion of cell wall polysaccharides in Arabidopsis. *Plant Cell* 25, 2633–2646. doi: 10.1105/tpc.113.112482

Gidda, S. K., Shockey, J. M., Rothstein, S. J., Dyer, J. M., and Mullen, R. T. (2009). Arabidopsis thaliana GPAT8 and GPAT9 are localized to the ER and possess distinct ER retrieval signals: functional divergence of the dilysine ER retrieval motif in plant cells. *Plant Physiol. Biochem.* 47, 867–879. doi: 10.1016/j.plaphy.2009.05.008

Girard, A.-L., Mounet, F., Lemaire-Chamley, M., Gaillard, C., Elmorjani, K., Vivancos, J., et al. (2012). Tomato GDSL1 is required for cutin deposition in the fruit cuticle. *Plant Cell* 24, 3119–3134. doi: 10.1105/tpc.112.101055

Graça, J., Schreiber, L., Rodrigues, J., and Pereira, H. (2002). Glycerol and glyceryl esters of w-hydroxyacids in cutins. *Phytochemistry* 61, 205–215. doi: 10.1016/S0031-9422(02)00212-1

Guzman-Puyol, S., Benitez, J. J., Dominguez, E., Bayer, I. S., Cingolani, R., Athanassiou, A., et al. (2015). Pectin-lipid self-assembly: influence on the formation of polyhydroxy fatty acids nanoparticles. *PLoS One* 10:e0124639. doi: 10.1371/journal.pone.0124639

Heredia-Guerrero, J. A., Benitez, J. J., and Heredia, A. (2008). Self-assembled polyhydroxy fatty acids vesicles: a mechanism for plant cutin synthesis. *BioEssays* 30, 273–277. doi: 10.1002/bies.20716

Hollenbach, B., Schreiber, L., Hartung, W., and Dietz, K. J. (1997). Cadmium leads to stimulated expression of the lipid transfer protein genes in barley: implications for the involvement of lipid transfer proteins in wax assembly. *Planta* 203, 9–19. doi: 10.1007/s00050159

Ingram, G., and Nawrath, C. (2017). The roles of the cuticle in plant development: organ adhesions and beyond. *J. Exp. Bot.* 68, 5307–5321. doi: 10.1093/jxb/erx313

Jetter, R., Kunst, L., and Samuels, A. L. (2006). "Composition of plant cuticular waxes," in *Biology of the Plant Cuticle*. eds. M. Riederer and C. Müller (Oxford: Blackwell Publishing), 145–181.

Jetter, R., and Riederer, M. (2016). Localization of the transpiration barrier in the epi- and intracuticular waxes of eight plant species: water transport resistances are associated with fatty acyl rather than alicyclic components. *Plant Physiol.* 170, 921–934. doi: 10.1104/pp.15.01699

Kim, H., Lee, S. B., Kim, H. J., Min, M. K., Hwang, I., and Suh, M. C. (2012). Characterization of glycosylphosphatidylinositol-anchored lipid transfer protein 2 (LTPG2) and overlapping function between LTPG/LTPG1 and LTPG2 in cuticular wax export or accumulation in *Arabidopsis thaliana*. *Plant Cell Physiol.* 53, 1391–1403. doi: 10.1093/pcp/pcs083

Kondo, S., Hori, K., Sasaki-Sekimoto, Y., Kobayashi, A., Kato, T., Yuno-Ohta, N., et al. (2016). Primitive extracellular lipid components on the surface of the charophytic alga *Klebsormidium flaccidum* and their possible biosynthetic pathways as deduced from the genome sequence. *Front. Plant Sci.* 7:952. doi: 10.3389/fpls.2016.00952

Kremer, J. R., Mastronarde, D. N., and McIntosh, J. R. (1996). Computer visualization of three-dimensional image data using IMOD. *J. Struct. Biol.* 116, 71–76. doi: 10.1006/jsbi.1996.0013

Lashbrooke, J., Cohen, H., Levy-Samocha, D., Tzfadia, O., Panizel, I., Zeisler, V., et al. (2016). MYB107 and MYB9 homologs regulate suberin deposition in angiosperms. *Plant Cell* 28, 2097–2116. doi: 10.1105/tpc.16.00490

Lee, S. B., Go, Y. S., Bae, H. J., Park, J. H., Cho, S. H., Cho, H. J., et al. (2009). Disruption of glycosylphosphatidylinositol-anchored lipid transfer protein gene altered cuticular lipid composition, increased plastoglobules, and enhanced susceptibility to infection by the fungal pathogen *Alternaria brassicicola*. *Plant Physiol.* 150, 42–54. doi: 10.1104/pp.109.137745

Lee, S. B., and Suh, M. C. (2018). Disruption of glycosylphosphatidylinositol-anchored lipid transfer protein 15 affects seed coat permeability in Arabidopsis. *Plant J.* 96, 1206–1217. doi: 10.1111/tpj.14101

Lewandowska, M., Keyl, A., and Feussner, I. (2020). Wax biosynthesis in response to danger: its regulation upon abiotic and biotic stress. *New Phytol.* 227, 698–713. doi: 10.1111/nph.16571

Lewinson, O., Orelle, C., and Seeger, M. A. (2020). Structures of ABC transporters: handle with care. *FEBS Lett.* 594, 3799–3814. doi: 10.1002/1873-3468.13966

Lopez-Marques, R. L., Poulsen, L. R., Bailly, A., Geisler, M., Pomorski, T. G., and Palmgren, M. G. (2015). Structure and mechanism of ATP-dependent phospholipid transporters. *Biochim. Biophys. Acta* 1850, 461–475. doi: 10.1016/j.bbagen.2014.04.008

Luo, B., Xue, X. Y., Hu, W. L., Wang, L. J., and Chen, X. Y. (2007). An ABC transporter gene of *Arabidopsis thaliana*, *AtWBC11*, is involved in cuticle development and prevention of organ fusion. *Plant Cell Physiol.* 48, 1790–1802. doi: 10.1093/pcp/pcm152

Manrich, A., Moreira, F. K. V., Otoni, C. G., Lorevice, M. V., Martins, M. A., and Mattoso, L. H. C. (2017). Hydrophobic edible films made up of tomato cutin and pectin. *Carbohydr. Polym.* 164, 83–91. doi: 10.1016/j.carbpol.2017.01.075

Martin, L. B. B., and Rose, J. K. C. (2014). There's more than one way to skin a fruit: formation and function of fruit cuticles. *J. Exp. Bot.* 65, 4639–4651. doi: 10.1093/jxb/eru301

Martin, L. B. B., Romero, P., Fich, E. A., Domozych, D. S., and Rose, J. K. C. (2017). Cuticle biosynthesis in tomato leaves is developmentally regulated by abscisic acid. *Plant Phys.* 174, 1348–1398.

Mastronarde, D. N. (2005). Automated electron microscope tomography using robust prediction of specimen movements. *J. Struct. Biol.* 152, 36–51. doi: 10.1016/j.jsb.2005.07.007

Mazurek, S., Garroum, I., Daraspe, J., De Bellis, D., Olsson, V., Mucciolo, A., et al. (2017). Connecting the molecular structure of cutin to ultrastructure and physical properties of the cuticle in petals of *Arabidopsis*. *Plant Physiol.* 173, 1146–1163. doi: 10.1104/pp.16.01637

McFarlane, H. E., Shin, J. J. H., Bird, D. A., and Samuels, A. L. (2010). *Arabidopsis* ABCG transporters, which are required for export of diverse cuticular lipids, dimerize in different combinations. *Plant Cell* 22, 3066–3075. doi: 10.1105/tpc.110.077974

Nawrath, C., Schreiber, L., Franke, R. B., Geldner, N., Reina-Pinto, J. J., and Kunst, L. (2013). Apoplastic diffusion barriers in Arabidopsis. *Arabidopsis Book* 11:e0167. doi: 10.1199/tab.0167

Panikashvili, D., Shi, J. X., Bocobza, S., Franke, R. B., Schreiber, L., and Aharoni, A. (2010). The Arabidopsis DSO/ABCG11 transporter affects cutin metabolism in reproductive organs and suberin in roots. *Mol. Plant* 3, 563–575. doi: 10.1093/mp/ssp103

Panikashvili, D., Shi, J. X., Schreiber, L., and Aharoni, A. (2009). The Arabidopsis *DCR* encoding a soluble BAHD acyltransferase is required for cutin polyester formation and seed hydration properties. *Plant Physiol.* 151, 1773–1789. doi: 10.1104/pp.109.143388

Panikashvili, D., Shi, J. X., Schreiber, L., and Aharoni, A. (2011). The Arabidopsis ABCG13 transporter is required for flower cuticle secretion and patterning of the petal epidermis. *New Phytol.* 190, 113–124. doi: 10.1111/j.1469-8137.2010.03608.x

Philippe, G., Geneix, N., Petit, J., Guillon, F., Sandt, C., Rothan, C., et al. (2020a). Assembly of tomato fruit cuticles: a cross-talk between the cutin polyester and cell wall polysaccharides. *New Phytol.* 226, 809–822. doi: 10.1111/nph.16402

Philippe, G., Sørensen, I., Jiao, C., Sun, X., Fei, Z., Domozych, D. S., et al. (2020b). Cutin and suberin: assembly and origins of specialized lipidic cell wall scaffolds. *Curr. Opin. Plant Biol.* 55, 11–20. doi: 10.1016/j.pbi.2020.01.008

Pighin, J. A., Zheng, H. Q., Balakshin, L. J., Goodman, I. P., Western, T. L., Jetter, R., et al. (2004). Plant cuticular lipid export requires an ABC transporter. *Science* 306, 702–704. doi: 10.1126/science.1102331

Pyee, J., Yu, H. S., and Kolattukudy, P. E. (1994). Identification of a lipid transfer protein as a major protein in the surface wax of broccoli (*Brassica oleracea*) leaves. *Arch. Biochem. Biophys.* 311, 460–468. doi: 10.1006/abbi.1994.1263

Rautengarten, C., Ebert, B., Ouellet, M., Nafisi, M., Baidoo, E. E. K., Benke, P., et al. (2012). The Arabidopsis *DEFICIENT IN CUTIN FERULATE* (*DCF*) encodes a transferase required for feruloylation of ω-hydroxyfatty acids in cutin polyester. *Plant Physiol.* 158, 654–665. doi: 10.1104/pp.111.187187

Salminen, T. A., Blomqvist, K., and Edqvist, J. (2016). Lipid transfer proteins: classification, nomenclature, structure, and function. *Planta* 244, 971–997. doi: 10.1007/s00425-016-2585-4

Samuels, L., and McFarlane, H. E. (2012). Plant cell wall secretion and lipid traffic at membrane contact sites of the cell cortex. *Protoplasma* 249, 19–S23. doi: 10.1007/s00709-011-0345-7

Scott, M. G., and Peterson, R. L. (1979). Root endodermis in *Ranunculus acris*. 2. Histochemistry of the endodermis and the synthesis of phenolic compounds in roots. *Can. J. Bot.* 57, 1063–1077. doi: 10.1139/b79-130

Shanmugarajah, K., Linka, N., Grafe, K., Smits, S. H. J., Weber, A. P. M., Zeier, J., et al. (2019). ABCG1 contributes to suberin formation in *Arabidopsis thaliana* roots. *Sci. Rep.* 9:11381. doi: 10.1038/s41598-019-47916-9

Stefan, C. J., Manford, A. G., and Emr, S. D. (2013). ER-PM connections: sites of information transfer and inter-organelle communication. *Curr. Opin. Cell Biol.* 25, 434–442. doi: 10.1016/j.ceb.2013.02.020

Sterk, P., Booij, H., Schellekens, G. A., Vankammen, A., and Devries, S. C. (1991). Cell-specific expression of the carrot EP2 lipid transfer protein gene. *Plant Cell* 3, 907–921.

Ukitsu, H., Kuromori, T., Toyooka, K., Goto, Y., Matsuoka, K., Sakuradani, E., et al. (2007). Cytological and biochemical analysis of COF1, an Arabidopsis mutant of an ABC transporter gene. *Plant Cell Physiol.* 48, 1524–1533. doi: 10.1093/pcp/pcm139

Verrier, P. J., Bird, D., Buria, B., Dassa, E., Forestier, C., Geisler, M., et al. (2008). Plant ABC proteins - a unified nomenclature and updated inventory. *Trends Plant Sci.* 13, 151–159. doi: 10.1016/j.tplants.2008.02.001

Wu, H. X., Carvalho, P., and Voeltz, G. K. (2018). Here, there, and everywhere: The importance of ER membrane contact sites. *Science* 361:5835. doi: 10.1126/science.aan5835

Yadav, V., Molina, I., Ranathunge, K., Castillo, I. Q., Rothstein, S. J., and Reed, J. W. (2014). ABCG transporters are required for suberin and pollen wall extracellular barriers in Arabidopsis. *Plant Cell* 26, 3569–3588. doi: 10.1105/tpc.114.129049

Yang, W. L., Simpson, J. P., Li-Beisson, Y., Beisson, F., Pollard, M., and Ohlrogge, J. B. (2012). A land-plant-specific glycerol-3-phosphate acyltransferase family in Arabidopsis: substrate specificity, sn-2 preference, and evolution. *Plant Physiol.* 160, 638–652. doi: 10.1104/pp.112.201996

Yeats, T. H., Howe, K. J., Matas, A. J., Buda, G. J., Thannhauser, T. W., and Rose, J. K. C. (2010). Mining the surface proteome of tomato (*Solanum lycopersicum*) fruit for proteins associated with cuticle biogenesis. *J. Exp. Bot.* 61, 3759–3771. doi: 10.1093/jxb/erq194

Yeats, T. H., Martin, L. B. B., Viart, H. M. F., Isaacson, T., He, Y. H., Zhao, L. X., et al. (2012). The identification of cutin synthase: formation of the plant polyester cutin. *Nat. Chem. Biol.* 8, 609–611. doi: 10.1038/nchembio.960

Yeats, T. H., and Rose, J. K. C. (2008). The biochemistry and biology of extracellular plant lipid-transfer proteins (LTPs). *Protein Sci.* 17, 191–198. doi: 10.1110/ps.073300108

Yeats, T. H., and Rose, J. K. C. (2013). The formation and function of plant cuticles. *Plant Physiol.* 163, 5–20. doi: 10.1104/pp.113.222737

Zhao, Z. Z., Yang, X. P., Lu, S. Y., Fan, J. B., Opiyo, S., Yang, P., et al. (2020). Deciphering the novel role of AtMIN7 in cuticle formation and defense against the bacterial pathogen infection. *Int. J. Mol. Sci.* 21:5547. doi: 10.3390/ijms21155547

Conflict of Interest: The authors declare that the research was conducted in the absence of any commercial or financial relationships that could be construed as a potential conflict of interest.

The reviewer JP declared a past co-authorship with the author GP to the handling editor.

Publisher's Note: All claims expressed in this article are solely those of the authors and do not necessarily represent those of their affiliated organizations, or those of the publisher, the editors and the reviewers. Any product that may be evaluated in this article, or claim that may be made by its manufacturer, is not guaranteed or endorsed by the publisher.

frontiers in Plant Science

ORIGINAL RESEARCH
published: 07 January 2022
doi: 10.3389/fpls.2021.807723

The Response of Tomato Fruit Cuticle Membranes Against Heat and Light

José J. Benítez[1], Ana González Moreno[2], Susana Guzmán-Puyol[3], José A. Heredia-Guerrero[3], Antonio Heredia[2] and Eva Domínguez[3]*

[1] Instituto de Ciencia de Materiales de Sevilla, Centro Mixto Consejo Superior de Investigaciones Científicas-Universidad de Sevilla, Seville, Spain, [2] Departamento de Biología Molecular y Bioquímica, Instituto de Hortofruticultura Subtropical y Mediterránea "La Mayora", Universidad de Málaga-Consejo Superior de Investigaciones Científicas, Universidad de Málaga, Málaga, Spain, [3] Departamento de Mejora Genética y Biotecnología, Instituto de Hortofruticultura Subtropical y Mediterránea "La Mayora", Universidad de Málaga-Consejo Superior de Investigaciones Científicas, Estación Experimental La Mayora, Málaga, Spain

Two important biophysical properties, the thermal and UV-Vis screening capacity, of isolated tomato fruit cuticle membranes (CM) have been studied by differential scanning calorimetry (DSC) and UV-Vis spectrometry, respectively. A first order melting, corresponding to waxes, and a second order glass transition (T_g) thermal events have been observed. The glass transition was less defined and displaced toward higher temperatures along the fruit ripening. In immature and mature green fruits, the CM was always in the viscous and more fluid state but, in ripe fruits, daily and seasonal temperature fluctuations may cause the transition between the glassy and viscous states altering the mass transfer between the epidermal plant cells and the environment. CM dewaxing reduced the T_g value, as derived from the role of waxes as fillers. T_g reduction was more intense after polysaccharide removal due to their highly interwoven distribution within the cutin matrix that restricts the chain mobility. Such effect was amplified by the presence of phenolic compounds in ripe cuticle membranes. The structural rigidity induced by phenolics in tomato CMs was directly reflected in their mechanical elastic modulus. The heat capacity (Cp_{rev}) of cuticle membranes was found to depend on the developmental stage of the fruits and was higher in immature and green stages. The average Cp_{rev} value was above the one of air, which confers heat regulation capacity to CM. Cuticle membranes screened the UV-B light by 99% irrespectively the developmental stage of the fruit. As intra and epicuticular waxes contributed very little to the UV screening, this protection capacity is attributed to the absorption by cinnamic acid derivatives. However, the blocking capacity toward UV-A is mainly due to the CM thickness increment during growth and to the absorption by flavone chalconaringenin accumulated during ripening. The build-up of phenolic compounds was found to be an efficient mechanism to regulate both the thermal and UV screening properties of cuticle membranes.

Keywords: tomato fruit cuticle membrane, thermal characterization, UV-Vis screening, heat capacity, glass transition, fruit growth and ripening

OPEN ACCESS

Edited by:
Eduardo A. Ceccarelli, CONICET Instituto de Biología Molecular y Celular de Rosario (IBR), Argentina

Reviewed by:
Moritz Knoche, Leibniz University Hannover, Germany
Nikolai Borisjuk, Huaiyin Normal University, China

****Correspondence:***
José J. Benítez
benitez@icmse.csic.es

Specialty section:
This article was submitted to Plant Physiology, a section of the journal Frontiers in Plant Science

Received: *02 November 2021*
Accepted: *16 December 2021*
Published: *07 January 2022*

Citation:
Benítez JJ, González Moreno A, Guzmán-Puyol S, Heredia-Guerrero JA, Heredia A and Domínguez E (2022) The Response of Tomato Fruit Cuticle Membranes Against Heat and Light. Front. Plant Sci. 12:807723. doi: 10.3389/fpls.2021.807723

INTRODUCTION

The plant cuticle membrane (CM) is a hydrophobic extracellular layer that protects the outermost surface of fruits, leaves, seeds, petals, and green stems from the environment. One of the main functions of CM is to guard the plant against environmental stresses such as harmful irradiation, as well as thermal and mechanical damage and water loss (Domínguez et al., 2011; Heredia-Guerrero et al., 2018). The protective level of the cuticle membrane is conditioned by the amount and assembly of its components, i.e., the polyester cutin matrix, polysaccharides, waxes, and phenolics (López-Casado et al., 2007; Domínguez et al., 2011; Yeats and Rose, 2013). Waxes have been shown to play a major role in the protection against water loss whereas phenolic compounds have proven to be very effective in modulating the mechanical behavior of cuticle membranes (Domínguez et al., 2009; España et al., 2014). Over the last decades, the water permeability and mechanical properties of CMs have been extensively studied (Riederer and Schreiber, 2001; Khanal and Knoche, 2017); however, much less attention has been paid to the analysis of their thermal and UV-Vis screening response and, in particular, to their changes along fruit development.

Though, the structural modifications induced by temperature play a key role in the biophysics of the cuticle membrane, comparatively little work has been done on the thermal characterization of isolated CMs and their components, mostly on tomato fruit (Schreiber and Schönherr, 1990; Luque and Heredia, 1994, 1997; Casado and Heredia, 2001; Matas et al., 2004). Two main thermal events have been reported for isolated CMs, a first order wax melting and second order glass transition. The glass transition (T_g) entails a network relaxation and the appearance of conformational changes and segmental mobility within the biopolymer structure. Such rheological alteration of the cuticle membrane is associated with the modification of mass transfer between the epidermal plant cells and the environment (Schreiber and Schönherr, 1990) with foreseeable physiological and ecological consequences. In this sense, the modulation of T_g can be envisaged as an adaptation mechanism of plants to the environment (Matas et al., 2004).

Most of the research on the interaction of UV-Vis radiation with plant CMs has been concentrated on leaves (see reviews by Kolb and Pfündel, 2005; Pfündel et al., 2006; Karabourniotis et al., 2021). However, much less work has been focused on fruits (Ward and Nussinovitch, 1996; Krauss et al., 1997; Kolb et al., 2003; Solovchenko and Merzlyak, 2003). Excessive exposure, particularly to the higher energy UV component, induces photochemical reactions that may cause damage to proteins and the modification of the enzymatic activity that could have a negative effect on quality parameters such as texture, color and organoleptic and nutritional values of produce (Hollósy, 2002; Karabourniotis et al., 2021). However, under moderate UV exposure, the biosynthesis of flavonoids is stimulated (Awad et al., 2000; Luthria et al., 2006) to the point that UV-A irradiation can be proposed as farming and postharvest treatments to improve the antioxidant level of tomato fruits (Luthria et al., 2006; Dyshlyuk et al., 2020). Benefits of moderate UV exposure in the appearance (coloration) and susceptibility to russeting of apple fruit have also been reported (Khanal et al., 2020). Phenolic (either hydroxycinnamic acid derivatives or flavonoids) have been identified as responsible for the UV screening in fruits (Pfündel et al., 2006). In *V. vinifera berries* and in apple fruit, it has been proposed that their accumulation in the epidermal cells controls the UV screening capacity (Moskowitz and Hrazdina, 1981; Solovchenko and Merzlyak, 2003). Meanwhile, the role of cuticular phenolics seems to be restricted to be a primary shield against UV radiation under low levels of solar exposure, but no data on the characterization and response of isolated tomato fruit cuticle membranes to UV-Vis light have been found in the literature.

In this article, we have addressed the study of the thermal and UV-Vis screening properties of isolated tomato CMs and their changes throughout fruit development to provide new insights to the current knowledge in the field.

MATERIALS AND METHODS

Plant Material and Cuticle Membrane Isolation

Solanum lycopersicum L. "Cascada" plants were grown from seeds treated with a solution of chlorine bleach 50% (v/v) in distilled water, rinsed and incubated in the dark in a moist environment for several days until germination. Seedlings were then transplanted to plug trays containing 85% coconut fiber substrate and 25% plant-nutrient loaded zeolite and grown in an insect-proof glasshouse. At the four true-leaf growth stage, they were transplanted into soil in a multi-tunnel plastic greenhouse with a 0.5 m within-row and 1.5 m between-row spacing. Plants were watered when necessary using a nutrient solution, supported by string and pruned to a single stem. To harvest fruits at specific time-points, flowers were labeled at anthesis and vibrated to ensure fruit set.

Cuticle membranes were enzymatically isolated from tomato fruits at different stages of development following an enzymatic protocol (Petracek and Bukovac, 1995). Tomatoes were halved and immersed in an aqueous solution of a mixture of fungal cellulase (0.2% w/v) and pectinase (2.0% w/v) in sodium citrate buffer (50 mM, pH 3.7) and incubated for a week at 35°C with continuous agitation. Sodium azide (1 mM) was added to the citrate buffer to prevent microbial growth. After this period, flesh tissue could easily be removed. The cuticle membranes, with remnants of internal tissue, were incubated for another week in the enzymatic solution. At this point, the CM apparently did not have any remaining internal tissue debris. Another change in enzymatic solution was carried out then, and the samples incubated for a 3rd week. Cuticle membranes were then visually inspected and, if any residual tissue was still attached, incubated again with fresh enzymatic solution. This procedure was employed to avoid peeling the fruits or any other mechanical practice that could compromise CM's integrity, especially in immature fruits. Samples were then rinsed with distilled water, air dried on a flat Teflon surface, moved to Petri dishes and stored under dry conditions (Domínguez et al., 2008;

España et al., 2014). Waxes were removed by treatment with a hot (∼60°C) mixture of chloroform: methanol (2: 1, v:v) for 2 h. Polysaccharides were eliminated from previously dewaxed cuticle membranes to yield the cutin fraction by refluxing them in a 6 M HCl aqueous solution for 12 h (Matas et al., 2004). The developmental stage of fruits is defined as days after anthesis (daa). Samples were characterized at the hydration degree corresponding to their stabilization at room conditions (typically 20°C and 45% RH).

Infrared Spectroscopy

Attenuated Total Reflection (ATR-FTIR) spectra were obtained using a single reflection ATR accessory (MIRacle ATR, PIKE Technologies, Madison, WI, United States) with a diamond crystal at 45° incidence and coupled to a FT-IR spectrometer (FT/IR-6200, Jasco, Tokyo, Japan). All spectra were acquired with a liquid nitrogen cooled MCT detector in the 4000–6000 cm^{-1} range at 4 cm^{-1} resolution and by accumulating 50 scans. Band area calculation and ATR penetration depth correction were performed using the Jasco SpectraManager software V.2 (Jasco Corporation, Tokyo, Japan). Three samples at each daa stage were analyzed.

Mechanical Characterization

Uniaxial tensile tests were carried out with a Criterion 42 (MTS Systems, Eden Prairie, MN, United States) machine equipped with a low force (10 N) cell. Rectangular uniform pieces (5 mm × 15 mm) were cut and elongated at room conditions using a crosshead speed of 0.2 mm/min with a clamping distance of 7 mm. The Young's modulus (E) was calculated from the maximum slope of the stress-strain curve (typically around 1–2% strain). Ten replicates per specimen were analyzed.

Storage moduli (E′) were obtained at room conditions by Dynamic Mechanical Analysis (DMA) measurements using a Q800 analyzer (TA Instruments, New Castle, DE, United States) in tension mode. In these tests, the sample is stressed with a low amplitude sinusoidal force and the strain response is simultaneously decomposed into an instantaneous in-phase (elastic) and a delayed out-of-phase (viscous) components. The storage modulus (E′) corresponds to the pure elastic response of the sample. Experiments were repeated with five samples at each daa stage. A more detailed description of the procedure is provided elsewhere (Benítez et al., 2021).

Thermal Characterization

Samples for Differential Scanning Calorimetry (DSC) measurements were prepared by stacking punched 4.5 mm Ø discs inside a TZero (TA Instruments, New Castle, DE, United States) aluminum pan covered with a non-hermetic lid. The final sample weight was about 5 mg and was accurately determined for each specimen with 0.01 mg precision. The DSC equipment was a Q-20 (TA Instruments, New Castle, DE, United States) previously calibrated with indium (for temperature and enthalpy) and sapphire (for heat capacity) references. DSC thermograms consisted in a heat-cool-heat cycle from −70 to 100°C at 10°C/min under N_2 flow at 50 mL/min. Glass transition temperature (T_g) values were calculated from the second heating by the inflection method using the in-built TA Instruments Universal Analysis 2000 v. 4.5A software (TA Instruments-Waters LLC). Values were averaged from three measurements. The absence of temperature effects on the T_g was confirmed by the steadiness of values after sample pretreatments up to 150°C.

The heat capacity was obtained by non-isothermal modulated DSC (M-DSC) in the −5 to 55°C range after the DSC heat-cool-heat cycle. In M-DSC, a sine wave temperature signal of ± 1°C amplitude and 120 s period was superimposed to a linear temperature ramp of 1°C/min and the enthalpy variation was recorded. The reversible specific (Cp_{rev}) was calculated at each temperature by dividing the amplitude of the enthalpy variation signal by the sample weight. To minimize the contribution from the aluminum pan, those used for the sample and the reference were selected to differ in less than 0.05 mg. The sample consisted in circular pieces from about 20–25 different fruits, which is considered to be statistically representative, and no measurement repetition was performed.

UV-Vis Spectrometry

UV-Vis spectra were recorded using a Cary 300 (Agilent Technologies, Santa Clara, CA, United States) spectrophotometer equipped with a DRA-CA-30I integrating sphere (Labsphere Inc., North Sutton, NH, United States) and using a 8° wedge to collect the total (diffuse and specular) reflectance. Cuticle membranes were mounted on aluminum mask holders coated with barium sulfate (ODP97, Gigahertz-Optik GmbH, Türkenfeld, Germany) and always irradiated on the outer side, thus resembling the orientation of the fruit with respect to sunlight in nature and to account for the effect of the epicuticular wax layer on the intensity of reflected light. The total transmitted and reflected light intensity were collected in the 200–800 nm range. The absorbance spectrum (A) was obtained according to equation (I) (Solovchenko and Merzlyak, 2003):

$$A = \log((I_O - I_R)/I_T) \quad \text{(I)}$$

where (I_O) is the incident intensity (defined as 100%) and (I_R) and (I_T) the percentages of reflected and transmitted light at each wavelength, respectively.

Reflectance in a given region is defined as:

$$R = 100 - RT_{avg} \quad \text{(II)}$$

where RT_{avg} is the average of total reflectance values (as percentage) in that region. Analogously, the blockage is calculated by:

$$\text{Blockage} = 100 - TT_{avg} \quad \text{(III)}$$

where TT_{avg} is the average of total transmittance values (in percentage) in the defined region.

Statistical Analysis

Data are expressed as mean ± 1 SE and significance was determined by one-way ANOVA. Pearson's correlation analysis was performed using OriginPro, Version 2019 software

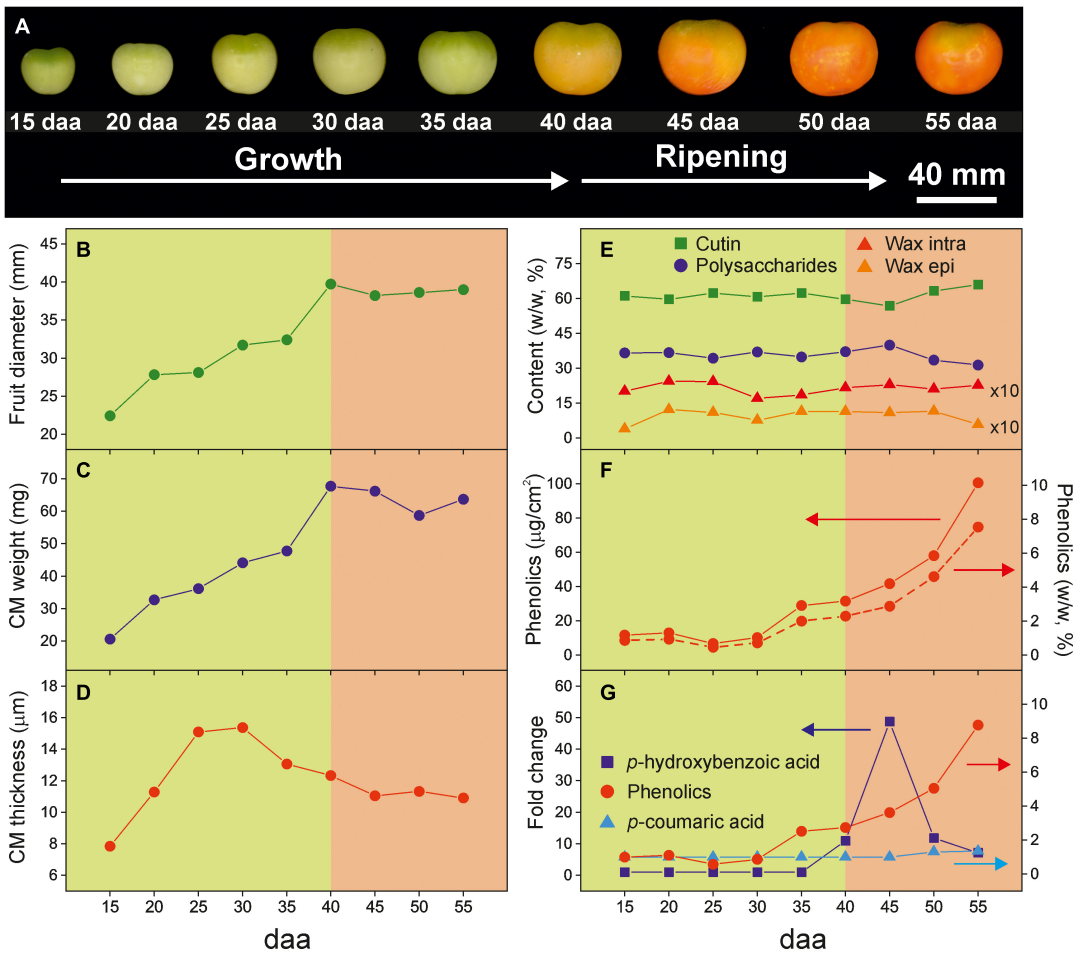

FIGURE 1 | (A) Visual aspect and parameters modification along tomato fruit growth and ripening [**(B)** fruit diameter, **(C)** CM weight, **(D)** CM average thickness, **(E)** CM composition, **(F)** phenolics content and **(G)** relative evolution of hydroxycinnamic acids and total phenolic compounds in the cuticle membrane] (adapted from Domínguez et al., 2008 and España et al., 2014).

(OriginLab Corporation, Northampton, MA, United States). Letters indicate significant differences ($P < 0.05$).

RESULTS

Fruit Development and Physical and Chemical Modification of the Cuticle Membrane

Figure 1 summarizes some of the physical, morphological and chemical modifications in tomato Cascada fruits and their isolated CMs along development. From 15 to 40 daa the fruit experiments a noticeable increment of size (**Figures 1A,B**). Such growth stage is characterized by a predominant green color tone, an increment of CM weight (**Figure 1C**) and thickness (**Figure 1D**) and relatively low phenolics content (**Figure 1F**). Above 40 daa, the fruit size remains constant and the average cuticle membrane thickness decreases slightly. However, this ripening period is characterized by an intense change in color and the accumulation of phenolic compounds in the CM. The overall cuticle membrane composition along the fruit development remains almost unaltered with cutin as the most abundant fraction followed by polysaccharides. Waxes and phenolics are minor components (**Figures 1E,F**). However, in the ripening stage, a small reduction in polysaccharides can be appreciated.

ATR-FTIR Analysis of Isolated Cuticle Membrane and Cutins

Tomato fruit CMs throughout development contain a ∼55–62% w/w of cutin (a fatty polyester matrix) with a 0.4–1.2% w/w and ∼2–2.4% w/w of epicuticular and embedded waxes, respectively, and a variable amount of phenolic compounds (0.3–7% w/w) that strongly increases with ripening (**Figures 1E,F**). They also have an important remnant polysaccharide fraction from the cell walls (31–40% w/w). The presence of such fractions can be detected in the ATR-FTIR spectra. **Figure 2A** shows the 700–1900 cm^{-1} region where characteristic ester bands ν(C=O) at 1731 and 1715 cm^{-1} (hydrogen bonded) as well

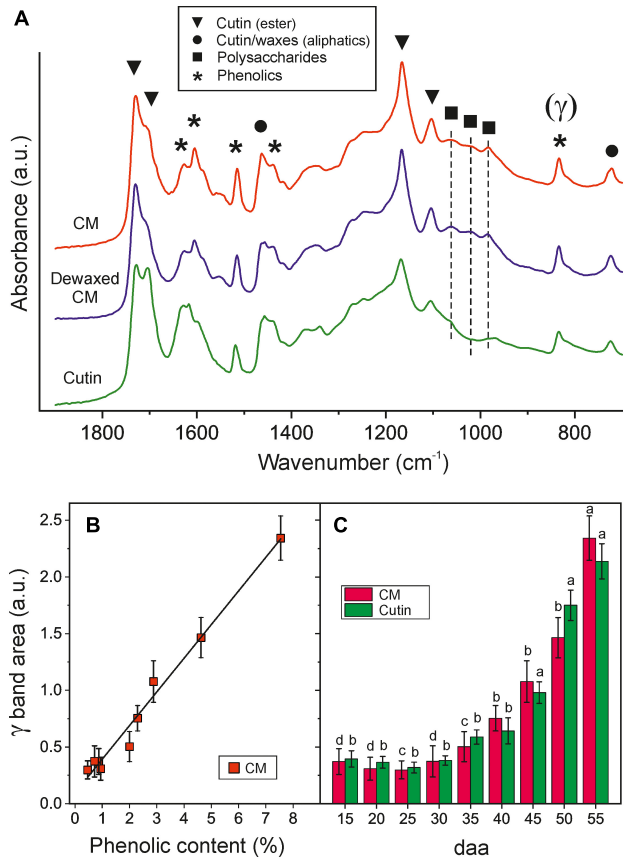

FIGURE 2 | (A) ATR-FTIR spectra of isolated and dewaxed CMs and cutins of ripe tomato fruit. Characteristic bands of cutin, polysaccharides, waxes and phenolics are labeled with symbols. **(B)** Correlation between the phenolics content and the ATR-FTIR γ band area in cuticle membranes. **(C)** Evolution of phenolics content by means of the ATR-FTIR γ band area in tomato CMs and cutins along fruit growth and ripening. Error bars represent ± 1 SE and letters indicate significant differences ($P < 0.05$).

as ν(C-O-C) at 1168 and 1105 cm^{-1} are observed (Heredia-Guerrero et al., 2014). Aliphatic chains in cutin and waxes are characterized by intense peaks at 2926 and 2854 cm^{-1} [$\nu_a(CH_2)$ and $\nu_s(CH_2)$, respectively, not shown] and weaker (CH_2) deflection modes at 1463 (scissoring) and 725 cm^{-1} (rocking). The presence of polysaccharides is revealed by ν(C-O), ν(C-C) and δ(C-O) peaks at 1053, 1034 cm^{-1} and 984 cm^{-1}, corresponding to cellulose, hemicellulose and pectin, respectively (Szymanska-Chargot and Zdunek, 2013). Phenolic compounds are detected by their ν(C=C) (1627 cm^{-1}), ν(C-C) (1605, 1515 and 1436 cm^{-1}) and γ(C-H) (835 cm^{-1}) modes (Ramírez et al., 1992; España et al., 2014).

Cuticle membranes dewaxing has no detectable effect on the ATR-FTIR spectrum, which is consistent with the low wax content. On the other side, polysaccharide removal is evident from the intense reduction of bands at 1053 and 984 cm^{-1} and the elimination of the 1034 cm^{-1} peak in cutins. Bands corresponding to phenolics remain unaltered, which suggests that embedded phenolics withstand both the organic solvent extraction and the polysaccharide hydrolysis. The normalized γ band area at 835 cm^{-1} has proven to be an accurate parameter to quantify the amount of phenolics *in situ* with no need for CM processing and depolymerization (**Figure 2B**). Accordingly, ATR-FTIR data confirmed the intense accumulation of phenolics in the ripening stage (40–55 daa) and their affinity for the cutin matrix (**Figure 2C**).

Differential Scanning Calorimetry of Tomato Cuticle Membranes and Cutins

Figure 3 shows the DSC thermograms of isolated CMs as well as those after dewaxing and polysaccharide removal (cutin) for immature green (20 daa) (**Figure 3A**) and red ripe (55 daa) (**Figure 3B**) tomato fruits. The full thermogram series are compiled in **Supplementary Figure 1**. As observed, the main thermal event is the second-order transition from a rigid glassy state to a more relaxed and dynamic rubbery conformation (T_g). Such glass transition is characteristic for amorphous polymers and displays a sharp profile in immature and mature green CMs. The glass transition becomes systematically broader, less defined and displaced toward higher temperature while ripening. Dewaxing has virtually no effect on T_g values of CMs, however, the removal of polysaccharides significantly diminishes the T_g of the cutin fraction. In addition to the glass transition, in isolated cuticle membranes, a weak endothermic peak around 55°C caused by the melting of the small fraction of intra and epicuticular waxes (∼3% w/w) can be detected. As expected, this melting is absent in dewaxed CMs and in cutins.

The developmental time course of T_g values of CMs, dewaxed CMs and cutins is observed in **Figure 4A**. The plots show the systematic lower values of cutins with respect to CMs and reveal the sharp increment of the glass transition temperature above 35 daa and up to full ripening at 55 daa. The inset (**Figure 4B**), remarks the reduction of T_g (δ T_g) after wax and polysaccharide removal. Such reduction is variable and very low after dewaxing, but very noticeable after polysaccharide removal, particularly during ripening (above 35 daa).

A significant and positive correlation between the areas of the ATR-FTIR γ band, an indicator of phenolic content, and T_g values can be observed for isolated CMs and cutins ($r = 0.978$, $P < 0.01$ and $r = 0.985$, $P < 0.01$, respectively) along fruit development (**Figure 5A**). Such structural rigidity induced by phenolics in tomato cuticle membranes is also reflected in their mechanical response with a positive and significant correlation between the T_g and the **Young's** (E) and storage (E′) moduli ($r = 0.916$, $P < 0.01$ and $r = 0.966$, $P < 0.01$, respectively) (**Figure 5B**).

Reversible Heat Capacity of Tomato Fruit Cuticle Membranes and Cutins

Reversible heat capacity (Cp_{rev}) values versus temperature for isolated tomato CMs and cutins are shown in **Figures 6A,B**, respectively. As observed, the heat capacity grows almost linearly with temperature. The main deviation from this trend is caused by the occurrence of the glass transition within the temperature range analyzed. Deviations are particularly visible

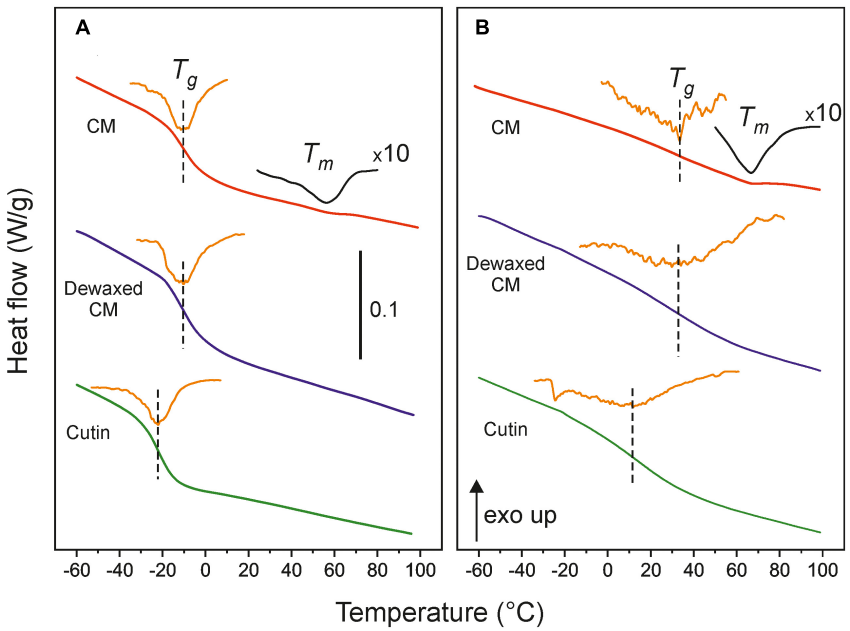

FIGURE 3 | DSC thermograms of isolated and dewaxed cuticle membranes and cutins of **(A)** immature green (20 daa) and **(B)** red ripe (55 daa) tomato fruits. The orange line is the derivative of the heat flow signal and marks the T_g value. For CMs, an expanded heat flow trace (×10) is included to facilitate the visualization of the wax melting peaks. The bar in **(A)** represents a 0.1 W/g heat flow variation.

in CMs because their T_g values are higher than those of the corresponding cutins (**Figure 4**); also in samples where the transition in very sharp, as in 35 and 40 daa CMs and in cutins above 35 daa (see **Supplementary Figure 1**). Additionally, in cuticle membranes and above 50–55°C, the beginning of wax melting causes an increment of heat capacity.

In general, the Cp_{rev} curves displace toward lower values and increment their slope with fruit development. Such effects can be better visualized in **Figures 6C,D**, where the average Cp_{rev} value in the (0 to 50°C) interval and the slope of the curve (αCp_{rev}) above the glass transition are, respectively, plotted versus fruit daa. The (0 to 50°C) interval for average Cp_{rev} calculation has been selected as representative for the temperature range experimented by fruits along growth and ripening.

It is interesting to notice that the average Cp_{rev} of CMs are lower than those of cutins, **Figure 6C**. This is very likely due to the contribution of the polysaccharide fraction of the cuticle membrane, as the heat capacities of cellulose, hemicellulose and pectin are reported to be in the 1.2–1.5 J/g°C range at room temperature (Blokhin et al., 2011; Domínguez et al., 2011; Mohd Rasidek et al., 2018; Qi et al., 2020). Considering an average Cp_{rev} = 1.75 J/g°C for cutin and 1.3 J/g°C for polysaccharides and their relative abundances in CMs (64 and 36%, respectively), the calculated Cp_{rev} for cuticle membranes is 1.59 J/g°C. Thus, polysaccharides cause a theoretical reduction of 0.16 J/g°C in the cutin matrix, quite close to the average 0.12 J/g°C experimental difference observed (**Figure 6C**).

It is also worth noticing that average Cp_{rev} values slightly decrease in the ripening stage. This is partially due to the fact that heat capacity increases noticeably when crossing the glass transition. CMs of immature and mature green fruits in the 0–55°C range are always above their T_g, and, consequently, the contribution of higher Cp_{rev} values is larger than in cuticle membranes of ripe fruits.

UV-Vis Absorption and Blocking Capacity of Tomato Fruit Cuticle Membranes

Figure 7A shows the changes in the total transmittance UV-Vis spectra of tomato CMs during growth and ripening. The shape of the curves resembles the pattern of a selective optical filter with a sharp transition from a low transmission region in the UV to a highly transparent one in the visible range (Krauss et al., 1997; Karabourniotis et al., 2021). The cut-off wavelength progressively displaces during fruit development from about 350 nm for the immature and mature green CMs to 525 m for red ripe ones. The maximum transmittance gradually decreases during the whole 15–55 daa period from about 70 to 53%. Interestingly, a small peak of transmittance was detected around 260 nm, within the UV-C region, that slowly decreased with development.

The UV-Vis blockage capacity of tomato cuticle membranes displays a complex trend with fruit growth and ripening (**Figure 7C**). While the screening against UV-B is extremely high with an average value of 99% for the whole developmental period, a similar level of protection against UV-A is only attained in CMs of breaker and ripe tomatoes (45–55 daa). Although CMs of immature and mature green fruits (15–30 daa) show an average ∼75% UV-A blockage, with a small increase trend, a steep transition from very low to high transmittance was observed for

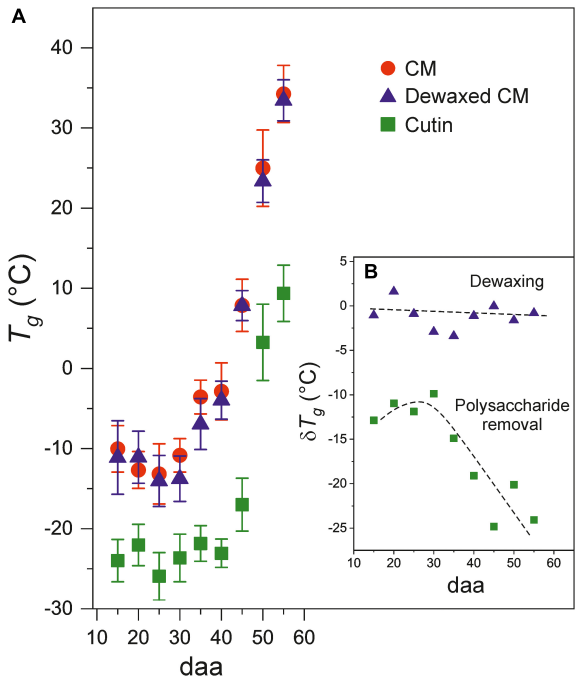

FIGURE 4 | (A) Evolution of T_g for CMs, dewaxed CMs and cutins along fruit development. **(B)** T_g variation (δT_g) after dewaxing (triangles) and polysaccharide removal (squares) from cuticle membranes. Error bars represent ± 1 SE.

these cuticle membranes within the UV-A region (**Figure 7A**). A similar small increase in the Vis blocking is detected within the 15–30 daa period, with a plateau at 35 daa, and a more prominent increase during ripening. CM dewaxing did not have an effect on UV-B blocking at any stage of development and a very minor influence in UV-A blockage. A higher, yet still slight, effect is observed for Vis screening indicating that waxes play a small role in blocking the incident radiation.

The outer surface of tomato CMs shows little reflectance within the UV-B and most of the UV-A regions while it is moderately reflective in the visible range (400–800 nm). Maximum values of total reflectance (RT) ranges from 20 to 45% but without any clear relation with the developmental stage (**Figure 7B**). Reflectance is conditioned by many factors such as the CM surface topography, the total wax content and the structure and composition of the epicuticular wax layer (Vogelmann, 1993; Ward and Nussinovitch, 1996; Petit et al., 2014). A more detailed analysis of the reflectance of tomato CMs as a function of fruit growth and ripening is provided in **Figure 7D**, where values within each spectral region have been averaged. As observed, average reflectance values in the visible region are quite constant (∼30%). However, dewaxing causes an important 35% reduction (values ∼20%), which confirms the important contribution of waxes to the ability of cuticle membranes to reflect visible light. On the other hand, UV reflectance (UV-A + UV-B) is significantly low (∼9%) and wax removal does not have any effect, as reported by Koch and Barthlott (2006).

The absorbance spectra of tomato CMs during fruit development are shown in **Figure 8A**. Peaks detected at 235, 310, and 380 nm are assigned to the π → π*electron transitions in conjugated (C = C) bonds, hydroxycinnamic acid derivatives and flavonoids, respectively (Cockell and Knowland, 1999; Kolb et al., 2003; Pfündel et al., 2006). The absorbance at 380 nm increases with fruit development and significantly and positively correlates ($r = 0.958$, $P < 0.01$) with phenolics accumulation (**Figure 8B**).

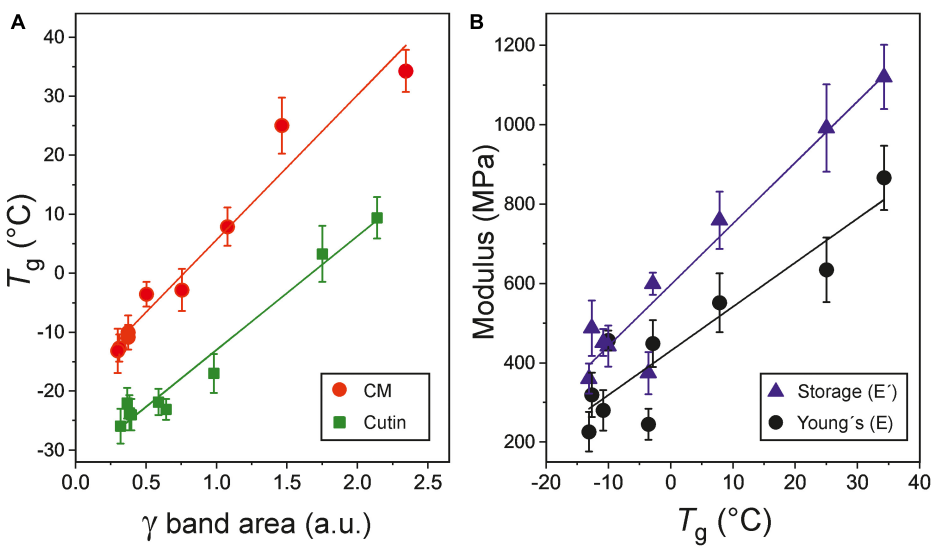

FIGURE 5 | (A) Correlation between the glass transition temperature (T_g) and phenolics content, as monitored by the ATR-FTIR γ band, in CMs and cutins of tomato fruit. **(B)** Direct relationship between the Young's (E) and storage (E′) moduli and the glass transition temperature (T_g) in tomato fruit cuticle membranes. Error bars represent ±1 SE.

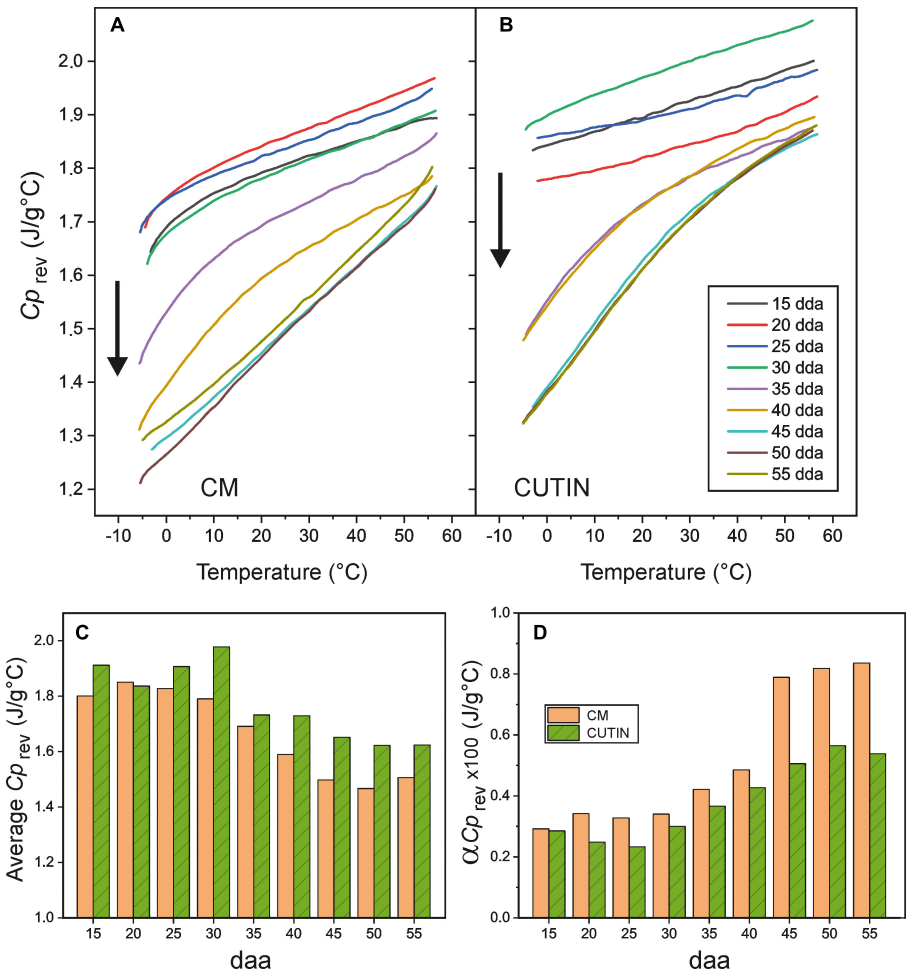

FIGURE 6 | Reversible heat capacity values (Cp_{rev}) for **(A)** cuticle membranes and **(B)** cutins of tomato fruit in the (–5 to 55°C) temperature interval. Arrows highlight the curve evolution with daa time. **(C)** Average heat capacity values in the (0–50°C) interval and **(D)** slope of the linear region of the curves (αCp_{rev}) for CMs and cutins along fruit growth and ripening.

Absorbance at 235 and 310 nm seems to follow an analogous trend though the accuracy of values may be conditioned by difficulties in assessing the base line of spectra and the proximity to band saturation.

DISCUSSION

Phenolic Compounds and Polysaccharides Modulate the Glass Transition Temperature of Tomato Fruit Cuticle Membranes

Differential scanning calorimetry results demonstrate that the glass transition temperature (T_g) of tomato CMs clearly depends on the developmental stage of the fruit. Thus, in immature and mature green fruits, the T_g occurs at temperatures below zero indicating that, during the growing period the cuticle membranes are in a more viscous and fluid state. However, during ripening, the T_g strongly increases to temperatures that reach 20–35°C, well within the average temperature of tomato plant growth. This implies that during daily (and seasonal) fluctuations in temperature, the fruit CM of ripening tomatoes can be oscillating between a rigid and a viscous state. It is well known that water acts as a plasticizer reducing the T_g of a sample. Although the analysis has been carried out with dry samples and, in the fruit, the CM is expected to have a certain degree of hydration, the magnitude of the reported T_g reduction with hydration (Matas et al., 2004) is not expected to alter this conclusion.

Intracuticular waxes have been reported to behave as fillers within the cuticle membrane framework (Luque and Heredia, 1994; Petracek and Bukovac, 1995; Tsubaki et al., 2013). Fillers occupy the space in between chains in the CM structure and reduce the free volume available for motions. Consequently, intracuticular waxes can shift the transition from the glassy to the viscous state to higher temperatures. This is in agreement with the reduction of ~1.5°C in the T_g observed in dewaxed CMs at all stages of development. This is a small reduction in

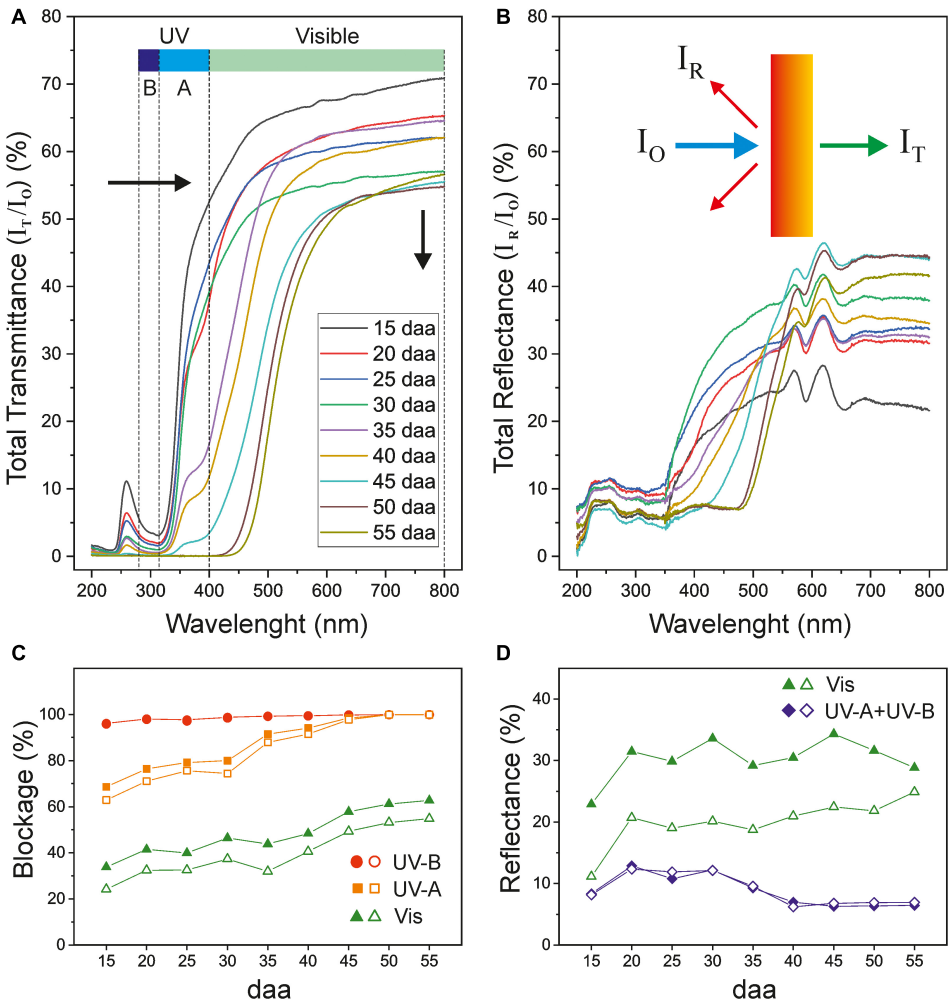

FIGURE 7 | (A) Total transmittance and **(B)** total reflectance spectra of isolated tomato CMs along fruit growth and ripening. Black arrows in **(A)** show the spectra displacement along fruit development. **(C)** Blockage and **(D)** reflectance percentages of UV and visible light of tomato fruit cuticle membranes during growth and ripening. Open symbols correspond to dewaxed CMs.

T_g but it should be taken into account that waxes are minor CM components in tomato (Domínguez et al., 2008). Thus, in species with a higher intracuticular wax load, a more prominent change in T_g could be expected.

Phenolic compounds have also been described as fillers that could explain the increment of T_g in CMs (Luque and Heredia, 1994). Whereas the amount of waxes does not exhibit significant changes during fruit development (**Figure 1E**), this is not the case for phenolic compounds (**Figure 1F**). Tomato fruit cuticle membranes display a low amount of phenolics during most of the growing period that notably increases during ripening reaching a maximum at the red ripe stage. Thus, phenolics would have a minor contribution to the T_g during growth, but play a major role in the dramatic increase of T_g during ripening, as indicated by the linear correlation in **Figure 5A**. However, the role of phenolics does not seem to be merely restricted to fill nanomeric cavities within the cuticle membrane by bonding to free groups in the polymeric framework. Tentatively, they are also involved in bridging polymeric chains as cross-linkers and thus incrementing the elastic modulus (Domínguez et al., 2009; España et al., 2014; Benítez et al., 2021). Such behavior would explain the observed correlation between the glass transition temperature and mechanical elasticity (**Figure 5B**). It is worth mentioning that "rigidity" in terms of restriction to the internal and segmental motions of chains induced by temperature (T_g) is not the same concept as "rigidity" as the structure response to an external mechanical stress (elastic modulus). However, both parameters generally correlate in cross-linked polymers.

The polysaccharide fraction of the cuticle membrane seems to have an important effect on the glass transition since its removal causes a notable decrease in T_g. Thus, during the growing period, when the amount of phenolics is low, the extraction of polysaccharides reduces the T_g value about 11°C (**Figure 4B**). This is compatible with a highly interwoven distribution of polysaccharides within the polyester cutin framework in the CM, giving rise to a closer arrangement

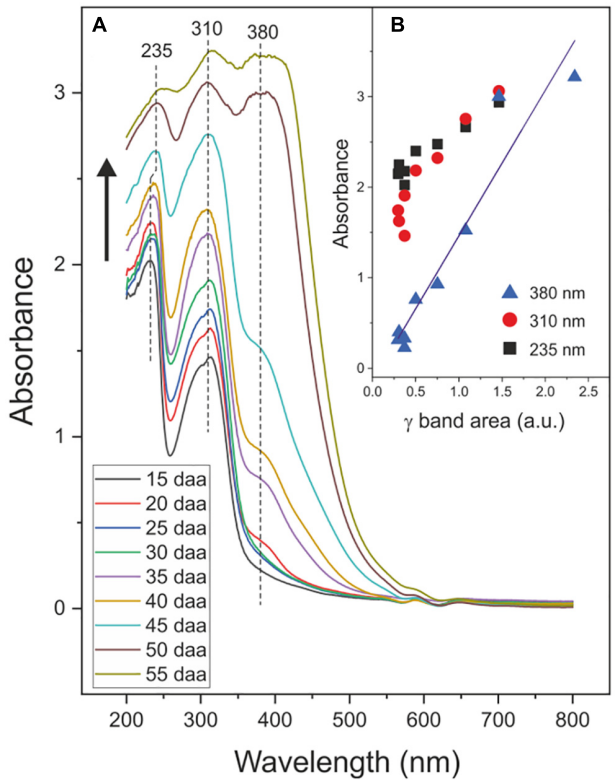

FIGURE 8 | (A) Absorbance spectra of isolated tomato CMs during fruit growth and ripening. Black arrow indicates the evolution of spectra with the developmental stage. **(B)** Relationship between the absorbance at 235, 310, and 380 nm and the phenolic content *via* the quantification of the ATR-FTIR γ band.

of chains that restricts their internal motions. Furthermore, the accumulation of phenolics during ripening notably and progressively increment the T_g reduction after polysaccharide removal (**Figure 4B**), which suggests an enhanced bonding between polysaccharides and cutin phases mediated by phenolic compounds. An analogous model has been proposed to explain the mechanical reinforcement induced by phenolics in tomato fruit cuticle membranes (Benítez et al., 2021). The analysis of the FT-IR data of cutin samples can provide additional support to the hypothesis of a strong binding or interaction between polysaccharides and the cutin polyester matrix. Thus, the ATR-FTIR spectrum of cutin shows the development of a band at 1704 cm^{-1} in parallel to the removal of cellulose, hemicellulose and pectin from the CM (**Figure 2A**). This band can be assigned to new free carboxylic acid groups resulting from the disassembling of polysaccharides. Moreover, ATR-FTIR analysis did not show any detectable degradation of the polyester matrix or loss of the phenolic peaks, an indication that CM dewaxing and polysaccharide removal by hydrolysis are selective and effective treatments. Consequently, the accumulation of phenolics, and their interaction with both the cutin and the polysaccharide fractions, could be a strategy to regulate the transition of cuticle membranes from a rigid to a viscous state and to adapt their rheology to the requirements of fruit development. Therefore, during fruit growth, the CM is always in the viscous state, which facilitates molecular diffusion processes. As the fruit ripens, the transition temperature threshold notably increases and the mass transfer across the CM would be reduced and become highly dependent on the environmental temperature and its daily fluctuations.

The Cuticle Membrane Helps to Regulate the Heat Transference Between the Fruit and the Environment

The heat capacity of tomato CMs within the 5–50°C range is significantly higher than the one of atmospheric air (∼1 J/g°C) (**Figure 6**). This means that under a thermal flux from the external environment, the cuticle membrane is capable to act as a heat sink and to moderate the temperature increment of the internal plant tissues. Though the amount of CM is small if compared with the total mass of the fruit, the thermal regulatory capacity of cuticle membranes may contribute to palliate potential temperature damages to the plant. Interestingly, the average heat capacity of cutins and CMs is reduced during ripening and coinciding with phenolic accumulation (**Figure 6C**). However, such decrease can be compensated with the higher Cp_{rev} increment with temperature (αCp_{rev}), particularly in cuticle membranes (**Figure 6D**). This means that in hot environments, the thermal regulation of ripe fruit CMs reaches similar values to those of immature and mature green ones.

Tomato Fruit Cuticle Membranes Effectively Block UV Radiation by Absorption

The tomato fruit CM prevents most of the harmful UV-B radiation to reach the cell and provides a very efficient barrier that virtually blocks UV-B light. This is in good agreement with the reported literature on the cuticle membrane of woody species (Krauss et al., 1997). Interestingly, this almost complete protection is present from the very early stages of growth. However, the blockage of UV-A is clearly dependent on the stage of development, with CMs from immature green fruits displaying the highest transmittance and a virtually zero transmittance at the red ripe stage. Considering the low reflectance of tomato CMs in the UV region (**Figure 7D**), the blockage capacity in such region has to be ascribed to the absorption by phenolics. However, whereas in the UV-B region the small amount of phenolics present in tomato fruit CMs from early stages of development (España et al., 2014) may be enough for a total reduction of transmittance, this is not the case for the UV-A region of the spectra. Indeed, an increase in UV-A blockage is observed within the 15–30 daa period of development, although the amount of CM phenolics remains relatively constant (España et al., 2014). A more detailed analysis reveals a significant and positive correlation ($r = 0.965$, $P < 0.05$) between the UV-A blockage and the average thickness of the cuticle membrane in the 15–30 daa period (**Supplementary Table 1** and **Supplementary Figure 2**). Hence, it can be concluded that, at low phenolics content, the

modification of the UV-A blockage capacity mainly depends on CM thickness. However, such UV-A blockage-thickness relationship is not reproduced for CMs during ripening since thickness does not increase and yet the blockage is almost 100%. It should be reminded that tomato fruit CMs accumulate the flavonoid chalconaringenin during ripening (España et al., 2014). Whereas cinnamic acids absorb within the UV-B region, flavonoids have been reported to mainly absorb within the UV-A region (Kolb et al., 2003; Pfündel et al., 2006). Therefore, the complete blockage of UV-A observed in CMs from ripening tomato fruits could be attributed to the chalconaringenin accumulated as the tomato changes from mature green to red ripe, and not to the additional increase of cinnamic acid derivatives also observed during ripening (**Figure 1G**). Phenolic compounds have been reported in the epi and intracuticular wax fractions and suggested to play an important role in the optical properties of the cuticle membrane (Karabourniotis and Liakopoulos, 2005). However, it can be concluded that waxes (both intra and epicuticular) contributes very little to the UV screening capacity of tomato fruit CMs, an almost negligible 0.2% in the UV-B region and around a 5% in UV-A at the immature and mature green stages that diminishes as the fruit ripens.

In summary, the tomato fruit cuticle membrane seems to protect the epidermal cells from harmful UV light by a combined strategy of phenolic accumulation and CM thickness modification; with cinnamic acid derivatives protecting from UV-B and CM thickness and chalconaringenin accumulation playing a role in UV-A blockage during fruit growth and ripening, respectively. Therefore, the accumulation of phenolics in the cuticle membrane is a very efficient tool to modulate the amount of UV radiation that reaches the internal tissues and constitutes a strategy of plants to adapt to environmental sunlight levels.

DATA AVAILABILITY STATEMENT

The raw data supporting the conclusions of this article will be made available by the authors, without undue reservation.

AUTHOR CONTRIBUTIONS

JB, ED, and AH conceived and planned the research. JB and AGM performed the experiments. SG-P helped in the analysis of UV-Vis data. JB, JH-G, and ED wrote the article with contributions and supervision of all authors. All authors approved the submitted text.

FUNDING

This work was supported by grant RTI2018-094277-B/AEI/10.13039/501100011033 from Agencia Estatal de Investigación, Ministerio de Ciencia e Innovación, Spain (co-financed by the European Regional Development Fund, ERDF). JH-G acknowledges the support by the Spanish "Ministerio de Ciencia, Innovación y Universidades" project RYC2018-025079-I/AEI/10.13039/501100011033 (co-financed by the European Social Fund, ESF). SG-P thanks the support of the PIE project 202040E003 funded by the Spanish Research Council (CSIC). AGM gratefully acknowledges the MINECO FPU grant (FPU17/01771).

SUPPLEMENTARY MATERIAL

The Supplementary Material for this article can be found online at: https://www.frontiersin.org/articles/10.3389/fpls.2021.807723/full#supplementary-material

REFERENCES

Awad, M. A., de Jager, A., and van Westing, L. M. (2000). Flavonoid and chlorogenic acid levels in apple fruit: characterization of variation. *Sci. Hortic.* 83, 249–263. doi: 10.1016/S0304-4238(99)00124-7

Benítez, J. J., Guzmán-Puyol, S., Vilaplana, F., Heredia-Guerrero, J. A., Domínguez, E., and Heredia, A. (2021). Mechanical performances of isolated cuticles along tomato fruit growth and ripening. *Front. Plant Sci.* 12:787839. doi: 10.3389/fpls.2021.787839

Blokhin, A. V., Voitkevich, O. V., Kabo, G. J., Paulechka, Y. U., Shishonok, M. V., Kabo, A. G., et al. (2011). Thermodynamic properties of plant biomass components. Heat capacity, combustion energy, and gasification equilibria of cellulose. *J. Chem. Eng. Data* 56, 3523–3531. doi: 10.1021/je200270t

Casado, C. G., and Heredia, A. (2001). Specific heat determination of plant barrier lipophilic components: biological implications. *Biochim. Biophys. Acta* 1511, 291–296. doi: 10.1016/S0005-2736(01)00285-1

Cockell, C. S., and Knowland, J. (1999). Ultraviolet radiation screening compounds. *Biol. Rev. Camb. Philos. Soc.* 74, 311–345. doi: 10.1017/s0006323199005356

Domínguez, E., España, L., López-Casado, G., Cuartero, J., and Heredia, A. (2009). Biomechanics of isolated tomato (*Solanum lycopersicum*) fruit cuticles during ripening: the role of flavonoids. *Funct. Plant Biol.* 36, 613–620. doi: 10.1071/FP09039

Domínguez, E., Heredia-Guerrero, J. A., and Heredia, A. (2011). The biophysical design of plant cuticles. *New Phytol.* 189, 938–949. doi: 10.1111/j.1469-8137.2010.03553.x

Domínguez, E., López-Casado, G., Cuartero, J., and Heredia, A. (2008). Development of fruit cuticle in cherry tomato (*Solanum lycopersicum*). *Funct. Plant Biol.* 35, 403–411. doi: 10.1071/FP08018

Dyshlyuk, L., Babich, O., Prosekov, A., Ivanova, S., Pavsky, V., and Chaplygina, T. (2020). The effect of postharvest ultraviolet radiation on the content of antioxidant compounds and the activity of antioxidant enzymes in tomato. *Heliyon* 6:e03288. doi: 10.1016/j.heliyon.2020.e03288

España, L., Heredia-Guerrero, J. A., Segado, P., Benítez, J. J., Heredia, A., and Domínguez, E. (2014). Biomechanical properties of the tomato (*Solanum lycopersicum*) fruit cuticle during development are modulated by changes in the relative amounts of its components. *New Phytol.* 202, 790–802. doi: 10.1111/nph.12727

Heredia-Guerrero, J. A., Benítez, J. J., Domínguez, E., Bayer, I. S., Cingolani, R., Athanassiou, A., et al. (2014). Infrared and Raman spectroscopic features of plant cuticles: a review. *Front. Plant Sci.* 5:305. doi: 10.3389/fpls.2014.00305

Heredia-Guerrero, J. A., Guzman-Puyol, S., Benítez, J. J., Athanassiou, A., Heredia, A., and Domínguez, E. (2018). Plant cuticle under global change: biophysical implications. *Glob. Chang. Biol.* 24, 2749–2751. doi: 10.1111/gcb.14276

Hollósy, F. (2002). Effects of ultraviolet radiation on plant cells. *Micron* 33, 179–197. doi: 10.1016/s0968-4328(01)00011-7

Karabourniotis, G., and Liakopoulos, G. (2005). "Phenolic compounds in plant cuticles: physiological and ecological aspects," in *Advances in Plant Physiology*, Vol. 8, ed. A. Hemantaranjan (Jodhpur: Scientific Publishers), 33–47.

Karabourniotis, G., Liakopoulos, G., Bresta, P., and Nikolopoulos, D. (2021). The optical properties of leaf structural elements and their contribution to photosynthetic performance and photoprotection. *Plants* 10:1455. doi: 10.3390/plants10071455

Khanal, B. P., and Knoche, M. (2017). Mechanical properties of cuticles and their primary determinants. *J. Exp. Bot.* 68, 5351–5367. doi: 10.1093/jxb/erx265

Khanal, B. P., Mekonnen, S. B., and Knoche, M. (2020). Shading affects fracture force and fracture strain of apple fruit skins. *Sci. Hortic.* 274:109651. doi: 10.1016/j.scientia.2020.109651

Koch, K., and Barthlott, W. (2006). Plant epicuticular waxes: chemistry, form, self-assembly and function. *Nat. Prod. Commun.* 1, 1067–1072. doi: 10.1177/1934578X0600101123

Kolb, C. A., Kopeckı, J., Riederer, M., and Pfündel, E. E. (2003). UV screening by phenolics in berries of grapevine (*Vitis vinifera*). *Funct. Plant Biol.* 30, 1177–1186. doi: 10.1071/FP03076

Kolb, C. A., and Pfündel, E. (2005). Origins of non-linear and dissimilar relationships between epidermal UV absorbance and UV absorbance of extracted phenolics in leaves of grapevine and barley. *Plant Cell Environ.* 25, 580–590. doi: 10.1111/j.1365-3040.2005.01302.x

Krauss, P., Markstädter, C., and Riederer, M. (1997). Attenuation of UV radiation by plant cuticles from woody species. *Plant Cell Environ.* 20, 1079–1085. doi: 10.1111/j.1365-3040.1997.tb00684.x

López-Casado, G., Matas, A. J., Domínguez, E., Cuartero, J., and Heredia, A. (2007). Biomechanics of isolated tomato (*Solanum lycopersicum* L.) fruit cuticles: the role of the cutin matrix and polysaccharides. *J. Exp. Bot.* 58, 3875–3883. doi: 10.1093/jxb/erm233

Luque, P., and Heredia, A. (1994). Glassy state in plant cuticles during growth. *Z. Naturforsch. C* 49, 273–275. doi: 10.1515/znc-1994-3-419

Luque, P., and Heredia, A. (1997). The glassy state in isolated cuticles: differential scanning calorimetry of tomato fruit cuticular membranes. *Plant Physiol. Biochem.* 35, 251–256.

Luthria, D. L., Mukhopadhyay, S., and Krizek, D. T. (2006). Content of total phenolics and phenolic acids in tomato (*Lycopersicon esculentum* Mill) fruits as influenced by cultivar and solar UV radiation. *J. Food Compos. Anal.* 19, 771–777. doi: 10.1016/j.jfca.2006.04.005

Matas, A., Cuartero, J., and Heredia, A. (2004). Phase transitions in the biopolyester cutin isolated from tomato fruit cuticles. *Thermochim. Acta* 409, 165–168. doi: 10.1016/S0040-6031(03)00357-5

Mohd Rasidek, N. A., Mad Nordin, M. F., Yusoff, Y. A., Tukuyama, H., and Nagatsu, Y. (2018). Effect of temperature on theology behaviour of banana peel pectin extracted using hot compressed water. *J. Teknol.* 80, 97–103. doi: 10.11113/jt.v80.11467

Moskowitz, A. H., and Hrazdina, G. (1981). Vacuolar contents of fruit subepidermal cells from *Vitis* species. *Plant Physiol.* 68, 686–692. doi: 10.1104/pp.68.3.686

Petit, J., Bres, C., Just, D., Garcia, V., Mauxion, J.-P., Marion, D., et al. (2014). Analyses of tomato fruit brightness mutants uncover both cutin-deficient and cutin-abundant mutants and a new hypomorphic allele of GDSL Lipase. *Plant Physiol.* 164, 888–906. doi: 10.1104/pp.113.232645

Petracek, P. D., and Bukovac, M. J. (1995). Rheological properties of enzymatically isolated tomato fruit cuticle. *Plant Physiol.* 109, 675–679. doi: 10.1104/pp.109.2.675

Pfündel, E. E., Agati, G., and Cerovic, A. G. (2006). "Optical properties of plant surfaces," in *Biology of the Plant Cuticle*, Vol. 23, eds M. Riederer and C. Müler (Oxford: Blackwell), 216–249.

Qi, C., Hou, S., Lu, J., Xue, W., and Sun, K. (2020). Thermal charactgeristics of birch and its cellulose and hemicelluloses isolated by alkaline solution. *Holzforschung* 74, 1099–1112. doi: 10.1515/hf-2019-0285

Ramírez, F. J., Luque, P., Heredia, A., and Bukovac, M. J. (1992). Fourier transform IR of enzymatically isolated tomato cuticular membrane. *Biopolymers* 32, 1425–1429. doi: 10.1002/bip.360321102

Riederer, M., and Schreiber, L. (2001). Protecting against water loss: analysis of the barrier properties of plant cuticles. *J. Exp. Bot.* 52, 2023–2032. doi: 10.1093/jexbot/52.363.2023

Schreiber, L., and Schönherr, J. (1990). Phase transitions and thermal expansion coefficients of plant cuticles. The effects of temperature on structure and function. *Planta* 182, 186–193. doi: 10.1007/BF00197109

Solovchenko, A., and Merzlyak, M. (2003). Optical properties and contribution of cuticle to UV protection in plants: experiments with apple fruit. *Photochem. Photobiol. Sci.* 2, 861–866. doi: 10.1039/b302478d

Szymanska-Chargot, M., and Zdunek, A. (2013). Use of FT-IR spectra and PCA to the bulk characterization of cell wall residues of fruits and vegetables along a fraction process. *Food Biophys.* 8, 29–42. doi: 10.1007/s11483-012-9279-7

Tsubaki, S., Sugimura, K., Teramoto, Y., Yonemori, K., and Azuma, J. (2013). Cuticular membrane of Fuyu Persimon fruit is strengthened by triterpenoid nano-fillers. *PLoS One* 8:e75275. doi: 10.1371/journal.pone.0075275

Vogelmann, T. C. (1993). Plant tissue optics. *Annu. Rev. Plant Physiol. Plant Mol. Biol.* 44, 231–251. doi: 10.1146/annurev.pp.44.060193.001311

Ward, G., and Nussinovitch, A. (1996). Gloss properties and surface morphology relationships of fruits. *J. Food Sci.* 61:973977. doi: 10.1111/j.1365-2621.1996.tb10914.x

Yeats, T. H., and Rose, J. K. C. (2013). The formation and function of plant cuticles. *Plant Physiol.* 163, 5–20. doi: 10.1104/pp.113.222737

Conflict of Interest: The authors declare that the research was conducted in the absence of any commercial or financial relationships that could be construed as a potential conflict of interest.

Publisher's Note: All claims expressed in this article are solely those of the authors and do not necessarily represent those of their affiliated organizations, or those of the publisher, the editors and the reviewers. Any product that may be evaluated in this article, or claim that may be made by its manufacturer, is not guaranteed or endorsed by the publisher.

frontiers in Plant Science

ORIGINAL RESEARCH
published: 24 January 2022
doi: 10.3389/fpls.2021.786933

Minimum Leaf Conductance (g_{min}) Is Higher in the Treeline of *Pinus uncinata* Ram. in the Pyrenees: Michaelis' Hypothesis Revisited

*Amauri Bueno[1†], David Alonso-Forn[2†], José Javier Peguero-Pina[2,3], Aline Xavier de Souza[1], Juan Pedro Ferrio[2,4], Domingo Sancho-Knapik[2,3] and Eustaquio Gil-Pelegrín[2]**

[1] Chair of Botany II – Ecophysiology and Vegetation Ecology, Julius von Sachs Institute of Biological Sciences, University of Würzburg, Würzburg, Germany, [2] Unidad de Recursos Forestales, Centro de Investigación y Tecnología Agroalimentaria de Aragón, Zaragoza, Spain, [3] Instituto Agroalimentario de Aragón -IA2, CITA-Universidad de Zaragoza, Zaragoza, Spain, [4] Aragon Agency for Research and Development (ARAID), Zaragoza, Spain

OPEN ACCESS

Edited by:
Howard Scott Neufeld, Appalachian State University, United States

Reviewed by:
Anna Lintunen, University of Helsinki, Finland
David Rosenthal, Ohio University, United States
Wenzhi Zhao, Northwest Institute of Eco-Environment and Resources, Chinese Academy of Sciences (CAS), China

***Correspondence:**
Eustaquio Gil-Pelegrín
egilp@cita-aragon.es

† These authors have contributed equally to this work

Specialty section:
This article was submitted to Plant Physiology, a section of the journal Frontiers in Plant Science

Received: 30 September 2021
Accepted: 17 December 2021
Published: 24 January 2022

Citation:
Bueno A, Alonso-Forn D, Peguero-Pina JJ, de Souza AX, Ferrio JP, Sancho-Knapik D and Gil-Pelegrín E (2022) Minimum Leaf Conductance (g_{min}) Is Higher in the Treeline of Pinus uncinata Ram. in the Pyrenees: Michaelis' Hypothesis Revisited. Front. Plant Sci. 12:786933. doi: 10.3389/fpls.2021.786933

The search for a universal explanation of the altitudinal limit determined by the alpine treeline has given rise to different hypotheses. In this study, we revisited Michaelis' hypothesis which proposed that an inadequate "ripening" of the cuticle caused a greater transpiration rate during winter in the treeline. However, few studies with different explanations have investigated the role of passive mechanisms of needles for protecting against water loss during winter in conifers at the treeline. To shed light on this, the cuticular transpiration barrier was studied in the transition from subalpine *Pinus uncinata* forests to alpine tundra at the upper limit of the species in the Pyrenees. This upper limit of *P. uncinata* was selected here as an example of the ecotones formed by conifers in the temperate mountains of the northern hemisphere. Our study showed that minimum leaf conductance in needles from upper limit specimens was higher than those measured in specimens living in the lower levels of the sub-alpine forest and also displayed lower cuticle thickness values, which should reinforce the seminal hypothesis by Michaelis. Our study showed clear evidence that supports the inadequate development of needle cuticles as one of the factors that lead to increased transpirational water losses during winter and, consequently, a higher risk of suffering frost drought.

Keywords: cuticular waxes, minimum leaf conductance, Michaelis' hypothesis, treeline, *Pinus uncinata*

INTRODUCTION

The alpine treeline determines the forest altitudinal limit. The transition from the sub-alpine forest to the alpine tundra, also known as the "tension zone" (Griggs, 1934), is formed by the forest mass opening, leading to isolated specimens. These specimens develop forms away from the typical tall, erect timber-sized tree as they approach the altitudinal limit of distribution (Wardle, 1965, 1968). Exposed trees frequently have the characteristic "flagged" crown structure shaped by continual exposure to freezing winds, which becomes progressively more stunted, culminating in prostrate individuals, called Krummholz (Marr, 1977).

The search for a universal explanation of this altitudinal limit for tree occurrence has given rise to different hypotheses, including specific physiological causes associated with the harsh conditions suffered by shoots (see Fernández et al., 2017 and references therein). During winter, the water

uptake is limited by low soil temperatures, while the warm atmosphere and solar radiation increase evaporative demand, producing what is known as "frost drought" (Michaelis, 1934; Tranquillini, 1976; Sakai and Larcher, 1987; Körner, 2012). This water imbalance would promote death by needle desiccation in subalpine conifers. However, this phenomenon is not generally accepted as the leading cause for the existence of the alpine treeline (Mamet and Kershaw, 2013; Nakamoto et al., 2013). When accepted, there is no consensus on the environmental factors and the underlying physiological mechanisms involved, resulting in coexisting different interpretations about the majority presence of dry needles at the end of winter. Mayr et al. (2003, 2006) showed these drought signals as a consequence of frost drought that prevents water uptake and possibly amplified by repeated freeze-thaw cycles that increase the susceptibility of the xylem to embolism. Other studies have emphasized the role of leaf passive mechanisms for protection against desiccation as the thickness of the entire epidermal complex (hypodermis, epidermis, and cuticle) comparing populations with an extreme altitudinal difference (Baig and Tranquillini, 1976). These tools would comprise key factors to understand the recurrence of wilted and brown needles in the treeline specimens. Specifically, the main protective barrier of the leaves is the cuticle, a cutin matrix impregnated and coated with cuticular waxes whose primary function is to prevent uncontrolled water loss (Riederer and Schreiber, 2001; Schuster et al., 2017; Bueno et al., 2019).

The role of the cuticle is critical when stomata remain closed to reduce transpiration, such as during prolonged winter drought, as occurs with evergreen plant species in cold environments. Under these conditions, plant transpiration is determined by water diffusion through passive systems such as the cuticle (Gil-Pelegrín, 1993). Michaelis (1934), who first raised this idea, proposed that an inadequate "ripening" of the cuticle caused the greater transpiration rate during winter in the treeline. This phenomenon would be caused by the shortening of the vegetative period as a result of the temperature reductions at these altitudes. The increased cuticular water loss rate could explain the "frost drought" damage suffered by specimens at the treeline during the winter (Michaelis, 1934). Otherwise, Hadley and Smith (1983, 1986) proposed that the extreme abrasion of the cuticle (e.g., wind blow, ice crystals, or snow) caused the excessive water loss in the treeline more than an inadequate maturation during summer.

Therefore, few studies with different but not excluding explanations have investigated the role of passive needle mechanisms in protecting tree line conifers from winter water loss (Sakai and Larcher, 1987; Körner, 2012). Specifically, there is a lack of studies comparing very precise measurements of cuticular properties and cuticular waxes with minimum needle conductance (g_{min}) in populations with small altitudinal differences. To shed light on this, the cuticular transpiration barrier was studied in the transition from subalpine *Pinus uncinata* forests (thereafter Forest) to alpine tundra at the upper limit of the species in the Pyrenees (thereafter Krummholz). This upper limit of *P. uncinata* was selected here as an example of the ecotones formed by conifers in the temperate mountains of the northern hemisphere.

In this study, we revisited Michaelis' hypothesis (1934) and, thus, tested whether (i) specimens of *P. uncinata* living in the Krummholz display higher values of g_{min} than those specimens living in the Forest and (ii) whether changes in g_{min} between Krummholz and Forest are associated with changes in cuticle thickness and quantitative/qualitative changes in cuticular composition. To test these hypotheses, we have measured g_{min} at 25°C, cuticle thickness, and chemical composition for specimens of *P. uncinata* grown both at the Krummholz and Forest populations.

MATERIALS AND METHODS

Study Site

Twigs of *P. uncinata* were collected on October 30th of 2019 in Sierra de las Cutas (Ordesa y Monte Perdido National Park, Huesca, Spain). The study was carried out in two nearby populations of a *P. uncinata* in the Spanish Pyrenees, the so-called Forest (42°38′10″N, 0°03′07″W, 2,150 m a.s.l.) and Krummholz (42°38′15″ N, 0°03′12″ W, 2,200 m a.s.l.) **Figure 1A**.

Both populations are found on calcareous soil with an average annual precipitation of 1,698 mm and an average winter snow cover of 63.2 cm. Although in the study area the snowfall is assured, there are periods with little snow cover due to the strong wind and continental conditions (see **Supplementary Figure 1A**). The coldest month is February with a minimum average temperature (T_{min}) of −4.8°C and a maximum average temperature (T_{max}) of 3°C; the warmest month is July with a T_{min} of 9.7°C and a T_{max} of 16.8°C (**Figure 1B**). Due to the altitude and soil porosity, the trees of the forest reached 7.6 ± 1.3 m in height and those of Krummholz 0.44 ± 0.01 m at their highest points. Tree height was measured with a Bitterlich relascope.

The analysis of the main climatic parameters that define the study site has been carried out based on the information collected by the Goriz observatory during the years 1981–2018. The refuge, with a slope, aspect and elevation very similar to those of the sampling area, is located at an altitude of 2,215 m a.s.l. on the southern slopes of the Monte Perdido massif located in the Ordesa y Monte Perdido National Park (Serrano-Notivoli et al., 2018).

The specimens selected as models of the typical monopodial bearing of the species were located within the central band of the pine forest that develops on the southern slope of the Sierra de las Cutas. Specifically, south-exposed, current-year needles from the first whorl of branches were sampled in Forest population. The collection of shoots in the Krummholz forms (see **Figure 1C** and **Supplementary Figure 1B**) was carried out in the central part of the tree, avoiding its most peripheral parts, damaged by local factors (permanence of snow and shading, especially).

Minimum Needle Conductance

Five fascicles (two needles per fascicle) per tree from 10 trees were collected in each one of the studied populations and were fully hydrated in a humid chamber overnight before the measurements. The water-saturated weight (SW) was determined for each group of five fascicles using an analytical balance (MC-1 AC210S, Sartorius; precision 0.1 mg), and the dry weight (DW) was obtained after oven drying the samples at 90°C for 24 h. The fresh weights (FW) during needle-drying experiments were

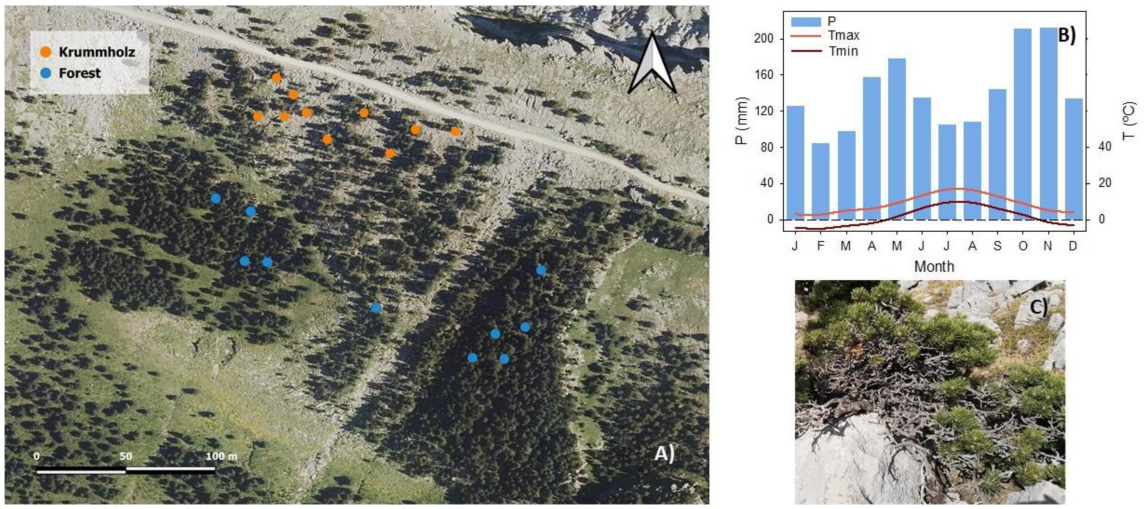

FIGURE 1 | (A) Orthoimage obtained from the Spanish National Plan for Aerial Orthophotography (PNOA) corresponding to the year 2018 of Sierra de Las Cutas in the Spanish Pyrenees. Each point in the image corresponds to an individual (n = 10 per population). **(B)** Climograph of the study site, obtained from the climatic data of the Goriz Refuge located in the Ordesa y Monte Perdido National Park (Huesca, Spain) collected during the years 1981–2018. The monthly average precipitation (P), the monthly average maximum (Tmax), and minimum (Tmin) temperature are shown (Serrano-Notivoli et al., 2018). **(C)** Specimen of *Pinus uncinata* with the characteristic Krummholz mat shape.

used to calculate the relative water deficit (RWD) according to the following:

$$RWD = 1 - \frac{FW - DW}{SW - DW}$$

A flatbed scanner (CanoScan LiDE 120, Canon, Tokyo, Japan) was used to obtain high-resolution images of the needles and using the ImageJ image analysis software (Wayne Rasband/NIH, Bethesda, MD, United States) needle area was measured. Total needle surface area (A_{needle}) was estimated from measurements of needle width (w) and length (l), and it was assumed that this area approximates a semi-cylinder:

$$A_{needle} = \pi \left(\frac{w}{2}\right)^2 + \left(\frac{w}{2}\right) \pi \, l + w \, l$$

Minimum needle conductance (g_{min}) was determined from the consecutive weight loss of desiccating needles in darkness and at close to 0% relative humidity, following the methodology described by Bueno et al. (2020). The same needles used for RWD were used for g_{min} measurement.

g_{min} is the lowest conductance a needle can reach when stomata are maximally closed due to desiccation. Water-saturated needles were sealed with high melting paraffin wax (Paraplast Plus, Leica Biosystems, IL, United States). Subsequently, the sealed needles were placed in a closed container with a temperature of approx. 25°C. The air temperature and humidity were monitored using a digital thermo-hygrometer (Testoterm 6010, Testo, Lenzkirch, Germany). Silica gel (Envirogel, London, United Kingdom) was used to control the moisture, obtaining a relative humidity close to 0%. The weight of desiccating needles was determined as a function of desiccation time using an analytical balance (MC-1 AC210S, Sartorius, Gotinga, Germany; precision 0.1 mg). The transpiration rate (J) was calculated from the change in fresh weight (ΔFW) with time (t) divided by the A_{needle}:

$$J = \frac{\Delta FW}{\Delta t \times A_{needle}}$$

The cuticular water conductance (g) was calculated from the transpiration rate (J) divided by the driving force for water loss from the outer epidermal cell wall to the surrounding atmosphere. The driving force for the vapor-based conductance corresponds to the difference between the saturation concentrations of water vapor at the temperature of the needle ($C_{\text{wv sat needle}}$) and the surrounding atmosphere ($C_{\text{wv sat air}}$) multiplied by the water activity in the epidermal apoplast (α_{apo}) and the atmosphere (α_{air}):

$$g = \frac{J}{\left(\alpha_{apo} \times C_{wv\ sat\ needle}\right) - \left(\alpha_{air} \times C_{wv\ sat\ air}\right)}$$

The water activity of the atmosphere (α_{air}) over silica gel is nearly zero. The water activity in the apoplast adjacent to the inner side of the cuticle (α_{apo}) is assumed to be close to one. Thus, the active driving force for cuticular transpiration in the setup used was the saturation concentration of water vapor at actual needle temperature ($C_{\text{wv sat needle}}$). The corresponding water vapor saturation concentrations at needle temperature were derived from tabulated values (Nobel, 2009). The cuticular water conductance at a given dehydration point was plotted vs. the respective RWD.

Anatomical Measurements

Sections of 1 mm × 1 mm of 6 needles from each population were cut and processed for anatomical measurements as described in

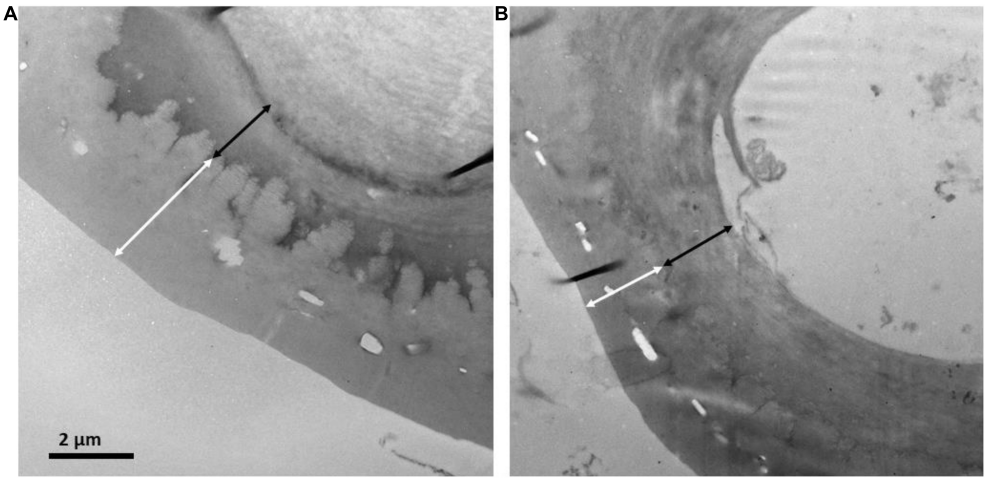

FIGURE 2 | Transmission electron micrographs of the cuticle and outer cell wall for needles of *P. uncinata* grown at **(A)** Forest and **(B)** Krummholz populations. The white arrows represent cuticle thickness and the black arrows represent cell wall thickness.

Peguero-Pina et al. (2016). Semi-thin (0.8 µm) and ultrathin (90 nm) cross-sections were cut with an ultramicrotome (Reichert and Jung model Ultracut E). Semi-thin cross-sections were stained with 1% toluidine blue and viewed under a light microscope (Optika B-600TiFL, Optika Microscopes, Ponteranica, Italy). Ultrathin cross-sections were contrasted with uranyl acetate and lead citrate and viewed under a transmission electron microscope (H600, Hitachi, Tokyo, Japan). Light and electron microscopy images were analyzed with ImageJ software[1] to determine needle anatomical characteristics (**Figure 2**). Light micrographs were used to measure the thickness of the epidermis and hypodermis. Electron micrographs were used to measure the thickness of the cuticle and the outer cell wall of epidermal cells. Each anatomical trait was measured on six different fields of view per section, that is a total of 36 fields of view per population.

Chemical Analyses of Cuticular Waxes

This section is taken *verbatim* from Bueno et al. (2020). Cuticular waxes were extracted by dipping the whole needles twice into trichloromethane (≥99.8%, Roth) at room temperature for 1.5 min. *N*-tetracosane (C_{24}; ≥99.5%, Sigma-Aldrich) was added as an internal standard, and the solutions were reduced to dryness under a gentle flow of nitrogen. Dry cuticular wax samples were derivatized with *N,O*-bis(trimethylsilyl)trifluoroacetamide (BSTFA, Marchery-Nagel) in pyridine (≥99.5%, Roth) at 70°C for 30 min. Quantification of cuticular wax compounds was performed with a gas chromatograph equipped with a flame ionization detector and an on-column injector (7890A, Agilent Technologies). Separation of compounds was carried out on a fused silica capillary column (DB1-ms; 30 m length × 0.32 mm inner diameter, 0.1 µm film thickness, Agilent Technologies) with hydrogen as a carrier gas. The temperature program consisted of injection at 50°C for 2 min, raised by 40°C min^{-1} to 200°C, held at 200°C for 2 min, and then raised by 3°C min^{-1} to 320°C and held at 320°C for 30 min. Qualitative analysis was carried out using a gas chromatograph equipped with a mass spectrometric detector (5975 iMSD, Agilent Technologies) following the same gas chromatographic conditions but using helium as the carrier gas. Cuticular wax compounds were identified by comparing a query mass spectrum with reference mass spectra in a library *via* spectrum matching and quantitated against the internal standard.

[1]http://rsb.info.nih.gov/nih-image/

Statistical Analyses

The normality of data distribution was tested with Shapiro–Wilk test. To check equality of variances we applied Fisher's F-test and the Mann – Whitney U test for those non-normally distributed. Student's *t*-tests were used to compare values of g_{min}, anatomical traits, and cuticular wax composition between Forest and Krummholz populations. g_{min} and anatomical traits means are presented along with their standard error and wax composition mean values are presented along with their standard deviation. All statistical analyses were performed in the R software environment (version 4.0.0, R Core Team, 2020).

RESULTS

The first stage of drying curves for needles of both populations was characterized by high conductance that decreased with leaf dehydration until reaching a plateau of constant needle conductance values (g_{min}), after reaching maximum stomatal closure (**Figure 3**). The value of g_{min} for needles from Krummholz (0.210 ± 0.018 mmol H_2O m^{-2} s^{-1}) was 1.5-fold higher ($p = 0.005$, **Figure 4**) than that measured for Forest needles (0.142 ± 0.012 mmol H_2O m^{-2} s^{-1}).

Regarding anatomical traits, it should be highlighted that cuticle was thicker ($p < 0.001$, **Figures 2**, **5**) in needles from the Forest population (3.62 ± 0.66 µm) in comparison to the Krummholz population (2.87 ± 0.43 µm). By contrast, the thicknesses of the epidermis, hypodermis, and the outer cell

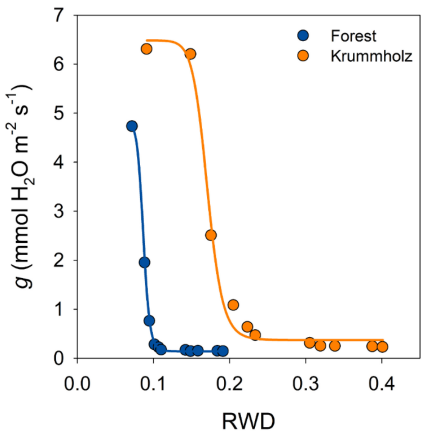

FIGURE 3 | Cuticular water conductance (*g*) as a function of the relative water deficit (RWD) for a single representative tree of each one of the studied populations of *P. uncinata* (Forest and Krummholz). A sigmoidal four-parameter curve is fitted to guide the eye. The transition between the declining stage and the plateau stage of needle conductance represents stomatal closure. After maximum stomatal closure, needle conductance remains constant, representing the minimum needle conductance (g_{min}).

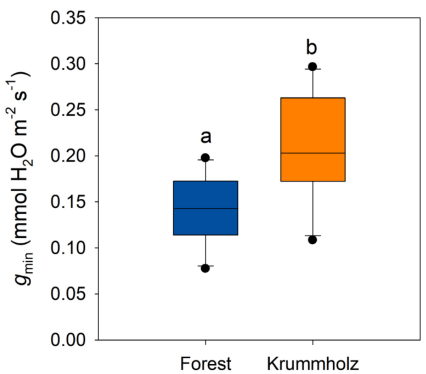

FIGURE 4 | Minimum leaf conductance (g_{min}) for needles of *P. uncinata* grown at Forest and Krummholz populations, obtained from drying curves at 25°C. Different letters indicate statistically significant differences ($p < 0.05$) between both populations.

wall of epidermal cells did not differ between both populations ($p = 0.879$, $p = 0.352$, and $p = 0.802$, respectively, **Figure 5**). Needle length was 5.2 ± 0.2 cm in Forest and 3.1 ± 0.1 cm in Krummholz (data not shown).

The cuticular wax load was higher for needles from Forest (35.2 ± 6.3 μg cm^{-2}) compared with those from Krummholz (22.9 ± 5.1 μg cm^{-2}). Non-acosan-10-ol was the major cuticular wax constituent for both Forest (15.9 ± 3.8 μg cm^{-2}) and Krummholz (9.2 ± 2.3 μg cm^{-2}), values statistically different when compared between populations ($p = 0.017$) (**Figure 6**). Among the other identified compounds, none is exclusive to one population, however, the relative contributions of single compounds in each of the populations do not always follow the same pattern. Thus, long-chain alkanoic acids between C_{28} and C_{32}, heptacosan-10-ol, non-acosan-7,10-ol and non-acosan-10,13-ol abundancy was higher in Forest needles; short-chain alkanoic acids from C_{20} to C_{24} and primary alkanols do not shown differences between populations; and C_{32} methyl ester was more abundant at the Krummholz population (**Figure 6**).

DISCUSSION

Our results demonstrate that the specimens of *P. uncinata* living in the transition with alpine tundra and the upper limit of the species (Krummholz population) displayed higher values of g_{min}, lower values of cuticle thickness and total cuticular wax load than those living in the adjacent subalpine forest. Nonetheless, we still stress that these findings should be interpreted carefully and should not be extrapolated to other plant species and environments since there is strong evidence that g_{min} in some species correlates neither with cuticular wax load nor cuticular thickness (Schreiber and Riederer, 1996; Riederer and Schreiber, 2001; Schuster et al., 2017; Bueno et al., 2020). In addition, it must be taken into account that the values of g_{min} have a great variation and can differ among plant organs or even between the two sides of a single leaf (Diarte et al., 2020; Márquez et al., 2022).

Among the components found in cuticular waxes, non-cacosan-10-ol is the most abundant, being about ten times more abundant than the others (**Figure 6**). Non-acosan-10-ol is the main constituent of the tubular microcrystalline wax aggregates that have been described for the stomatal antechambers of coniferous needles, conferring an additional resistance to stomatal transpiration (Jetter and Riederer, 1994; Dommisse et al., 2007). Thus, this compound would be discarded in the comparison of cuticular waxes strictly related to g_{min}. However, it results in the fact that wax production is generally lower in Krummholz needles.

Michaelis (1934) proposed that a greater residual transpiration rate during winter is produced due to an inadequate maturation of the cuticle in the needles from the treeline. This hypothesis was revisited by Wardle (1974) and Tranquillini (1979), again suggesting this idea as a general cause to explain the existence of an upper treeline. In fact, Baig and Tranquillini (1976) showed that residual transpiration in needles from upper limit specimens of *Pinus cembra* and *Picea abies* was higher than those measured in specimens living in the lower levels of the subalpine forest. In addition, these authors also revealed that the upper limit specimens displayed lower thickness values of the entire epidermal complex (hypodermis, epidermis, and cuticle), which for the cuticle was attributed to a shorter summer developmental time.

We have obtained similar results to those in Baig and Tranquillini (1976) in terms of differences in g_{min} and cuticle thickness, which should reinforce the seminal hypothesis by Michaelis (1934). Further, the contribution of the different wax fractions to the cuticular transpiration barrier of *P. uncinata* is still to be determined. In fact, most of the studies concerning Krummholz physiology at the upper treeline do not confirm Michaelis' hypothesis (Hadley and Smith, 1983, 1986; Grace, 1990). Some of them associated the damage found

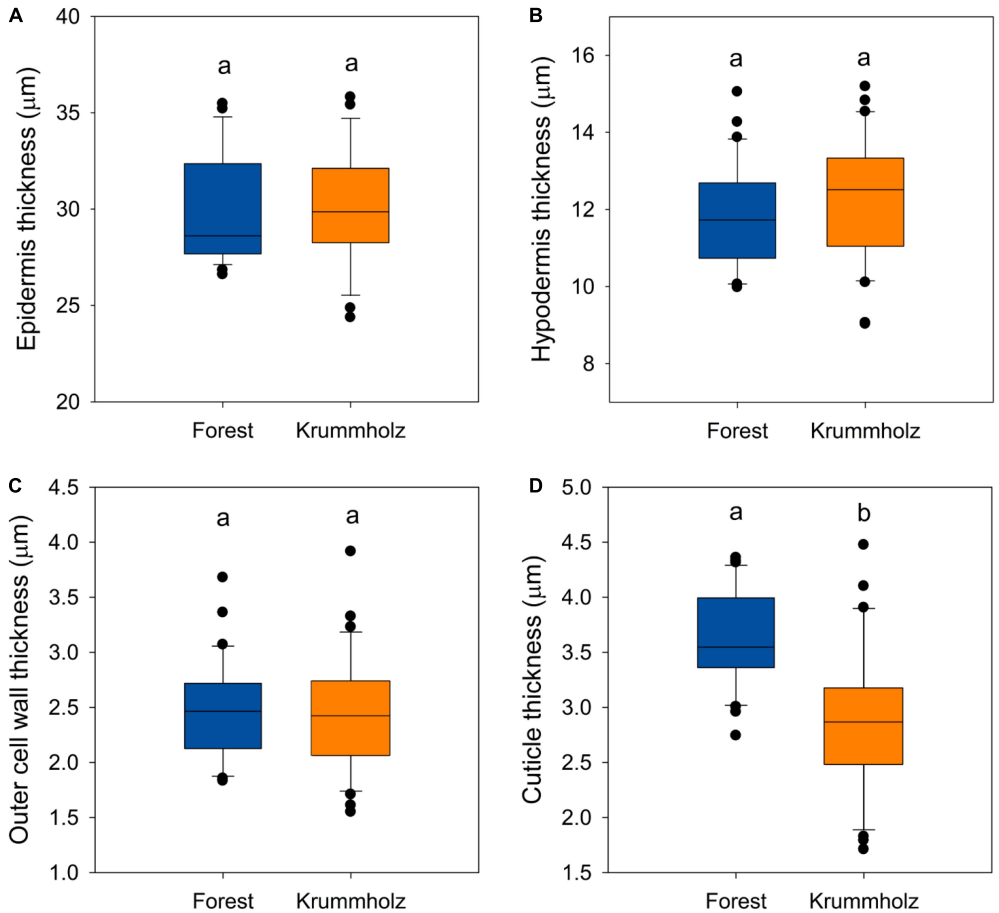

FIGURE 5 | The thickness of the **(A)** epidermis, **(B)** the hypodermis, **(C)** the outer cell wall of the epidermis, and **(D)** the cuticle for needles of *P. uncinata* grown at Forest and Krummholz populations. Different letters indicate statistically significant differences ($p < 0.05$) between both populations.

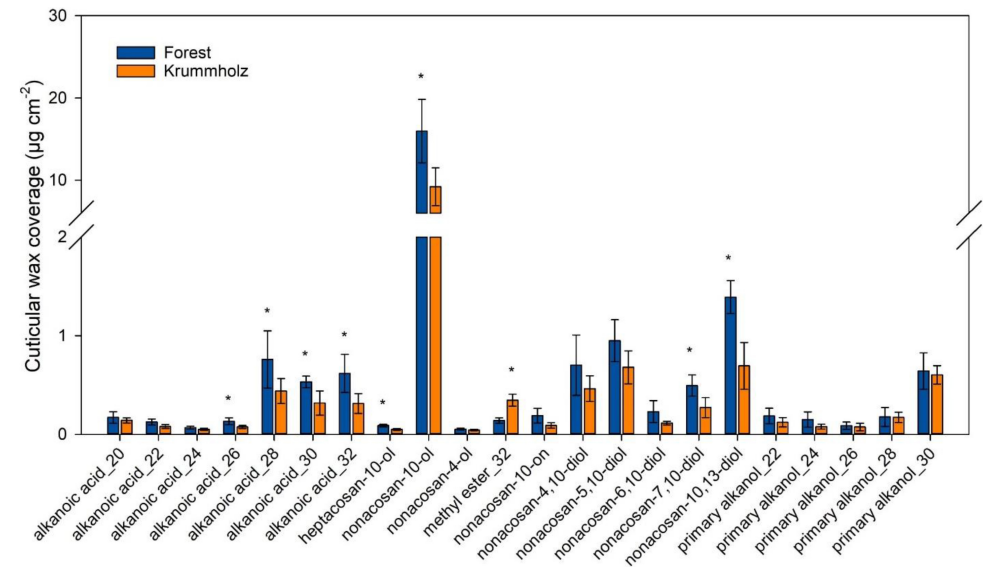

FIGURE 6 | Contribution of single compounds to the cuticular wax coverage of *P. uncinata* needles grown at Forest and Krummholz populations ($n = 5$; mean ± standard deviation). Asterisks indicate statistically significant differences ($p < 0.05$) between both populations.

in Krummholz needles to direct winter damage rather than inadequate development during the vegetative period. In this sense, Grace (1990) reported higher winter transpiration in needles of *Pinus sylvestris* in United Kingdom at treeline but he did not find signs of inadequate cuticular development in needles. Besides that, Hadley and Smith (1983, 1986) also found a higher g_{min} in the subalpine conifers constituting the upper treeline in Wyoming (United States), but they explained such difference through the abrasion in the cuticle caused by harsh environmental conditions that can occur in the treeline during winter. Nevertheless, our measurements were carried out during autumn in current-year needles, which minimizes the possibility of winter degradation factors, such as abrasion and stomatal dysfunction, contributing to the higher g_{min} and thinner cuticle thickness in Krummholz trees (Hadley and Smith, 1983, 1986). Instead, our results favor the Michaelis (1934) hypothesis of inadequate cuticle development.

However, it cannot be assumed that worldwide alpine treelines result from inadequate cuticle development (Körner and Paulsen, 2004). Thus, *Pinus pumila* shows no correlation between cuticle characteristics and needle mortality at treeline when comparing two Krummholz populations growing at high altitude with different wind exposures (Nakamoto et al., 2012). Otherwise, Anfodillo et al. (2002) studying *Picea abies* and *Pinus cembra* in the Dolomites along a broad altitudinal gradient, found that these species have thicker cuticles at higher elevations. However, in our study, it is hard to assume that a climatic gradient associated with changes in altitude can modify in such way the cuticle of both growth forms. This would be a big difference compared to the study of Baig and Tranquillini (1976) in which the differences in altitude between populations are approximately 1,000 m, while here it is close to 50 m. The effect of several and continuous alterations of the apical dominance by continuous over pruning, modify the growth pattern from the typical tall, erect timber-sized tree to the stunted Krummholz. Furthermore, it could also be suggested that this over pruning alters the carbon allocation patterns and/or carbohydrate status of the needle so that trees have less carbon available to develop their cuticles, suggesting a trade-off between carbon assimilation and water loss with g_{min} (Machado et al., 2021). This may be a factor that should be explored to explain this modified functioning.

The differences found in the present study in terms of g_{min} and cuticle thickness between Forest and Krummholz populations may increase the risk of "frost drought" in the treeline (Michaelis, 1934; Tranquillini, 1976). However, other factors besides g_{min} and cuticle thickness should be considered when analyzing the possible existence of "frost drought" in the treeline. For instance, the occurrence of a high number of freeze-thaw events could promote massive embolism and needle desiccation during winter in the alpine treeline (Mayr et al., 2006). One might think that the continuous loss of shoots due to "frost drought" condition their stunted form significantly, modifying its nature and the performance of its needles. In this sense, one might wonder if the lower cuticle development, the smaller needle size, the lower cuticle thickness and the greater g_{min} in Krummholz specimens have a causal relationship, however, this is only a mere hypothesis that should be tested in further studies.

Therefore, the upper treeline is a complex phenomenon that probably cannot be explained from a single point of view, and more research is needed to provide a general explanation for its existence. Our study showed clear evidence that supports the inadequate development of needle cuticles as one of the factors that lead to increased transpirational water losses during winter and, consequently, a higher risk of suffering frost drought. However, other factors associated with the harsh conditions suffered by shoots during winter (i.e., cuticle abrasion or a high number of freeze-thaw events) may also increase the risk of "frost drought" and should be considered when analyzing the upper treeline.

DATA AVAILABILITY STATEMENT

The original contributions presented in the study are included in the article/**Supplementary Material**, further inquiries can be directed to the corresponding author.

AUTHOR CONTRIBUTIONS

EG-P, AB, and DA-F conceived the idea and collected the plant material. EG-P and JP-P conceptualized and supervised the project. AB, DA-F, JF, and DS-K contributed to the conception and design of the study. DA-F performed the minimum needle conductance measurements. JP-P and DA-F achieved the anatomical measurements and analyzed the data and wrote the first draft of the manuscript. AS performed the chemical analyses of cuticular waxes. All authors contributed to manuscript revision, read, and approved the submitted version.

FUNDING

The work of DA-F was supported by an FPI-INIA contract BES-2017-081208. AS was a recipient of a doctoral fellowship from the Brazilian National Council for Scientific and Technological Development (CNPq). DA-F, JF, JP-P, DS-K, and EG-P acknowledge the financial contribution by Reference Group H09_20R (Gobierno de Aragón, Spain).

ACKNOWLEDGMENTS

We thank Markus Riederer (University of Würzburg, Germany) for helpful discussions and valuable suggestions.

SUPPLEMENTARY MATERIAL

The Supplementary Material for this article can be found online at: https://www.frontiersin.org/articles/10.3389/fpls.2021.786933/full#supplementary-material

Supplementary Figure 1 | Specimens of *Pinus uncinata* from Krummholz population in Sierra de Las Cutas, Spanish Pyrenees. **(A)** Krummholz tree at the upper limit of the species, partially covered with snow. **(B)** Krummholz specimen with signs of browning and lesions on the needles.

REFERENCES

Anfodillo, T., Pasqua, di Bisceglie, D., and Urso, T. (2002). Minimum cuticular conductance and cuticle features of *Picea abies* and *Pinus cembra* needles along an altitudinal gradient in the Dolomites (NE Italian Alps). *Tree Physiol.* 22, 479–487. doi: 10.1093/treephys/22.7.479

Baig, M. N., and Tranquillini, W. (1976). Studies on upper timberline: morphology and anatomy of Norway spruce (*Picea abies*) and stone pine (*Pinus cembra*) needles from various habitat conditions. *Can. J. Bot.* 54, 1622–1632. doi: 10.1139/b76-174

Bueno, A., Alfarhan, A., Arand, K., Burghardt, M., Deininger, A.-C., Hedrich, R., et al. (2019). Temperature effects on the cuticular transpiration barrier of two desert plants with water-spender and water-saver life strategies. *J. Exp. Bot.* 70, 1613–1625. doi: 10.1093/jxb/erz018

Bueno, A., Sancho-Knapik, D., Gil-Pelegrín, E., Leide, J., Peguero-Pina, J. J., Burghardt, M., et al. (2020). Cuticular wax coverage and its transpiration barrier properties in *Quercus coccifera* L. leaves: does the environment matter? *Tree Physiol.* 40, 827–840. doi: 10.1093/treephys/tpz110

Diarte, C., de Souza, A. X., Staiger, S., Deininger, A., Bueno, A., Burghardt, M., et al. (2020). Compositional, structural and functional cuticle analysis of Prunus laurocerasus L. sheds light on cuticular barrier plasticity. *Plant Physiol. Biochem.* 158, 434–445. doi: 10.1016/j.plaphy.2020.11.028

Dommisse, A., Wirtz, J., Koch, K., Barthlott, W., and Kolter, T. (2007). Synthesis of (S)-Nonacosan-10-ol, the Major Component of Tubular Plant Wax Crystals. *Eur. J. Org. Chem.* 21, 3508–3511.

Fernández, V., Bahamonde, H. A., Peguero-Pina, J. J., Gil-Pelegrín, E., Sancho-Knapik, D., Gil, L., et al. (2017). Physico-chemical properties of plant cuticles and their functional and ecological significance. *J. Exp. Bot.* 68, 5293–5306. doi: 10.1093/jxb/erx302

Gil-Pelegrín, E. (1993). *Estudios ecofisiológicos sobre Pinus uncinata* Mill. en el límite superior del bosque. Ph. D. Thesis. Madrid: Universidad Autónoma de Madrid.

Grace, J. (1990). Cuticular water loss unlikely to explain treeline in Scotland. *Oecologia* 84, 64–68. doi: 10.1007/BF00665596

Griggs, R. F. (1934). The edge of the forest in Alaska and the reasons for its position. *Ecology* 15, 80–96. doi: 10.2307/1932778

Hadley, J. L., and Smith, W. K. (1983). Influence of wind exposure on needle desiccation and mortality for timberline conifers in Wyoming, USA. *Arct. Alp. Res.* 15, 127–135.

Hadley, J. L., and Smith, W. K. (1986). Wind effects on needles of timberline conifers: seasonal influence on mortality. *Ecology* 67, 12–19. doi: 10.2307/1938498

Jetter, R., and Riederer, M. (1994). Epicuticular crystals of nonacosan-10-ol: In-vitro reconstitution and factors influencing crystal. *Planta* 195, 257–270.

Körner, C. (2012). *Alpine treelines: Functional ecology of the global high elevation tree limits*. Basel: Springer.

Körner, C., and Paulsen, J. (2004). A world-wide study of high altitude treeline temperatures. *J. Biograogr.* 31, 713–732. doi: 10.1111/j.1365-2699.2003.01043.x

Machado, R., Loram-Lourenço, L., Farnese, F. S., Alves, R. D. F. B., de Sousa, L. F., Silva, F. G., et al. (2021). Where do leaf water leaks come from? Trade-offs underlying the variability in minimum conductance across tropical savanna species with contrasting growth strategies. *New Phytol.* 229, 1415–1430. doi: 10.1111/nph.16941

Mamet, S. D., and Kershaw, G. P. (2013). Environmental Influences on Winter Desiccation of *Picea glauca* Foliage at Treeline, and Implications for Treeline Dynamics in Northern Manitoba. *Arct. Alp. Res.* 45, 219–228. doi: 10.1657/1938-4246-45.2.219

Márquez, D. A., Stuart-Williams, H., Farquhar, G. D., and Busch, F. A. (2022). Cuticular conductance of adaxial and abaxial leaf surfaces and its relation to minimum leaf surface conductance. *New Phytol.* 233, 156–168. doi: 10.1111/nph.17588

Marr, J. W. (1977). The development and movement of tree islands near the upper limit of tree growth in the southern Rocky Mountains. *Ecology* 58, 1159–1164. doi: 10.2307/1936937

Mayr, S., Gruber, A., and Bauer, H. (2003). Repeated freeze–thaw cycles induce embolism in drought stressed conifers (Norway spruce, stone pine). *Planta* 217, 436–441. doi: 10.1007/s00425-003-0997-4

Mayr, S., Hacke, U., Schmid, P., Schwienbacher, F., and Gruber, A. (2006). Frost drought in conifers at the alpine timberline: xylem dysfunction and adaptations. *Ecology* 87, 3175–3185. doi: 10.1890/0012-9658(2006)87[3175:fdicat]2.0.co;2

Michaelis, P. (1934). Ökologische Studien an der alpinen Baumgrenze. V. Osmotischer Wert und Wassergehalt während des Winters in verschiedenen Höhenlagen. *Jahrb. Wiss. Bot.* 80, 337–362.

Nakamoto, A., Ikeda, T., and Maruta, E. (2012). Needle browning and death in *Pinus pumila* in the alpine region of central Japan were not related to mechanical damage of cuticle and cuticle thickness. *Can. J. For. Res.* 42, 167–178. doi: 10.1139/x11-153

Nakamoto, A., Ikeda, T., and Maruta, E. (2013). Needle browning and death in the flagged crown of *Abies mariesii* in the timberline ecotone of the alpine region in central Japan. *Trees* 27, 815–825. doi: 10.1007/s00468-012-0836-y

Nobel, P. S. (2009). *Physicochemical and environmental plant physiology*, 4th Edn. Oxford: Academic Press.

Peguero-Pina, J. J., Sisó, S., Sancho-Knapik, D., Díaz-Espejo, A., Flexas, J., Galmés, J., et al. (2016). Leaf morphological and physiological adaptations of a deciduous oak (*Quercus faginea* Lam.) to the Mediterranean climate: a comparison with a closely related temperate species (*Quercus robur* L.). *Tree Physiol.* 36, 287–299. doi: 10.1093/treephys/tpv107

R Core Team (2020). *R: A Language and Environment for Statistical Computing*. Vienna: R Foundation for Statistical Computing. Available online at: https://www.R-project.org/

Riederer, M., and Schreiber, L. (2001). Protecting against water loss: analysis of the barrier properties of plant cuticles. *J. Exp. Bot.* 52, 2023–2032. doi: 10.1093/jexbot/52.363.2023

Sakai, A., and Larcher, W. (1987). "Frost survival of plants: responses and adaptation," in *Ecological studies*, Vol. 62, ed. W. Larcher (Berlin: Springer).

Schreiber, L., and Riederer, M. (1996). Ecophysiology of cuticular transpiration: comparative investigation of cuticular water permeability of plant species from different habitats. *Oecologia* 107, 426–432. doi: 10.1007/BF00333931

Schuster, A. C., Burghardt, M., and Riederer, M. (2017). The ecophysiology of leaf cuticular transpiration: are cuticular water permeabilities adapted to ecological conditions? *J. Exp. Bot.* 68, 5271–5279. doi: 10.1093/jxb/erx321

Serrano-Notivoli, R., Buisán, S., Abad Pérez, L. M., Sierra Álvarez, E., Rodríguez Ballesteros, C., López Moreno, J. I., et al. (2018). "Tendencias recientes en precipitación, temperatura y nieve de alta montaña en los pirineos (Refugio de Góriz, Huesca)," in *El clima: aire, agua, tierra y fuego*, eds M. Gómez, J. Pedro, et al. (Madrid: Asociación Española de Climatología), 267–280.

Tranquillini, W. (1976). "Water Relations and Alpine Timberline," in *Water and Plant Life. Ecological Studies (Analysis and Synthesis)*, Vol. 19, eds O. L. Lange, L. Kappen, and E. D. Schulze (Berlin: Springer Verlag), 473–491. doi: 10.1007/978-3-642-66429-8_29

Tranquillini, W. (1979). *Physiological ecology of the alpine timberline*. Heidelberg: Springer-Verlag.

Wardle, P. (1965). A comparison of alpine timberlines in New Zealand and North America. *N Z. J. Bot.* 3, 113–135. doi: 10.1080/0028825X.1965.10876989

Wardle, P. (1968). Engelmann spruce (*Picea engelmannii* Engel.) at its upper limits on the Front Range, Colorado. *Ecology* 49, 483–495. doi: 10.2307/1934115

Wardle, P. (1974). "Alpine timberlines," in *Arctic and alpine environments*, eds J. O. Ives and R. G. Barry (London: Methuen).

Conflict of Interest: The authors declare that the research was conducted in the absence of any commercial or financial relationships that could be construed as a potential conflict of interest.

frontiers | Frontiers in Plant Science

ORIGINAL RESEARCH
published: 12 May 2022
doi: 10.3389/fpls.2022.840061

Chemical Composition of Cuticle and Barrier Properties to Transpiration in the Fruit of *Clausena lansium* (Lour.) Skeels

Hua Huang[1], Ling Wang[2], Diyang Qiu[1] and Yusheng Lu[1]**

[1] *Institute of Fruit Tree Research, Guangdong Academy of Agricultural Sciences; Key Laboratory of South Subtropical Fruit Biology and Genetic Resource Utilization, Ministry of Agriculture and Rural Affairs, Guangdong Provincial Key Laboratory of Tropical and Subtropical Fruit Tree Research, Guangzhou, China,* [2] *Sericultural & Agri-Food Research Institute Guangdong Academy of Agricultural Sciences, Key Laboratory of Functional Foods, Ministry of Agriculture and Rural Affairs, Key Laboratory of Agricultural Products Processing, Guangzhou, China*

OPEN ACCESS

Edited by:
Antonio Heredia, University of Malaga, Spain

Reviewed by:
Jinwei Suo, Zhejiang Agriculture and Forestry University, China
Isabel Lara, Universitat de Lleida, Spain

***Correspondence:**
Hua Huang
huangw0109@gmail.com
Yusheng Lu
luyusheng@gdaas.cn

Specialty section:
This article was submitted to Plant Physiology, a section of the journal Frontiers in Plant Science

Received: *20 December 2021*
Accepted: *22 March 2022*
Published: *12 May 2022*

Citation:
Huang H, Wang L, Qiu D and Lu Y (2022) Chemical Composition of Cuticle and Barrier Properties to Transpiration in the Fruit of Clausena lansium (Lour.) Skeels. Front. Plant Sci. 13:840061. doi: 10.3389/fpls.2022.840061

The plant cuticle, as a lipid membrane covering aerial plant surfaces, functions primarily against uncontrolled water loss. Herein, the cuticle chemical composition and the transpiration of wampee fruit (*Clausena lansium* (Lour.) Skeels) at the green, turning, and yellow stages in cultivars of "Jixin" and "Tianhuangpi" were comprehensively studied. The coverage of wax and cutin monomers per unit of fruit surface area at the green stage was lower in "Jixin" than in "Tianhuangpi" and increased gradually during development. Cutin monomers accumulated ranging from 22.5 μg cm^{-2} (green) to 52.5 μg cm^{-2} (turning) in "Jixin" and from 36.5 μg cm^{-2} (green) to 81.7 μg cm^{-2} (yellow) in "Tianhuangpi." The total composition of waxes ranged between 6.0 μg cm^{-2} (green) and 11.1 μg cm^{-2} (turning) in "Jixin," while they increased from 7.4 μg cm^{-2} (green) to 16.7 μg cm^{-2} (yellow) in "Tianhuangpi." Cutin monomers were dominated by ω-, mid-dihydroxy fatty acids (over 40%), followed by multiple monomers of α,ω-dicarboxylic acids with or without added groups, α-monocarboxylic acids with or without ω- or mid-chain hydroxy or mid-epoxy groups, primary alcohols, and phenolics. The very-long-chain (VLC) aliphatic pattern of cuticular waxes was prominently composed of *n*-alkanes (ranging from 21.4% to 39.3% of total wax content), fatty acids, primary alcohols, and aldehydes. The cyclic waxes were dominated by triterpenoids (between 23.9 and 51.2%), sterols, and phenolics. Water loss in wampee fruit exhibited linear changes over time, indicating an overall monofunctional barrier to transpiration. Permeance for water in wampee fruit was higher at the green stage than at the yellow stage in both "Jixin" and "Tianhuangpi," which showed a negative correlation with the changes of VLC *n*-alkanes. The results showed the cuticular chemicals, including cutin monomers and waxes, in wampee fruit and further indicated the potential contributions of the cuticular chemical composition to the physiological functions in fruits.

Keywords: wampee fruit, cuticular waxes, cutin monomers, transpiration, barrier properties

INTRODUCTION

Clausena lansium (Lour.) Skeels, named wampee or "huangpi (黄皮)" in Chinese for the yellow skin in ripe fruits, is a typical subtropical to tropical fruit. Wampee is native to south China and is also planted in other regions of southern Asia (Rodrigues et al., 2018). Almost all parts of the wampee, including leaves, seeds, roots, and fruits, contain abundant carbazole alkaloids, triterpenoids, and amides, exhibiting strong antioxidant, anticancer, and anti-inflammatory activities (Prasad et al., 2010; Shen et al., 2017; Peng et al., 2019). Therefore, wampee is potentially an economically important plant due to its nutritional and medicinal value.

The plant cuticle is a continuous lipid membrane covering all the aerial plant organs against uncontrolled water loss, pathogen infection, and cracking (Yeats and Rose, 2013). This extracellular membrane has been well studied and is composed of soluble waxes, containing very-long-chain aliphatics and cyclic triterpenoids; the cutin matrix is constructed by C_{16}- and C_{18}-type fatty acid derivatives as well as a small content of phenolics (Jetter et al., 2008; Fich et al., 2016). It has long been established that the barrier to nonstomatal transpiration in plants is largely provided by the cuticle, especially the wax pattern (Riederer and Schreiber, 2001). In addition, both cutin polymers and waxes provide a mechanical barrier to pathogen invasion or as signal components involved in the germination of conidia (Hansjakob et al., 2010; Serrano et al., 2014). Though the phytochemicals of various organs in wampee have been widely investigated, the chemical compositions of the outermost cuticle have not yet been addressed.

Wampee belongs to the Rutaceae family being a distant relative of citrus, and the size of the fruit resembles grape berry and cherry fruit (Rodrigues et al., 2018). Unlike citrus, in which the peel tissue of fruits is independent of the edible parts, the peel adheres together with the pulp in wampee fruit. Wampee is a perishable fruit, which is susceptible to mechanical damages, browning, and disease infection after harvest (Shao et al., 2020). Meanwhile, pathogen invasion as a factor-causing fruit softening and cracking has been a concern in wampee fruit production (Zhou et al., 2015). It has been widely reported that the chemical composition and the structural arrangements of the cell wall or cuticle, as well as the fruit surface properties, are pivotal in maintaining the fruit quality (Ríos et al., 2015; Winkler et al., 2020). Accordingly, the peel tissues may play important roles in affecting fruit quality changes during development and postharvest storage.

In addition, the most popular product of wampee is dried fruit. Therefore, the desiccation process is important for product quality. The tolerance to desiccation in seeds increases during development (Fu et al., 2008), and the drying conditions are also important for the quality of the final product (Chokeprasert et al., 2005). Therefore, elucidating the characteristics of water loss and its barrier property to transpiration might be helpful in improving the production of dry wampee. However, the transpiration property and the potential barrier property of the hydrophobic cuticle in wampee fruit are still unclear.

The goal of this study was to characterize the chemical composition of cuticles and the potential effect of various cuticular components on the transpiration barrier properties in wampee fruit. Previous studies on the varieties of wampee fruit have found that the sour wampee fruit with a common dark yellow surface contained higher antioxidants and a higher antioxidant activity than the sweet wampee fruit with a light yellow surface (Ye et al., 2019). In this study, "Jixin," the common sour wampee fruit, and "Tianhuangpi," with high sugar content and sweet flavor, were selected to be comparatively studied. Changes in cuticle composition, including waxes and cutin monomers, as well as the transpiration at the green, turning, and yellow ripe stages, were studied in detail. The chemical composition of the cuticle and the potential contributions to the transpiration barrier properties in wampee fruit are also comprehensively discussed.

MATERIALS AND METHODS

Plant Materials and Reagents

Wampee fruits (*Clausena lansium* (Lour.) Skeels) at the green (about 60 days after anthesis, DAA), turning (about 75 DAA), and yellow ripe (about 90 DAA) stages in cultivars of "Jixin" and "Tianhuangpi" were harvested from an orchard in Guangzhou, P. R. China (23°30'N, 113°30'E). The fruits were transported back to the laboratory immediately, and the fruits with uniformity of shape, color, and size were selected for further experiments. At each developmental stage, 15 individual fruits were selected to determine the transpiration, and at least 10 fruits were used to isolate the cuticular membranes for further chemical analysis. All the experimental reagents used were in analytical grade and were prepared following the methods given in the previous reports (Huang and Jiang, 2019).

Preparation of Cuticular Membranes From Wampee Fruit

Cuticular membranes from wampee fruit at different stages were prepared following the previous methods with minor modifications (Huang and Jiang, 2019). The fruits with uniform shape and size at each stage were randomly selected to isolate cuticular membranes. Because of different fruit sizes during development, peel disks from the middle position of wampee fruit at the green, turning, and yellow stages were prepared using a puncher with diameters of 0.5, 0.8, and 1.0 cm, respectively. The cuticular membranes were isolated by immersing the peel disks in 10 mM citric acid buffer containing 1% (w/v) pectinase and 1% (w/v) cellulase (Beijing Solarbio Science & Technology Co., Ltd., Beijing, China) and incubated under 37°C for 2–3 days. Once most of the tissues were removed from the fruit skin, the cuticular membranes were then washed by 10 mM sodium tetraborate decahydrate (Solarbio Science and Technology Co., Ltd., Beijing, China) to absorb the contamination of free fatty acids. The cuticular membranes were further rinsed with distilled water and air-dried for further analysis.

Cuticular Wax and Cutin Monomer Extraction

Cuticular waxes and cutin monomers were extracted in series from isolated cuticular membranes according to the previous methods with minor modifications (Huang et al., 2017). The isolated cuticular membranes were completely dipped in chloroform (Guangzhou Chemical Reagent Factory, China) with a mild temperature of around 40°C to better release the soluble waxes. The extraction time was set for 2 min. Each sample was extracted three times and combined with the extracts. Then, *n*-tetracosane (Sigma–Aldrich, Shanghai, China) was added as an internal standard to evaluate the cuticular contents. The solvent in the extracts was evaporated by gentle nitrogen gas until they dried for further analysis. After that, the membranes that have been removed of soluble waxes were subsequently depolymerized in boron trifluoride with methanol (BF_3-methanol, 10%, ∼1.3 M, Sigma–Aldrich, Shanghai, China) and incubated for 16 h at 70°C. After membranes were lysed, *n*-dotriacontane (Sigma–Aldrich, Shanghai, China) as an internal standard was added. Saturated aqueous sodium chloride solution and chloroform were added in series to extract the cutin monomers. The organic phase was collected and evaporated to dryness under a gentle stream of nitrogen gas for further analysis.

Gas Chromatography–Mass Spectrometry

To detect the chemical composition of cuticular waxes and cutin monomers, the above-prepared extracts were derivatized with pyridine (Shanghai Aladdin Bio-Chem Technology Co., Ltd., Shanghai, China) and *N,O*-bis (trimethylsilyl) trifluoroacetamide (BSTFA, Sigma–Aldrich, Shanghai, China) for 30 min at 70°C. The chemical components were analyzed using a temperature-controlled capillary gas chromatography (7890B GC System; Agilent Technologies, USA) instrument equipped with a mass spectrometric detector (*m*/*z* 50–750, MSD 5977B; Agilent Technologies, USA). Single compounds were identified based on their electron ionization mass spectra using authentic standards, the mass spectral library of Wiley 10th (John Wiley & Sons), NIST 2014 (W10N14), or by interpretation of the spectra information, including the retention times and fragments of m/z, which were analyzed by comparison with data from the literature (Holloway, 1982; Jetter et al., 2008) or online database (https://www.lipidmaps.org/resources/lipidweb/lipidweb_html/index.html).

To quantify wax and cutin monomer components, the extracts were analyzed using a capillary gas chromatography instrument equipped with a flame ionization detector (7890A, GC System; Agilent Technologies, Santa Clara, CA, USA) and on-column injection with a capillary column (30 m × 0.32 mm, DB-1 ms, 0.1 μm film; J&W Scientific, Agilent Technologies, USA). To separate cuticular wax compounds, 1-μL samples were injected at 50°C; after 2 min at 50°C, the temperature was raised to 200°C at 40°C min^{-1} and held for 2 min and then raised to 320°C at 3°C min^{-1} and held for 30 min. For separation of the cutin monomers, 1-μL samples were injected at 50°C; after 1 min at 50°C, the temperature was raised to 150°C at 10°C min^{-1} and held for 2 min and then raised to 320°C at 3°C min^{-1} and held for 30 min. The area under the peaks was compared with that of the internal standards to obtain the quantity of cuticular waxes and cutin monomers. Five repetitions for each cultivar at each stage were performed for both wax and cutin analysis. The average chain length of the VLC acyclic compounds was calculated following the methods reported by Huang et al. (2017).

Determination of Fruit Transpiration

The transpiration of the fruit at different stages was determined gravimetrically by recording the weight loss with the extension of time (Huang et al., 2017). In brief, an intact fruit without any defects in a total of 12–15 samples from each developmental stage and cultivar was carefully selected. Before measurement, fruit samples were saturated with water by dipping fruit stalks in water overnight. Then, the fruit pedicel scars were sealed with paraffin wax to avoid stalk water loss. The weight loss of fruit vs. time was recorded every 2 h over six times and extended to over 24 h, and the atmosphere temperature was controlled at 25°C. The measurement was taken using an analytic electronic balance with a precision of 0.1 mg (BSA-224S, Sartorius, Beijing, China). The dynamic changes in accumulative transpiration (flux of water vapor, F in g m^{-2}) per unit of fruit surface area (A, m^2) vs. time (Δt) were analyzed. The fruit surface area was obtained by regarding the fruit as an ellipsoid or a sphere shape. Subsequently, permeance for water (P in m s^{-1}) of wampee fruit was obtained according to the transpiration rate *via* a driving force:

$$P = \frac{F}{A^* C_w^* (a_{fruit} - a_{air})}$$

The concentration of water vapor under the saturated status (C_w) was referred to from the tabulated values (Nobel, 2009). The fruit water activity (a_{fruit}) was assumed as a unit. The air water activity (a_{air}) over silica gel was regarded to be close to zero.

Statistical Analysis

Statistical analyses of all the experimental data were performed by SPSS (23, IBM Corp., Armonk, NY, USA) and SigmaPlot 12.5 (Systat Software, Inc., San Jose, CA, USA). Comparison analyses were carried out by one-way analysis of variance, and the differences between the two groups were analyzed at a level of 0.05. All the graphs were performed by SigmaPlot 12.5.

RESULTS

Changes in Fruit Surface Area at Different Developmental Stages

The fruit shape differed among the variety of cultivars and had different developmental stages. The fruit resembled an ellipsoid at all the developmental stages in "Jixin" (**Figure 1A**). In contrast, it was close to an ellipsoid shape at the green stage and shifted to a more sphere-like shape at the turning and yellow stages in "Tianhuangpi" (**Figure 1B**). Fruit size, measured as the surface area, increased gradually with the development and was calculated on the basis of the assumed shape of the fruit. The fruit surface area was the lowest at the green stage and increased rapidly by 70% from 7.3 cm^2 (green) to 12.7 cm^2 (turning) and

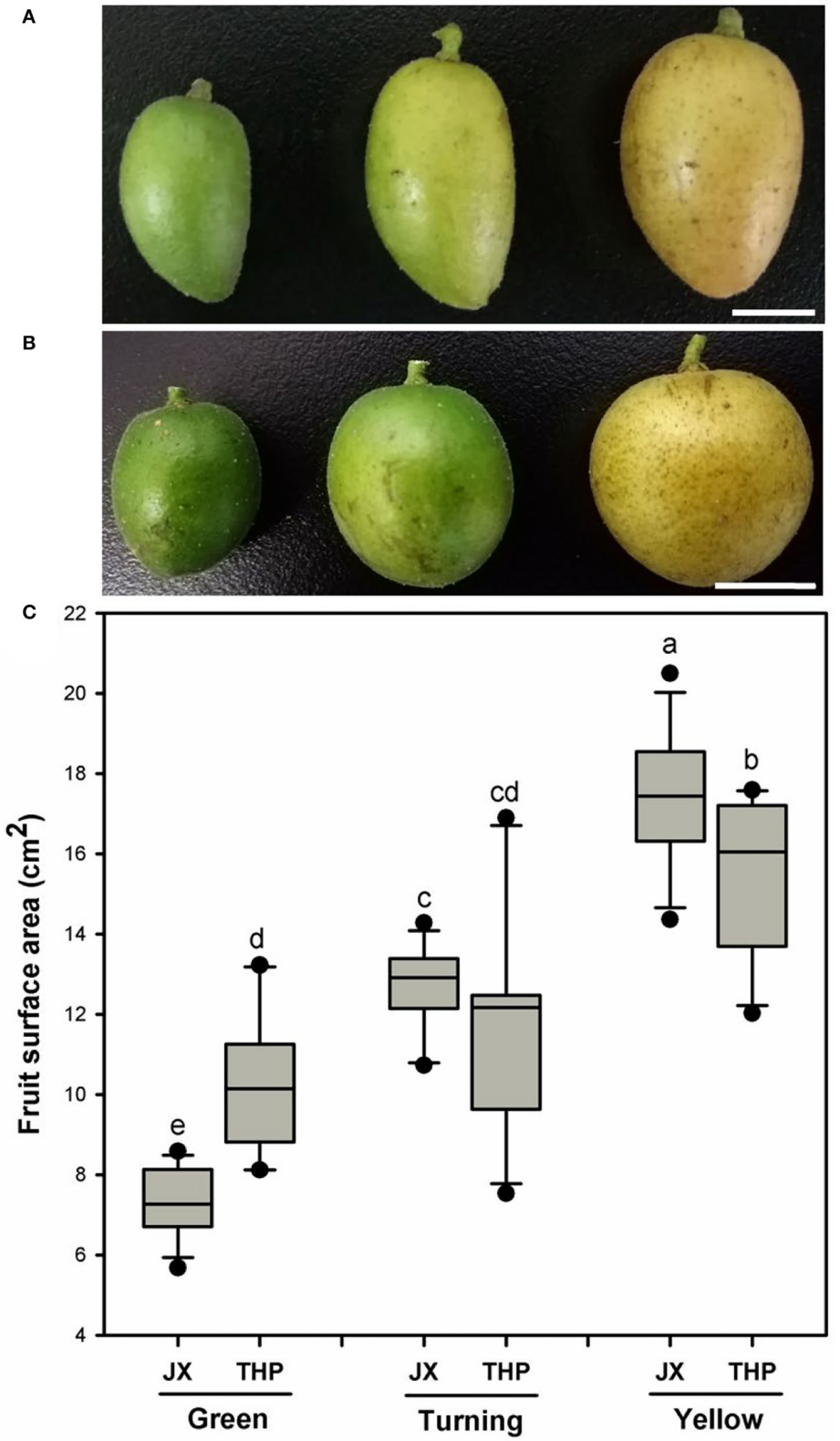

FIGURE 1 | Changes in fruit appearance and surface area changes at different developmental stages for wampee (*Clausena lansium* (Lour.) Skeels). The overall changes of "Jixin" —JX **(A)**, and "Tianhuangpi" —THP **(B)**, as well as the fruit surface areas **(C)** at the green, turning, and yellow ripe stages. Data are presented as the mean ± standard deviation ($n = 12$). Scale bars in **(A)** and **(B)** are 1 cm. Different letters indicate the significant differences at the level of 0.05.

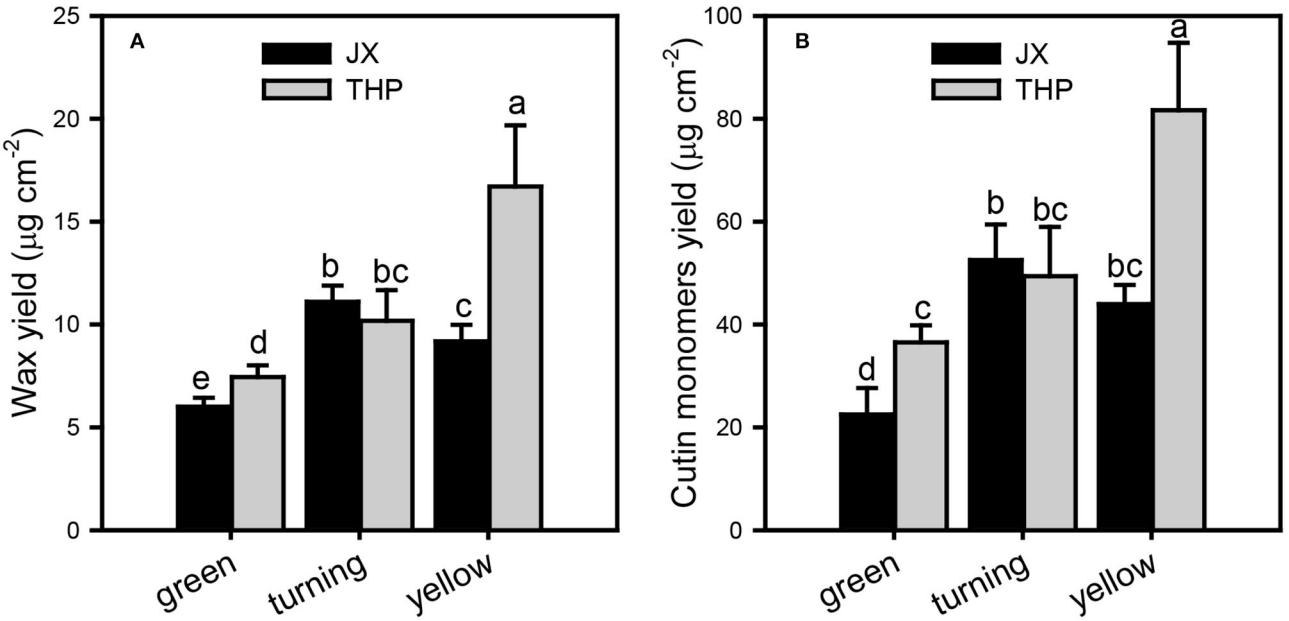

FIGURE 2 | The overall cuticular chemical composition in wampee fruit (*Clausena lansium* (Lour.) Skeels). Total cuticular waxes **(A)** and total cutin monomers **(B)** in the three developmental stages of "Jixin" —JX and "Tianhuangpi" —THP. Data are presented as the mean ± standard deviation ($n = 5$). Different letters indicate the significant differences at the level of 0.05.

TABLE 1 | Overall cuticular chemicals including waxes and cutin monomers of wampee fruit (*Clausena lansium* (Lour.) Skeels) in two cultivars of "Jixin" and "Tianhuangpi".

	"Jixin"			"Tianhuangpi"			Unit
	Green	Turning	Yellow	Green	Turning	Yellow	
Aliphatics	1.91 ± 0.49^{c}	4.21 ± 0.68^{b}	3.97 ± 0.59^{b}	1.97 ± 0.29^{c}	4.50 ± 1.68^{abc}	8.27 ± 2.10^{a}	μg cm^{-2}
Cyclics	2.64 ± 0.37^{c}	4.48 ± 0.83^{ab}	3.73 ± 0.25^{b}	4.07 ± 0.64^{b}	3.88 ± 0.35^{b}	5.41 ± 0.45^{a}	μg cm^{-2}
Aliphatics/cyclics	0.73 ± 0.22^{bc}	0.97 ± 0.28^{ab}	1.07 ± 0.23^{ab}	0.50 ± 0.15^{c}	1.19 ± 0.52^{ab}	1.52 ± 0.29^{a}	ratio
ACL	28.01 ± 0.81^{ab}	28.76 ± 0.21^{b}	29.29 ± 0.01^{a}	28.46 ± 0.28^{b}	29.22 ± 0.13^{a}	29.08 ± 0.13^{a}	carbons
C16/C18 monomers	9.14 ± 1.68^{ab}	7.15 ± 1.11^{b}	6.49 ± 0.68^{b}	10.83 ± 1.02^{a}	7.58 ± 0.82^{b}	7.44 ± 1.56^{b}	ratio
Wax/cutin	0.28 ± 0.07^{a}	0.21 ± 0.03^{a}	0.21 ± 0.01^{a}	0.20 ± 0.01^{a}	0.21 ± 0.07^{a}	0.21 ± 0.05^{a}	ratio
Cuticle yield	32.81 ± 6.04^{d}	71.71 ± 8.08^{b}	59.66 ± 4.47^{bc}	50.91 ± 4.73^{c}	66.30 ± 8.89^{bc}	109.21 ± 16.60^{a}	μg cm^{-2}

The cuticle yield, coverage of VLC aliphatics, cyclics (μg cm^{-2}), the ratio of total wax vs. cutin monomers, aliphatics vs. cyclics, and C_{16}- vs. C_{18}-type monomers in cutin, and the weight average chain length (ACL) of aliphatics in waxes.

Data are given as mean values with standard deviation ($n = 5$).

Different letters indicate the significant differences at the level of 0.05.

to 17.3 cm^2 in the yellow fruit (2.5-fold of the green fruit) in "Jixin." It increased slowly by 15% from 10.3 cm^2 (green) to 11.8 cm^2 (turning) and by 35% in the yellow fruit (13.7 cm^2) in "Tianhuangpi" (**Figure 1C**).

Cuticular Chemicals Detected in Wampee Fruit

The overall accumulation of waxes and cutin monomers per unit of surface area was lower in "Jixin" than in "Tianhuangpi." The contents of cuticle chemicals were lowest at the green stage, increased until the turning stage, and decreased thereafter in "Jixin." In contrast, they accumulated gradually during the whole development of "Tianhuangpi" (**Figure 2**). Cuticular wax was covered between 6.0 μg cm^{-2} (green) and 11.1 μg cm^{-2} (turning) in "Jixin" and ranged from 7.4 μg cm^{-2} (green) to 16.7 μg cm^{-2} (yellow) in "Tianhuangpi" (**Figure 2A**). Cutin monomers accumulated from 22.5 μg cm^{-2} at the green stage to 52.5 μg cm^{-2} at the turning stage in "Jixin" and varied from 36.5 μg cm^{-2} at the green stage to 81.7 μg cm^{-2} at the yellow stage in "Tianhuangpi" (**Figure 2B**). As a result, the ratio of total wax over cutin monomers was maintained at around 0.21 (**Table 1**).

Accumulation of Cutin Monomers

Numerous cutin monomer families were detected in the wampee fruit cuticle. Similar to the changes in total cutin monomers, most classes of cutin monomers exhibited lower coverage in

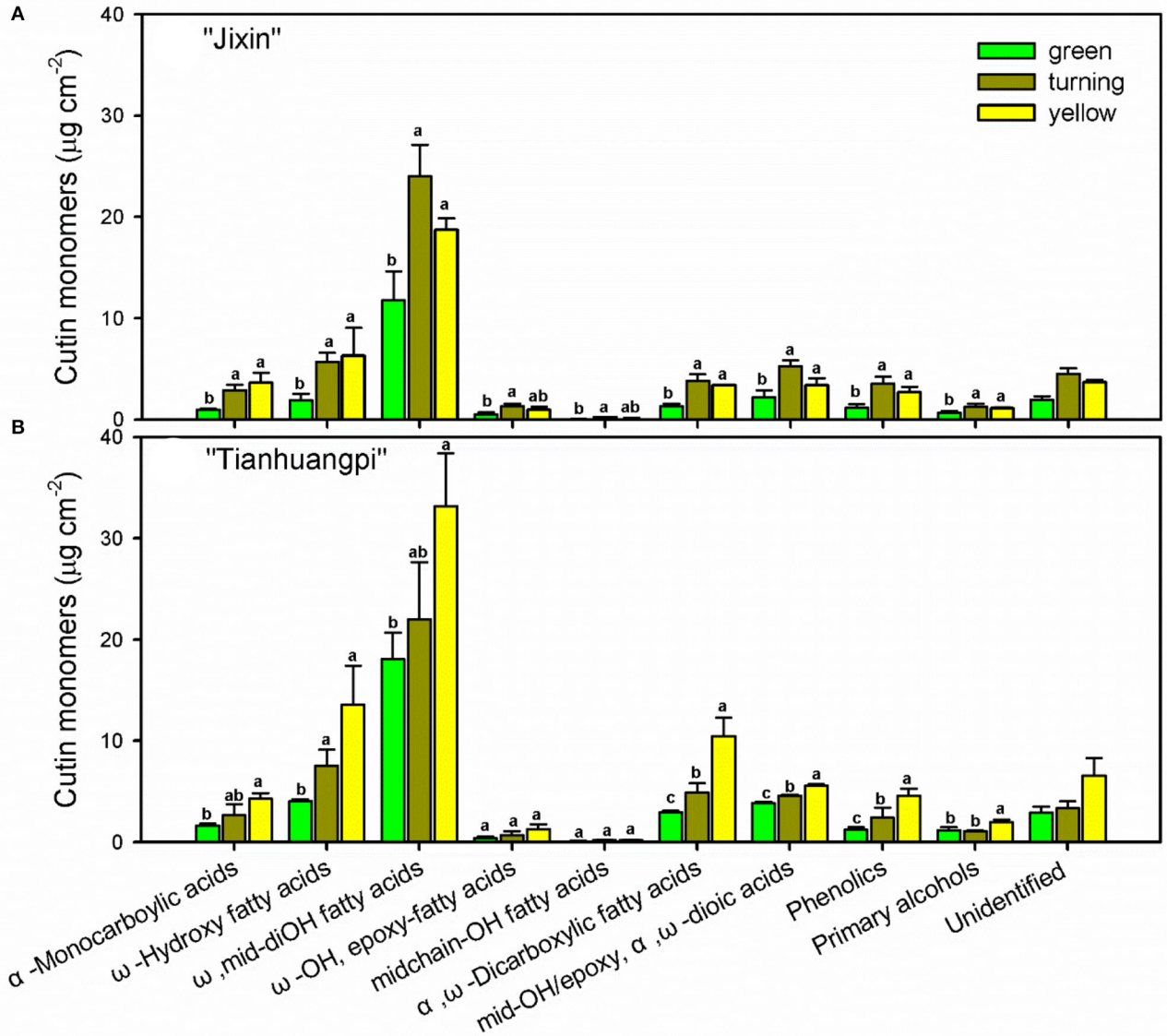

FIGURE 3 | Chemical compositions of cutin monomers in wampee fruit (*Clausena lansium* (Lour.) Skeels). Fruits at the green, turning, and yellow stages of two cultivars **(A)** "Jixin" and **(B)** "Tianhuangpi" were comparatively analyzed. Data are given as means ± standard deviation ($n = 5$). Different letters indicate the significant differences at the level of 0.05.

"Jixin" compared with "Tianhuangpi" (**Figure 3**). The homologs of ω-, mid-dihydroxy fatty acids (varying from 42.7 to 52.2% of total monomers) were the prominent cutin monomers, followed by α,ω-dicarboxylic acids with or without added hydroxy or epoxy groups, α-monocarboxylic acids with or without ω- or mid-chain hydroxy groups, primary alcohols, and phenolics (**Figure 3**). The most abundant monomer was 9(10),16-dihydroxyhexadecanoic acid, which ranged from 11.3 μg cm^{-2} (green) to 22.7 μg cm^{-2} (turning) in "Jixin" and between 17.4 μg cm^{-2} (green) and 31.8 μg cm^{-2} (turning) in "Tianhuangpi" (**Supplementary Materials**—cutin monomers). In addition, ω-OH C_{16} fatty acids (4.4 μg cm^{-2} to 5.0 μg cm^{-2} in "Jixin" and 7.7 μg cm^{-2} to 8.2 μg cm^{-2} in "Tianhuangpi"), α,ω-dicarboxylic C_{16} acids (5.1 μg cm^{-2} to 6.4 μg cm^{-2} in "Jixin" and 6.8 μg cm^{-2} to 9.4 μg cm^{-2} in "Tianhuangpi"), and 7(8)-OH-α,ω-dicarboxylic C_{16} acids (7.4 μg cm^{-2} to 9.8 μg cm^{-2} in "Jixin" and 6.9 μg cm^{-2} to 10.4 μg cm^{-2} in "Tianhuangpi") were also detected as abundant monomers in wampee fruit cuticles (**Supplementary Materials**—cutin monomers). The other monomers were detected in <5 μg cm^{-2} and increased slightly during development (**Figure 3** and **Supplementary Materials**—cutin monomers). Similarly, α-monocarboxylic acids with mid-OH (C_{15}) or with ω-OH and mid-epoxy groups (C_{18}) were detected in a small amount. Monofunctional fatty acids ranged from C_{16} to C_{32} with C_{16}, C_{18}, and C_{30} being the most abundant. Small amounts of

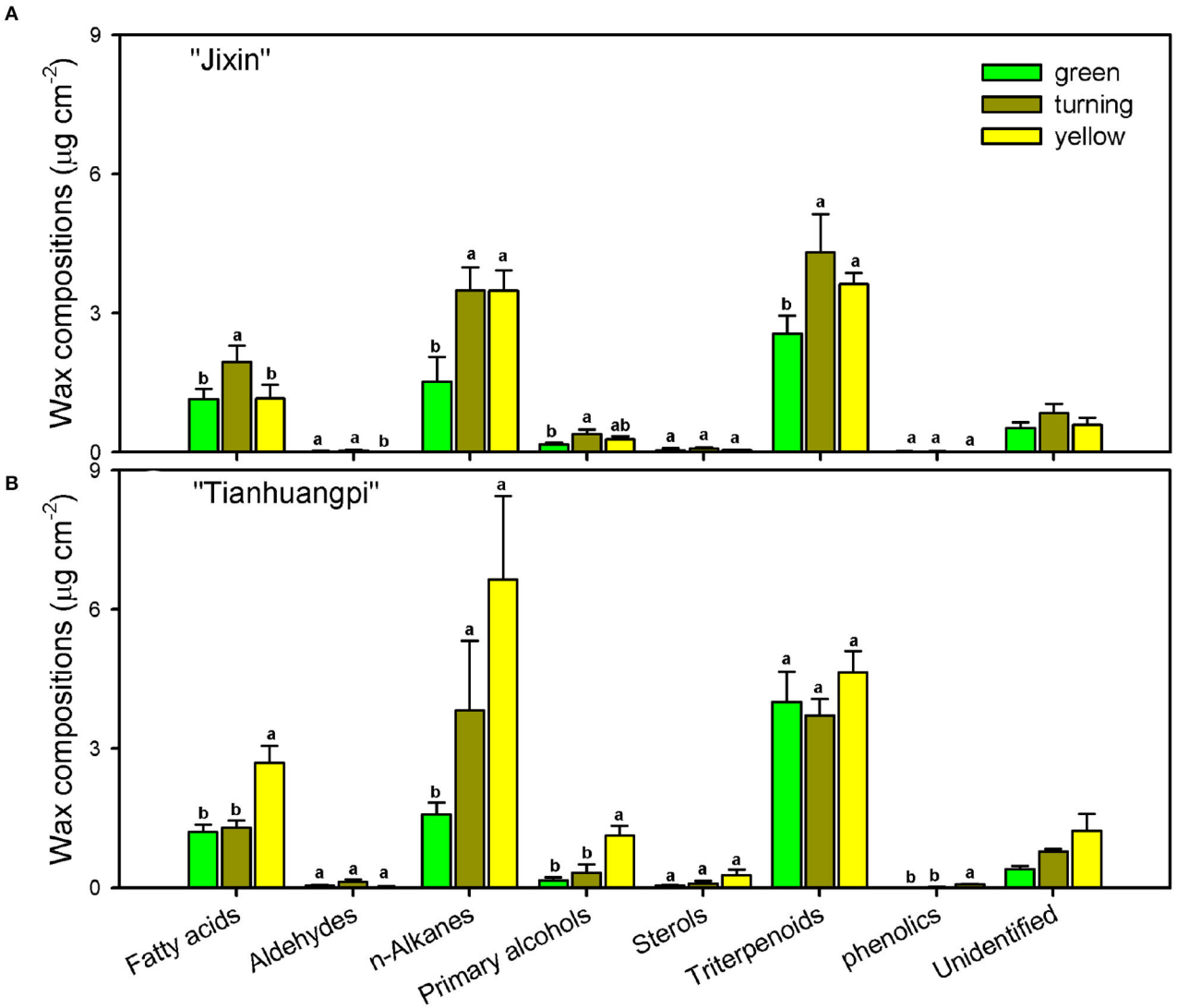

FIGURE 4 | Chemical compositions of cuticular waxes in wampee fruit (*Clausena lansium* (Lour.) Skeels). Fruits at the green, turning, and yellow stages of two cultivars **(A)** "Jixin" and **(B)** "Tianhuangpi" were comparatively analyzed. Data are given as means ± standard deviation ($n = 5$). Different letters indicate the significant differences at the level of 0.05.

primary alcohols, from C_{24} to C_{31}, and coumaric acid and their derivatives as phenolics were also detected (**Figure 3** and **Supplementary Materials**—cutin monomers). The most prominent components in cutin, C_{16}- and C_{18}-type monomers, exhibited a decreasing trend in their ratio from 9.1 to 6.5 in "Jixin" and from 10.8 to 7.4 in "Tianhuangpi" (**Table 1**).

Chemical Composition of Cuticular Waxes

The accumulation of VLC aliphatic components in waxes varied from 1.9 μg cm^{-2} (green) to 4.2 μg cm^{-2} (turning) in "Jixin" and increased by 4-fold from 2.0 μg cm^{-2} (green) to 8.3 μg cm^{-2} (yellow) in "Tianhuangpi" (**Table 1**). The content of cyclics increased from 2.6 μg cm^{-2} (green) to 4.5 μg cm^{-2} (turning) in "Jixin" and from 4.1 μg cm^{-2} (green) to 5.4 μg cm^{-2} (yellow) in "Tianhuangpi" (**Table 1**). It is also noteworthy that the relative contents of VLC aliphatics and cyclics in total waxes appeared in stable ratios in "Jixin" (between 0.7 and 1.1) while increasing by 3-fold (0.5 to 1.5) in "Tianhuangpi" during fruit development (**Table 1**).

The aliphatic components were dominated by *n*-alkanes, followed by fatty acids, primary alcohols, and aldehydes in waxes (**Figure 4** and **Supplementary Materials**—waxes). The most abundant VLC *n*-alkanes accumulated with homolog carbon chains from C_{21} to C_{33} and were dominated by C_{29} (6.0–14.9% in "Jixin", and 5.9–15.3% in "Tianhuangpi") and C_{31} (7.0–12.7% in "Jixin", and 6.2–13.7% in "Tianhuangpi"), which were lower in the green stage than in other stages (**Figure 5A** and **Supplementary Materials**—waxes). Fatty acids

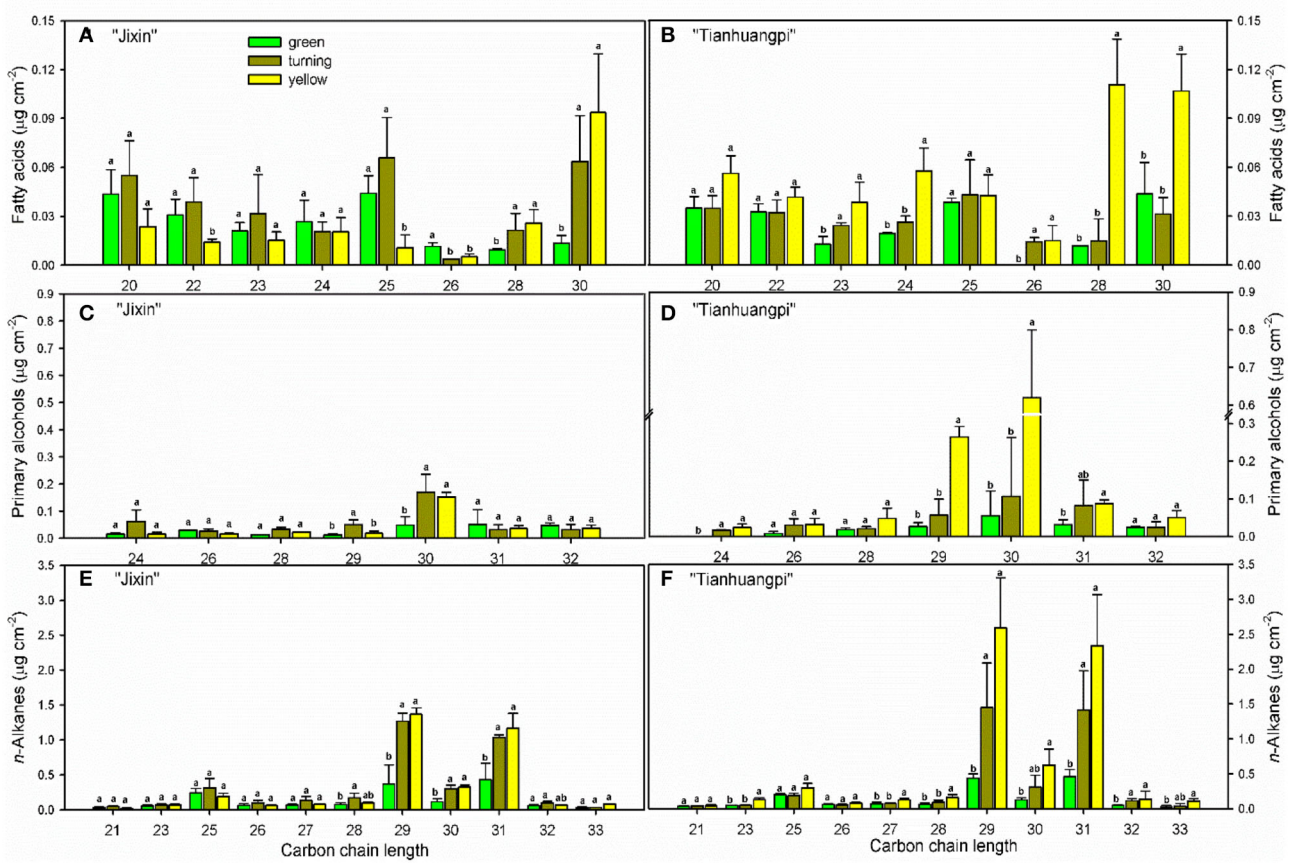

FIGURE 5 | Carbon chain-length distribution and content of aliphatics in wampee fruit (*Clausena lansium* (Lour.) Skeels). **(A,B)** fatty acids, **(C,D)** primary alcohols, and **(E,F)** *n*-alkanes in fruits at the green, turning, and yellow stages of "Jixin" and "Tianhuangpi" were comparatively analyzed, respectively. Data are given as means ± standard deviation ($n = 5$). Different letters indicate the significant differences at the level of 0.05.

from C_{20} to C_{30} were mainly even-numbered carbon chains with an increasing trend for C_{28} and C_{30} during development (**Figure 5B** and **Supplementary Materials**—waxes). Similar to fatty acids, primary alcohols accumulated as even-numbered carbon chains between C_{24} and C_{32} and changed mostly in C_{30} (**Figure 5C** and **Supplementary Materials**—waxes). Only a small amount of C_{30} for aldehydes was detected in wampee fruit waxes (**Supplementary Materials**—waxes).

The cyclics in the waxes of wampee fruits were found to be mainly triterpenoids and sterols. Triterpenoids as the prominent cyclic components comprised various members, the most abundant being uvaol (37.2– 40.3% in "Jixin" and 23.9–51.2% in "Tianhuangpi"), followed by lupeol, α-amyrin, β-amyrin, σ-amyrin, and taraxerol (**Figure 6**). These triterpenoids were detected to maintain relatively stable levels from the green to yellow ripe stages in both "Jixin" and "Tianhuangpi" (**Figure 6** and **Supplementary Materials**—waxes). Campesterol, stigmasterol, and β-sitosterol were detected as the sterol constituents, in which stigmasterol and β-sitosterol increased notoriously during development. In addition, small amounts of tocopherols as phenolic components were also detected (**Figure 6** and **Supplementary Materials**—waxes).

Cuticular Transpiration of Wampee Fruit

Transpiration was measured at different developmental stages by continually recording the weight loss. As shown in **Figure 7A**, water loss in weight per unit of the surface area of wampee fruit at different stages exhibited linear changes over time ($r^2 > 0.99$). Plant transpiration has been reported to be regulated either by the surface stomata exhibiting a dynamic process named drying curve or by the hydrophobic barrier contributed by the cuticle with linear changes of water loss (Burghardt and Riederer, 2003; Zeisler-Diehl et al., 2017). The transpiration of wampee fruit exhibited linear changes during the measured time period extending up to 24 h or even longer. This indicated a single main factor affecting the barrier property for transpiration in wampee fruit. Taking the driving force into account, permeance for water in wampee fruit was lower in "Tianhuangpi" than in "Jixin" at both green and yellow stages. In contrast, water permeability exhibited the lowest levels at the yellow ripe stage in both "Jixin" and "Tianhuangpi" (**Figure 7B**). Permeance for water varied between 2.0×10^{-4} m s^{-1} (green) and 1.7×10^{-4} m s^{-1} (yellow) in "Jixin" and from 1.6×10^{-4} m s^{-1} (green) to 1.4×10^{-4} m s^{-1} (yellow) in "Tianhuangpi" (**Figure 7B**).

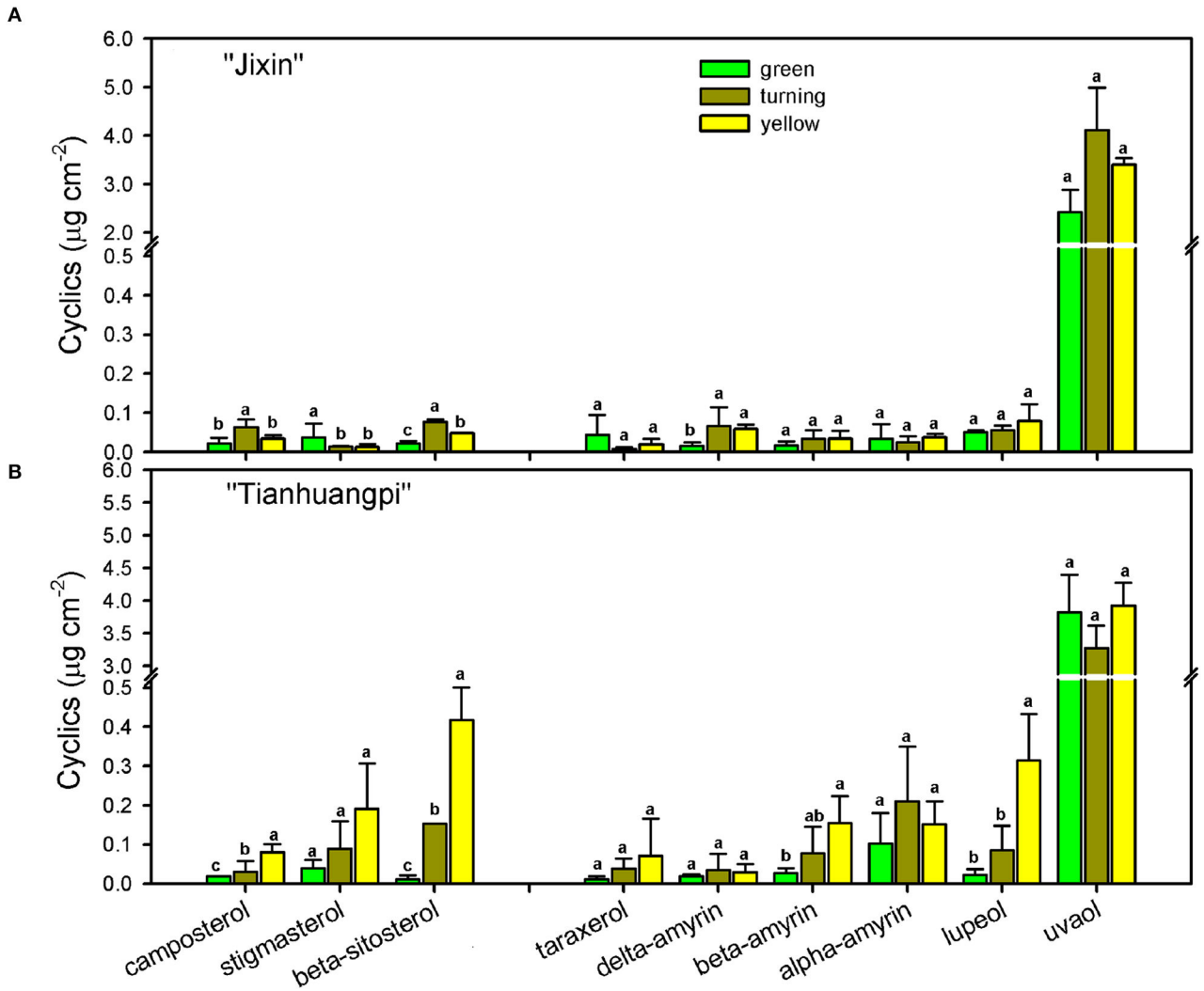

FIGURE 6 | Changes in sterols and triterpenoids as cyclic pattern in wax mixtures of wampee fruit (*Clausena lansium* (Lour.) Skeels). Fruits at the green, turning, and yellow stages of two cultivars **(A)** "Jixin" and **(B)** "Tianhuangpi" were comparatively analyzed. Data are given as means ± standard deviation ($n = 5$). Different letters indicate the significant differences at the level of 0.05.

DISCUSSION

Wampee fruit is rich in phytochemicals with antioxidant and anticancer activities (Prasad et al., 2009; Ye et al., 2019). However, the main part of peel tissues, the outer cuticle, has not been previously studied. The cutin matrix was constructed by numerous monomers dominated by 9/10,16-dihydroxy fatty acids, varying from 38.9% in yellow "Tianhuangpi" to 50.3% in green "Jixin" of total monomers (**Figure 3** and **Supplementary Materials**—cutin monomers). Monomers of ω-, mid-dihydroxy fatty acids as the main cutin components have been reported in many other fruits, especially in tomatoes (Leide et al., 2007), peppers (Parsons et al., 2013), pitayas (Huang and Jiang, 2019), olives (Huang et al., 2017), and selected northern berries (Järvinen et al., 2010). However, the main monomer components in the wampee fruit cuticle were different from those of the citrus fruit (species in the same family as wampee), in which ω-hydroxy fatty acids with mid-chain oxo-group dominated in cutin monomers (Wang et al., 2016). Besides the cutin monomers, *n*-alkanes ranged from 21.4% in green "Tianhuangpi" to 39.3% in yellow "Tianhuangpi" as the main aliphatics, while triterpenoids varied between 28.2% in yellow "Tianhuangpi" and 53.6% in green "Tianhuangpi" as cyclic components (**Figure 5A** and **Supplementary Materials**—waxes). The *n*-alkanes and triterpenoids have also been found as prominent compounds in waxes in tomatoes (Leide et al., 2007) and cherries (Belge et al., 2014).

The cutin monomers and waxes accumulated in similar chemical classes but exhibited cultivar- and development-related variability in wampee fruit. The coverage of waxes and cutin monomers, as well as their variety of components, was overall lower in "Jixin" than in "Tianhuangpi" (**Figures 3**, **4**

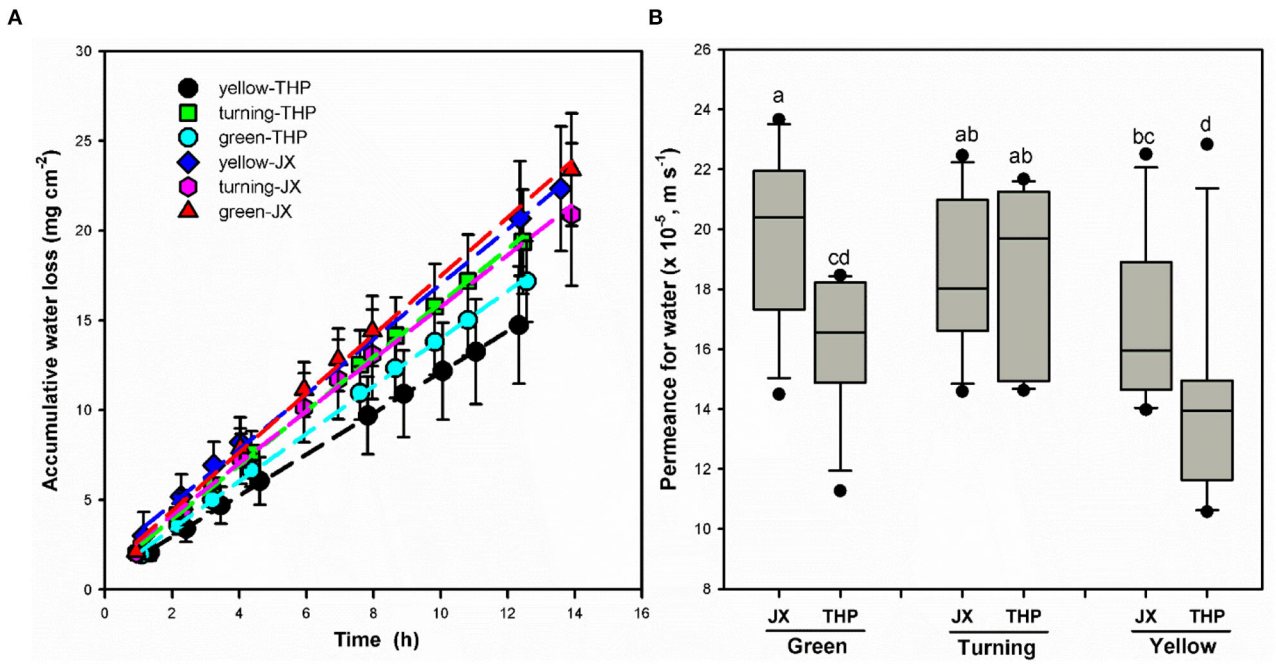

FIGURE 7 | (A,B) Transpiration in wampee fruit (*Clausena lansium* (Lour.) Skeels) at the green, turning, and yellow stages of "Jixin" —JX and "Tianhuangpi" —THP. Data are given as means ± standard deviation ($n = 15$). Different letters indicate the significant differences at the level of 0.05.

and **Supplementary Materials**—cutin monomers and waxes). Similar cultivar-related differences were reported in sweet cherries (Belge et al., 2014), olives (Diarte et al., 2019), grape berries (Yang et al., 2021), and northern berries (Järvinen et al., 2010). In addition, cuticular components in mass per unit of fruit surface area were accumulated in lower levels in the green fruit and were highest at the turning stage in "Jixin", while they increased gradually in "Tianhuangpi" during development (**Figures 3**, **4** and **Supplementary Materials**). The surface waxes increased gradually in mass in bayberry and grape berry fruits and peaked at 85 and 81 DAA, respectively, while exhibiting a slightly decreasing trend thereafter (Simpson and Ohlrogge, 2016; Arand et al., 2021). It has also been mentioned that both cutin monomers and waxes exhibited an increasing trend during development in tomato (Leide et al., 2007) and cherry (Peschel et al., 2007). In citrus fruits, the distant relatives of wampee, the accumulation of cutin monomers increased with the expansion of the fruits and peaked at 180 DAA (color turning stage), whereas waxes increased through the whole developmental period till 240 DAA (Wang et al., 2016). As a result, the cultivar and developmental time differences in wampee fruit exhibited the typical berry characteristics on the basis of the changes in cuticular chemical composition.

The cuticle functions as an extracellular membrane covering plant surfaces and is largely affected by the chemical constituents and their structural arrangements (Riederer and Schreiber, 2001). On the basis of the above chemical analysis, wampee fruit forms a similar berry fruit cuticle, which plays an important role against nonstomatal transpiration, pathogen infection, and fruit cracking. The *n*-alkanes, dominated by C_{29} and C_{31}, as well as the main carbon chain of C_{30} for fatty acids, primary alcohols, and aldehydes were the main VLC aliphatic components (**Figure 5** and **Supplementary Materials**—waxes). In addition, the VLC aliphatics in mass per surface area were lower at the green stages and increased following the development of the fruit in both "Jixin" and "Tianhuangpi." Consequently, the overall carbon chain aliphatics indicated by average chain length shifted from C_{28} to C_{29} during development (**Table 1**). As the efficiency of the hydrophobic barrier to transpiration is largely contributed by the VLC aliphatic compounds (Leide et al., 2007), changes in VLC components may influence the water status in wampee fruit.

Similar to the changes in cuticular chemicals, transpiration of wampee fruit also exhibited cultivar and developmental time differences. It has been reported that transpiration of plant tissues was mainly regulated by stomata and the outermost hydrophobic cuticle. When stomata are open, the dynamic water loss is evidenced as a drying curve, which shows a rapid initial water loss and slows down following the closing of stomata (Burghardt and Riederer, 2003). In contrast, the behavior is linear for transpiration *via* nonstomatal surfaces or when most stomata are closed (Zeisler-Diehl et al., 2017). In this study, the linear dynamic changes of water loss even during prolonged measurements, indicating a single barrier for transpiration, were largely contributed by the cuticle in wampee fruit. Water permeability was generally lower in "Tianhuangpi" than in "Jixin" and showed the highest level at the green stage with a decreasing trend during development (**Figure 7**). Simultaneously, the overall VLC aliphatics on total waxes,

especially the major pattern of *n*-alkanes, C_{29} and C_{31}, increased in both mass per surface area and relative level during fruit development (**Supplementary Materials**—waxes). Accordingly, a negative correlation between the accumulation of VLC *n*-alkanes and the water permeability was found ($r^2 = 0.84$, $p < 0.01$). It has been verified that the VLC aliphatics, especially hydrocarbons, are pivotal in regulating the transpiration in plants to adapt to water-deficit stresses (Kosma et al., 2009; Patwari et al., 2019; Dimopoulos et al., 2020). The increase of VLC aliphatics, in both amount and relative level, may enhance the hydrophobic crystalline zones in the cuticle (Riederer and Schreiber, 1995; Huang et al., 2017), thus slowing down the transpiration in wampee fruit during development.

It is noteworthy that triterpenoids, another major family of wax compounds, accumulated steadily in mass per surface area but decreased in the relative level during fruit development (**Figures 5**, **6**). It has been mentioned that the triterpenoids were largely detected in the intracuticular layer in plants (Jetter and Riederer, 2015; Arand et al., 2021). In wampee fruit, uvaol as the major triterpenoid was released together with cutin monomers, which was embedded in the cutin matrix. The abundant triterpenoids were implicated to function as fillers embedding in the cutin matrix to plasticize and enhance the mechanical properties of the cuticle (Tsubaki et al., 2013; España et al., 2014). Cutin monomers polymerize as a matrix to provide scaffolding for the accumulation of waxes and also enhance the mechanical support in the cuticle (Fich et al., 2016). In tomatoes, cutin deficit was found to accelerate fruit softening and susceptibility to pathogen infection (Isaacson et al., 2009; Yeats et al., 2012). During the development of wampee fruit, the amount of triterpenoids and cutin monomers increased per surface area, while the relative level of total wax content and total cutin monomers decreased remarkably (**Figures 3**, **6** and **Supplementary Materials**). These changes may induce the alteration in the arrangement of cuticular chemicals on a spatial level.

In addition, berry fruits are susceptible to cracking during development or at the ripening stage such as in cherries, grape berries, plums, and tomatoes (Khadivi-Khub, 2014). As wampee fruit exhibits similar characteristics to these berry fruits, the increase of chemical components in the cuticle might be important to enhance the barrier so as to protect from fruit cracking. On the one hand, the fruit exhibits vigorous metabolism and high transpiration during development. Thus, it needs to accumulate waxes and cutin to enhance mechanical properties maintaining the fruit integrity during the expansion of fruit (Knoche and Lang, 2017). Though lower amounts of cuticular components accumulated in green fruit, the higher relative contents of triterpenoids and cutin monomers were important to strengthen the mechanical properties of the cuticle to protect fruit integrity. On the other hand, with the expansion of the fruit, the relative content of cuticular chemicals decreased in cyclics and cutin monomers, which may form a less tight cuticle, inducing cracking in ripe berries compared with young fruits (Knoche et al., 2004). In addition, as compared to green fruits, water permeability was lower in ripe fruit, which might be because of the maintenance of fruit quality following the ripening of the fruit (**Figure 7**). It should be noted that *n*-alkanes as one of the main wax components exhibited an increasing trend for both mass per surface area and the relative content level (**Figure 5** and **Supplementary Materials**—waxes). It has also been proposed that the accumulation of *n*-alkanes was probably taking part in enhancing the tolerance to cracking in cherry fruits (Ríos et al., 2015). Therefore, the decline of the relative level in cyclics and cutin monomers may broaden the space in the cuticle to embed the *n*-alkanes, thus forming a better barrier to transpiration in wampee fruit at the ripe stage.

In conclusion, this study reports the detailed chemical composition of waxes and cutin monomers as well as their potential effects on the transpiration barrier properties in wampee fruit. The cuticular chemical composition and transpiration properties exhibited cultivar and developmental time differences following the expansion of wampee fruit. Cuticular waxes were dominated by *n*-alkanes and triterpenoids, while ω-, mid-chain dihydroxy fatty acids were the prominent cutin monomers. The contents of cuticular chemical composition were higher in "Tianhuangpi" than in "Jixin" and were lower in green fruits. Transpiration was higher in the green fruit and decreased during development. In addition, the increase of *n*-alkanes, dominated by C_{29} and C_{31}, in both mass per area and relative content levels provided further insights into the importance of hydrocarbons to form hydrophobic barriers in the cuticle. To the best of our knowledge, this study provides the first approach to cuticle chemicals as well as to the physiological functions, taking transpiration as an example in wampee fruit. Further study on the effect of cuticles on fruit cracking and microbial infection is necessary.

DATA AVAILABILITY STATEMENT

The original contributions presented in the study are included in the article/**Supplementary Material**, further inquiries can be directed to the corresponding authors.

AUTHOR CONTRIBUTIONS

HH designed and performed most of the experiments and prepared the draft of the manuscript. LW and DQ contributed to part of the experiments and data analyses. YL took part in revising the manuscript and participated in funding acquisition. All authors approved the final version of the manuscript.

FUNDING

This work was supported by the Funding for Excellent Young Scientists of Guangdong Academy of Agricultural Sciences (R2021YJ-YB1005), Wild Plant Resources (Fruit Trees) Survey, Collection and Evaluation Project (2021KJ269), Funding of Young Scientist Cultivation for Institute of Fruit Tree Research, Guangdong Academy of Agricultural Sciences (2021-107), Common Technical Innovation Team of Guangdong Province on Preservation and Logistics of

Agricultural Products (2022KJ145), the Innovation Team of Modern Agricultural Industry Technology System in Guangdong Province of China (2021KJ116), the Special Financial Fund of Foshan-Guangdong Agricultural Science and Technology Demonstration City Project (2021), the National Tropical Plants Germplasm Resources Center, the Guangdong Basic and Applied Basic Research Foundation (2019A1515110611), Funding from Guangxi Key Laboratory of Fruits and Vegetables Storage-Processing Technology (2021-01), the "Pearl River Talent Plan" for Young Scientists Program of Guangdong Province [2018(2)], and special fund for scientific innovation strategy-construction of high level Academy of Agriculture science of Guangdong Academy of Agricultural Sciences (R2019QD-012).

SUPPLEMENTARY MATERIAL

The Supplementary Material for this article can be found online at: https://www.frontiersin.org/articles/10.3389/fpls.2022.840061/full#supplementary-material

REFERENCES

Arand, K., Bieler, E., Dürrenberger, M., and Kassemeyer, H. H. (2021). Developmental pattern of grapevine (*Vitis vinifera* L.) berry cuticular wax: Differentiation between epicuticular crystals and underlying wax. *PLoS ONE.* 16, e0246693. doi: 10.1371/journal.pone.0246693

Belge, B., Llovera, M., Comabella, E., Gatius, F., Guillén, P., Graell, J., et al. (2014). Characterization of cuticle composition after cold storage of "celeste" and "somerset" sweet cherry fruit. *J. Agric. Food Chem.* 62, 8722–8729. doi: 10.1021/jf502650t

Burghardt, M., and Riederer, M. (2003). Ecophysiological relevance of cuticular transpiration of deciduous and evergreen plants in relation to stomatal closure and leaf water potential. *J. Exp. Bot.* 54, 1941–1949. doi: 10.1093/jxb/erg195

Chokeprasert, P., Huang, T. C., Chen, H. H., Khotavivattana, S., and Oupadisskoon, C. (2005). Effect of drying conditions on qualities of dried wampee. *Agric. Nat. Resour.* 39, 416–423.

Diarte, C., Lai, P. H., Huang, H., Romero, A., Casero, T., Gatius, F., et al. (2019). Insights into olive fruit surface functions: a comparison of cuticular composition, water permeability, and surface topography in nine cultivars during maturation. *Front. Plant Sci.* 10, (1484).doi: 10.3389/fpls.2019.01484

Dimopoulos, N., Tindjau, R., Wong, D. C., Matzat, T., Haslam, T., Song, C., et al. (2020). Drought stress modulates cuticular wax composition of the grape berry. *J. Exp. Bot.* 71, 3126–3141. doi: 10.1093/jxb/eraa046

España, L., Heredia-Guerrero, J. A., Segado, P., Benítez, J. J., Heredia, A., and Domínguez, E. (2014). Biomechanical properties of the tomato (*Solanum lycopersicum*) fruit cuticle during development are modulated by changes in the relative amounts of its components. *New Phytol.* 202, 790–802. doi: 10.1111/nph.12727

Fich, E. A., Segerson, N. A., and Rose, J. K. C. (2016). The plant polyester cutin: biosynthesis, structure, and biological roles. *Annu. Rev. Plant Biol.* 67, 207–233. doi: 10.1146/annurev-arplant-043015-111929

Fu, J. R., Jin, J. P., Peng, Y. F., and Xia, Q. H. (2008). Desiccation tolerance in two species with recalcitrant seeds: *Clausena lansium* (Lour.) and *Litchi chinensis* (Sonn.). *Seed Sci. Res.* 4, 257–261. doi: 10.1017/S0960258500002245

Hansjakob, A., Bischof, S., Bringmann, G., Riederer, M., and Hildebrandt, U. (2010). Very-long-chain aldehydes promote in vitro prepenetration processes of Blumeria graminis in a dose-and chain length-dependent manner. *New Phytol.* 188, 1039–1054. doi: 10.1111/j.1469-8137.2010.03419.x

Holloway, P. J. (1982). "The chemical constitution of plant cutins," in *The Plant Cuticle*, Cutler, D. F, Alvin, K. L, Price, C. E (eds). *London: Academic Press. p.* 45–85.

Huang, H., Burghardt, M., Schuster, A., Leide, J., Lara, I., and Riederer, M. (2017). Chemical composition and water permeability of fruit and leaf cuticles of *Olea europaea* L. *J. Agric. Food Chem.* 65, 8790–8797. doi: 10.1021/acs.jafc.7b03049

Huang, H., and Jiang, Y. (2019). chemical composition of the cuticle membrane of pitaya fruits (*Hylocereus Polyrhizus*). *Agriculture.* 9, 250. doi: 10.3390/agriculture9120250

Isaacson, T., Kosma, D. K., Matas, A. J., Buda, G. J., He, Y., Yu, B., et al. (2009). Cutin deficiency in the tomato fruit cuticle consistently affects resistance to microbial infection and biomechanical properties, but not transpirational water loss. *Plant J.* 60, 363–377. doi: 10.1111/j.1365-313X.2009.03969.x

Järvinen, R., Kaimainen, M., and Kallio, H. (2010). Cutin composition of selected northern berries and seeds. *Food Chem.* 122, 137–144. doi: 10.1016/j.foodchem.2010.02.030

Jetter, R., Kunst, L., and Samuels, A. L. (2008). Composition of plant cuticular waxes. *Biol. Plant Cuticle.* 23, 145–181. doi: 10.1002/9780470988718.ch4

Jetter, R., and Riederer, M. (2015). Localization of the transpiration barrier in the epi- and intracuticular waxes of eight plant species: water transport resistances are associated with fatty acyl rather than alicyclic components. *Plant Physiol.*170, 921–934. doi: 10.1104/pp.15.01699

Khadivi-Khub, A. (2014). Physiological and genetic factors influencing fruit cracking. *Acta Physiologiae Plantarum.* 37, (1718). doi: 10.1007/s11738-014-1718-2

Knoche, M., Beyer, M., Peschel, S., Oparlakov, B., and Bukovac, M. J. (2004). Changes in strain and deposition of cuticle in developing sweet cherry fruit. *Physiologia Plantarum.* 120, 667–677. doi: 10.1111/j.0031-9317.2004.0285.x

Knoche, M., and Lang, A. (2017). Ongoing growth challenges fruit skin integrity. *CRC Crit Rev Plant Sci.* 36, 190–215. doi: 10.1080/07352689.2017.1369333

Kosma, D. K., Bourdenx, B., Bernard, A., Parsons, E. P., Lue, S., Joubes, J., et al. (2009). The impact of water deficiency on leaf cuticle lipids of arabidopsis. *Plant Physiol.* 151, 1918–1929. doi: 10.1104/pp.109.141911

Leide, J., Hildebrandt, U., Reussing, K., Riederer, M., and Vogg, G. (2007). The developmental pattern of tomato fruit wax accumulation and its impact on cuticular transpiration barrier properties: effects of a deficiency in a β-ketoacyl-coenzyme A synthase (LeCER6). *Plant Physiol.* 144, 1667–1679. doi: 10.1104/pp.107.099481

Nobel, P. (2009). *Physicochemical and Environmental Plant Physiology.* Oxford: Academic Press.

Parsons, E. P., Popopvsky, S., Lohrey, G. T., Alkalai-Tuvia, S., Perzelan, Y., Bosland, P., et al. (2013). Fruit cuticle lipid composition and water loss in a diverse collection of pepper (Capsicum). *Physiologia Plantarum.* 149, 160–174. doi: 10.1111/ppl.12035

Patwari, P., Salewski, V., Gutbrod, K., Kreszies, T., Dresen-Scholz, B., Peisker, H., et al. (2019). Surface wax esters contribute to drought tolerance in Arabidopsis. *Plant J.* 98, 727–744. doi: 10.1111/tpj.14269

Peng, W., Fu, X., Li, Y., Xiong, Z., Shi, X., Zhang, F., et al. (2019). Phytochemical study of stem and leaf of *Clausena lansium*. *Molecules.* 24, 3124. doi: 10.3390/molecules24173124

Peschel, S., Franke, R., Schreiber, L., and Knoche, M. (2007). Composition of the cuticle of developing sweet cherry fruit. *Phytochem.* 68, 1017–1025. doi: 10.1016/j.phytochem.2007.01.008

Prasad, K. N., Hao, J., Yi, C., Zhang, D., Qiu, S., Jiang, Y., et al. (2009). Antioxidant and anticancer activities of wampee (*Clausena lansium* (Lour.) Skeels) peel. *J. Biotechnol. Biomed. 2009,* 612805. doi: 10.1155/2009/612805

Prasad, K. N., Xie, H., Hao, J., Yang, B., Qiu, S., Wei, X., et al. (2010). Antioxidant and anticancer activities of 8-hydroxypsoralen isolated from wampee (*Clausena lansium* (Lour.) Skeels) peel. *Food Chem.* 118, 62–66. doi: 10.1016/j.foodchem.2009.04.073

Riederer, M., and Schreiber, L. (1995). "Waxes: the transport barriers of plant cuticles. Waxes—The Transport Barriers of Plant Cuticles," *in Waxes: Chemistry, Molecular Biology and Functions, Hamilton, R.J., (eds). West Ferry, Dundee: The Oily Press.* 6, 130–156.

Riederer, M., and Schreiber, L. (2001). Protecting against water loss: analysis of the barrier properties of plant cuticles. *J. Exp. Bot.* 52, 2023–2032. doi: 10.1093/jexbot/52.363.2023

Ríos, J. C., Robledo, F., Schreiber, L., Zeisler, V., Lang, E., Carrasco, B., et al. (2015). Association between the concentration of n-alkanes and tolerance to cracking in commercial varieties of sweet cherry fruits. *Scientia Horticulturae.* 197, 57–65. doi: 10.1016/j.scienta.2015.10.037

Rodrigues, S., de Brito, E. S., and de Oliveira Silva, E. (2018). "Wampee—*Clausena lansium"*, in *Exotic Fruits,* Rodrigues, S., de Oliveira Silva, E., de Brito, E.S. *(eds.). Academic Press. p.* 439–441. doi: 10.1016/B978-0-12-803138-4.00059-9

Serrano, M., Coluccia, F., Torres, M., L'Haridon, F., and Métraux, J. P. (2014). The cuticle and plant defense to pathogens. *Front. Plant Sci.* 5, 274. doi: 10.3389/fpls.2014.00274

Shao, Y., Jiang, Z., Zeng, J., Li, W., and Dong, Y. (2020). Effect of ethanol fumigation on pericarp browning associated with phenol metabolism, storage quality, and antioxidant systems of wampee fruit during cold storage. *Food Sci. Nutr.* 8, 3380–3388. doi: 10.1002/fsn3.1617

Shen, D. Y., Kuo, P. C., Huang, S. C., Hwang, T. L., Chan, Y. Y., Shieh, P. C., et al. (2017). Constituents from the leaves of Clausena lansium and their anti-inflammatory activity. *J Nat Med.* 71, 96–104. doi: 10.1007/s11418-016-1033-x

Simpson, J. P., and Ohlrogge, J. B. (2016). A novel pathway for triacylglycerol biosynthesis is responsible for the accumulation of massive quantities of glycerolipids in the surface wax of bayberry (*Myrica pensylvanica*) Fruit. *Plant Cell.* 28, 248–264. doi: 10.1105/tpc.15.00900

Tsubaki, S., Sugimura, K., Teramoto, Y., Yonemori, K., and Azuma, J. I. (2013). Cuticular membrane of Fuyu persimmon fruit is strengthened by triterpenoid nano-fillers. *PLoS ONE.* 8, e75275. doi: 10.1371/journal.pone.0075275

Wang, J., Sun, L., Xie, L., He, Y., Luo, T., Sheng, L., et al. (2016). Regulation of cuticle formation during fruit development and ripening in 'Newhall' navel orange (*Citrus sinensis* Osbeck) revealed by transcriptomic and metabolomic profiling. *Plant Sci.* 243, 131–144. doi: 10.1016/j.plantsci.2015.12.010

Winkler, A., Blumenberg, I., Schürmann, L., and Knoche, M. (2020). Rain cracking in sweet cherries is caused by surface wetness, not by water uptake. *Scientia Horticulturae.* 269, 109400. doi: 10.1016/j.scienta.2020.109400

Yang, M., Luo, Z., Gao, S., Belwal, T., Wang, L., Qi, M., et al. (2021). The chemical composition and potential role of epicuticular and intracuticular wax in four cultivars of table grapes. *Postharvest Biol. Technol.* 173, 111430. doi: 10.1016/j.postharvbio.2020.111430

Ye, Y., Chang, X., Brennan, M. A., Brennan, C. S., and Guo, X. (2019). Comparison of phytochemical profiles, cellular antioxidant and anti-proliferative activities in five varieties of wampee (*Clausena lansium*) fruits. *Int. J. Food Sci.* 54, 2487–2493. doi: 10.1111/ijfs.14205

Yeats, T. H., Martin, L. B. B., Viart, H. M. F., Isaacson, T., He, Y., Zhao, L., et al. (2012). The identification of cutin synthase: formation of the plant polyester cutin. *Nat. Chem. Biol.* 8, 609–611. doi: 10.1038/nchembio.960

Yeats, T. H., and Rose, J. K. C. (2013). The formation and function of plant cuticles. *Plant Physiol.* 163, 5–20. doi: 10.1104/pp.113.222737

Zeisler-Diehl, V. V., Migdal, B., and Schreiber, L. (2017). Quantitative characterization of cuticular barrier properties: methods, requirements, and problems. *J. Exp. Bot.* 68, 5281–5291. doi: 10.1093/jxb/erx282

Zhou, J. N., Liu, S. Y., Chen, Y. F., and Liao, L. S. (2015). First report of pantoea anthophila causing soft rot disease in *Clausena lansium* (Wampee) in China. *Plant Dis.* 99, 416–416. doi: 10.1094/PDIS-10-14-1025-PDN

Conflict of Interest: The authors declare that the research was conducted in the absence of any commercial or financial relationships that could be construed as a potential conflict of interest.

Publisher's Note: All claims expressed in this article are solely those of the authors and do not necessarily represent those of their affiliated organizations, or those of the publisher, the editors and the reviewers. Any product that may be evaluated in this article, or claim that may be made by its manufacturer, is not guaranteed or endorsed by the publisher.

Frontiers in
Plant Science

Cultivates the science of plant biology and its applications

The most cited plant science journal, which advances our understanding of plant biology for sustainable food security, functional ecosystems and human health.

Discover the latest Research Topics

See more →

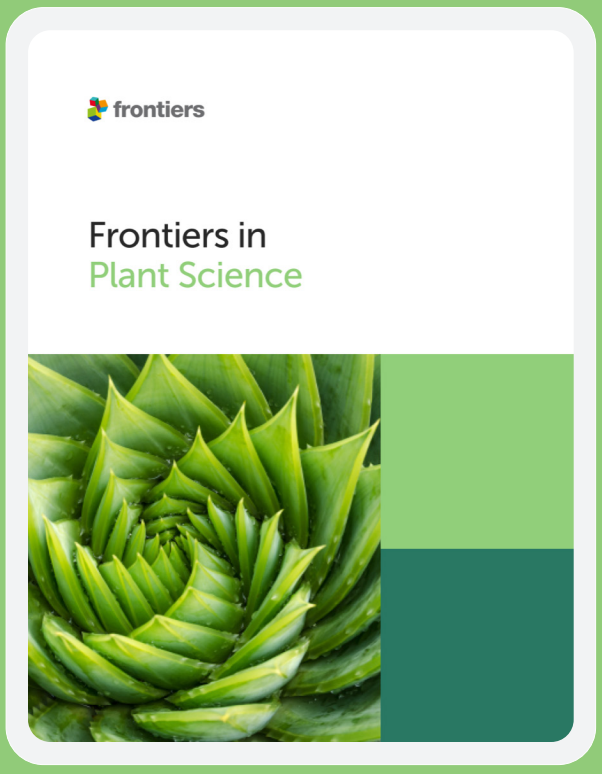

Frontiers

Avenue du Tribunal-Fédéral 34
1005 Lausanne, Switzerland
frontiersin.org

Contact us

+41 (0)21 510 17 00
frontiersin.org/about/contact